„HENRI COANDĂ”
AIR FORCE ACADEMY

ROMANIA

ASSOCIATION for
RESEARCH and EDUCATION

„GENERAL M. R. STEFANIK”
ARMED FORCES ACADEMY

SLOVAK REPUBLIC

AFASES 2016

ISSN, ISSN-L: 2247-3173
DOI:10.19062/2247-3173.2016.18.1

Volume I

Publishing House of "Henri Coanda" Air Force Academy

Str. Mihai Viteazu 160, Brasov 500183, ROMANIA
Phone: +40 268 423 421, Fax: +40 268 422 004
Webpage: www.afahc.ro/ro/editura/editura.html
E-mail: editura@afahc.ro

INTERNATIONAL SCIENTIFIC COMMITTEE

Presidents ship:

Air Flotilla General **Vasile BUCINSCHI**, PhD

Doc.Ing. **Jozef PUTTERA**, CSc.

Members:

Associate Professor Eng. **Marcel HARAKAL**, PhD

Professor Eng. **Milan SOPÓCI,** PhD

Associate Professor **Mária PETRUFOVÁ**, PhD

Associate Professor **Ludovic Dan LEMLE**, PhD

Professor **Gherman A. DE LA REZA**, PhD

Professor Eng. **Juraj MIČEK**, PhD

Professor **Mircea LUPU**, PhD

Professor **Corneliu UDREA**, PhD

Professor **Ştefan-Gheorghe PENTIUC**, PhD

Professor **Dorin BOCU**, PhD

Associate Professor **Răzvan - Lucian ANDRONIC**, PhD

Associate Professor **Ciprian Ioan RĂULEA**, PhD

Assistant Professor **Constantin Edmond CRACSNER**, PhD

Assistant Professor **Cătălin Marius GHERASIM**, PhD

Associate Professor **Otilia TODOR**, PhD

Associate Professor **Marilena TICUŞAN**, PhD

Associate Professor **Ioana LEPĂDATU**, PhD

Associate Professor **Maria Dorina PAŞCA**, PhD

Professor **Vladimir HORAK**, PhD

Professor **Vitalijs PAVELKO**, PhD

Associate Professor **Michael TODOROV**, PhD

Associate Professor **Valentin ILIEV**, PhD

Professor **Adrian STOICA**, PhD

Senior Researcher **Alexandru DUMITRACHE**, PhD

Professor **Sterian DĂNILĂ**, PhD

Professor **Ion FUIOREA**, PhD

Senior Researcher **Valentin SILVESTRU**, PhD

Professor **Romulus LUNGU**, PhD

Associate Professor **Alexandru Nicolae TUDOSIE**, PhD

Professor **Ioan NICOLAESCU**, PhD

Professor **Vasile NUȚU**, PhD

Associate Professor **Răzvan NECHIFOR**, PhD

Associate Professor **Mihai MIHĂILĂ-ANDRES**, PhD

Associate Professor **Cristian MOLDOVEANU**, PhD

Associate Professor **Ion PURICEL**, PhD

Professor **Mihail ANTON**

Professor **Constantin DUGULEANĂ**, PhD

Professor **Philippe DONDON**, PhD

Professor **Daniela ROSCA**, PhD

Professor **Adrian ROSCA**, PhD

Professor **Yann LEDOUX**, PhD

Professor **Patrick SEBASTIAN**, PhD

Professor **Thierry PALIN-LUC**, PhD

Professor **Robert SZABOLCSI**, PhD

Professor Eng. **Alex ŞTEFAN**, PhD

Professor **Maria DINESCU**, PhD

Professor **Petrică VIZUREANU**, PhD

Associate Professor **Slawomir AUGUSTYN**, PhD

Professor Eng. **Marian PEARSICA**, PhD

Associate Professor Eng. **Doru LUCULESCU**, PhD

ORGANIZING COMMITTEE

Chair:

Lt.Col. **Laurian GHERMAN**, PhD

***Members*:**

Lt.Col. **Ionică CÎRCIU**, PhD
Professor Eng. **Constantin ROTARU**, PhD
Col. Associate Professor **Laurenţiu POPESCU**, PhD
Assistant Professor Eng. **Vasile PRISACARIU,** PhD
Lt.col. **Eduard MIHAI**
Assistant Professor Eng. **Constantin STRÎMBU**, PhD
Assistant Professor Eng. **Liliana MIRON**, PhD
Assistant Professor **Gheorghe RADU**, PhD
Assistant Professor **Mihaela SMEADĂ**, PhD
Assistant Professor **Diana ILIŞOI**, PhD
Cpt. **Laura Maria SABOSLAI-FOTIN**
Assistant Professor **Mihaela GURANDA,** PhD
Psychologist **Mihaela OANCEA**

Static exhibition:

Col. **Vasile ŞANDRU**, PhD
Col. **Ovidiu MOŞOIU.** PhD
Lt.Col. **Sorin VÂNT**

Logistics:

Col. **Dumitru DINU**
Assistant Professor Eng. **Cristian CONSTANTINESCU**, PhD
Assistant Professor **Bogdan MUNTEANU**, PhD
Lt.Col. **Bogdan CHIOSEAUA,** PhD
Lt.Col. **Cristian ENE**
Lt.Col. **Marian OANĂ**
Lt.Col. **Ionel FEROIU**
Maj. **Daniel STEFĂNESCU**
WO **Marius TĂNASE**
WO **Călin DOBREAN**
WO **Deneş SZABO**
WO **Marius CODREANU**
WO **Marian MIHALACHE**

Secretariat:

WO **Sergiu OBREJA**
Eng. **Mariana GHINDĂOANU**
Eng. **Daniela OBREJA**
Inf. **Adina DOBRIŢOIU**


A CENTURY
OF ROMANIAN
AIR DEFENSE
1916 - 2016

CONTENTS

VOLUME I

REMOTELY AND PILOTED AIRCRAFT SYSTEMS / LAW AND POLICIES

ELECTRICAL AND ELECTRONICAL ENGINEERING / RENEWABLE ENERGY AND ENVIRONMENT

MECHANICAL ENGINEERING. MATERIALS AND TECHNOLOGY

APPLIED MATHEMATICS, COMPUTER SCIENCE, IT&C


A CENTURY
OF ROMANIAN
AIR DEFENSE
1916 - 2016

VOLUME II

SOCIO - HUMANITIES

MANAGEMENT


A CENTURY
OF ROMANIAN
AIR DEFENSE
1916 - 2016

THE AIRPORT TRACING &HANDLING IN THE NEAR FUTURE

Sławomir AUGUSTYN, Hanna TURZYŃSKA

National Defence University Warsaw, Poland, Aviation & Air Defence Institute,
(s.augustyn@aon.edu.pl, hannaturzynska@poczta.onet.pl)

DOI: 10.19062/2247-3173.2016.18.1.1

Abstract: *The article shows a new approach to the vision in design of airports. This approach allows for analysis and assessment in the forecasting a new way of the aviation project. Moreover, this aspect influences on safety of aircraft and security of passengers.*

Due to the extensive theme, the subject of research was limited to select all technical sciences areasassociated with a new system in the project process of the aircraft.

Key words*: aviation design, safety and security system, project process.*

1. INTRODUCTION

Nowadays airports already considered “cities” due to the millions of passengers who attend a day, but also the attractions and many other establishments have, making people feel good and more comfortable. Being considered a world apart, airports require a lot of supervision and safety by all employees who work there because of the many people who attend daily, as mentioned earlier.

One of the areas that most headaches gives airport managers are Tracking and Handling of baggage and cargo. It is a very complex process that requires many trained workers and adequate specialist in Ground Handling, and many security measures.

We will now explain all this complex process that will begin at check-in and will end only when the passenger to get back in the suitcase back, already at your destination [3].

Airports are vital parts of every kind of air transportation network and therefore day and night as well as under any weather condition, which allows aircraft operation, needed for perfect and safe handling services in any way. This includes provision of accurate de-icing and anti-icing of aircraft surfaces prior take off. Without proper treatment of an aircraft during snowy and iceconditions, the accumulation of frost, ice or snow changes the airflow over the aircraft wings, reducing the lift and increasing the drag. Ice and snow also adds to the total weight of an aircraft, increasing its required lift for takeoff. The combination of these effects can bring about significant consequences. The need to improve all-weather flying safety is absolutely necessary and beyond of any discussion. Two main factors are influencing the possibilities of avoiding ice on aircrafts and making it necessary to continuing optimizing the existing procedures: first economic reasons and second ecological reasons. For the economical approach a simple sentence is valid: An aircraft only makes money if it’s airborne [7]. Thus airlines want the overall turnaround process, which includes de- and anti-icing, at the gate, which includes de- and anti-icing, to be as short as possible. For environment protection the providers of de- and anti-icing services are legally forced to use a minimum of applicable chemicals, depending on the used technology. This part of the article discusses current procedures provided by Ground

Handling Operators as well as new ways in tracking by RFID system and to ensure ice-free aircraft surfaces, but does not discuss the possibilities of built-in technologies to protect the aircraft during flight.

2. A NEW WAY OF BAGGAGE TRACKING AND HANDLING

The passengers and baggage make boarding as easy and as quick as possible. A lot of the time they get it right and their flight leaves on time and without delay. But sometimes things happen that are out of their control and things seem to go wrong. For an example, you may have been called to the departure gate and the aircraft isn't there, your first thought is probably "Why am I here?''.To try and answer this question, and others, they have put together a timeline of what is happening while you are standing in a queue.

The boarding procedure starts when you get the call to go to the gate (normally an hour before the STD). You should try and make your way to the gate as soon as possible, but as long as you are there before the gate closes you'll be fine. Once you're at the gate, normally two queues will appear. The speedy boarders who have paid for up front seating, over wing seatsand families with children under 5, and passengers with reduced mobility and the other queue for the all remaining customers. About 30 minutes before take-off, there will be something called "Pre-boarding" this is when the staff at the gate will start to check ID documents and boarding passes (if appropriate) and you'll move through the gate. While this is happening it is quite common that the plane will have only just got to the gate. As soon as the plane has reached the gate, passengers are disembarked, their luggage is unloaded and the cabin is tidied by the cabin crew. Also in this time, extra catering may be brought on board and refuelling the plane will begin. All of this happens within the first 10 minutes after touchdown. As soon as refuelling is nearly complete, you'll be asked to start boarding the plane. You're boarding pass isn't required after your check at the gate, so you can walk straight onto the plane and take your seat. Just remember your seat number. While you are doing this the plane will finish refuelling and your hold luggage will be loaded. This part of the process should only take 10-15 minutes. Once you are all on board and sat down, the cabin doors will close along with the hold doors and you'll be nearly ready to take off [6].

Airlines have tinkered with different boarding systems almost since the days of Orville and Wilbur Wright, who tossed a coin to decide who would fly first aboard their biplane. Plenty of people have offered ideas for improvement, but no perfect method has ever emerged. Most airlines let first-class and other elite customers board first. After that, some carriers fill the rear rows and work toward the front. Others fill window seats and work toward the aisle. Some use a combination of the two. Airlines have also tried other tricks, like letting people board early if they do not have aisle-clogging carry-on bags. It's not trivial stuff. With many flights full, anxious passengers know that boarding late means there might not be any room left in the overhead bin. And it matters to the airlines. Slow boarding creates delays, which mean missed connections, unhappy customers and extra costs. Delta's Early Valet service will offer to have airline employees take carry-on bags at the gate and put them in the bins above assigned seats. The airline wants to see if its own workers can load the bins faster than passengers [1].

According to a method, the first seat to board would be the back window, followed by the third-to-back window on the same side, and so on up the aisle.

People need about two rows to stow their stuff, the model showed.Then the other side of the plane would board outside-first, back-to-front.When all the window seats were seated, the middle seat passengers would file in, back to front-allowing for multiple people to sit at the same time. Travelers don't always come in single-servings-What about

for families or people who are traveling together?-According to this question: fill the even-numbered rows first, starting on one side of the plane and moving to the other.Then repeat with the add-numbered rows.This method also beat out the competition, boarding twice as fast as starting in the back.

Today many world airports or we can say almost everyone, using the RFID system as tracking and baggage handling.

An RFID system consists basically of one antenna, a transceiver, which is the signal reading and transfers the information to a reader device, and also a transponder or RF tag (radio frequency), which should contain the circuit and the information to be transmitted. These labels can be present in people, animals, products, packaging, in short, in different equipment [4].

Thus, the antenna transmits information by issuing the integrated circuit signal to transmit its information to the reader, which in turn converts the radio waves from RFID to digital information. Now, after converted, they can be read and understood by a computer to then have your data analyzed.

For this, the transponders should be attached in bags and on passengers' tickets at check-in, so that there is a unique ID for both the purpose of enabling the tracking of baggage all the way and identification of their respective owners.

With regard to the utilized transponders, for safety is the type read-only, i.e., no information in addition to the serial assigned at registration, must be registered. Therefore, no luggage identification or passenger will be changed to avoid possible fraud. In cases of additional information will be registered in a central database, at the time a suitcase go through an RFID reader and its serial is captured.

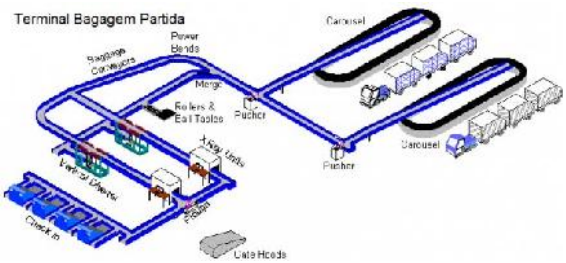

FIG. 1. The tracking of bags made by f RFID readers system
source:www.waspbarcode.com

The tracking of bags will be made by means of RFID readers, shown in Figure 1. They will be present at times when the bags are in and out of the aircraft. Readers should be attached to conveyor belts to indicate whether the case is in connection, going to another aircraft, or if she is going to the landing section.

We can say that this system is quite functional and mostly effective in the way it is used in international airports.

Although effective are increasingly lost luggage throughout the world and many of them end up never return to their respective owners, this is due to the fact that air traffic is increasingly rising. This system is used by the Lost and Found (telecommunications software) by almost all airports worldwide with this tracking system.

A measure which can help this system is very introducing a GPS chip. This chip could help us understand exactly the precise location of a suitcase or a load that may be lost. Despite the RFID system is quite effective often is lost bags between location stations, but also we have a GPS chip know for sure where the suitcase is, what will help Handling Ground companies and will help companies air service level.

3. POSSIBLE FUTURE OF DE-ICING TECHNOLOGY

The infrared (IR) de-icing technology involves melting frost, ice, and snow from aircraft surface with infrared energy. IR energy systems are based on natural gas- or propane-fired emitters that are used to melt frost, ice, and snow. Infrared energy does not heat up the surrounding air and tests have shown that it has negligible effect on the aircraft cabin inside temperature. Among others Radiant Energy Corporation with the InfraTek™ system is one provider of this kind of technology. The InfraTek™ system consists of infrared generators, so-called Energy Processing Units (EPUs), located in an open-ended, hangar-type structure. The EPUs are fueled by natural gas and generate IR energy waves to melt and evaporate frost, ice, and snow. If the aircraft surface is dry, the IR waves are reflected. Although these systems are as fast as conventional ADFs, more ecofriendly and way cheaper some disadvantages can interfere a widely usage: the huge physical size of systems such as InfraTek™ make planning and design for quite complex.

Also, due to the aircraft processing capacity of an InfraTek™ type system, an IR facility can be a bottleneck during peak traffic hours. While IR systems reduce the need for ADFs, thus limiting the environmental impact from these fluids, the system cannot provide anti-icing protection. Some anti-icing fluid use is still required to ensure holdover times [5].

Tempered Steam Technology (TST) uses a mix of air and steam-infused air to melt ice on aircraft surfaces and then pure hot air to dry the surface. Several tests have been conducted during the 2006 – 2007 de-icing season. The new device demonstrated the ability to deice and dry up to 6 cm of snow and up to 2 cm of ice in about 10 minutes. TST can thus prove to be useful for frost removal and pre-de-icing applications, potentially reducing the volume of Type I ADF needed to deice an aircraft.

Several additional projects are researching for new technologies and testing systems which are still under development:

1. Polaris Thermal Energy Systems, Inc. has been evaluating warm fuel as a de-icing method. If the wing fuel tanks are infused with heated fuel, frost, ice, and snow will not be able to develop on the aircraft wing surface. This will reduce the amount of ADF needed to deice the aircraft.
2. At the Dartmouth's Thayer School of Engineering, Dr. Victor Petrenko is working on pulse electro-thermal de-icing. This method uses short pulses of electricity to break the ice.
3. Foster-Miller, Inc. is trying to develop technology that will provide anti-icing protection by coating the aircraft surface. This surface treatment will not require ADF usage.

Deciding on and installing a new de-icing system is quite complex, especially with the expansion of various new technologies and environmental regulations. At this stage, it looks like no technology can escape at least some ADF usage, which means that airports will always need to contain the environmental impact of these fluids. Does it make more sense for airports to invest and change their systems to accommodate new de-icing technology that uses less ADFs or to invest in advancing new glycol collection and recycling systems? It seems that particularly major airports will not be able to avoid large capital expenditure associated with de-icing operations.

Flight delays, lost luggage, messing with changed routes, which will take off fields - airports can be quite stressful. What if technology can make the whole history of air transport more efficient and even enjoyable? In view of this, the airport operators have invested almost 7 billion. euro IT services last year experimenting with automated check - in navigation applications and new ways for quick checks on security stations and

passport control. In the future we can expect a laser scanners for security, virtual shopping walls, gates and biometric holographic assistants that will improve our experience and travel at the same time will raise the profits of operators. Airports may even become destinations in themselves - filled with technology terminals that enchant and amaze us.

For example Jewel expansion of Changi Airport in Singapore. It will open in 2018 and his grand design of steel and glass will include five floors above ground and five below it , a huge indoor park with native flora and hiking trails , as well as the tallest indoor waterfall in the world - 40 meter "Rain Vortex" with their own sounds and lights. Security measures with which it will have will be the last generation and some of them even have no analogue in the world as it will be introduced for the first time.

Annoying airport operations such as registration will increasingly be automated. Airports London Heathrow and Amsterdam Schiphol is already testing the self-catering biometric gates that use technology for face recognition. A Japanese Nippon Airways provide their guests “smart tags” allowing them to be checked quickly navigate the airport and receive messages in real time for their flights. Gatwick airport in London, meanwhile, builds largest automated baggage area in the world that will allow you to check in your luggage for 12 hours before the flight by simply dropping it on the conveyor belt. From a security perspective, this will allow sufficient time for people who check baggage to do their job peaceful and inspect baggage being problematic or even threaten the security of passengers and the airport. Technology Face Detection is now increasingly entering a requirement in airport security. This technology continues to evolve and constantly improve for its reliability and security saves time and money. Gatwick Airport, for example, uses the technology for face recognition to ensure that time spent in the queue checks always less than five minutes. The faces of the passengers are monitored at four points during the passage through security to get feedback about how long it takes your process. This data is combined with the expected changes in traffic and can actively open and close checkpoints by sending emails to staff phones. Recognition technology people can develop to the recognition of facial expressions or body movements that suggest that someone can carry contraband or may be a security risk, experts say, although such technology could fall foul activists privacy.

X-ray laborious process can also be changed. US firm Genia Photonics has created a „molecular laser scanner " that penetrates clothing and other organic matter to reveal traces of explosives or drugs. The technology, which some analysts say will eventually occur at airports , scanning several people simultaneously and works a distance of 50 meters.

Making airports more efficient and pleasant is one thing, but dealing with the expected increase in air traffic is another. The number of passengers is expected to reach 7.3 billion by 2034, more than double the 3.3 billion in 2014, according to a forecast by the International Air Transport Association. This will probably mean that our skies will become increasingly congested, causing more flight delays and emissions of carbon dioxide [8].

All these increasing performance require constant development and improvement of new and optimized security systems to be both highly effective and timesaving. Since the dawn of its creation, the civilian air transport is one of the fastest growing and dynamic sectors. Its importance is crucial for the economy globally. For this reason, the level and security measures must constantly meet the growing demands of this type of transport to ensure its full and normal functioning.

4. CONCLUSION& ACKNOWLEDGMENT

In the new boarding process, passengers get a boarding number at the gate, which will be based on their seat number.When boarding begins, the numbers will be displayed in a sequence on screens at the gate.

After passengers with reduced mobility,those travelling with children and SkyPriority members have boarded, the new process will come into effect.The order in which the numbers will be displayed ensures that passengers with a window seat board first, starting at the rear of the aircraft.

Next, passengers seated in the middle seats can board, after which the passengers with aisle seats will be allowed to board.This ensures that passengers can wait their turn in the boarding lounge, rather than having to queue up in long lines at the gate.

In summary that the RFID system is one of the nominees for the screening of baggage, but like any system or model always has some flaws and is always room for improvement. The inclusion of a GPS chip can in the future to improve this system, which is almost perfect.

REFERENCES

[1] Augustyn S., *Human factors in aviation safety investigations*. Kosice: ActaAvionica 2011
[2] Federal Aviation Administration. *Ground Deicing and Anti-icing Program*. Circular No. 120-60B.
[3] Federal Aviation Administration. *Pilot Guide Large Aircraft Ground Deicing*. Circular No. 120-58.
[4] Federal Aviation Administration. *Design of Aircraft Deicing Facilities*. Circular No. 150/5300-14B.
[5] Airport Cooperative Research Program. *Deicing Planning Guidelines and Practices for Stormwater Management Systems*. Report 14.
[6] Airport Cooperative Research Program. Deicing Practices. Fact Sheet 4.
[7] Hessing, H., Knoesel, E., & Sharkey, I. *Infrared Aircraft Deicing Facility at John F. Kennedy International Airport.*
[8] Environmental Protection Agency. *TDD for Proposed Effluent Limitation Guidelines and Standards for the Airport* De-icing Category. July 2009.
[9] http://lechicgeek.boardingarea.com/improving-boarding-process-airlines-ramps-sliding-seats/
[10]http://thepointsguy.com/2012/10/travel-science-improving-airplane-boarding-procedures/
[11]http://www.easyjet.com/en/help/at-the-airport/boarding
[12]http://news.yahoo.com/airlines-try-save-time-speedier-boarding-process-201152323--finance.html

FLIGHT SAFETY INTRODUCTION FOR STUDENT PILOTS

Oliver CIUICĂ[*], Eduard MIHAI[*], Carmen ȘTEFAN[**]

"Henri Coandă" Air Force Academy, Braşov, Romania (oliverciuica@yahoo.com, mishued@outlook.com), [**] Romanian Aviation Academy (carmen.garnita@gmail.com)

DOI: 10.19062/2247-3173.2016.18.1.2

Abstract: *Human factors represent one of the most important issues for aviation safety. More over when we are talking about the pilots and their first flights. The message of this article is to discover and to discuss where from we came, where we are and where we are going from the flight safety point of view.*

Keywords: *first flight, safety, training, discover, learning.*

1. INTRODUCTION

As flight instructors in Romanian Air Force Training School and also as a team members for the PSCD project "Study regarding limitations and human performance in flight activity" it was interesting to observe the "human factors" that we had to deal with. Their wish to fly as soon as possible and as much as they can, made me look back in time to my first years of flight.

During the ground school I asked the young pilots: "Are you ready for flying?". They answered to me in one voice:"Yes we are!". I knew that it wasn't at all like that because they didn't know anything about what the flight mean. In the plane you are not a passenger. You are a pilot. You have to be the word of law, the decision maker, the one who knows everything.

After they learned the basics of the flight such as the cockpit management, air navigation, rules of the air and so on I gave them one simple scenario: Enter in the cockpit and start the engine. Nobody could tell me the right way to do that. For me it was easy to describe the sequences due to my experience and my skills resulted in years of flight and training.

After this episode none of them answered that they are ready to fly.

2. FEELING THE NEED OF SAFETY

We say it once more about the necessity of a flight simulator for the first phase of training [1]. This will increase, for sure, the flight safety level. It can be a real safety generator. Otherwise, we will still use the phrase "Every pilot starts with a bag full of luck and an empty bag of experience. The trick is to fill the bag of experience before he empty the bag of luck." [2]

Our studies and researches in aeronautical safety field led us to reorganize the flight preparation and briefings using the theoretical concepts in the domain. First of all we put their theoretical knowledge in a logical order and after that we discussed about the flight safety approaches for a better perception and understanding. For this we split the safety domain into some areas [3]:

- Decision making;
- Communication;
- Workload management;
- Error management;
- Situational awareness;
- Stress;
- Risk management.

After hours of theoretical classes and some exams the students were able to fly, obviously with a flight instructor first. The training started from the simplest to the complex mode and we pointed in every stage what they have to do, where to look and why, how to communicate and how to act in different stages of flight or attitudes of the plane.

After around ten sorties for every student new challenges arrived for us. We had to deal with different types of human characters, different kind of people, males or females. Approximately 60 % from them were deeply involved in the learning process, being self-taught, asking questions, trying to simulate the last flight or the next one (chair flight). The other part, around 40 % was less involved.

The aviation professional culture reflects the attitudes and the values associated to the flight. It has a direct impact for the safety and the performances of this organization. There are some organizations where the safety is sensed in a different way but beside that the professional culture gives an important meaning for the work safety and for the impact that this has upon the employees. In the case regarding the pilots the safety is associated by the pride and the pleasure for their job, for the work that they love and for doing it well. There is a positive component of pilot's culture that is given by the need of "professional pride", but also a negative one that is present on their mind as the feeling of invulnerability because of the belong to an elite professional group.

Most of the pilots think that their emergency situations decisions are all correct like in all other normal situations, that their performances are not affected by the personal or stress factors. That is why the fail to recognize the human performances limits is a general issue between airmen and this attitude can lead to the lone aviator stereotype that does not need the colleagues help. This kind of behavior must be erased at once.

After studying the five hazardous attitudes of human factors, we could face this challenge, because we had the "antidote" [4]:

Name	Description	Antidote
Antiauthority	"Don't tell me..."	Follow the rules; they're usually right.
Impulsivity	"Do something quickly!"	Not so fast-Think first!
Invulnerability	"It won't happen to me..."	It could happen to me!
Macho	"I can do it."	Taking chances is foolish.
Resignation	"What's the use?"	I'm not helpless.

3. LEARNED LESSONS

At the aviation organizational level are present dangerous attitudes and behaviors of the airmen. Pilots have always been regarded as elite, empowered and invincible, who are not willing to admit failure. The whole history of aviation is based on the pilot as a hero who often compensates for the shortcomings of the aircraft capabilities. This attitude

prevents informing, the pilots being not ready to admit they were wrong, they do not want to hear anything about errors and they are looking to those who have made mistakes as "unwise", away from their "standards".

Throughout career, experienced pilots have fallen prey or been tempted by one or more of the following dangerous behaviors:

- Pressure from the group (wrong decision based on an emotional response due to the colleagues pressure, without an objective assessment of the situation);
- Mental jam (the inability to recognize and react to the changing of the circumstances, different from those anticipated or planned);
- Focusing on landing (clouding the mind and focusing on landing under distress, storm, strong wind, without giving importance to alternatives action);
- Flying too low (determined by the desire to "take a look" down below the minimum allowable level of the mission);
- Loss of control on the situation (the actions are determined by external factors, those that the pilot cannot control them);
- Flying with insufficient fuel (can be a consequence of excessive confidence, ignoring the rules, shortcomings in the flight plan);
- Continue the VFR flight (Visual Flight Rules) in IMC (Instrument Meteorological Condition);
- Exceeding the technical limitations of the airplane by overestimating their abilities;
- Ignoring the flight plan, the plane check before the flight or the check-lists.

Motivating the students to be aware of everything that is part of the safety chain, for us it was not easy. We could do this only practicing and discussing some case studies. They understood that the career they are training for, as a military pilot, is not an easy one. First of all they are alone in the cockpit, they have to do a lot of work – flying the plane, communication, reading the instruments, setting the control panels, etc. Secondly, they will train for war missions where, maybe, the battle will depend on their success.

Continuing the training, after their first solo flights, they realized that being alone up there is not an easy thing to do. The quality of the flight was higher comparing to the ones with the instructor. Their attention regarding the situation awareness (SA) was increased and all the parameters on board were the necessary ones. For the manner that they flew it is a reverse of the coin, the fact that all of them were tired and some accusing minor muscles pain. Practicing more and more solo flights, their skills and cockpit management improved.

At this point of training, we considered necessary to review the safety areas from the beginning: Decision making; Communication; Workload management; Error management; Situational awareness; Stress and Risk management. The meaning and the objectives of these domains were better understood because they were able to explain to themselves from practice.

It was a long process to observe and to do the best to put into practice the values of the flight safety. All the pilot students came into the Air Force Academy leaded by some movies, challenges, and the beauty of flight. After at least two years of practical training (around 70 hours of flight) they start to change their perception. 70 % of them reconsider their need to know, the limits of their own behavior even the next step in career. Somewhere, around 30 % are staying at the same level but reviewing their attitude regarding personal knowledge four or five years later after graduation.

It is useless to say that the self example of instructor is the light that will guide the pilots over their career. That’s why the teaching process has to be done like never before, the human resource being aware of what this mean to the youngest pilots.

The big challenge of current aviation is to achieve more efficient and safe flights. For the optimally function of man-aircraft-environment system it is necessary to create a state of balance between its elements that are achieved by:

- Efficient correlation of flight components to achieve man-mission system reliability, which would not be influenced by variations of the internal human element nor the external mission elements;
- Development of safety research, discovering the causes of accidents and setting safety standards;
- Acceleration of the acquisition process of modern aircraft, operating techniques, maintenance and service;
- Keeping the pilots at a high level of specialized training using flight simulators solution;
- Optimize the activities of all personnel categories involved in carrying out the flight;
- Awareness of the important role that each individual plays in the system functioning.

4. CONCLUSIONS

It is hard to achieve a good safety culture in this period of time. The training hours are reduced, the number of the planes or helicopters, the same. We still have trained pilots capable for air operations in all weather conditions, day or night, but for how long?! The new rumors regarding the pension law increase the necessity to stay focus on the flight safety for at least next two years. Would we be able to stay at the same status?! The remaining pilots will be under 40 years old. This is a good thing, but less experienced. Since 20 years ago the system is trying to fill the gaps between generations and this filling is not complete. More and more we have to learn from the others mistakes. We don't have enough time to do them all; but for this a lot of lessons learned have to be written and disseminated in a complete form and at all levels.

In our point of view the focus on individual training during the school is mandatory. Here, at this level, is the best period of time and age to gather all the needed information and skills for an airman. After graduation and the licensing it is very useful to go to the next level of safety training where the accent of training process will be oriented towards the CREW RESOURCE MANAGEMENT, the one that affect the standards and the limits of air operations.

The feeling of calmness and confidence that SAFETY offers is achieved through the combined effort of all personnel, specialized and qualified to obtain the best results in the field.

Any inaccuracies, errors, malfunctions are aimed to be completed and resolved before they become potential risks to the safety of flight, whose main objective is to reduce risk, limit the casualties and minimize material losses.

Our next steps in safety researching will be focused on how the students deal with Workload (WL) - Situational Awareness (SA) – Performance.

REFERENCES

[1] J. Kozuba and A. Bondaruk, *Flight simulator as an essential device supporting the process of shaping pilot's situational awareness*, AFASES 2014 22-24 May 2014;

[2] http://www.allowe.com/laughs/book/Rules%20Of%20The%20Air.htm, *Rules of the air*, accessed on 17th of April 2016;

[3] P. Croucher, *Single pilot CRM*, 2006, p. 18;

[4] http://flighttraining.aopa.org/magazine/1999/September/199909_Features_Hazardous_Attitudes.html, accessed on 19th of November 2015;

[5] I. M. Dumitru and M. Boşcoianu, *Human factors contribution to aviation safety*, AFASES 2015 28-30 May 2015;
[6] H. Amin, *Promoting a safety culture in aviation*, http://harisamin.hubpages.com/hub/Safety-Culture-in-Aviation accesed on 28th of May 2015.

The authors wish to thank the "Henri Coandă" Air Force Academy of Braşov for supporting the research necessary for writing this article through project PSCD 2015-104 "Study on the limits of human performance and flight activity".

AIR FORCE AND AEROSPACE ENGINEERING

MODERN TECHNOLOGIES FOR THE REALIZATION OF THE PUMA HELICOPTER BLADE

Ion DINESCU

"Henri Coandă" Air Force Academy, Brasov, Romania

DOI: 10.19062/2247-3173.2016.18.1.3

Abstract: *The main pales represent the helicopters` vital organ. Concerning the flight's security, the pales are the vital organ because a pale's breaking has as a consequence the total destruction of the whole device (plane) because of the lack of poise.*

This paper presents some of the characteristics that concern their building (construction) and materials used in the aeronautic constructions.

Keywords: *technologies, materials, helicopter, blade, construction.*

1. INTRODUCTION

The blades for helicopters have been made out of a composite of wood and metal. The demands concerning the mechanical resistance, the dimensional precision, the humidity and corrosion resistance have changed the structure and technology of execution [1; 3; 4].

The reduction of the unstationary vibrations that drive on each blade is made with the incorporation of some piezo-electrical materials within the structure of the blade.

The recent research for the control of the anisotropic blade, are using the drive on the fibers of the composite structure, the model being experimented on the blade of the main rotor of the Sikorsky H-34 helicopter.

2. ASPECTS OF THE REALIZATION OF THE BLADE

During the flight, the helicopter blades are subdued to very big aerodynamic speed differences while a complete rotation of the engine that can lead to the helicopter's lack of poise [5; 6].

In practical cases this phenomenon is combated by the continuous change of the blade's incidence within its swivel around its longitudinal axle (the changing of the cyclical steep).

On the other hand, the blade is simultaneously subdued to a lifting effort and to the action of the centrifugal force that, once geometrically summed up, could determine an azimuth direction of the blade, case in which at the embedding, towards the log, the flexion of the body of the blade would be cipher.

This direction being valid at every rotation that takes place during a flight, led to the idea of ensuring the blade a second joint called "joint with rotative motion" around an ZZ' axle. Adding a third joint around the YY' axle, in order to absorb the inequality of the resistance when moving ahead, led to a log "totally articulated" universally used, but pretty complicated mechanically speaking [6].

The way in which every joint works ca be observed in figure number 1.

The usage of plastics in what concerns the accomplishment of blades allowed, without reaching the breaking boundary, eliminating two joints, a rotor head being obtained "completely rigid", but still having the incidence variation. This way, the joint with rotative motion and of the alternative motion have been replaced with the litheness of the blade [2; 4].

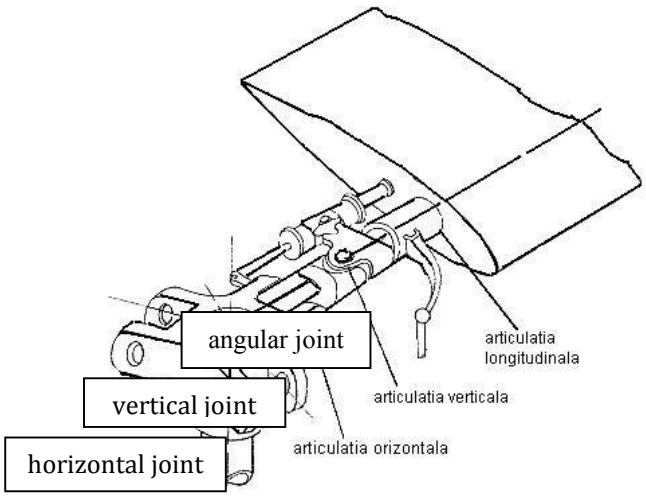

FIG.1. Joint for moving the Puma helicopter blade

The solution embraced determines the growth of the flexion efforts within the embedding, efforts easily taken over by the plastic coverage, because of their great resistance. The efforts are constantly variating, but can be absorbed, because the coverages can almost unlimitedly resist to the alternating tensions.

The ratio between the value of the resistance and the density is a lot higher than in the case of the materials for aeronautic constructions (duralumin, steel), allowing the alleviation of the blades and at the same time the diminishing of the forces. Plus, the reduced density allows the utilization of some more dense materials, less subdued to the local deformation, facilitating the avoidance of the panels' "swelling". The vulnerability is also reduced at the impact of the projectiles when talking about military helicopters, the corrosion disappears and the vibrations during the flight are reduced. The fabrication process is relatively easy and quick and the selling price of the blade is also reduced, despite the high prices of these materials [7].

The main blades represent the vital organ of the helicopter, fulfilling the following distinct functions:

- they create the pulling force, necessary for the maintaining in the air;
- they create the pulling force needed for the heading;
- it serves as a commanding organ for the maintaining of the balance during the flight and for the changing of the flight direction.

3. COMPOSITE MATERIALS FOR THE REALIZATION OF THE BLADE

The blade made out of composite materials (figure number 2) has the same realization:

- *the longeron (1)* – made out of glass fibre (network) impregnated with epoxidic resin that incorporates the attaching jacks of the helicopter's blade;

- *the coverage (2)* – made out of two layers of texture made of carbon fibers impregnated with epoxidic resin and a layer of glass fiber on the outside;
- *the filling (3)* – made for the aerodynamic profile of the blade, built of a plastic honeycomb structure and rigid foam;
- *the trailing edge of the wing (4)* – made out of a gathering of glass and carbon fibers;
- *the end of the blade (5)* – where are being fixed the static and dynamic balancing masses;

the leading wing edge (6) – made out of steel armours.

The low density of the composite materials allows when having an equal weight a supra-dimensioning of the areas solicited by tiredness, so then the making of a new blade longer and wider, with higher performances. [1; 3; 4; 7].

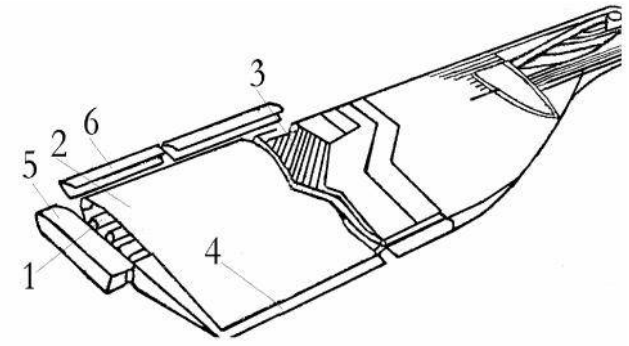

FIG.2. Constituent materials of blade
Puma helicopter

4. MODERN TECHNOLOGIES FOR THE REALIZATION OF THE BLADE

The component parts of the composite blade, as well as the blade itself are being made in special molding devices [2; 4]. The assembling is being made in iron chills warmed up and maintained at 40°C while assembling the components, and then the polymerization of the resin to be done at 120°C, 0.8÷0.9 bars, for 2 hours.

The fabrication begins by the positioning of the layer used for the coverage of protection (glass fiber texture), followed by carbon fiber textures and by the assembling of the other components. The steps must be executed with the maximum of accuracy. The smallest impure material depositions are compromising for the quality of the solder.

The longeron is made out of a bunch of glass fibers – Rowing type – impregnated with epoxidic resin, rapped on a special device. The rapping of every bunch is being made with the help of a special technology that ensures the profile. The checking of the profile is made on a checking device.

The honeycomb structure is being made at the blade's profile on a milling machine.

After the demoulding of the blade the adjusting and finishing operations are made.

Then the solder of the attacking board is next, in a special device with heating that re-feeds an interstice well determined and then controlled.

Composite materials are a new technology that will find increased use in new helicopter structure. Titanium alloy technology also enables lighter wight helicopter, high temperature flight environment.

For a higher speed precission of helicopters, medium density plastic composites should be used, such as fiberglass reinforced phenolic resins containing hylon, silica, graphite or carbon.

These have good resistance to erosion, allow high surface temperatures and exhibit good insulation performance.

Medium density plastic composite materials char at high temperature but generally maintain their thickness and aerodynamical shape. They are usually fabricated by wrapping fiberglass tape over a metal form mandrel, so that the grain of the finished unit is oriented for minimum erosion. After winding, the tape is cured, machined as necessary and assembled with other components using adhesives and sealants.

5. CONCLUSIONS & ACKNOWLEDGMENT

The composite materials, thanks to their extraordinary qualities, which they have imposed in high fields, at which the classical materials do not correspond, represent an efficient way of reducing the consumption in their fabrication as well as in exploitation.

The assessment of helicopter materials technologies addresses five new enabling technologies. These are composite structure materials and reduced parts count structure.

Graphite epoxy and aluminium or aluminium alloys are attractive choices for lighter weight structure. Graphite epoxy and aluminium alloys have hight strength to weight ratio, are easily fabricated, have a good corrosion resistance, and are low in cost.

The strength to weight capability of advanced composites is very high. In addition to small diameter fibers, advanced composite structures have long, continuous fibers and a fiber/matrix ratio that is greater than 50% fibers by volume. Fibers can be: carbon (graphite), kevlar, boron, ceramic, silicon carbide quartz, glass, polyethylene and others.

Also the low density of composites further reduces the weight compared to metals.

Graphite fiber composite materials have extremely high modulus of elasticity resulting in low strain and deflection compared to metals.

However, a note of caution, unlike metals that generally yield gracefully before ultimate failure, composite fibers generally fail suddenly without yield.

Aeronautical and spatial constructions work in very difficult conditions compared to those at which are subdued the structures belonging to the building of the machines. As a consequence, the utilization of the composite materials in aeronautics still remains a field in which a lot of research can be done.

REFERENCES

[1]. Dinescu, I., Eftimie, L., Cătana, D. *Tehnologia materialelor, Tehnologii de bază,* Editura Lux Libris, Braşov (1997).

[2]. Dinescu, I., *Tehnologia materialelor, Materiale tehnologice,* Editura Academiei Aviaţiei şi Apărării Antiaeriene "HENRI COANDĂ", Braşov (2000).

[3]. Dinescu, I., s.a. *Studiu privind utilizarea materialelor compozite în construcţiile aerospaţiale,* Buletinul ştiinţific al Sesiunii naţionale de comunicări ştiinţifice 1-2 noiembrie 2002, Academia Forţelor Aeriene "HENRI COANDĂ", Braşov, pag. 41-50 (2002).

[4]. Dinescu, I., Smeada, M., Stoicanescu, M. *Materiale moderne utilizate în tehnica militară***,** Editura Academiei Fortelor Aeriene "HENRI COANDĂ", Braşov (2012).

[5]. Ispas, Şt. *Materiale* compozite, Editura Tehnică, Bucureşti (1987).

[6]. Marinescu, A., Anghel, V. *Aerodinamica si dinamica elicopterului*, Editura Academiei Române, Bucureşti (1992).

[7]. Smeada, M., Dinescu, I., Stoicanescu, M. *Materiale metalice şi nemetalice utilizate în tehnica militară***,** Editura Academiei Fortelor Aeriene "HENRI COANDĂ", Braşov (2012).

STUDY ON THE ELECTROMAGNETIC INTERFERENCE OF THE MICROSTRIP-FED PATCH ANTENNA OF AN AIRCRAFT RADAR ALTIMETER

Nicușor-Nicolae DRUȚĂ[*], Daniel ZVÎNCU[*], Mădălina Nela DASCĂLU[**]

[*]Military Technical Academy, Bucharest, Romania (nicu_dnn@yahoo.com, daniel.zvincu@gmail.com), [**] "Dunărea de Jos" University of Galați

DOI: 10.19062/2247-3173.2016.18.1.4

Abstract — *This paper aims to address the issue of electromagnetic compatibility in the field of aviation, an issue increasingly discussed in the nowadays electromagnetic context. Aircrafts incorporate a large number of complex systems, which must be able to perform complex functions in various operating conditions, and also to simultaneously operate without disturbing each other.*

Keywords: *radar altimeter; microstrip-fed patch antenna; Sim4life; FDTD.*

1. INTRODUCTION

Aircrafts operate in both natural electromagnetic field (lightnings, electrostatic discharges) and manmade electromagnetic field (radars, broadband emissions), thus emphasizing the significance of studying this complex and important area.

On most severe conditions, the electromagnetic interferences can cause potentially dangerous situations or even accidents on board of the aircrafts. In these cases, the high precision navigation devices on board of the aircraft register malfunctions, misleading the pilots or even failing to function properly.

The radar altimeter system is a solid-state, phase modulated/pulsed system which measures absolute altitude. The radar altimeter system consists of one receiver-transmitter device (R/T), one R/T mount, one receiving antenna, and one transmiting antenna. Each antenna is a microstrip patch type and sealed with a fiberglass cover for protection. They are mounted on the bottom of the aircraft on special mounts to permit the proper angle between them.

This paper illustrates how a microstrip-fed patch antenna used by the radar altimeter can be modeled and analyzed numerically with Sim4Life. From the results, some relevant quantities, i.e., the reflection coefficient and near-field and far-field radiation patterns are extracted and displayed.

Sim4Life is a 3-D full wave simulation environment based on the Finite-Difference Time-Domain method (FDTD), developed and provided by Zurich Med Tech (ZMT). The software is designed to address the electromagnetic TCAD needs of the wireless and medical sectors in terms of antenna design, EMC and dosimetry.

2. FINITE-DIFFERENCE TIME-DOMAIN FORMULATION

2.1. Discretization of Maxwell's Equations

The Finite-Difference Time-Domain method (FDTD) proposed by Yee in 1966 is a direct solution of Maxwell's curl equations in the time domain. The electric- (E-field) and magnetic-field (H-field) components are allocated in space on a staggered mesh of a Cartesian coordinate system (as shown in the following figure). The E- and H-field components are updated in a leap-frog scheme according to the finite-difference form of the curl surrounding the component. The transient fields can be calculated when the initial field, boundary, and source conditions are known.

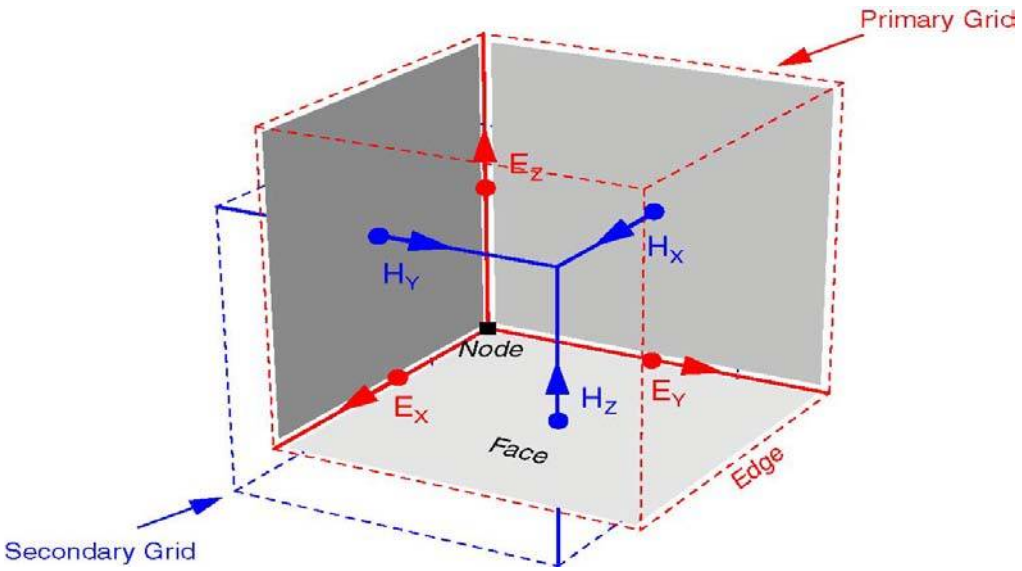

FIG. 1. 3D Yee cell showing the E- and H-field components in the staggered grid

Maxwell's curl equations are discretized by means of a second-order finite-difference approximation both in space and in time in an equidistantly spaced mesh. The first partial space and time derivatives lead to

$$\frac{\partial F(i,j,k,n)}{\partial x} = \frac{F^n(i+1/2,j,k) - F^n(i-1/2,j,k)}{\Delta x} + O\left[(\Delta x)^2\right] \tag{1}$$

$$\frac{\partial F(i,j,k,n)}{\partial t} = \frac{F^{n+1/2}(i,j,k) - F^{n-1/2}(i,j,k)}{\Delta t} + O\left[(\Delta t)^2\right] \tag{2}$$

with F^n as the electric (E) or magnetic (H) field at time $n \cdot \Delta t$, i, j, and k are the indices of the spatial lattice, and $O\left[(\Delta x)^2\right]$ and $O\left[(\Delta t)^2\right]$ are error terms.

The central differences to Maxwell's curl equations are applied to obtain:

$$\nabla \times \vec{H} = \frac{\partial}{\partial t}\varepsilon\vec{E} + \sigma_e\vec{E} \tag{3}$$

$$\nabla \times \vec{E} = \frac{\partial}{\partial t}\mu\vec{H} + \sigma_h\vec{H} \tag{4}$$

with σ_e as the electric and σ_h as the magnetic losses for the proposed allocation of the fields in space and time. The result is, e.g., the FDTD equation above for the E_x component.

$$\frac{E_x\big|_{i.j,k}^{n+1} - E_x\big|_{i.j,k}^{n}}{\Delta t} = \frac{1}{\grave{o}_{i,j,k}}\left(\frac{H_z\big|_{i.j+1/2,k}^{n+1/2} - H_z\big|_{i.j-1/2,k}^{n+1/2}}{\Delta y} - \right.$$
$$\left. - \frac{H_y\big|_{i.j,k+1/2}^{n+1/2} - H_y\big|_{i.j,k-1/2}^{n+1/2}}{\Delta z} - \sigma_{i,j,k} E_x\big|_{i.j,k}^{n+1/2}\right) \tag{5}$$

With the approximation

$$E_x\big|_{i.j,k}^{n+1/2} = \frac{E_x\big|_{i.j,k}^{n+1} + E_x\big|_{i.j,k}^{n}}{2} \tag{6}$$

E_x can be reduced to the unknown E_x^{n+1} of the new time step, which yields

$$E_x\big|_{i.j,k}^{n+1} = \left(\frac{1 - \frac{\Delta t \sigma_{i,j,k}}{2\grave{o}_{i,j,k}}}{1 + \frac{\Delta t \sigma_{i,j,k}}{2\grave{o}_{i,j,k}}}\right) E_x\big|_{i.j,k}^{n} + \left(\frac{\frac{\Delta t}{\grave{o}_{i,j,k}}}{1 + \frac{\Delta t \sigma_{i,j,k}}{\grave{o}_{i,j,k}}}\right)$$
$$\left(\frac{H_z\big|_{i.j+1/2,k}^{n+1/2} - H_z\big|_{i.j-1/2,k}^{n+1/2}}{\Delta y} - \frac{H_y\big|_{i.j,k+1/2}^{n+1/2} - H_y\big|_{i.j,k-1/2}^{n+1/2}}{\Delta z}\right) \tag{7}$$

This procedure can be used to derive Maxwell's curl equations, which may be discretized to generate explicit expressions for all six field components.

2.2. Numerical Stability

For the explicit finite-difference scheme to yield a stable solution, the time step used for the updating must be limited according to the Courant-Friedrich-Levy (CFL) criterion. For the FDTD formulation of Maxwell's equations on a staggered grid, this criterion reads

$$\Delta t \le \frac{1}{c\sqrt{\frac{1}{(\Delta x)^2} + \frac{1}{(\Delta y)^2} + \frac{1}{(\Delta z)^2}}} \tag{8}$$

where Δx, Δy, and Δz are the mesh steps of a Cartesian coordinate system and *c* is the speed of light within the material of a cell.

From this equation, it is clear that the time step is directly related to the cell size. The cell size therefore has a significant impact on the computational requirements of a simulation. In an equidistantly spaced mesh, a reduction of the mesh step size by a factor

of two increases the necessary storage space by a factor of eight and the computation time by a factor of 16(!). For non-uniform meshes, the impact of the smallest mesh cell size on storage space is not that significant. Nevertheless, the time step must be chosen for the smallest cell in the mesh, which has an impact on the overall simulation time as well.

2.3. The modeling of Microstrip-Fed Patch Antenna

The structure is a microstrip-fed patch antenna placed on a grounded dielectric substrate of a thickness of 1.52 mm with a permittivity ε = (3.38 - j 0.0074)ε_0, as it is shown in Fig. 1. The modeling section demonstrates how geometries that are not always trivial to build, like the proposed one, can be easily handled by making use of a wide variety of advanced and highly customizable modeling tools.

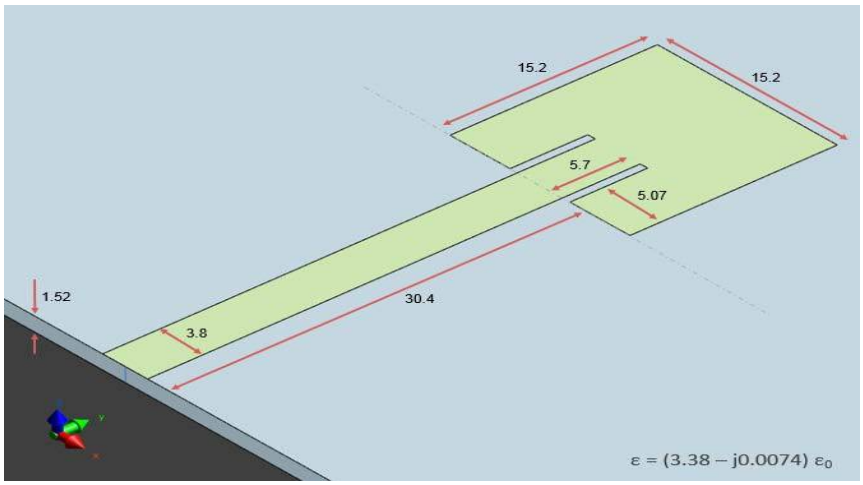

FIG. 2. Microstrip-fed patch antenna modeled in Sim4Life

The FDTD method requires that the model and the surrounding computational domain be spatially divided into cells, where the FDTD equations are applied. Sim4Life has a sophisticated grid generation engine that always seeks to automatically generate suitable settings for the user, taking into account the model characteristics, the type of simulation, etc.

For the microstrip-fed patch antenna modeled, the total number of cells is approximately 432.4 kCells.

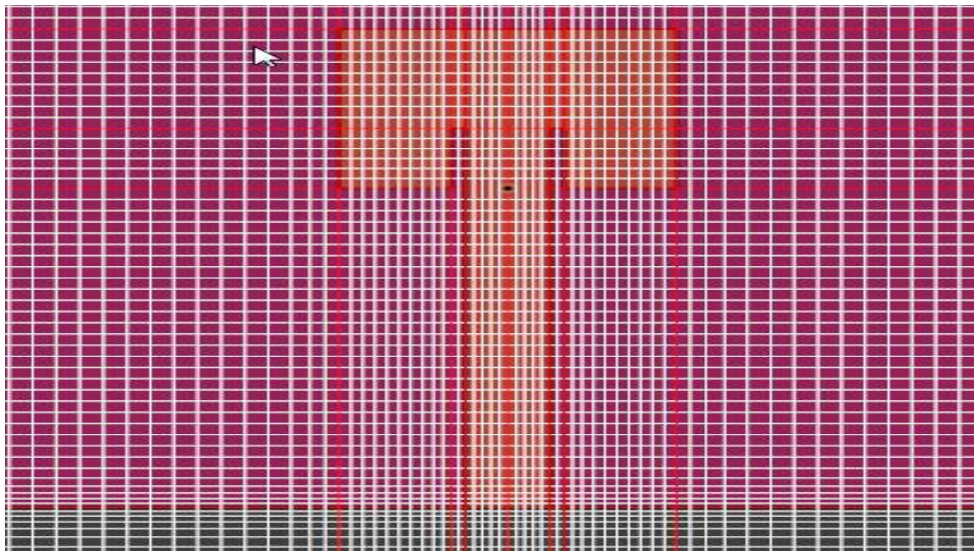

FIG. 3. The grid lines for Microstrip-fed patch antenna modeled in Sim4Life

Voxels view Fig. 4 shows how dielectric materials and PEC are rendered in different ways; the voxel edges of PEC objects are highlighted.

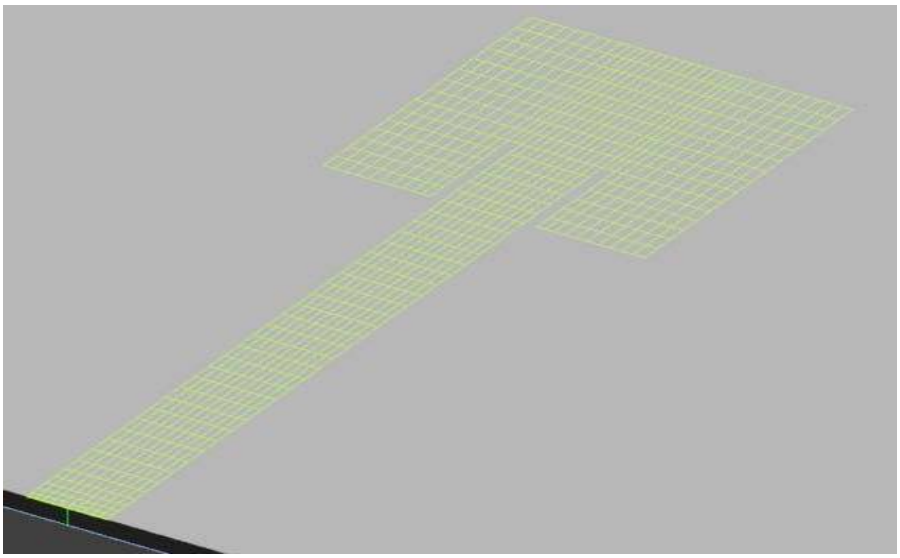

FIG. 4. Voxels view for Microstrip-fed patch antenna modeled in Sim4Life

For the excitation of electromagnetic fields, Sim4Life offers various source structures. The excitation signal used for this simulation is *Gaussian* (a modulated Gaussian pulse). The *Center Frequency* (defines the center frequency of the modulated Gaussian pulse) is 5 GHz and *Bandwidth* (defines the bandwidth of the modulated Gaussian pulse) is 5 GHz. The signal looks like in Fig. 5.

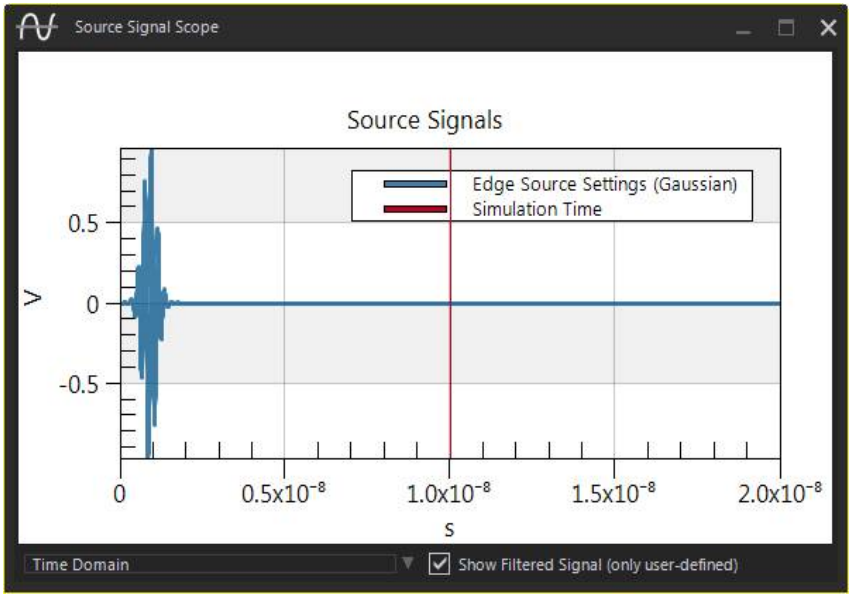

FIG. 5. The excitation source

For the recording of field components, parameter extraction and data visualization, Sim4Life offers a variety of sensor types designed for various purposes. These sensor objects are part of the CAD model, which means that they automatically adapt their geometrical resolution to the grid used for the simulation. Most of the sensors can record either time domain quantities or extract frequency domain results. Selected sensor for this simulation is far-field sensor and the extracted frequency is 5.17 GHz.

3.1. The reflection coefficient

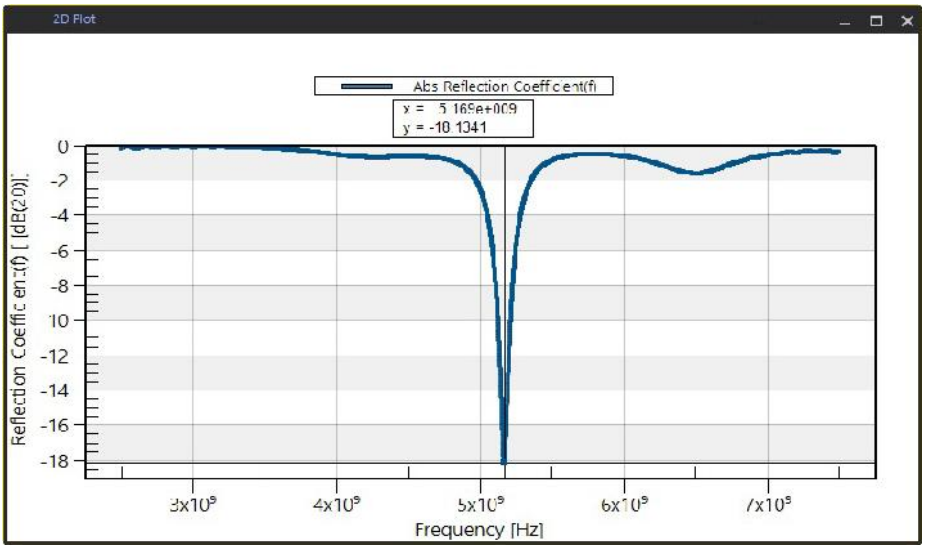

FIG. 6. The reflection coefficient

The table below shows Sim4Life results. The values Fmin and Fmax are the frequency values at which the reflection coefficient is equal to -10 dB. The bandwidth, BW, is defined as BW = Fmax - Fmin; while the central frequency, Fc, is Fc = (Fmax + Fmin)/2.

Table 1 - Table With **Sim4Life** Results

	Fmin (GHz)	Fmax (GHz)	Fc (GHz)	BW
S4L	5.13	5.213	5.172	0.083

3.2. Real Magnitude of E-field.

Fig.7 show the magnitude of the electric field distribution of the microstrip patch antenna of Fig. 2 computed by Sim4Life. The E-field distribution shows clearly that the desired mode has been excited along the microstrip line.

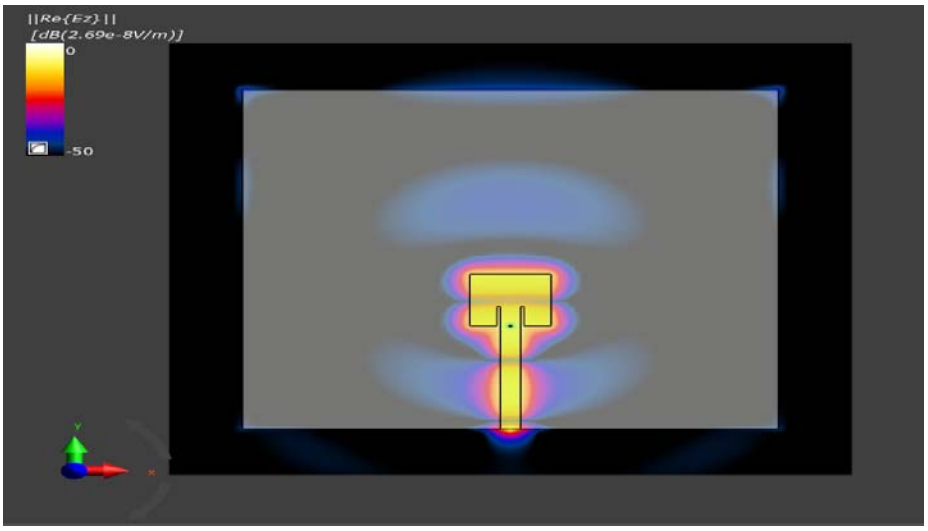

FIG. 7. Real Magnitude of the z-comp of E-field

3.3. Far-Field Radiation Pattern Extraction

An antenna radiation pattern is defined in the IEEE standard as “the spatial distribution of a quantity which characterizes the electromagnetic field generated by an antenna”.

The 3-D Far-Field Viewer Fig. 8 displays the far-field and related chart types within the 3-D model. Each RMS (root mean square) far-field quantity is represented in a spherical coordinate system as a sphere whose local radius and color index are proportional to the value of the quantity in the direction defined by angles theta (θ) and phi (Φ).

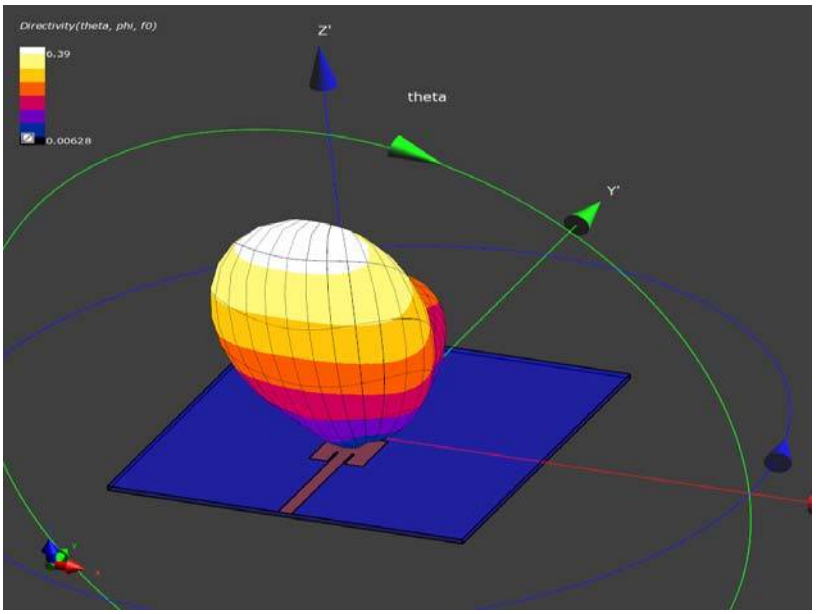

FIG. 8. Spherical Viewer showing the far-field directivity

The sphere is represented by a quadrangular mesh whose resolution is parameterized by the number of longitudes along (Φ) and the number of latitudes along (θ). As the number of longitudes or latitudes increases, the level of detail increases, so does the level of detail and the calculation time.

4. CONCLUSIONS

This paper illustrates how the microstrip-fed patch antenna is modeled, simulated, and analysed in Sim4Life. The modeling of the geometry is described, including details such as how the domain is spatially divided into cells. Following this, explanations for setting up the relevant simulation are discussed and finally, an overview and explanation of some of the results obtained from the simulation is presented (the reflection coefficient, near-field and far-field radiation patterns).

In order to determine the electromagnetic field interferences, three types of methods of investigation can be used: the experimental, analytical, and the numerical methods. Experimental methods are time consuming and sometimes the results are subject to hazard and do not allow much flexibility in changing the parameters of analysis. Field evaluation leads to accurate solutions by using analytical methods or to approximate solutions by using numerical methods.

A key conclusion is that, FDTD method has a powerful ability to provide, in a straightforward manner, wideband results for complex antenna structures comprised of, or adjacent to, arbitrary configurations of inhomogeneous materials. This robustness allows the use of the FDTD method to confidently test proposed novel antenna on the computer before they are built.

Electromagnetic interferences are increasing in the current aeronautical context due to the increasing number of electronic circuits on board aircrafts, resulting in higher electromagnetic disturbance sensitivity, collaborated with decreasing distances between electrical circuits and the framework sensitivity to electromagnetic interferences. This phenomenon’s effects can endanger the flight safety of aircrafts and therefore it must be extensively studied and understood in order to prevent it.

5. ACKNOWLEDGMENT

The modelling and the simulation of the microstrip-feed patch antenna were performed using the Sim4Life software. The research was conducted during an Erasmus + stage at the Electromagnetic Compatibility Laboratory of the Universitat Politècnica de Catalunya, Escola Tècnica Superior d'Enginyeria de Telecomunicacio de Barcelona, Barcelona, Spain.

6. REFERENCES

[1] Sadiku M. N. O.. *"Numerical Techniques in Electromagnetics"*. Second Edition. Boca Raton, London, New York Washington, D.C.: CRC Press, 2000.

[2] Allen Taflove, Susan C. Haginess, "*Computational Electrodynamics: The Finite-Difference Time-Domain Method*", 3rd ed. Norwood, MA: Artech House, 2005.

[3] Maloney J. G., G. S. Smith and W. R. Scott Jr, *"Accurate computation of the radiation from simple antennas using the finite-diference time-domain method"*, IEEE Trans. Antennas and Propagation, Vol. 38, 1990.

[4] Yee, K.S.. "*Numerical solution of initial boundary-value problems involving Maxwell's equations in isotropic media"*. IEEE Trans. Ant. Prop., vol. AP-14, 1996, May. pp.. 302–307.

[5] Umran S. Inan , Robert A. Marshall *"Numerical Electromagnetics-The FDTD Method"* United States of America, New York, Cambridge University Press, 2011.

[6] John L. Volakis, Kubilay Sertel. *"Integral Equation Methods for Electromagnetics"*, SciTech Publishing Inc.

[7] Taflove A., K. R. Umashankar, B. Beker, F. A. Harfosuh and K. S. Yee *"Detailed FDTD analysis of electromagnetics fields penetrating narrow slots and lappeds joints in thick conducting screens"*, IEEE Trans. Antennas and propagation, Vol. 40, 1992, pp. 357-366.

[8] Umashankar K. R., A. Taflove, *"A novel method to analyze electromagnetic scattering of complex objects"*, IEEE Trans. Electromagnetic Compatibility, Vol. 24, 1982, pp. 397-404.

[9] Ovidiu Gabriel Avădănei, Gabriel Banciu, Ioan Nicolaescu, Liviu Nedelcu, *"Superior Modes in High Permittivity Cylindrical Dielectric Resonator Antenna Excited by a Central Rectangular Slot"* , IEEE Trans. Antennas and Propagation, Vol. 60 , Issue 11 , pp.5032 – 5038.

AIR FORCE AND AEROSPACE ENGINEERING

AN ADVANCED NEURAL NETWORK-BASED APPROACH FOR MILITARY GROUND VEHICLE RECOGNITION IN SAR AERIAL IMAGERY

Victor-Emil NEAGOE, Serban-Vasile CARATA, Adrian-Dumitru CIOTEC

"Politehnica" University of Bucharest, Bucharest, Romania (victor.neagoe@upb.ro)

DOI: 10.19062/2247-3173.2016.18.1.5

Abstract: *The paper presents a novel neural network approach for automatic target recognition (ATR) in the synthetic aperture radar (SAR) aerial imagery; this is applied to identify military ground vehicles. The proposed ATR algorithm consists of a processing cascade with the following stages: (a) object detection using a pulse-coupled neural network (PCNN) segmentation module; (b) a first feature selection module using Gabor filtering (GF); (c) a second feature selection module using principal component analysis (PCA); (d) a support vector machine (SVM) classifier improved by using virtual training data generation (VTDG) with concurrent self-organization maps (CSOM). The proposed model has been applied for the recognition of three classes of military ground vehicles of the former Soviet Union represented by the set of 2987 images of the MSTAR public release database. The experimental results have confirmed the method effectiveness, leading to a total success rate of 97.36%.*

Keywords: *Automatic target recognition (ATR), aerial SAR imagery; military ground vehicles; pulse-coupled neural network (PCNN) segmentation, support vector machine (SVM), concurrent self-organizing maps (CSOM).*

1. INTRODUCTION

In peace or war, the fate of millions can depend on the analysis of images gathered by radar or other imaging sensors. These images might reveal a significant truth, like the 1962 U-2 pictures of Soviet missiles in Cuba [19]. In military intelligence and military reconnaissance, knowledge is power and one way to get to know your opponent is to watch him from the air or from space. But it is not so simple. Enemy countermeasures, natural atmospheric disturbances and daunting technical challenges complicate the task. Even when you are watching your enemy under the best conditions, you may not understand what you are looking at. The defense image interpreters are usually concerned with images gathered from aircraft or satellites and have to be able to recognize objects and interpret their meaning [19]. The recent advances try to substitute the human image interpreters by *Automatic Target Recognition (ATR)* based on artificial intelligence. Target objects are often military vehicles as those shown in Fig. 1 considered for the MSTAR public release database used to experiment our ATR proposed method.

(a) (b) (c)

FIG. 1. Three military vehicles of the former Soviet Union: (a) BMP2 (infantry fighting vehicle); (b) BTR70 (armored personnel carrier); (c) T72 (tank).

Radar imagery brings the advantage of independence from a passive illumination source, such as sunlight or starlight, thus offers imaging capability at night and through clouds. Modern day radar imaging systems are capable of comparatively high resolution by using synthetic aperture radar (SAR) imagery [2]. The area of Automatic Target Recognition (ATR) for SAR imagery is an ongoing research in many branches of the military and large research institutions [6], [7], [16], [17], [20]. On the other side, there has been an increasing interest in using artificial neural networks (ANN) for image processing and pattern recognition [1], [2], [7], [11], [12], [13], [14], [15], [17]. A typical target recognition system consists of a detection module (filtering and segmentation) and a recognition module (feature selection and classification) [1]. Moreover, the speckle noise specific to SAR images makes segmentation and recognition difficult tasks [2], [6]. We further propose application and development of new and challenging neural network models both for target detection (filtering and segmentation) and also for classification tasks. *The segmentation uses the pulse-coupled neural network (PCNN)* model based on the implementation of the mechanisms underlying the visual cortex of cat [9], [10], [14], [15]. The visual cortex is the part of the brain that receives information from the eye. The waves generated by each iteration of the PCNN algorithm create specific signatures of the scene used for segmentation (target detection as a first processing step of the present approach), namely to decide for each pixel its potential belonging to a certain object. Second processing step means object feature selection performed firstly using Gabor filtering [4], [5], [8] and refined by the second step based on the application of principal component analysis (PCA). The fourth processing stage of the method corresponds to support vector machine (SVM) classification using an improved training based on *virtual training data generation (VTDG) by concurrent self-organizing maps (CSOM)* [12], [14]. The proposed method is applied for military ground vehicle recognition in aerial images, being experimented for Moving and Stationary Target Acquisition and Recognition (MSTAR) public release database.

2. ATR PROCESSING CASCADE

The flowchart of the proposed ATR model is shown in Fig. 2. It consists of the following processing stages : (a) object detection using a pulse-coupled neural network (PCNN) segmentation module; (b) a first feature selection module using Gabor filtering (GF); (c) a second feature selection module using principal component analysis (PCA); (d) a support vector machine (SVM) classifier improved by using virtual training data generation (VTDG) with concurrent self-organization maps (CSOM).

FIG. 2. Flowchart of the neural network-based ATR cascade.

2.1. PCNN segmentation. PCNN is a biological inspired type of neural network; its functions are found in the visual cortex of mammals [10],It is a single layered, two-dimensional, laterally connected network of pulse-coupled neurons. There exists a one-to-one correspondence between the image pixels and network neurons. The PCNN equations are given below [10]:

$$F_{ij}[n] = \exp(-\alpha_F) * F_{ij}[n-1] + V_F \sum_k \sum_l M_{ijkl} Y_{kl}[n-1] + S_{ij} \quad (1)$$

$$L_{ij}[n] = \exp(-\alpha_L) * L_{ij}[n-1] + V_L \sum_k \sum_l W_{ijkl} Y_{kl}[n-1] \quad (2)$$

$$U_{ij}[n] = F_{ij}[n]\left(1 + \beta L_{ij}[n]\right) \quad (3)$$

$$E_{ij}[n] = E_{ij}[n-1]\exp(-\alpha_E) + V_E Y_{ij}[n-1] \quad (4)$$

$$Y_{ij}[n] = \begin{cases} 1, & if\ U_{ij}[n] > E_{ij}[n] \\ 0, & otherwise \end{cases} \quad (5)$$

where α_F, α_L, and α_E are the time constants; V_F, V_L, and V_E are the magnitude adjustments; β is the linking strength of the PCNN. Each neuron is denoted with indices (i, j), and one of its neighboring neurons is denoted with indices (k, l). Feeding component $F_{ij}[n]$is combined with linking component $L_{ij}[n]$into neuron's internal activity $U_{ij}[n]$. The neuron receives input signals via feeding synapse M_{ijkl}, and each neuron is connected to its neighbors such that the output signal of a neuron modulates the activity of its neighbors via linking synapse W_{ijkl}. The pulse is able to feed back to modulate the threshold $E_{ij}[n]$ via a leaky integrator, raising the threshold by magnitude V_E that decreases with time constant α_E. During iterations, when a neuron's internal activity $U_{ij}[n]$ exceeds its dynamic threshold $E_{ij}[n]$, a pulse is generated (firings).

The PCNN model has proved to be very suitable for image segmentation [6], [9], [10], and [15]. To obtain an improved segmentation performance, we have proposed to run in parallel two PCNN segmentation models, one for n iterations and second for m iterations (see Fig. 3). The results of these two segmentations are added, and as a result the objects have been accentuated and any remaining noise is faded in the background. A good relation between n and m has proved to be m = n + 3. The segmentation is finished by thresholding the PCNN output image.

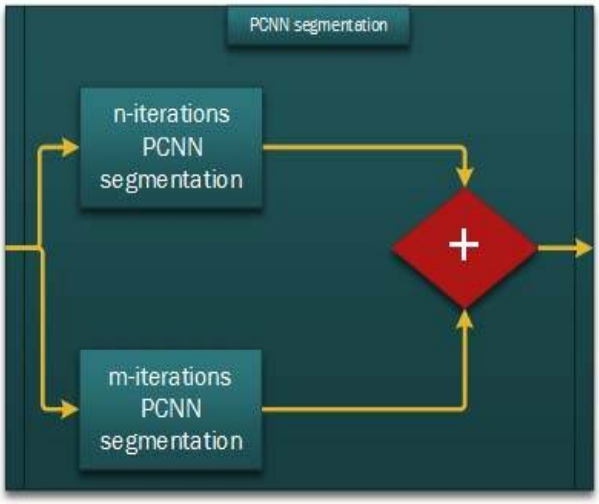

FIG. 3. Image segmentation using a combination of two parallel PCNN models.

2.2. Gabor Filtering (GF) as a first feature selection stage. First feature selection step has been performed by the standard 2-D Gabor filter [3], [4], [5], [8], [16]. It accepts the segmented images, from PCNN segmentation stage and provides an output column vector, consisting of the Gabor features. The feature vectors are normalized to zero mean and unit variance. The output GF vector has the length (m*n*u*v)/(d1*d2), where m and n represent the image with and height, u is the number of scales, v is the number of orientations, d1 is the factor of down sampling along rows and d2 is the factor of down sampling along columns.

2.3. Principal Component Analysis (PCA) as a second feature selection stage. We have applied PCA [1] to transform the GF output belonging to a (m*n*u*v)/(d1*d2)-dimensional space into a reduced p-dimensional space.

2.4. Support vector machine (SVM) classifier using an improved training based on virtual training data generation (VTDG) by concurrent self-organizing maps (CSOM). In order to improve training set quality, we use the innovative idea to build a training set composed by virtual samples only that completely substitute the input original samples [12]. The structure of the VTDG-CSOM is shown in Fig. 4. The steps of the proposed algorithm are the following:

a. Building M pattern subsets. One splits the original labeled sample set into M pattern subsets corresponding to each class, where M is the number of classes.
b. Training of each of the Self-Organizing Map modules SOM (k) (k=1,…, M). One uses the SOM unsupervised algorithm [11], [12], [13] to train each of the SOM modules. Namely, each SOM module has been trained only with the samples having the same label with the neural module label.
c. Virtual training data generation. After training, the weight vectors of the SOM modules have become virtual samples that substitute the input real samples, building an improved training set to obtain a more accurate classifier.

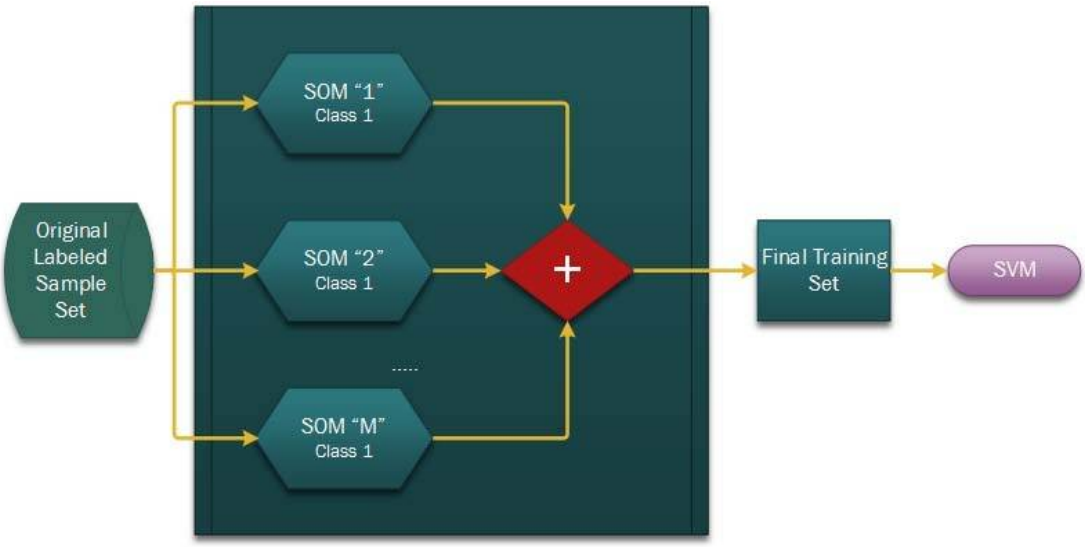

FIG. 4. Flowchart of the VTDG-CSOM.

3. EXPERIMENTAL RESULTS

3.1. MSTAR-database of military ground vehicles. We have intended to test the proposed model for the special defense application regarding identification of military ground vehicles. This why we have chosen MSTAR as a standard dataset for automatic target recognition (ATR) tasks. It is performed at the Redstone Arsenal, Huntsville, AL by the Sandia National Laboratory (SNL) using a Synthetic Aperture Radar (SAR) sensor platform. The collection was jointly sponsored by DARPA and Air Force Research Laboratory as part of the Moving and Stationary Target Acquisition and Recognition (MSTAR) program. SNL used an X-band SAR sensor in one foot resolution spotlight mode. Three classes of military ground vehicles of the former Soviet Union have been considered for our experiments from MSTAR database: BMP2 (infantry fighting vehicle), BTR70 (armored personnel carrier), and T72 (tank). We have chosen 2987 images of 128 x 128 pixels, using two depression angles: 15 degrees and 17 degrees. One chooses 1622 images corresponding to the 17-degree depression angle for training, while the other 1365 pictures corresponding to the 15-degree depression angle are considered for test.

3.2. Experimental performances. For our experiments, the image sizes are m=n=128. For PCNN, we have chosen the iteration parameters n = 21 and m = 24 to give the best results. We have denoted by RS (Reference Segmentation) the method consisting of median filtering, histogram equalization, and thresholding [18]. A comparison of PCNN versus RS performances may be subjectively evaluated in Fig. 5.

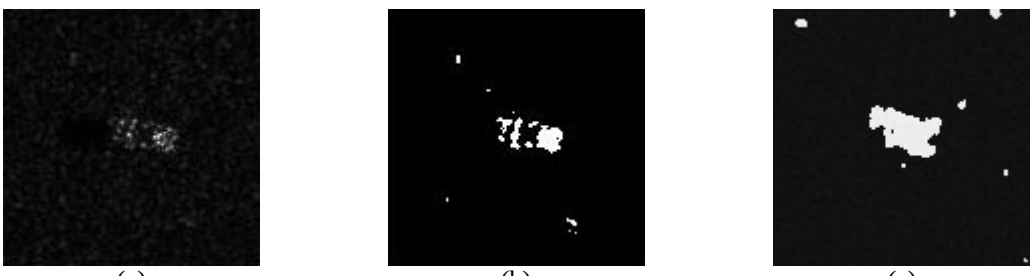

(a) (b) (c)

FIG. 5.(a) The original SAR image (BMP2); (b) Image obtained by reference segmentation (RS); (c) Image segmented with PCNN method (n = 21, m = 24).

The chosen GF parameters are u = 5, v = 21, d1 = d2 = 4, and consequently, the output of GF is a 107520-dimensional feature vector. After PCA, the GF output vector dimensionality is reduced to p=500. The experimental performances are shown in Table 1.

Table 1 – Maximum recognition score for MSTAR dataset.
R= (number of virtually generated training data using CSOM)/ (number of original training data).

Cascade	Maximum correct recognition score [%]	Parameters
PCNN-GF-PCA-{VTDG-CSOM}-SVM	97.36	R=3.25; rectangle sheet CSOM modules of sizes: (48x47), (28x27), (48x47); SVM of RBF type; gamma=0.0001
PCNN-GF-PCA- SVM	94.06	SVM of RBF type; gamma=0.0001
RS-GF-PCA-SVM	86.15	SVM of RBF type; gamma=0.01

4. CONCLUSIONS

The present paper has proposed a neural network-based ATR method using the synthetic aperture radar (SAR) imagery for the special application of military ground vehicle recognition. The proposed ATR has the following processing stages: PCNN segmentation for object detection; first feature selection stage using Gabor filtering (GF); second feature selection stage with PCA; SVM classification using an original neural-network procedure called VTDG-CSOM. Two of these stages are based on advanced neural networks: PCNN segmentation and VTDG-CSOM procedure for improvement of SVM classification performance. The experiments are performed using the dataset of military ground vehicles MSTAR (Moving and Stationary Target Acquisition and Recognition).

A comparison of PCNN versus RS performances subjectively evaluated in Fig. 3 can point out the objective advantage of PCNN segmentation over RS. For classical SVM classifier, Table 1 shows that PCNN segmentation leads to a 94.06% classification score versus 86.15% score obtained by the RS segmentation.

Table 1 also shows the advantage of the virtual data generation (VTDG) using CSOM in order to improve SVM classification. By substituting the original training samples with virtual samples generated by VTDG-CSOM model (the number of virtual samples being about R=3.25 times bigger than the number of original samples), one obtains an increasing of recognition score from 94.06% to 97.36%. Both neural network approaches (that of PCNN segmentation and also that of VTDG-CSOM classification) lead to the increasing pf classification performance from 86.15% to 97.36%, meaning a total score improvement of 11.21%.

REFERENCES

[1] M. Bishop, *Pattern Recognition and Machine Learning*, Springer, New York, 2006.
[2] C.H. Chen, *Signal and Image Processing for Remote Sensing*, 2nd Edition, CRC. Press, New York, 2012.
[3] M. Haghighat, S. Zonouz, M. Abdel-Mottaleb, Identification Using Encrypted Biometrics, in *Computer Analysis of Images and Patterns*, *Lecture Notes in Computer Science*, Volume 8048, Springer, Berlin Heidelberg, pp. 440-448, 2013.
[4] J.K. Kamarainen, V. Kyrki, H. Kälviäinen, Fundamental Frequency Gabor Filters for Object Recognition, *Proc. 16th International Conference on Pattern Recognition (ICPR'02)*, vol. 1, August 11-15, 2002, Quebec (Canada), pp. 628-631.
[5] J.K. Kamarainen, V. Kyrki, H. Kälviäinen, Robustness of Gabor Feature Parameter Selection, *Proc. IAPR Conference on Machine Vision Applications (IAPR MVA 2002)*, Dec. 2002, pp. 132–135.

[6] J.A. Karvonen, Baltic Sea Ice SAR Segmentation and Classification Using Modified Pulse-Coupled Neural Networks, *IEEE Trans. on Geoscience and Remote Sensing*, Vol. 42, No. 7, pp. 1566-1574, July 2004.
[7] S. Kidera, T. Kirimoto, Accurate and Robust Automatic Target Recognition Method for SAR Imagery with SOM-based Classification, *IEICE Transactions on Communications*, Vol. E95-B No.11, pp. 3563-3571, Nov. 2012.
[8] V. Kyrki, J.K. Kamarainen, H. Kälviäinen, Simple Gabor Feature Space for Invariant Object Recognition, *Pattern Recognition Letters*, vol. 25, issue 3, pp. 311–318, Feb. 2004.
[9] G. Kuntimad and H.S. Ranganath, Perfect Image Segmentation Using Pulse Coupled Neural Networks, *IEEE Trans. on Neural Networks*, Vol. 10, No. 3, pp. 591-598, May 1999.
[10] Y. Ma, K. Zhan, Z.Wang, *Applications of Pulse-Coupled Neural Networks*, Springer, Heidelberg-New York, 2010.
[11] V.E. Neagoe and A. Ropot, Concurrent Self-Organizing Maps - A Powerful Artificial Neural Tool for Biometric Technology, pp. 291-298, in: *Harbour Protection Through Data Fusion Technologies*, Edited by: Shahbazian, E; Rogova, G; DeWeert, MJ, NATO Science for Peace and Security Series-C: Environmental Security, Springer, 2009.
[12] V.E. Neagoe, A.D. Ciotec, New Approach for Accurate Classification of Hyperspectral Images Using Virtual Sample Generation by Concurrent Self-Organizing Maps, *Proc. IEEE Internat. Geoscience and Remote Sensing Conf. (IGARSS 2013)*, July 21-26 2013, Melbourne (Australia), pp. 1031-1034.
[13] V.E. Neagoe, R.M. Stoica, A.I. Ciurea, L. Bruzzone, F. Bovolo, Concurrent Self-Organizing Maps for Supervised/Unsupervised Change Detection in Remote Sensing Images, *IEEE Journal of Selected Topics in Applied Earth Observations and Remote Sensing*, Vol. 7, No. 8, pp. 3525-3533, August 2014.
[14] V.E. Neagoe, S. V. Carata, A. D. Ciotec, Automatic target recognition in SAR imagery using Pulse-Coupled Neural Network segmentation cascaded with virtual training data generation CSOM-based classifier, *Proc. 2015 IEEE International Geoscience and Remote Sensing Symposium (IGARSS 2015)*, Milano, Italy, July 26-31, 2015, pp.3274-3277.
[15] H.S. Ranganath and G. Kuntimad, Object Detection Using Pulse Coupled Neural Networks, *IEEE Trans. on Neural Networks*, Vol. 10, No. 3, pp. 615-620, May 1999.
[16] H. Ruohong, Y. Ruliang, SAR Target Recognition Based on MRF and Gabor Wavelet Feature Extraction, *IEEE International Geoscience and Remote Sensing Symposium (IGARSS 2008)*, July 2008, vol. 2, pp. II-907–II-910.
[17] N.M. Sandirasegaram, *Automatic Target Recognition in SAR Imagery using a MLP Neural Network*, Technical Memorandum, Defence Research and Development Canada (DRDC), Ottawa, TM 2002-120, Nov. 2002.
[18] M. Sezgin, B. Sankur, Survey over Image Thresholding Techniques and Quantitative Performance Evaluation, *Journal of Electronic Imaging*, Vol. 13, no 1, pp. 146–165, Jan. 2004.
[19] A. Streicher, E-Learning for radar image interpreters, in: *New Security Learning*, http://www.newsecuritylearning.com/index.php/feature/105-e-learning-for-radar-image-interpreters.
[20] Y. Sun, Z. Liu, S. Todorovic, J. Li, Adaptive boosting for SAR automatic target recognition, *IEEE Transactions on Aerospace and Electronic Systems*, vol. 43, issue 1, pp. 112–125, Jan. 2007.

AIR FORCE AND AEROSPACE ENGINEERING

A QUICK LOOK OVER THE ROMANIAN GROUND BASED AIR DEFENCE

Marius RĂDULESCU*, Vasile ŞANDRU**

*Electromecanica State Own Company, Ploieşti (marius@elmecph.ro)
**"Henri Coandă" Air Force Academy, Braşov, Romania (svasile1966@yahoo.com)

DOI: 10.19062/2247-3173.2016.18.1.6

Abstract: *The paper work proposes a short review of the Romanian Ground Base Air Defense today and try to identify few ways of development into the next future, focusing on the Land and Air Force belonging systems. An important point is the revealing the significance of networking and flexible integration of the sensors, C3I capability and the firing units, allowing the growth of the Air Defense power by addition of the new own or allied units on the existing and compatible pattern. While some systems are completely obsolete and will be replaced, others are susceptible to follow a life cycle up-grading program and certain equipments must be purchased. As a conclusion, the Air Defense is a very dynamic branch of the armed forces and represents a priority in the operational and financial effort to setup a credible armed deterrence.*

Keywords: *equipment, missile, integration, system*

1. INTRODUCTION

The Air Defense takes a major role in the military capability of a state, because is a component characterized by:

- early action
- rapid reaction
- great inhibitive factor

in case of an aggression. This capability prevents the effective use of the enemy's most important asset – the air power.

Building in the peace-time even a solid defense against planes, drones and missiles imposes to an enemy more precautions for a conflict planning and in many aspects forces him to not considers the easy scenarios.

As a general view, AD assures also relatively safe area for other components forming so called National Defense, Safety and Public Order System (SNASOP).

The AD has three initial destinations:

- covers the critical military and civilian infrastructures
- assures the protection of military force
- gives time to react for the political deciders

Together with Intelligence, Special Forces, Communications and Aviation, the Air Defense is in the first line of the state defense.

2. THREATS

Today the air threat rapidly evolves due to the technological advance in software, micro-electronics and precision mechanics mainly. Alongside the fighter-bombers,

helicopters and a wide range of UAV's, some new target categories came to challenge the air defense, including the cruise missiles (CM) and air-to-surface missiles (ASM).

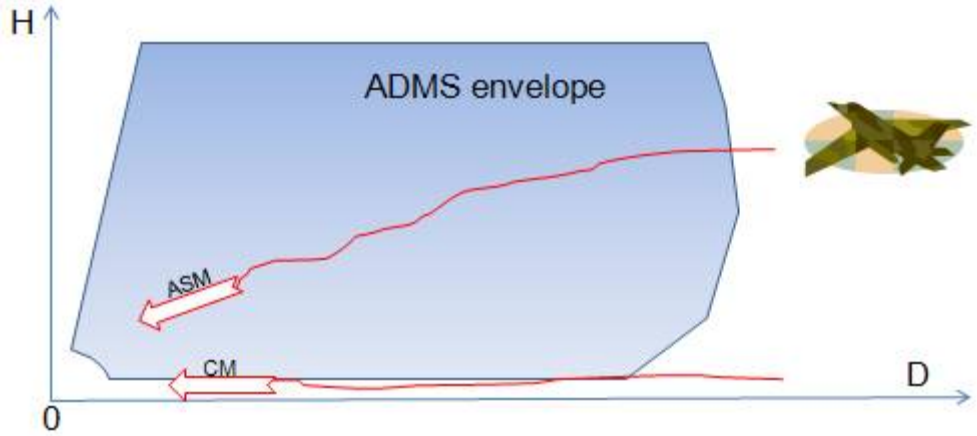

FIG. 1. AIR DEFENCE MISSILE SYSTEM vs. HEAVY TARGETS

The CM as well as the ASM, both stand-off launched, are very difficult targets and imposes high performances to ADMS (Air Defense Missile System). Their low RCS (Radar Cross Section), almost unpredictable trajectory and reduced vulnerability required to ADMS an accurate tracking, quick reaction and high hit-to-kill probability.

3. THE AD SYSTEMS EFFICACY

Contrary to some wrong expectations, the real AD efficacy is dramatically lower than that claimed by sellers or obtained in ideal conditions in field range firings. If values presented in [12] for gun systems or in [9] for common missile systems will be considered, easily may be calculates that no reasonable tactical disposal could delivery enough fire power to assure the target destruction.

Table 1. THE EFFICACY OF SOME AD SYSTEMS

	Missile system		Gun system	
	A	B	C	D
SSKP	0.22	0.33	0.7	0.2
No of rds	1	1	560	70
No of weapons	6 … 7	4	9	42

Even the most advanced missile systems, for that producers claim high kill probability (around 90%), reach this performances in the controlled field range scenarios, while real, with strong jamming environment and in presence of a very maneuverable target, the parameter is lower (between 60% and 40%) [6].

Another limitation is strictly connected to the cost of the target kill operation (i.e. unit elements work and missiles [4], [5]) vs. the value of the target itself.

4. THE STRUCTURE AND THE VOLUME OF THE ROMANIAN GBAD (GROUND BASED AIR DEFENCE)

The Ground Forces disposed by a number of fighting brigades, supported by an AD battalion each and a number of independent AD regiments assigned to the divisional structures. The AD battalions are equipped with small caliber automatic cannon (2 x 30, 2

x 35 tracked and 2 x 35 self-propelled), as well as with VSHORAD (Very Short Range Air Defense) local-built missile systems (CA-94 and CA-95).

FIG. 2. CLOSE RANGE AD EQUIPMENT OF THE GROUND FORCES

These provide an acceptable protection level today, but only at close range (2.5 to 4.5 km) and will become obsolete in the next future.

At the infantry and mechanized units, the close AD is supported by the heavy machine-guns of the armored vehicles.

FIG. 3. THE 12.7 MM, 14.5 MM AND 25 MM WEAPONS ON MBTs, APCs AND IFVs

Generally these are effective against low flying rotary or fixed wing aircraft and UAV's at a range of 1 to 2 km.

Regarding the equipment of the AD regiments, the Russian origin SA-8 and SA-6 ADMS have enough good engagement performances, but their technical resource is almost consumed. However, these are susceptible to perform a life cycle up-grading program [4], [5], going even to the missile replacement [8], 9], [10].

FIG. 4. SHORAD/MRAD EQUIPMENT OF THE GROUND FORCES

The Air Force operates a MRAD missile brigade and a number of Air Force Base AD battalions. The equipment consists on the last variant of Russian made SA-2, now at the end of life cycle and Hawk missile system which attend an up-grade program to the Hawk-XXI standard, while the AFB AD battalions retains the ageing radar-controlled S-60 57mm semiautomatic gun system.

FIG. 5. AD EQUIPMENT OF THE AIR FORCE

The Air Force launched a RFI document (Request for Information) concerning an acquisition of a VSHORAD/SHORAD systems destined for the AFB's (Air Force Base) protection mainly, and the self-defense means of the Deveselu NATO strategic area assure coverage for a large part of Romanian infrastructure.

The Navy has on-board specialized and quite different AD systems. The Danube units operate multi barrel 14.5 mm and 30 mm systems, while Black Sea units are equipped with Russian made 30 mm (AK-230 and AK-630), 2 x 57mm and 76 mm (AK-176 and AK-276) radar controlled gun systems, the OTO Melara 76 mm Super Rapido gun and a board version of CA-94 missile system. Counting the numerical limitation of the naval systems and the specific requirements, we consider these a separate chapter regarding the object of this paper work.

5. MODERN AD DEVELOPMENT CONCEPTS

Integrated Battle Management Center (IBMC) including a Sensors Fusion sub-system represents the expression of coordination between the forces categories in time of a military operation. A C^4I (Command, Control, Communications and Informatics) system supports the action of a skilled staff, capable to use all available forces to fulfill its mission. High performance battle management software, containing likely scenarios comes to assure an advanced efficiency of the staff work [1], [3].

Concerning the AD, these conduct to better target allowance, concentrates enough fire-power on target, permits good IFF dialogue to avoid the blue-on-blue engagements and offer stealthiest pattern for the own firing units.

In other sense, a network with territorial distributed terminals, compatible with NATO data link protocols (ATDL-1, Link 11b, Link 16) is necessary to be setup in peace-time even. That allowed to enhance a zone AD protection adding own supplementary sensors and FU (Firing Units) or allies. This capability called Plug-and-Fight confers flexibility and quick power growth for a dedicated AD operation in a system open architecture [6].

The stability reached by the Commercial off-the-shelf (COTS) components opens the perspective to solve many technical problems [7], mainly regarding the integration jobs, in local industrial facilities.

7. PRIORITIES

Maintaining of the yet-effective AD systems - Today, some AD systems can be up-grade yet while others are complete obsolete and must be replaced. This imposes few urgent up-grading programs, in time of systems life cycle:

- Hawk improvement to XXI standard
- SA-6 Kub flexibility enhancement

In parallel an effort to develops in country in partnership with adequate foreign companies, the elements of the future VSORAD/SHORAD integrated system deserve to be start.

Slowly replacement of the obsolete systems - In this matter may proceeds to a standardization or guns caliber and type of missiles inside of the specific classes. An actual trend looks to build FU based on dual-use high performance missiles, for SHORADs especially [9].

Development of the industrial infrastructure - This work looks first for maintenance and partial production of the AD ammunitions (projectiles and missiles spare parts) mainly. The task supposes a coherent multi-year politics, supporting programs in the fields of:

- equipment acquisition
- systems up-grade
- equipment integration
- research and development (some of these in partnership)
- teaching and advanced training facilities (including the field range modernization)

8. CONCLUSIONS

Using a system open architecture and a common line developed missile family, the C^4I operational command can integrates different AD assets that are existing in field at a moment, like 3D surveillance radars, MRADs and semi-fixed (towed) SHORADs of the Air Force and the highly mobile SHORADs of the Army units, until at the piece level [2].

The local industrial facilities and also the local (Romanian) R&D capabilities may support a consortium to accomplish the AD systems engineering and integration work, and can assume the organization of a training facility, a maintenance facility or even a local Centre of Excellence for Missile Systems.

REFERENCES

[1] Băluţă, S., Pearsică, M., Axente, C., *The command and control structure of the mobile Short Range Air Defence systems*, The International Session of XI-th Scientific Papers, AFASES 2009 - Scientific Research and Education in the Air Force, 20-22 May, Brasov, I.S.B.N. 978-973-8415-67-6, p. 19

[2] Constantinescu, D., Rădulescu, M., *Euro-Atlantic integration for a high-performance Romanian SHORAD*, Proceedings of the 11th International Scientific Conference „Strategies XXI", National Defence University „CarolI", Bucharest, April 2 – 3, 2015, ISSN 2285-8318, Vol. 2, p. 59

[3] Oglage, L., *Conducerea forţelor şi mijloacelor de apărare antiaeriană din fâşia diviziei pentru NATO,* Forţele Terestre nr. 2 din 2009, Buletin de teorie militară editat de Statul Major al Forţelor Terestre, http://www.rft.forter.ro/2009_2_t/02-fenmil/05.htm

[4] Rădulescu, M., Calefariu, E., Boşcoianu, M., Ciufudean, C., *Aspects Regarding Technical and Economic Upgrade Elements in the Case of an A.D. Missile System*, Proceedings of the 14th WSEAS Conference - Advances in Mathematical and Computational Methods, ISBN: 978-1-61804-117-3, Sliema, Malta, 7 – 9 November, 2012, p. 236

[5] Rădulescu, M., Şandru, V., *Prelungire de resursă, revitalizare şi modernizare pentru complexele de rachete antiaeriene*, Revista Gândirea Militară Românească nr. 5 pp. 70–79/2013 ISSN 1454-0460

[6] Rădulescu, M., Mihăilescu, C., Marinescu, M., *Some Aspects of the Air Defense Missiles Up-Grading,* New Challenges in Aerospace Sciences Conference (NCAS 2013), pp 129-133, ISSN 2344-4762, ISSN L 2344-4762, Bucharest, Romania, 7-8 November, 2013

[7] Rădulescu, M., Mihailescu, C., *New possibilities for multilayered air defence in an open architecture systems*, The 2nd edition of New Challenges in Aerospace Science International Conference, NCAS 2015, Bucharest, Romania, 5-6 November 2015

[8] Rădulescu, M., Şandru, V., *Advanced use of the e-resources in the research activities regarding to missile integrated systems development*, code 10.12753/2066-026X-14-120, 10th International Conference ''eLearning and Software for Education'', Book of Abstracts, Bucharest, April 24-25, 2014, ISSN 2360-2198, p.97

[9] Rădulescu, M., Şandru, V., *SHORAD solutions for the Air Forces systems up-grade*, International Conference of Scientific Paper, AFASES 2015, Vol. 1, p.99, Braşov, 28-30 May 2015

[10] Şandru V., Rădulescu M., Ciufudean C, Boşcoianu E. C., *Critical Aspects Regarding the Integration of Low Cost Up-grade Architecture in High-technology Assets for Defense*, Mathematical Methods for Information Science and Economics, WSEAS Conferences, Montreux, 2012, ISBN: 978-1-61804-148-7
[11] Şandru, V., Rădulescu, M., *Requirements for ground-based air defense integrated systems*, RECENT Journal vol 14 Nr 3 (39), 2013, pp.186-190, Universitatea Transilvania, Braşov, ISSN 1582-0246
[12] Şandru, V., Boşcoianu, M., *Comparative analyse regarding to kill probability one of the main criteria of Air Defense integrated systems*, Revista INCAS BULLETIN, Vol 6 Issue 3 / 2014 pp. 57-67, ISSNL 2066 – 8201, DOI:10.13111 / 2066 – 8201.2014.6.3, Bucureşti

SIMPLIFIED MATHEMATICAL MODEL FOR AIRCRAFTSRESPONSE CHARACTERISTICS

Constantin ROTARU, Oliver CIUICĂ, Eduard MIHAI, Ionică CÎRCIU, Radu DINCĂ

[*]"Henri Coandă" Air Force Academy, Braşov, Romania
(rotaru.constantin@afahc.ro, oliverciuica@yahoo.com, mishued@outlook.com, circiuionica@yahoo.co.uk, radu_mihai1989@yahoo.com)

DOI: 10.19062/2247-3173.2016.18.1.7

Abstract: *Human performance modeling provides a complementary technique to develop systems and procedures that are tailored to the pilot's tasks, capabilities, limitations and also, offers a powerful technique to examine human interactions across a range of possible operating conditions. From an initial review of past efforts in cognitive modeling, it was recognized that no single modeling architecture or framework had the scope to address the full range of interacting and competing factors driving human actions in dynamic and complex environments.*

The paper presents two mathematical compensatory models, based on the aircraft dynamics characteristics and frequency responses.

Keywords: *aircraft dynamics , Laplace transform, frequency response.*

1. INTRODUCTION

Human performance models were developed and applied to flight operations in order to predict errors and evaluate the impact of new information technologies and new procedures on flight crew performance.The usefulness of the human performance modeling to the design and evaluation of the aircraft technology is determined by the core capabilities – visual attention allocation, workload, crew interactions, procedures, situation awareness and error prediction [1]. The modeling efforts revealed that human performance models, even those cognitive architectures that have traditionally been used in the context of psychological laboratory experiments, can indeed be useful tools for complex, context dependent domains such as aviation. Specifically, the tools can be used to address the design and evaluations of aviation displays, procedures and operations.

These models can be used to inform display design and the allocation of information so as to optimize efficient scan patterns and increase the uptake of relevant information in a timely manner. Although the analysis and understanding of the airplane as an isolated unit is important, for many flight situations it is the response of the total system, made up of the human pilot and the aircraft, that must be considered. Many tasks performed by the pilots involve them in activities that resemble those of a servo control system, so, the pilot can be modeled by a set of constant coefficients linear differential equations [2, 3]. Much of research in the field of human pilot describing functions hasconcentrated on the pilot's performance in a single degree of freedom compensatory tracking task with random system inputs, where the pilot controls a single state variable through the actuation of a single control. A compensatory display is one in which the tracking error is presented, regardless of the source of error.

2. PILOT MODEL

Due to the complex nature of the situation it is possible to model the pilot in many ways and to measure the model by employing a variety of techniques. One of the most successful approaches to the measurement problem utilizes power spectral density measurements of signal circulating in the control loop. The human pilot could be replaced by a mathematical model consisting of two parts (Fig. 1): the linear describing function (written in Laplace transform notation), $Y(s)$, and the remnant, $n(t)$. Since a linear model is never able to describe the pilot completely, $Y(s)$ is insufficient by itself, and it is necessary to include the remnant $n(t)$, which is the signal that must be added in order to have all the time signals circulating in the system [4]. The $Y(s)$ selected to describe the pilot in any particular task is chosen so as to minimize that part of the input signal to the aircraft which arises from $n(t)$. Thus, the linear pilot model that results is that which accounts for as much pilot input to the aircraft as possible, and a measure of its adequacy is the fraction of the pilot input to the aircraft accounted for by $Y(s)$.

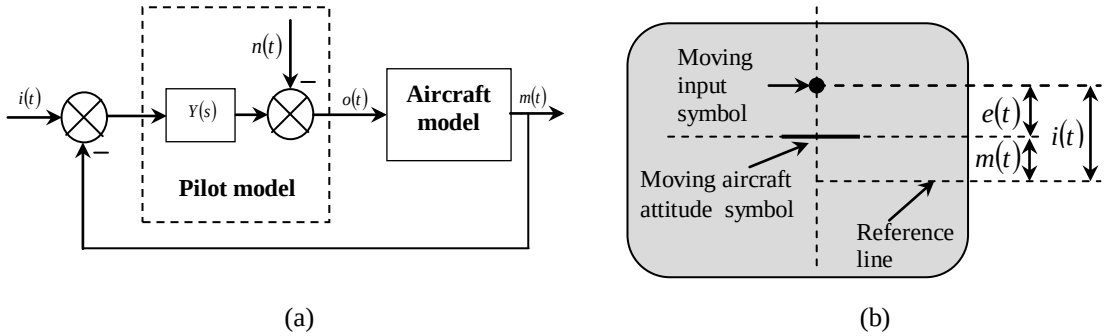

FIG. 1. Linear model of the pilot-aircraft system (a) and displayed variables (b)

According to the Fig.1, the pilot must control the aircraft response $m(t)$ in such a fashion that is matches as closely as possible the desired aircraft response. The pilot does this by viewing the instantaneous error $e(t)$ and altering his input to the aircraft (Fig. 2). It is found that the pilot's control technique is influenced by the type of input $i(t)$, the dynamics of the control system, the type of display and the dynamics of the aircraft. Although $e(t)$ is available in both cases, only the pursuit display separates the error into its components and conveys this information to the pilot. The single degree of freedom tracking task with a pursuit display is identical to the compensatory task, except that the displayed variables are different. In the compensatory task only $e(t)$ are displayed, whereas in the pursuit task both $i(t)$ and $m(t)$ are separately displayed. The data that pilots utilize to fly can be found on cockpit display panels and qualitatively different from the cues used in correspondence judgments (Fig. 2). They are data rather than cues in that they are precise, reliable indicators of whatever they are designed to represent. In the electronic environment of the cockpit, the primary task of the pilot is to supervise and monitor systems and information displays to ensure consistency of the information and to restore them when disruptions occur.

All the possible airspeed and altitude conditions of an aircraft are visualized in the flight envelope, where every aircraft performs the specific mission for which it has been designed. Within this flight envelope, desirable flying qualities are defined as a combination of characteristics both in terms of piloting the aircraft as well as in terms of the aircraft response in itself [5, 6]. Specifically, this includes the analysis of three factors: control authority (the pilot's capability to generate appropriate aerodynamic and thrust forces and moments), pilot workload (the physical effort while the pilots applies

physical forces through its arms and feet to the control commands in the cockpit of the aircraft), and pilot compensation (the mental effort by the pilot while at the controls of the aircraft).

(a) (b)

FIG. 2. Aircraft cockpit (a) and human pilot workload (b)

The aircraft dynamical equations are nonlinear in the inertia terms and in the kinematical variables. The external force, especially the aerodynamic one, may contain inherent nonlinearities. In the automatic and powered control systems used in aerospace vehicles, there occur nonlinear control elements such as limiters, switches, and others. The human pilot is the ultimate in time-varying nonlinear systems.

3. AIRCRAFT CONTROL CHARACTERISTICS

Two control paths that the pilot employs for compensatory and precognitive control were considered. For compensatory control, the pilot observes errors between the desired and the actual response of the aircraft and applies the control to reduce or eliminate the error. If the pilot has the ability to observe the task command directly, the aircraft can be controlled to immediately follow that command without waiting for the error to develop. With a priori knowledge of the aircraft behavior, the pilot can shape these control commands to achieve the desired response.

Two models of the pursuit task are presented in fig. 3, where the pilot is represented by a pair of describing functions $(Y_1(s), Y_2(s))$ or $(Y_3(s), Y_4(s))$ since the pilot is considered to have two inputs and one output. The function $g(t)$represents the turbulence acting on the controlled aircraft.

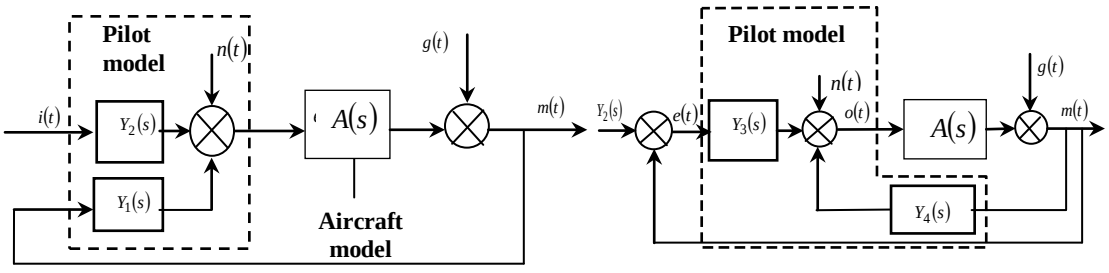

(a) (b)

FIG. 3. Compensatory task with pilot model (a) and the model of the pursuit task (b)

The response of the aircraft to either control inputs or disturbances may be represented by the transfer function of the aircraft with respect to the controls or by the transfer

function of the aircraft with respect to the disturbances. The control input is defined both by the pilot's open-loop inputs in response to the command and the pilot closed-loop inputs in reaction to the error between the command and the aircraft's actual response.

The first element of the control system that the pilot encounters is the control inceptor, namely, stick, pedals, throttle and thrust-vector levers. Nonlinear characteristics typical of most mechanical control devices must be considered, including hysteresis, breakout force and changes in the force gradient with control deflection.

4. HIMAN PILOT MATHEMATICAL MODEL

To carry out analyses of the aircraft's flying qualities, it is necessary to have a mathematical representation of the pilot. Pilot models are typically represented in transfer function form that relate the pilot's control output in response to perceived error in the aircraft's response compared to the desired command,

$$Y_p = K_p \frac{T_L \cdot s + 1}{T_I \cdot s + 1} \cdot \frac{e^{-\tau \cdot s}}{T_P \cdot s + 1} \tag{1}$$

The first element of the transfer function is the gain, K_p, that determines the amount of control the pilot commands in proportion of the perceived error. The pilot can also perform dynamic compensation such lead (T_L - lead time constant) and lag (T_I - lag time constant), as indicated in the equation (1). Elements that cannot be adjusted are associated with the transport delay, τ, involving visual observation and mental processing of the information. The human muscle structure cannot respond instantaneously to command to move and exhibit a lag in response, which is represented by the term T_p in the equation (1). The observed variation of the T_p with forcing function bandwidth ranges from $0.1\,s$ to $0.6\,s$. The time delay represented by the $e^{-\tau \cdot s}$ term is due sensor excitation, nerve conduction, computational lags and other data processing activities in the central nervous system. The parameter τ is considered constant because it appears to be invariant with forcing function and controlled element dynamics for either single or dual random-appearing inputs tasks. The representative values for time delay are of the order of $\tau = 0.2\,s$ and the time lag T_p is approximately $0.1\,s$.

The expression $K_p(T_L \cdot s + 1)/(T_I \cdot s + 1)$ represents the major element in that adaptive capability of the pilot which allows him to control the dynamic devices. Its function is the modification of the stimulus signal into a suitable man-machine system operation.

The form of the pilot transfer function shown in the equation (1) was identified from aerospace publications and laboratory measurements acquired from human subjects. Pilot workload consists of both the mental and physical effort required to control the aircraft to achieve the desired response. Mental effort, which is difficult to quantify, is associated with anticipation required to generate lead to compensate for poor aircraft response characteristics. Physical workload can be described as the work the pilot must expend in moving the control inceptors against their resisting force. An example for an open-loop bank angle response to aircraft lateral control is

$$A(s) = \frac{L_{\delta_A}}{s(s+1)} \cdot \frac{1}{T_A \cdot s + 1} \tag{2}$$

where L_{δ_A} is the lateral control sensitivity, T_R is the roll mode time constant and T_A is the control surface actuator time constant.

For the longitudinal aircraft control, the simplified system of equations has the form

$$\begin{bmatrix} s\cdot U_1 - Z_\alpha & -s\cdot U_1 \\ -\left(M_{\dot\alpha}s + M_\alpha\right) & s^2 - sM_q \end{bmatrix} \cdot \begin{bmatrix} \alpha(s) \\ \theta(s) \end{bmatrix} = \begin{bmatrix} Z_{\delta_e} \\ M_{\delta_e} \end{bmatrix} \delta_e(s) \tag{3}$$

wheres is the Laplace transform parameter. The other variables in the above equation are the longitudinal control derivatives, the pitch and attack angles (θ and α) and the elevator command δ_e [7, 8].

In order to obtain the dynamic response characteristics of the human pilot, we have made laboratory measurements acquired from human subjects, for control forces of the stick, pedals, throttle and aircraft command surfaces. We have estimated the time delay, the lead and lag time constants of the pilot model represented in transfer function form and also we built up the mathematical model of the whole system "pilot and aircraft".

5. NUMERICAL RESULTS

The impulse and step responses are calculated for an aircraft with the following parameters: wing span, $8\,m$; mean aerodynamic chord, $1.5\,m$; sweep angle, 18°; mass of aircraft $3000\,kg$; I_{xx} moment of inertia, $1000\,kg\cdot m^2$; I_{yy} moment of inertia, $6200\,kg\cdot m^2$; I_{zz} moment of inertia, $6800\,kg\cdot m^2$; I_{xz} product of inertia, $200\,kg\cdot m^2$; flight Mach number, *0.7*. Some numerical results are presented in the following figures.

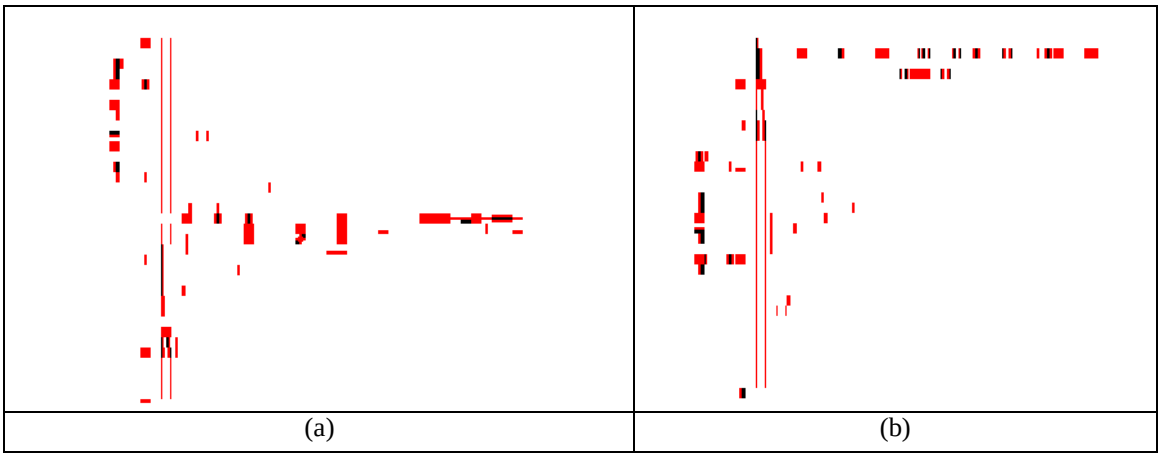

(a) (b)

FIG. 4. Impulse response (a) and step response (b) for the aircraft elevator command

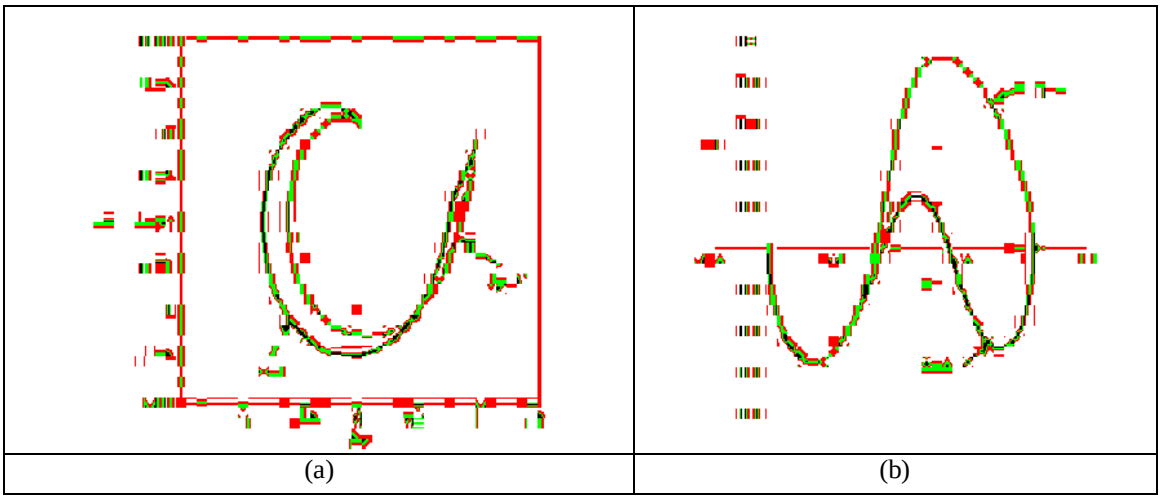

(a) (b)

FIG. 5. Polar plot of pilot-aircraft transfer function in lateral (a) and longitudinal (b) movements

The dynamic characteristics of the integrated "pilot-aircraft" system were studied with the frequency-response method. The middle line (red color) in fig. 5 corresponds to the following parameters: $K_p = 1$; $T_L = 2$; $T_P = 0.5$; $\tau = 0.15$.

CONCLUSIONS

The assessment of handling or flying qualities of airplane depends on pilot skills. When the pilot flies an aircraft he forms subjective opinions concerning the suitability of the man-machine system for performing the assigned task. In arriving at an assessment he is influenced by many parameters. These range over a wide spectrum and include the response to external disturbances, the ease with which instruments can be read, mission, visibility, weather conditions and the familiarity of the pilot with the present aircraft and mission. To be able to asses aircraft handling qualities and human performances, one must have a measuring technique with which any given aircraft characteristics can be rated. If the pilot is expected to assume manual control the system should be structured that he is either kept actively in the control loop at all times or is constantly made aware of the feel of the present aircraft configuration through some auxiliary task which he can practice on during critical phase of the flight.

REFERENCES

[1] J. A. Franklin, "*Dynamics, Control, and Flying Qualities of V/STOL Aircraft,*" AIAA Education Series, Reston, Virginia, USA, 2002.

[2] M. R. Napolitano, "*Aircraft Dynamics. From Modeling to Simulation,* John Wiley & Sons, Inc.,USA, 2012.

[3] C. E. Moldoveanu, A. Giovannini, H. C. Boisson, *Turbulence receptivity of longitudinal vortex-dominated flows* Lecture Notes in Computational Science and Engineering, Vol. 69: BAIL 2008 - Boundary and Interior Layer Proceedings of the International Conference on Boundary and Interior Layers - Computational and Asymptotic Methods, Limerick, Springer Verlag, Berlin, pag. 227 – 236, ISBN: 978-3-642-00604-3, July, 2008.

[4] C. E. Moldoveanu, A. Giovannini, H. C. Boisson, P. Şomoiag, *Simulation of Wake Vortex Aircraft in Ground Effect,* INCAS Buletin, Volum 3, nr. 1/2011, pag.55-61, ISSN 2066-8201, 2011.

[5] C. E. Moldoveanu, F. Moraru, P. Şomoiag, H. C. Boisson, A. Giovannini, *Turbulence Modelling Applied to Aircraft Wake Vortex Study,* MTA Review, Volum XXI, nr. 1/ 2011, ISSN 1843-3391, (2011).

[6] A. N. Tudosie, *Supersonic Air Inlet Control System Based On The Inner Channel Minimum Cross-Section Position Control,*International Conference on Military Technologies ICMT 2009, Brno, Czech Republic, 2009.

[7] A. N. Tudosie, *Aircraft Jet Engine Exhaust Nozzle Controller Based on Turbine Pressure Ratio Sensor with Micro-Jet System,* Proceedings of the 11th International Conference on Applied and Theoretical Electricity (ICATE), Craiova, 2012.

[8] C. Rotaru and I. Sprintu, "*State Variable Modeling of the Integrated Engine and Aircraft Dymanics*", 10th International Conference on Mathematical Problems in Engineering, Aerospace and Sciences (ICNPAA 2014)", Volume 1637, pp. 889-898, 2014.

THE CONCEPT OF CAPABILITY DEVELOPMENT COMMAND, CONTROL AND RECONNAISSANCE OF AIR FORCE

***Milan SOPÓCI*[*]*, Marek WALANCIK*[**]

[*]Armed Forces Academy of general M. R. Štefánik in Liptovský Mikuláš (milan.sopoci@aos.sk), [**]Academy of Business in Dabrowa Górnicza (mwalancik@wsb.edu.pl)

DOI: 10.19062/2247-3173.2016.18.1.8

Abstract: *The article deals with present conception of command, control and reconnaissance of Air Forces Slovak republic (AF SR). On one hand shows present state and on the other hand it shows trend for future years according rules and requirements NATO. The article pointed to that for all changes it need to change organizational structure and large defence sources for modernization weapons systems and armament.*

Key words: *Air Forces, command, control, reconnaissance, modernization, armament,*

1. INTRODUCTION

The submission of Concept development capabilities command, control and reconnaissance Air Force emerged from the conclusions of the expert group's Strategic Defence Review, the Ministry of Defence for the needs of elaboration of the Development Plan OS SR until the Year 2024th.

The aim of the concept of development capability command, control and reconnaissance Air Force is to analyze the current situation and proposal for further procedure development command, control and reconnaissance Air Force of the Armed

Forces of the Slovak Republic. It should provide the basic framework for the development of requirements for complex and interrelated development of all aspects of operational capabilities (area doctrines, organizational structures, training, arming, preparing leaders, staff development, infrastructure and interoperability). Further developing the command, control and reconnaissance Air Force of the Armed Forces of the Slovak Republic should ensure the elimination of negative trends and achieve the necessary operational capabilities for the smooth execution of the tasks under the relevant general statutes, the

Defence Strategy, from Slovakia's membership in NATO, EU and to ensure the fulfillment of commitments under international agreements of the Slovak Republic. Further developing the command, control and reconnaissance Air Force, the Armed Forces of the Slovak Republic should ensure the elimination of negative trends and achieve operational capabilities necessary for the smooth execution of the tasks of protection and defense of airspace, national and international crisis management.

2. CURRENT STATUS OF COMMAND, CONTROL AND RECONNAISSANCE IN THE AIR FORCE(1).

Command, control, radar and radio survey of the Air Force is ensured by forces and means of the brigade command, control and reconnaissance (bvrps Zvolen), which is equipped with LETVIS, 3D medium range radars (P-37, ST-68 MSK), radar rangefinder short range (RL-4AM), radar altimeter (PRV-16) and the system of radio-technical means RATES (KRTP-81E, KRTP-86E). Last year, elements of command, control and reconnaissance provide airy sovereignty of the Slovak Republic within NATINADS, assigned forces and means operating center (OPCEN) and companies of radar recco of brigade command, control and reconnaissance (bvrps) in continuous mode. In the area of responsibility of the air force was captured by emergency means, tracking and locking 407,442 air objects (which is an average of 60 per hour). After evaluation of air objects and allocated to that identity was radar information send as a complete picture of air situation (RAP - Recognized Air Picture) on the CAOC Uedem in Germany. Air navigators (RRBP) of central point of guidence (CMN) made 1439 guidances for air objects.

BVRP organizational structure comprises:

- Operations Centre
- Recco radar batalion
- command support company

3. IMPLEMENTATION OF TRAINING

Bvrps staff training is mainly focused on the changing workplace of declared forces for SACEUR as well as other units providing emergency system Air Force. The staff is trained according to national criteria at the level required prerequisite for further increasing the level of training in preparation for the evaluation TACEVAL. The performance of tasks is affected by both a lack of fullness units at the expense of overtime and on the other hand, the limited amount of flight hours of fighter aircraft. Further increasing the number of trained personnel is dependent on personal repletion units and the allocation of financial resources earmarked for training. OPCEN is the main control unit NATINADS and Emergency system of Air Forces. Its staff is dedicated to the management of forces and means within NATINADS. At present OPCEN 84.5% manning of these critical expertise. Of this number it is to ensure shift operation intended 85%. Continuous service is ensured in 24 hour shifts._Current state of training of personnel is at 97% according to national criteria. The main components include OPCEN CRC, CMN and StrROP. Achieving NATO FOC is conditional upon retraining personnel for training and training centers NATO.

CRC since 2006 is declared unit under the command of SACEUR. CRC exercise command and control forces and means in carrying out defense of the airspace of the Slovak Republic within NATINADS. Its staff performs continuous monitoring and evaluation of airborne objects within the airspace SR / NATO within range radars . The service is carried out in continuous mode. Current state of training of personnel at the level is 92%. according to national criteria. Achieving NATO FOC is conditional upon retraining personnel in training centers NATO. CMN serves to ensure the continued provision of air traffic control services. Its staff performs continuous management of air traffic in the allocated area of responsibility and ensures the fulfillment of tasks of combat use of fighter aircraft the Air Forces and NATO in the airspace of the Slovak Republic.

Current state of training of personnel is at 59% according to national criteria. Achieving NATO FOC is conditional upon retraining personnel in training centers NATO.

Centre for control of operations serves as a command post of commander of the Air Force to perform tasks in a state of safety and during the combat readiness It is a tool commander in solution of crisis situations and duties of National Crisis Management. Manages and coordinates the activities Air patrol and rescue service and participates in cooperation with other components of the integrated rescue system SR. . Currently, 96% of manning of expertise. Current state of training of personnel is at 96%. The main task of the recco radiolocation batalion is to provide command and control to six radar recco companies and two companies of radiotechnical reconnaissance in performing continuous radar and radio recco of airspace SR / NATO within range of their technical means. The main task of these units is to implement a continuous survey RL Airspace SR / NATO emergency changes (identifying, monitoring and evaluation of airborne objects), maintenance, repair and adjustment of radar systems.

4. WEAPONS

Currently, the basic command and control system of the Air Force SR is system LETVIS. This system is its primary purpose designed for the collection, processing and distribution of information on airborne objects, completed to the functionality of planning and management of combat operations of active means.

Radar reconnaissance

The armament of the brigade command, control and recco is the six pieces of three-dimensional (3D) radar medium-range P-37MSK and two pieces of ST-68 MSK, 4 pieces of two-dimensional (2D) radar short range RL-4AM and 3 radar altimeter PRV-16 . The current technique, except RL-4AM is of Russian origin. All the equipment is built based on outdated elements base, which always makes it difficult to procure spare parts for its operation and maintenance. SR as a member state of the EU and NATO has a common border with Ukraine, is therefore a priority coverage eastern borders (Schengen border) focal radiolocation field for small and medium altitudes (below 3,000 meters). This tasks can not comply with the current technology.

Radio-reconnaissance

The armament of the brigade command, control and survey are two sets of radio-recco KRTP-81E and KRTP-86E. They are mobile radio-technical reconnaissance means designed to analyze radio-signals, identification and tracking air and ground targets. Technical life KRTP- 81E-up in 2016 and KRTP-86E in 2019.

5. TARGET STATE COMMAND, CONTROL AND RECONNAISSANCE IN THE AIR FORCE (2,3).

Organizational structure.

Wing command, control and survey will formed, which is to provide command and control of forces and means earmarked to the standby system of Air Forces SR, that perform continuous radar survey of the airspace of the Slovak Republic in the integrated air defense system of NATO - NATINADS.

In addition to the tasks of command, control and reconnaissance within a NATINADS Wing command, control and reconnaissance ensure:

- Support and ensuring the Air Force Command,

- Radio-technical reconnaissance (ELINT) to support news alert system (SVS) ,
- Intelligence support for the General Staff of the Slovak Armed Forces, military SIGINT center and ISTAR,
- Meteorological support OS SR.

The primary role of personnel management is to ensure the continuous staffing the professional soldiers with the required skills and expertise in the ranks to achieve the desired state(4).

This is directly for:

- To provide new, efficient replenishment system and training of key personnel,
- Ensure better links between education at school and training facility in NATO,
- Create the conditions for continuous career growth and stabilization of the staff.

Training

Staff training will be carried out after the purchase of new vehicles from 2016 to 2020 (2017-2021). Suppliers of equipment shall be provided under a contract for purchase of equipment and execution of operator training instructors manufacturer of military education to the highest level of operation and maintenance in conformity with the technical documentation in the Slovak Republic. The number and duration of training is also part of the contract. The Training Supervisor shall issue a certificate of competency to train additional staff. Further training new personnel will be carried out by personnel holding a certificate own forces and means.

Within the deadlines specified by the SHAPE / HQ Allied Air Command Ramstein achieve and maintain the required level of training to implement the CRC certification TACEVAL. To achieve adequate NATO staff qualifications CRC and CMN is necessary to ensure that they are sending to the foreign professional training attested by valid certification NATO.

Weapons

Command and Control System It will be necessary to complete the enlargement process classified (classified) part of the network system LETVIS in recco radar companies.

Radar and radio survey

Tips and amount of resources radar and radio survey needed for variation

amendment, based on a study of the current radar coverage of the Slovak territory and analysis of current status of radar and radio equipment, the figure 1

Elements of reconnaissance

In accordance with the above documents, strategic defense review and program plan armaments needed replacement of 6 pieces P-37MSK for 3D medium range from 2016 and 4 pieces RL-4AM for 3D small range since 2017.

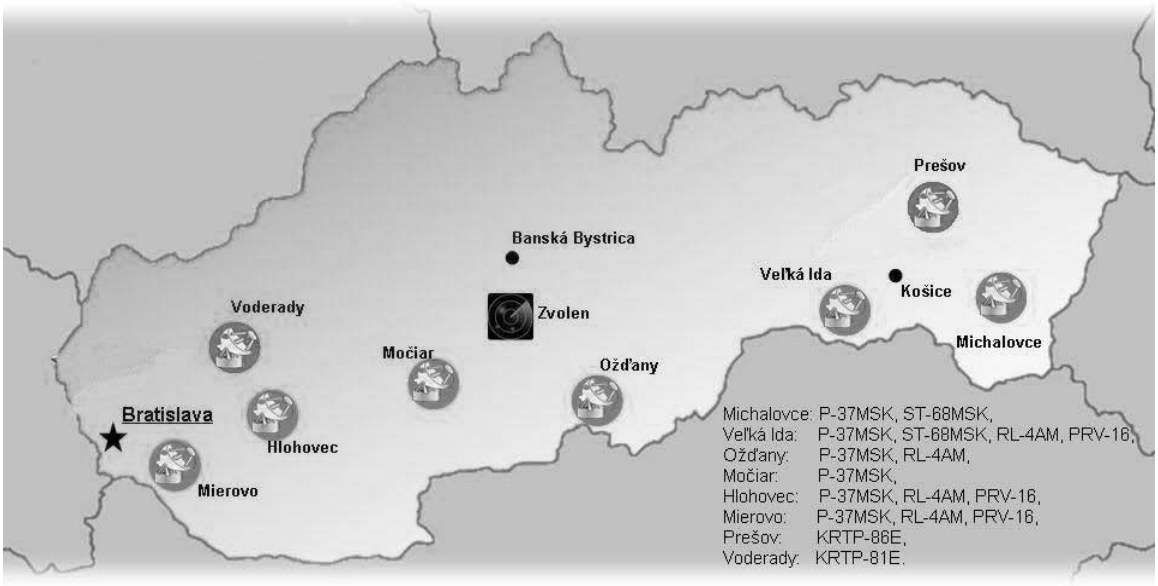

FIG.1. Reconnaissance system of Slovak Air Forces

As part of the purchase will also address the need to purchase a special work for repairs that takes into account the technologies used and the above prophylactic work, including the creation of adequate storage facilities for the storage of special components . In accordance with these documents it requires the purchase of 2 pieces of new mobile radio-technical reconnaissance means in the years 2016 and 2018 as a replacement for KRTP-81E and KRTP-86E.

C**ONCLUSIONS**

Development capabilities command, control and reconnaissance Air Force of the Armed Forces of the Slovak Republic should ensure the elimination of negative trends, both in terms of available financial and material resources, as well as in training for staff to achieve and maintain the necessary operational capabilities for the smooth execution of the tasks of defense a national crisis management._To develop competency command, control and research will be needed by 2024 to implement a series of gradual measures consisting:

- The preparation of CRC and realization evaluation of TACEVAL,
- Ensuring the resources for infrastructure maintenance,
- Variations in the implementation of radar and radio equipment.

To procure new radar technology and key security technologies is necessary to ensure the maintenance of existing operational capabilities and regular:

- Supplementing staff,
- Training and education of personnel
- Providing resources for the maintenance of safety equipment,
- Ensuring the resources for infrastructure maintenance.

REFERENCES

[1] *Evaluation of AF SR* , NADC team, Zvolen 2003.
[2] *Long-term plan of the structure and development of the Slovak Armed with a planning perspective to 2024*, MOD SR, Bratislava, 2014
[3] *Conception of command, control and reconnaissance of Air Forces Slovak Republic*, MOD Bratislava 2014
[4] Sopóci, M. – Walancik, M.: *Conception of competences development of Air Defence of Armed Forces. In. AFASES international conference*, AFA Brašov 2015, ISSN 2247-3173.

PROTECH „IN-HOUSE" SOFTWARE AN ALTERNATIVE FOR PROJECTILE'S DRAG COEFFICIENT EVALUATION IN CASE OF SMALL TOLERANCES OF ITS GEOMETRICAL DIMENSIONS

George SURDU*, **Cristian MOLDOVEANU****, **Șomoiag PAMFIL****

*Research Center for Navy, Constanța, Romania
** Military Technical Academy, Romania

DOI: 10.19062/2247-3173.2016.18.1.9

Abstract: *In this paper is described a software product for projectile's drag coefficient evaluation in case of small finite differences of projectile's geometrical dimensions. The software is useful for engineers who work in research and ammunition design when is necessary to evaluate the preliminary projectile drag coefficient and its implications on trajectory. The paper offers an evaluation of projectile's drag coefficient by two different methods: numerical simulation using the flow around the projectile shape and using ProTech design software. The evaluation is made with two different software products, a fluid mecanics one and the "in-house" ProTech software instrument, by comparing the results for drag coefficient obtained using four different projectile shapes.*

Keywords: *drag coefficient, ammunition, aerodynamics, projectile, aerodynamic configuration*

1. INTRODUCTION

The evaluation of the aerodynamic parameters of a projectile's shape assumes to calculate theirs variations taking into account geometrical tolerances of the projectile's geometrical shape.

This variation can be evaluated using some numerical methods specialized on fluid flow evaluation in general and high-speed flow simulation around aerodynamic configurations in particular, which are not in this case a useful instrument. For this reason, was developped an "in-house" software instrument named ProTech that is based on analytic methods. This software instrument has the main purpose to evaluate the projectile's drag coefficient tolerances and the influences of these tolerances on drag coefficient without using a large amount of resources.

This instrument offers to engineers or field test specialist of ammunitions an important standalone software that serves in projectile geometrical modification evaluation, ballistic table evaluation, and projectile's trajectory evaluation using drag coefficient modifications caused by small tollerances of projectile's dimensions.

Some of these instruments can represent a cheap and handy alternative for field-testing but cannot replace the experimental tests. Specialist for preliminary evaluation and implications can use these instruments.

The study has two main objectives: drag coefficient evaluation using the ProTech "in-house" software instrument for four different shapes of projectiles and compare the results with the ones obtained by flow simulation, and the other goal is to make known in a few words the capabilities of the ProTech "in-house" software.

ProTech software is a project financially supported within the project entitled "Horizon 2020 - Doctoral and Postdoctoral Studies: Promoting the National Interest through Excellence, Competitiveness and Responsibility in the Field of Romanian Fundamental and Applied Scientific Research", contract number POSDRU/159/1.5/S/140106. This project is co-financed by European Social Fund through Sectoral Operational Programme for Human Resources Development 2007-2013. Investing in people!

This software has implemented a series of mathematical models developped to execute: statistical evaluation of a ballistic or geometrical parameter, projectile's drag coefficient evaluation taking into account his geometrical tolerances, projectile's trajectory study using projectile's drag coefficient tolerances.

Taking into account, the capabilities briefly presented before the ProTech software instrument contains three main evaluation modules: statistic calculus module named StatTech, drag coefficient module named AeroTech and trajectories evaluation module named BalextTech.

The diagram, for the software modules presentation and theirs icons identification, is presented in Fig. 1.

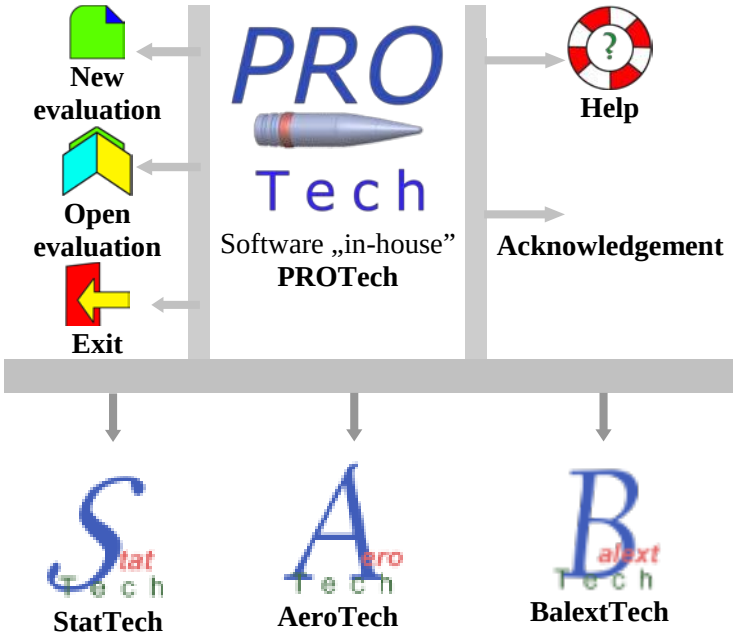

FIG. 1. ProTech sofware diagram

(Source: Authors database presented in [1])

For the presented study, we used the AeroTech module, which represents only the drag coefficient evaluation capability from the ProTech "in-house" software instrument.

Using Protech and a flow simulation software will be compared a few results obtained for four different geometrical configurations of projectiles of 23 mm and 30 mm caliber.

2. NUMERICAL DATA AND 3D MODELS USED FOR DRAG COEFFICIENT EVALUATION

In this study, we used four projectile geometrical configurations. For these configurations, the 3D models of them are presented in Fig. 2, Fig. 3, Fig. 4 and Fig. 5.

FIG. 2. Projectile 23x152B for ZSU canon 3D virtual model, configuration 1-23

(Source: Authors database presented in [1])

FIG. 3. Projectile 23x260 for Rikhter 23-R canon 3D virtual model, configuration 2-23

(Source: Authors database presented in [1])

FIG. 4. Projectile 30x165 for Gsh-30 canon 3D virtual model, configuration 3-30

(Source: Authors database presented in [1])

FIG. 5. Projectile 30x210B for NN-30 canon 3D virtual model, configuration 4-30

(Source: Authors database presented in [1])

All four configurations presented before are use to evaluate the drag coefficient using the flow around projectile and the analytical implemented in ProTech software instrument.

The mathematical model [1, 2, 3] for drag coefficient estimation uses projectile's geometrical dimensions (Fig. 6).

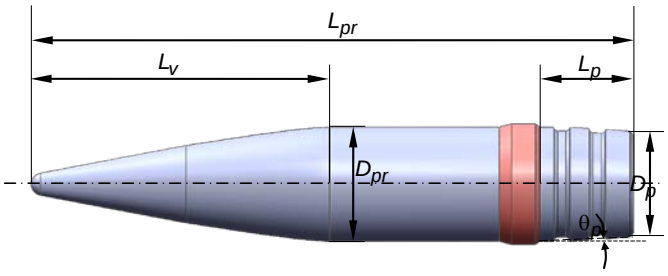

FIG. 6. Projectile's dimensions used (Source: Authors database presented in [1])

These dimensions are: L_{pr}– projectile's total length, L_v- ogive length, L_p- tronconical length, D_{pr} - transversal section diameter, D_p - projectile back – side diameter, θ_p – angle for projectile's tronconical part.

These four configurations of projectiles have the ballistic characteristics presented in Table 1.

Table 1. Projectiles ballistic characteristics

Configuration	Weight [kg]	Initial velocity [m/s]	Total length [mm]
1-23	0.190	970	98.6
2-23	0.175	850	102.35
3-30	0.400	860	139.7
4-30	0.3285	1050	118.6

Source: Authors own database [1]

In Table 1 are presented the ballistic parameters of the four configurations of projectiles and all these data were used for numerical flow 3D simulation and analytical calculation with ProTech software. The numerical evaluations were made for three Mach numbers taking into account their initial velocity.

The numerical results obtained by simulation for every configuration are compared with the results obtained using ProTech's drag coefficient module AeroTech. In addition, the drag coefficient evauaton using ProTech is based on Siacci's law as reference law.

3. NUMERICAL RESULTS

The drag coefficient evaluation with the ProTech software application was made using the geometrical data presented in Table 2. the dimension presented n Table 2 are acording the dimensions presented in Fig. 6.

Table 2. Configurations geometrical parameters

	Configuration			
Parameter	1-23	2-23	3-30	4-30
D_{pr} [mm]	23	23	30	30
L_{pr} [mm]	98.6	102.35	139.7	118.6
L_v [mm]	51.89	40.4	82.8	39.8
L_p [mm]	3.9	6.1	3	5.7
θ_p [deg]	45	45	60	6

Source: Authors own database [1]

The flow simulation was made in the flow simulation scenarios presented in Table 3, Table 4, Table 5 and Table 6 for each configuration separately.

Table 3. Flow design scenarios data for configuration 1-23

Parameter	Flow scenario		
Free stream Mach number value [-]	2.7	2.8	2.9
Free stream density [kg/m^3]	1.22		
Reference surface [m^2]	0.000415476		

Source: Authors own database [1]

Table 4. Flow design scenarios data for configuration 2-23

Parameter	Flow scenario		
Free stream Mach number value [-]	2.5	2.6	2.7
Free stream density [kg/m3]	1.22		
Reference surface [m2]	0.000415476		

Source: Authors own database [1]

Table 5. Flow design scenarios data for configuration 3-30

Parameter	Flow scenario		
Free stream Mach number value [-]	2.5	2.6	2.7
Free stream density [kg/m3]	1.22		
Reference surface [m2]	0.000706858		

Source: Authors own database [1]

Table 6. Flow design scenarios data for configuration 4-30

Parameter	Flow scenario		
Free stream Mach number value [-]	3.0	3.1	3.2
Free stream density [kg/m^3]	1.22		
Reference surface [m^2]	0.000706858		

Source: Authors own database [1]

Drag coefficient was evaluated using the flow field around each of these four configurations presented before. The results for the pressure field and Mach distribution for each configuration are presented in Fig. 7 to Fig. 14.

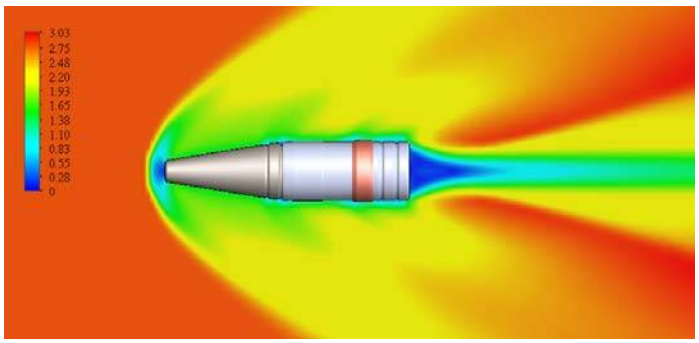

FIG. 7. Mach field for 1-23 configuration at 2.9 Mach free stream velocity

(Source: Authors database presented in [1])

As we can see in Fig. 7 the flow around the projectile's geometrical configurations is with shock waves one. This flow is characteristic for all four configurations and is a symetrical flow around the projectile's main axis. The pressure distribution field is in acordance with the flow as we can observe in Fig. 8. The sresults obtaind for the othe other three configurations will be only exposed without any explanations because the flows around them has the same charatheristics.

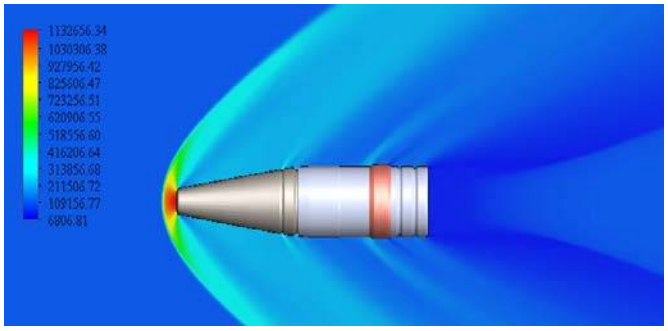

FIG. 8. Pressure field for 1-23 configuration at 2.9 Mach free stream velocity

(Source: Authors database presented in [1])

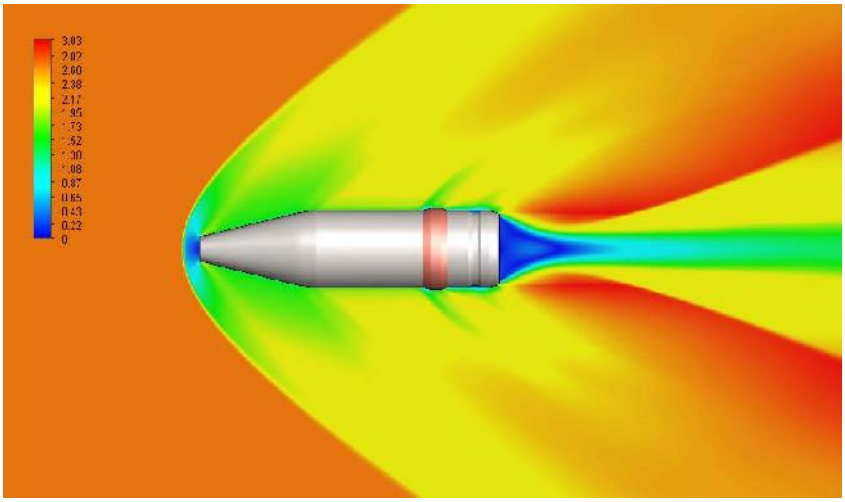

FIG. 9. Mach field for 2-23 configuration at 2.7 Mach free stream velocity

(Source: Authors database presented in [1])

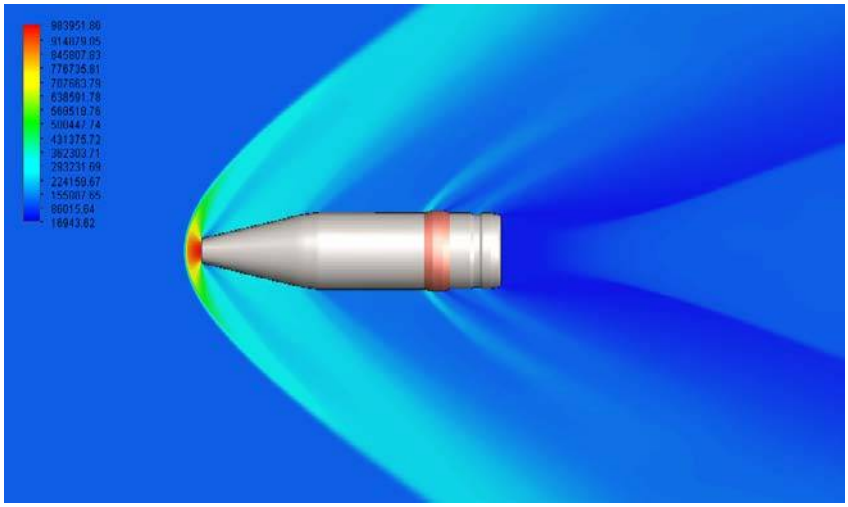

FIG. 10. Pressure field for 2-23 configuration at 2.7 Mach free stream velocity

(Source: Authors database presented in [1])

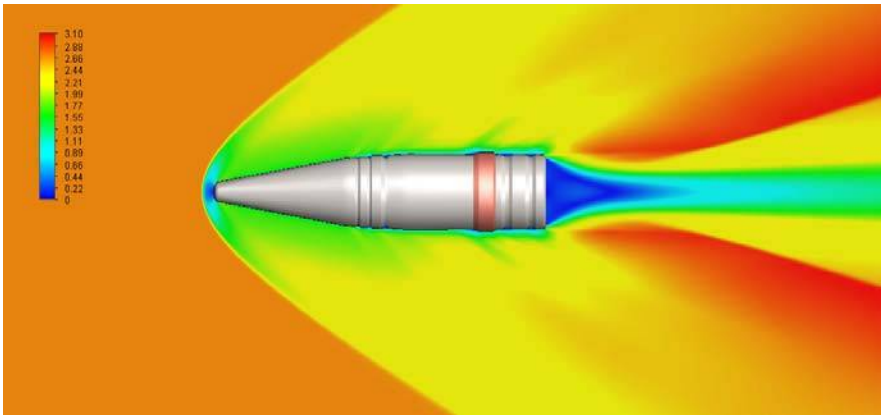

FIG. 11. Mach field for 3-30 configuration at 2.7 Mach free stream velocity

(Source: Authors database presented in [1])

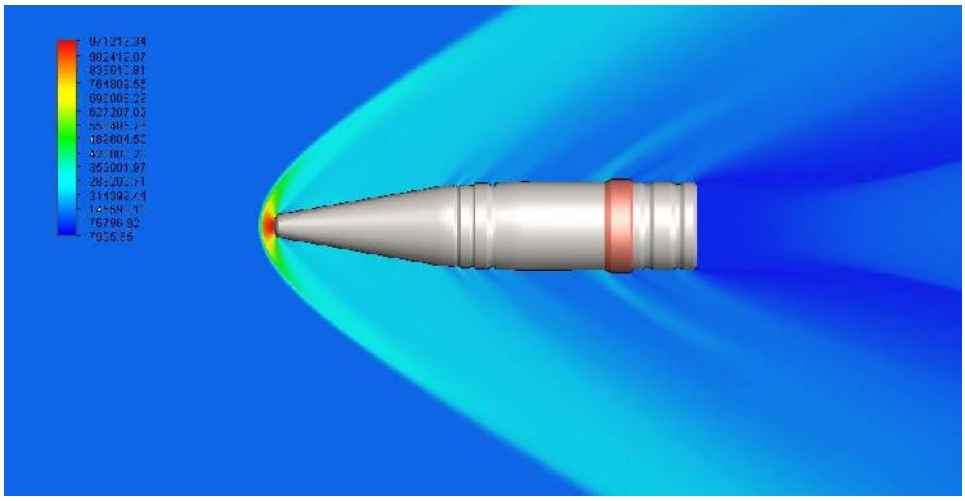

FIG. 12. Pressure field for 3-30 configuration at 2.7 Mach free stream velocity

(Source: Authors database presented in [1])

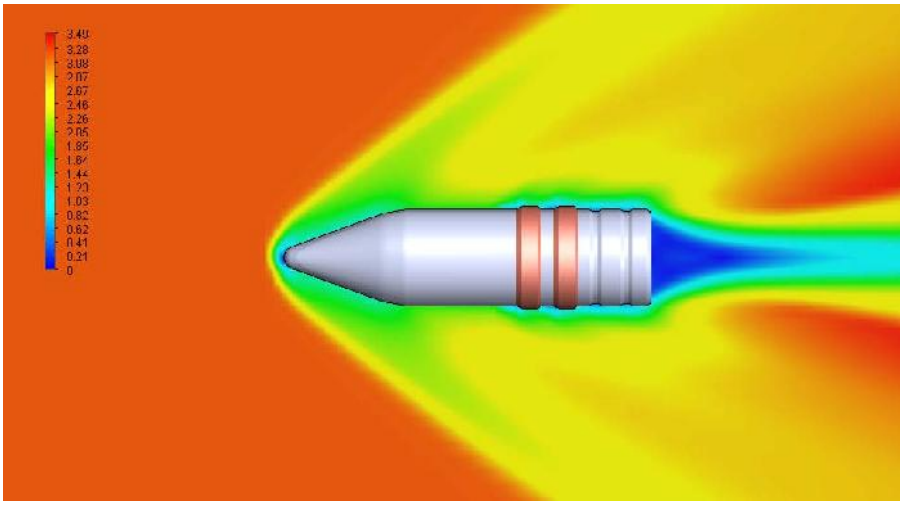

FIG. 13. Mach field for 4-30 configuration at 3.2 Mach free stream velocity

(Source: Authors database presented in [1])

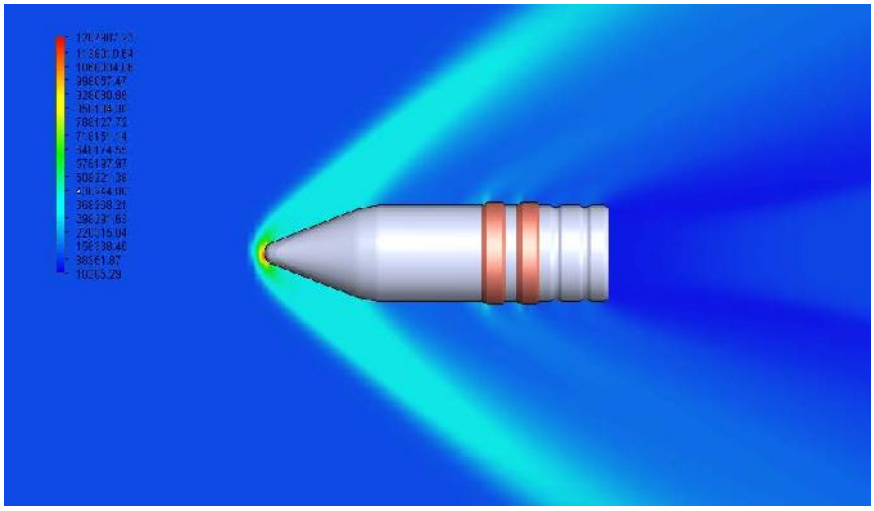

FIG. 14. Pressure field for 4-30 configuration at 3.2 Mach free stream velocity

(Source: Authors database presented in [1])

Drag coefficient for projectiles configurations obtained by simulation and using ProTech's software module AeroTech are compared and exposed in Table 7, Table 8, Table 9 and Table 10.

Relative deviation between the simulation results and ProTech results for drag coefficient value is calculated using the following relation:

$$dev\_rel[\%] = \left| \frac{C_{d\_flow} - C_{d\_ProTech}}{C_{d\_flow}} \right| \cdot 100 \quad (1)$$

in which: dev_rel represents the relative deviation, C_{d_flow} represents drag coefficient calculated using the flow field, $C_{d\_ProTech}$ represents the drag coefficient value calculated using ProTech software.

Table 7. Drag coefficient comparative results for configuration 1-23

	Mach = 2.7	Mach = 2.8	Mach = 2.9
Drag value ProTech	0.19823	0.194252	0.18993
Drag value flow simulation	0.19940	0.195711	0.18993
Relative deviation	0.583330	0.745732	0.00099

Source: Authors own database [1]

Table 8. Drag coefficient comparative results for configuration 2-23

	Mach = 2.7	Mach = 2.8	Mach = 2.9
Drag value ProTech	0.20134	0.19683	0.19232
Drag value flow simulation	0.19564	0.19182	0.19075
Relative deviation	2.91363	2.61403	0.82532

Source: Authors own database [1]

Table 9. Drag coefficient comparative results for configuration 3-30

	Mach = 2.5	Mach = 2.6	Mach = 2.7
Drag value ProTech	0.16515	0.16145	0.15775
Drag value flow simulation	0.16728	0.15861	0.15695
Relative deviation	1.27067	1.79178	0.50816

Source: Authors own database [1]

Table 10. Drag coefficient comparative results for configuration 4-30

	Mach = 3.0	Mach = 3.1	Mach = 3.2
Drag value ProTech	0.17690	0.17187	0.16851
Drag value flow simulation	0.17121	0.16676	0.16404
Relative deviation	3.32151	3.06356	2.72739

Source: Authors own database [1]

From the results analysis we can see easily that the relative deviation in absolute value is between 0.001 % and 3.33%, which means that the deviations are in the accepted limits of 3% to 10 %. We can consider accepted the results obtained with the ProTech software instrument.

4. CONCLUSIONS

The drag coefficient evaluation was made using two different methods by flow simulation evaluation and using ProTech software instrument.

The results obtained for drag coefficient using ProTech software was in good agreement with the results for it obtained with the flow simulation around the projectile geometrical configuration.

This result can be very useful for the projectile's trajectory evaluation. This can be done using the ProTech's trajectory evaluation module BalextTech.

The software "in-house" ProTech can be used with good results in: research, desing and development for armaments and ammunitions.

REFERENCES

[1] G. Surdu, *Cercetări privind influența caracteristicilor aerodinamice ale proiectilelor de calibru mic asupra dinamicii zborului și preciziei tragerii. Metode statistice de evaluare și instrumente software „in-house”*, Raport cercetare postdoc, POSDRU/ 159/ 1.5/S/140106, București, 2015;

[2] G. Surdu, *"In – house" software module for projectile's drag coefficient evaluation in case of small geometrical dimension tolerances: A solution for cost reducing*, Romanian Journal of Economics, Romanian Academy, online ISSN: 2344-4568, Bucharest, 2015;

[3] G. Surdu, V. Vasile, G. Slămnoiu, *Applications of probability theory to study the influence of projectile's mass tolerances on exterior balistic*, Review of the Air Force Academy, nr. 3 (27), vol. XII, p.101 – 104, Brasov, (2014).

[4] C. Rotaru, I. Cîrciu, C. Aramă, C.G. Constantinescu, *Aspects regarding velocity distribution in the secondary zone of a gas turbine combustor*, Review of the Air Force Academy, nr. 3 (30), p.33-38, Brasov, (2015);

[5] C. Rotaru, I. Cîrciu, C. M. Boscoianu, *Computational Methods for the Aerodynamic Design*, Review of the Air Force Academy, nr. 2 (17), p.43-48, Brasov, (2010).

AIR FORCE AND AEROSPACE ENGINEERING

THUNDERSTORM OCCURENCE AND ASSOCIATED FLIGHT HAZARDS IN THE SOUTHERN PART OF ROMANIA

Carmen STEFAN

Romanian Aviation Academy, Bucharest, Romania (carmen.garnita@gmail.com)

DOI: 10.19062/2247-3173.2016.18.1.10

Abstract: *This research work evaluates the thunderstorm occurrence and associated flight hazards in the southern part of Romania. This study focused on the monthly and annual occurrence, the trend of this flight hazard during the past six years. The statistical analyses employed were Simple and Multiple bar charts and correlations. It was observed from the analysis that thunderstorms occur mostly between March and October with an increasing trend of 71% for 2010 and 2014, and with a lower rate, between 10%-33% for 2011, 2012 and 2015, probably associated with the global warming. The monthly peak was registered in June, but August also became a month with a high probability of thunderstorm formation. A significant decrease with 28%-89% was also revealed for September.*

The study concluded that the thunderstorms occurrence in the studied area has significantly increased and it has more impact on delays than on diversions, but it is not the root cause of any incident/accident.

Keywords: *thunderstorm, occurrence, flight hazard*

1. INTRODUCTION

One of the most important flight hazard is the thunderstorm. When assessing accidents related with thunderstorms and other related impacts, it became obvious that the flight hazards associated where not always identified by the aviators. This weather phenomena significantly influence the safety and the operational activity of air traffic, particularly at the terminal areas. The serious consequences are excepting accidents, delays, diversions and sometimes cancellations of flights. The thunderstorms can be devastating as a typhoon, hurricane, tropical cyclone or a tornado. It is estimated that there are as many as 40,000 thunderstorm occurrences each day world-wide. A single cell of thunderstorm affects an area of 8 km. According to NTSB Aviation Accident and Incident Data Base [3, 8] most of the weather factors that caused or contributed to weather-related accidents are thunderstorms or weather phenomena associated with them.

Therefore, a good knowledge of this flight hazard becomes very important to aviators, in order to increase the flight safety and reduce the risks to a minimum.

As such, the purpose of this study is to determine the occurrence of thunderstorms in the southern part of Romania and the comparison with previous statistical data.

In order to achieve this aim, the following objectives were pursued to:

1. Determine the annual and monthly occurrence of thunderstorm over the southern part of Romania.
2. Analyze the variability/trend of thunderstorm occurrence in southern part of Romania.
3. Correlate with the global climate changes in the last years.
4. Determine the influence of thunderstorm on flight safety and operations.

2. ATMOSPHERIC PARAMETERS NECESSARY FOR THUNDERSTORM DEVELOPMENT

2.1 High relative humidity (sufficient water vapour to form and maintain the cloud). The amount of water vapour in the atmosphere plays an important part in the development of thunderstorm. In order to calculate the amount of water vapour in the atmosphere [1] the partial pressure of the water vapour , maximum water vpour pressure E and relative humidity RH are used.

$$RH = \frac{e}{E}100 \tag{1}$$

The saturation corresponds to a relative humidity of 100%. The empirical relation between E and temperature, t is as follows[3]:

$$E = 6.107\left(\frac{7.6326t}{10^{241.9+t}}\right) \tag{2}$$

For practical aviation purposes dew point temperature is used, τ, which is the temperature at which the relative humidity reaches 100%, by cooling at a constant pressure and maintaining the water vapour quantity constant. Its values may be determined using the formula [3]:

$$\tau = \frac{241.9\ln\frac{e}{6.107}}{7.6326 - \ln\frac{e}{6.107}} \tag{3}$$

Using a simple approximation [3] we may conclude that the temperature dew point is

$$\tau \approx t - \frac{100 - RH}{5} \tag{4}$$

or

$$RH \approx 100 - 5(t - \tau) \tag{5}$$

2.2 Atmospheric instability.

The Environmental Lapse Rate, γ value gives a clear indication [3] regarding the stability state of the atmosphere and can be written as function of temperature, t and altitude, z:

$$\gamma = -\frac{\partial t}{\partial z} \tag{6}$$

The conditional instability occurs if:

$$\gamma_S \prec \gamma \prec \gamma_D \tag{7}$$

The absolute instability occurs if:

$$\gamma \succ \gamma_D \tag{8}$$

where $\gamma_S = 1.8°C/1000ft$ is Saturated Adiabatic Lapse Rate and $\gamma_D = 3°C/1000ft$ is Dry Adiabatic Lapse Rate.

2.3 Indices used for TS determination

K_{index} is derived arithmetically as:

$$K_{index} = (t_{850mb} - t_{500mb}) + \tau_{850mb} - (t_{700mb} - \tau_{700mb}) \tag{9}$$

The difference between t_{850mb} and t_{500mb} is used to parameterize the vertical temperature lapse rate, γ. The temperature dew point at 850 mb, τ_{850mb} provides information on the moisture content in the lower level of the atmosphere. The vertical extent of the moist layer is represented by the difference between t_{700mb} and τ_{700mb} [1, 2].

TS probability (P_{TS})may be calculated using the formula:

$$P_{TS} = 4\left(K_{index} - 15\right) \tag{10}$$

Table1. Correlation between K_{index} and P_{TS}

K_{index} value	TS probability(P_{TS})
Less than 20	None
20 to 25	Isolated thunderstorms
26 to 30	Widely scattered thunderstorms
31 to 35	Scattered thunderstorms
Above 35	Numerous thunderstorms

2.3 Triggering action. The triggers or lifting forces are [4] convection, orographic uplift, convergence and frontal uplift. The source of lift (upward) is caused by the difference in air density and it is accomplished by several methods: differential heating, fronts, terrain.

3. THUNDERSTORM (TS) DEVELOPMENT

3.1 Types of thunderstorms. Thunderstorms are classified [4] as heat, or air mass thunderstorm (more common in summer) and frontal thunderstorm (more common in winter). Heat thunderstorms are isolated, most frequent over land in summer, formed by day, clear by night and associated with cols and weak lows. Frontal type thunderstorms are most frequent in winter, formed over land or sea, by day or by night, usually formed in a line at a cold front or occlusion, found in depressions or troughs, often accompanied by a squall line.

3.2 Life cycle of a thunderstorm. The life cycle of a thunderstorm cell lasts about 15-20 minutes for the initial and mature stages, and about 1.5 to 2.5 hours for the dissipating stage. During the initial stage, the currents are up draughts.

The second stage of development is the mature stage or Towering Cumulus stage and the currents are strong vertical up draughts and down draughts. In this stage, microbursts may appear, in a region with a diameter of 1 km to 4 km and a duration of 1 minutes to 5 minutes. The precipitations start to fall in this mature stage. Rising and falling water droplets will produce a considerable build-up of static electricity, usually of positive charge at the top of the cloud and negative at the bottom. The build-ups eventually lead to lighting discharge and thunder.

The third stage is the dissipating stage[3, 4], which is characterized by down draughts. The Cumulonimbus cloud usually reaches the tropopause and in the upper part of the cloud there will appear the anvil. Large variations in static charge in and around the cloud cause discharge in the form of lighting, which can appear in the cloud, from the cloud to the ground, or from the cloud to the air alongside.

3.3 Supercell thunderstorms (Severe local storms). Supercell thunderstorms are more common over continental land masses than over the maritime areas. Thunderstorms over mid-vest states of USA, north of Africa and west of Europe producing tornadoes are good examples.

3.4 Movement of a thunderstorm. The movement of a thunderstorm may be calculated using the following formula, during the winter:

$$v_{TS} = 0.80 v_{700mb} \quad (11)$$

and using the following formula for summer:

$$v_{TS} = 0.50 v_{500mb} \quad (12)$$

where v_{TS} = thunderstorm movement velocity, v_{700mb} = wind velocity at 700 mb and v_{500mb} = wind velocity at 500 mb.

Forecasting the occurrence of thunderstorm will be largely a matter of assembling the conditions necessary for the formation and the triggers. A combination of this two groups will indicate the probability of thunderstorms. Satellite images and computer modeling are used to predict this occurrence.

4. THUNDERSTORM HAZARDS

4.1 Turbulence. Turbulence can be severe both within cloud and their sides. Turbulence may be dangerous below the cloud, during take-off and landing and wind shear may also appear.

4.2 Hail. Hail may be expected at any height in the cloud, also below the cloud and below the anvil. Damaging hail can occur up to a height of 45,000 ft.

4.3 Icing. This weather phenomena may occur at all heights in the cloud, where the temperature is between 0°C and -40°C. Due the fact that Cumulonimbus cloud is a cumuliform cloud [4], inside the cloud there is a high concentration of large supercooled water droplets, which may result in severe clear icing.

4.4 Lightning. Lightning is most likely to occur within 5,000 ft of the freezing level. There are 3 effects that may be expected:

- It may cause a pilot temporarily blinded.
- Compasses may become totally unreliable.
- Some airframe damage may be caused, particularly with composite aircraft.

4.5 Static. This causes interference on radio equipment in the LF, MF, HF and VHF frequencies. St Elmo's fire may be caused by static and it results in purple rings of light, especially around the wing tips. This indicates[2, 4] that the air is electrically charged and lightning is probable, but it does not represent a hazard for flight.

4.6 Pressure variation. Local pressure variation may determine inaccurate altimeter readings as much as ±1000 ft at all heights.

4.7 Microburst. These are strong vertical down draughts [4, 9] in the cloud, which also move outwards by reaction from the ground. They are largely caused by descending raindrops, which cools the surrounding air by evaporation, the higher density accelerating the down draught still further. They have a horizontal development between 1km and 4 km and have a lifetime of about 4 minutes. They may cause severe turbulence and severe wind shear conditions. A warning sign of this weather phenomena is virga.

4.8 Water ingestion. If up draught speed approaches or exceeds the terminal velocity of raindrops which are falling, the resulting high concentrations of water can exceed the design limits for water ingestion in some turbine engine. That may cause engine flame-out and/or structural failure. Water ingestion may also affect Pitot heads.

4.9 Tornados. These are usually associated with severe thunderstorm and Tropical Revolving Storm [4], which often occur in the mid-west of USA, west of Europe and north of Africa.

5. DATA PRESENTATION AND ANALYSIS

5.1 Data presentation. The studied area is located between 44°N and 45°N, 24°E and 27°E and the analyzed data set includes parameters used to forecast the significant weather phenomena for aviation purposes. The analyzed period consists of six years (from 2010 to 2015).

The table 2. shows the total yearly frequency of TS occurrences during the last six years over the southern part of Romania and fig. 1 depicts the graphic representation of statistical data.

Table 2. Number of days with TS

Year	Total days number with TS
2010	51
2011	26
2012	32
2013	43
2014	53
2015	26

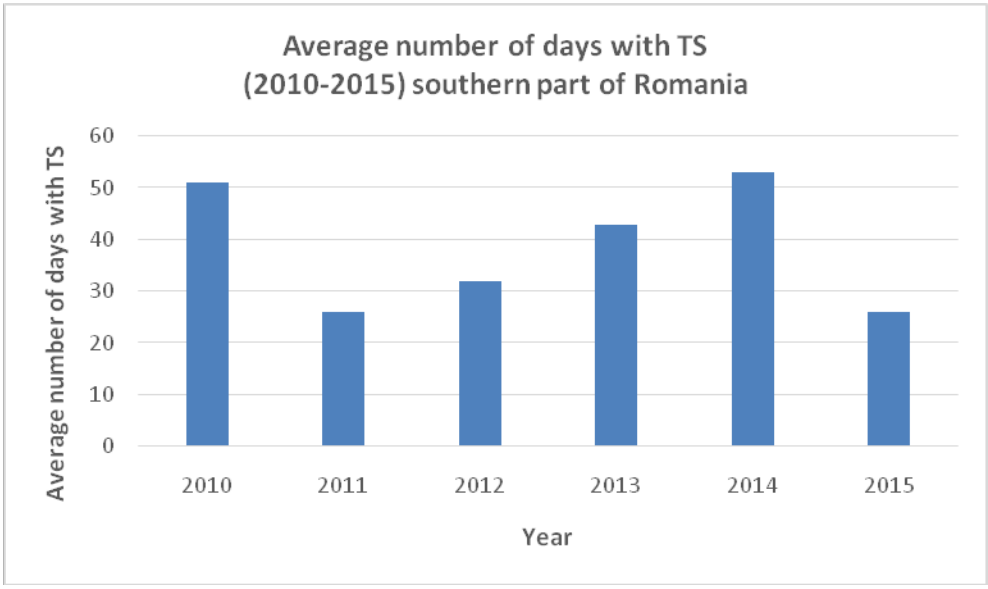

FIG. 1. Average number of days with TS in the southern part of Romania

In this area are three international airports that reported thunderstorms as follows:

- the table 3. shows the total yearly frequency of TS occurrences during the last six years at LROP and LRBS.

Table 3. Monthly frequency of TS occurrences for LROP and LRBS

Month	2010	2011	2012	2013	2014	2015
March	0	0	1	0	0	1
April	2	0	4	0	2	1
May	10	14	8	8	9	6
June	10	9	8	13	12	6
July	16	5	5	9	15	5
August	8	3	4	6	6	7
September	3	1	0	1	2	3
October	0	0	0	2	0	0
November	2	0	0	0	0	0
December	0	0	0	0	1	0

- the table 4. shows the total yearly frequency of TS occurrences during the last six years at LRCV.

Table 4. Monthly frequency of TS occurrences for LRCV

Month	2010	2011	2012	2013	2014	2015
March	0	0	1	0	0	1
April	2	0	4	0	2	1
May	10	14	8	8	9	6
June	10	9	8	13	12	6
July	16	5	5	9	15	5
August	8	3	4	6	6	7
September	3	1	0	1	2	3
October	0	0	0	2	0	0
November	2	0	0	0	0	0
December	0	0	0	0	1	0

The graphic representations of statistical data for LROP, LRBS and LRCV are depicted in Fig. 2 and Fig. 3.

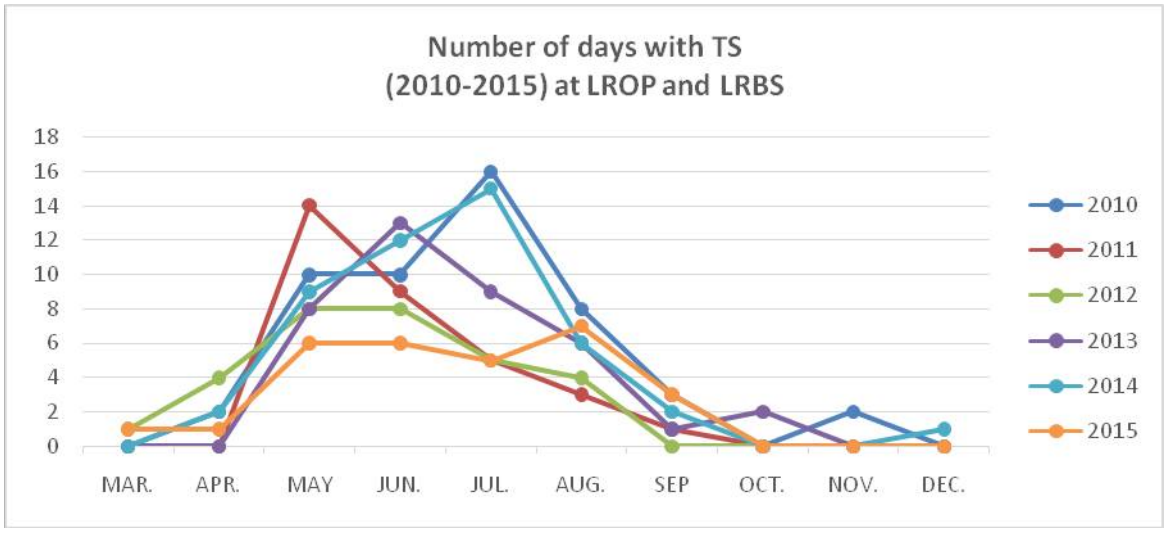

FIG. 2. Number of days with TS at LROP and LRBS

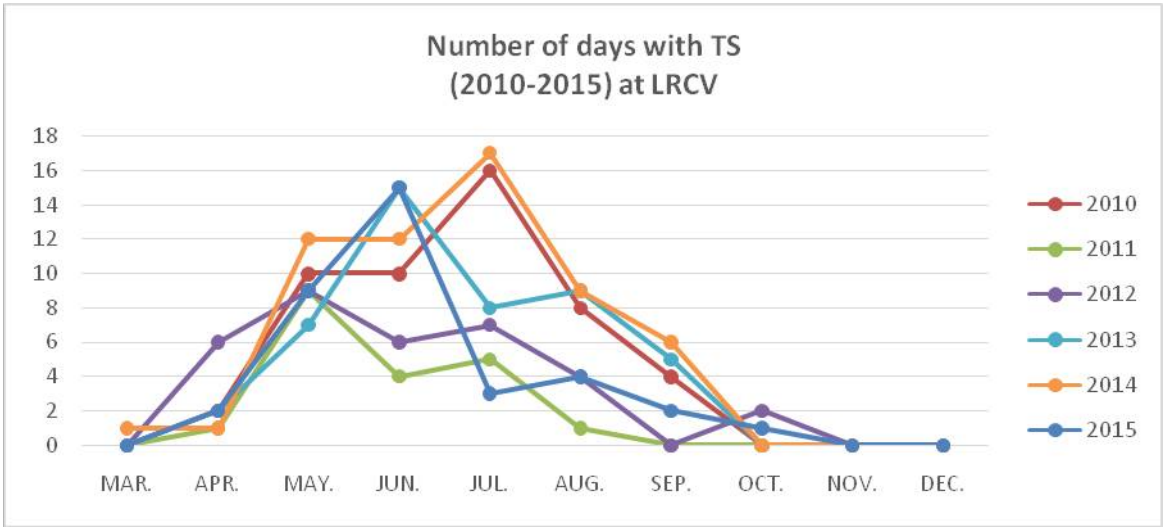

FIG. 3. Number of days with TS at LRCV

The graphic representations of percentages for LROP, LRBS and LRCV are depicted in Fig. 4 and Fig. 5.

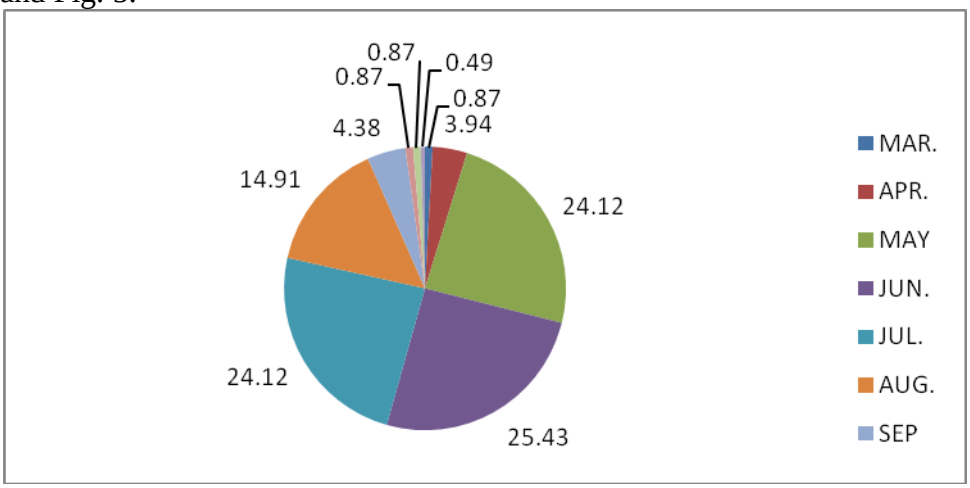

FIG. 4. Percentages of days with TS by months at LROP

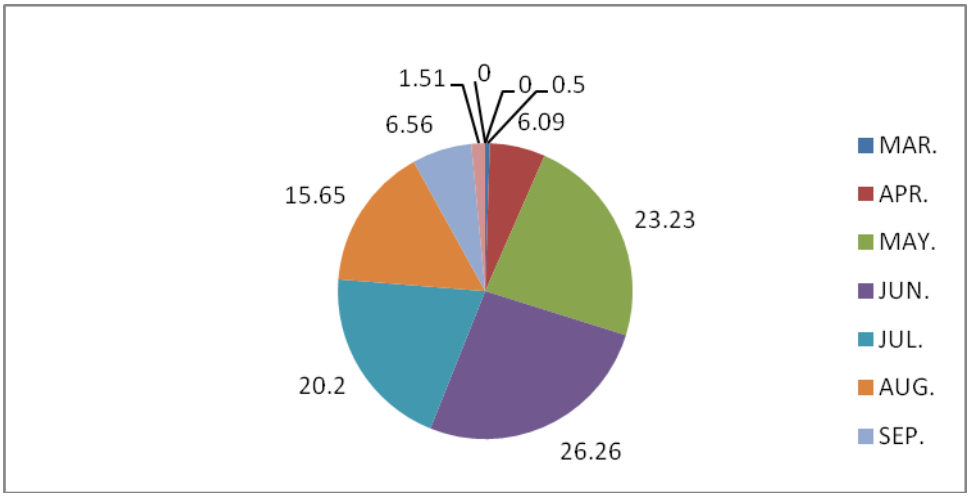

FIG. 5. Percentages of days with TS by months at LRCV

5.2 Data analyses. Statistical data indicate that thunderstorms form in the southern part of Romania mostly between March and October, and only in exceptional cases during December. Thunderstorms have not occurred during January and February within the studied period. The number of days with thunderstorms revealed by the study has increased by 71% for 2010 and 2014. A lower rate of increasing was recorded for 2011, 2012 and 2014.

The monthly peak was recorded in June, but August became a month with a high probability of thunderstorm formation, instead of September as previous studies depicted. The percentages decreasing for September vary between 29% and 89%. July also has become a month with a high number of thunderstorms. The presence of thunderstorms in the southern part of Romania has caused delays and even cancelations of flights, but never incidents/accidents. When thunderstorms have been reported within the southern part Bucharest FIR, the most common method to avoid the associated flight hazards was to divert.

CONCLUSIONS

The study indicates that in the last six years the number of days with thunderstorms has increased by almost 71%, during 2010 and 2014 and with smaller percentages between 10%-33% in 2011, 2012, 2013 and 2015, compared to previous studies. The study revealed that the peak of days number associated with thunderstorm was in 2010 and 2014. The monthly peak was registered in June, but also the fact that August became a month with a high probability of thunderstorm formation. A significant decrease with 28%-89% was also revealed for September.

This trend for TS occurrence is a general one for the central and eastern part of Europe. The growth may be connected with the global changes of climate. The observed trend of temperature and of the greenhouse gases concentrations may be the cause of this perturbation.

The presence of TS influences the flight safety, especially on the final approach causing delays, in some situations the alternate airport being used. During the other phases of flight the aviators use diversion, in order to avoid TS areas and the associated flight hazards. The operational activity was seriously affected during the days with TS, but no incident/accident related with this weather phenomena was registered in the southern part of Romania.

REFERENCES

[1] D. Borsan, *Fizica atmosferei*, Bucuresti, 1981;
[2] E. Aguado and J. E. Burt, *Understanding weather and climate*, USA, pp. 416–418, ISBN 978-0-13-149696-5;
[3] I.C. Enete, U. Ajator and K. C. Nwoko, Impacts of thunderstorm on flight operations in Port-Harcourt International Airport Omagwa, River State, Nigeria, *International Journal of Weather, Climate Change and Conservation Research*, vol. 1, no. 1, pp. 1-10, 2015;
[4]OXFORD AVIATION ACADEMY, *Meteorology*, England, 2009;
[5] ST. M. Stoenescu and D. Tistea, *Clima Romaniei*, Bucuresti, 1962;
[6] http://flightplan.romatsa.ro/init/meteo/opmet
[7] http://www.meteoromania.ro/anm/?lang=ro_ro
[8] http://www.ntsb.gov/_layouts/ntsb.aviation/index.aspx
[9] https://www.wunderground.com/history/

GROUND TEST FACILITY FOR A TURBOSHAFT-TYPE APU TG-16M FOR PASSENGER AIRCRAFT

Alexandru-Nicolae TUDOSIE

University of Craiova, Craiova, Romania (atudosie@elth.ucv.ro)

DOI: 10.19062/2247-3173.2016.18.1.11

Abstract: *This paper describes a ground facility for an APU, TG-16M-type.This kind of APU assisted some Russian (soviet) passenger aircraft during their ground engines' startup and also when the deicing electrical system was switched on. TG-16M turboshaft and generator embedded system together with its control panel and electrical sources are parts of the Aerospace Engineering Laboratories in University of Craiova facilities. One has realized a fuel supplying installation, an electrical supplying and control system, as well as an engine operating parameters' board apparatus panel. Tests results were used for some scientific contributions and papers, but the embedded system is also useful for aerospace students education (both for license and master studies); some specific results may be useful also for PhD studies.*

Keywords: *APU, turboshaft, engine, control, test, fuel, electrical generator.*

1. INTRODUCTION

An APU (which means Auxiliary Power Unit) allows an aircraft to operate autonomously, without reliance on ground support equipment, such as a ground electrical power unit, an engine start cart, or an external air-conditioning unit.

Some APUs are certified for use in flight, so those APUs can be used, as required, to provide an additional electrical power (in the event of the loss of an engine electrical generator); APUs can also be used as sources of electrical power for starter assist for an inflight engine relight, or to power the aircraft deicing (or anti-icing) system.

The auxiliary power unit TG-16M is a turboshaft-type turbo-engine, which spins up a 28 Volts DC electrical generator GSR-2000; this APU was used on soviet passengers airplanes Il-18 and An-24 type, as well as on some of their versions.

Il-18 airplane was a successful long range airliner, as well as a civil or military cargo plane, for several decades (starting with 1957 when it first flew), powered by four Ivchenko AI-20 turboprops engines, 3170 kW each. Airplane's main engines were started using a TG-16M APU, which was fitted in the rear part of the airplane's fuselage, in the tail-cone section, below the tail rudder.

An-24 (built in Soviet Union, then in Ukraine) was also a successful passenger airplane, but a short-medium range one. Its power installation consists of two Ivchenko AI-24 turboprop engines (driving four-bladed constant-speed reversible propellers, developing 1900 kW each), mounted in two nacelles under the wing; the TG-16M auxiliary power unit (APU) turboshaft engine was fitted in the left engine nacelle. Its destination was to assure electrical power during main engine start, as well as in flight deicing system electrical supplying, for some versions (such as An-24T).

The An-24T proved satisfactory in service, but its takeoff performance under "hot & high" (hot weather / high altitude) conditions left something to be desired. In cold weather

conditions, the flight surfaces deicing system, driving by engine bleed air, drew off too much excess power, with the result that it couldn't be used on takeoffs. In addition, the TG-16M APU didn't always provide as much power as needed. However, avoiding these extreme conditions, the above mentioned APU was a successful and safe assistant of the airplane's power system.

A straightforward solution of this issue was a new kind of extra power engine, such as the compact RU-19A-300 turbojet (designed by Tumansky-office). This engine was a combination between a classic APU and a booster engine, with a thrust of 2.16 kN. In spite of a higher overall (which required a redesign of the left engine nacelle, in order to accommodate the new RU-19A-300), this new engine proved all that was hoped for, providing adequate boost power under difficult take-off conditions, plenty of airflow for the deicing system, and plenty of electrical power for ground operation. The new obtained version of An-24 was called An-24RV.

The studied TG-16M-type APU was in service on an An-24T passenger airplane (former in use at Romanian Airliner Company *Romavia*), which belongs now to Aerospace Engineering Laboratories in the University of Craiova.

2. SYSTEM'S PRESENTATION

Ground test lab facility for the above-mentioned APU consists of: a) starting and test control panel; b) electric power lab sources; c) electrical consumers group; d) TG-16M APU (consisting of a turboshaft engine and a 28 V d.c. electric generator).

The studied TG-16M APU is mounted on an iron frame support (cart), as Fig.1 shows and consists of the main engine (turbo-shaft, with centrifugal compressor, inverted combustor, axial turbine, exhaust nozzle, fuel supply system, electrical system), the reduction gear and the electric power 28 Volts d.c. generator (with cool bleed air pipe).

Engine's fuel supply system is feeded from an external fuel tank (15 liter capacity), which is mounted on a flat sheet fixed on the upper engine crankcase and is connected to the engine through the lower fuel pipes common connection, before the isolating valve (see Fig. 1 and schematics in Fig. 4).

APU's cart has a pair of fixed wheels and a pair of adjustable wheels (directed by a beam), in order to facilitate the displacement in the laboratory. During the tests APU's cart is

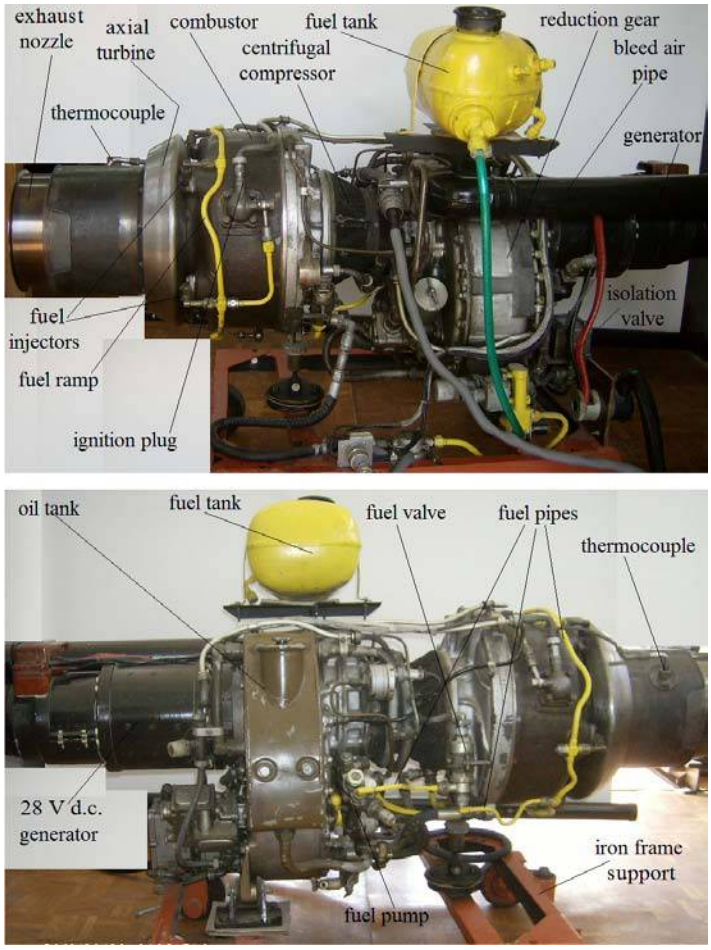

FIG. 1. APU TG-16M type on its ground cart (view from right side and from left side)

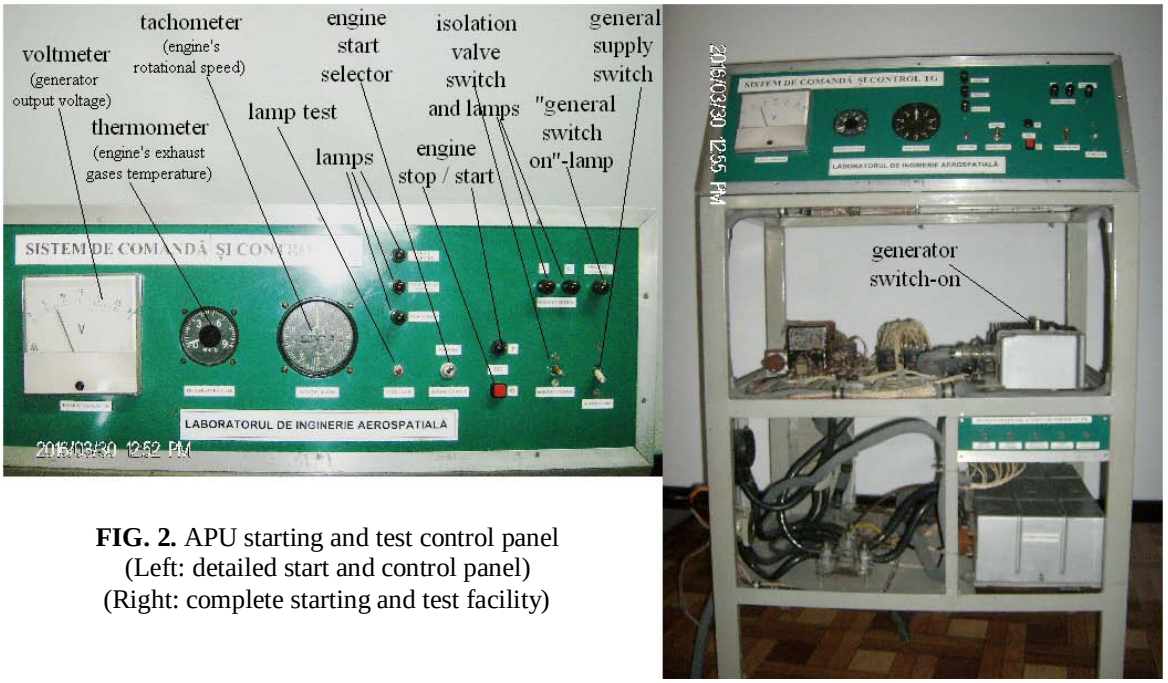

FIG. 2. APU starting and test control panel
(Left: detailed start and control panel)
(Right: complete starting and test facility)

secured by linking it to two short pillars stuck in the ground floor of the test facility.

The group of starting and test facilities is presented in Fig. 2 (detail in the right photo). Starting and test control panel is positioned on top of the facility (Fig. 2, left photo) and consists of three groups of elements: indicators (generator's output voltage, exhaust gases temperature, engine's shaft rotational speed), lamps (pilot lamps, for presence of electrical supply, for switch on/off, for complete start cycle) and buttons/switches (lamp test button, engine start and stop buttons, engine start mode selector). The mode selector for the engine start is a switch, which upper position commands a "hot start" (meaning an effective engine start), while lower position commands a "cold start" (meaning an engine start without flame/ignition, only with engine shaft spinning).

Electrical consumers group is not a specific facility, but it may be formatted occasionally, when the APU test with effective load is necessary. This group may contain resistors, converters or other electrical machines and drives, equipment which could absorb electricity (electrical power) supplied by APU's generator (see Fig. 3.a).

Power sources are standard equipment of the laboratory (see Fig. 3.b); for the APU test there are necessary: a high power 30 V d.c. source (for engine's start), as well as a common lab source (28 V d.c.).

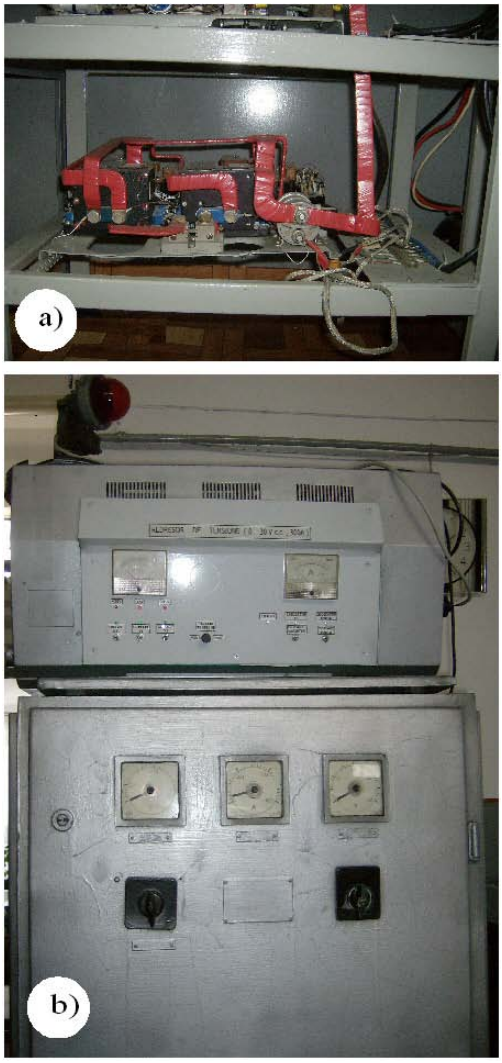

FIG. 3. Lab facilities: a) electric consumers group (resistors, electrical drives and machines); b) electric power sources.

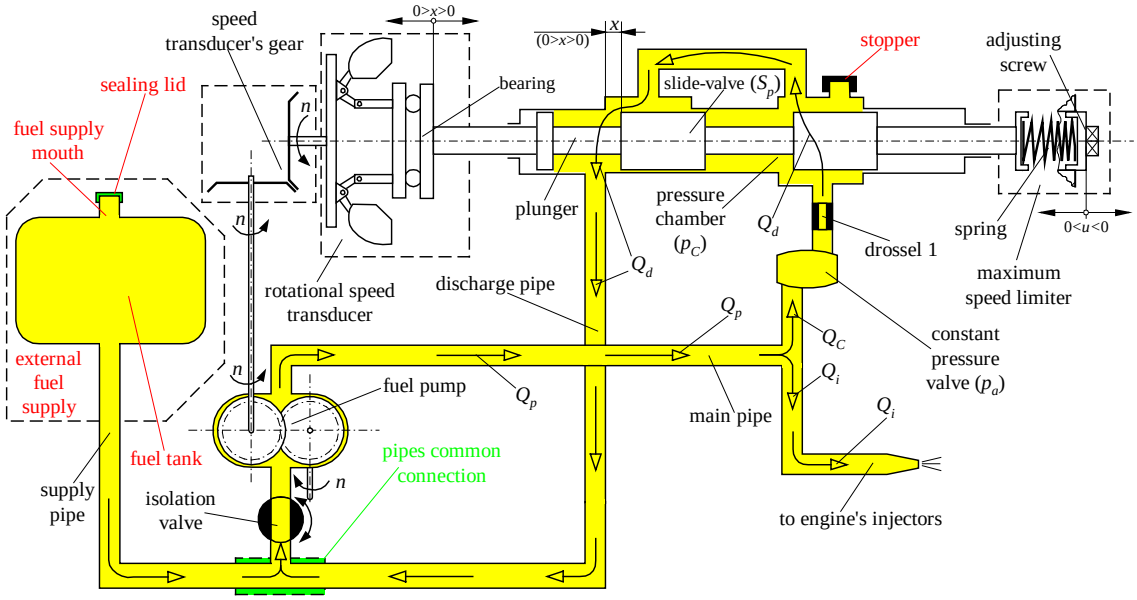

FIG. 4. APU fuel system with external supply

3. APU'S CONTROL SYSTEM WITH EXTERNAL FUEL SUPPLY

Unlike the way the APU is mounted on the airplane, on the ground test facility, because of some constraints, APU's fuel system had to undergo few structural changes.

The external fuel tank of the facility is smaller than any fuel tank of an airplane, it has no air pressuring system and it is refilled through an upper supply mouth, which is sealed with a lid after complete refueling.

Meanwhile, facility's external fuel tank has no booster-pump assistance for the APU's fuel supply, therefore it had to be mounted at a height of at least half meter from fuel pipes common connection level; consequently, fuel supply pressure at the APU's pump inlet is at most (0.04÷0.05) bar, which is too low and it could be lower than that in the secondary discharge pipe (from the second drossel of the transducer's pressure chamber), which would create a counterpressure in the common connection and would induce disturbances into fuel pump's input (supplying) circuit. In order to avoid this situation, the secondary discharge pipe had to be cancelled, so its drossel was sealed by a stopper (see Fig. 1 and Fig. 4, where the new fuel supply schematics is presented).

In fact, secondary discharge pipe and its drossel's role is to assure a small but permanent fluid (fuel) circulation through slide-valve's slots, even when main discharge circuit is closed (when slide-valve closes the main discharge slot); this fuel circulation transforms the basic distributor into a circulation distributor and prevents hydraulic shocks to occure when the slide-valve is repositioned during engine's transient (dynamical) regime.

Consequently, APU's fuel system operates a little different when mounted on the ground test facility, which, obviously, may be reflected by the mathematical model form, as well as by time step response curve(s).

4. APU'S BEHAVIOR ON GROUND TEST FACILITY

4.1. Mathematical model. For the TG-16M APU the mathematical model was determined and studied in [14], based on ground tests, developped on the above-described test facility. Most important consequence of the secondary discharge pipe cancellation is

that the fuel flow rate Q_R (given by eq. (4) in [14]) becomes null, so equation (6) modifies, as follows:

$$Q_C - Q_d = S_p \frac{\mathrm{d}x}{\mathrm{d}t} + \beta_f V_C \frac{\mathrm{d}p_C}{\mathrm{d}t}. \tag{1}$$

Furthermore, k_{RC} – co-efficient becomes also null, which modifies values of k_{xC} and a co-efficients, as follows

$$k'_{xC} = \frac{x_0}{(k_{CC} - k_{dC})p_{C0}}; \tag{2}$$

$$a' = k_{QC} k'_{xC} k_{es}. \tag{3}$$

Obviously, because of the reduced right member expression in Eq. (2) denominator, above described quantities become bigger, so embedded system's time constant $(\tau_m - a'\tau_x)$ is also affected, becoming smaller; meanwhile, the term $1 - k_f k_{pn} + a'$ becomes bigger, but system transfer function keeps its same form in [14]

$$H_n(\mathrm{s}) = -\frac{k_{cg}}{(\tau_m - a'\tau_x)\mathrm{s} + 1 - k_f k_{pn} + a'}. \tag{4}$$

4.2. Stability and quality. Stability conditions remain the same described in [14]; determined transfer function's co-efficients for the discussed embedded system are both positive, so this system is a stable one.

In terms of system's quality, it remains asimptotic stable (studied system being a first order one). Transfer function's co-efficient values changes induce time behavior changes. Because of time constant decreasing, the embedded system becomes faster and its stabilisation time becomes smaller; meanwhile, because of the second term increasing, system static error grows (in absolute value), as curves in Fig. 5 show.

Studies were performed based on embedded system block diagram with transfer functions (Fig. 4 in [14]), where appropriate modifications were realized, using Matlab-Simulink. One has studied system's step input time response for both cases: APU on the ground test facility, respectively APU on the airplane.

Co-efficients were determined for the first case (when the fuel system is connected as shown in Fig. 5) during the ground tests, by measurements and analitical estimations, studying both idle regime and several regimes with different electrical generator's loads (power consumption inputs).

System's behavior as presented in [14] was obtained based on the above determined co-efficients, completed with the estimated k_{RC} – co-efficient; this estimation was based on author's observations

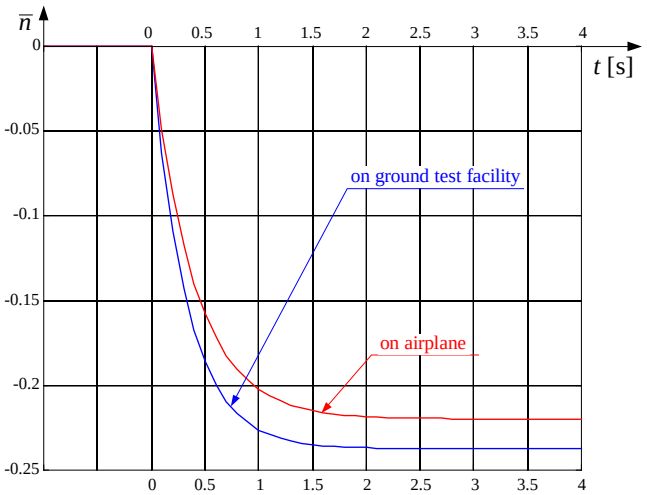

FIG. 5. System's quality: engine's speed step responses for APU's ground test configuration comparing to APU's airplane configuration

and on literature specifications [2, 8, 11, 12], so Eq. (6) in [14] was formally completed and used for system mathematical model, as well as for the described studies.

CONCLUSIONS

The paper has presented a laboratory ground test facility for an APU, TG-16M-type, which has equipped an An-24T passenger airplane. Above mentioned lab test facility consists of : a) APU's frame support; b) starting and test control panel; c) electrical consumers group; d) electric power lab sources.

The involved APU's fuel system has undergone few changes on ground facility comparing to the aircraft fuel supply system, in order to avoid malfunctions due to the lack of an external fuel supply pump to assist the fuel tank.

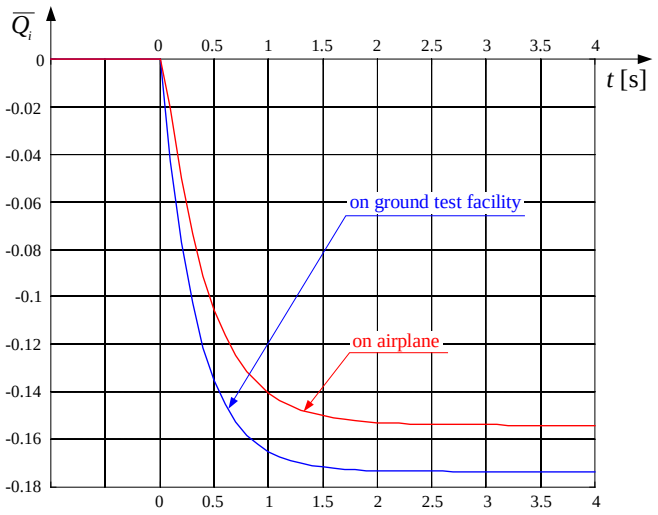

FIG. 6. System's quality: injection fuel flow rate parameter's step response for APU's ground test configuration comparing to APU's airplane configuration

Embedded system (turbo-shaft engine and electric generator) as controlled object was studied in [14], mathematical model's co-efficients being experimentally determined just with the described facility and/or analytically estimated. Embedded system has resulted as a first order system, just as its transfer function proves; consequently, system's stability is asymptotic-type (as shown in figures 5 and 6).

Comparing both embedded system time behaviors from the engine's speed, as well as from the injection fuel flow rate points of view, one has observed some differences. On ground test facility the embedded system is more rapid, its time response being around (1.8÷2.3) s, comparing to (2.2÷2.8) s onboard of the airplane. Meanwhile, static error has grown on ground test facility: as Fig. 4 shows, speed non-dimensional parameter has a higher static error by 10%, while injection fuel flow rate parameter (see Fig. 6) has a higher static error by 12%.

However, APU behavioral differences are small and doesn't matter in terms of teaching (from didactical point of view), nor in the experimental studies of engine's equipment and its electrical system.

Although the ground test facility was designed specifically for a TG-16M-type APU, some parts of starting and test control panel, as well as electric power lab sources and electrical consumers group can be used for other APUs or turbo-engines tests.

Lab test ground facility, as well as the embedded system engine+generator is useful for didactical demonstrations and training, as well as for scientific researches of master and PhD students.

REFERENCES

[1] Abraham, R. H. *Complex dynamical systems*, Aerial Press, Santa Cruz, California ,1986;
[2] Dinca, L. *On-board Hydro-pneumatic Equipment and Systems*, Universitaria Publisher, Craiova, 2008;
[3] Gorinevsky, D., Dittmar, K., Milaraswamy, D., Nwadiogbu, E., Model-based Diagnostics for an Aircraft Auxiliary Power Unit, *IEEE Conference on Control Applications, Glasgow, Scotland, 18-20 September, 2002*;
[4] Ispas, St., *Turbojet engine*. Tehnica Publisher, Bucuresti, 1984;
[5] Lungu, R., Tudosie, A., Dinca, L. *Fluid Mechanics and Technical Thermodynamics*. SITECH Publisher, Craiova, 2004;
[6] Lungu, R. *Flight Apparatus Automation*. "Universitaria" Publisher, Craiova, 2000;
[7] Mattingly, J. D. *Elements of Gas Turbine Propulsion.* McGraw-Hill, New York, 1996;
[8] Mattingly, J. D., Heiser, W. H., Pratt, D. T. *Aircraft Engine Design*. AIAA Education Series, Reston (VA), 2002;
[9] Rotaru, C., Andres-Mihăilă, M., Matei, P.G. An Extended Combustion Model for the Aircraft Turboet Engine, *International Journal of Turbo & Jet Engines*, Volume 31, Issue 3, Pp. 229-237, ISSN 0334-0082, DOI 10.1515/tjj-2013-0048, 2014.
[10] Rotaru, C., Sprinţu, I. State Variable Modeling of the Integrated Engine and Aircraft Dynamics, *10th International Conference on Mathematical Problems in Engineering, Aerospace and Sciences* (ICNPAA 2014), Volume 1637, pp. 889-898, DOI 10.1063/1.4904661, 2014.
[11] Rotaru, C., Arghiropol, A., Barbu, C., Boşcoianu, M. Some Aspects Regarding Possible Improvements in the Performances of the Aircraft Engines, *Proceedings of the 6th IASME/WSEAS International Conference on Fluid Dynamics and Aerodynamics*, ISBN 978-960-6766-98-5, pages 196-201, Greece, 2008;
[12] Tudosie, A. N. *Aerospace Propulsion Systems Automation*. University of Craiova Inprint, Craiova, 2005;
[13] Tudosie, A. N. *Aircraft Gas-Turbine Engine's Control Based on the Fuel Injection Control* in Aeronautics and Astronautics, Max Mulder (Ed), INTECH, Rijeka, Croatia, 2011.
[14] Tudosie, A. N. *Turboshaft-type APU For Aircraft As Controlled Object*. Unpublished, 2016.
[15] ****** *TG-16M -Technical description and overhaul manual*.

AIR FORCE AND AEROSPACE ENGINEERING

TURBOSHAFT-TYPE APU FOR AIRCRAFT AS CONTROLLED OBJECT

Alexandru-Nicolae TUDOSIE

University of Craiova, Craiova, Romania (atudosie@elth.ucv.ro)

DOI: 10.19062/2247-3173.2016.18.1.12

Abstract: *This paper describes a case study of an aircraft auxiliary power unit (APU) considered as controlled object. Considering the specific case of a TG-16M power unit (which is an embedded system: a gas turbine turboshaft and an electrical 28 V DC generator), one has established the mathematical model of this system, based on its non-linear motion equations; operating with the finite difference method, one has obtained the linear and adimensional form of the mathematical model. Equations' co-efficient were experimentally established and/or calculated, during the ground lab tests of a TG-16M at the Aerospace Engineering Laboratory, University of Craiova. Based on the system's mathematical model, one has also performed some studies concerning its stability and quality, using Matlab® Simulink simulations.*

Keywords: *APU, gas turbine, fuel, rotational speed, control, electrical power, generator.*

1. INTRODUCTION

An auxiliary power unit (APU) is a small gas turbine engine that provides electrical power and/or compressed air to aircraft consumers, which enables them to operate autonomously, without reliance on specific ground support equipment (such as an electrical power unit/battery/generator, an external air-conditioning unit, or a high pressure air unit/battery).

This "supplementary" power is used to start the main propulsion engines, to provide pressurized air for aircraft environmental control systems, to provide electrical power for aircraft lighting, avionics and on-board galleys on the ground and, additionally, to provide backup and emergency power in flight [3]. APUs can provide power for almost all functions of the airplane while it is on the ground, except propulsion.

The main and most important purpose of the APU is to provide the power to start the aircraft main engine(s). An aircraft's gas turbine engine needs to be accelerated to rotate at an extremely high speed for it to provide an adequate amount of air compression to keep it spinning.

Depending on its destination and design, the APU can provide electric power, hydraulic power, pneumatic power or all three of them. Connecting APU to a hydraulic pump, it allows the crew to operate hydraulic equipment (such as the flight controls, aerodynamic brakes or flaps). Having one of these functions, such an APU is also useful for a backup, if there is an engine failure. APUs are critical to aircraft safety, as they supply backup electricity, as well as the compressed air, in place of a failed main engine generator, or of a dead engine.

Small airplanes do not need an APU, as those engines are started using an electric motor (electric starter), supplied by batteries. Meanwhile, big aircrafts are started by an air turbine motor or powerful electric starters and thus the need for the APU to power

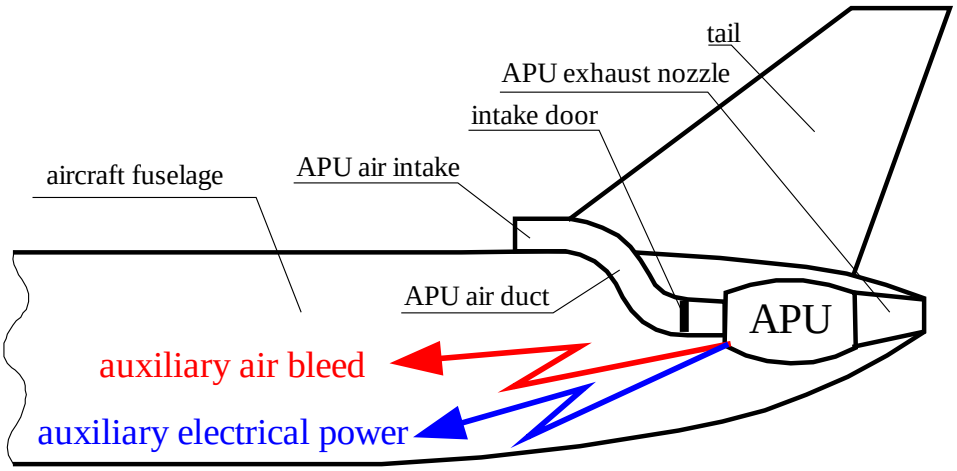

FIG. 1. APU's positioning on aircraft

them. Before the engine gets turned, one needs to start the APU (usually by battery or a hydraulic accumulator).

APU's are often positioned in the tails of aircraft (rear fuselage, as Fig. 1 shows), in the rear of one of engines' nacelles, or in the landing gear bay, ranging from larger turboprops to jets. On most jets, the APU is installed in the far aft tail-cone section, so as to isolate it as much as possible from other systems in the event of an APU fire. Like the aircraft's main engines, an APU must be installed behind a firewall. It also needs its own fire detection and extinguishing system.

The APU can be started utilizing only the aircraft battery(s) (accumulators) and, once running, it will provide to aircraft systems electrical power, hydraulic pressure, as well as bleed air for air conditioning (and/or for main engine(s) start, depending on its (their) starting solutions).

Because the APU is often operated on the ground, dual fire-control panels are sometimes installed, one in the cockpit and one accessible from the aircraft's exterior. This allows an APU fire to be fought from either location. Since an APU is usually not closely monitored by the crew once it is started, most are designed to shut down automatically in case of a fire or loss of oil pressure [3].

Some APUs are only for ground use (engine start, air conditioning), but if certified for use in flight, the APU can be used, as required, to provide an additional source of electrical power in the event of the loss of an engine generator. It can also be used as a source of bleed air for supplementary air conditioning, as well as for starter assist for an in-flight engine relight, or to power the air-conditioning packs if the event conditions or company policy dictate that the takeoff should be conducted with the main engine bleed air turned off. The APU is normally left off in flight, but it may be turned on for certain long-haul flights, or for overwater (transoceanic) flights, as an extra precaution.

2. SYSTEM'S PRESENTATION

The studied TG-16M APU is turboshaft-type, similar to a turboprop engine (obviously, without propeller), which spins up a dedicated 28 V DC electrical generator via a planetary gear. It operates as auxiliary electrical power source for an airplane (such as An-24T short-haul passenger airplane, or the old Il-18 medium-haul passenger airplane); it is positioned in the rear of starboard AI-24 engine's nacelle.

As Fig.2 shows, APU is broken up into three main sections – the power section, the gearbox and the electrical generator. The power section consists of the gas generator

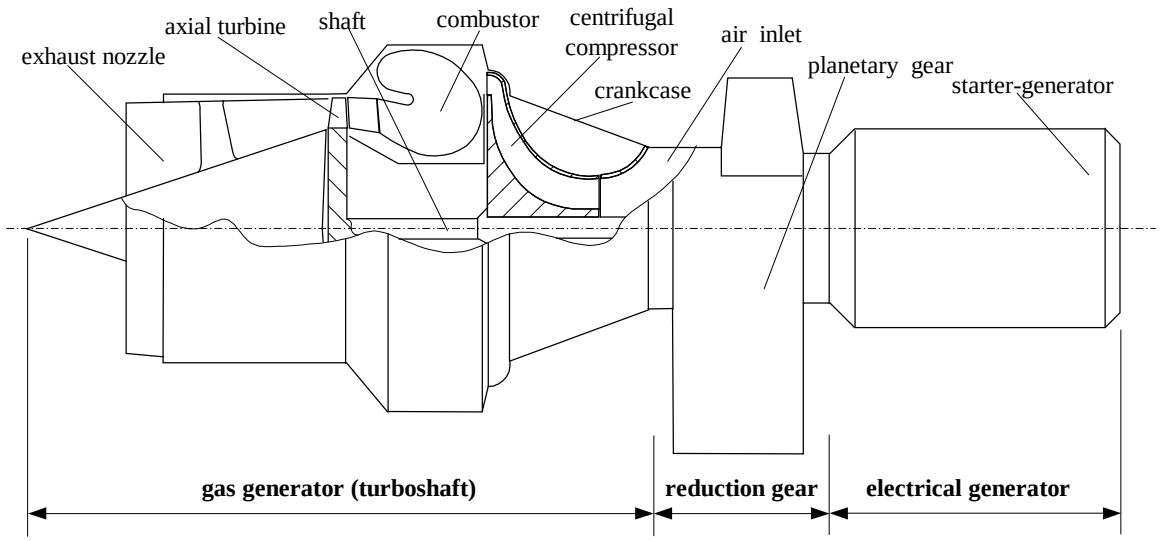

FIG. 2. APU's main parts

portion of the engine and produces all the power for the entire APU (engine's compressor, reduction gear and electrical generator).

APU's main shaft is driven by a single stage axial turbine (which is the gas generator turbine); it spins up the engine's centrifugal compressor, as well as the electrical generator via the planetary reduction gear. The gas generator has a compact inverted flow combustor, where the injected fuel is mixed with the compressed air (delivered by the compressor) and burned into hot gases, which are expanded in the engine's turbine, then discharged through the exhaust nozzle.

So, turbine's mechanical work should cover the necessary work of the compressor, of the gear, as well as of the electrical generator.

3. NON-LINEAR MOTION EQUATIONS

Non-linear mathematical model consists of APU-system main parts' non-linear equations; relevant main parts are: APU's main shaft, rotational speed transducer, fuel pump and fuel control system. Figure 3 contains fuel system's technical schematic.

3.1. Shaft equation. Shaft motion equation involves turbine (M_T), compressor (M_C), gear (M_g), friction (M_{fr}) and electrical generator (M_{EG}) torques, as follows:

$$M_T - M_C - M_g - M_{fr} - M_{EG} = \frac{\pi J}{30}\frac{\mathrm{d}n}{\mathrm{d}t}, \tag{1}$$

where J is spool's axial moment of inertia and n – shaft rotational speed.

Assuming that M_g and M_{fr} torques are nearly constant and low values, they may be neglected for further studies. Meanwhile, one can affirm that turbine torque (M_T active torque) depends on the injection fuel flow rate Q_i and on the shaft speed *n*; compressor torque M_C depends only on the shaft speed [11, 12], while generator torque M_{EG} depends both on the shaft speed and on the load current amperage I_{cg} (M_C and M_{EG} being resistant torques).

3.2. Fuel control system equations. As fig. 3 shows, injection fuel flow rate Q_i (which supplies engine's combustor) is established as the difference between pump's

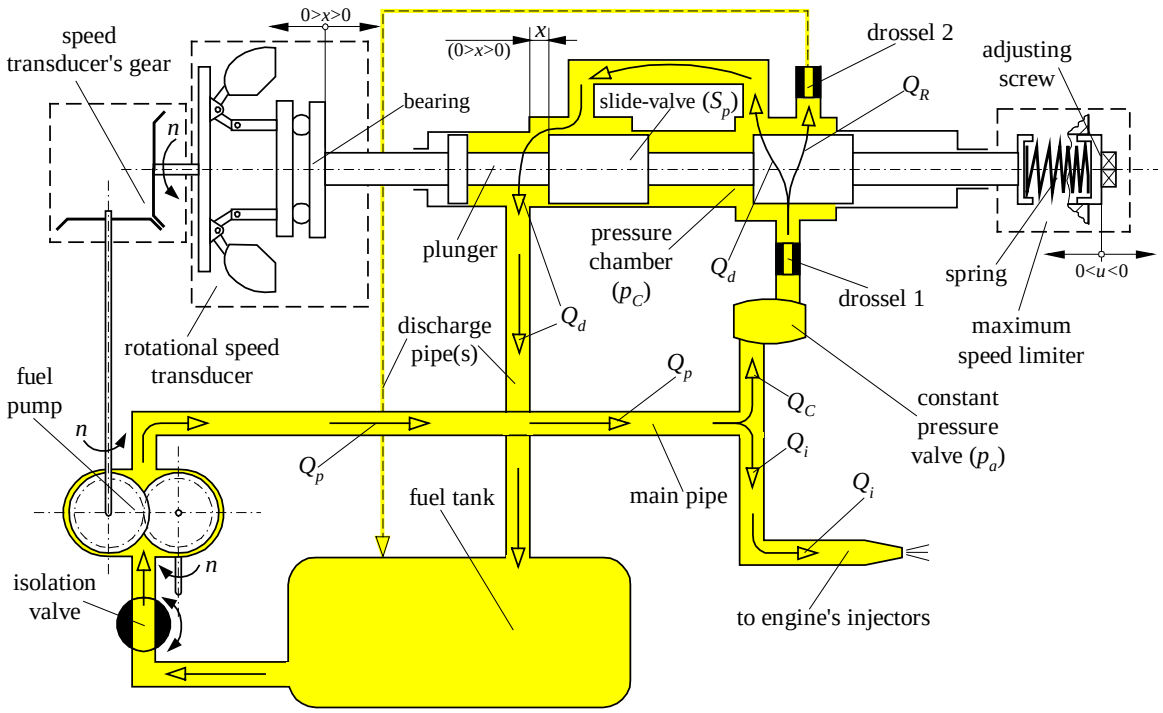

FIG. 3. APU's fuel system

flow rate Q_p and control flow rate Q_C (which is recirculated and sent to the fuel tank). In the pressure chamber the control flow rate is split into two streams: Q_R – through the second drossel and Q_d – through the variable slot of plunger's slide valve and further through the discharge pipe back into the fuel tank. So, discharged flow rate Q_d depends on the plunger's displacement *x*, which results from engine's effective speed *n* and from preset speed value n_p (given by the adjusting screw's displacement *u*).

Motion equation for the fuel system are, as follows:

$$Q_i = Q_p - Q_C, \tag{2}$$

$$Q_C = \mu_d \frac{\pi d_1^2}{4} \sqrt{\frac{2}{\rho}} \sqrt{p_a - p_C}, \tag{3}$$

$$Q_R = \mu_d \frac{\pi d_2^2}{4} \sqrt{\frac{2}{\rho}} \sqrt{p_C - p_{dc}}, \tag{4}$$

$$Q_d = \mu b x \sqrt{\frac{2}{\rho}} \sqrt{p_C - p_{dc}}, \tag{5}$$

$$Q_C - Q_R - Q_d = S_p \frac{\mathrm{d}x}{\mathrm{d}t} + \beta_f V_C \frac{\mathrm{d}p_C}{\mathrm{d}t}, \tag{6}$$

where p_a is the fuel supplying pressure (assumed as constant, because of the constant pressure valve on the main pipe), p_C – command pressure, p_{dc} – discharging pipes fuel

pressure (very low value, comparing to p_a and p_C, so negligible), μ,μ_d – flow co-efficients, d_1,d_2 – drossel's diameters, S_p – piston (slide-valve) surface area, ρ – fuel density, β_f – fuel compressibility co-efficient (practically null, so negligible, as the terms involving it), V_C – pressure chamber's volume, b – slide-valve's discharge slot width.

For further studies the above-presented equations should be simplified, by linearisation and adimensionalization. Meanwhile, one has to consider for the mathematical model the fuel pump's equation, as well as the speed transducer equation.

4. SYSTEM'S MATHEMATICAL MODEL

4.1. Linearised motion equations. Non–linear equations can be brought to a linear form, using the finite difference method, assuming the small perturbation hypothesis; formally, any variable or parameter X should be considered as $X = X_0 + \Delta X$, where X_0 is parameter's steady state regime's value, ΔX – parameter's deviation and $\overline{X} = \dfrac{\Delta X}{X_0}$ the non-dimensional deviation. Consequently, the above-presented equations become

$$\left(\frac{\partial M_T}{\partial n}\right)_0 \Delta n + \left(\frac{\partial M_T}{\partial Q_i}\right)_0 \Delta Q_i - \left(\frac{\partial M_C}{\partial n}\right)_0 \Delta n - \left(\frac{\partial M_{EG}}{\partial n}\right)_0 \Delta n - \left(\frac{\partial M_{EG}}{\partial I_{cg}}\right)_0 \Delta I_{cg} = \frac{\pi J}{30}\frac{\mathrm{d}}{\mathrm{d}t}\Delta n, \tag{7}$$

$$\Delta Q_i = \Delta Q_p - \Delta Q_C, \tag{8}$$

$$\Delta Q_C = -\mu_d \frac{\pi d_1^2}{4}\sqrt{\frac{1}{2\rho(p_a - p_{C0})}}\Delta p_C = -k_{CC}\Delta p_C, \tag{9}$$

$$\Delta Q_R = \mu_d \frac{\pi d_2^2}{4}\sqrt{\frac{1}{2\rho p_{C0}}}\Delta p_C = k_{RC}\Delta p_C, \tag{10}$$

$$\Delta Q_d = \mu b\sqrt{\frac{2p_{C0}}{\rho}}\Delta x + \mu b x_0\sqrt{\frac{1}{2\rho p_{C0}}}\Delta p_C = k_{dx}\Delta x + k_{dC}\Delta p_C, \tag{11}$$

$$\Delta Q_C - \Delta Q_R - \Delta Q_d = S_p\frac{\mathrm{d}}{\mathrm{d}t}\Delta x. \tag{12}$$

4.2. Non-dimensional linear equations. Using some appropriate chosen amplifying terms, the above-presented linearised equations can be transformed in non-dimensional forms; after applying the Laplace transformation, one obtains the system's linear non-dimensional mathematical model, as follows:

$$(\tau_m \mathrm{s} + 1)\overline{n} = k_f\overline{Q_i} - k_{cg}\overline{I}_{cg}, \tag{13}$$

where $k_{mR} = \left(\dfrac{\partial M_C}{\partial n}\right)_0 + \left(\dfrac{\partial M_{EG}}{\partial n}\right)_0 - \left(\dfrac{\partial M_T}{\partial n}\right)_0$, $\tau_m = \dfrac{\pi J}{30k_{mR}}$, $k_f = \dfrac{1}{k_{mR}}\dfrac{Q_{i0}}{n_0}\left(\dfrac{\partial M_T}{\partial Q_i}\right)_0$ and

$$k_{cg} = \frac{1}{k_{mR}} \frac{Q_{i0}}{I_{cg0}} \left(\frac{\partial M_{EG}}{\partial I_{cg}} \right)_0 ;$$

$$\overline{Q}_i = \overline{Q}_p - \overline{Q}_C , \tag{14}$$

$$\overline{Q}_C = -k_{QC} \overline{p}_C , \tag{15}$$

$$(\tau_x \mathrm{s} + 1)\overline{x} = \frac{1}{k_{xC}} \overline{p}_C , \tag{16}$$

where $k_{QC} = k_{CC} \frac{Q_{C0}}{p_{C0}}$, $k_{xC} = \frac{x_0}{(k_{CC} - k_{RC} - k_{dC}) p_{C0}}$, $\tau_x = \frac{S_p}{k_{dx}}$.

Together with Eq. (13), (14) and (15), in order to build the mathematical model, one has to consider also fuel pump's equation (16), as well as transducer's equation (17) (together with their own annotations, given by [12]):

$$\overline{Q}_p = k_{pn} \overline{n} , \tag{17}$$

$$\overline{x} = k_{es} \overline{n} - k_u \overline{u} . \tag{18}$$

Some observations should be made, concerning the above presented equations. Terms containing p_{dc} and β_f in Eq (4), (5) and (6) can be neglected. Meanwhile, the term containing $\overline{u}$ can be excluded, because adjustments concerning maximum engine speed value are made during ground tests.

System's block diagram with transfer functions, built using Eq. (13)…(18), is depicted in Fig. 4.

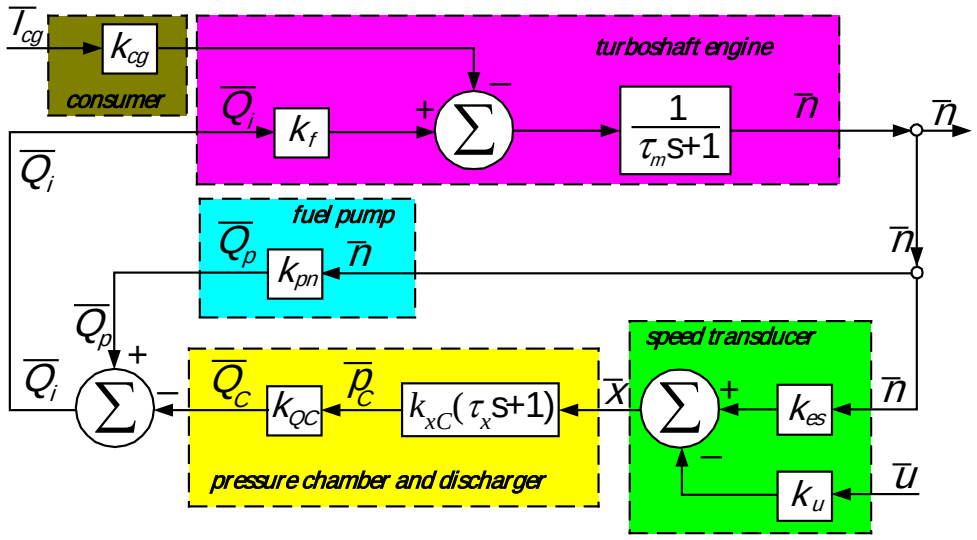

FIG. 4. System's block diagram with transfer functions

4.3. System's transfer function. The above-mentioned equations may be transformed into a much simpler single equation, which expresses the dependence $\bar{n} = f\left(\bar{I}_{cg}\right)$ and represents system's transfer function:

$$\left[\left(\tau_m - a\tau_x\right)\mathrm{s} + 1 - k_f k_{pn} + a\right]\cdot \bar{n} = -k_{cg}\bar{I}_{cg}, \tag{19}$$

equivalent to

$$\bar{n} = -\frac{k_{cg}}{\left(\tau_m - a\tau_x\right)\mathrm{s} + 1 - k_f k_{pn} + a}\bar{I}_{cg}, \tag{20}$$

where $a = k_{QC}k_{xC}k_{es}$, so the transfer function expression is

$$H_n(\mathrm{s}) = -\frac{k_{cg}}{\left(\tau_m - a\tau_x\right)\mathrm{s} + 1 - k_f k_{pn} + a}. \tag{21}$$

5. SYSTEM'S STABILITY AND QUALITY

System's transfer function is a first order one; for system's stability it is compulsory that its characteristic polynomial co-efficients have the same sign. Consequently, system's stability condition should be

$$\left(\tau_m - a\tau_x\right)\left(1 - k_f k_{pn} + a\right) > 0. \tag{22}$$

The term a is strictly positive (because of its definition formula(s)); meanwhile, from [11] and [12] it results that, in order to obtain a stabile engine-fuel pump connection, the term $1 - k_f k_{pn}$ must be strictly positive. Consequently, from Eq. (22) only the first term remains to be discussed, so $\tau_m - a\tau_x > 0$, which gives (considering formulas for a and τ_m)

$$S_p < \frac{k_{dx}}{k_{QC}k_{xC}k_{es}}\tau_m. \tag{23}$$

If $1 - k_f k_{pn} < 0$, the engine-fuel pump connection is unstable, which means that a supplementary condition is required, in order to keep the same condition (23). Consequently, for $1 - k_f k_{pn} + a > 0$, the supplementary condition is

$$a > \left|1 - k_f k_{pn}\right|, \tag{24}$$

otherwise the term $\tau_m - a\tau_x$ should become negative, and the (23)-condition becomes

$$S_p > \frac{k_{dx}}{k_{QC}k_{xC}k_{es}}\tau_m. \tag{25}$$

System's quality was studied for two situations: a) idling engine (without generator's load) b) step input of the electrical load $\bar{I}_{cg}$; results (step responses) are presented in Fig. 5 and were calculated using a Matlab-Simulink simulation, based on system's block diagram with transfer functions (in Fig. 4). System's co-efficients were experimentally and analytically determined, using a ground test facility for an APU (TG-16M type).

CONCLUSIONS

The paper has studied an APU as controlled object. The APU consists of a single shaft turbo-engine which spins up an electrical generator through a planetary gear. From its non-linear motion equations one has determined the linear non-dimensional mathematical model, as well as its transfer function.

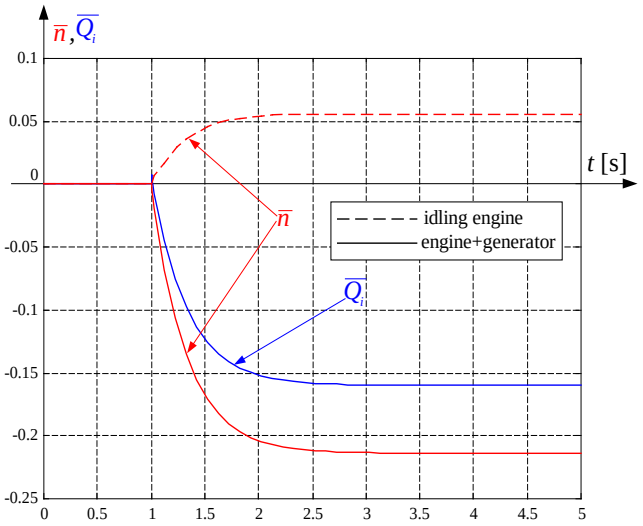

FIG. 5. System's quality (time step response)

The above studied system is a first order one, its transfer function having a first-degree characteristic polynomial, which has simplified its stability studies. One has obtained a condition for the stability, which gives an information about how to choose the plunger's slide valve frontal surface area S_p with respect to the gas turbine engine time constant τ_m and to the gas turbine engine's fuel system geometry (effective diameters), as well as to flow rate co-efficients values.

System's quality studies shows that both the idling engine and the embedded system engine+generator have stabile aperiodic behavior, as seen in Fig. 5. The system is affected of static errors (positive for idling engine, negative otherwise), especially when the generator supplies external consumers, the bigger the consumers' electrical power are.

This study was realized only for ground test operation, but it may be extended to other APUs, as well as for some different flight regimes.

REFERENCES

[1] Abraham, R. H. *Complex dynamical systems*, Aerial Press, Santa Cruz, California ,1986;
[2] Dinca, L. *On-board Hydro-pneumatic Equipment and Systems*, Universitaria Publisher, Craiova, 2008;
[3] Gorinevsky, D., Dittmar, K., Milaraswamy, D., Nwadiogbu, E., Model-based Diagnostics for an Aircraft Auxiliary Power Unit, *IEEE Conference on Control Applications, Glasgow, Scotland, 18-20 September, 2002*;
[4] Ispas, St., *Turbojet engine*. Tehnica Publisher, Bucuresti, 1984;
[5] Lungu, R., Tudosie, A., Dinca, L. *Fluid Mechanics and Technical Thermodynamics*. SITECH Publisher, Craiova, 2004;
[6] Lungu, R. *Flight Apparatus Automation*. "Universitaria" Publisher, Craiova, 2000;
[7] Mattingly, J. D. *Elements of Gas Turbine Propulsion*. McGraw-Hill, New York, 1996;
[8] Mattingly, J. D., Heiser, W. H., Pratt, D. T. *Aircraft Engine Design*. AIAA Education Series, Reston (VA), 2002;
[9] Rotaru, C., Andres-Mihăilă, M., Matei, P.G. An Extended Combustion Model for the Aircraft Turbojet Engine, *International Journal of Turbo & Jet Engines*, Volume 31, Issue 3, Pp. 229-237, ISSN 0334-0082, DOI 10.1515/tjj-2013-0048, 2014.
[10] Rotaru, C., Sprinţu, I. State Variable Modeling of the Integrated Engine and Aircraft Dymanics, *10th International Conference on Mathematical Problems in Engineering, Aerospace and Sciences* (ICNPAA 2014), Volume 1637, pp. 889-898, DOI 10.1063/1.4904661, 2014.
[11] Rotaru, C., Arghiropol, A., Barbu, C., Boşcoianu, M. Some Aspects Regarding Possible Improvements in the Performances of the Aircraft Engines, *Proc. of the 6th IASME/WSEAS International Conference on Fluid Dynamics and Aerodynamics*, ISBN 978-960-6766-98-5, pp. 196-201, Greece, 2008;
[12] Tudosie, A. N. *Aerospace Propulsion Systems Automation*. Univ. of Craiova Inprint, Craiova, 2005;
[13] Tudosie, A. N. *Aircraft Gas-Turbine Engine's Control Based on the Fuel Injection Control* in Aeronautics and Astronautics, Max Mulder (Ed), INTECH, Rijeka, Croatia, 2011.

MOTIVATION AND LEADERSHIP- SPECIFIC AREAS OF THE MILITARY ORGANIZATION IN THE SPIRIT OF ORGANIZATIONAL CULTURE

Mihai VIȚALARIU, Ovidiu MOȘOIU

"Henri Coandă" Air Force Academy, Braşov, Romania

DOI: 10.19062/2247-3173.2016.18.1.13

Abstract: *The military organization-integral part of society, includes a complex ensemble of material and spiritual virtues, rules of conduct and cultural models, attitudes and skills created and adopted by its members over time. The exposing to the military environment requirements has different effects according to the person's socialization level, to the cognitively and rational abilities and also, to the adherence at the norms and virtues system.*

Changing society generally involve socio-professional military values that change towards the effective functioning of the military organization. The reconfiguration of the military organization's values system in agreement with the civilian society ones overlaps with the maintaining of specific professional values, to the professional soldiers. In peacetime and in war, defending and respecting the values submitted by military culture represents the best sign of the professional performance of professional military.

Keywords*: culture, organizational culture, military organizational culture, military organization, motivation, leader, military leader, spiritual leader, leadership.*

1. INTRODUCTION

In the most accepted sense, culture includes all acquisitions that the company has made over time in science, art, education, humanity in general. Also culture is a vector of human development and evolution of individual training as a member of society, creation and strengthening of his personality.

Often used in all the social life domains, the culture term played its role in the organizational psyhosociology by being a form of organizational culture. As a recognition and stability element of a specific organization, it defines an ensemble of spiritual and material virtues, rules of conduct and cultural models, skills and attitudes specific to an organization formed, adapted and internalized by all its members over time.

As an organization with tradition which followed the society over time, the military constitution has also an organizational culture which distinguish it between the others governmental organizations.

2. THE MILITARY ORGANIZATIONAL CULTURE REPORTED TO THE NATIONAL ORGANIZATIONAL CULTURE

Generating, maintaining, recording and transmission of values that define the future of the military, is a very important aspect of the organizational culture of the military organization. Those values "*can be found in terms of discipline, authority, loyalty and respect, hierarchy, collaboration and cooperation, sense of duty, the subordination of*

individual interests to those of the group responsibility, mind body and spirit of sacrifice" [1]

The military professional culture is the one that adds to the qualities and abilities of the modern professional soldier, by time, all these values which are indispensable qualities and that he can assume by only intense intellectual effort, through experience, special training and high specialization. Knowing those allows all who want to choose the military career *"to argue their actions according to understanding their role in the organization, of the need of assuming the norms and values, and the requirements imposed by the member position in the organization or military leader, too"*. [2]

Acquiring the values promoted by the organizational culture is essential to the developing and evolution of the professional military. The soldier's motivation to choose the military career and achieving performance over it represents one of the aspects which is decisively influenced by the cultural values of the organization.

Practising the military profession is realized only by the ones who acquire the required abilities and are able to pass the specialization and competence criteria requested by the military constitution. Choosing this profession is a vocation problem, being wanted and assumed by the person in his deepest thoughts.

The most efficient motivational factors are the inherited ones, which come from the inner experiences of the person, from self-assessment about his work and from his beliefs about the signification and importance of his work. Service performed in the public interest, the specific of the military organization which imposes significant restrictions to its members, requires from the soldiers a directed orientation to the inner motivator factors trying to counterbalance the low level of the extrinsically ones.

In these circumstances we consider that the reasoning professional military status is achieved by the ascension of his hierarchical, camaraderie and spirit of the body, respect for truth, loyalty and honour, morals and ethics.

The internalization of the military values for the soldier is basic in his motivation process for the professional performance. Reporting to the person's military environment represents an active and complex process in which the values and military norms inter-combine, on one side, and the individual attitudes, on the other side. This exposure to the military environment requests can have different effects according to his rational and cognitively abilities, to its socialization level and to adherence to the virtues and norms system.

Bulding a military carachter, a skill-based fighter, a leader, a specialist, educator and citizen occurs by following training programs in military educational institutions and through socialization performed by exposure to organizational culture. Similarly produce intrinsic motivation and necessary purchases for professional military performance by assuming responsibly and actively to high spiritual and moral values of the individual sought to defend the professional execution of their choice, even these values. When the beliefs and values are internalized and assumed, they crystallize into the mind and became the hard material of the professional intrinsic motivation. The motivational factors operate continuously and give deep efficiency and performance , but also quality and consistence to the professional soldier actions.

The social and economic influences can have an unfavourable perception according to the purpose and sense of the military institution, perception which can determine a reduced effort from the state regarding rewarding the military work. Often this reward materialized in paying the principal extrinsic motivator of work, and it does not compensate properly the conditionings and privations of military service. This thing undermines dignity and creates dissatisfactions inside the military organization, finally acting like a negative motivator

factor on people. The issues outlined above necessarily require professional military orientation to a predominantly intrinsic motivation.

With its action on the soldier, the organizational culture contributes to the fixation in the conscience of it, of the specific virtues of the institution and to enrich the personality with these ones, transforming them in motivations to performance and work, apart from the presented by the medical insurance, equipment, wage etc., becoming extrinsically motivation factors.

Nowadays, the military organization goes through a continuous process of adaptation to the realities of modern society, by acceding to the new values that characterizes a dynamic military structure. Professional norms and values of the military requires adapting to changes as a result of the transformation of the military and society in general. In the direction of functional efficiency of the military organization in line with the overall change of the society, changes socio-professional military values. This reconfiguration of the values system specific to the military organization, in agreement with the civil society ones, overlaps with the maintenance of specific professional military values.

Whereas the military culture is a part of the national culture and express the features of the society where it belongs, the military values are not in conflict with the civilian ones. The intrinsic motivations took people in provocative situations, internalize values and justify their social and moral implication, especially when they are confirmed by reactions from the reference group.

3. THE MILITARY ORGANIZATION LEADER- LANDMARK OF THE PROFESSIONAL PERFORMANCE

Understanding and fixing the new values is a process which the military leaders are responsible for. In their role as educator and trainer, leaders must bring the professional values in front of the subordinates, define and transmit values by common education and training as part of their socialization process.

Some factors which military leaders by their own and their subordinates must develop in order to motivate themselves to reach high performances, professional and social standards are high abilities, self-consciousness, collective thinking, body spirit, the need and ability of personal development, energy and connection to the primary values.

The military must not pursue only his personal interests, he is subordinated to the group interests, to the major interests than his group's, of the military organization and society as a whole. The professional military subordinates his personal interests and needs to the national ones, of the state and country, which he serves by vocation, by deep and conscious understanding of the highest moral and moral values of humanity. The professional military's motivation consists in his vocation to protect the others, in its ability to sacrifice for the common good.

The Commander "shall encompass the virtues of justice, humanity, wisdom, courage and austerity", as Sun Tzu (The Art of War) [3].

Time trends in management approach, namely leadership, based on man and his needs on his particular importance in organizational economy, promoting new valences of the leader, starting from the most important and necessary quality, the intelligence. "*The specialists keep under atention four types of intelligence that marked guidelines in this field overtime.* [4].

First of all, we talk about physical intelligence or competence of "to do" (PQ), the physical ability to do things, to achieve the objective of bringing out various tasks or assignments. Secondly we refer to intelligence or intellectual power to think and learn (IQ).

This type of intelligence allows the preparation of associations/ dissociations, analyzes, planning, development of strategies or solving situations.

The emotional intelligence (EQ) or communication skill, is the third type of intelligence, studied a lot nowadays by different people who want to show its importance. Actually, we must say in few details that through this intelligence type, the crossing from the traditional management to leadership is made.

The fourth form of intelligence, the spiritual one (SQ), represents the newest guidance and the ability of giving (the power of giving). Steinhard father, eminent philosopher, essayist and romanian linguist, said that *"you will gain by givin"*. In this way the message is sent through spiritual intelligence. *"Through this, the feed-back is complete and mutual and represents the leader's reply to the effort of the ones coordinated by him"*. [5] Also, it represents the form through the leader can use and transform the idea into material (action), by the most powerful arguments of leadership.

Value-based motivation is mainly attribute leaders with leadership style based on spiritual intelligence. *"The spiritual leader tries transforming the individual mental into collective mental"*. [6]

4. CONCLUSIONS

At the level of the military in leadership tasks, and through them, in execution positions, motivating the professional performance is also imposed through other motivational factors. In this case, the military leader's role interferes, managed by superior moral, social and ethical virtues, formed in the spirit of the highest values of the military institution.

At present, the military leaders can be leaders defined by emotional and spiritual intelligence, leaders whose personality consolidates by respect for the values promoted by the particular military organizational culture directly obtained from the basic values of humanity, thing that makes possible to reach a superior level of motivation in subordinates. This type of leader is relevant to maintaining and transmitting the institutional values, known as development vectors of people, and which leads the professional military's actions towards performance.

The professional soldier is a protector and a promoter of ethical and moral virtues of highest level. The building of this leader is based on abilities and leading to the human resources (HR) as main sample of the military organization's action. They are able to combine the belligerent and violent appearance of the war with the sacrifice for the rest, for their defence and security.

The type of leader with high emotional, physical and spiritual intelligence is specific to technical specializations from the military environment, especially to anti-aircraft artillery and rocket military, in the Romanian army who celebrate the centenary of their specialization's foundation, in 2016.

REFERENCES

[1] Sava Ionel Nicu, Tibil Gheorghe, Zulean Marian, coordonatori, în *„Armata și societatea, culegere de texte de sociologie militară"*, editura Info-Team, București, 1998;
[2] Jianu Alexandru, *"Cultura organizației militare, dimensiune definitorie a construcției prospective a liderilor militari"*, în volumul *„Psihologie Militară"*, editura UNAp, București, 2011;
[3] Mendes Cardoso Alberto, *"Cele treisprezece momente. Analiza operei lui Sun Tzu"*, editura Economică, București, 2002;
[4] Goleman Daniel, *„Inteligența emoțională"*, editura Curtea Veche, București, 2002;
[5] Zohat Danah, Marshall Ian, *„Inteligența spirituală"*, editura Vellant, București, 2011;

[6] Iacob Carmen Mihaela, *„Profilul psihologic al liderului militar, tipurile de inteligență și noul lider în organizația militară”,* Facultatea de administra ție publică, SNSPA, București, 2010;
[7] Iacob Florin Alexandru, *„Leadership și motivație în organizația militară”,* Facultatea de comunicare și relații publice, SNSPA, București, 2012;
[8] Mihai Eduard, Moşoiu Ovidiu *„Analysis of the romanian air force squadron organizational culture”*, in Review of the Air Force Academy, Vol XII, No 2(26) Brasov, Romania, 2014;
[9] Belu Daniela, *„The psyhological and statistic instruments used to measure capacity to be motivated – the basis of leadership”*, in Review of the Air Force Academy, Vol XI, No 2(24) Brasov, Romania, 2013;
[10] Codreanu Aura, *„Organisational comunication patterns underllying the concept of organisational behavior”*, in Review of the Air Force Academy, Vol XI, No 1(16) Brasov, Romania, 2010;

AIR FORCE AND AEROSPACE ENGINEERING

EMULSION EXPLOSIVES DETONATION VELOCITY DETERMINATIONS USING TIME DETECTORS

Neculai-Daniel ZVINCU[*], Nicușor-Nicolae DRUȚA[*], Lavinia Valentina BOCEA[**]

[*]Military Technical Academy, Bucharest, Romania (daniel.zvincu@gmail.com, nicu_dnn@yahoo.com), [**] Craiova University of Medicine and Pharmacy (lavinia_bocea@yahoo.com)

DOI: 10.19062/2247-3173.2016.18.1.14

Abstract: *The present work assesses the detonation velocity of emulsion explosives using time arrival detectors such as electrically charged ionized pins and optical fibers probes. They record the arrival time of an object (it's free surface) or wave. Results obtained for emulsion explosives are presented for both types of experiments. Also, numerical simulations were created in order to have a good results comparison.*

Keywords: *emulsion explosives, detonation velocity, ionised pins, optical fibers, DYNA 2D.*

1. INTRODUCTION

Detonation velocity determination of an explosive can be achieved while using detectors that record the arrival time of the particles or waves. These detectors trigger a signal on arrival of a pulse. Ionised pins electrically charged and optical fibers are important examples, and the first models being used in such determinations. Other methods for determining thedetonation velocity of explosives involves ultra-fast cameras, X-rays or holography (hologram).

Studies on the shock wave propagation driven by Graham, Asay and Chhabildas concluded that the mechanical devices can not be used for determinations of such type due to the speed at which events occur.

Detonation velocity determinations were conducted for emulsion explosives.

2. EMULSION EXPLOSIVES

Emulsion explosives are consisted of a matrix and a sensitiser. The matrix is formed by mixing ammonium nitrate (ammonium nitrate), water and a mineral oil, the last being added in order to reach a stoichiometric ratio with an emulsifying agent which improves the mixture of the emulsion. Matrix can not detonate without adding a sensitizer. Sensitizers are usually glass microspheres filled with air, diameter of about 100 μm or cenospheres, ash microspheres, sorted by size and density.

Emulsion explosives (EMX) are widely used in mining.

Emulsion explosives have a number of significant properties: good detonation parameters, are less sensitive to heat and mechanical action, detonation velocity can vary widely depending on manufacturing technology and composition.

Theoretically, the detonation of explosive emulsion has not been studied adequately. Several mechanisms have been proposed to describe this phenomenon. A "hot spot"

model was proposed by Deribas, while Sil'vestrov chose an empirical model based on three parameters chosen from the condition of similarity with data obtained experimentally.

Medvedev chose adiabatic compression mechanism as the most suitable to describe the phenomenon of detonation of emulsion explosives. This mechanism is applicable to all porous heterogeneous explosives, and is best suited for emulsion explosives sensitizers glass microspheres.

The combustion of the emulsion is shown schematically in Figure 1 (three stages). The scheme shows the burning surface indicated by gray and black, respectively glass microspheres as white circles. Three stages of combustion are shown (left to right):

- Initial phase, with a low burning surface
- Increase of sphere burning phase, with a maximum area of combustion
- Burning behind Chapman-Jouguet point (CJ) phase, burning a small area.

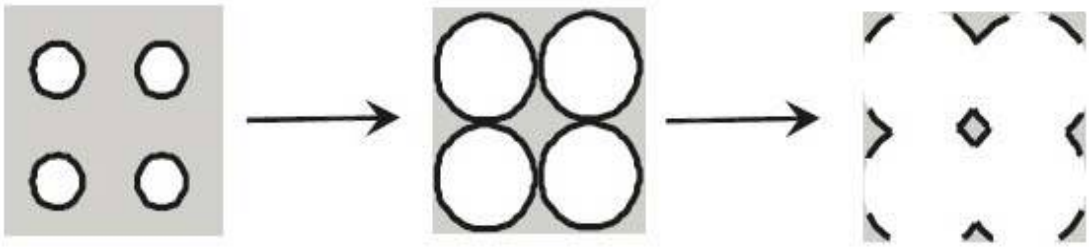

FIG. 1"Burning spheres" phenomena

The maximum of heat released is achieved when the total area of "burning spheres" reaches the maximum value. The total maximum area of "burning spheres of " is achieved when the spheres are densely packed. Even for densely packed spheres with identical diameter the minimum porosity is 0.26.

3. EXPERIMENTAL METHODS OF DETERMINING THE DETONATION VELOCITY: ELECTRICALLY CHARGED IONISED PINS METHOD

This method consisted in detonating charges with diameters of 15 mm, 19 mm, 25 mm and 32 mm; length of 220 mm. Six ionized pins with diameter of 1 mm were placed in the explosive charge at a known distance one apart from each other. The probes were connected to an electric circuit and an oscilloscope.

The shock wave when passing through the probe generates an electrical discharge materialized in the form of signal peaks (peaks) on the oscilloscope. Knowing the distance between the ionised pins and having the time periods signals were generated by the oscilloscope, the detonation velocity variation could be measured.

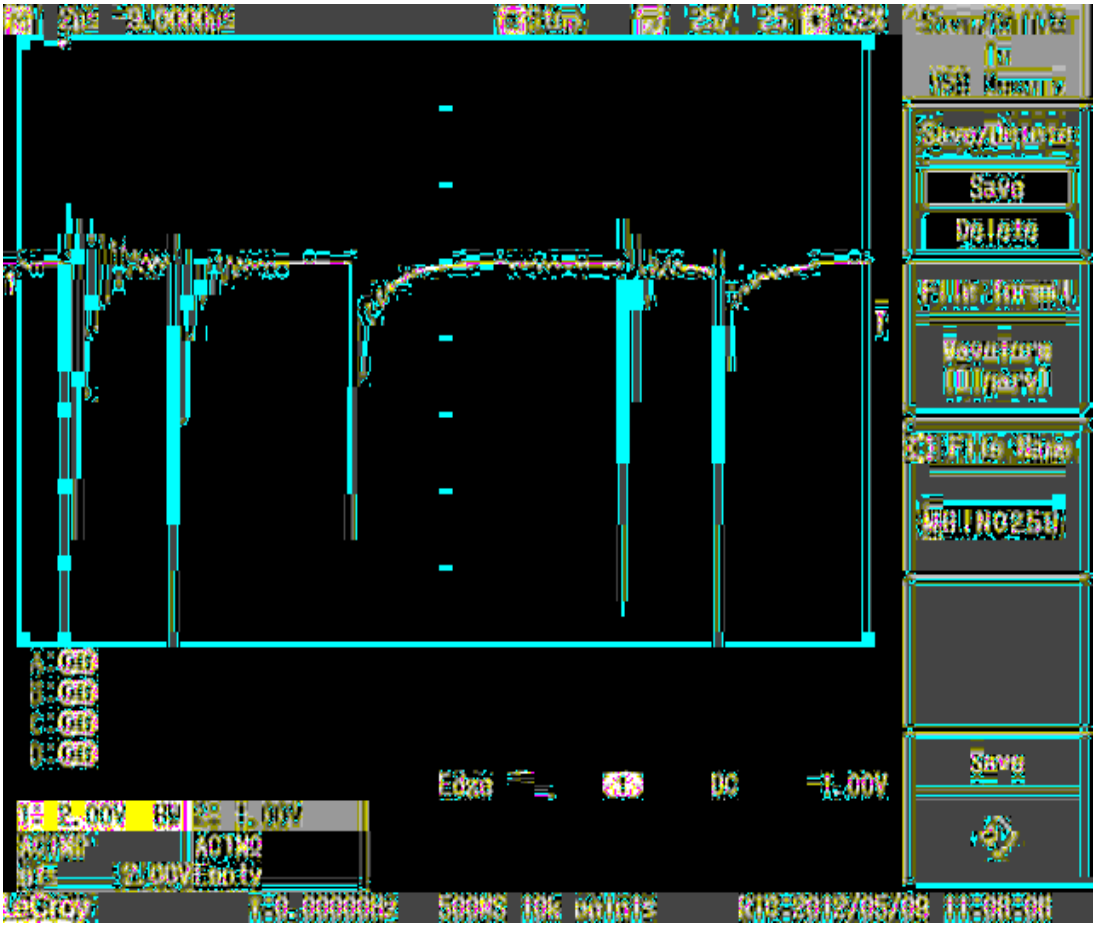

FIG. 2 Oscilloscope signal peaks generated by the shock wave passing through ionised pins

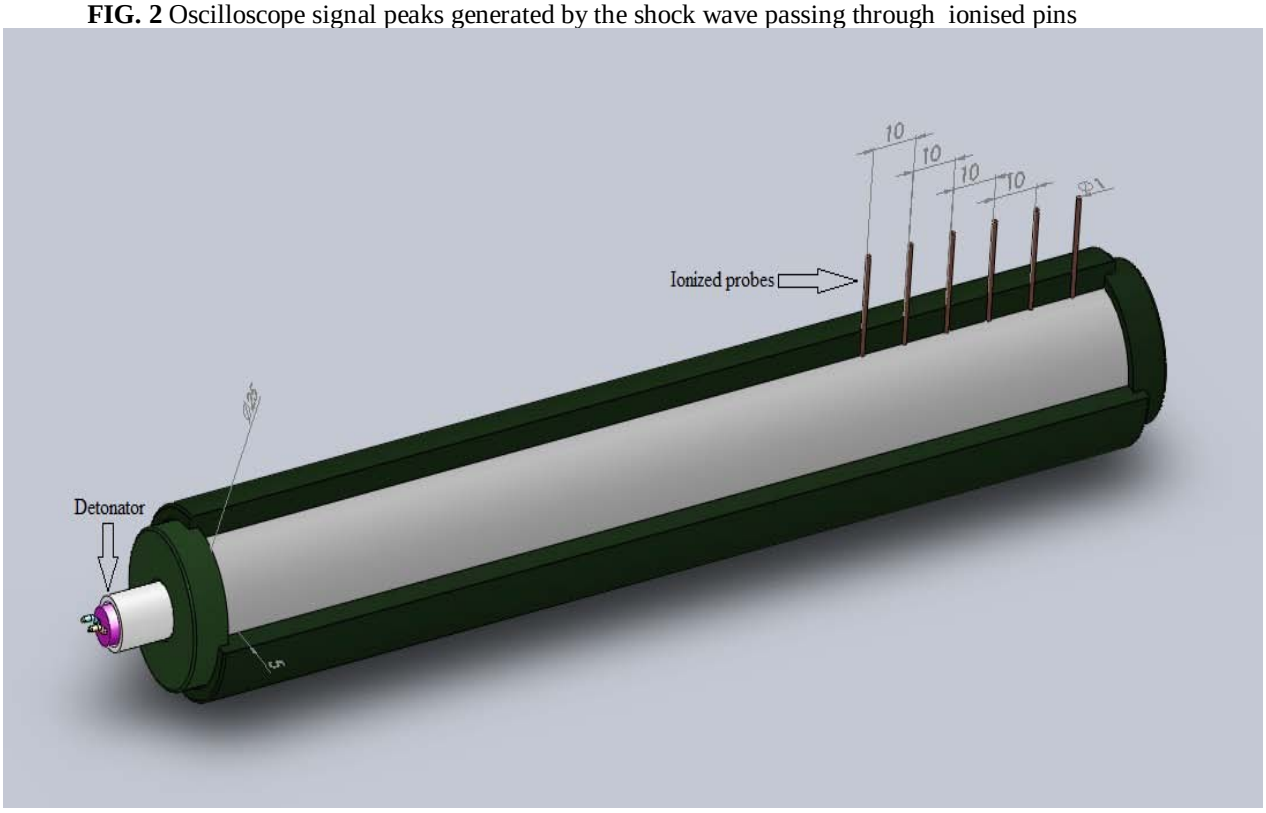

(a)

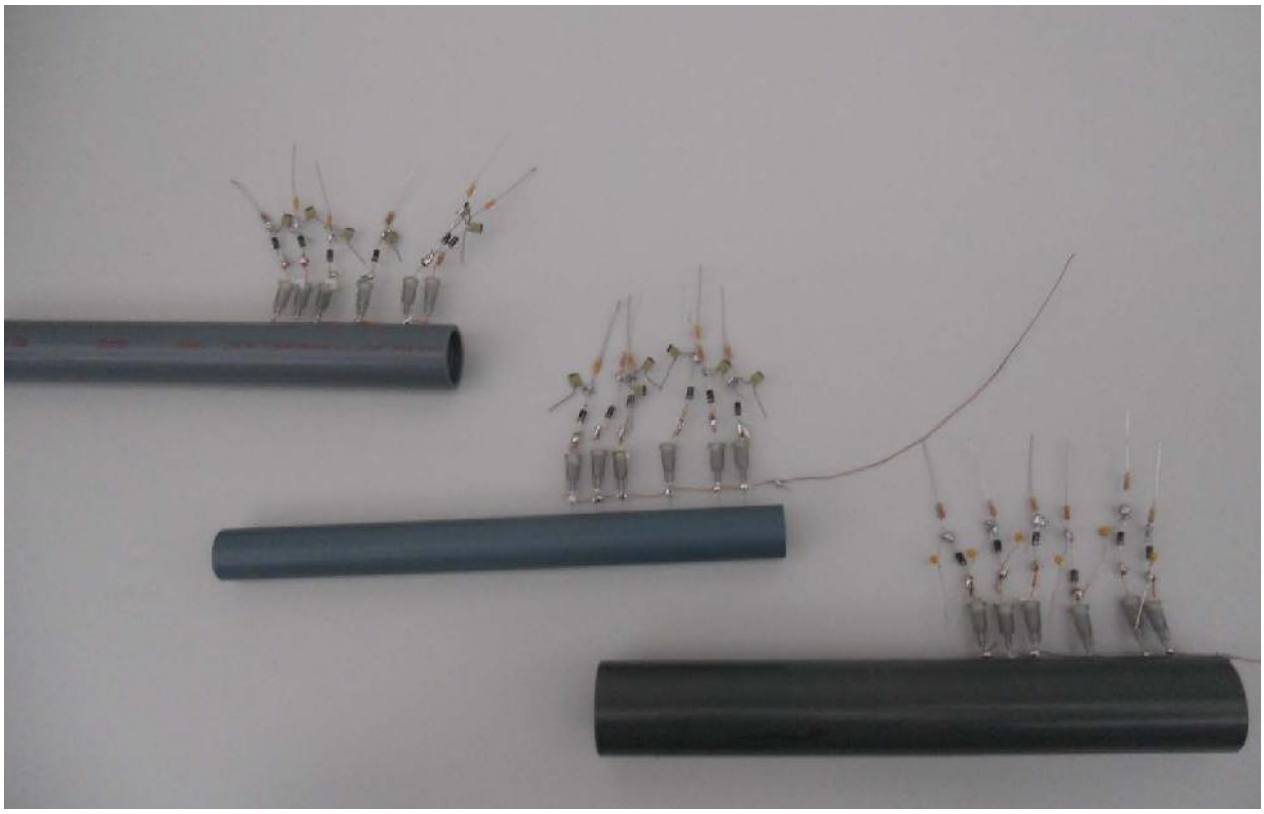

(b)

FIG. 3 Ionised pins inserted in explosive charge (Solidworks graphic and photo)

4. EXPERIMENTAL METHODS OF DETERMINING THE DETONATION VELOCITY: OPTICAL FIBERS EXPERIMENTAL APPARATUS

The detonation velocity was measured at the end of the explosive charge with a length of 220 mm and 25 mm diameter. PVC tubes with a thickness of 5 mm were used as confinement forms.Optical fiber probes with diameters of 250 microns were used for the detonation wave velocity measurements. One end of the optical fiber (MFOP) is placed inside the explosive charge (3 mm), perpendicular to the direction of propagation of the detonation wave, the other end being connected without intermediate optical equipment to the "streak" HAMAMATSU C-7700 camera.

These experiments allow evaluation of detonation with an error rate of 2-3 percent. At the end of the explosive charge a PMMA plate has been attached, with optical fibers embedded, to access speed of the shock wave induced in the PMMA plate by the detonation wave.

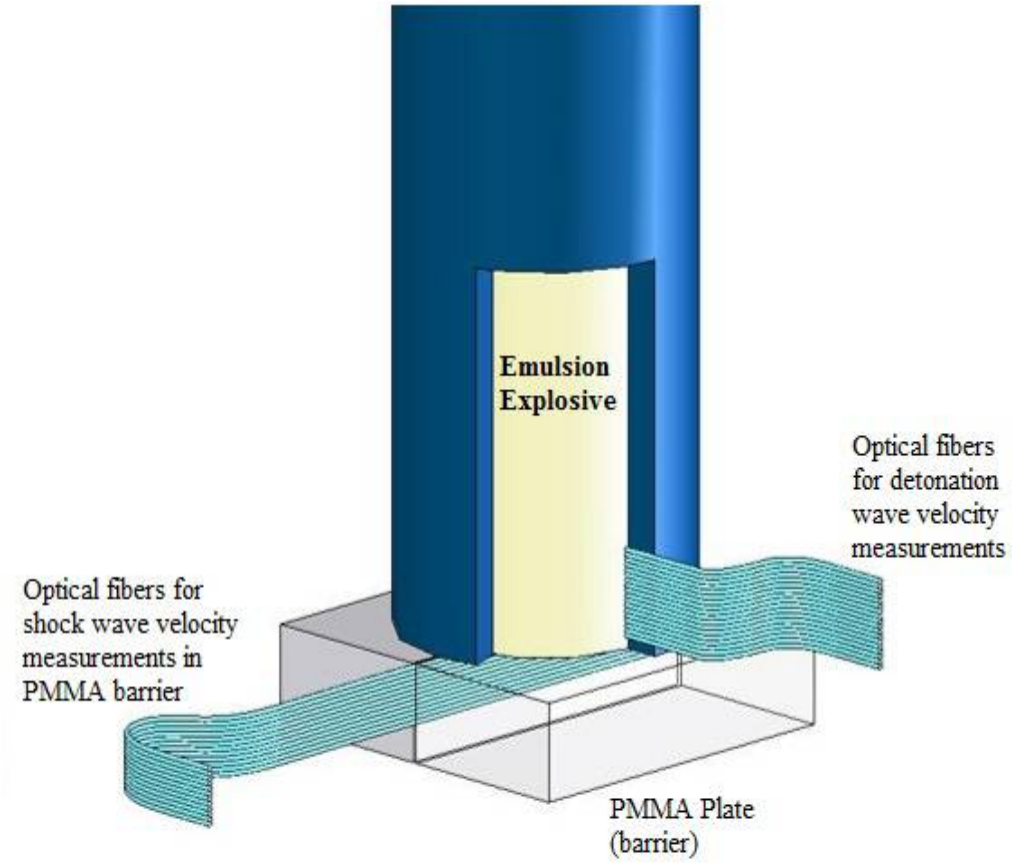

FIG. 4. Design of experimental model used for detonation velocity determinations using streak HAMAMATSU C-7700 camera

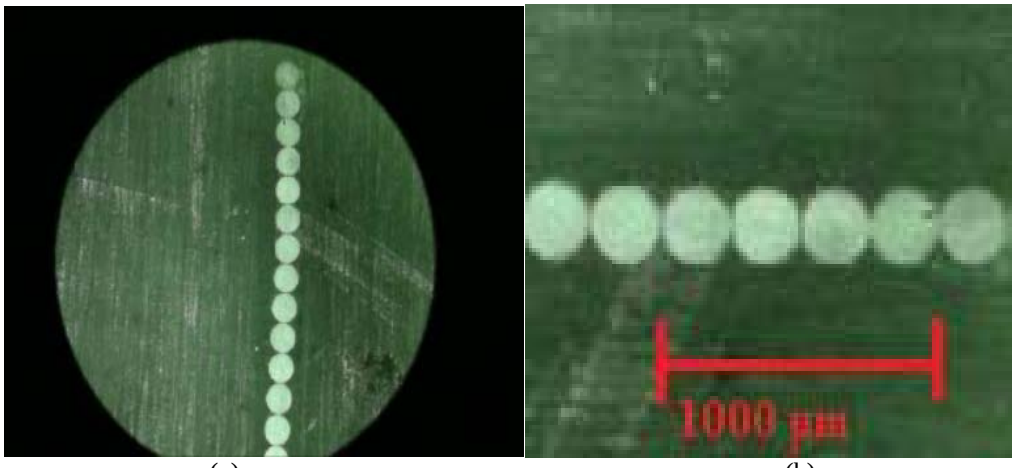

(a) (b)

FIG.5 Microscopic view of optical fibers

5. NUMERICAL SIMULATIONS

Numerical simulations were created, following the experimental model to have a wide range of results and to see the differences between them. Simulations were conducted using free-trial version of DYNA 2D software from Hydrosoft International company. This package contains the DYNA 2D, MAZE and ORION programs.

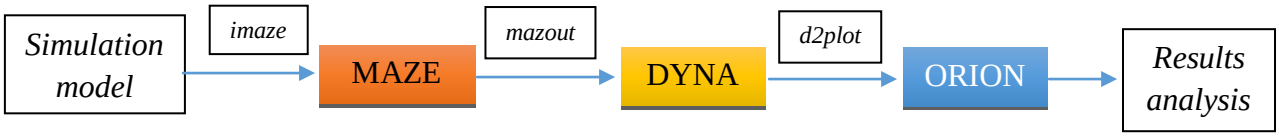

FIG. 6 Simulations Diagram

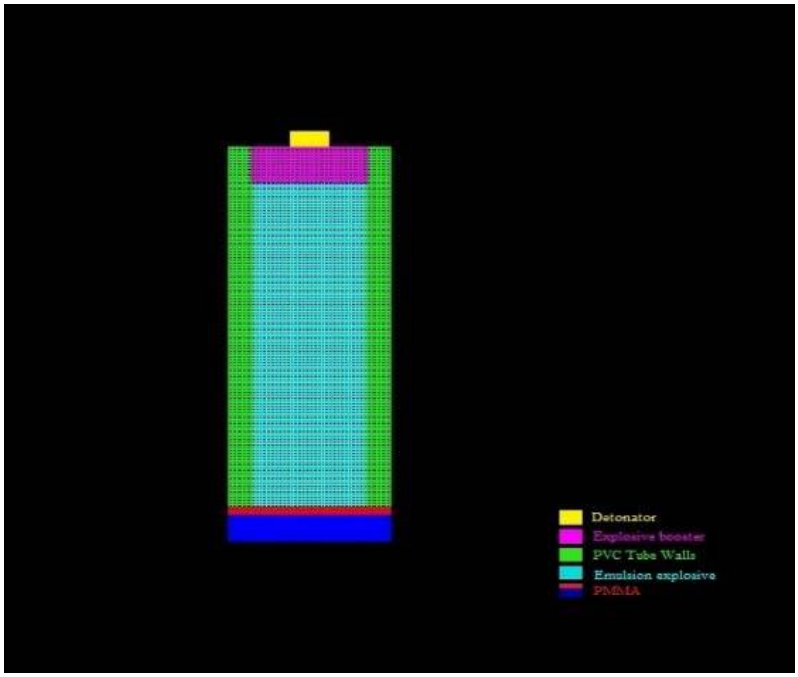

FIG. 7 Simulated Model

6. RESULTS OBTAINED

Table 1 contains the results obtained for the first time detector experimental setup, the ionised pins.

Table 1. Results obtained using ionised pins

	Charge Interior Diameter [mm]	Density [g/cm^3]	HGMB [%]	Detonation Velocity [mm/μs]
Experiment 1	25	1.041	5	**4.762**
Experiment 2	25	0.974	5	**4.560**
Experiment 3	32	1.023	5	**4.990**
Experiment 4	19	1.076	5	**4.386**
Experiment 5	15	1.073	5	**4.207**
Experiment 6	25	0.795	20	**3.514**

Next, the values for the detonation velocity obtained using the streak camera and the optical fibers are shown.

Table 2. Results obtained using ionised pins

Experiment	Density [g/cm^3]	Detonation Velocity [mm/μs]
Experiment 1	1.05	**4.892**
Experiment 2	1.12	**4.713**
Experiment 3	1.20	**4.628**
Experiment 4	1.32	**4.415**

For the numerical simulation, the results are presented in Table 3.

Table 3. Results obtained using ionised pins

Charge Interior Diameter [mm]	Length [mm]	Detonation Velocity [mm/μs]
15	100	**4.436**
19	100	**4.5996**
25	100	**4.7079**
32	100	**4.8736**
50	100	**5.1397**

7. AKNOWLEDGEMENTS

Both the experimental work and the numerical modelling and simulations for detonation velocity determinations of emulsion explosives were performed during Erasmus and Erasmus + stages at Departamento de Engenharia Mecânica / Faculdade de Ciencias e Technologia of Universidade de Coimbra, Portugal.

8. REFERENCES

[1] Mendes R., Ribeiro J., Plaksin I., Campos J. *"Non ideal detonation of emulsion explosive mixed with metal particles"*, 2010
[2] Medvedev E., Fomin V. M., Reshetnyak A. Yu. "*Mechanism of detonation of emulsion explosives with microballoons*", 2010
[3] Deribas, A.A., Medvedev A.E., Reshetnyak A.Yu., Fomin V.M. "*Detonation of emulsion explosives containing hollow microspheres*" Dokl. Phys. **389**, 163–165, 2003
[4] Guide to Streak Cameras – HAMAMATSU PHOTONICS K.K. , System Divisions
[5] Goga D. "*Explozivi și pirotehnie*", Editura Academiei Tehnice Militare
[6] Rotariu T. "*Chimia Explozivilor*", București, 2010

AIR FORCE AND AEROSPACE ENGINEERING

STUDY OF THE TURBOJET ENGINES AS PROPULSION SYSTEMS FOR THE UNMANNED AERIAL VEHICLES

Irina-Carmen ANDREI, Mihai Leonida NICULESCU,
Mihai Victor PRICOP, Andreea CERNAT

INCAS – National Institute for Aerospace Research "Elie Carafoli"
Bucharest, Romania (andrei.irina@incas.ro, icandrei28178@gmail.com
niculescu.mihai@incas.ro, pricop.victor@incas.ro, bobonea.andreea@incas.ro)

DOI: 10.19062/2247-3173.2016.18.1.15

Abstract: *The use of jet engines as propulsion systems for Unmanned Aerial Vehicles UAV's represents a actual challenge. For a large class of UAV's, providing more advantages with respect to the turboprop and turboshaft engines, as well as super-charged V12 piston engines, the small to medium size turbojet engines represent a more effective option. The research presented in this paper is focused on the thermo-dynamical analysis of a small sized turbojet. The single-spool turbojet engine model was used for the performance analysis; the one-dimensional engine cycle design was used to calculate the turbojet performances for a specified range of flight altitude and Mach number, as well as various engine operational regimes. From the numerical simulations have been expressed new parameter correlations, e.g. thrust - fuel flow, which will contribute to the deduction of a control law for the fuel flow. The objectives of the thermo-dynamical analysis have been fulfilled, with the calculated engine operating maps (i.e. variation of performances with altitude, flight Mach number and engine rotational speed), universal map of the engine; in addition, this analysis provides the values for significant engine parameters which are required by the engine's dynamic study.*

Keywords*: Unmanned Aerial Vehicle UAV, jet engines, turbojet, modeling, performances, engine maps*

1. INTRODUCTION

There is a large class of UAV and RPV [6] - [9] and a continuous demand for their use in both civil and military applications. Their main design goal is to satisfy the conditions imposed by the profile mission, in conjunction with other criteria such as simple construction and lower costs for manufacturing, operating and maintenance.

- **Why the turbojet engine**?

The turbojet engine it is a convenient solution, due to the simplicity of construction (single-spool), ease of operating and maintenance and lower costs.

Taking into account the vehicle flight mission profile, the thrust provided by the engine should range a good match. Thrust augmentation if necessary for the same family type of engine, which may be required by the demand of increasing the weight of the vehicle, can be obtained by increasing the turbine (stagnation) inlet temperature T3T, as well as the increasing of the air flow rate and pressure ratio. Nevertheless, in case of the same family of engines (with the preservation of the same outer diameter, which means

the air flow rate remains unchanged) remain two options, that is to have higher T3T and pressure ratios. In case of a turbojet equipped with centrifugal compressor, the largest and convenient value for the pressure ratio is about 5, Babak [21]; centrifugal compressors with pressure ratios slightly higher than 6, (as it is the case of the TURMO IV C turboshaft engine), develop embedded supersonic areas on the impeller and rotor, with the consequent occurrence of shock waves, followed by separation and/or re-attachment of the boundary layer, all of these being potential sources for energy and pressure losses. In case of the axial compressor, still keeping the subsonic flow within the axial stage, the pressure ratio can be increased with the addition of axial stages. As proven in practice, [4]-[5], due to safety reasons, axial compressors designed for single-spool turbojet engine constructions are efficient (i.e. operate with lower loss levels) if the pressure ratio is higher than 6 but less than 12 up to 15. Twin spool constructions are used if pressure ratios range from 15 up to 25, since these do operate farther from the surge margin; twin spool constructions can be found at turbojet, turbofan and turboprop engines. For large pressure ratios (over 30-35) the triple spool constructions are more efficient

For UAV's and RPV's, the most convenient from the economy standpoint is to select a small or small to medium sized turbojet, propulsion system "on-the-shelf", which means already designed, build and manufactured. A small or small to medium sized turbojet is usually a single-spool construction, with centrifugal compressor and (one or two staged) axial turbine. A potential increase of thrust, engaging as few changes as possible and reduced costs, is the increasing of the turbine inlet temperature (e.g. with about 100 up to 300 degrees, generating the boost of thrust with about 300 [N]), while the values of airflow rate and pressure ratio are maintained unchanged, which from the construction standpoint mean the maintaining of the same cross section diameter and the same compressor. The increasing of turbine inlet temperature requires less modifications on the combustor level. The selection and/ or the purchasing of an engine built and manufactured in Europe, represents a better option to support the development of EU industry.

- **Which are the objectives of the analysis**?

1. The objectives of the analysis of the turbojet engine as a recommended solution, are the modeling and simulation;
2. The purpose of **modeling and simulation** of a jet engine (thus the turbojet being included) is to do the steady state analysis and further the transient analysis.
3. The methods for analyzing the performances of the turbojet engine and its dynamic control are grouped so that A.1// - *Steady state analysis* and A.2// - *Transient analysis* will be described and explored;

A. The **steady state analysis** consists in the investigation of the operating, equilibrium states, thus the performances of the jet engine being determined.

B. The **transient analysis** reveals the dynamic behavior of a jet engine and allows engine's control; the design and management of the aircraft engine controls are based on the results of transient analysis.

As principle, the construction of a TURBOJET ENGINE Model supposes the completion of the steady state analysis and the transient analysis.

The steps for completing the performance analysis (i.e. steady state analysis) /A/ are:

A.1 - computation of the Brayton cycle at Sea Level Static SLS and ISA conditions;

A.2 - calculation of turbojet performances, such that to build the engine's Operation Maps:

A.2.1 - Altitude Map,

A.2.2 - Velocity Map,
A.2.3 - Rotor Speed Map,
A.3 - calculation of engine's Universal Map.

This paper is focused on the turbojet performance analysis, with the application to the J85 single spool turbojet engine, as Test Case.

The steps for completing the dynamic analysis /B/ are:

- selecting the state variables and relevant first order differential equations
- selecting the output equations
- investigation of the operating states
- perform Taylor linearization to obtain linear models
- combine individual linear models (corresponding to the main parts of the engine) in order to form a composite model describing the turbojet engine operation all over the whole operating area
- constructing a simulation model (e.g. in Simulink ambient)
- constructing a design model
- flight path cycle analysis and further optimizations

For a applications such as experimental aircrafts, powered gliders and UAV, UCAV systems, RPV, the use of turbojet engines as propulsion systems is an increasingly prevalent option; its convenience is due to the lower costs in purchasing, operation and maintenance, as well as inter-changeable features. In most cases, small sized turbojet engines are used, which are characterized by simplicity in construction, such as single-shaft engine with single-stage axial or radial compressor, annular combustion chamber, single-stage axial turbine, and stationary exhaust jet. In the compressor intake there is a brushless starter generator, which enables the starting from the board network and power generating in course of the engine operation. In this paper will be presented the first part, that is the steady-state analysis, providing the turbojet engine's performance analysis.

2. PERFORMANCE ANALYSIS OF TURBOJET ENGINE

2.1 PROBLEM STATEMENT AND FRAMEWORK

Performance Analysis of Turbojet Engine, also referred as **Thermodynamic Analysis** supposes the completion of three phases.

The first phase consists in calculating at SLS, ISA conditions (i.e. "*fixed point*", which usually means altitude H = 0 [km] and flight velocity V = 0 [m/s]) of the engine's performances (*Thrust*, *Specific Thrust*, *Specific Fuel Consumption*) and the determination of the engine's thermodynamic cycle (i.e. Brayton cycle).

The second phase consists in calculating the engine's performances at different flight regimes and rotor speed, which usually are expressed by **ENGINE's OPERATING MAPS** (i.e. **ALTITUDE MAP, VELOCITY MAP, SPEED MAP**.

The third phase, which consists in calculating of the **ENGINE's UNIVERSAL MAP**, completes the performance analysis. The results obtained following the performance analysis of the engine allow to study the dynamic behaviour of the engine and to do the numerical simulations.

Since not all the engine's design parameters are given, it comes out that at first hand, one must identify the missing parameters. In case of the turbojet engine, this is done by repeating the calculation of the Brayton cycle, until there is obtained a match with a specified parameter, usually the turbojet engine's thrust.

2.2 IDENTIFICATION OF MISSING THERMODYNAMIC ENGINE PARAMETERS

The main engine parameters which must be known (being given or determined) before performing the thermodynamic analysis are given below; J85 turbojet engine is the Test Case.

Compressor Pressure Ratio π_c^* (1) defined as the ratio of stagnation pressures at compressor exit versus inlet.

$$\pi_c^* = \frac{p_2^*}{p_1^*} \quad (1)$$

$$\pi_c^* = 8.3 \quad (2)$$

Turbine inlet temperature T3T (also referred as T_3^*) is determined from the relation (8) expressing the specific work of turbine (3) as the specific enthalpy drop between turbine exit and turbine inlet; the operating law for the single-spool turbojet is (4), with the meaning that the specific work produced by the turbine is used to produce specific work on compression (5) (the bleed and auxiliary flow rates can be neglected, as less than 2% of engine air flow rate); compressor pressure ratio is defined as the ratio of stagnation pressures at compressor exit versus inlet (4); specific enthalpy is proportional with the temperature and constant pressure specific heat *Cp* , with different values for air (6.1) and mixture of burned gas (6.2); expressing the turbine specific work as a function (7) of the stagnation temperatures at turbine inlet T_3^* and turbine exit T_4^*, then relation (8) is deduced :

$$l_T^* = i_3^* - i_4^* \quad (3)$$

$$l_T^* = l_c^* \quad (4)$$

$$l_c^* = i_2^* - i_1^* = i_1^* \cdot \frac{\left((\pi_c^*)^{\frac{k-1}{k}} - 1\right)}{\eta_c^*} \quad (5)$$

$$C_p = 1.005 \left[\frac{kJ}{kgK}\right] \quad (6.1)$$

$$C_{pg} = 1.165 \left[\frac{kJ}{kgK}\right] \quad (6.2)$$

$$l_T^* = i_3^* - i_4^* = C_{pg} \cdot (T_3^* - T_4^*) \quad (7)$$

$$T_3^* = T_4^* - \frac{l_T^*}{C_{pg}} \quad (8)$$

$$T_3^* = 1250\ [K] \quad (9)$$

Note that for the specified operating regimes one can deduce also the **T3T operating control law**, expressing its variation with the % of the rotor speed regimes [%rpm]; next, the automatic controls of the engine/ fuel systems can be designed. E.g. Max starting = 100, Nominal -97, Cruising = 91, Cruising lowered = 84, Idle ground = 50.

Airflow rate $\dot{M}_a$ [kg/s] is determined after a performing a number of iterations for the Brayton cycle, with the consequent calculation of the turbojet engine performances (i.e. specific thrust F_{sp} $\left[\frac{Ns}{kg}\right]$, thrust F $[N]$ and specific fuel consumption C_{sp} $\left[\frac{kg}{Nh}\right]$),

$$\dot{M}_a = 20.43 \left[\frac{kg}{s}\right] \quad (10)$$

Other engine parameters which must be determined before performing the thermodynamic analysis are listed downwards. These values have been trimmed such that to match the given thrust and specific fuel flow.

- **adiabatic efficiency on compression** η_c^* (11) defined as the ratio of specific work on compression and ideal specific work . From experience, centrifugal compressors have slightly lower values of adiabatic efficiencies with respect to axial flow compressor. In this case $\eta_c^* = 0.85$.

$$\eta_c^* = \frac{l_{c\_id}^*}{l_c^*} \tag{11}$$

- **adiabatic efficiency on turbine expansion** η_t^* (12) defined as the ratio of ideal specific work of turbine and its specific work. In this case $\eta_t^* = 0.89$.

$$\eta_t^* = \frac{l_t^*}{l_{t\ id}^*} \tag{12}$$

- **mechanical (shaft) efficiency** η_m (13) defined as the ratio of specific work consumed by compressor and specific work produced by turbine; in case of a single spool turbojet engine, $\eta_m = 1$. In, since there are no mechanical losses between compressor and turbine.

$$\eta_m = \frac{l_c^*}{l_t^*} \tag{13}$$

- **pressure loss at engine intake** σ_{da}^* (14) defined as the ratio of the stagnation pressures at intake exit versus inlet; $\sigma_{da}^* = 0.92$.

$$\sigma_{da}^* = \frac{p_1^*}{p_H^*} \tag{14}$$

- **pressure loss in combustor** σ_{ca}^* (15) defined as the ratio of the stagnation pressures at compressor exit versus combustor exit; $\sigma_{ca}^* = 0.98$.

$$\sigma_{ca}^* = \frac{p_3^*}{p_2^*} \tag{15}$$

- **combustion efficiency** $\xi_{ca} = 0.998$
- **exhaust nozzle velocity** $\varphi_{ar} = 0.940$

2.3 PURPOSE OF CALCULATIONS

a) the determination of **turbojet engines performances** (i.e. specific thrust $F_{sp}\ \left[\frac{Ns}{kg}\right]$ (47), thrust $F\ [N]$ (48), specific fuel consumption $C_{sp}\ \left[\frac{kg}{Nh}\right]$ (49), for all flight envelope and engine operating regimes;

b) the influence of altitude, flight Mach number and rotor speed [rpm] on inlet air flow rate (50) and compressor pressure ratio (55) - (58), was taken into account when calculating the turbojet engine performances, when operating at altitude, at specified flight velocity and engine regime [%rpm];

c) in addition, **Brayton cycle** (the variation of specific enthalpy [kJ/kg] versus specific entropy [kJ/kgK], at SLS, ISA conditions, Fig. 1 ;

2.4 THE BRAYTON CYCLE AND ENGINE PERFORMANCES

For the turbojet engine operating at **Sea Level Static SLS** and **International Standard Atmosphere ISA conditions** (i.e altitude *H* = 0 [km] and flight velocity *V* = 0 [m/s]), is calculated the Brayton cycle, Fig. 1.

3. MATHEMATICAL MODEL

3.1 HYPOTHESIS

The mathematical model of a turbojet engine describing its behavior as close to reality is based on the following **HYPOTHESIS**:

- the working fluid is considered perfect gas,
- two species:

A. // **air** // - from intake to compressor,

B. // **burned gas** // - within combustor, turbine and exhaust unit,

- fuel specific power, for JET A, JET A1 and/or JET B (aviation kerosene): $P_{CI} = 43500 \left[\frac{kJ}{kg}\right]$,
- ratio of specific heat $k = \frac{C_p}{C_v}$, see Table 1.
- constant pressure specific heat $C_p \left[\frac{kJ}{kgK}\right]$:
- gas constant $R \left[\frac{kJ}{kgK}\right]$; the relation between R and C_p is (16):

$$C_p = R \cdot \frac{k}{k-1} \tag{16}$$

Table 1 - Properties of the working fluids

Fluid	k	C_p [kJ/kg/K]	R [J/kg/K]
Air	1.4	1.005	287.3
Burned Gas	1.33	1.165	288.4

3.2. BASIC EQUATIONS

Basic equations (17) - (46) for computing the **turbojet engine performances** (algorithm defined by equations / relations ordered as entries in work flow):

- SLS, ISA conditions: $p_0 = 1.01325\,[bar]$ (17.1), $T_0 = 288\,[K]$ (17.2) and $i_0 = C_p \cdot T_0\ [kJ/kg]$, (18)
- conditions at engine inlet (intake) - station 0 (SLS) or H (flight) :
- *if* H = 0 [km] *then* $p_1^* = \sigma_{d\alpha}^* \cdot p_0\ [bar]$, (19.1), $T_1^* = T_0\ [K]$ (19.2), and $i_1^* = C_p \cdot T_1^*\ [kJ/kg]$ (20),

if H > 0 *then* $p_1^* = p_H^* \cdot p_0\ [bar]$ (21.1), $T_1^* = T_H^*\ [K]$ (21.2) and $i_1^* = C_p \cdot T_1^*\ [kJ/kg]$ (22),

where $T_H = T_0 - 6.5 \cdot H\ [km],\ [K]$ (23) and $p_H = p_0 \cdot \left(\frac{T_H}{T_0}\right)^{5.2553}$ (24) *and* $T_H^* = T_H + \frac{V^2}{2 \cdot C_p}$ (25) or $T_H^* = T_H \cdot \left(1 + \frac{(k-1)}{2} \cdot Mach^2\right)$ (26) *and* $p_H^* = p_H \cdot \left(1 + \frac{(k-1)}{2} \cdot Mach^2\right)^{\left(\frac{k-1}{k}\right)}$ (27)

- dynamic pressure ratio:

$$\pi_d^* = \frac{p_H^*}{p_H} = \left(\frac{T_H^*}{T_H}\right)^{\left(\frac{k-1}{k}\right)} = \left(1 + \frac{(k-1)}{2} \cdot Mach^2\right)^{\left(\frac{k-1}{k}\right)} = \left(\Theta(Mach)\right)^{\left(\frac{k-1}{k}\right)} \tag{28}$$

- conditions at compressor inlet - station 1^*: $p_1^* = \sigma_{da}^* \cdot p_H^*$ (29.1), $T_1^* = T_H^*$ (29.2), $i_1^* = i_H^*$ (30)
- conditions at combustor inlet - station 2^*:

$$p_2^* = \pi_c^* \cdot p_1^* \text{ (31)}, \qquad i_2^* = i_1^* \cdot \left(1 + \frac{\left((\pi_c^*)^{\frac{k-1}{k}} - 1\right)}{\eta_c^*}\right) \text{ (32)}, \qquad T_2^* = \frac{i_2^*}{C_p} \text{ (33)}$$

- conditions at turbine inlet - station 3^*:

$p_3^* = \sigma_{ca}^* \cdot p_2^*$ (34), $\cdot T_3^*$ from equation (8), $i_3^* = C_{pg} \cdot T_3^*$ (35)

- fuel flow coefficient (from energy balance eqn. in combustor):

$$m_c = \frac{(i_3^* - i_2^*)}{(\xi_{ca} \cdot p_{ci} - i_3^*)} \text{ (36)}$$

- burned gas flow coefficient (from mass balance eqn. in combustor):

$$m_g = 1 + m_c \text{ (37)}$$

- fuel flow coefficient: $m_c = \frac{M_c}{M_a}$ (38)
- burned gas flow coefficient: $m_g = \frac{M_g}{M_a}$ (39)
- conditions at turbine exit - station 4^*:

$i_4^* = i_3^* - l_t^*$ (40), $T_4^* = \frac{i_4^*}{C_{pg}}$ (41); $p_4^* = \frac{\delta_t^*}{p_3^*}$ (42),

- where δ_t^* is the pressure ratio in turbine, and it comes out from the expression of specific work in turbine. $\delta_t^* = \left(1 - \frac{l_{t\,id}^*}{i_3^*}\right)^{-\left(\frac{kg}{kg-1}\right)}$ (43)
- conditions at nozzle exit - station 5:

case: full exhaust nozzle expansion: $p_5 = p_H$ (44.1) , then the thrust obtained is maximum

case: partial exhaust nozzle expansion:

$$p_5 = p_{cr} < p_H \text{ (44.2)}, \qquad p_{cr} = \left(\frac{2}{kg+1}\right)^{\left(\frac{kg}{kg-1}\right)} \cdot p_4^* \text{ (45)}$$

- velocity of expelled gas c_5 [m/s], (46):

$$c_5 = \varphi_{ar} \cdot \sqrt{2 \cdot \left\{ \left[i_3^* \cdot \left(1 - \pi_d^* \cdot \sigma_{da}^* \cdot \pi_c^* \cdot \sigma_{ca}^*\right)^{-\left(\frac{kg-1}{kg}\right)} \right] - i_1^* \cdot \left[\frac{(\pi_c^*)^{\frac{k-1}{k}} - 1}{\eta_c^* \cdot \eta_t^* \cdot \eta_m} \right] \right\}} \qquad (46)$$

3.3. DEFINITIONS OF TURBOJET ENGINE PERFORMANCES

Relations (47) - (49) define the **turbojet engine performances** (i.e. thrust *F* [N],, specific thrust F_{sp} [Ns/kg] and specific fuel consumption C_{sp} [kg/Nh] or **TFC**,

- **specific thrust** $F_{sp} = m_g \cdot c_5 - V, \left[\frac{Ns}{kg}\right]$ (47)
- **thrust** $F = F_{sp} \cdot \dot{M}_a, [N]$ (48)
- **specific fuel consumption** $C_{sp} = \frac{3600 \cdot m_c}{F_{sp}}, \left[\frac{kg}{Nh}\right]$ (49)

3.4. THE INFLUENCE OF ALTITUDE, FLIGHT MACH NUMBER AND ROTOR SPEED ON AIRFLOW RATE AND COMPRESSOR PRESSURE RATIO

Equations (50) - (58) express the **influence of altitude, flight Mach number** and **rotor speed** on inlet **air flow rate** (50) and **compressor pressure ratio** (55) - (58):

- Airflow rate (50) is influenced by the change of altitude and flight Mach number, by the means of the variation of compressor pressure ratio, dynamic pressure ratio and the ratio of static pressures al altitude H [km] versus SLS:

$$\dot{M}_a = \dot{M}_{a_0} \cdot \frac{\pi_c^*}{\pi_{c_0}^*} \cdot \pi_d^* \cdot \frac{p_H}{p_0} \tag{50}$$

- specific work on compression (51) changes with the square of rotor speed (52)

$$l_c^* = l_{c_0}^* \cdot \bar{n}^2 \tag{51}$$

- rotor speed % (52) represents the ratio of speeds at operating versus nominal engine regime:

$$\bar{n} = \frac{n}{n_{NOMinal}} \tag{52}$$

- the relations between specific work of compressor, compressor pressure ratio, intake enthalpy and rotor speed, are (53) for SLS, ISA conditions and (54) for the flight at altitude:

$$l_{c_0}^* = i_0 \cdot \left(\frac{\left(\pi_{c_0}^*\right)^{\frac{k-1}{k}} - 1}{\eta_{c_0}^*} \right) \tag{53}$$

$$l_c^* = i_H^* \cdot \left(1 + \frac{\left(\left(\pi_c^*\right)^{\frac{k-1}{k}} - 1\right)}{\eta_c^*} \right) \tag{54}$$

- the influence of altitude, flight Mach number and rotor speed on compressor pressure ratio (55) - (58) is deduced from relations (53), (54) and (51); the ratio of compressor efficiencies at operating regime versus nominal can be taken about 1.0 (as initial approximation or in case that the universal compressor map is not available):

$$\pi_c^* = \left[1 + \left(\left(\pi_{c_0}^*\right)^{\frac{k-1}{k}} - 1 \right) \cdot \frac{i_0}{i_H^*} \cdot \bar{n}^2 \cdot \frac{\eta_c^*}{\eta_{c_0}^*} \right]^{\left(\frac{k}{k-1}\right)} \tag{55}$$

$$\pi_c^* = \left[1 + \left(\left(\pi_{c_0}^*\right)^{\frac{k-1}{k}} - 1 \right) \cdot \frac{i_0}{i_H^*} \cdot \bar{n}^2 \right]^{\left(\frac{k}{k-1}\right)} \tag{56}$$

$$\pi_c^* = \left[1 + \left(\left(\pi_{c_0}^*\right)^{\frac{k-1}{k}} - 1 \right) \cdot \frac{i_0}{i_H^*} \cdot \bar{n}^2 \right]^{\left(\frac{k}{k-1}\right)} \tag{57}$$

$$\pi_c^* = \left[1 + \frac{l_{c\,id}}{i_H^*} \cdot \bar{n}^2 \right]^{\left(\frac{k}{k-1}\right)} \tag{58}$$

3.5. THE TURBOJET ENGINE'S OPERATING MAPS

Definitions of turbojet engine's OPERATING MAPS, (i.e. the variation of the jet engine performances: thrust F [N], specific thrust F_{sp} [Ns/kg] and specific fuel consumption C_{sp} [kg/Nh] or TSFC, with altitude, flight velocity and engine rotational regime)

ENGINE OPERATING MAPS are represented by: 1/ **ALTITUDE MAP**, Fig. 1; 2/ **VELOCITY MAP**, Fig. 2 and 3/ **SPEED MAP**, Fig. 3.

(1) - ALTITUDE MAP is defined as the variation of the jet engine's performances (i.e. thrust F [N],, specific thrust F_{sp} [Ns/kg] and specific fuel consumption C_{sp} [kg/Nh] or TSFC) with respect to altitude H [km], while the flight velocity and rotor speed [%rpm] are constant, their values being usually taken for SLS, ISA conditions

Thrust	$F = f(H)]_{\substack{V=0 \\ n\%=1}}$
Specific thrust	$F_{sp} = f(H)]_{\substack{V=0 \\ n\%=1}}$
Specific fuel consumption	$C_{sp} = f(H)]_{\substack{V=0 \\ n\%=1}}$
Altitude Map	

(2) - VELOCITY MAP is defined as the variation of the jet engine's performances (i.e. thrust F [N],, specific thrust F_{sp} [Ns/kg] and specific fuel consumption C_{sp} [kg/Nh] or TSFC) with respect to flight velocity $\boldsymbol{V}$ [m/s] or its equivalent, flight Mach number, while the altitude H [km] and rotor speed [%rpm] are constant, their values being usually taken for SLS, ISA conditions

Thrust	$F = f(V)]_{\substack{H=0 \\ n\%=1}}$		**Thrust**	$F = f(M)]_{\substack{H=0 \\ n\%=1}}$	
Specific thrust	$F_{sp} = f(V)]_{\substack{H=0 \\ n\%=1}}$		**Specific thrust**	$F_{sp} = f(M)]_{\substack{H=0 \\ n\%=1}}$	
Specific fuel consumption	$C_{sp} = f(V)]_{\substack{H=0 \\ n\%=1}}$		**Specific fuel consumption**	$C_{sp} = f(M)]_{\substack{H=0 \\ n\%=1}}$	
Velocity Map			**Velocity Map**		

(3) - SPEED MAP is defined as the variation of the jet engine's performances (i.e. thrust F [N],, specific thrust F_{sp} [Ns/kg] and specific fuel consumption C_{sp} [kg/Nh] or TSFC) with respect to rotor speed [rpm] or its equivalent engine operational regime [%rpm], while the altitude $\boldsymbol{H}$ [km] and flight velocity $\boldsymbol{V}$ [m/s] are constant, their values being usually taken for SLS, ISA conditions

Thrust	$F = f(V)]_{\substack{H=0 \\ n\%=1}}$		**Thrust**	$F = f(M)]_{\substack{H=0 \\ n\%=1}}$	
Specific thrust	$F_{sp} = f(V)]_{\substack{H=0 \\ n\%=1}}$		**Specific thrust**	$F_{sp} = f(M)]_{\substack{H=0 \\ n\%=1}}$	
Specific fuel consumption	$C_{sp} = f(V)]_{\substack{H=0 \\ n\%=1}}$		**Specific fuel consumption**	$C_{sp} = f(M)]_{\substack{H=0 \\ n\%=1}}$	
Speed Map			**Speed Map**		

3.6. THE TURBOJET ENGINE'S UNIVERSAL MAP

Definitions of UNIVERSAL ENGINE MAP, (i.e. the variation of non-dimensional parameters of thrust F [N],, specific thrust F_{sp} [Ns/kg] and specific fuel consumption C_{sp} [kg/Nh] or TSFC, in case of a jet engine)

UNIVERSAL ENGINE MAPS are represented in coordinates **THRUST PARAMETER** and **SPECIFIC FUEL CONSUMPTION PARAMETER** versus either **flight Mach number** or **SPEED PARAMETER**.

The **UNIVERSAL ENGINE MAP** is defined in two equivalent ways, expressing the variation of Thrust parameter and Specific fuel consumption parameter with respect to Mach number, for a constant Speed parameter, or vice-versa :

UNIVERSAL ENGINE MAP - definition # **1**	
$\frac{F}{p_1^*} = f(M)\Big\|_{\frac{n}{\sqrt{T_1^*}}=const.}$	**Thrust parameter**
$\frac{C_{sp}}{\sqrt{T_1^*}} = f(M)\Big\|_{\frac{n}{\sqrt{T_1^*}}=const.}$	**Specific fuel consumption parameter**
$\frac{n}{\sqrt{T_1^*}} = constant$	**Speed parameter**

UNIVERSAL ENGINE MAP - definition # **2**	
$\frac{F}{p_1^*} = f\left(\frac{n}{\sqrt{T_1^*}}\right)$	**Thrust parameter**
$\frac{C_{sp}}{\sqrt{T_1^*}} = f\left(\frac{n}{\sqrt{T_1^*}}\right)\Big\|_{M=c}$	**Specific fuel consumption parameter**
$M = constant$	**Flight Mach number**

Universal Map

4. RESULTS

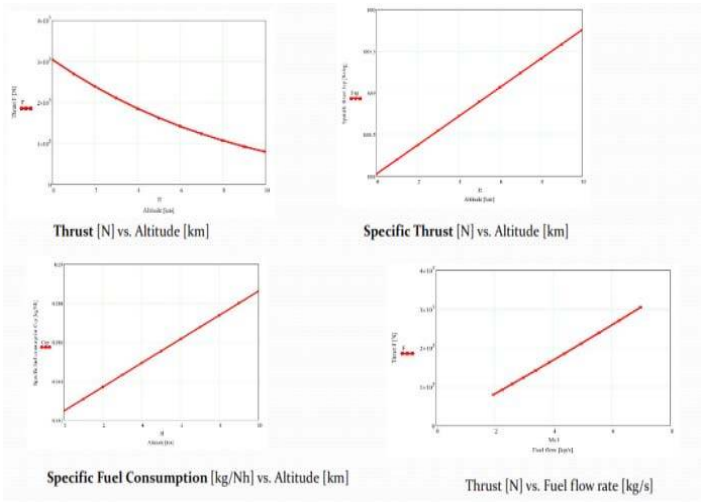

FIG. 1 - ALTITUDE MAP

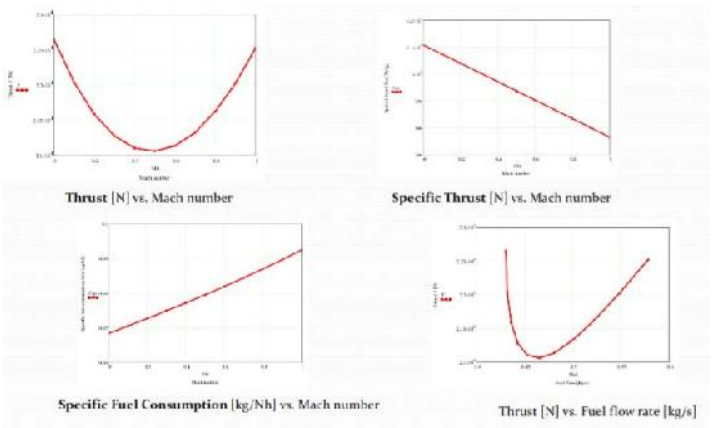

FIG. 2 - VELOCITY MAP

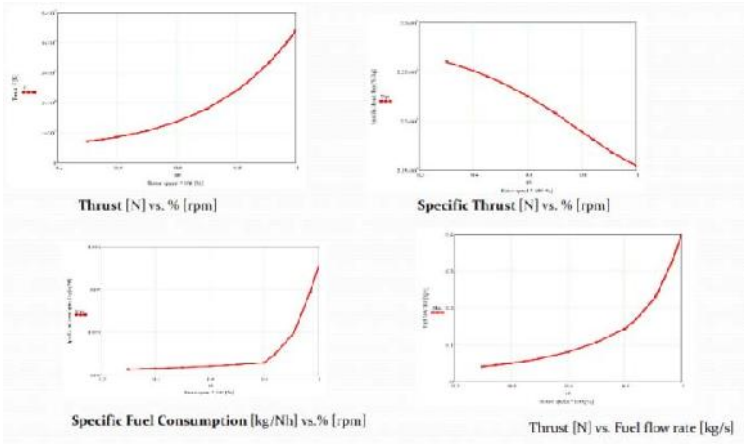

FIG. 3 - SPEED MAP

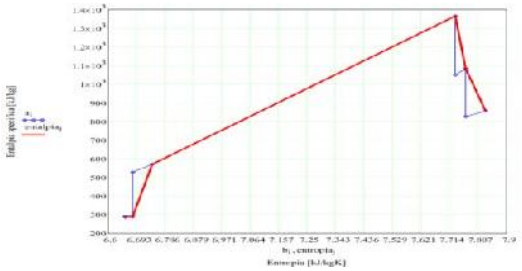

FIG. 4 - J 85 turbojet Brayton cycle (at SLS, ISA conditions)

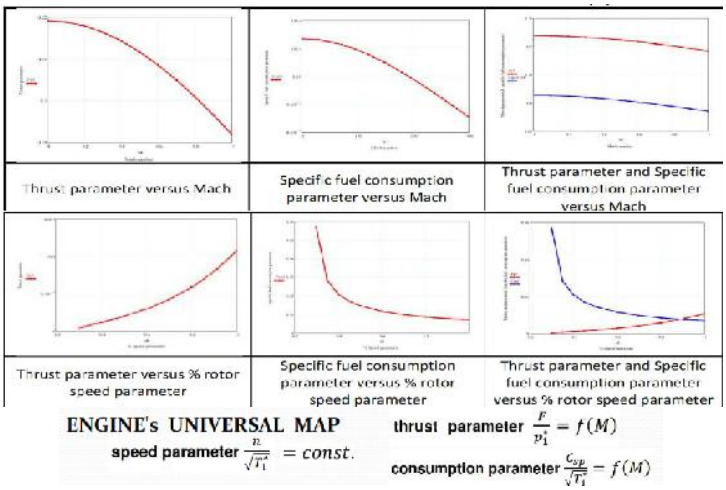

The turbojet engine's **OPERATING MAPS** are: 1/ **ALTITUDE MAP**, 2/ **VELOCITY MAP** and3/ **SPEED MAP**, followed by 4/ **UNIVERSAL MAP**, with the appropriate calculation of the thrust parameter and specific fuel consumption parameter.

3. CONCLUSIONS & ACKNOWLEDGMENT

The focus of this study is the performance analysis for a single spool turbojet, which was completed within a thorough research; its results were expressed graphically, as the turbojet engine's operational and universal maps. The engine's performances calculated from the in-house codes match the engine data from catalogues.

The authors would like to express their gratitude to the INCAS - National Institute of Aerospace Research "Elie Carafoli" Bucharest for the support while carrying on research activities within the Flow Physics Department, Numerical Simulations Unit, as well as the

documentary research. The results presented in this paper are correlated to the current research activities regarding the jet propulsion systems, carried on within INCAS.

REFERENCES

[1] J. D. Mattingly, *Elements of Propulsion and Gas Turbine and Rockets*, American Institute of Aeronautics and Astronautics Education Series, Inc. Reston, VA,.

[2] L. C. Jaw, J. D. Mattingly, *Aircraft Engine Controls: Design, System Analysis And Health Monitoring*, American Institute of Aeronautics and Astronautics, Inc. Reston, VA, 2009, p. 331.

[3] NAP.edu/10766, *5 Propulsion Technologies, Uninhabitated Air Vehicles, Enabling Science for Military Systems*, The National Academies Press

[4] ***, Rolls Royce, *The Jet Engine*, fifth edition, ISBN 0 902121 2 35, The Technical Publications Department Rolls-Royce plc, Derby, England

[5] ***, Powerplant, JAA ATPL Training, JEPPESEN, Atlantic Flight Training Ltd

[6] Junghsen Lieh, Eric Spahr, Alireza Behbahani, John Hoying, *Design of Hybrid Propulsion Systems for Unmanned Aerial Vehicles*, 47th AIAA/ASME/SAE/ASEE Joint Propulsion Conference & Exhibit, 31 July - 03 August 2011, San Diego, California, AIAA 2011-6146

[7] Anna Marcellan, An exploration into the potential of microturbine based propulsion systems for civil Unmanned Aerial Vehicles, M Sc Thesis, T U Delft, 2015

[8] S. Bagassi, G. Bertini, D. Francia, F. Persiani, Design Analysis for Hybrid Propulsion, 28 th INTERNATIONAL CONGRESS OF THE AERONAUTICAL SCIENCES, ICAS 2012

[9] **Z. GORAJ, M. SZENDER,** Techniques and Critical Technologies Applied for Small and Mini UAVs – State of The Art and Development Perspectives

[10] S. Yarlagadda, *Performance analysis of J85 turbojet engine matching thrust with reduced inlet pressure to the compressor*, PhD Thesis, The University of Toledo, Ohio, 2010, Theses and Dissertations, Paper 1022, http://utdr.utoledo.edu/theses-dissertations

[11] Jan Janikovich, *Gas Turbine Transient Performance Modeling for Engine Flight Path Cycle Analysis*, Cranfield University, School of Engineering, Gas Turbine Engineering Group, PhD Thesis, 2010.

[12] Wilfried Wisser, *Generic Analysis Methods for Gas Turbine Engine Performance, The development of the gas turbine simulation program GSP*, PhD Thesis, NLR and TU Delft, 2015.

[13] ***, *Compressor and Turbine Maps for Gas Turbine Performance Computer Programs*, Issue 3, GasTurb GmbH, 2013

[14] NASA Technical Memorandum **TM X-3014**, *A generalized hybrid computer program for studying turbojet or turbofan engine dynamics*, John Szuch, Cleveland, Ohio, 1974

[15] S. M. Eastbourn, *Modeling and simulation study of a dynamic turbofan engine using Matlab Simulink*, M. Sc. A.E. Dissertation, Wright State University, 2012

[16] Dr. I. Andrei, A. Stanescu, *Issues on modeling and simulation of a mixed flows turbofan*, Caius Iacob Conference, 2015

[17] Stan Zak, *Turbojet Engine Modeling*, School of Electrical and Computer Engineering, Purdue University, Academic Course, 2014.

[18] S. Mahmoud, D. McLean, *Effective optimal control of an aircraft engine*, AIAA Journal, 1991, pp. 21-27

[19] F. Zare, Dr. Arpad Veress, K. Beneda, *Simplified mathematical model for a single spool and no by-pass jet engine*, RTK Conference, BME, 2013

[20] N. U. Rahman, J. F. Whidborne, *A numerical investigation into the effect of engine bleed on performance of a single-spool turbojet engine*, Procs. of the Institution of Mechanical Engineers, Part G: Journal of Aerospace Engineering, vol. 222, no. 7, 939-949, 2008

[21] M. Babak, *Effective computational procedure for high pressure ratio centrifugal compressor*, TechSoft Engineering & SVS FEM Konfererence ANSYS 2009

[22] H. Asgari, X. Chen, R. Sainudin, *Modeling and simulation of gas turbines*, Intl. Journal Modelling, Simulation and Control, 2013.

[23] S. C. Uysal, *High by-pass ratio turbofan engines aero-thermodynamic design and optimization*, PhD Thesis, The Graduate School of Natural and Applied Sciences, Middle East Technical University, 2014

[24] NASA Technical Memorandum 83446 (NASA - TM 83446), *Digital Computer Program for Generating Dynamic Turbofan Engine Models (DIGTEM)*, C.J. Daniele, S. M. Krosel, J. R. Szuch, E. J. Westerkamp, Lewis Research Center, Cleveland, Ohio, 1983
(May, 2016).

COMPARATIVE STUDY BETWEEN GLOBAL POSITIONING SYSTEMS USED ON REMOTELY PILOTED AIRCRAFT SYSTEMS

Attila Laszlo BOER, Marius Cristian LUCULESCU, Luciana CRISTEA, Sorin Constantin ZAMFIRA, Ion BARBU

Transilvania University of Braşov, Romania (aboer@unitbv.ro, lucmar@unitbv.ro, lcristea@unitbv.ro, zamfira@unitbv.ro, ibarbu@unitbv.ro)

DOI: 10.19062/2247-3173.2016.18.1.16

Abstract: *The paper presents a comparative study on Global Positioning Systems that can be used on Remotely Piloted Aircraft Systems (RPAS). Neo-M8N and Neo-6 from U-blox were taken into account. The study focuses on the interfacing with a microcontroller development system and errors positioning data obtained under the same conditions. Experimental data show that receiving conditions have significant impact on the accuracy of results. For position and altitude the NEO-M8N receiver provides higher accuracy under good receiving conditions. The compass calibration is mandatory before bearing measurements.*

Keywords: *Remotely Piloted Aircraft System, Global Positioning System, microcontroller.*

1. INTRODUCTION

The Global Positioning System (GPS) is a satellite-based navigation system that was developed as a military application in the 1970s. GPS is a one-way-ranging system, i.e. users can only receive the signals [1].

GPS consists of a constellation of satellites, known as Initial Operational Capability. The satellite orbits are nearly circular and their period is about 12 hours.

GPS involves three major components:

- the space segment, which consists of the 24-sattelite constellation;
- the control segment, which consists of a worldwide network of tracking stations;
- the user segment, which includes all users.

Using a receiver the user can determine his position anywhere in the world (providing that GPS signal is available). The signal contains the coordinates of the satellites as function of time. GPS ensures very accurate timing and frequency signals using atomic clocks on the satellites [1-3].

The precision of GPS data depends on both the GPS receiver and the observing conditions. In the last years several studies were published regarding GPS data accuracy and reliability [4-7]. In the present work we will compare the accuracy of GPS data obtained with the NEO-M8N and NEO-6M GPS receivers, which can be used on Remotely Piloted Aircraft Systems.

2. THE NMEA PROTOCOL

NMEA stands for the National Marine Electronics Association. In 1983 the association adopted the NMEA 0183 format for interfacing marine electronic devices. It

has been updated several times, the latest release being v4.10 published in early May 2012.

The NMEA data streams include information on latitude, longitude, time, altitude and other variables. The data is sent in form of sentences. Each sentence starts with a dollar sign "$" and ends with a carriage-return line-feed <CR><LF>.

In the present article we will restrict our discussion to one sentence only, the GGA: Global Positioning System fix data. The general structure of the GGA sentence has the following form [1,2]:

$GPGGA,092750.000,5321.6802,N,00630.3372,W,1,8,1.03,61.7,M,55.2,M,,*76

We are interested in fields 3+4 (latitude), 5+6 (longitude) and 10+11 (altitude). The advantage of the NMEA standard is that being an ASCII format it is very easy to parse using standard command line tools such as awk, perl or python (for more details see section 3).

Most GPS receivers available on the market support the NMEA 0183 standard.

3. HARDWARE AND SOFTWARE SETUP

Our hardware setup consists of a standard GPS receiver connected to a Raspberry Pi 2 board via serial and i2c interfaces.

The Raspberry Pi is a single-board computer developed by the Raspberry Pi foundation. During the last years several generations have been released. The second generation, which has been used in our hardware setup, was released in February 2015. All models feature an ARM compatible CPU. The board uses SD cards to store the operating system (mainly Linux variants) and programs. Lower level input-output is provided by the GPIO pins (general purpose input/output) along the edge of the board. The pins support common protocols such as serial or i2c. In our setup the serial interface was used for the GPS data and the i2c interface for the compass [8,9].

As GPS receivers the NEO-6M and NEO-M8N have been used. The NEO-6 series has been designed with low power consumption and low cost in mind. The NEO-M8N GPS receiver incorporates the HMC5883L digital compass and includes an internal Flash that allows firmware updates. Both modules work with a baud rate of 38400 and incorporate power and fix indicator LEDs [10,11].

In order to display the NMEA protocol sentences transmitted by the GPS receiver via the serial port (/dev/ttyAMA0 in the case of the Raspberry Pi board) we can use the following bash script:

```
#!/bin/bash
i="0"
while [ $i -lt 200 ]
do
    OUTPUT=$(cat /dev/ttyAMA0 | ./script1.sh | ./script2.sh)
    if [[ ${OUTPUT} ]]; then
            echo ${OUTPUT}
            i=$[$i+1]
    fi
    sleep 1
done
```

script2.sh uses the standard UNIX command line utility "awk" to parse the NMEA sentences and to extract the information regarding latitude, longitude and altitude.

awk -F, '/\$GPGGA/ {print strftime("%Y-%m-%d "), $2, (substr($3,0,2) + (substr($3,3) / 60.0)), $4, (substr($5,0,3) + (substr($5,4) / 60.0)), $6, $10; fflush();}'

The digital compass is connected via the i2c interface at address 0x1e. Data acquisition has been done using the following Python script [12,13]. It outputs the coordinates x, y and z.

```
#!/usr/bin/python
import smbus
import time
import math
import sys

bus = smbus.SMBus(1)
address = 0x1e

def read_byte(adr):
    return bus.read_byte_data(address, adr)

def read_word(adr):
    high = bus.read_byte_data(address, adr)
    low = bus.read_byte_data(address, adr+1)
    val = (high << 8) + low
    return val

def read_word_2c(adr):
    val = read_word(adr)
    if (val >= 0x8000):
        return -((65535 - val) + 1)
    else:
        return val

def write_byte(adr, value):
    bus.write_byte_data(address, adr, value)

write_byte(0, 0b01110000)
write_byte(1, 0b00100000)
write_byte(2, 0b00000000)

for i in range(0,500):
      x_out = read_word_2c(3)
      y_out = read_word_2c(7)
      z_out = read_word_2c(5)
      print x_out, y_out, z_out
      sys.stdout.flush()
      time.sleep(0.1)
```

Bearing in the x-y plane can be computed as:

$$\alpha = \operatorname{atan}\left(\frac{y}{x}\right) \quad (1)$$

This value should be corrected taking into account the so called magnetic declination, i.e. the angle on the horizontal plane between magnetic north and true north.

4. EXPERIMENTAL RESULTS

We studied the accuracy of GPS data provided by the NEO-6M and NEO-M8N receivers. A number of approximately 200 measurements have been taken both in good and difficult receiving conditions.

Table 1 shows the standard deviation of latitude, longitude, altitude and bearing, respectively the localization error in meters. As we can observe receiving conditions and radio interference might have a very pronounced impact on the accuracy of results.

The localization error was computed using the following formula:

$$d = R\sqrt{a^2 + b^2} \tag{2}$$

where R is Earth's radius (6371 km) and

$$a = \Delta\lambda \cdot \cos\varphi_m \tag{3}$$

$$b = \Delta\varphi \tag{4}$$

Where φ being the latitude and λ the longitude and φ_m denotes the mean value of latitude.

Table 1. Standard deviation of latitude, longitude, altitude and bearing, respectively the localization error

GPS receiver	STDEV for latitude (seconds)	STDEV for longitude (seconds)	STDEV for altitude (m)	Localization error (m)	STDEV for bearing (degrees)
NEO-6M (good conditions)	< 0.18	< 0.18	10.44	< 6.783	0.1253
NEO-6M (difficult conditions)	0.688	1.547	8.29	39.597	0.2172
NEO-M8N (good conditions)	< 0.18	< 0.18	4.26	< 6.783	0.4762
NEO-M8N (difficult conditions)	0.218	0.784	19.78	18.229	1.1965

Figure 1 shows the values for the altitude during the 200 measurements for both the NEO-6M (red) and NEO-M8N (blue) modules. We must note that air pressure sensor is the most accurate way to measure altitude, however it needs to be calibrated whenever a reliable reference is available or when at sea level.

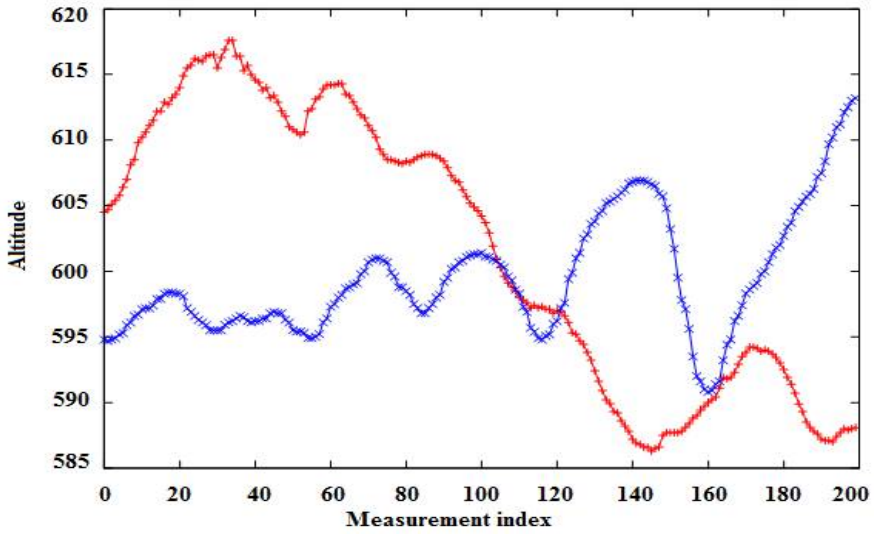

FIG. 1. Values for the altitude for both the NEO-6M (red) and NEO-M8N (blue) modules.

In order to display accurate values for the bearing, we must be calibrate the compass. We start by rotating the device in the horizontal plane and we register the values for the *x* and *y* coordinates. If we plot the values we notice that the circle isn't centred around the origin (see Fig. 2).

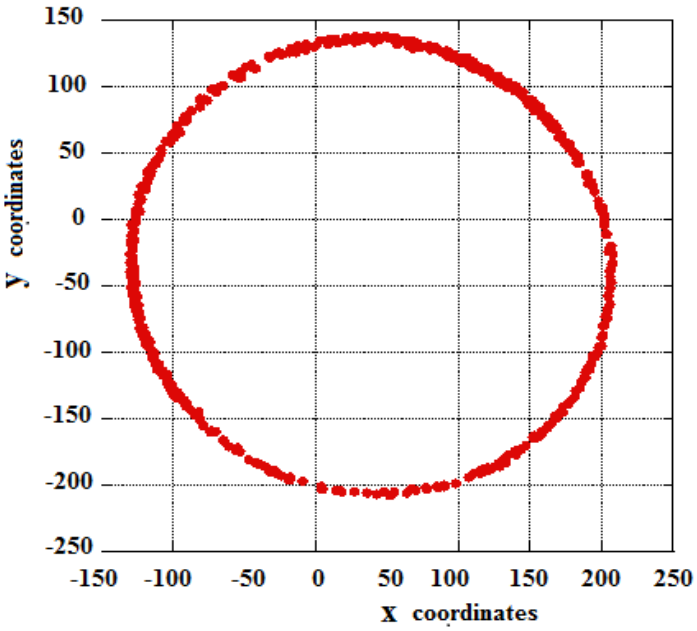

FIG. 2. x and y coordinates in compass calibration

The x and y offset can be computed as:

$$x_{offset} = \frac{x_{min} + x_{max}}{2} \qquad y_{offset} = \frac{y_{min} + y_{max}}{2} \tag{5}$$

Table 2 shows the offset values for both GPS receivers. We note that the NEO-6M module has an unusually high offset along the y axis.

Table 2. The offset values for both GPS receivers

GPS receiver	x_{offset}	y_{offset}
NEO-6M	38	-170
NEO-M8N	39	-35

5. FINAL REMARKS

We studied GPS data accuracy for the NEO-6M and NEO-M8N receivers. The hardware setup consists of a GPS receiver, which connects to a Raspberry Pi 2 board via serial and i2c interfaces. Experimental data shows that receiving conditions have significant impact on the accuracy of results.

For position and altitude the NEO-M8N receiver provides higher accuracy under good receiving conditions. We have shown that compass calibration is mandatory before bearing measurements.

For the NEO-M8N the offsets along the x and y axis were moderate, however for the NEO-6M unusually high y offset was detected.

AKNOWLEDGMENT

This paper was realized within the Partnerships Programme in priority domains-PN-II, which runs with the financial support of MEN-UEFISCDI, Project no. PN-II-PT-PCCA-2013-4-1629.

REFERENCES

[1] Ahmed El-Rabbany, *Introduction to GPS – the global positioning system*, Artech House, Boston, London (2002).
[2] E. D. Kaplan, C. J. Hegarty, *Understanding GPS - Principles and Applications*, Artech House, Boston-London (2006).
[3] G. Xu - GPS - Theory, Algorithms and Applications 2nd ed., Spinger Verlag (2007).
[4] C. Cai et. al., *An analysis on combined GPS/COMPASS data quality and its effect on single point positioning accuracy under different observing conditions*, Advances in Space Research 54 818-829 (2014).
[5] G. I. Emel'yantsev et. al., *Improving the accuracy of GPS compass for small-sized objects*, Gyroscopy and Navigation 6 166-171 (2015).
[6] X. Li et. al., *Accuracy and reliability of multi-GNSS real-time precise positioning: GPS, GLONASS, BeiDou, and Galileo*, Journal of Geodesy 89 607-635 (2015).
[7] K. Liu et. al., *Improving Positioning Accuracy Using GPS Pseudorange Measurements for Cooperative Vehicular Localization*, IEEE Transactions on Vehicula 63 (2014).
[8] P. Hongyan et. al., *Drive design for ship GPS navigation equipment based on Linux operating system*, International Conference on Educational and Network Technology (ICENT) (2010).
[9] S. Monk, *Programming the Raspberry Pi - Getting started with Python*, Mc Graw Hill (2013).
[10] NEO-6 u-blox 6 GPS Modules Data Sheet. Available at https://www.ublox.com/sites/default/files/products/documents/NEO-6_DataSheet_(GPS.G6-HW-9005).pdf, accessed on 02 April 2016
[11] NEO-M8N u-blox GNSS module Data Sheet. Available at https://www.u-blox.com/sites/default/ files / NEO-M8N-FW3_DataSheet_(UBX-15031086).pdf, accessed on 02 April 2016
[12] Mark Lutz, *Learning Python*, Publisher O'Reilly, (2013).
[13] Connecting and calibrating a HMC5883L Compass on the Raspberry Pi, http://blog.bitify.co.uk/2013/11/connecting-and-calibrating-hmc5883l.html, accessed on 02 April 2016

THEORETICAL CONSIDERATIONS ON POSSIBLE INSURANCE OF DRONES AGAINST DAMAGE AND THEFT

Catalin CIOACA*, Florin OLTEANU**

*"Henri Coandă" Air Force Academy, Braşov, Romania (catalin.cioaca@afahc.ro)
** Transilvania University from Brasov, Romania, (olteanu_florincatalin@yahoo.com)

DOI: 10.19062/2247-3173.2016.18.1.17

Abstract: *The diversity of missions and drones use areas has led to the development of their performance and thus the increasing the risks to which they are subjected. Material damage, which may be suffered or caused by drones due to risk manifestation, can reach high values, so it is recommended an optional insurance of drones from damage and theft.*

Keywords: *drone, risk, damage, theft, optional insurance*

1. INTRODUCTION

In the last few years, the terms "unmanned aircraft system", "unmanned aerial vehicle", "remotely piloted aircraft system" and "drone" are becoming synonymous with two things: a death dealing machine flying high above Afghanistan and hobbyist equipments that are popping up everywhere [1]. "Drone" historically refers to an unmanned aircraft system which exists to act as a target for live-fire air defense weapons training by armed forces [2]. Popular culture, particularly the media, uses the term "drone" as a generic descriptor for all classes of unmanned aircraft systems [2]. For this scientific approach, we chose to use the term "drone" because it is expressed best the class equipment for which we are trying to develop insurance policies.

Drone, according to specialty literature [3, 4, 5], are both air vector with equipments placed on board and ground command - control station that can operate either by remote control or autonomously. In recent years the technical performance of drones developed, in maximum speed, flight autonomy or operational ceiling.

With the development of technical performance arising from limitations and requirements drones diversified along with the fields of use. They are no longer the preserve of military missions but became accessible to civilians users such as legal entities or individuals [6, 7].

The diversifying of the areas of use of drones, the increasing complexity and difficulty of flying missions that are used for risk diversification led to accidental damage and theft. On the other hand, with the increased performance of drones their prices increased. Considering the latter, material damage caused by these risks can reach high levels. Therefore, it is increasingly imperative that these risks can be transferred by drones' owners to insurance companies by the conclusion of an optional insurance for damage and theft.

This paper examines some aspects of the optional insurance contract regarding the damage and theft of drones, such as: the object of insurance, insured risks, situations in which compensation may be guaranteed exclusions in accordance with the law [8, 9, 10, 11].

2. CONSIDERATIONS REGARDING THE OPTIONAL INSURANCE CONTRACT OF DRONES

The optional insurance contract applied to the drones can be made after the known model of voluntary insurance contract of auto theft and damages, known by the acronym CASCO [8, 9].

The necessary elements to drones optional insurance contract conclusion are: the insured object (approved according to law) [8, 9, 10, 11]; the existence of a contract of compulsory insurance for damages caused to third parties; operator (authorized) and specifying conditions of use (weather, missions), shown in Fig. 1.

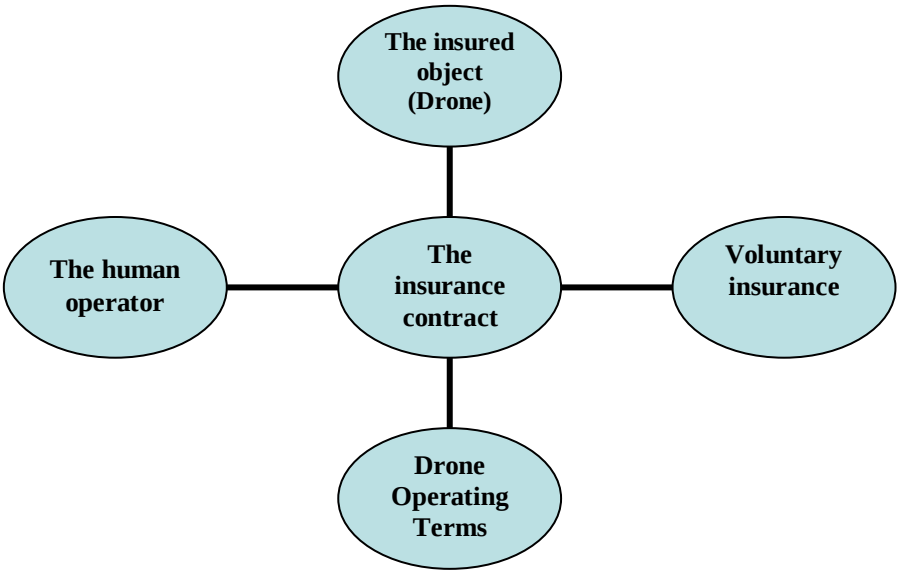

FIG. 1 Necessary elements for optional insurance contract conclusion

2.1 Object of insurance. The object of insurance in case of damage and theft of drone's are the following categories: natural and legal persons; structures of the national defense, security and public order. The drones that are not registered at Romanian Civil Aeronautical Authority or National Military Aviation Authority and don't have the compulsory insurance for damages to third parties can not be insured.

2.2 Insured risks. Safety Risk Management (SRM) is the tool that:

1. ensures that risks associated with operations/ activities are managed effectively;
2. allows obtaining approvals to conduct such operations;
3. enables pricing/ cost of insurance.

Thus, insurance becomes an integral part of risk management that provides financial compensation when the safety management system has failed to prevent an accident or a loss has been suffered due to an unforeseen event [12, 13]. Insurance is one of the present requirements related to drone operations by the side of privacy and data protection, operational safety and liability.

Insurance can be taken in the following *categories of risk*:

a. Basic risks such as collisions, accidental collisions with other bodies outside the ensured drone, its fall (on the ground in the ravine, water, etc.), falling bodies on the drone.

b. A number of additional risks, such as:

- ✓ fire, lightning, explosion, falling aircraft and sonic boom;
- ✓ natural disasters: earthquakes, floods of natural causes and landslides;

- ✓ atmospheric phenomena, a category which includes: hail, windstorm, weight of snow or ice and avalanche;
- ✓ theft and vandalism, namely: total theft, burglary and / or robbery and vandalism.

2.3 Situations of granting compensation for damage of the drones. Drones belonging to military organizations are compensated in situations such as: during any military applications (if accidentally hit by flying objects); during any military applications, (where drones are hit by bullets, or projectiles used by tanks, artillery and anti-aircraft except drones used as targets); during the conduct of surveillance missions and reconnaissance of targets; during the course of rescue missions; during the training and instruction program conducted in authorized institutions; aeronautical rallies.

Drones belonging to legal persons are compensated in the following situations:

- Flying surveillance of their targets or third parties that are requested;
- Flights for rescue operations;
- Flights authorized or licensed for the transmission of images or footage of events such as concerts, sporting events, weddings, and so on;
- Training flights.

Drones belonging to individuals are compensated in the following situations: pleasure flights and authorized filming of events.

2.4 General exclusions. They do not include insurance and no liability for:

A) damage of drones due to events such as:

- ✓ war (declared or not), invasion or action of an external enemy, civil war, revolution, rebellion, insurrection, military dictatorship, conspiracy, strikes, civil unrest, terrorism;
- ✓ confiscation, expropriation, nationalization, requisition, seizure, destruction or damage by order of any de jure or de facto government or any public authority;
- ✓ atomic explosion, radiation or radioactive infestations as a result of using atomic energy or fissile materials;
- ✓ pollution or contamination of any kind and from any cause.

B) damage of drone in the following cases :

- ✓ the event was caused deliberately or by gross negligence of the insured, the beneficiary, user, contractor or any other person treated them. Is deemed to be serious misconduct, situations such as leaving/ maintenance drone in hangars / unlocked room, not taking measures to change the locks of the hangar / premises as a result of an attempted theft by forcing locks or loss or theft of keys and so on;
- ✓ at the time of the event the drone was operated by a person who is not licensed in that category;
- ✓ the event was produced during handling drone drunk, under the influence of narcotics or drugs that are not compatible with the permission of handling drone;
- ✓ after the event, the person handling drone refuses to submit harvest biological samples to determine alcohol or consumption of goods / drugs or medication or does leave the place of the event without prior approval from the authorized authority when the incident occurred as a result of crime;
- ✓ drones damaged/ destroyed during flights in the airspace of other states when the flight is not authorized / approved by the State;
- ✓ drones damaged/ destroyed during flights over areas of private individuals or legal entities, when these flights are made without their consent and authorized institutions;
- ✓ drones damaged/ destroyed during flights over areas of state institutions, national companies, autonomous bodies when these flights are not approved by them;

- ✓ drones damaged/ destroyed during flights over areas of military or intelligence services organizations, when these flights are not approved by them;
- ✓ drones damaged/ destroyed because they did not respect flight altitudes and distances from airports, recommended by the aeronautical authorities;
- ✓ drones damaged/ destroyed while being used in acts of terrorism.

An insurance contract for damage and theft of drones also includes a number of elements, among which may be mentioned: definition of the terms used in the agreement: the insured, the insurer, customer, contractor, road, compensation, franchise, period of insurance, an so on; conclusion of insurance; commencement and termination liability insurer; insured period; insurance premiums; policyholder obligations and special obligations after the occurrence of the insured risk; finding and paying compensation; final provisions.

CONCLUSIONS

Due to the many risks to which drones are subjected during ground and flight operation and the fact that the damage that can affect drones that can have a high value and major implications on the development of business in the future, a contract of optional flexible and personalized insurance is required.

The voluntary insurance damage and theft of drones contract offers complementary advantages to the compulsory insurance contract by protecting all or part of the initial investment on technical system configured or in the case of the upgrade during operation considered in the contract under the aeronautical specific legislation.

This paper is required to be continued with the development of a software model for calculating insurance premiums in multi-criteria concept, starting from existing models used in CASCO insurance.

AKNOWLEDGMENT

The authors wish to thank the Transilvania University of Brasov and "Henri Coandă" Air Force Academy of Brasov for supporting the research necessary for writing this article.

REFERENCES

[1] Ezvid, *Drone vs UAV? What's the difference?*. Available at http://www.ezvid.com/drone-vs-uav-whats-the-difference, accessed on 28 Jan, 2016;
[2] Australian Certified UAV Operators Inc., *What do we call them: UAV, UAS or RPAS*. Available at http://www.acuo.org.au/industry-information/terminology/what-do-we-call-them/, accessed on 5 Feb, 2016;
[3] UAS Yearbook, Unmanned aircraft systems – The Global Perspective 2013/2014, Blyenburg & Co, june 2014, Paris, ISSN 1967-1709, 244 p., Available at www.uvs-info.com, accessed on 15 Jan, 2016;
[4] DoD Dictionary of Military and Asociated Terms, J P 1-02, US DoD, Washington DC, 2003;
[5] Unmanned Aircraft System (UAS) ROADMAP 2005-2030, US DoD, Washington DC, 2005, 213p;
[6] Department of Defence, *Unmanned Aerial Vehicles and Uninhabited Combat Aerial Vehicles*, USA, 2004;
[7] Prisacariu V., Cîrciu I., Luchian A., Unmanned aircraft vehicle (UAV) in the Romanian airspace. An overwiev, *Journal of Defence Resources Management*, vol. 5, issue 1(8) 2014, ISSN 2068-9403, p.123-128;
[8] Lungu N.C., *Asigurări de bunuri*, Editura Universităţii ,,Alexandru Ioan Cuza", Iaşi, ISBN: 978-973-703-485-4, 2010.
[9] Badea B.G., *Manualul agentului de asigurări*, Bucureşti, Editura Economică, ISBN 978-973-709-376-9, 2008;

[10] Reglementare Aeronautica Civila Romana RACR-AZAC *Admisibilitatea la zbor a unor categorii de aeronave civile*, Ed. 01/2007, Publicat in Monitorul Oficial nr. 637 din 18/09/2007 prin Ordinul ministrului transporturilor nr. 806/2007, Available at http://www.caa.ro/media /docs/C.2.2.b_RACR-AZAC_Ed_1.pdf;

[11] UAS Ordonanţa Guvernului nr. 29/1997 privind *Codul aerian civil*, republicată, consolidata la 25.10.2011, disponibil la http://www.caa.ro/media/docs/A.3.1_OG_29-1997_Codul_Aerian.pdf;

[12] Prisacariu V., Boşcoianu M., Luchian A., *Innovative solutions and UAS limits*, REVIEW OF THE AIR FORCE ACADEMY, 2(26)/2014, Braşov, Romania, ISSN 1842-9238; e-ISSN 2069-4733, p51-58;

[13] *** Global Aerospace, *What You Need to Know About Drone Insurance*. Available at http://www.global-aero.com/what-you-need-to-know-about-drone-insurance/, accessed on 10 March, 2016.

REMOTELY AND PILOTED AIRCRAFT SYSTEMS / LAW AND POLICIES

RISK PLANNING IN AVIATION SCIENTIFIC RESEARCH PROJECTS

Catalin CIOACA*, Sebastian POP**

*"Henri Coandă" Air Force Academy, Braşov, Romania (catalin.cioaca@afahc.ro)
** Transilvania University from Braşov, Braşov, Romania
(aerodrone.uav@gmail.com)

DOI: 10.19062/2247-3173.2016.18.1.18

Abstract: *Aviation scientific research projects, a field recognized as one very risky, require an effective risk management system ever since the stage of proposal of the design and implementation capabilities. The paper does not propose to redefine specific steps of risk management projects process. Its main objective is to highlight the importance of simple approaches for successful decisions, even from the planning stage. The result of the research is the design based on a simple qualitative approach, an initial risk management plan for MASIM research project.*

Keywords: *risk planning, aviation project, risk management plan, MASIM*

1. INTRODUCTION

The projects are all interrelated activities which take place according to a plan in order to achieve certain results in a limited period of time [1]. For aviation projects, using knowledge, competencies, skills, tools and specific techniques has resulted in the development or improvement of airports, making electronic or mechanical, aircraft development and introduction of a new system for air traffic control or discovery of material with special properties.

The risk in research projects may take the form of total failure (expected results do not materialize) or partial failure (expected results outside the triangle to materialize in time - cost - quality) of the scientific initiative [2]. In this context, risk analysis systematically uses available information to determine how often events may occur (specific or nonspecific) and the magnitude of their impact on the project [3].

Promoting a risk culture plays an important role for the success of scientific research projects. In the team / research consortium this translates by highlighting the benefits of risk management activities, which are often perceived as useless and resource intensive [4]. Project competitions discourage the identification of risk through the design of funding applications, because they are perceived as weakness. Reality has shown that a good balance between funding and results of the project is achieved when there are viable action plans for achieving the objectives of risk management activities thus adding value to the project.

Project risk management attempts to anticipate and provide a solution regarding the uncertainties that pose a threat to project objectives and terms [5]. In aviation projects, small or complex, a risk management strategy should follow two main directions: to identify as many potential risks as possible and, then, to decide how to deal with them [6].

To achieve the objective, the first part of the paper addresses the positioning of research projects in aviation on the quality-time-cost diagram and the second part details the process of

risk management specific to the MASIM project, which results in the design of the original risk management plan.

2. RISK MANAGEMENT IN RESEARCH AND DEVELOPMENT PROJECTS

The risk of undesirable events in socio-technical processes exist and can not be completely eliminated. Accordingly, research and development projects should be conducted taking into account that there are always risks that require effective management throughout the lifecycle of the project and favorable circumstances that can add value to the project.

The risk note present in all projects may be enhanced by the following factors: the project takes longer; the time between the planning and execution phase is extended; the experience of the project manager, of the project team and the partners in the consortium is narrower; methodology and technology to which called for the project is newer and less known [7]. Specifically, research projects are trying to move beyond the current boundaries of knowledge, which further increases the uncertainty in the results, regarded as objectives to be achieved [6].

In terms of project management one should distinguish between risk and uncertainty. If regarding the risk one can make possible scenarios of events occurrence, in case of uncertainty the probability of occurrence and impact can not be identified.

Starting from the definition of risk offered by Opran (2002) “the probability of losing” there can be identified within the projects a series of forms of this loss, depending on the weight of three main factors: time, cost and quality (Figure 1). Thus, if the final product must meet high performance requirements, then that project will be situated close to the peak "quality" [8].

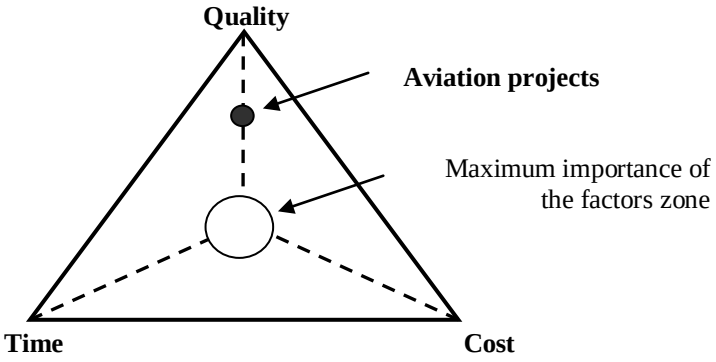

FIG. 1. Positioning diagram in aviation projects

Risk management is the set of methods and means by which the uncertainty is managed, as the basis of risk factors in order to reach the planned objectives. Risk approach as a enhancer factor for progress, turns risk management into a tool that enhances decision-making under uncertainty.

In research and development, the risk is often interpreted in limiting terms, with a negative impact on the goals. The peculiarities of these activities are a enhancer of the risk factor [9]: the uncertainty of the discoveries; the need for creative freedom; the scientific result is a public good; the effect in time of the results; the difficulty of assessing the effects.

3. RISK MANAGEMENT IN MASIM PROJECT

The air system project multi-agent with mobile earth station information management (MASIM) has as main objective the design, development and prototype testing of an innovative system of multi-agent aerial mini-platforms.

In terms of typology [10], MASIM project is primarily a manufacturing project (air mini-platforms), but it includes elements that place it in the category of IT Projects (it develops and introduces a new software).

The MASIM project contains innovative elements in all systems and components and integrates the latest technologies (microelectronics, ICT, software algorithms and composite materials), which can be an additional source of risk.

Through its architecture design and the implementation of a quality product, the simplicity in operation by operators with medium-level qualifications and attractive proposed MASIM captures product market's attention in completely new niche. MASIMs system efficiency, expressed through unique capabilities in saving lives and properties is the objective of end users.

The risk management for scientific MASIM research project is the process of covering the following steps: setting the context; risk identification; analyzing, evaluating and prioritizing risks; developing and implementing the risk management plan; monitoring initial results and improving the initial plan [1].

Although listed as a separate entities these stages interact with each other and with other areas of project management throughout the projects life cycle.

1. Describing the context

Scientific research is based on two pillars: human resources and finance. Unfortunately for Romania, this structure continues to be a weakened one evens at the opening date of the competition, at least for the following reasons:

- a ratio of researchers reported the total active population of 3.64%, compared to 9.2% in Europe [11];
- the lack of internationally recognized researchers in the field;
- Romania’s negative image of due to academic plagiarism scandals, fake diplomas or imposture of Romanian universities [12]
- Romania had the lowest research and development intensity in the EU, at a value of less than a quarter of the EU average [13];
- Romania has not obtained European funding for any grant from 2007 to 2013 in the context of allocating 10 billion EUROs for research [14].

In such a context, project planning could not exclude the possibility of continuing the underfunding trend of research during the project, with repercussions on the objectives set and on the maintaining of the research teams formed.

2. Risk identification

Once the context being set it moved on to the identification of the potential risks based on the analysis of the source and of the problem and the methods used were: checklist, identifying risks based on objectives and risk identification scenarios. Thus, they were grouped into six categories: financial risks; risks related to the project team/ consortium; risks related to information provision; risks related to the context in which research is carried out; risks related to infrastructure and equipment; risks compromising the investigation due to extreme natural phenomena or anthropogenic factors.

3. Analysis, assessment and risks prioritization

In order to analyze identified risks available information from previous research projects were used to determine which is the probability of occurrence of specified events (table 1) and what could be the impact of the consequences of these events [15].

Table 1. Probability Score

Score	**Describing the probability**		
3	Probable	***High,*** it can occur several times during the projects life cycle	> 0,7
2	Possible	***Potential,*** It can occur at least once during the projects life cycle	0,3 ÷ 0,7
1	Improbable	***Low,*** It occurred at least once in similar projects	< 0,3

The potential impact is evaluated based on criteria drawn from the specific research and innovation activity on a descriptive scale of three levels: major, moderate and minor (tab. 2). Prioritizing risks is in relation to level of risk tolerance, which is periodically reset by the project manager depending on the context of projects internal and external environment.

Table 2. Risk Matrix

		impact				
		Minor	Moderate	Major		
probability		1	2	3	**detection difficulty**	
3	Probable	**1, 2, 3**			3	Difficult
2	Posible	**4, 6, 9**			2	Average
1	Improbable	**12, 18, 27**			1	Easy

A useful approach is that of the three regions of risk assigning (tab. 3):

Table 3. Risk levels

Risk index interpretation		
Unacceptable 12 - 27	**- treatment, regardless of cost**	The probability and the consequences are unacceptable, regardless of the benefits. It requires significant cuts, regardless of cost.
Tolerable 4 - 9	**- reduction is possible, but the abatement costs exceed results**	The probability and consequences are alarming. The risk is acceptable provided the measures for its mitigation are applied to an acceptable level.
Acceptable 1 - 3	**- ensuring that risks remain the same** **- monitoring**	The consequences are very unlikely or insufficiently server to produce concern. The risk is accepted as such. It is nevertheless recommended risk mitigation measures.

- Denied region, when the risk is considered unacceptable, whatever benefits it might bring and where risk treatment is imperative regardless of cost;

- Tolerability region, where the risk is tolerable only if the reduction is impossible or if the costs outweigh the damage reduction;

- Acceptance region, where the level of risk is considered negligible.

Factors affecting decisions on risk tolerance include: identification and analysis of treatment of risk needs; prioritizing risk treatment; determining the activities to be undertaken; determining routes to follow.

Risk ranking is done according to the risk index and in situations of equality the impact is the shootout criterion.

4. Development and implementation of the initial risk management plan

Exits of the risk identification and analysis stage are contained in the original plan risk management. The main elements of the risk management plan include roles and responsibilities; risk categories; defining likelihood and impact; risk tolerances reviewed; risk response planning. In the trigger stage of the MASIMO project the risk management plan presented in Appendix 1 was conducted.

Introduction of the criterion of difficulty of detecting as multiplier of risk index is based on considerations relating to the possibility of risk prevention in the context of the difficulty of identifying its causes.

The risk manager has the responsibility, the authority and the resources to implement the risk management plan. By implementing the plan we have conducted a planned response to risk, which was adapted to the significance of the response and realistic in the context of project risk.

5. *Monitoring results and improving the original plan*

With the execution of the project it starts the actual testing of the transposed planning in terms of change management that occur. Monitoring results include the analysis of activities of residual risks, identifying new risks, upgrade risk management plan and evaluate the effects of it throughout the lifecycle of the project.

CONCLUSIONS

Scientific research projects in aviation have a strong innovation embodied by generating partial solutions to identified problems or needs.

Planning scientific research projects in aviation is an important factor in the success or a sure way to failure. The successful approach of risks in the planning stage is based on: identifying those responsible; building and maintaining an environment of consensus among stakeholders (financier, contractor, partners, beneficiaries); identify tools and techniques of risk management; developing strategies for risk reduction.

Plans and risk management strategies are monitored and reviewed throughout the projects life cycle and project management ensures that any amendments are applied.

The risk in a research-innovation project is inevitable and accentuated by the paradox that it has variable costs (which depend on the chosen solution) and fixed benefits (given the purpose and objectives). Conducting such a project is based on certain resource consumption, and future estimates (eg. Technological or fiscal policies), which induces a state of uncertainty of project management when determining the best option.

Risk management in scientific research projects associated with aviation becomes extremely important for all stakeholders: the donor – by identifying the balance between project results and financial resources allocated; the managers – by improving decision-making for targeting; the project team – by identifying sources of risk and approach solutions; the beneficiaries – by the contribution to meeting the needs and adding value to the investments.

AKNOWLEDGMENT

This work was accomplished through the Partnerships Program in priority fields - PN II, developed with the support of MEN-UEFISCDI, PN-II-PT-PCCA-2013-4-1349, MASIM project no. 255/2014.

REFERENCES

[1] A. Bârgăoanu, *Managementul proiectelor. Curs*, „David Ogilvy" National School of Political and Administrative Studies 2004. Available on: http://www.umfiasi.ro/masterate/Suporturi%20de%20curs/Facultatea%20de%20Bioinginerie/Managementul%20proiectelor/Managementul%20proiectelor%20Bargaoanu.doc.

[2] J. Schuyler, *Risk and Decision Analysis in Projects* (Cases in project and program management series), Project Management Institute, Pennsylvania, Newton Square, 2001.

[3] Z. Kremljak, C. Kafol, *Types of Risk in a System Engineering Environment and Software Tools for Risk Analysis*, 24th DAAAM International Symposium on Intelligent Manufacturing and Automation, 2013. *Procedia Engineering* 69 (2014) 177 – 183.

[4] MITRE, *Risk Identification*, September 2013. Available on: http://www.mitre.org/publications/systems-engineering-guide/acquisition-systems-engineering/risk-management/risk-identification.

[5] C. Cioaca, Qualitative Risk Analysis Methods In Aviation Projects, *Journal of Defense Resources Management*, No. 1(2), 2011.

[6] T.G. Flouris, D. Lock, *Managing Aviation Projects from Concept to Completion*, Ashgate Publishing, 2009.

[7] S.E. Portny, *Project Management for Dummies*, Wiley Publishing, Inc. 2001.

[8] C. Opran (coord.), S. Stan, S. Năstasă, B. Abaza, *Managementul proiectelor*. Available on: www.comunicare.ro, Bucureşti, 2002.

[9] C. Igor, G. Cuciureanu, *Riscurile ce intervin în procesul de realizare a proiectelor de cercetare-dezvoltare în Republica Moldova*. Analiza opiniei cercetătorilor (directorilor de proiecte). Available on: http://idsi.md/files/file/publicatii/Riscurile%20ce%20intervin%20in%20procesul%20de%20realizare%20a%20proiectelor%20de%20cercetare_dezvoltare%20in%20RM.pdf.

[10] T.G. Flouris, D. Lock, *Aviation Project Management*, Ashgate Publishing, 2008.

[11] I. Corina, Golgota cercetării românesti: cercetătorii români nu cedează si cer sprijin Uniunii Europene, Interviu ziare.com, 2013. Available on: http://www.danbadea.net/2013/04/29/golgota-cercetarii-romanesti-cercetatorii-romani-nu-cedeaza-si-cer-sprijin-uniunii-europene/.

[12] M. Sergiu, Europa a oferit 10 miliarde euro pentru cercetare. România, singura ţară care nu a atras nici un euro. Interviu Petre Badica, 2014. Available on: http://www.romanialibera.ro/special/investigatii/europa-a-oferit-10-miliarde-euro-pentru-cercetare--romania--singura-tara-care-nu-a-atras-nici-un-euro--ungaria-%E2%80%93-90-milioane--germania-%E2%80% 93-1-5-miliarde-325518.

[13] National Conference of Research and Innovation (CNCI), *Rolul cercetării si inovării în societatea modernă*, 7-9 Noiembrie 2012, Bucuresti. Available on: http://cnci.ancs.ro/raport_conferinta.pdf.

[14] P. Badica, Europa a oferit 10 miliarde euro pentru cercetare. România, singura ţară care nu a atras nici un euro. Available on: http://www.romanialibera.ro/special/investigatii/europa-a-oferit-10-miliarde-euro-pentru-cercetare--romania--singura-tara-care-nu-a-atras-nici-un-euro--ungaria-%E2%80%93-90-milioane--germania-%E2%80%93-1-5-miliarde-325518.

[15] D.F. Cooper, S. Grey, G. Raymond, P. Walker, *Project Risk Management Guidelines. Managing Risk in Large Projects and Complex Procurements*, John Wiley & Sons Ltd, 2005.

Risk management plan

Risk ID	Risk description	P.	I.	D.d.	Risk score	Risk control measures	Responsible
1. Financial risks							
1.1.	Reducing or stopping funding	3	3	1	**9**	Continuous monitoring of resource consumption and budget corrective action is taken when necessary. Identification of several alternative technologies or constructive. Review the expectations of the parties involved. A structured review of the project documentation, including plans, objectives or previous records project.	Project director
1.2.	Not providing funding for certain expenditure items	2	2	1	**4**		Project director
1.3.	Failure funding deadlines	2	3	1	**6**		Project director
1.4.	Erroneous estimate of the project cost	1	3	2	**6**		Project director Project leaders Economic leaders
2. Risks related to project team / consortium							
2.1.	Lack of qualified specialists for project execution	2	2	1	**4**	All partners must provide qualified human resources and provide specialized training.	Project director
2.2.	Issues related to hiring and keeping young professionals	1	2	1	**2**	Using the platform for publishing project vacancies.	Project director Project leaders
2.3.	Breaking the rules of good conduct in research	1	2	1	**1**	Promoting cooperation and collegiality in order to facilitate the exchange of ideas, mutual constructive criticism and mutual verification of results.	Each researcher Ethics committee
2.4.	Compromise of classified information	1	2	2	**4**	Allowed access to classified information with respect for the principle of "need to know" basis only to persons who hold valid security clearances or access authorization.	Each researcher
2.5.	Breach of confidentiality on intellectual property	1	1	1	**1**	The partners have negotiated an agreement on intellectual property rights, in accordance with national and European regulations, which came into	Project director Project leaders

						force with the actual start of the project.	
2.6.	The multidisciplinary nature of partners	2	2	2	**8**	Project management is structured to ensure ease of communication between technology providers and users, monitoring project progress and developments.	Project director Risk management learders
2.7.	Underestimating the effort required to complete each project	3	2	3	**18**	Continuous monitoring of resources and taking corrective actions when necessary.	Project leaders
2.8.	Underestimating the time needed to produce results	3	2	3	**18**	To ensure the successful completion of the work and the validity of their results, each work package contains necessarily planning, validation and quality assurance.	Project leaders
2.9.	Getting technical results of lower quality than projected	2	2	3	**12**	A technical team with the participation of project responsible will review the technical aspects of the project on each work package. This ensures that the project remains focused on the initial technical objectives. The results are revalued throughout the project life cycle to ensure their validity in terms of end user needs.	Project director Project leaders Scientific leaders
3. Risks related to information provision							
3.1.	Lack of or reduced quality of data needed	2	2	2	**8**	Including in the consortium partner institutions with experience. Free access for researchers to databases of scientific publications in the workplace through research organization to which they belong or a partner organization.	Scientific leaders
3.2.	Difficulties in obtaining the necessary data	2	1	1	**2**		Scientific leaders
3.3.	Limited access to current scientific results	1	2	3	**6**		Scientific leaders
4. Risks related to the context in which research takes place							
4.1.	Incomplete and inadequate	2	2	3	**12**	Compliance of the European Aviation	Scientific leaders

	legislation in the field					Safety Agency regulations on: certification of aircraft and operators, special authorization (under Art. 8 of the Chicago Convention).	
4.2.	Slow procedure for conducting the procurement process	2	2	1	**4**	Establish in advance the timing of the whole process. Creating and updating a database of systematic observation and monitoring market development trend. Choosing the right procedure for awarding a public procurement contract.	Economic leaders
4.3.	Difficulties in information flow between partners	3	3	3	**27**	Establishing communication strategy: the main way of transmitting information will be official documents, meetings, telephone conferences, e-mail sites. The project defines structured management processes. Based on these, decisions and procedures for resolving conflicts will be reported in a qualitatively and will be approved later.	Project manager Project leaders
4.4.	Lack of support from decision makers	1	3	3	**9**	Inviting decision-makers at events dedicated to disseminating the results of the milestones of the project.	Project manager Project leaders
4.5.	Delay in obtaining the approvals, permits and certificates needed	2	3	2	**12**	Assigning responsibilities and following of the algorithm for obtaining approvals, permits and certifications in accordance with regulations.	Assistant manager
4.6.	Communication problems with end users and market	2	3	3	**18**	Ensuring interaction with target groups through	Project director Project leaders

						communication networks of all partners.	
5. Risks related to the infrastructure and equipment							
5.1.	Unsatisfactory infrastructure and research conditions	1	3	2	**6**	An inventory of equipment, technologies and information systems existing in the partners involved. Improving institutional cooperation.	Scientific leaders
5.2.	Lack of modern testing equipment	2	3	2	**12**		Scientific leaders
5.3.	The disposal of existing equipment	3	3	1	**9**	The Technical Commission will review technical aspects of the project and control activities and technical directions.	Scientific leaders
6. Risks to discredit the research due to extreme natural phenomena							
6.1.	The occurrence of major force events (earthquake, fire, flood, war, terrorist attack)	1	2	2	**4**	Partner claiming force majeure has the obligation to notify other members of the consortium within five (5) days and also inform them of the date of cessation of the situation. Identification of variants of further research by overlapping responsibilities and completion of the research team. Regularly updating security plans for mitigating the consequences.	Project director Project leaders Risk management leaders
6.2.	Loss of research documentation for technical reasons	2	3	1	**6**	Making rescue operations (backup) at the end of each stage. The possibility of allocating funds for data recovery operations.	Assistant manager

SYNTHESIS AND STUDY OF THE MATHEMATICAL MODEL OF A TRICOPTER

Martin KAMBUSHEV, Stefan BILIDEROV, Yavor VARBANOV

Faculty "Aviation", Dolna Mitropolia, Bulgaria (m_kambushev@yahoo.com, biliderow_ss@yahoo.com,yavor_office@mail.bg)

DOI: 10.19062/2247-3173.2016.18.1.19

Abstract: *In this report is synthesized and studied the mathematical model of a tricopter. The stabilization of a tricopter in angular velocity and angle is presented.*

Keywords: *tricopter, mathematical model, stabilization*

1. INTRODUCTION

Regardless of the various types of classification of unmanned aerial vehicles which we have been witness to in the last years, they are divided into two basic kinds – airplanes and helicopters. The helicopter class incorporates the so-called copters.

The application of copters has so far been limited by the capacity of their batteries and by the payload of the different configurations.

One useful configuration is that of the tricopter, which can be seen as quite exotic in terms of steering. For the purposes of this research the cheapest possible design has been selected, where all the three rotors rotate in the same direction. This design features the use of a tilting tail rotor to counterbalance the summary reactive moment of the whole tricopter. The construction schematics of the tricopter that has been developed is shown on Fig. 1.

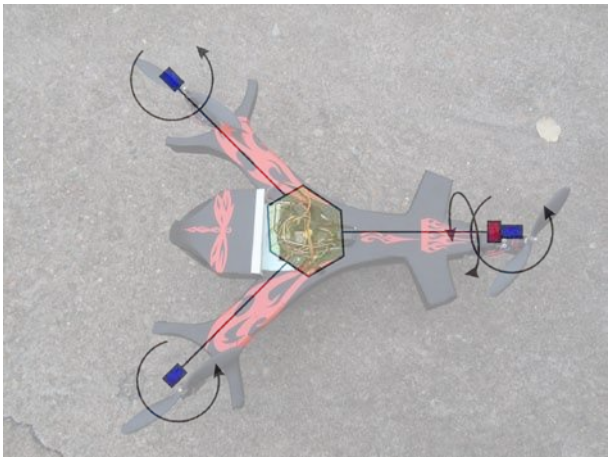

FIG. 1. Construction schematics of the tricopter

The development of computer technology in its two main spheres – hardware and software, made it possible for a large array of new technologies to be implemented in the process of developing and using unmanned aerial vehicles.

Many of these technologies have originated from various universities, for example the Arduino series of controllers and Raspberry Pi class of computers.

Their software base has been developed using primarily Open Source platforms, which makes them easily accessible when designing unmanned aerial vehicles' automatic control systems.

There is a rule regarding the unmanned aerial vehicles' automatic control systems which states that the closer the mathematical model incorporated in the control algorithms is to reality, the more precise the flight control will be.

Following that rule a mathematical model of a tricopter based on a physical model of one such aircraft is presented and studied in the current paper. Stabilization along the axes of the tricopter's body-fixed coordinate system based on the angular velocities and the angle of deflection of the tail rotor is viewed. Fig. 2 depicts the tricopter in flight.

FIG. 2. The studied tricopter in flight

2. SINTHESIZING A COMPLETE MATHEMATICAL MODEL OF A TRICOPTER

The process of synthesizing a working mathematical model of a tricopter passes through several stages. First, the limitations which have to be considered while developing the model are defined. A tricopter is defined as a rigid body with 6 DOF. Thus, the Euler differential equations for quantity of movement and kinetic moment alteration are used for the development of the mathematical model of the tricopter [3]:

$$m.\frac{d\vec{V}}{dt} = \sum \vec{F} \tag{1}$$

where: $\frac{d\vec{V}}{dt}$ is the absolute acceleration in a stationary coordinate system;

$\sum \vec{F}$ is the sum of the external forces acting on the tricopter.

$$\frac{d\vec{K}}{dt} = \sum \vec{M} \tag{2}$$

where: $\frac{d\vec{K}}{dt}$ is the kinetic moment; $\sum \vec{M}$ is the summary moment along the axes of a body-fixed coordinate system.

Through equations (1) and (2) is described the forward and rotary motion of a tricopter. In Fig. 3 is shown the distribution of the external forces and moments acting on a tricopter.

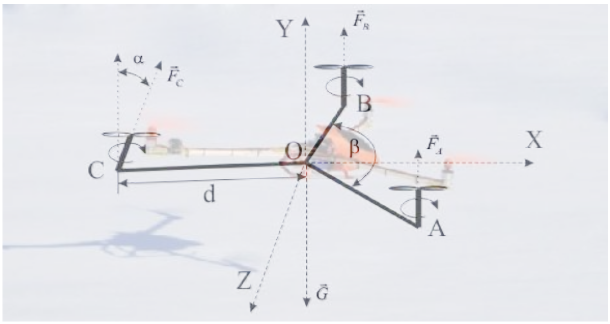

FIG. 3. Diagram of the forces and moments acting on the tricopter

Projecting the external forces from equation (1) along the axes X, Y, Z of the tricopter's body-fixed coordinate system the equations in (3) are worked out, which define the forward movement of the vehicle.

$$\begin{aligned}
&\sum F_x = -G.\sin(\ );\\
&\sum F_y = F_A + F_B + F_C.\cos(\alpha) - G.\cos(\gamma).\cos(\ );\\
&\sum F_z = F_C.\sin(\alpha) + G.\sin(\gamma).\cos(\ ).
\end{aligned} \tag{3}$$

where: F_A, F_B, F_C is the thrust of the engine-propeller system for each of the tricopter's arms; ϑ, γ, ψ are the angles of roll, pitch and yaw; α is the angle of deflection of the tail rotor.

Each of the forces or a combination of the three forces of thrust generated by the tricopter's engines define moments along the axes of the fixed body coordinate system.

Moreover, the propellers of the tricopter generate reactive moments due to the reaction of the air to their rotation.

In reference to Fig. 3, in the equations of the moments along the axes X, Y, Z of the fixed body coordinate system we have the correlations (4):

$$\begin{aligned}
&\sum M_x = (F_A - F_B).\sin\left(\beta/2\right).d;\\
&\sum M_y = F_C.\sin(\alpha).d - \left(M_{A_{yp}} f(F_A) + M_{B_{yp}} f(F_B) + M_{C_{yp}} f(F_C, \cos(\alpha))\right);\\
&\sum M_z = (F_A + F_B).d.\cos\left(\beta/2\right) - F_C.\cos(\alpha).d + M_{C_{zp}} f(F_C.\sin(\alpha)).
\end{aligned} \tag{4}$$

where: $M_{A_{yp}}, M_{B_{yp}}, M_{C_{yp}}, M_{C_{zp}}$ are the reactive moments generated by the propellers and projected along the axes of the fixed body coordinate system; β is the angle between the arms of the tricopter; d is the length of the tricopter's arm.

The differential equations of the movement of the tricopter are worked out by projecting equations (1) and (2) along the axes of the fixed body coordinate system, which give us the linear and angular velocities in this coordinate system. The forces and moments form equations (3) and (4) constitute the right side of the equations.

The three equations of Euler defining the relation between the angular velocities and the angles of roll (γ), pitch (υ) and yaw(ψ) are used to determine the position in space of the tricopter in relation to a stationary coordinate system. The differential equations are as follows (5):

$$\begin{aligned}
\frac{d\vartheta}{dt} &= \omega_y.\sin\gamma + \omega_z.\cos\gamma \\
\frac{d\gamma}{dt} &= \omega_x - tg\vartheta.(\omega_y.\cos\gamma - \omega_z.\sin\gamma) \\
\frac{d\psi}{dt} &= \frac{\omega_y.\cos\gamma - \omega_z.\sin\gamma}{\cos\vartheta}
\end{aligned} \tag{5}$$

To solve the equations for the movement of the tricopter, for the forces of thrust (F_A, F_B, F_C) and the reactive moments $(M_{A_p}, M_{B_p}, M_{C_p})$ are used the results obtained in (1).

A system of nine differential equations describing the model of the position in space of the tricopter is obtained after the substitution of expressions (3) and (4) in equations (1) and (2) and the addition of the equations from (5) to the system. This is the system of equations (6).

The model of the tricopter's position in space presented with these equations is designed as an S function of a Simulink diagram in a MATLAB-SIMULINK environment.

What is convenient about this method is that it extends Simulink capabilities through the introduction of an additional non-standard block which can be created using Matlab, C, C++ or Fortran. Next, the function is compiled in a MEX file and is dynamically linked with MATLAB execution engine, thus, enabling the S function to be automatically loaded and executed.

$$m.\left(\frac{dV_x}{dt} + \omega_y.V_z - \omega_z.V_y\right) = -G.\sin$$

$$m.\left(\frac{dV_y}{dt} + \omega_z.V_x - \omega_x.V_z\right) = F_A + F_B + F_C.\cos\alpha - G.\cos\gamma.\cos$$

$$m.\left(\frac{dV_z}{dt} + \omega_x.V_y - \omega_y.V_x\right) = F_C.\sin\alpha + G.\sin\gamma.\cos$$

$$I_x.\frac{d\omega_x}{dt} + (I_z - I_y).\omega_y.\omega_z = (F_A - F_B).d.\sin\left(\frac{\beta}{2}\right)$$

$$I_y.\frac{d\omega_y}{dt} + (I_x - I_z).\omega_z.\omega_x = F_C.\sin\alpha.d - \left(M_{A_{yp}}.f(F_A) + M_{B_{yp}}.f(F_B) + M_{C_{yp}}.f(F_C.\cos\alpha)\right)$$

$$I_z.\frac{d\omega_z}{dt} + (I_y - I_x).\omega_x.\omega_y = (F_A + F_B).d.\cos\left(\frac{\beta}{2}\right) - F_C.\cos\alpha.d + M_{C_{zp}}.f(F_C.\sin\alpha)$$

$$\frac{d}{dt} = \omega_y.\sin\gamma + \omega_z.\cos\gamma$$
$$\frac{d\gamma}{dt} = \omega_x - tg\ .(\omega_y.\cos\gamma - \omega_z.\sin\gamma) \quad (6)$$
$$\frac{d\psi}{dt} = \frac{\omega_y.\cos\gamma - \omega_z.\sin\gamma}{\cos}$$

In Fig. 4 can be seen the S function of the system of equations (6) presented in a Simuklink diagram

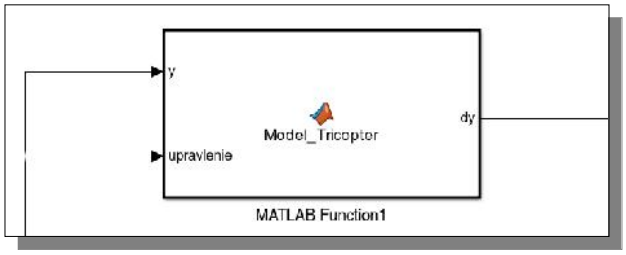

FIG. 4. The S function presented as a simulink diagram

After linearizing the non-linear model, the system's intrinsic numbers equal zero which means that the model is on the border of stability.

In Fig. 5 and Fig. 6 are presented the graphs showing the changes in the angular velocities along the axes of the fixed body coordinate system and the angles of roll, pitch and yaw.

Fig. 7 illustrates the movement of the tricopter with an open-loop control system.

In order to control the tricopter it is necessary for the open-loop system to be closed by means of a feedback connection. The closed-loop system is illustrated in the Simulink diagram in fig. 8[4].

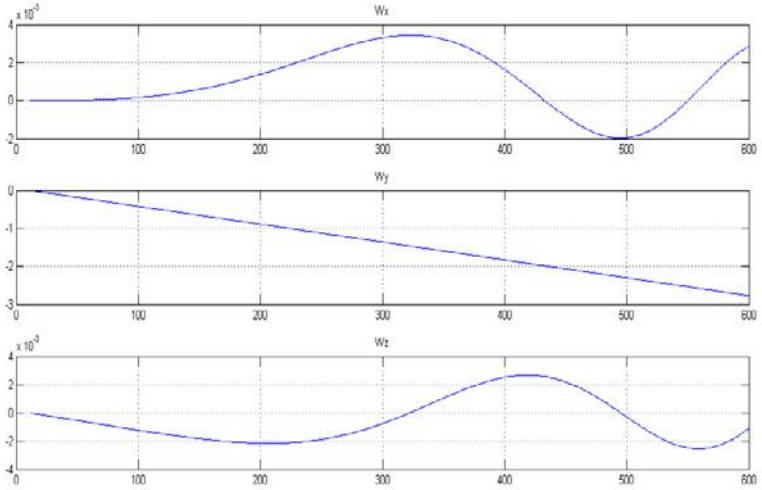

FIG. 5. Changes in the angular velocities of an open-loop system

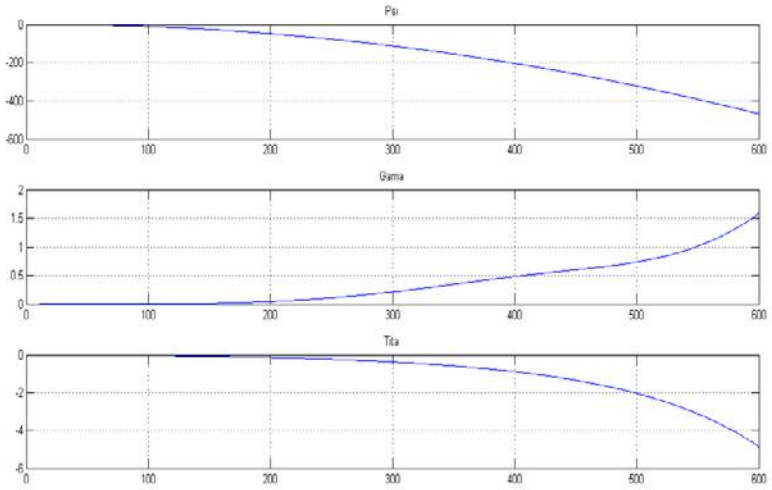

FIG. 6. Changes in roll, pitch and yaw angles of an open-loop system

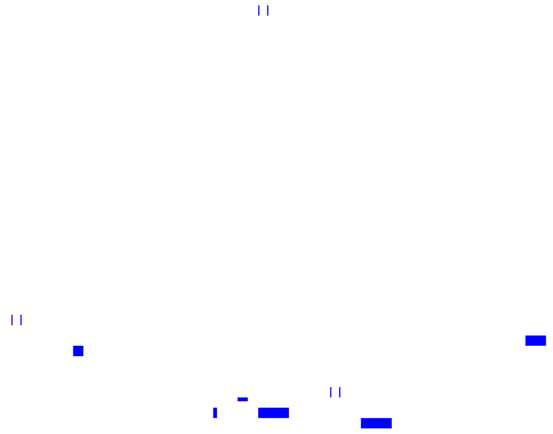

FIG. 7. Spacial movement of an open-loop system

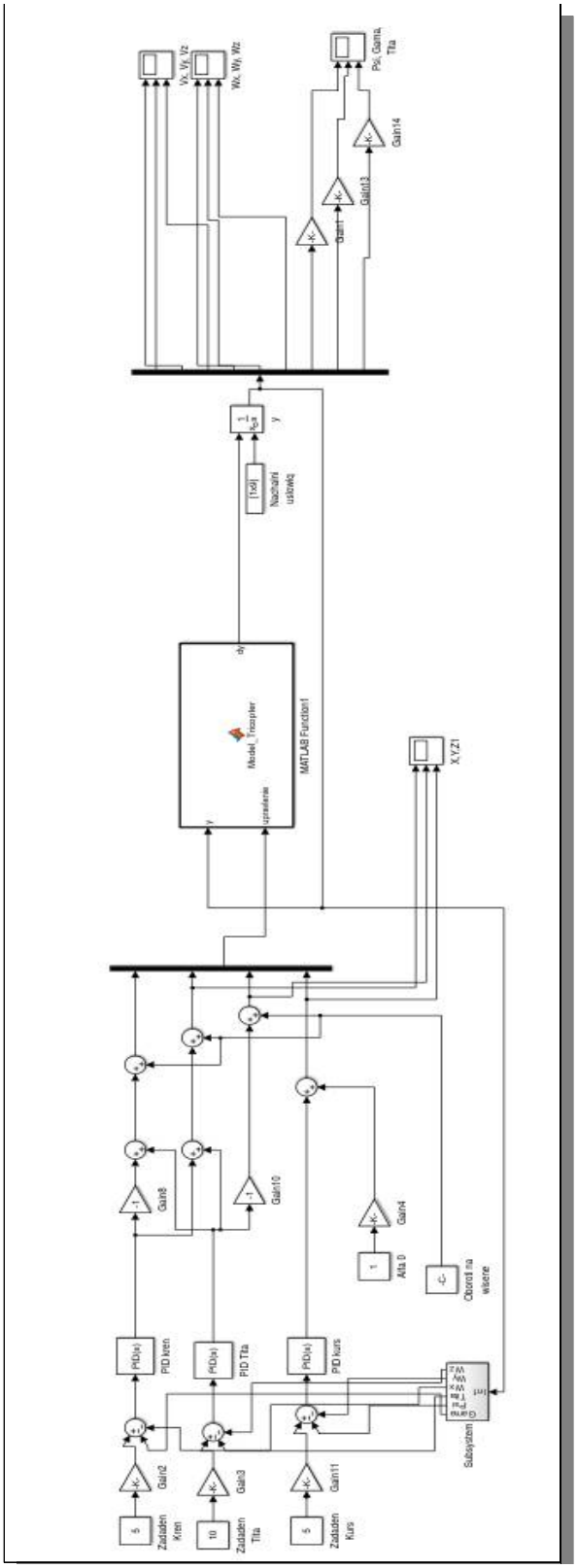

FIG. 8. A simulink diagram of the model with a feedback connection closed-loop system

The case of PID control is studied, using part of the condition vector in the feedback connection [5]. In figures 9 and 10 are shown the changes in the angular velocities along the axes of the fixed body coordinate system and in the roll, pitch and yaw angles, and the picture in fig. 11 shows the tricopter in flight.

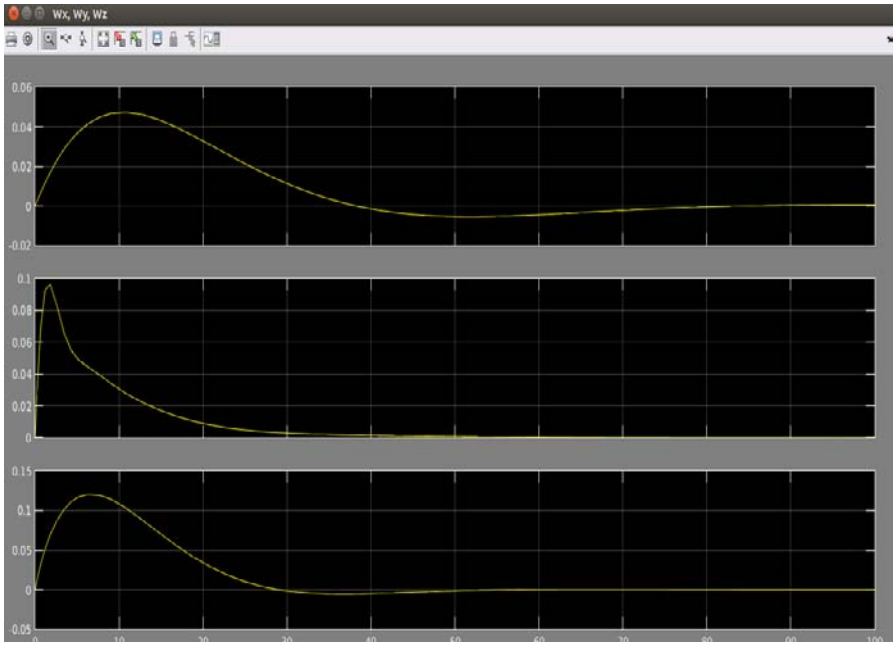

FIG. 9. Changes in the angular velocities of a closed-loop system

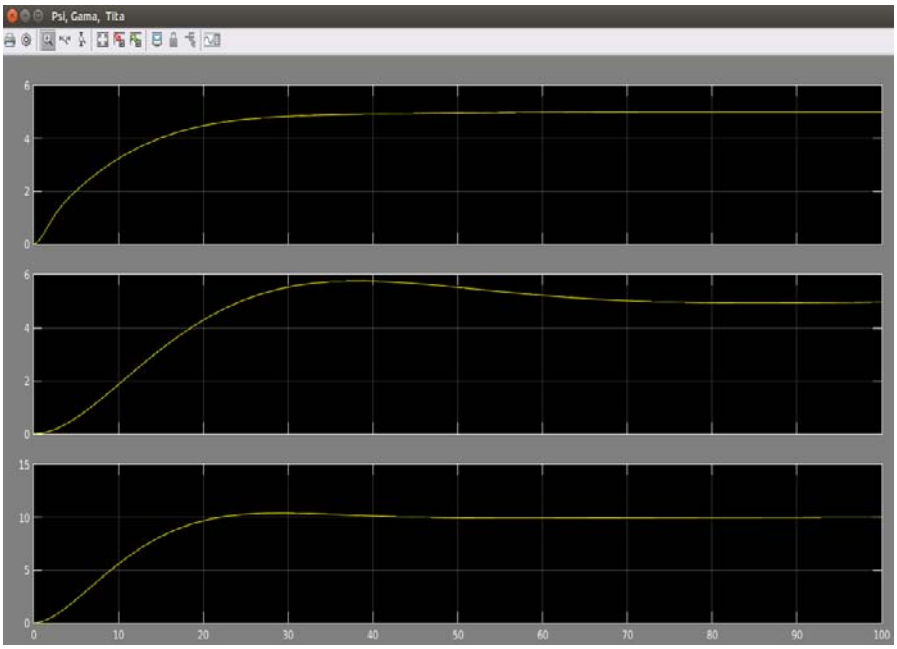

FIG. 10. Changes of roll, pitch and yaw angles of a closed-loop system

FIG. 11. The tricopter in flight

3. CONCLUSIONS AND ACKNOWLEDGEMENTS

In the current paper is developed a mathematical model of the spatial movement of a tricopter.

The open-loop system model is on the border of stability. The closed system model uses PID regulator.

After closing the system it becomes controllable, and the PID regulator's coefficients are automatically adjusted in the MATLAB-Simulink environment.

It can be clearly seen from the results that the PID regulator stabilizes the angular velocities, helping to achieve the predefined angles of divergence.

REFERENCES

[1] Biliderov S.S., Kambushev M.M. *Evaluation of experimentally obtained characteristics of an engine-propeller system for small unmanned aerial vehicles.* Dolna Mitropolia, 2013;
[2] Veleva E., Karakoleva S. *Numerical methods practicum with Matlab*. University of Rousse, Rousse, 2004;
[3] Lisenko N.M. *Dynamics of flight*. Sofia, 1977;
[4] Stevens B.L., Lewis F. L. *Aircraft control and simulation.* John Wiley&Sons, 2003*;*
[5] Tewari A. *Modern control design*. New York, John Wiley&Sons, 2002;

REMOTELY AND PILOTED AIRCRAFT SYSTEMS / LAW AND POLICIES

LEACH IN MULTI-AGENT HYBRID ROBOT ARCHITECTURES

Andrei-Mihai LUCHIAN[*], Cristian-George CONSTANTINESCU[**]

[*]Transilvania University, Brașov, România, [**]Air Force Academy "Henri Coandă", Brașov, România

DOI: 10.19062/2247-3173.2016.18.1.20

Abstract:*In the last decade research in wireless sensor networks has drawn attention due to the advantage regarding surveillance of phenomena's in different backgrounds. The life extension of networks, scalability and balance of recharging are just a few important parameters for wireless sensor networks. Grouping the nodes is an efficient technique to obtain such results. In this paper we will introduce an algorithm for energy efficiency in node groups based on a LEACH protocol. LEACH (Low Energy Adaptive Clustering Hierarchy) is one of the most known solutions of node grouping in the last decade being proposed for any type of wireless sensor networks. LEACH protocols use TDMA (Time Division Multiple Access) based on a MAC protocol which optimizes the energy consumption. The proposed protocol will be used in a simulation program. As we can observe in the accompanying results, there is a slight reduction of energy consumption compared to the classical protocols.*

Key words: *WSN (Wireless Sensor Networks), LEACH protocol, lifetime extension of networks*

1. INTRODUCTION

Routing in WSN architectures represents a though challenge due to its distinctive characteristic: ad-hoc networks and cellular networks.

Over time there had been a lot of proposals regarding the algorithms due to its advantages in WSN applications and architectures.

Based on theadopted network, the protocols for WSN can be classified as:

- Flat network routing
- Hierarchical network routing
- Location-based network routing. [1]

Flat network routing is characterized by the use of all the nodes to fulfill the location and routing requirements.

Hierarchical network routing divides the network into groups to achieve scalability and energy efficiency. The most known version of it is LEACH. [2]

Location-based network routing uses the localization data of the nodes to commute the route. The location information can be provided using Global Positioning System (GPS), such a system being attached to each node.

While creating the topology of a network we can observe the fact that the routing setting process for a WSN is influenced by energy consumption.

LEACH protocols can reduce the alert because it doesn't need information regarding the location of the node or ways to manage the access point into the node. In doing so we reduce the energy that is used by a node and increasing its life support. We must point out that there are still issues regarding the location of mobile objects. Thus a new demand has appeared, protocols must support mobile nodes.

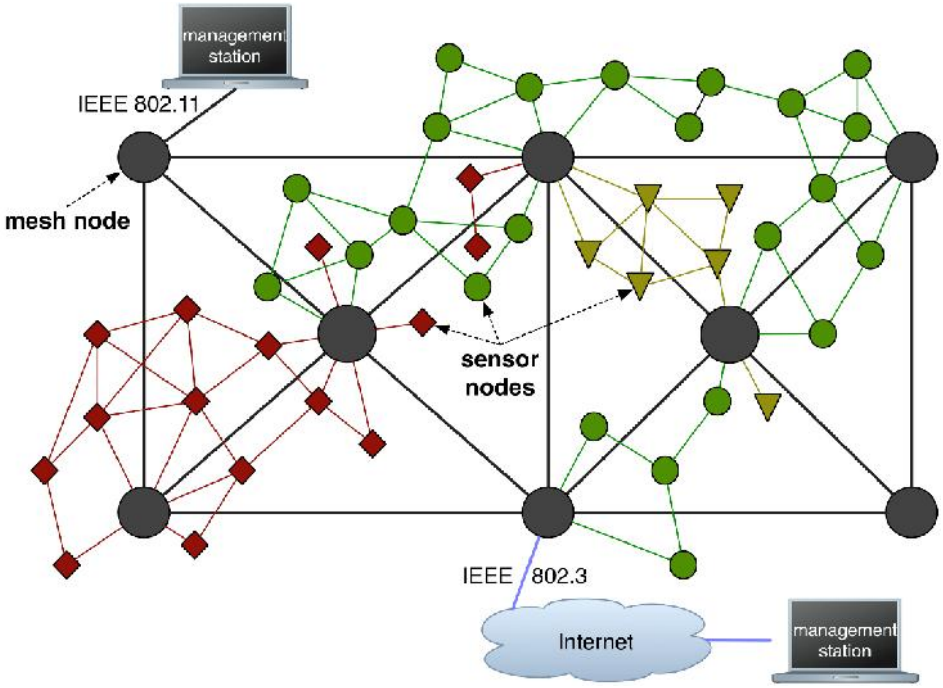

FIG. 1. WSN network structure [3]

2. LEACH

Node grouping is a hierarchical method for architectural structures. Using this method,nodes can streamline the radio resources and extend the lifetime of the batteries. Inside a group aggregations and fusions take place so it can reduce the volume of information that is transmitted to the cluster head. [2]

LEACH: The main idea is to create a group of nodes with sensors that are based on the signal power and use of the main node as a router so it can transfer data through the other nodes. This is a dynamic mechanism. At the beginning of the process, the group cluster head is chosen randomly based on the energy consume. Then each node with a sensor called “n” generates a random number between 0 and 1 and this number is being compared with a well-established limit called “T(n)”. If the random number is lower than T(n), that would mean that the node will become the cluster head in this process. If not, it will become a simple node in the group. T(n) is defined as [2], [4]:

$$T(n) = \frac{P}{1 - P\left(r \bmod \frac{1}{P}\right)} \qquad \forall n \epsilon G \qquad (1)$$

P=is the probability of cluster heads over all nodes in the network;

r=the number of rounds of selection;

G= is the set of nodes that are not selected in round $\frac{1}{P}$

After they become cluster heads, they send a message to the other nodes informing them who are the cluster heads. The other nodes will select the next cluster heads depending on the power of the signal from the message received. For each round the clusters heads are changed so it can equally disperse the energy consume, prolonging the lifetime of all nodes in this way. [4]

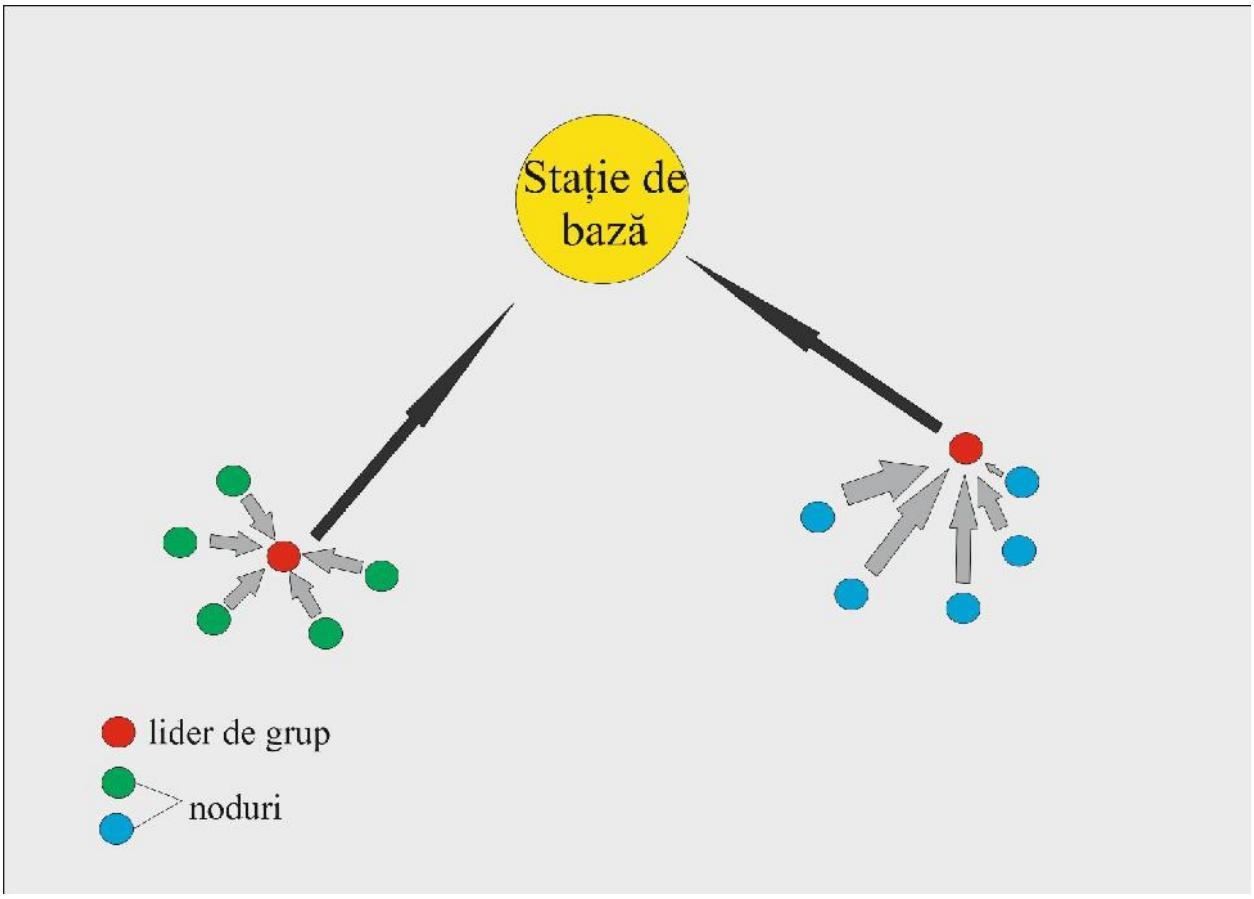

FIG.2. LEACH scheme

3. LEACH IN UAS

3.1. HISTORICAL DEVELOPMENT

In complex media software the airship and soil equipment must communicate in real time. Historically speaking, the designers of these systems have developed them as independent systems connected through LEACH-type complex, with a system management program included. Recently, air and ground platforms have become the main pillar in data transmission. Image intelligence offers clean information through data-flow, thus enhancing the evolution of the system.

UAV's require a tight connection with ground platforms. In the last decade, developers had made huge investments in data link and protocols. This fact influenced the range and time of flight, sensors, and the functionality of the system. There are a lot of widgets that offer data transmission, but data-links aimply create a route for an image signal and another for radio communications between air and ground platforms.

Having LEACH connections, the network can extend to an end-to-end signal which has a coherent architecture. Using end-to-end design developers could access information from any node, thus simplifying their information distribution. Of course, by combining different types of platforms for different types of missions the developers have stumbled upon new demands.

3.2. UAV-UGV

The composition of the UAV-UGV systems can be divided into three subsystems: air platform, ground platform and command center. Each subsystem has its own challenges.

3.2.1. Air and ground platforms

UAVs and UGVs are limited due to the operating environments, where battery resistance quality and the weight of the aircraft can be decisive factors. These subsystems must contain a flight computer, WSN, load management, and a weapon system if it is possible. The components will be interconnected in a variety of serial-buses and networks having a live operating system capable of real time data transmission.

3.2.2. Command center

Through assimilation this system is alike with a classic work station. The operating system (OS) is LINUX or WINDOWS with a diversity of applications for air and ground platforms, and with digital review of the data acquired. These three subsystems must contain data-link connections separate from the communication links so that the data-flow will not be affected.

3.2.3. Image Intelligence UAS

Of course, for a good functionality the applications of the system must work together and not as individual software's. Within a large range of missions, it is impossible to think that a single application can handle all the objectives. A single system was used in the past for a variety of missions, thus leading to large expanses regarding maintenance and software creation.

Nowadays, military architectural companies have upgraded the classical UAV, UGV systems in US (unmanned system) systems or combinations of platforms which can be used in a large diversity of missions. The advanced optic systems allowed these platforms to work in any weather conditions and in any environment. The issues of these systems are mainly the disconnections of the wireless satellite connection due to electromagnetic interference. Electromagnetic interference appears because of frequency similarity, thus reducing the imagery of the platforms in missions, resulting mistakes or even failure due to insufficient information.

3.2.4. Numerical simulation of LEACH in UAS

We realized a numerical simulation for a bunch of LEACH connections inside UAS systems, especially for a WSN in an UAS system.

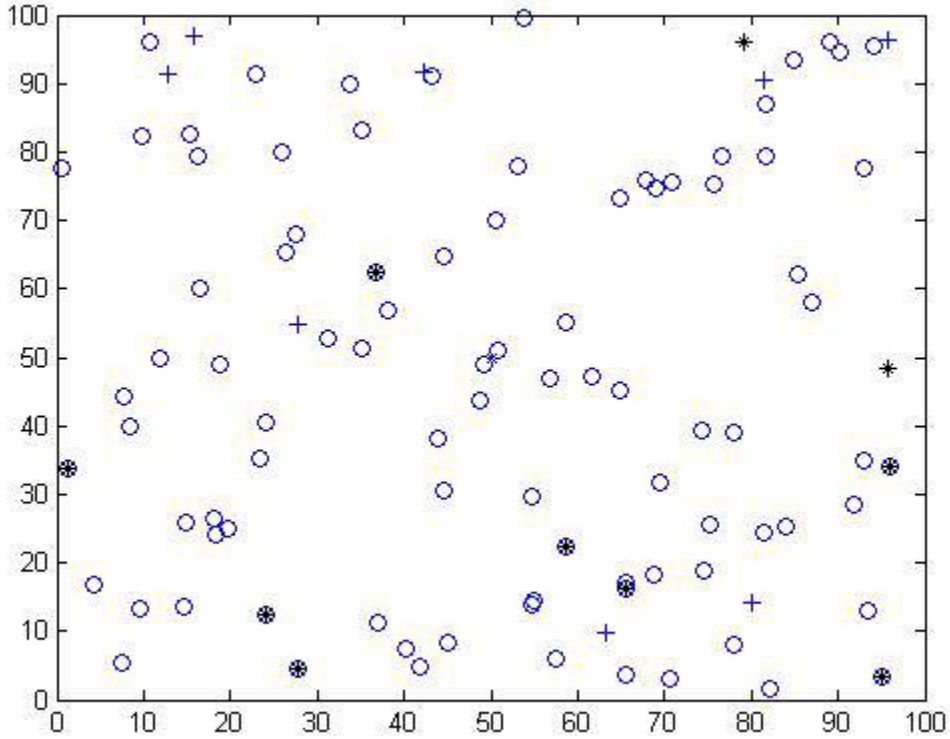

FIG. 3. LEACH in UAS

The nodes closer to the base are the first nodes that die. The further a node is from the base, the greater chances for it to die in case we start a direct transmission between the nods. The sensors that remain alive (simple circles) and the nodes that die (colored circles) have been through different stages of data transmission, so that we can find their weaknesses, but also to find the cluster heads (group leaders) which are symbolized with "+". [7], [8], [9], [10].

4. CONCLUSSIONS

LEACH protocols are appropriate for WSN when all the sensors from the nodes are identical and are charged with the same quantity of energy. Thus, each node knows the rate of energy consumption, being capable of controlling the rate transfer and distance. All the "communication ways" in the nodes are identical.

Any node can communicate with any other node, even if this node is a base station.

The base station is fixed point, which is far away from the wireless networks. Thus, we can ignore the energy consumption of the base station, assuming that the energy supply is from an external network and it has enough energy for its functionality. [5], [6]

Each node has data for transfer at each process.

The nodes with sensors are not static points (fixed points). They are in continuous movement.

REFERENCES

[1] Lu, Ye Ming and Vincent W. S. Wong, *"An energy-efficient multipath routing protocol for wireless sensor networks*" research articles. Int. J.Commun. Syst., 20(7):747--766, 2007.

[2] W. Heinzelman, A. Chandrakasan and H. Balakrishnan, *"Energy-efficient communication protocols for wireless microsensor networks"* Proceedings of the Hawaii International Conference on Systems Sciences, Jan. 2000.

[3] http://home.inf.unibe.ch/~rvs/research/mancom.html

[4] W. Heinzelman, A. Chandrakasan and H. Balakrishnan, *"An application-specific protocol architecture for wireless microsensor networks"*, IEEE Transactions on Wireless Communication, vol. 1, no.4, pg. 660-670, 2002.

[5] T.C. Hou, T.J.Tsai, *"An access-based clustering protocol for multihop wireless ad hoc networks"*, IEEE Journal on Selected Areas in Communication, July 2001

[6] M.Joa-Ng, I.T.Lu, *"A Peer-to-peer Zone-based Two-level link state routing for mobile Ad Hoc Networks"*, IEEE Journal on Selected Areas in Communications, Special Issues on Ad-hoc Networks, August 1999

[7] A. Manjeshwar, D.P. Agrawal, TEEN, *"A protocol for enhanced efficiency in wireless sensor networks"* Proceedings of the 1st International Issues in Wireless Networks and Mobile Computing, San Francisco, CA, April 2001

[8] A. Manjeshwar, D.P. Agrawal, APTEEN, *"A hybrid protocol for efficient routing and comprehensive information retrieval in wireless senson networks"* Proceedings of the 2nd International Issues in Wireless Networks and Mobile Computing, Ft. Lauderdale, FL, April 2002

[9] P. Agwarwal and C. Procopiuc, *"Exact and approximation algorithm for clustering"*, in Proc. 9th Annual. ACM-SIAM Symp. Discreet Algorithms, Baltimore, MD, January 1999

[10] Prisacariu V., Cîrciu I., Cioacă C., Boşcoianu M., Luchian A., *Multi aerial system stabilized in altitude for information management*, Review of the Air Force Academy, ISSN 1842-9238; e-ISSN 2069-4733, 3/2014, p89-94

KINEMATIC ANALYSIS FOR MULTI-COPTER UAV LANDING GEAR

Doru LUCULESCU[*], Vasile PRISACARIU[*], Octavian ISĂILĂ[**]

[*]Air Force Academy Henri Coandă, Braşov, Romania (doru_luculescu@yahoo.com, aerosavelli73@yahoo.com), [**]The Training, Study and Research Institute for UVS, ITSC-SVFP, Mediaş, Romania (office@vehiculefarapilot.ro)

DOI: 10.19062/2247-3173.2016.18.1.21

Abstract: *The multi-copter UAV landing gear is used for ground station and shock damping for landings. The materials used in the construction of landing gears are selected by using a simple criterion: minimal mass versus maxim resistance at shocks. Article contains an evaluation of a kinematics mechanism quadrilateral landing gear is mounted on a multicopter.*

Keywords: *UAV, multi-copter, landing gear, mechanism, kinematic analysis*

Symbols:

n	*The number of elements for the mechanism, including fixed elements*	p	*The number kinematic couplings of the mechanism*
m	*Movement restrictions*	c_i	*Constrain level for kinematic couple*
q	*Number of independent outlines of the mechanism*	b	*The number of free space for the gradations that are used (mobility number)*
b_j	*The number of free space for the gradations used in the closed chain*	f_i	*The connectivity of kinematic couple (the number of free space for the gradations)*

1. INTRODUCTION

The multi-copter UAV's are one of the most stable and fast unmanned aerial vehicles which offers a large applicability in all types of missions, such as: data acquisition, registration, direct transmissions, and flight at low altitude, all at a low cost. The actual development rate proves the fact that they are especially used in data acquisition due the variety of sensors on it. [3, 7].

The imagery sensors are usually mounted in the center of the aerial vector for a wide range in the field vision. Fixed landing gear does not offer an advantage for the sensor mounted, see figure 1, thus the constructors resorted to retractable landing gear which enhanced data acquisition, see figure 2.

The multi-copter UAV landing gear is used for ground station and shock damping for landings. The materials used in the construction of landing gears are selected by using a simple criterion: minimal mass versus maxim resistance at shocks. Some of the materials used are: duralumin, glass fiber and carbon. The elements for the landing gear could have a pipe or rod shape, with a circular or square section [7].

Looking at the landing gear functions (turnover, station and shock damping) we will present a series of data and an analysis of a landing gear for a UAV type multi-copter.

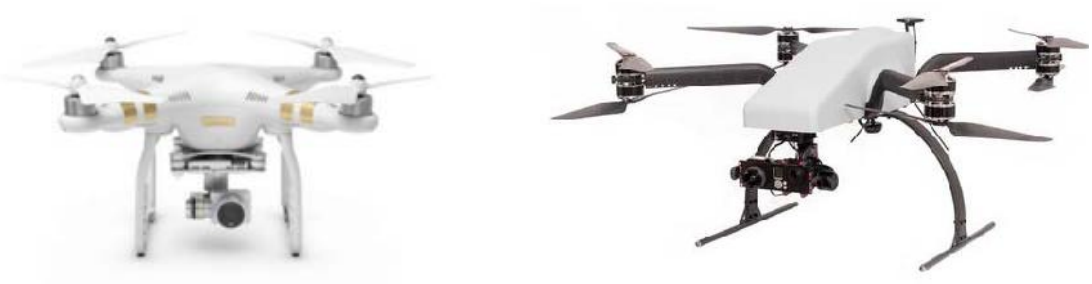

(a) (b)

FIG.1. Multi-copter with fixed landing gear, a.DJI Phantom 3 [1], b.Bird-pilot X8 [2]

a b

FIG.2 UAV type multi-copter with retractable landing gear, a.DJI Inspire 1 [1], b. DJI S1000 [4]

2. THEORETICAL REFERENCES

From the constructor's point of view, the landing gear chosen for analysis is the one with a linkage mechanism (quadrilateral mechanism) which has 4 closed kinematic couples, where the contact between the two kinematic elements is realized through permanent steerage, see figure 3.

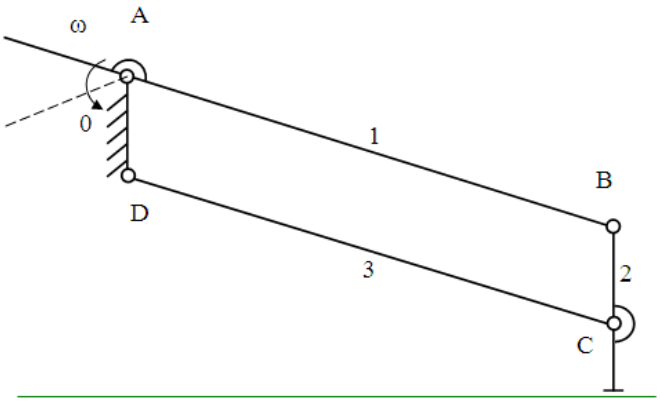

FIG. 3 Kinematics scheme for the landing gear mechanism

A plan mechanism with a high rate of mobility requires four fundamental kinematic couples. The chosen landing gear represents a determined kinematic chain (desmodromic) in which the position of the components depends on the position of one kinematic parameter (angle or movement), and the mobility rate for the plan mechanism (Grubler-Cebîşev-Kuţbah equation) is accordance with the fast calculation method, [11] which is written (equation 1, 2, and 3):

$$M = 6 \cdot (n-1) - \sum_{i=1}^{p} c_i \quad (1)$$

$$M = b(n-p-1) + \sum_{i=1}^{p} f_i \quad (2)$$

$$M = \sum_{i=1}^{p} f_i - \sum_{j=1}^{q} b_j \quad (3)$$

For plane mechanism with b=3 the mobility rate is (equation. 4):

$$M = -3 + \sum_{i=1}^{p} f_i \quad (4)$$

3. THE ANALYSIS OF A RETRACTABLE LANDING GEAR FOR UAV TYPE MULTI-COPTER

3.1. Landing gear type parallelogram with four support points

This type of landing gear could be equipped with wheels for the realization of turnovers or sled, both cases offering a high stability on the ground. The support base on the sole for a light weighted multi-copter is optimized in the following way: components versus a high stability at station on ground, respecting the minimal ground fuselage (e) which will be adopted according to the standard dimensions of the video sensor (see figure 4b)

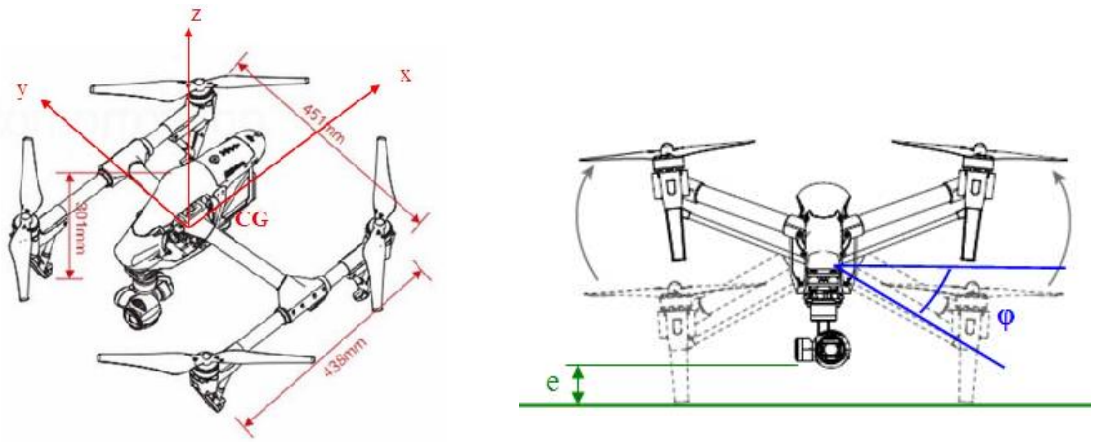

a b

FIG. 4 Dimensions and the extreme positions of the landing gear

a- base dimensions for multi-copter, b- ground clearance and the semi-angle of the retractable landing gear

The design process includes the conceptual stage where the mechanism of the landing gear is analyzed through a series of parameters: dimensional, positional, angular and kinematic, depending on the mobility rate that it has. For movement element for the landing gear we use a servomechanism with the following characteristics, see table 1.

Table 1. Servomechanism characteristics [6]

Servo model	Futaba 3153	Tension	4.8 – 6 V
Modulation	Digital	Torsion	1.4-1,7 kgcm
Motor type	Brushless	Mass	9,6 g

3.2. The analysis of the quadrilateral landing gear

The kinematic analysis of the mechanism is reduced to the study of the structural groups, so it can determine the trajectories for some points in the mechanism, the position of the mechanism for the know data of the leader element, speed and angular accelerations for head elements, speed and angular accelerations for some random point in the mechanism.

We will take into consideration the fact that the balance mechanism contains a RRR diode, with the geometry presented in figure 5, and the analysis data in table 2. The kinematic mechanism has three mobile elements (m=3) and four inferior kinematic couples (i=4), see figure 5. The mechanism is analyzed with the help of a software, SAM 6.1 [5, 9, and 12], and the values are from table 2. This software allows design, analysis and optimization of simple and complex plan mechanisms.

Table2. Parameters for kinematic mechanism

Training element 6	30 mm	Execution Element 4	49 mm
Element 2	49 mm	Element 3	230 mm
Element 1	230 mm	Actuation lever angle	60^0
Analysis time	6 sec		

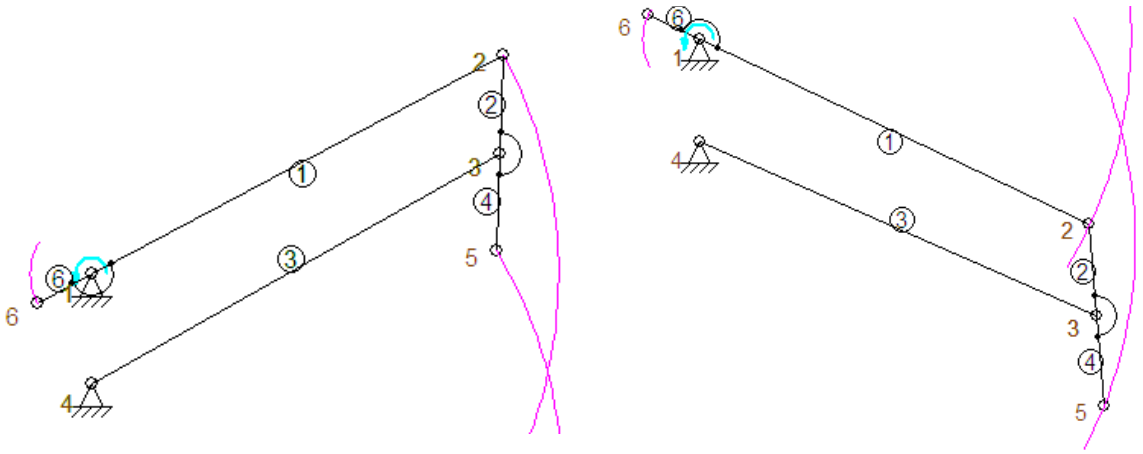

FIG.5. Extreme positions of the kinematic mechanism for the landing gear [9]

The analysis shows a series of position and speed parameters in figure 6 and figure 7 and table 3.

Table3 Kinematic characteristics

Time [s]	x(6) [mm]	y(6) [mm]	x(5) [mm]	y(5) [mm]
0	243	501	470	527
3	239	517	503	411
6	244	532	475	297

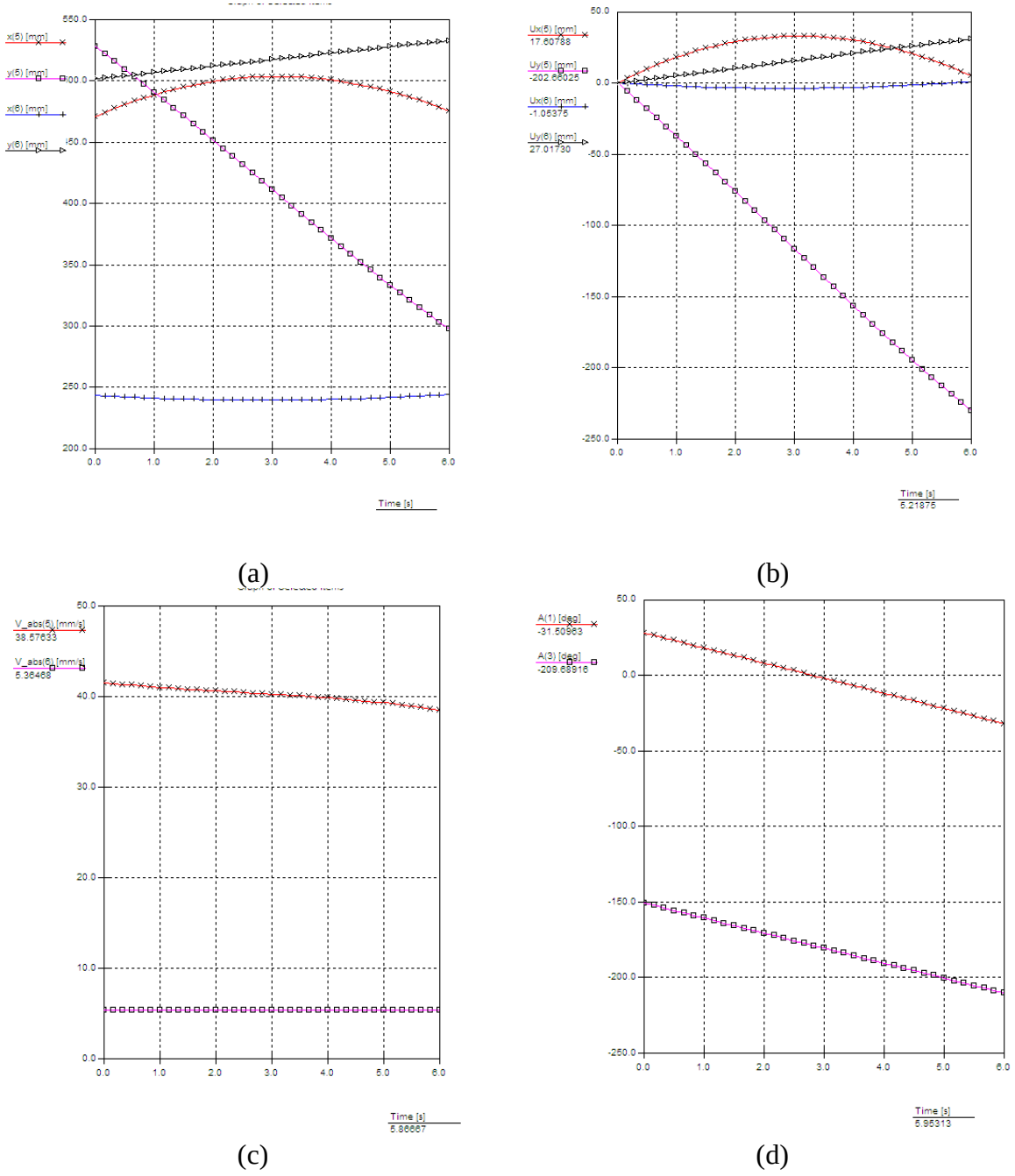

FIG. 6 Theoretical position parameters for the landing gear

Absolute speeds of input nodes (N6) and output (N5) can be seen in Figure 6c (node 6 constant speed, node 5 having quasi-linear variation). It is seen in Figure 6d a development parallel angle (A1 and A3) of the two arms (1 and 3) of the mechanism to be analyzed.

3. CONCLUSSIONS

SAM 6.1 integrates pre-processing, numerical analysis, post-processing and optimization mechanisms (only professional module) in an easy to use software environment, mechanisms can be designed free or module wizard.

To minimize errors and optimize kinematics mechanisms shaping plane and spatial systems in UAVs composition may require a dimensional study developed at the spare parts or assemblies.

The software kinematics analysis of the mechanism is the base of dimensional design of the chain command for a landing gear (for UAV). A complete analysis would be realized in a further research where we will optimize mass and kinematics for the landing gear using a minimal time for retraction.

ACKNOWLEDGMENT

The current article benefited from the documentary support of "Henri Coandă" Air Force Academy of Braşov and ITSC-SVFP of Mediaş, Romania, [8].

REFERENCES

[1] http://www.dji.com, consulted at 04.03.2016
[2] http://www.directindustry.com/prod/birdpilot-gmbh/product-162555-1691172.html, consulted at 04.03.2016
[3] Fahlstrom P.G., Gleason T.J., *Introduction to UAV systems*, fourth edition, aerospace series, 2012 John Wiley & Sons Ltd., ISBN 978-1-119-97866-4, 280p
[4] http://www.dji.com/product/spreading-wings-s1000-plus, consulted at 02.03.2016
[5] Luculescu D., Prisacariu V., *Method for determining the failure of flaps mechanism*, Review of the Air Force Academy, 2(26)/2014, Braşov, Romania, ISSN 1842-9238; e-ISSN 2069-4733, p41-44.
[6] *Futaba catalog*, 24p, copyright 2009-3002065, Brochure No. FUTZ2009 disponible at http://downloads.hobbico.com/catalogs/futz2009-futaba-catalog.pdf , consulted at 15.04.2016
[7] Backer A., Dutton S., Kelly D. (2004), *Compozite Materials for Aircraft Structures, AIAA*, Editura American Institute of Aeronautics and Astronautics, ISBN 978-1563475405
[8] http://vehiculefarapilot.ro/despre-noi, consulted at 01.04.2016
[9] Artas, SAM 6.1 *The ultimate mechanism designer*, manual 2010, 160p.
[10] Tao Wang, Tao Zhao, Hao Du, Mingxi Wang, *Transformable aerial vehicle*, US Patent – US20140263823 A1, disponible at http://www.google.com/patents /US20140263823 consulted at 04.04.2016
[11] Creţu Simona Mariana, *Mecanisme – Analiză structurală. Teorie şi aplicaţii*, Editura Sitech, Craiova 2010, ISBN 978-606-11-0760-5, 160p
[12] Luculescu D., *The driveline analysis of hyper sustentation devices*, International conference "Scientific Research and Education in Air Force" AFASES 2014, ISSN 2247-3173, Braşov, Romania.

CFD ANALYSIS FOR UAV OF FLYING WING

Dumitru PEPELEA, Marius Gabriel COJOCARU, Adrian TOADER, Mihai Leonida NICULESCU

National Aerospace Research, Bucureşti, Romania
(pepelea.dumitru@incas.ro, cojocaru.gabriel@incas.ro, toader.adrian@incas.ro, niculescu.mihai@incas.ro)

DOI: 10.19062/2247-3173.2016.18.1.22

Abstract: *The range of unmanned aerial aircraft (UAV) is developing continuously generating new constructive solutions from small size and mass to those, which are comparable to piloted aircraft. The main reason of UAV use is due to lower cost of design, realization and operation (on flight hour) in comparison with human piloted aircraft. This paper presents the CFD analysis on a UAV tailless, after a 3D scanned real model.*

Keywords: *CFD, UAV, flying wing, aerodynamic parameters*

Symbols and acronyms

ρ	*Air density*	C_D	*Drag coefficient*
V	*Air velocity*	C_L	*Lift coefficient*
α	*Angle of attack*	*MAC*	*Medium aerodynamic chord*
p	*Relative static pressure*	*SIMPLE*	*Semi IMplicit Pressure Linked Equation*
A	*Reference area*	*STL*	*Stereo Lithography (CAD files)*

1. INTRODUCTION

The range of unmanned aerial aircraft (UAV) is developing continuously generating new constructive solutions from small size and mass to those, which are comparable to piloted aircraft. The main reason of UAV use is due to lower cost of design, realization and operation (on flight hour) in comparison with human piloted aircraft. According to references [1, 2, 3, 4] UAV development included the flying wing (tailless) operating lonely or in network, see Fig. 1, [13, 14].

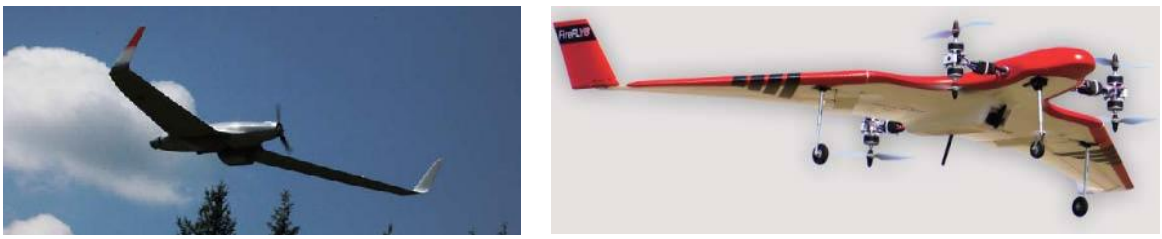

(a) (b)

FIG. 1 Flying wing UAV, a.Hirrus-TeamNet), b. FireFLY6 flying wing-tricopter

Constructive solutions of flying wing UAV are characterized by a series of requirements and exploitation limits on whole cycle of conception, fabrication and testing. UAV requirements and exploitation limits can be grouped on the following

categories: design concepts, aero-mechanical, materials and technologies, testing methods, flight safety and security and economical [5, 6, 7, 15 and 16].

2. CFD STUDIES FOR FLYING WING UAV

2.1. Preprocessing of model

The mock-up geometry was rebuilt with Ansys DesignModeler and Catia starting from scanned digital model (STL format) see Fig. 2, [8].

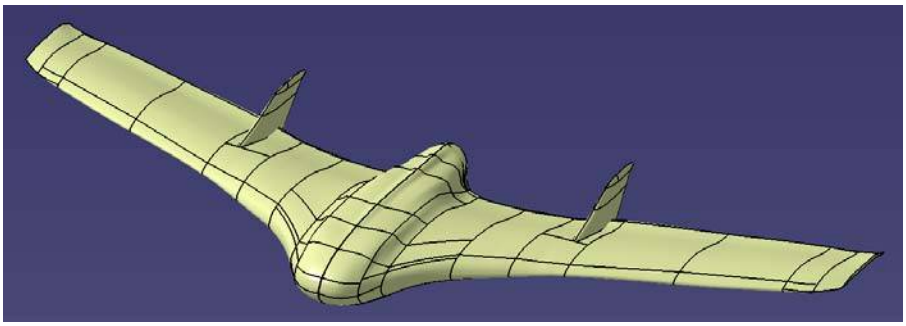

FIG. 2 CFD model of flying wing

The mesh was generated with Numeca/Hexpress and has 3.8 millions of hexahedral cells. The grid is refined to properly capture the leading and trailing edge curvature the junction between wing and vertical empennage, see Figs. 3 and 4, [11, 12].

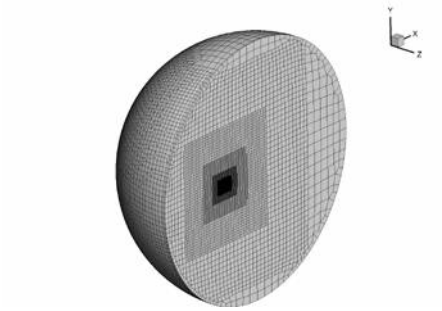

FIG. 3 Computational domain and mesh

FIG. 4 Mesh on flying wing surface

2.2. Computational Cases

The solver used in this study was Ansys Fluent [8]. In order to reduce the computational effort, a symmetry plane was introduced.

The governing equations are the Euler system. Furthermore, the fluid is assumed incompressible because the infinite upstream velocity is low (30 m/s). To solve numerically the Euler system, we used the SIMPLE algorithm due to its robustness and convergence rate for incompressible flows [9, 10]. The computational cases are given in table 1.

Table 1.Computational cases

Velocity (V)	30 m/s									
Angle of attack $\alpha(^0)$	-6	-4	-2	0	3	3	9	12	15	18

The reference values used to obtain lift and drag coefficients and relative pressure are given in Table 2.

Table 2.Reference parameters

p	101325 Pa	ρ	1,225 kg/m^3
A	0.29 m^2	V	30 m/s

2.3. Results and discussions

The CFD results are given in table 3 and in Figs. 6-9.

Table 3 CFD results

V	30 m/s									
α	-6^0	-4^0	-2^0	0^0	3^0	6^0	9^0	12^0	15^0	18
C_L	0,074	0,227	0,383	0,538	0,760	0,944	1,012	1,007	0,926	0,901
C_D	0,005	0,007	0,0013	0,023	0,043	0,070	0,154	0,234	0,286	0,325
C_L/C_D	15,113	31,400	29,133	23,763	17,660	13,514	6,581	4,294	3,238	2,771

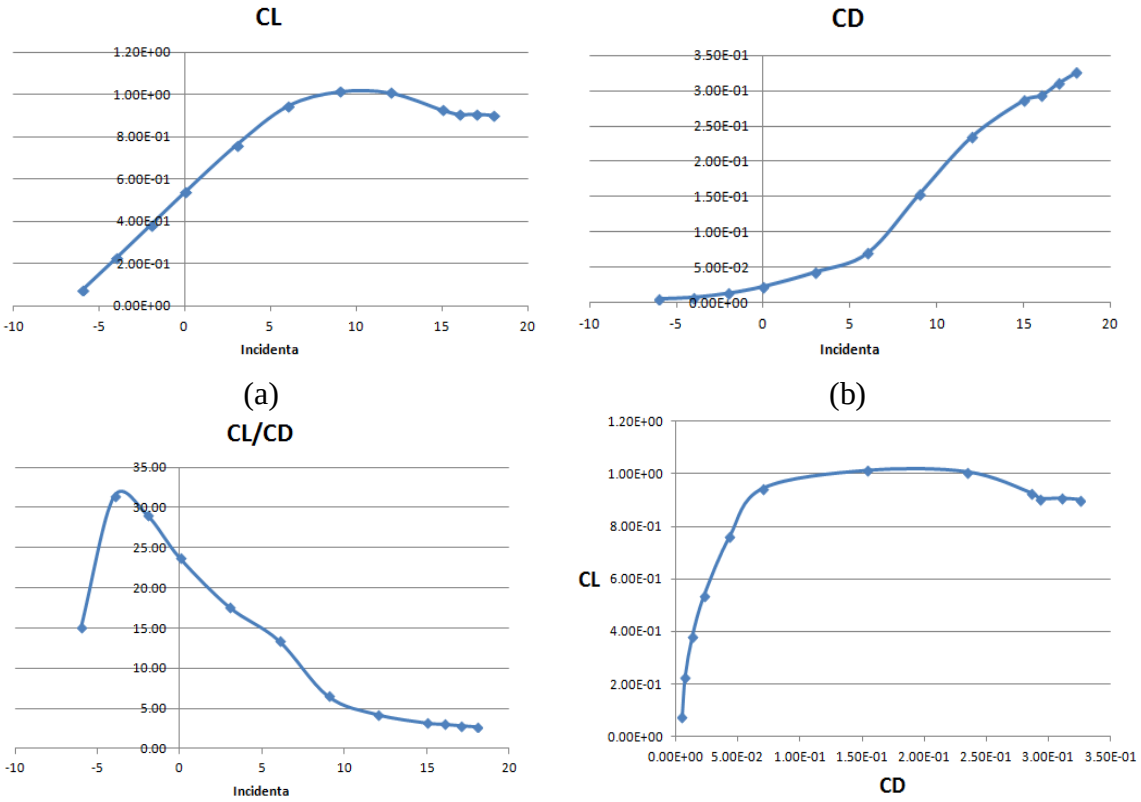

FIG. 5 Computed aerodynamic parameters, a- lift coefficient, b-drag coefficient, c, d-lift to drag ratio (C_L/C_D)

According to table 3 and Fig. 5, the maximal value of lift coefficient is at angle of attack of 9^0; significant increase of drag coefficient is observed from angles of attack greater than 6^0.

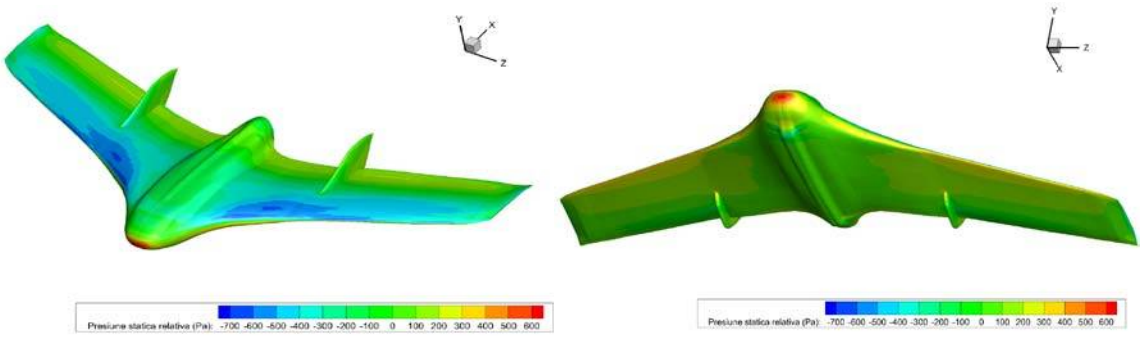

FIG. 6 Relative static pressure (Pa) at angle of attack of 0^0 (suction side-pressure side)

The position of model in the scanned geometry was considered at angle of attack of 0^0. One observes an incidence phase difference from the visualization of CAD model and from the comparison between CFD and wind tunnel results, see Fig. 6.

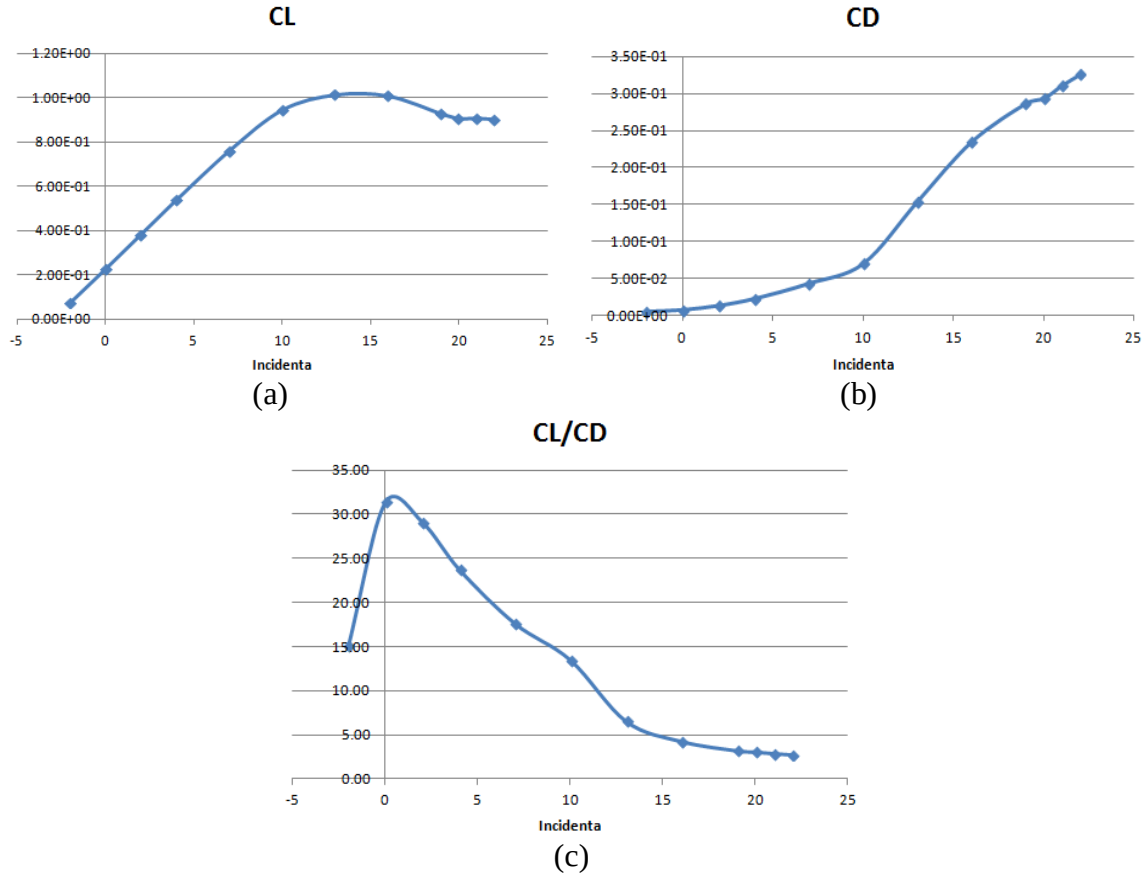

FIG. 7 Aerodynamic parameters of a incidence phase difference of 4^0

One observes that the maximal lift coefficient is achieved for the angle of attack in the range 12^0 to 13^0, see Fig. 7a; a significant increase of drag coefficient appears at angles of attack higher that 10^0 and the maximal lift to drag ratio is at angle of attack of around 1^0, see Fig. 7c. The pressure difference on the pressure side and suction side of wing gives the lift. This is clearly illustrated in Fig. 8 and Fig 9.

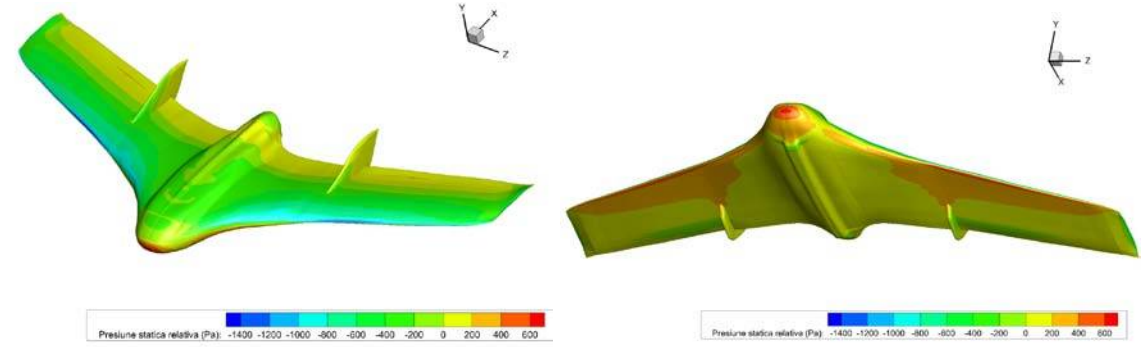

FIG. 8 Relative static pressure distribution on the suction side (left side) and pressure side (right side) for angle of attack of 3^0

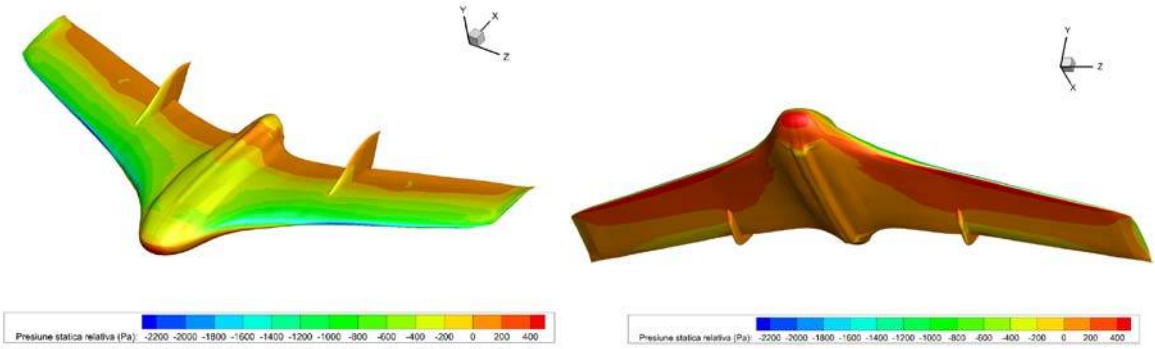

FIG. 9 Relative static pressure distribution on the suction side (left side) and pressure side (right side) for angle of attack of 6^0

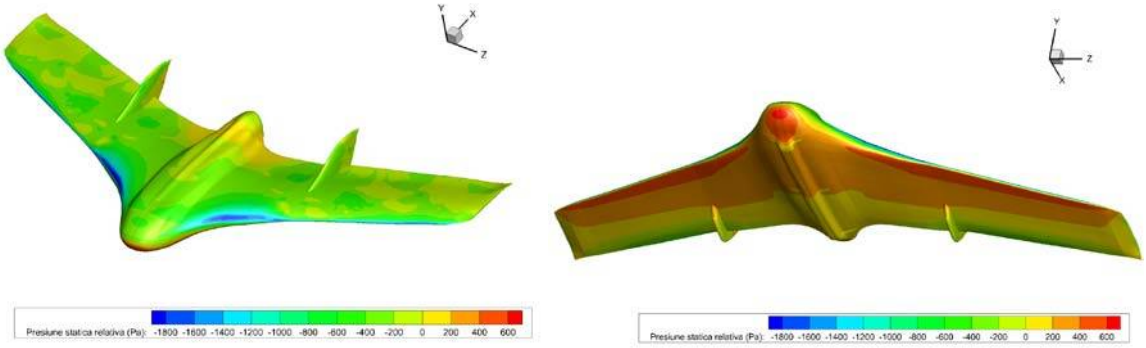

FIG. 10 Relative static pressure distribution on the suction side (left side) and pressure side (right side) for angle of attack of 12^0

3. CONCLUSIONS AND NEW RESEARCH DIRECTIONS

This CFD analysis for a flying wing UAV shows that the aerodynamic optimization is necessary. Furthermore, the CFD results have to be validated with the experimental ones obtained in subsonic wind tunnel. The above analysis shows the aerodynamic characteristics for a flying wing UAV obtained through 3D scan and simplified geometry in junction zones (wing- vertical empennages).

For a better analysis, it is necessary a finer mesh, which is suitable for RANS computations. Moreover, it is necessary to increase the number of test cases for a velocity range from 0 to 35 m/s and an angle of attack range from -10° to 20°. The future CFD

analyses could include the flights with the gliding angle up to 10° and with different twist angles.

ACKNOWLEDGMENT

This work is supported by the Executive Agency for Higher Education, Research, Development and Innovation Funding (UEFISCDI) under MASIM project (PN-II-PT-PCCA-2013-4-1349).

REFERENCES

[1] *Unmanned Aircraft System ROADMAP 2005-2030*, US DoD, Washington DC, 2005, 213p.
[2] UAS Yearbook, *Unmanned aircraft systems, The Global Perspective 2014/2015*, Blyenburg & Co, june 2014, Paris, ISSN 2270-6062, 240 p., available at www.uvs-info.com.
[3] Austin R., *Unmanned Aircraft Systems – UAVs design, development and deployment*, Aerospace series, Wiley and Sons Ltd publication, 2010, ISBN 978-0-470-05819-0, 365p.
[4] Prisacariu V., Cîrciu I., Cioacă C., Boşcoianu M., Luchian A., *Multi aerial system stabilized in altitude for information management*, REVIEW OF THE AIR FORCE ACADEMY, 3(27)/2014, Braşov, Romania, ISSN 1842-9238; e-ISSN 2069-4733, p 89-94.
[5] Prisacariu V., Boşcoianu M., Luchian A., *Innovative solutions and UAS limits*, REVIEW OF THE AIR FORCE ACADEMY, 2(26)/2014, Braşov, Romania, ISSN 1842-9238; e-ISSN 2069-4733, p51-58.
[6] Reglementările aeronautice române RACR-AZAC, 2007, http://www.caa.ro, consulted at 03.04.2016
[7] Directiva de navigabilitate privind aeronavele civile motorizate fără pilot uman la bord (UAV) DN 14-02-001, available at http://www.caa.ro/pdf/Directiva%20identificare %20UAV.pdf, consulted at 01.03.2014
[8] ANSYS FLUENT User's Guide 14, 2011, 2948p
[9] Patankar S. V., Spalding D., *A calculation procedure for heat, mass and momentum transfer in three dimensional parabolic flows*. 15:1787—1806, 1972
[10] Dănăilă S. Berbente C., *Metode numerice in dinamica fluidelor*, Editura Academiei Române, Bucureşti, 2003.
[11] Cojocaru, M. G., Niculescu, M. L., & Pricop, M. V. (2015). Aero-Acoustic assessment of installed propellers. *INCAS Bulletin*, ISSN 2066-8201, 7(2), p 53.
[12] Tomac, M. and Eller, D., 2011. From geometry to CFD grids—an automated approach for conceptual design. *Progress in Aerospace Sciences*, *47*(8), pp.589-596.
[13] http ://www.aft.ro, consulted at 01.04.2016
[14] http://www.birdseyeview.aero consulted at 04.04.2016]
[15] Prisacariu V., Boscoianu M., Cîrciu I., *Morphing wing concept for small UAV*, APPLIED MECHANICS AND MATERIALS, Vol. 332 (2013) pp 44-49, ISSN: 1662-7482, © (2013) Trans Tech Publications, Switzerland, doi:10.4028/www.scientific.net /AMM.332.44 OPTIROB 2013.
[16] Udroiu R., Applications of additive manufacturing technologies for aerodynamic tests, ACADEMIC JOURNAL OF MANUFACTURING ENGINEERING, **ISSN** 1583-7904, VOL. 8, ISSUE 3/2010

UNMANNED AERIAL SYSTEM (UAS) IN THE CONTEXT OF MODERN WARFARE

Vasile PRISACARIU[*], Adrian MURARU[**]

[*]"Henri Coandă" Air Force Academy, Braşov, Romania (aerosavelli73@yahoo.com)
[**]"Transilvania" University Braşov, Romania (muraruady@gmail.com)

DOI: 10.19062/2247-3173.2016.18.1.23

Abstract: *With the cybernetic implementation the modern battlefield will impact weapons systems which expands the uses of robotic systems and minimizes the use of human factors, keeping a rational integration between man and machine. Modern technologies offered by unmanned vehicles can provide a viable alternative to atypical confrontations. The article proposes an overview of the characteristics of UAS under modern conflicts.*

Keywords*: UAS, modern conflict, Signus, Airstrato*

Acronims

CDL	*Common Data Link*	*GCS*	*Ground Control Station*
UAS	*Unmanned Aerial System*	*IMINT*	*IM*agery *INT*elligence
ATO	*Air Tasking Order*	*KFOR*	*Kosovo FORce*
OSCE	*Organization for Security and Cooperation in Europe*	*CAOC*	*Combined Air Operations Centre*
STANAG	*Standardization NATO Agreement*		

1. INTRODUCTION

Modern conflicts have a number of issues with accuracy, efficiency and speed in which it carries out military action primarily for the protection of their military, here are some basic characteristics of military conflicts, characteristics that relate directly to systems of combat used (see Figure 1): the introduction of modern technologies and remote management of technical systems; reducing their costs and losses both own and collateral; interoperability between manned and unmanned systems; modern tactics and strategies based on smart sensors, mobility and targeted actions; informational war, protection and management of data flow [1, 2, 5].

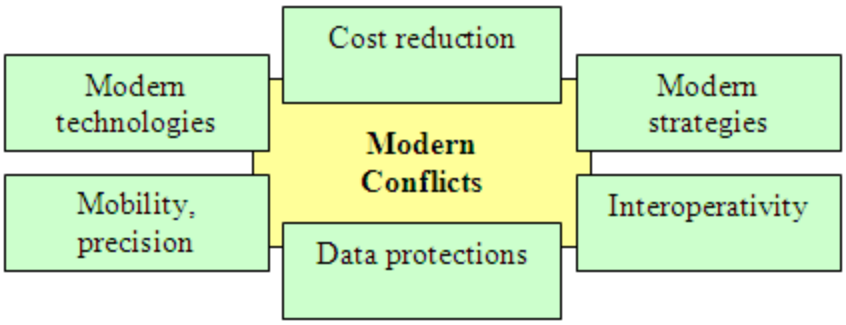

FIG. 1 The characteristics of modern confrontations

The needs of modern battles involves issues regarding the provision of humanitarian logistics to civilian population affected and protecting the civil economy, effectiveness of economic structures, the continuity in the provision of basic utilities to the population

since the war is not against the people themselves, the civilian population is not directly involved .

Modern fights are dominated by many atypical features: unequal war, asymmetric confrontation, enemy present but undetectable which means increasing security for own troops in asymmetrical warfare, anti-terrorism and reducing military involvement in dangerous missions through the transition from human controlled systems to unmanned.

Modern technologies offered by unmanned vehicles can provide a viable alternative to atypical confrontation, asymmetric battlefield, the guerrilla terrorist acts, all these issues require tailored strategies nonspecific, classical concept of the battlefield. An unmanned airborne system in modern conflicts remodels the concept of utilization in the modern airspace of sensor systems and information resultant [26, 29 and 30].

According to specialized references [1, 3-7] acquisition and use of UAS sites cannot be done without some risks and challenges, see Figure 2. To minimize these risks we should considered some benchmarks, such as the concept for use in operations; payloads; intercommunication with earth station (GCS), human factors involved in direct operations; lethal and non-lethal airborne weapons systems, existing UAS fleet. Such an evaluation aims to identify existing solutions necessary armed forces.

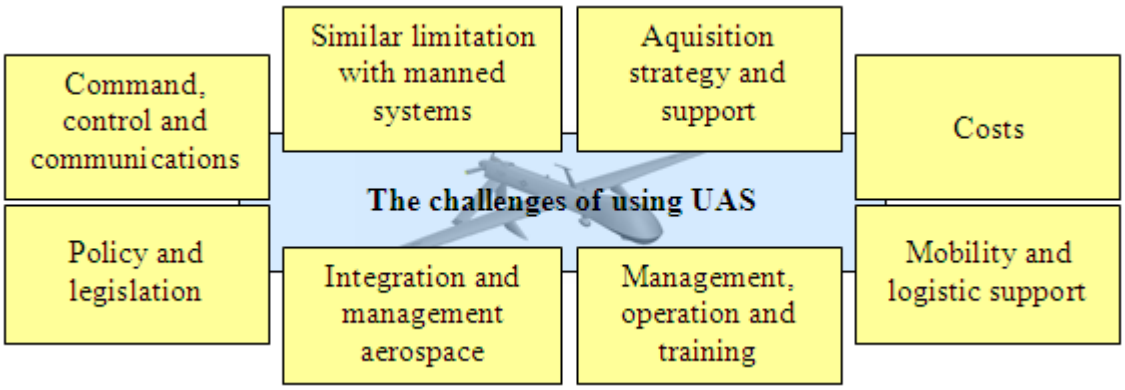

FIG. 2 The challenges of using UAS

Using a UAS in a hostile environment reduces risk and allows launching of guided munitions accurately from outside the range of enemy forces and means. The availability of a UAS is determined by the capacity and quality of the payload in most existing vehicles being represented by different types of sensors. The sensors carry differ in type and performance in accordance with UAS's role and mission requirements.

All payloads specialized in the field of IMINT (Imagery Intelligence) are characterized by sensitivity that they have in building and finally expressed the image quality that is given by resolution, [6, 7].

2. THE USE OF UAV SYSTEMS IN NATO STRUCTURES

A number of basic requirements have been accepted to a common level by policy makers, it is desired that UAS can operate in all categories of airspace to be available on all weather conditions, with a range of sensors, to be multirole with greater autonomy and stealth abilities, interoperable and low cost.

UAS integration in NATO's current operations immediately raised a range of questions from various military fields. One of the main questions was how to be responsible for UAS flight in formation bombardment manned platforms and provide commanders the confidence that no matter what, with or without man, the mission will be fulfilled.

NATO experience operations highlight the need to resolve fundamental problems to give the alliance necessary capability to solve an increasing number of operations and also to execute geographical areas outside of the territories of the member countries. In the new strategic environment, how forces are subject to hazards of a higher complexity require a new perspective on collective defense and how NATO operates.

NATO members have begun to look at the issue from a perspective based on capabilities instead of a traditional one, with an approach based on threat. The new "formula" must equip NATO with a well-developed and interoperable set of capabilities that allow commanders to work in this new era of globalization and asymmetric conflicts. In this process of transformation, unmanned aircraft systems already play a remarkable role enabling commanders to be better prepared to meet the demands of emerging modern battlefield and to design forces in any way they see fit. Reducing threats to allied forces is one of the main factors that are taken into account. In addition, increasing demand for UAS NATO is promoted by a wide variety of tasks that UAS can perform.

The presence of unmanned aircraft in theaters in the Balkans dates back to 1994. In 1995 RQ-1 Predator flew for the US for the first time operational mission over Bosnia [8, 9, 10], See Figure 3. In October and November 1998 RQ-1 Predator flying from Hungary to the US helped European Organization for Security and Cooperation (OSCE - Organization for Security and Cooperation in Europe) through verification missions over Kosovo [11], See Figure 3. German armed forces have used CL-289 Luna based in Macedonia. Immediately after these and other NATO members have carried out their own missions with UAVs, [12].

FIG. 3 RQ-1 Predator [8]

FIG. 4 CL-289 Luna [12]

The activity of NATO and USA throughout the air campaign was coordinated by the Combined Air Operations Center (CAOC - Combined Air Operations Centre) in Vicenza Italy. Each UAS mission over the Balkans had to be included in each day Air Load Order (ATO Air Tasking Order) with consequent difficulties in coordination. Another obstacle was important to combat conflict mitigation. The situation became more complicated after the deployment of KFOR and because of the increasing activities of transport helicopters.

Lessons identified and analyzed in UAS's deployment in the former Yugoslavia contribute positively to the success of NATO operations and the evidence from different scenarios outside NATO, UAS have become a new priority for many European NATO members, [13].

3. ISSUES OF STANDARDIZATION AND INTEROPERABILITY

To exploit the unique operational capabilities of UAS in civil and military operations, several technical issues must be addressed and resolved. UAS sites should have the same level of compliance as manned aircraft in the air traffic management, communications, navigation and surveillance needs where it intends to operate. According to specialized

references, [24 and 25] standardization and interoperability efforts include a series of standards issued, summarized as follows:

STANAG 3680 constitutes a glossary of terms and definitions.

STANAG 4586 includes NATO standards for interfacing control systems of UAS (data transmission, command, control and interface operator-system), it describes five levels of interoperability: from capturing and transmitting data received from the sensors to complete control and monitoring of aircraft including unmanned launch and recovery.

STANAG 4609: the standard of the captured images;

STANAG 4626: refers to the modular avionics architecture

STANAG 4660 it contains recommendations UAS command and control data link

STANAG 4670 it includes recommendations for the training of UAV operators.

STANAG 4671 the needed for UAV systems to meet the requirements of airworthiness. It requires a minimum standard of airworthiness for an UAV fixed wing as exemplified in documents such as 14 CFR Part 23 and EASA CS-23, while we recognize that there are several features for UAV systems that require compromises and additional subparts.

STANAG 7085 contain recommendations on data transmissions CDL.

STANAG 5066 refers to the communication errors.

STANAG 7023 it contains recommendations on primary format for images.

STANAG 7192 SD It contains recommendations on medical references for operators of UAVs.

It is also relevant to mention a series of recommendations that include STANAG cycle for operating picture, [27]:

- STANAG 3377: The report text, picture and annotated maps;
- STANAG 4545: Secondary image format;
- STANAG 4559: Library inteface for image standards;
- STANAG 4575: Advance interface for data storage;
- STANAG 4607: The format for the mobile ground target indicator;
- STANAG 4633: Common format for emiting reports.

4. UAS NATIONWIDE

Global and European trends have defined nationally a series of steps for design and implementation of robotic systems both small UAV categories and at close range [14, 18]. In what follows we present the top national projects in this area funded by commercial entities.

Signus

Signus was designed and built by TEAMNET Bucharest, Romania, see Figure 5 for mission data acquisition of the land and sea borders, with performance similar against other UAV of the same class (eg. RQ-7 Shadow 200). A number of features and performance are shown in Table 1. Signus supports the same ground station used to Hirrus, capable of mission data acquisition in real time used for the management of emergencies, environmental monitoring, agriculture, transport network utilities and communication routes (roads, railways, river, maritime) [15, 19].

Table 1. Characteristics

Span/ lenght (m)	5,2 / 3,8	G_{max} / G_{ut} (kg)	150/ 45
V_{max} / V_{cr} (km/h)	230 / 140	Autonomy (h)	2
Engine (CP)	32 / 61	Range (km)	150

FIG. 5 Signus [15]

FIG. 6 Airstrato Explorer [16]

Airstrato

It's a UAV designed by ARCA Space (USA) having its first test flight in 2014, see Figure 6 and technical characteristics of Table 2. Its performance is comparable to aerial robotic systems operational, with a cost ranging between $ 80-140000. There are two models version Airstrato Explorer and Pioneer. Both are constructed of reinforced composite materials and feature electric motors powered from internal batteries and photovoltaic, they are launched airborne pneumatic catapult and recovered by ballistic parachutes. US air transport avionics systems compatible, includes a pilot PLC internal equipment providing flight status information and computer system ADS-B flight. Connections between vector air and ground station are encrypted with standard AS 256, [28].

Air applications for Strato may include: border protection land / sea, disaster management, reconnaissance, communications relay, sea traffic control and scientific activities [16, 17, 20].

Table 2 Technical characteristics Airstrato Explorer

Span/ lenght (m)	16 / 7	V (km/h)	170
G_{max}/G_{ut} (kg)	230	Engine	6 x electric
Autonomy (h)	20	Altitude (m)	18000

Argus

Aviation vector realized by INAV S.A. Bucharest is at the stage of data acquisition demonstrator missions in areas of interest. Argus is built in 3 versions XL (Figure 7) XS Argus (Figure 7b) and Argus L, equipped with recovery systems [14, 22]. All versions have ground control stations equipped with telemetry and video transmission; technical characteristics are shown in Table 3.

a

b

FIG. 7 Argus XL (a), Argus XS (b), [22]

Table 3. Caracteristici tehnice Argus XL

Span/ lenght (m)	5 / 4,1	V_{max} / V_{cr} (km/h)	300 / 210
G_{max} / G_{ut} (kg)	140 / 40	Range (km)	300
Autonomy (h)	1,5		

CONCLUSION

The cybernetic implementation in the modern battlefield will impact weapons systems that expand the uses of robotic systems and the human factors will be minimized, keeping a rational integration between man and machine. Impact of information technology stems from a series of advances in both hardware and software that innovative concepts and materials on military technical systems.

UAVs can currently carry identification, observation, surveillance, air support of military actions, assessment of actions or strikes, acquisition targets and laser indication, in the military field.

Improving system reliability for UAS is an important goal to ensure efficient use in combat. Current levels of reliability UAS sites have a negative impact on utility operational procurement costs and their acceptance in aerospace regulations. The costs associated with improving reliability must be optimized both in relation to the purchase price, maintenance costs and less quantifiable benefits proposed by specific missions.

UAS technology will be integrated into a well-developed doctrine, tactics, techniques and mature procedures. A good level of integration airspace is essential to getting the full potential that unmanned platforms they provide.

AKNOWLEDGMENT

The authors wish to thank the "*Transilvania*" University of Braşov and "*Henri Coandă*" Air Force Academy of Braşov for supporting the research necessary for writing this article.

REFERENCES

[1] Balaceanu I., Râpan F. şi alţii , *Inteactiunea strategiilor in conflictele armate moderne*, Editura Universităţii de Apărare "Carol I", Bucureşti 2010, ISBN 978-973-663-853-4, 300p.

[2] Prisacariu V., *The UAVs in the theatre of operations and the modern airspace system*, RECENT 3 (39)/2013, ISSN 1582-0246. p 169-180

[3] Isache L., *Avioanele fără pilot uman la bord, tehnică de viitor pentru forţele armate,* Gândirea militară românească, 6/2006, ISSN 1454-0460, p108-117, www.gmr.mapn.ro,

[4] Ştir M., *Angajarea sistemelor aeriene fără pilot în acţiunile militare*, Gândirea militară românească 6/2010, ISSN 1454-0460 print, ISSN 1842-8231 online, p24-41

[5] Paraschiv C.V., *Proiect de cercetare PNCDI, Platformă aeriană autonomă cu modul de luptă strategic* – PAMLUS, ttp://mail.incas.ro/PNCDI2_ Program4/81 025/index.html, consulted on 04.08.2015

[6] *OSD UAV Roadmap 2002-2027*, Office of the Secretary of Defense Acquisition, Technology, & Logistics, Air Warfare, December 2002.

[7] *Unmanned Aircraft System (UAS) ROADMAP 2005-2030*, US DoD, Washington DC, 2005, 213p.

[8] http://defense-update.com/products/p/predator.htm, consulted on 04.02.2016

[9] Jones C.A., *Unmanned aerial vehicles (UAVS) an assessment of historical operations and future possibilities*, AU/ACSC/0230D/97-03, 76p, available at https://fas.org/irp/program/collect/docs/97-0230D.pdf

[10] Thirtle M.R., Johnson R.V., Bidder I.L., *The Predator ACTD: a case study for transition planning to the formal acquisition process*, 19980220 045, 107p, 2003, available at http://www.dtic.mil/dtic/tr/fulltext/u2/a337401.pdf,

[11] Haave C.E.,. Haun, P.M, *A-10s over Kosovo the victory of airpower over a fielded army as told by the airmen who fought in operation Allied Force*, Air University Press Maxwell Air Force Base, Alabama, 365p, 2003, available at www.dtic.mil /dtic/tr/fulltext/u2/a421682.pdf

[12] *Germany: A review of uav programmes and initiatives*, 4p, available at http://uvs-info.com/phocadownload/05_3h_2004/21_overview_germany.pdf, consulted on 12.02.2016

[13] Manolache Diana, Chiş C., *NATO bombing in the former republic of Yugoslavia*, AFASES 2015, ISSN 2247-3173, p 61-69.

[14] Prisacariu V., Cîrciu I., Luchian A, *Unmanned aircraft vehicle (UAV) in the Romanian airspace. An overview.* JOURNAL OF DEFENSE RESOURCES MANAGEMENT, vol.4 issue 1(8)/2014, ISSN: 2068-9403, eISSN:2247-6466, ISSN-L: 2247-6466, p123-128.
[15] http://www.rumaniamilitary.ro/uav-uri-romanesti-signus, consulted on 04.03.2016
[16] ARCA, *Airstrato. The most amazing air robot in the world*, 4p, 2014, disponibil la http://www.arcaspace.com/docs/ARCA_AirStrato_Press_Release.pdf, consulted on 05.02.2016
[17] http://www.arcaspace.com/en/airstrato.htm, consulted on 24.02.2016
[18] Magdalena I., *Unmanned air vehicles in Romania. Steps to the future*, AFASES 2015, vol I., ISSN 2247-3173, p55-60.
[19] Clavert J., Geffard J-C., Maloney P., *RQ-7B Shadow Achieved Performance Model Verification Final Report*, 2011, U.S. Department of Transportation, Federal Aviation Administration, DOT/FAA/TC-TN11/8, 31p, available at www.tc.faa.gov/its /worldpac/techrpt/tctn11-8.pdf
[20] http://www.militaryfactory.com/aircraft/detail.asp?aircraft_id=1300, consulted on 11.01.2016
[21] Blyenburg P. *Overview of the European UAS Community*, p120-138, available at http://uvs-info.com/phocadownload/05_3b_2010/P120-138_Overview-of-the-European-UAS-community_PVB.pdf
[22] INAV service offer, disponibil la http://www.inav.ro/eng/downloads/INAV-Services%20offer-extended%20version.pdf
[23] http://www.eurocontrol.int/mil/public/standard_page/atm_mil_uav.html, consulted on 09.01.2016
[24] NSA NATO Standardisation Agency, *STANAG 4586, ediţia a 3-a, Standard interface of UAV system (UCS) for NATO interoperability*, NSA/1235(2012)4586, 2012, 509
[25] Reg Austin, *Unmanned Aircraft Systems UAVs design, development and deployment*, Aerospace Series, ISBN 978-0-470-05819-0, 2010, 365p
[26] Muraru A., *An overview on the concept of uav survivability*, International conference of scientific paper AFASES 2011, ISSN: 2247- 3173, p1231-1236.
[27] *Integration of Motion Imagery into the STANAG 4559 Data Model*, 2014, 12p, available at www.gwg.nga.mil/misb/docs/rp/RP0813.1.pdf
[28] Intel, *Intel® Advanced Encryption Standard (AES) New Instructions Set*, 323641-001, Revision 3.0, 2010, 81p
[29] Boscoianu M, Cioacă, C., Rau C., Circiu I, *Concerted Systems for Increasing the Survivability of the Aircraft against Terrorist Threats*, Applied Mechanics and Materials, Vol. 325-326 (2013), Trans Tech Publications, doi:10.4028/www.scientific.net/AMM.325-326.756, pp. 756-760.
[30] Muraru A., Cioaca C, Boscoianu M.**,** *Modern Sense and Avoid Strategies for UAV***,** la the 9th International Scientific Conference New Trends in Aviation Development, Technical University Kosice – Faculty of Aeronautics, Gerlachov-High Tatras, September 16-17, 2010, Slovak Republic, ISBN 978-80-553-0475-5

REMOTELY AND PILOTED AIRCRAFT SYSTEMS / LAW AND POLICIES

AN H_∞ DESIGN METHOD FOR THE PITCH ATTITUDE HOLD AUTOPILOT OF A FLYING UAV

Adrian-Mihail STOICA, Petrisor-Valentin PARVU, Costin ENE

"Politehnica" University of Bucharest, Romania (adrian.stoica@upb.ro, parvupv@gmail.com, ene.costin27@gmail.com)

DOI: 10.19062/2247-3173.2016.18.1.24

Abstract: *The paper presents an H_∞ loop shaping method for the design of the automatic flight control system of an unmanned air vehicle's (UAV's) longitudinal dynamics. The design objectives include robust stabilization with respect to modeling uncertainties, pitch angle tracking of an ideal model and reduced sensitivity with respect to low frequency measurement errors. The design is illustrate by a case study for a flying wing UAV.*

Keywords: *UAV, pitch attitude hold autopilot, loop shaping, robust stability, ideal model tracking*

1. INTRODUCTION

The applications based on Unmanned Air Vehicle's (UAV's) received much attention over the last decades. Among them, the flying wing configuration of the UAVs was intensively analyzed due to their advantages concerning the reduced drag and the fuel consumption. A disadvantage of this configuration with respect to the classical one is its instability which fact requires an automatic control system able to stabilize the aircraft and to provide acceptable maneuverability qualities. The design problem of such a system has been previously considered in the control literature (see e.g. [1], [2], [3]). The proposed design methods include both classical techniques based for instance on the well-known PID (Proportional Integral Derivative) control laws, optimal approaches based on the linear quadratic problem, the H_∞ norm minimization and nonlinear methods including nonlinear inversion, etc ([4], [5], [6], [7], [8]). The methods mentioned above have advantages and drawbacks; the main difficulty in choosing the control design method is to ensure a trade-off between the complexity of the automatic flight control system and its performances. The actual applications require a wide spectrum of performances including not only the stabilization of the aircraft but also robustness with respect to modeling uncertainties and flying conditions changes, time response performances and reduced sensitivity to disturbances and measurement errors.

The aim of this paper is to present a design methodology for the Pitch Attitude Hold (PAH) autopilot of a flying wing configuration. The design procedure is illustrated and investigated for the Hirrus UAV designed and manufactured by a private Romanian company in collaboration with academics from Faculty of Aerospace Engineering of University "Politehnica" of Bucharest. The design approach is based on a modified version of the so-called two degrees of freedom (2 DOF) H_∞ loop-shaping able to accomplish simultaneously several objectives as robustness stability, model tracking and disturbances attenuation requirements. The original 2 DOF H_∞ method presented in [9] have been previously used for the autopilot design of the aircraft longitudinal and lateral

dynamics (see [10], [11], [12]). In the present paper the 2 DOF H_∞ loop-shaping procedure is used for the design of the PAH autopilot of UAV with flying wing configuration. The paper is organized as follows: in the second section, the design objectives and the design model of the UAV are presented. The design procedure of the PAH autopilot is presented in the third section. The numerical results obtained in a case study for the Hirrus UAV are presented and analyzed in the fourth section. The paper ends with some final remarks.

2. DESIGN MODELS AND AUTOPILOT SYNTHESIS OBJECTIVES

The Hirrus platform illustrated in Fig. 1 has a flying wing configuration with the wingspan 3.2 m, length 1.2 m, maximum takeoff weight 6.5 kg, cruising speed of 80 km/h and with a maximum payload of 1 kg.

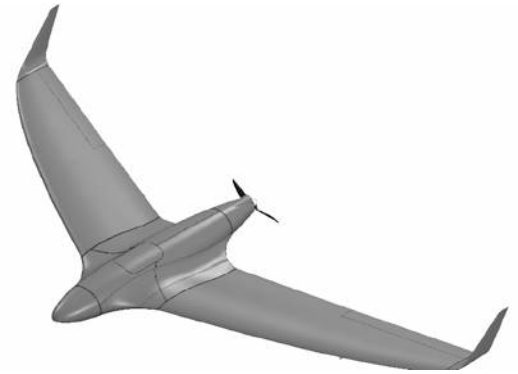

FIG.1. Hirrus UAV [13]

The longitudinal dynamics of the UAV is approximated by the following linearized nominal model:

$$\dot{x}(t) = Ax(t) + B\delta_e(t) \tag{1}$$

where the state vector $x(t)$ includes the perturbational values of the longitudinal speed u, of the angle of attack a, of the pitch rate q and of the pitch angle θ, respectively, with respect to their trimming conditions. The control input δ_e is the elevator deflection. The matrices arising in the above model corresponding a to the nominal flight conditions $V = 15\,\mathrm{m/sec}$ and $h = 10\,\mathrm{m}$ are

$$A = \begin{bmatrix} -1.3374e-02 & 1.3589e+00 & 0 & -9.07036e+00 \\ 1.2592e-01 & -1.1151e+01 & -5.0437e+01 & -1.4134e+00 \\ -7.2028e+00 & 1.3765e+03 & -3.5594+01 & 2.6574e-01 \\ 0 & 0 & 1 & 0 \end{bmatrix}, B = \begin{bmatrix} -6.4712e-03 \\ 3.6575e-02 \\ -7.7492e+00 \\ 0 \end{bmatrix} \tag{2}$$

The eigenvalues of the state matrix from the above system are $\{$-2.3362e+01 ± 2.6320e+02i; -1.6714e-02 ± 1.1328e-01i$\}$ showing that the UAV's phugoid poles are very close from the imaginary axis of the complex plane. This fact shows that in the absence of an automatic flight control system the time responses of the pitch angle are very slow. The measured outputs considered in this application are $y = [\alpha, q, \theta]^T$. The design objectives for the PAH autopilot are the following

(DO1) Robust stabilization of the longitudinal dynamics;

(DO2) Zero steady state value for the tracking error θ_{com}-$\theta(t)$ for piecewise constant values of the commanded pitch angle θ_{com} ;

(DO3) Shorter time responses of the pitch angle at constant commands;

(DO4) Reduced sensitivity with respect to low frequency measurement errors and robust stability with respect to modeling uncertainties.

3. THE DESIGN APPROACH OF THE PAH AUTOPILOT

In order to accomplish the design objective (DO2) defined in the previous section one introduces a *reference model* having the transfer function

$$H_m(s)=\frac{\omega_m^2}{s^2+2\xi_m\omega_m s+\omega_m^2} \tag{2}$$

where the natural frequency ω_m and the damping factor ξ_m are chosen such that the settling time is much shorter than in the case of uncontrolled phugoid. Thus, for $H_m(s)=10/(s^2+0.8s+10)$ the settling time is $t_s = 5.33\text{sec}$ and the damping ratio is $\xi_m = 0.12$. The control configuration used for the PAH autopilot is presented in Fig. 2.

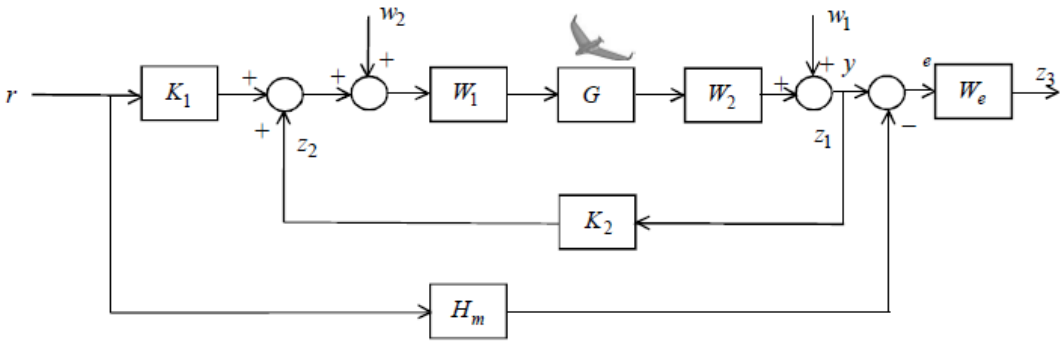

FIG. 2. PAH Autopilot configuration with 2 DOF

The two components K_1 and K_2 of the PAH autopilot are designed in order to accomplish the design objectives (DO1)¸ (DO4). In the above figure, W_1 is a stable dynamic weighting and $W_2 > 0$ is a positive weighting, chosen in order to provide the sensitivity reduction to measurements errors and robustness stability performances. The dynamic weighting $W_e(s)$ as a low-pass filter aiming to improve the tracking performance at low frequency commands for θ_{com} (see e.g. [15]). The control system $K = [K_1 \quad K_2]$ are determined such that it stabilizes the configuration from Fig. 2 and minimizes the H_∞ norm of the mapping $u_1 \to y_1$, where

$$u_1=\begin{bmatrix}\theta_{com}\\ w_1\\ w_2\end{bmatrix} \quad \text{and} \quad y_1=\begin{bmatrix}z_1\\ z_2\\ z_3\end{bmatrix}.$$

Reducing the H_∞ norm of the dependence from θ_{com} to z_3 implies to accomplish the tracking performances of the reference model output. In fact the control configuration from Fig. 2 may be regarded as the following H_∞ - norm minimization problem.

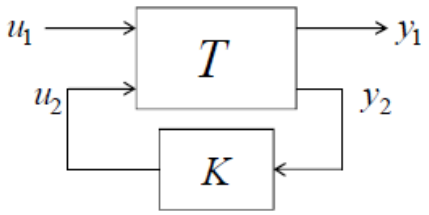

FIG. 3. The $H_¥$ -norm minimization problem

where T denotes the so-called *generalized system* obtained from the Fig.2 taking into account that u_2 and y_2 coincide with the control input and with the measurement vector, respectively, namely $u_2 = \delta_e$ and $y_2 = [\alpha, q, \theta]^T$. The generalized system T has the state-space realization of the following form

$$\begin{aligned} \dot{x} &= Ax + B_1u_1 + B_2u_2 \\ y_1 &= C_1x + D_{11}u_1 + D_{12}u_2 \\ y_2 &= C_2x + D_{21}u_1 + D_{22}u_2 \end{aligned} \tag{3}$$

Denoting by (A_m, B_m, C_m) a minimal state-space realization of the ideal model H_m given in (3), by (A_s, B_s, C_s) a minimal realization of the *shaped system* $G_s = W_2GW_1$ and by (A_w, B_w, C_w) a realization of the dynamic weighting W_3 it follows that

$$A = \begin{bmatrix} A_s & 0 & 0 \\ 0 & A_m & 0 \\ B_wT_rC_s & -B_wC_m & A_w \end{bmatrix}, B_1 = \begin{bmatrix} 0 & -H \\ B_m & 0 \\ 0 & B_wT_r \end{bmatrix}, B_2 = \begin{bmatrix} B_s \\ 0 \\ 0 \end{bmatrix}, C_1 = \begin{bmatrix} C_s & 0 & 0 \\ 0 & 0 & 0 \\ D_wT_rC_s & -D_wC_m & C_w \end{bmatrix}$$

$$C_2 = \begin{bmatrix} 0 & 0 & 0 \\ C_s & 0 & 0 \end{bmatrix}, D_{11} = \begin{bmatrix} 0 & I \\ 0 & 0 \\ 0 & D_wT_r \end{bmatrix}, D_{12} = \begin{bmatrix} 0 \\ W_u \\ 0 \end{bmatrix}, D_{21} = \begin{bmatrix} I & 0 \\ 0 & I \end{bmatrix},$$

where $T_r = [0 \quad 0 \quad 1]$ selects the regulated output θ from the measurement vector y, namely $T_r y = \theta$ and where $H = -ZC_s$, Z standing for the stabilizing solution of the Riccati equation ([15])

$$A_sZ + ZA_s^T - ZC_s^TC_sZ + B_sB_s^T = 0.$$

The positive weighting W_u has been introduced in the matrix D_{12}. It weights the control variable δ_e in order to reduce its amplitude for the saturation avoidance. Solving the above H_∞ norm

minimization problem one obtains the 2 DOF controller $K = [K_1 \quad K_2]$, representing for the PAH autopilot with the structure shown in Fig. 4.

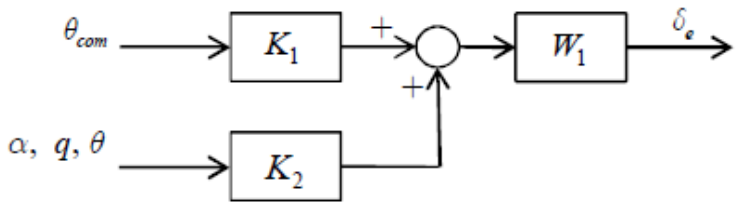

FIG.4. The 2 DOF autopilot

4. CASE STUDY FOR THE HIRRUS UAV

Before illustrating the design methodology presented above one notices from Fig. 5 that in the absence of the autopilot, the time response at step commands for the pitch angle is large due to the very small damping ratio of the phugoid.

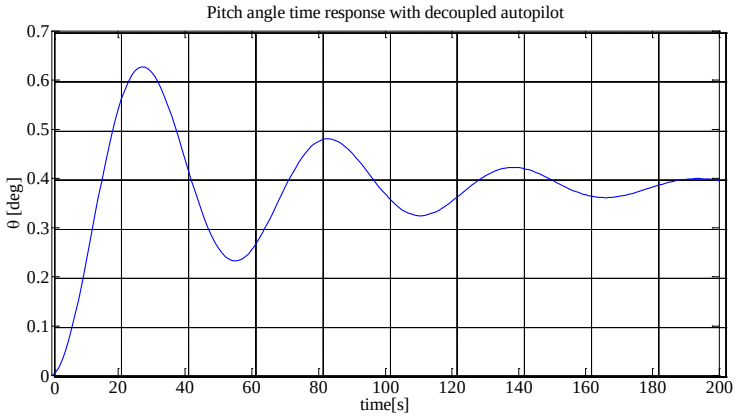

FIG.5. Pitch angle time response to unit step command

In order to improve the flying qualities of the UAV we used the design methodology presented in the previous section. One considered the linear model (1), (2) of the Hirrus UAV and then the H_∞ norm minimization problem for the system (4) have been solved using the following values for the weighting coefficients

$$W_1(s) = \frac{10^5}{100s+1},\ W_2 = I_3 \text{ and } W_e(s) = \frac{10^6(0.01s+1)}{100s+1}.$$

Two cases have been considered, corresponding to two different values of the weighting W_u penalizing the control variable δ_e, namely $W_u = 10$ and $W_u = 1000$, respectively. The time response of the error tracking for these two situations are presented in Fig. 6 and Fig. 7, respectively.

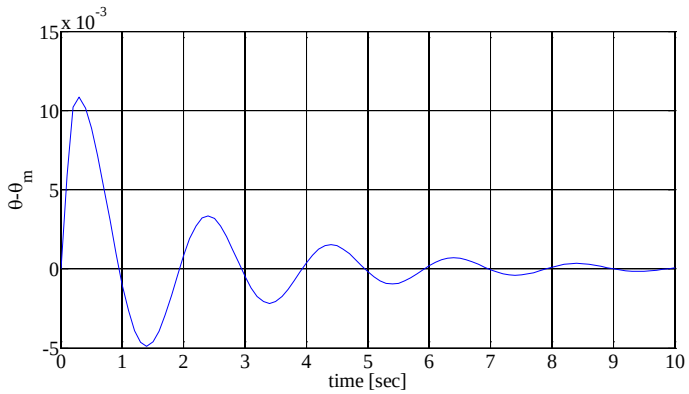

FIG. 6. Tracking error time response for W_u = 10

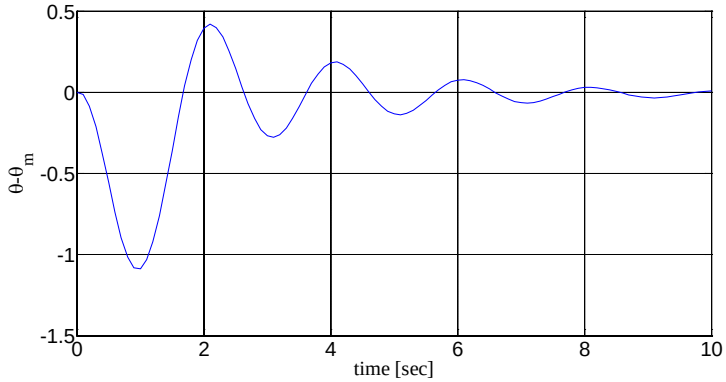

FIG. 7. Tracking error time response for W_u = 1000

The time response control δ_e for the two cases are given in Fig. 8 and Fig. 9, respectively.

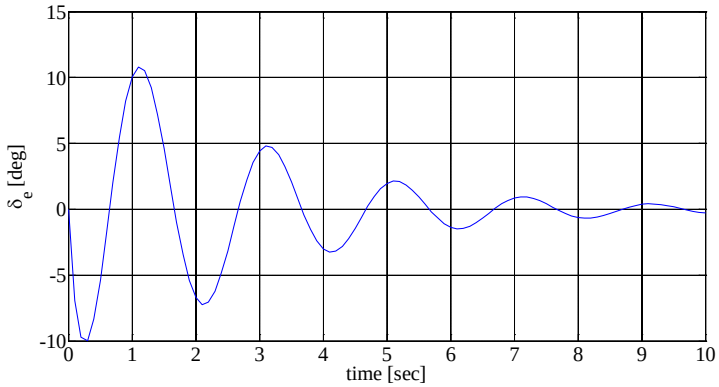

FIG. 8. Control variable δ_e time response for W_u = 10

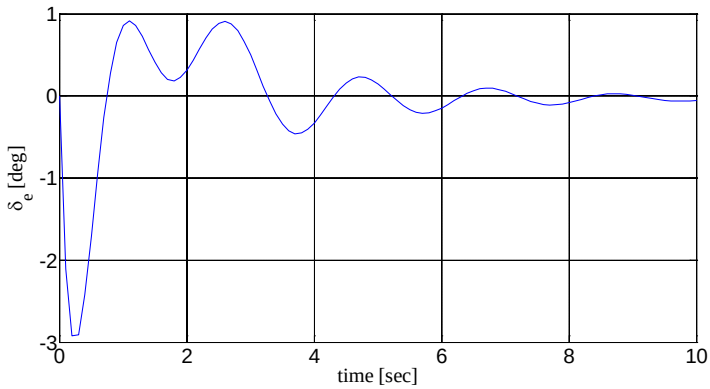

FIG. 9. Control variable δ_e time response for W_u = 1000

From the above plots it follows for both cases the settling time has been considerably reduced with respect to the case when the autopilot is not coupled. Moreover one also notices that when increasing the weighting W_u one obtains a smaller magnitude of the control variable but the tracking error of the ideal model response increases.

5. FINAL REMARKS

A modified loop-shaping H_∞ method with two degrees of freedom is presented for the design of the pitch attitude hold autopilot of an unmanned air vehicle. The numerical results and simulations indicate that the proposed approach is appropriate for acquiring robust stability, tracking of ideal model output and reduced sensitivity performances. These performances may be accomplished using a moderate complexity controller.

AKNOWLEDGMENT

This paper has been supported by MEN-UEFISCDI, Program Partnerships, Projects PN-II-PT-PCCA- 2013-4-1349 and PN-II-PT-PCCA- 2011-3.1-1560.

REFERENCES

[1] G. Stenfelt and U. Ringertz, Lateral Stability and Control of Tailless Aircraft Configuration, *Journal of Aircraft*, vol. 46, no. 6, pp. 2161-2164, 2009.
[2] A.D. Ngo, W.C. Reigelsperger and S.S. Banda, *Tailless Aircraft Control Law Design Using Dynamic Inversion and μ-Synthesis*, Proceedings of the 1996 IEEE International Conference on Control Applications, September 15-18, 1996, Dearborn, MI, pp. 107-112, 1996.
[3] M. Voskuijl, G. La Rocca and F. Dircken, *Controllability of Blended Wing Body Aircraft*, Proceedings of the 26th International Congress of the Aeronautical Sciences (ICAS), USA, 2008.
[4] R.W. Beard and T.W. Mclain, *Small Unmanned Aircraft: Theory and Practice*, Princeton University Press, 2012.
[5] R.J. Adams, J.M. Buffington, A.G. Sparks and S.S. Banda, Robust Multivariable Flight Control, Springer Verlag, 1994.
[6] B.L. Stevens and F.L. Lewis, *Aircraft Control and Simulation*, Wiley-Interscience,1992.
[7] A.-M. Stoica: L_1 *Controller Design for a Flying Wing Unmanned Aerial Vehicle*, Proceedings of ICMERA, 24-27 October 2013, Bucharest, Romania, 2013.
[8] V.G. Nair, M.V. Dileep and V.I. George, Aircraft yaw control system using LQR and fuzzy logic controller, *International Journal of Computer Applications*, vol. 45, no. 9, pp. 25-30, 2012.
[9] D. McFarlane and K. Glover, A loop shaping design procedure using $H_¥$ synthesis, *IEEE Transactions on Automatic Control*, vol. 37, no. 6, pp. 759-769, 1992.
[10] G. Papageorgiou, K. Glover, A. Smerlas and I. Poslethwaite, $H_¥$ Loop Shaping in *Robust Flight Control. A Design Challenge*, edited by J.F. Magni, S. Bennani and J. Terlouw, Springer-Verlag, pp. 64-80, 1997.
[11] G. Papageorgiou, K. Glover and R. A. Hyde, The $H_¥$ Loop Shaping Approach, in *Robust Flight Control. A Design Challenge*, edited by J.F. Magni, S. Bennani and J. Terlouw, Springer-Verlag, pp. 464-483, 1997.
[12] J. Lopez, R. Dormido, S. Dormido and J.P. Gomez, A Robust $H_¥$ Controller for an UAV Flight Control System, *Scientific World Journal, Hindawi Publishing Corporation*, Article ID 403236, 2015.
[13] User Guide for mini UAS Hirrus v1.2, Autonomous Flight Technology, 2015.
[14] D. McLean, *Automatic Flight Control Systems*, Prentice Hall International, 1990.
[15] D.C. McFarlane and K. Glover, *Robust Controller Design Using Normalized Coprime Factor Plant Descriptions*, Springer-Verlag, 1990.
[16] K. Glover, All optimal Hankel Norm Approximations of linear multivariable systems and their $L_¥$ -error bounds, *International Journal of Control*, Vol. 39, pp. 1115-1193, 1984.
[17] MIL-STD-1797A. *Flying Qualities of Piloted Aircraft*, 1997.

REMOTELY AND PILOTED AIRCRAFT SYSTEMS / LAW AND POLICIES

UAV OPERATOR TRAINING – BEYOND MINIMUM STANDARDS

Róbert SZABOLCSI

Óbuda University, Budapest, Hungary (szabolcsi.robert@bgk.uni-obuda.hu)

DOI: 10.19062/2247-3173.2016.18.1.25

Abstract: *Unmanned Aerial Vehicle (UAV) operators are key element of the Unmanned Aircraft Systems (UAS). Any technical system even UAS can fail if operating staff is not prepared well-enough to that proper level of skills ensuring safe operation of UAVs. There are many initiatives both for UAV military and civil operators to find minimum levels of training ensuring safe flight and ground operations. However, guidance available for the Military still not ratified by many NATO member-countries. Some of the NATO-members made their reservations related to frame regulations and guidance to clarify their standpoints in the training and education organizations responsible for training of designated UAV operators. This paper will combine basic principles of the guidance available in the field of military regulations with the civil regulations defined by appropriate EASA PART volumes.*

Keywords: *UAV, UAS, Designated UAV operator, UAV operator training.*

1. INTRODUCTION

Present days there are many ideas and initiatives about UAV designated operator training. Common feature here is that those available both military and civilian guidelines are defining training minimums and there are no upper limits in any means of it.

The training itself means to train UAV operators being educated in secondary grammar schools, in vocational training or in higher education institutions. The basic idea of the training is to train UAV operators able to handle UAVs safely both in flight and in ground operations.

In-spite of the existing guidelines being military or civil many countries made their reservations allowing taking into consideration experiences gained from operating UAVs in national airspaces under supervision of the national authorities.

2. LITERATURE REVIEW

The UAV airworthiness certification is analyzed in deep details in reference works of the author in [4, 5, 6, 7]. These papers are dealing only with many possible measures of compliance of the UAVs proposed by the author. Secondly, measure of compliance can be determined with that of pre-defined ones available in standards, guidelines, and handbooks.

Of course, to fly UAV safely it is necessary to own an educated and well-trained team being responsible for the flight safety, in general. There is a long lasting argue whether UAV operator is a pilot with its means. The military regulation goes far ahead to that of the civilian one, so this paper will analyze thoroughly two basic guidelines and regulations, which are the NATO STANAG 4670 [1] and The Joint Minimum Training

Standards of the Joint Staff [3]. As a rule any NATO standard can be serve as national rule if it is ratified by lawmakers. Due to sensitivity of the problem of the UAV operators' training still many NATO-member countries are in debt with ratification of the basic NATO document titled STANAG 4670/ATP–3.3.7 [2]. In close to that of STANAG 4670/ATP–3.3.7 principles goes The Joint Minimum Training Standards of the Joint Staff. These two basic documents derive guidelines for the principles of the training systems, and derive the syllabus in general. What is important, the basic norms are defined for the minimum levels of the skills of the operators, and, there are no formal upper limits for the syllabi of the training systems.

3. THE NATO STANAG 4670/ATP–3.3.7 TRAINING GUIDANCE

The first and basic document of NATO STANAG 4670 PFP(NNAG-JCGUAV)D(2006)001-Rev2 was issued with request of ratification 13 September 2006, till 1 December 2006. There are many years had flown by, and still, a UAV designated operator training is a matter of argue between many organizations. The latter version of this regulation is called as NATO STANDARD ATP-3.3.7 (Edition B, Version 1) from 22 April 2014.

The ATP-3.3.7 standard has some records of specific reservations, including those that were recorded at time of the promulgation, and are as follows below:

1) Belgium:
    a. will continue to deliver own training syllabi;
    b. will implement elements of BUQ Levels III and IV.
2) Canada:
    a. will not use term UAS;
    b. the UAV classification of CDN is not consistent with scheme used by NATO;
    c. will implement STANAG 4670 directed to training for the equivalent Canadian classification of the UAS.
3) Estonia: will use in dependence of UAS/UAV capabilities.
4) France:
    a. will not apply to class I drones;
    b. French Navy will apply as it receives the training equipment needed for the implementation;
    c. French Army will not apply because it departs too much from its practices and equipment.
5) Great Britain:
    a. reservation due to metrics;
    b. reservation to special regimes i.e. Stall Recovery, Dead Reckoning Navigation, Precision Radar Approaches;
    c. reservation due to classification of the UAVs.
6) Italy: will recognize Basic UAS Qualifications in accordance with this document.
7) The Nederland:
    a. will mutually recognize UAS operators' training;
    b. recognition and accreditation of qualifications issued by foreign authorities will be done by NLD Military Aviation Authority (MAA NLD);
    c. possible fly under Visual Meteorologic Conditions (VMC).
8) USA:
    a. UAS bases its training on CJCSI 3255.01 document [3];

b. some subject knowledge requires higher standards than existing requirements of the USA.

From the list of reservations given above easy to understand that still there are many differences between UAV manufacturers and UAV users, and sometimes it is cannot be bridged, the only possibility is to keep reservations in the given fields differing much.

The NATO STANAG 4670/ATP-3.3.7 training guidance based upon three documents, namely:

1) Chairman, CJCSI 3255.1, Joint Unmanned Aircraft Systems minimum training standards, originally dated 17 July 2009, Change 1, dated 31 October 2011, current version as of 4 September 2012;
2) AAP-03, Edition J, Version 1, dated November 2011;
3) AAP32)A), Change3, dated January 2002.

The basic idea of the STANAG 4670 regulation is to segment four levels of basic UAS qualifications (BUQ). The trend here is when it is feasible and applicable the knowledge, skills and abilities (KSA) requirements bring closer to that of International Civil Aviation Organization (ICAO) requirements defined for manned aircraft of the civil aviation.

There are many initiatives to classify UAVs and UASs leading to the diversity of available classification [8]. To understand levels of BUQ [2] gives detailed classification of the UAS (see **FIG. 1.**).

NATO UAS CLASSIFICATION

Class	Category	Normal Employment	Normal Operating Altitude	Normal Mission Radius	Primary Supported Commander	Example Platform
Class III (> 600 kg)	Strike/ Combat*	Strategic/National	Up to 65,000 ft	Unlimited (BLOS)	Theatre	Reaper
	HALE	Strategic/National	Up to 65,000 ft	Unlimited (BLOS)	Theatre	Global Hawk
	MALE	Operational/Theatre	Up to 45,000 ft MSL	Unlimited (BLOS)	JTF	Heron
Class II (150 kg - 600 kg)	Tactical	Tactical Formation	Up to 18,000 ft AGL	200 km (LOS)	Brigade	Hermes 450
Class I (< 150 kg)	Small (>15 kg)	Tactical Unit	Up to 5,000 ft AGL	50 km (LOS)	Battalion, Regiment	Scan Eagle
	Mini (<15 kg)	Tactical Subunit (manual or hand launch)	Up to 3,000 ft AGL	Up to 25 km (LOS)	Company, Platoon, Squad	Skylark
	Micro ** (<66 J)	Tactical Subunit (manual or hand launch)	Up to 200 ft AGL	Up to 5 km (LOS)	Platoon, Squad	Black Widow

*Note: In the event the UAS is armed, the operator should comply with the applicable Joint Mission Qualifications in ATP-3.3.7 (STANAG 4670) and the system will need to comply with applicable air worthiness standards, regulations, policy, treaty, and legal considerations.

**Note: UAS that have a maximum energy state less than 66 Joules are not likely to cause significant damage to life or property, and do not need to be classified or regulated for airworthiness, training, etc. purposes unless they have the ability to handle hazardous payloads (explosive, toxins, chemical/ biological agents, etc.).

FIG. 1. NATO UAS Classification.

The ATP-3.3.7 using MTOW data defines three UAS classes, which are important whilst to derive BUQ for four levels leaning on KSA–requirements.

In [1, 2, 3] a rating scale for UAS operators' skills was established to make difference between BUQ levels of the operators. Appropriate and certified BUQ levels provide strong foundation for the UAS operations both in military or civil applications. The Basic UAS Qualification include basic understanding of the weather, aerodynamics, human factors, operational risk management, and finally, flight regulations for the type of the airspace in which the UAS operates.

Before to start with BUQ Qualification levels' definitions it is important to understand and be familiarized with the airspace classification (see **FIG. 2.**)

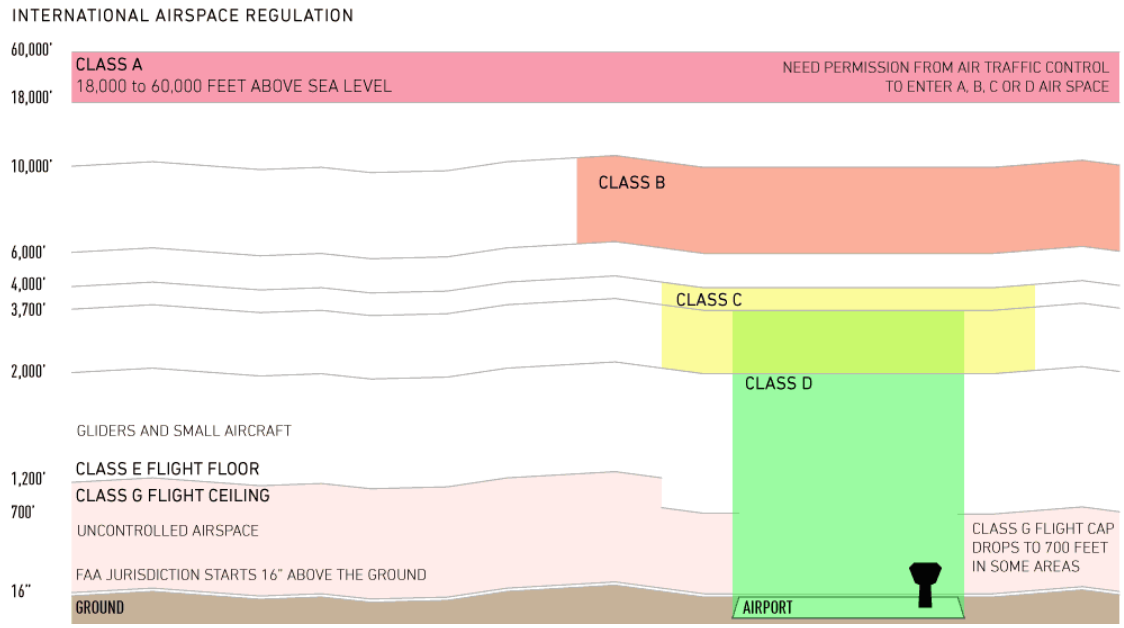

FIG. 2. International Airspace Classification (Accessed at: www.google.com)

References [1, 2, 3] define following four BUQ levels as they defined below:

1) BUQ Level I: knowledge and skills required to operate under Visual Flight Rules (VFR) in ICAO Classes E, F, and G, and Restricted/Combat airspace below 3000 ft above ground level (AGL). NATO Class I, Micro and Mini UAS operators are to be trained to BUQ Level I.
2) BUQ Level II: knowledge and skills required to operate under VFR in ICAO Class D, E, F and G, and Restricted/Combat airspace below 5000 ft AGL. NATO Class I, Small UAS operators must be trained to BUQ Level II.
3) BUQ Level III: knowledge and skills required to operate under VFR in all ICAO airspace except Class A below 18.000 ft AGL or Flight Level (FL) 180. NATO Class II, Tactical UAS operators must be trained to BUQ Level III.
4) BUQ Level IV: knowledge and skills required to operate under VFR and Instrument Flight Rules (IFR) in all airspace. NATO Class III UAS, MALE/HALE and Strike/Combat UAS operators must be trained to BUQ Level IV.

The BUQ levels given above are cumulative ones. Therefore, to meet higher requirements, operators must meet all the requirements of the lower levels as well.

The general aeronautical knowledge content is defined by following areas:

1) Airspace structure and operating requirements;
2) ATC procedures and rules of the air;

3) Aerodynamics;
4) Aircraft systems;
5) Performance;
6) Navigation;
7) Meteorology;
8) Communication procedures (Aeronautical English, ICAO Level 4)
9) Mission preparation.

The basic guideline followed by rulemakers is that the achieved level of competence of the UAS operators must be maintained, its currency and proficiency must be adequate to that existing national minimum standards and requirements. The principle of expiration is followed: all operators must subjected to periodic theoretical, practical and medical examination of the designated military examiners [1, 2, 3].

The basic aeronautical module is not explained yet, and its content belongs to those training organizations leading theoretical and practical training syllabi in UAS operator training.

The UAS operator training programs target to train UAV operators having pre-defined skills are divided into three main areas as follows:

1) Subject knowledge;
2) Task knowledge;
3) Task performance.

In these categories subcategories are defined with attributes to measure compliance to the given level of skills and knowledges of the UAS operators [1, 2, 3].

4. THE USA DoT FAA CIVIL REGULATIONS

Besides military training syllabi of UAS designated operators worth to mention the civil regulations. Of course, the national training programs may differ, but the FAA regulations are in the focus of attention of training organizations and experts not depending of its feature.

In 2015 a set of new norms were issued and published by FAA, which deals with UAS operators training and operators' responsibility, too. The UAV being flown is supposed to have wet weight less than 25 kgs (55 lbs), with no lower weight limits. These basic principles defined by FAA are as follows [8]:

1) UAV operators must be at least 17 years old;
2) Pilots of small UAV would be considered for "operator" instead of "pilot" widely applied and used;
3) UAV operators would be required to:
    a. pass an initial aeronautical knowledge test at an FAA–approved knowledge test center;
    b. be vetted by the Transportation Security Administration;
    c. obtain an unmanned aircraft operator certificate with a small UAS rating (like existing pilot airman certificates, never expires);
    d. pass a recurrent aeronautical knowledge test every 24 months;
    e. make available to the FAA, upon request, the small UAS for inspection or testing, and any associated documents/records required to be kept under the proposed rule;
    f. report an accident to the FAA within 10 days of any operation that results in injury or property damage;

g. conduct a preflight inspection, to include specific aircraft and control station systems checks, to ensure the small UAS is safe for operation.

It is easy to point out that there are many common points between military and civilian standpoints. As for the military training organizations, for the civil approved training organizations there is no strict regulations about aeronautical knowledge, and secondly, how it will be examined after 24 months.

CONCLUSIONS

The UAS operator training is a crucial point of the modern UAS systems. The flight safety assured by him/her, effectiveness of the flight mission execution depends on him/her. There are many regulations defining framework of the training system, however, many open items being investigated latter are remaining still. In many planned training syllabi the module of the aeronautical sciences still not defined, however, there are effective methods, tools and experiences gained from the conventional training systems of the manned aircraft used by EASA PART 66, for instance. The future work will be devoted to the comparison of the existing civil and military training syllabi by the module of Aeronautical sciences. Moreover, the minimums are defined without upper limits, and, there is an arising question how to find constraints for upper limits, if it is worth to be investigated.

REFERENCES

[1] NATO STANAG 4670 (Edition 1) *Recommended Guidance for the Training of Designated Unmanned Aerial Vehicle Operator (DUO)*, NATO Standardization Agency, 2006.

[2] ATP–3.3.7 – NATO STANAG 4670 (Edition 3) *Guidance for the Training of Unmanned Aircraft Systems (UAS) Operators*. NATO Standardization Agency, 2014.

[3] *Joint Unmanned Aircraft Systems Minimum Training Standards*, Joint Chiefs of Staff, CJCSI 3255.01, Washington, D.C., 20318, 2012.

[4] R. Szabolcsi, *A New Concept of the Basic Terms and Definitions for Measuring the UAV and UAS Systems Compliance with Airworthiness Criteria*. Bolyai Szemle, ISSN 1416-1443, XXIII(1), pp(5-18), 2014.

[5] R. Szabolcsi, *A New Concept of the Unmanned Aerial Vehicles Flying and Handling Qualities*. Bolyai Szemle, ISSN 1416-1443, XXIII(1), pp(19-26), 2014.

[6] R. Szabolcsi, *A New Approach of Certification of the Airworthiness of the UAV Automatic Flight Control System.* Revista Academiei Fortelor Terestre/Land Forces Academy Review, ISSN 2247-840x, eISSN 1582-6384, 4/2014:(76), pp(423-431), 2014.

[7] R. Szabolcsi, *Lateral/Directional Flying Qualities Applied in UAV Airworthiness Certification Process*. Revista Academiei Fortelor Terestre/Land Forces Academy Review, ISSN 2247-840x, eISSN 1582-6384, 3/2014:(75), pp(336-346), 2014.

[8] USA DoT FAA, 14 CFR Parts 21, 43, 45, 47, 61, 91, 101, 107, and 183. Docket No.: FAA-2015-0150; Notice No. 15-01, 2015.

UNMANNED AERIAL VEHICLE IN MILITARY OPERATIONS

Gheorghe UDEANU, Alexandra DOBRESCU, Mihaela OLTEAN

"Nicolae Bălcescu" Land Forces Academy, Sibiu, Romania (office@armyacademy.ro, alexa_papy@yahoo.com, mihaela.oltean91@yahoo.com)

DOI: 10.19062/2247-3173.2016.18.1.26

Abstract: *Unmanned Aerial Vehicles (UAVs) make significant contributions to the war fighting capability of operational forces. The assumption is that piloted, remotely piloted, and autonomous vehicles have advantages and disadvantages in military operations, and that these vary in strategic significance for different levels of conflict.*

Since it is essential for the U.S. defense establishment to consider the strategic and technological implications of these types of aerial vehicles, this study is devoted to addressing the issues raised by the new generation of aerial vehicles. As technological advances increase the lethality of weapons on the modern battlefield, it is inevitable that UAVs will reduce the risks to humans in combat. If there is a fundamental constraint on the development of UAVs, it is that technology promises to find purely unmanned solutions to combat but cannot deliver on that promise. Political and military authorities should approach with caution the prospect of a world in which automated systems select military targets and employ lethal ordnance.

Keywords: *drones, strike, military operations, UAV;*

Acronyms

UAV(S)	*Unmanned aerial vehicles (systems)*	*UCAV*	*Unmanned combat aerial vehicles*
IMINT	*Imagery intelligence*	*HVT*	*High Value Targets*
GCS	*Ground Control Station*	*IS(TA)R*	*Intelligence, Surveillance, (Target Acquisition) and Reconnaissance*

1. INTRODUCTION

1.1. UAV history

The UAV is an acronym for Unmanned Aerial Vehicle, which is an aircraft with no pilot on board. UAVs can be remote controlled aircraft (e.g. flown by a pilot at a ground control station) or can fly autonomously based on pre-programmed flight plans or more complex dynamic automation systems. UAVs have most often been associated with the military but they are also used for search and rescue, surveillance, traffic monitoring, weather monitoring and firefighting, among other things.

The beginning of UAVs started with the Austrian attack against the city of Venice with unmanned balloons loaded with explosives. That was the earliest recorded use of an UAV. Although some of the balloons worked and successfully managed to bomb The Republic, others were caught in a change of wind and blown back over Austrian lines, [1].

Later, during World War I and shortly after, using A.M. Low's radio control techniques, the Royal Flying Corps' Ruston Proctor Aerial Target was built in 1916. The concept was to develop a small, very simple aircraft, pack it with explosives and then guide it into a designated target. Shortly after, on 12th of September, Hewitt-Sperry

Automatic Airplane made its first flight. These two concept planes are considered the ancestors of today's cruise missiles, [2, and 7].

World War II reveals more unmanned aerial torpedo concepts developed by US Army Air Forces and Navy. Functioning on the same radio-controlled principle, many aircraft were modified to become flying bombs, some of which are: Culver "PQ-8", Culver PQ-14 Cadet, B-17 Flying Fortress and B-24 Liberator, [3].

Cold War brings an innovative use of an UAV, other than aerial torpedoes. It seemed like gathering information with an unmanned flying vehicle is safer and more efficient. To gather data from nuclear tests, several B-17 Flying Fortresses were transformed into drones in 1946. Reconnaissance drones were also built in the 1960s like the early, not so specialized Ryan Fire bee. Others followed, using a more advanced technology: YQM-94 B-Gull Compass Cope B and Lockheed D-21, [4, 5, and 6], see figure 1.

(a) (b)

FIG. 1. UAVs history, a. YQM-94 B-Gull Compass Cope B, [5] b. Lockheed D21B [6].

1.2. Classification and missions of the UAVs

The large variety of UAVs can be classified according to several characteristics like role, range, weight, endurance, maximum altitude, wing loading, engine type etc.
Classification by role for military area: ISTAR, UCAV, multi-purpose, radar and Communication Relay, aerial delivery and resupply, research and development.

UCAV stands for unmanned combat aerial vehicles. This category contains aircraft that are highly maneuverable and are able to engage in air to air combat and also provide precision weapon delivery to surface targets, see Figure 2 and Table 1.

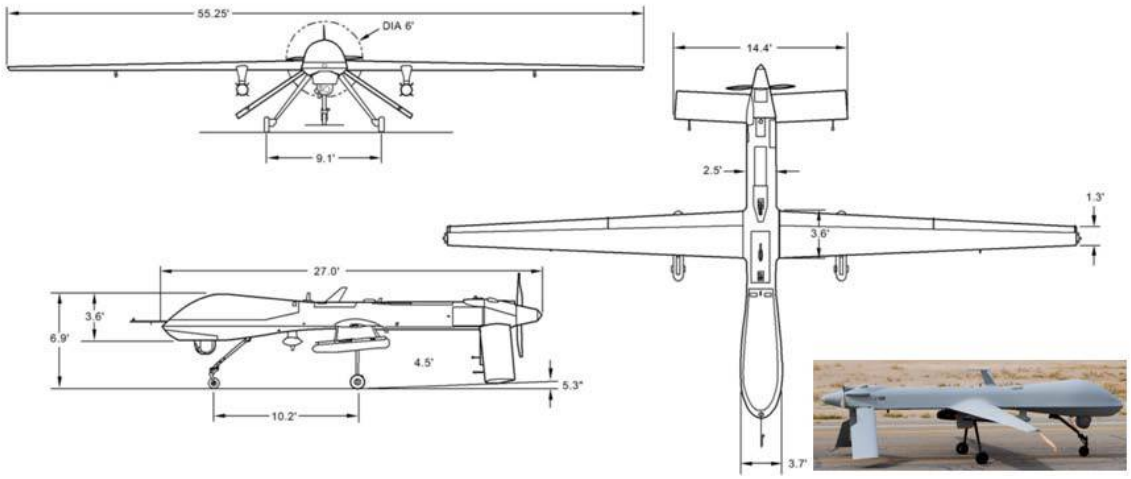

FIG.2. UCAV – MQ1 B Predator [12]

Table1. MQ-1 Predator features

Span	14,8 m	Empty weight	512 kg
Engine - Rotax	115 hp	Max. loaded	1020 kg
Maximum speed	217 km/h	Range	1100 km
Service ceiling	7600 m	Endurance	24 h

ISTAR is a system using UAVs to gather enemy information, locate target and petrol hostile air space without risking lives of the operators. Gathering such information by reconnaissance UAVs is more effective and voids putting soldier lives at risk.

Radar and communication relay UAVs are essentially an aerodynamic balloon filled with helium and air and are used for low-level surveillance system that uses aerostats as radar platforms, provide low-level trafficking or also provide television and radio signals.

Multi-purpose UAVs are usually modified reconnaissance UAVs that are weaponized. Their primary mission is usually interdiction and conducting armed reconnaissance against critical, perishable targets. These UAVs can also and strike using self-guided weapons.

The UAV in *Aerial/Supply delivery* category are designed for pin-point delivery of small cargo items such as ammunition and food supplies to Special Forces. The only UAV in this category is the CQ-10 Snow Goose.

The most important missions of the UAV for a civil area is: data acquisition and monitoring (e.g pipe line and power line survey, border patrol, crisis management), sports and recreation, commercial flights (e.g. agricultural operations), communications (e.g. retranslations data) and research, [13].

Considering the complexity and dangerousness of nowadays modern battlefield, the use of UAVs in military operations is mandatory. The UAV (Unmanned Aerial Vehicle), also known as UAS (Unmanned Aerial System) or commonly known as a drone is a powered, aerial vehicle that does not carry a human operator, uses aerodynamic forces to provide vehicle lift, can fly autonomously or be piloted remotely, can be expendable or recoverable, and can carry a lethal or non-lethal payload, [8, 9, and 10], see of communications from a UAV mission in Figure 3.

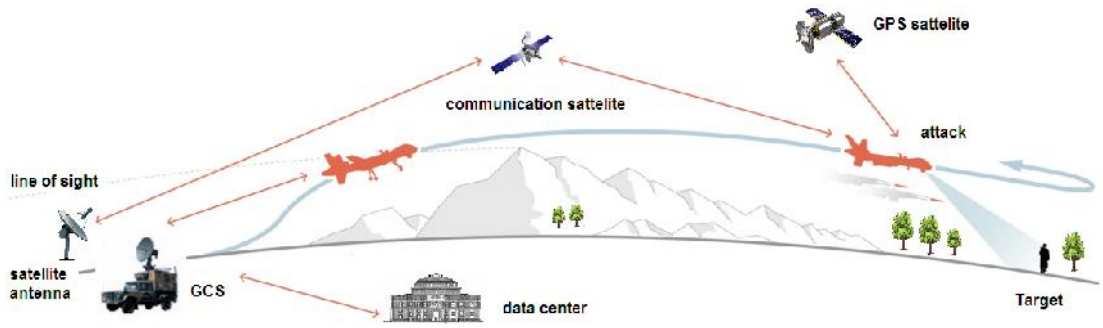

FIG.3. Data communication

2. UAV USE IN MILITARY OPERATIONS

2.1. ISTAR UAVs

ISTAR stands for information, surveillance, target acquisition, and reconnaissance. ISTAR is a practice that links sensors functions together in order to enhance battlefield functions in order to assist the combat force and manage the information collected.

UAVs enhance the ISTAR scheme through IMINT, which provide an comprehensive display of the battlefield. UAVs have proved their importance in ISTAR system in all the modern wars. The UAVs have reduced significantly the risks of collecting imagery from the battlefield, excluding the human pilot from the equation, [9, and 10].

2.2. UCAVs

An unmanned combat aerial vehicle is an UAV equipped for striking targets. It was develop in order to reduce the risk of the human pilots being behind enemy lines. The combat UAVs are capable of neutralizing targets deep in the battlefield with extreme precision and minimal collateral damage.

Combat UAVs have been successfully used in battle in Afghanistan, Pakistan, Yemen and many other battlefields. It has proved efficient and precise and the use of combat UAVs it's widespread along modern operational environments, [9, and 10].

2.3. Multi-purpose UAVs

Multi-purpose UAVs are a combination of ISTAR and Combat UAVs. The complexity of the system is an engineering challenge that was launched in 2002 by the US army. The challenge was to equip the aircraft with a high sensitivity imagery sensor and to make it capable of carrying a large amount of ammunition. General Atomics Aeronautical Systems has answered the challenge with MQ-1C Gray Eagle, [9, and 10].

3. UAV AGAINST TALIBAN

3.1. Who are the *Taliban*?

11 September 2001 was the date when the entire world started to be aware of the *Taliban.* The *Taliban* movement has its roots in religious schools in Pakistan for Afghan refugees, who fled the soviet regime. In 1994 Mullah Omar mobilized for the first time a group of 30 persons to rise against the governor of Kandahar. Soon the *Taliban* started to look good in the eyes of the oppressed people and got a lot of followers. With help from USA the in 1996 the movement became the government of Afghanistan. Starting from 1996 up until 2001 Afghanistan faced a civil war with between the mujahedeen and the *Taliban* movement. In 2001 a USA lead NATO military operation started in Afghanistan.

3.2. Why were the UAVs used against the *Taliban*?

One of the most notable uses of the UAVs has been in the counterterrorism role, both as an *intelligence, surveillance and reconnaissance* (ISR) platform and as an on-call strike platform. These armed UAVs are operated both by the U.S. Air Force and, in some cases (as with operations conducted over Pakistan), the CIA. Even before the 9/11 attacks, the armed Predator then in development were being considered as a means not only of keeping tabs on Osama bin Laden but also of killing him. Since then, armed UAVs have proved their worth both in the offensive strike role against specific targets and as a means of maintaining a constant level of threat, [11].

The insurgency type of battle the *Taliban* adopted along with the rough terrain and unknown environment for the multinational force set the perfect grounds for drone strikes against high value targets (HVT). Starting with late 2001 US drone strikes proved

effective against high value targets. Hidden locations, rough mountains, deep caves and insurgency techniques had made it almost impossible to the infantry to reach the targets. The need of a highly precise and versatile weapon appeared; that weapon proved to be the MQ-1 Predator UAV. Armed with Hellfire missiles, the Predator annihilated the HVTs that the infantry couldn't with the minimum effort and casualties, and most of the time without collateral damage.

Because in Afghanistan there were conducted US-NATO operations like Enduring Freedom and ISAF and later operation Resolute Support, most of the HVT of the *Taliban* movement were hiding in Pakistan. Status of Forces Agreement didn't allowed any *"foot"* operation in Pakistan, therefore the only resort of the coalition in order to neutralize the threat was to use air strikes against the strongholds of the *Taliban* leaders. The most versatile option was the UAVs like MQ-1 Predator and his larger cousin MQ-9 Reaper.

The use of the drones in current warfare operations is very controversial. There are a lot of supporters, but in the same time a lot of people and organizations are blaming the use of drones especially for the inhuman treatment towards their victims and the number of civilian casualties. At the beginning of drone usage their attacks haven't been so precise and the number of civilian victims was bigger than the number of targets killed. As the time passed the strikes became more precise and effective in the same time.

3.3 Statistics of drone strikes in Pakistan

Since 2010 the number of civilian casualties dropped from close to 20% to under 5% in 2015. The value of the targets, the impossibility of infantry troops to attack, the low number of civilian casualties and the zero loss in coalition soldiers has proved that the drones were the best choice for this type of action, see Figure 3.

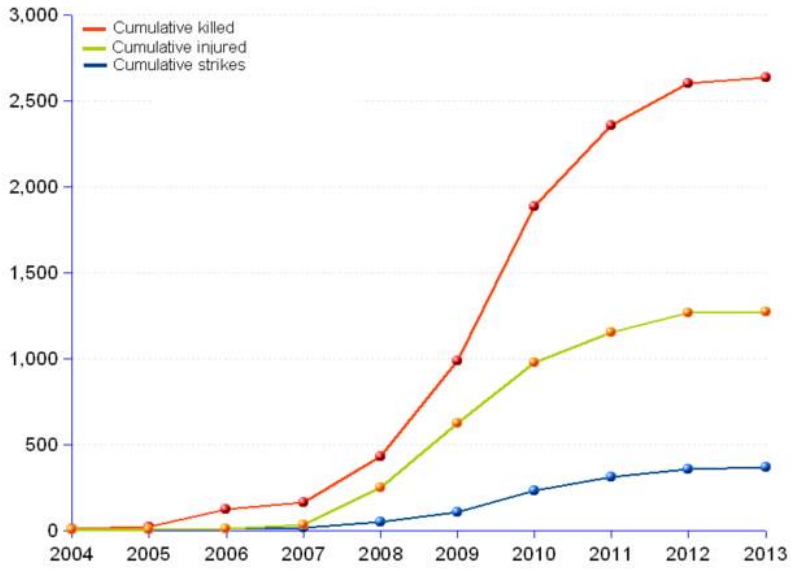

FIG. 3. Evolution UAV in military actions in Pakistan [14]

As displayed in the chart the trend is ascending, but the number of strikes has dropped in order to prioritize the targets and to reduce the collateral damage. In the same time the *Taliban* movement has lost its popularity both in Afghanistan and Pakistan.

As the years passed, the drone strikes became more precise and effective. The number of civilian killed in drone strikes has dropped significantly and the number of targets annihilated with has increased. The attacks aimed to neutralize more than one target at a time, therefore the use of the drones required more planning then before.

Public opinion played a very strong role in the change of modus of operandi for drone strikes. The decision of using drones was debated too much and the politics had to restrict the use of drones against Pakistani targets. As displayed in the chart below, the drones had increased in efficiency and accuracy and the number of collateral damage has dropped significantly. Although the number of civilians killed has decreased the public opinion has continued to accuse the use of drones against *Taliban.*

Drones are still used today in modern operational environment and had earned their place in battle. Although there have been strong controversies related to the use of drones, many high value targets were neutralized by drone strikes and a lot of soldiers' lives were saved.

CONCLUSIONS

The UAVs have a long history, but their capabilities have just started to be discovered. The military purposes, like ISTAR and strike, haven't been exploited to the maximum yet. Civilian uses of the unmanned aerial vehicles are developing every day from just entertainment up to research and rescue vehicles.

There is no doubt that recent technological advances have increased the military value of UAVs. For example, control systems have been perfected to the point where the operator needs far less experience with operating vehicles, and can focus on delivering weapons. Nor is it clear that UAVs will be less expensive to operate than their manned counterparts.

While automation can assist humans, we have not reached the point where technology will allow automated systems to make decisions about the use of lethal military force. If the objective behind the development of UAVs is find technological solutions for saving human lives in combat, it should not divert the technological community from finding better ways to integrate humans and machines into the most effective system for making the best possible decisions in war.

To reduce operating costs and losses in human and material UAV missions, synchronization strategy should include a number of areas of analysis, such as organization and doctrine, logistics and training, leadership and personnel, facilities and legislation.

AKNOWLEDGMENT

The authors wish to thank the "*Nicolae Balcescu*" Land Force Academy of Sibiu for supporting the research necessary for writing this article.

REFERENCES

[1] http://www.ctie.monash.edu.au/hargrave/rpav_home.html, consulted at 16.04.2016
[2] Barnhart R.K., Hottman S.B., Marshall D.M., Shappee E., *Introduction to unmanned aircraft systems*, CRC Press, 2012, ISBN 978-1-4398-3520-3, 215p.
[3] Heyman J., United States Military Aircraft, disponible at https://usmilitaryaircraft.files.wordpress.com /2015/04/airf-pq.pdf
[4] Ehrhard T.P., *Airforce UAVs – The secret history*, Mitchell Institute Press, 2010 Air Force Association, 88p.
[5] https://upload.wikimedia.org/wikipedia/commons/6/66/Boeing_YQM-94A_Compass_Cope_B_ USAF .jpg,consulted at 19.04.2016

[6] http://www.nationalmuseum.af.mil/Visit/MuseumExhibits/FactSheets/Display/tabid/509/Article/195778 lockheed-d-21b.aspx, consulted at 19.04.2016
[7] John David Blom, *Unmanned Aerial Systems: A Historical Perspective*, Institute PressCombat Studies Institute Press US Army Combined Arms Center Fort Leavenworth, Kansas, ISBN 978-0-9823283-0-9, 2010, 153p
[8] Prisacariu V**.,** *The UAVs in the theatre of operations and the modern airspace system*, RECENT 3 (39)/2013, ISSN 1582-0246. p 169-180
[9] Glade D., Unmanned Aerial Vehicles: *Implications for Military Operations*, Occasional Paper No. 16 Center for Strategy and Technology Air War College, Air University Maxwell Air Force Base, 2000, 39p.
[10] *OSD UAV Roadmap 2002-2027*, Office of the Secretary of Defense Acquisition, Technology, & Logistics, Air Warfare, December 2002.
[11] https://www.stratfor.com/weekly/armed-uav-operations-10-years, consulted at 25.04.2016
[12] http://smm.solidmodelmemories.net/Gallery/displayimage.php?pid=6018, consulted at 26.04.2016
[13] Catalin Cioacă, Vasile Prisacariu, *A Project Solution for Non-Cooperative Identification of Targets in the Land Forces*, in Review of The Air Force Academy, nr. 1 (18), 2011, ISSN 1842-9238, www.afahc.ro/revista/revista.html
[14] http://stats.areppim.com/stats/stats_dronewar_pak.htm, consulted at 27.04.2016

REMOTELY AND PILOTED AIRCRAFT SYSTEMS / LAW AND POLICIES

CONCEPTUAL DESIGN OF A VTOL REMOTELY PILOTED AIRCRAFT FOR EMERGENCY MISSIONS

Razvan UDROIU, Madalina Ioana BLAJ

Transilvania University of Brasov, Romania (udroiu.r@unitbv.ro, blaj_madalina2006@yahoo.com)

DOI: 10.19062/2247-3173.2016.18.1.27

Abstract: *This paper is focused on the design of a tilt-wing VTOL (Vertical Takeoff and Landing) remotely piloted aircraft. A tilt-X (X being wing or rotor) UAV has a hybrid configuration for taking the advantages of both fixed-wing and rotary-wing aircraft. This paper presents a short overview regarding the tilt-X concept and in the last part it is proposed a conceptual design of a tilt wing UAV, having a main mission of solving the emergency cases. The conceptual design was done with the help of software tools like as XFLR and CATIA.*

Keywords: *tilt wing, UAV, VTOL, conceptual design, emergency mission*

1. INTRODUCTION

In the literature there are many similar terms that can define the commonly known terms of drone. Thus, some similar terms are the following: remotely piloted aircraft systems (RPAS), unmanned-aircraft vehicle system (UAVS), remotely piloted aerial vehicle (RPAV), unmanned air systems (UaS) [10], unmanned aircraft system (UAS) [11] and unmanned aerial vehicle (UAV) [11]. The term unmanned aircraft system (UAS) was adopted by the United States Department of Defense [11], having four main components: the aircraft, the payload depends of flight missions, the control station and the data link. The interaction between operator and the UAS is facilitate through the data link, usually located in the control station.

The Vertical Takeoff and Landing (VTOL) aircrafts combine the advantages of the fixed-wing and rotary-wing aircrafts. Fixed-wing aircrafts take the advantage of high lift-to-drag ratio, fuel-efficient flying, and high-speed flying. Rotary-wing aircrafts can take-off and landing vertically and hover flying. Also, Vertical Short Takeoff and Landing (VSTOL) aircrafts is a more general terms that include VTOL concept.

According to [1], VSTOL aircrafts can be divided in the following main categories, see Fig. 1: augmented power plan for hover, combined power plant for hover, separate power plant and hover and same propulsion system for hover and forward flight. Tilt-X aircrafts are the hybrid vehicle that use the same propulsion system for forward flight and hover.

Basset and all [3] has distinguished the following main categories of rotorcraft or Tilt – X aircrafts, see Fig. 2:

1. Tilt Blade Tip-Path-Plane being the helicopter. The blade of the helicopter main rotor is tilted by using cyclic controls;

2. Tilt-Body can be considered like an multi rotors vehicle that tilted the whole aircraft based on the aerodynamic forces;

3. Tilt-Rotor can be a Rotoprop or Verticopter, consisting in one or more rotors that are tilted entirely. Rotorprop consists in one tail rotor used in hover and low speeds like a classical anti-torque rotor and at higher speeds like a pusher rotor. Verticopter has two tiltable coaxial contra-rotating rotors;

4. Tilt Wing combined, rotors with wings, propellers or other auxiliary propulsion;

5. Combined solutions between rotors and wing functions depending on the flight phase. These include Variable rotor radius (VRR) and Stoppable rotor (SR).

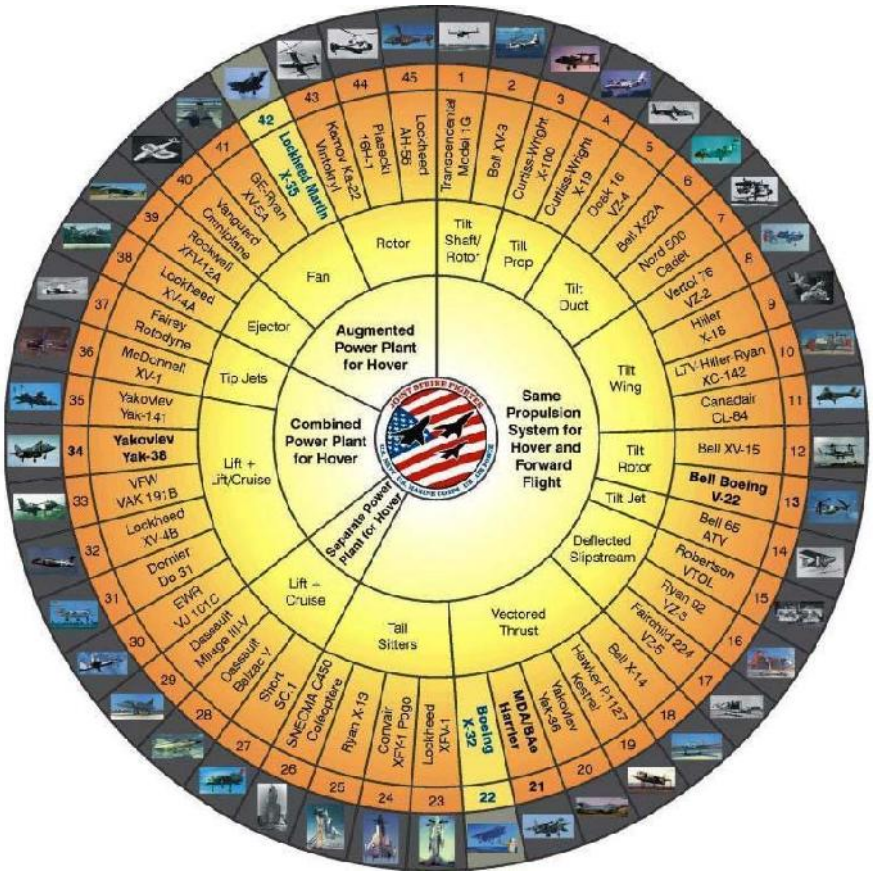

FIG. 1 VSTOL wheel of the aircraft and propulsion concepts [1]

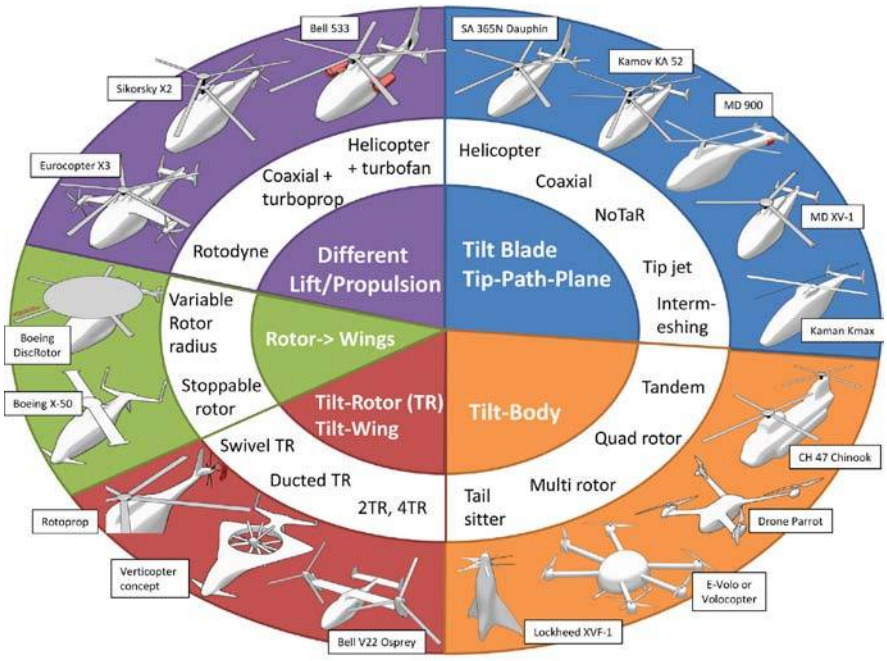

FIG. 2 Rotorcraft concepts [3]

Four categories of Tilt-X concepts are usually used worldwide as follows, Tilt-rotor, Tilt-wing, Tilt-jet and Tilt-duct.

The focus of this paper is on the tilt- wing UAV design.

2. TILT-X ANALYSIS FROM AIRCRAFTS TO UAV

Flight envelope of the tilt-wing is wider flight envelope from hover to high-speed and high altitude range than the flight envelope for Conventional Take Off and Landing (CTOL), Vertical Take Off and Landing (VTOL), as seen in Fig.3.

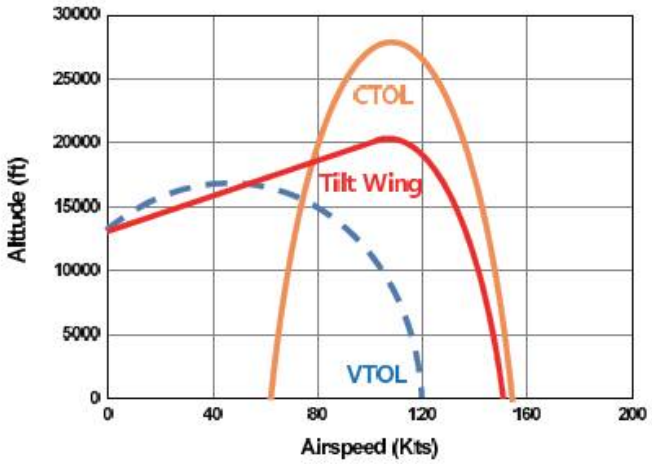

FIG. 3 Flight envelope [4]

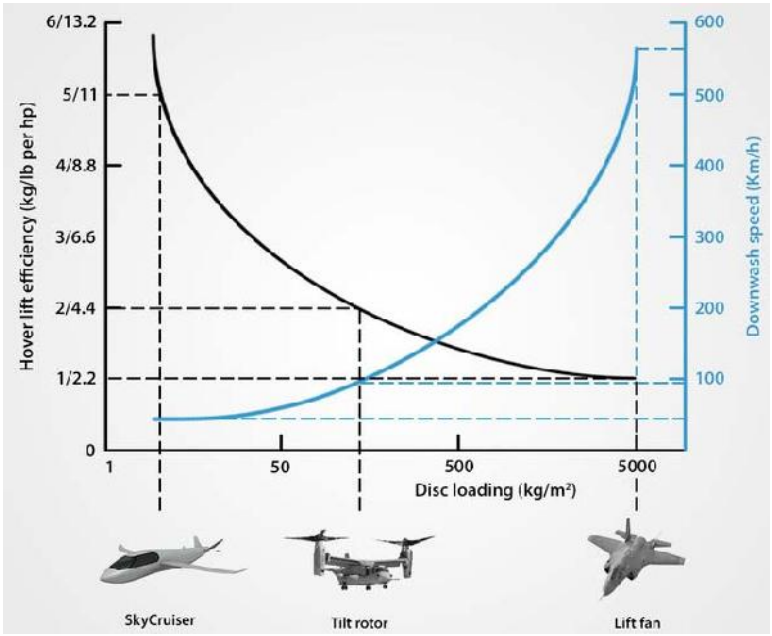

FIG. 4 Hover efficiency versus disc loading. Lower disc loading is more efficient, meaning less power is required to hover. [2]

Typically, the helicopter or multicopter have a lower disc loading and the lift fan systems have massive disc loading and typically require all the power of their powerful jet turbine engines to take off and land vertically [2]. Tilt- X aircrafts have a medium disc loading and a medium hover lift efficiency, see Fig. 4.

Some most popular example of tilt-X aircrafts are the following: Hiller X-18, XC 142, Canadair CL 84, Agusta Westland AW609, Bell Boeing V-22 Osprey etc.

In the field of tilt-X UAV concept has been developed some studies for military and civil application. As results of these we mention some UAV, like as Bell Boeing Eye, Bell Boeing Quad Tilt Rotor and NASA GL-10 Greased Lightening, see Fig. 5 and 6.

a

b

FIG. 5 Tilt-wing UAV, NASA GL-10 Greased Lightening (a) [6], Quad Tilt Rotor (b) [9]

a

b

FIG. 6 Tilt-rotor UAV, Ripmax VTOL (a) [7], Bell Eagle Eye (b), [8]

A tilt-wing aircraft operates in two main flight mode: airplane mode with the wing in horizontal position (conventional forward flight) and helicopter mode (vertical takeoff and landing) with the wing rotated up. It is similar to the tilt-rotor design where only the propeller and engine rotate.

The tilt-wing design offers certain advantages in vertical flight relative to a tilt-rotor but less control during hovering flight. Thus the tilt-wing is able to apply more of its engine power to lifting because the slipstream from the rotor strikes the wing on its smallest dimension. The tilt-rotor generally has better hover efficiency than tilt-wing, because the tilted vertically wing represents a large surface area for crosswinds to push.

3. ONE TILT-WING UAV FOR EMERGENCY MISSIONS

The main purpose of this work is to design an UAV like a ambulance-delivery drone that can improve global health. This UAV should be enable to automatically flown to any emergency situation and quickly delivery to any location a first aid payload box. This payload can consists in the following components: an automated external defibrillator (AED), medical toolkit, drugs, blood bag, insulin injection etc, as shown in fig. 7. An automated external defibrillator (AED) is a portable electronic device that automatically diagnoses the life-threatening cardiac arrhythmias of ventricular fibrillation and ventricular tachycardia in a patient. The firs aid toolkit can be used to guide citizens to make non-technical lifesaving procedures. Also, the ambulance-delivery UAV can automatically flown to villages with / without medical staff.

Generally the UAV development process consists in the following main steps: market analysis and customer requirements, mission specifications, conceptual design, preliminary design, detailed design, prototype manufacturing, flight test, and UAV production.

FIG. 7 Ambulance-delivery UAV

The UAV conceptual design was started by analysis the market needs, the current competitors and the applications in some emergency fields. First step has consisted in choosing the best configuration from several possible configurations.

Also, the establishing of the mission specification is an important input data to design a new aircraft or UAV. Usually, UAV mission specifications come depending on customer requirements.

The preliminary design of an UAV supposes using some software products like as Profili, XFLR, Advanced Aircraft Analysis (AAA) [12] etc. The parameters resulted after

the preliminary design are used to define the geometry of the UAV and used as input data to 3D computer aided design of the UAV.

The UAV presented in this paper using a contra-rotating rotors, have the general characteristics as shown in the table 1. The mission specification of the ambulance-delivery UAV consists in the following main segments: take-off, climb, tilting the wing, cruise, tilting the wing, descend and landing.

Table 1. Tilt – wing UAV characteristics

Tilt – wing UAV characteristics	**Value**
Length	2000 mm
Wing span	2800 mm
Wing mean aerodynamic chord	334 mm
Wing airfoil	MH 44
Aspect ratio	8,4
MTOW	40 kg
Payload capacity	10 kg

The ambulance-delivery UAV was 3D designed using the advanced computer aided design (CAD) software, CATIA by Dasault Systems [5].

The 3D CAD model of the ambulance-delivery UAV, in the main flight configurations, is shown in fig. 8.

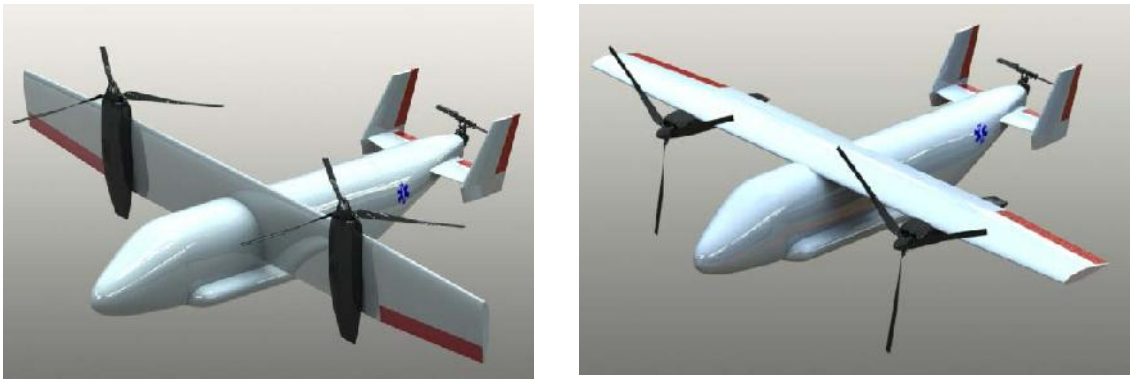

(a) (b)

FIG. 8. Flight configuration of the ambulance-delivery UAV (a) helicopter configuration mode (take off/ landing/ hover) (b) airplane configuration mode

CONCLUSIONS

The development of UAVs having Vertical Takeoff and Landing is crucial for operating in populated areas.

In the first part of this paper is presented a short review about VTOL unmanned aircraft system. The second part of the paper propose a new tilt-wing UAV focused on emergency missions. The main advantages of the proposed concepts are the following:

1. automatically flown to any emergency situation and quickly delivery to any location a first aid kit;
2. the possibility of operate on short distance in town, delivering first aid kit in order to operate without specialized personnel, coordinated by video-call;

3. the possibility of operate on long distance (around 70-120 km) in villages, delivering first aid kit, drugs, etc in order to operate with medical staff;

4. flight capability of takeoff / vertical landing.

The next steps in order to develop the ambulance-delivery UAV are, the aerodynamic optimization for different flight configurations, building a prototype from composite materials, flight tests and implementation of this UAV in the medical system.

REFERENCES

[1] ***, VSTOL Wheel of Misfortune, International V/STOL Historical Society, available at http://vertipedia.vtol.org/vstol/wheel.htm, accessed on 20 Apr. 2016;

[2] ***, Disc Loading and Hover Efficiency, Krossblade Aerospace Systems LLC, available at http://www.krossblade.com/disc-loading-and-hover-efficiency/, accessed on 15 Apr. 2016;

[3] P. M. Basset, A. Tremolet and T. Lefebvre, Rotary Wing UAV Pre-Sizing: Past and Present Methodological Approaches at Onera, *Journal AerospaceLab*, issue 8, pp. 1-12, 2014;

[4] S. Hong, J. Jeong, S. Kim, J. Suk and Ji In Jung, *Longitudinal Flight Dynamics of a Single Tilt-wing Unmanned Aerial Vehicle*, 19th IFAC Symposium on Automatic Control in Aerospace, 2013;

[5] ***, User manual for Catia v5, Dassault Systems, 2014;

[6] ***, Ten-Engine Electric Plane Completes Successful Flight Test, NASA, available at http://www.nasa.gov/langley/ten-engine-electric-plane-completes-successful-flight-test, accessed on 20 Apr. 2016;

[7] ***, Ripmax Transition VTOL ARTF, available at http://www.ripmax.com/Item.aspx?ItemID=A-RMX200, accessed on 20 Apr. 2016;

[8] ***, Bell Eagle Eye Tilt-rotor UAV, United States of America, available at http://www.naval-technology.com/projects/belleagleeyeuav/, accessed on 20 Apr. 2016;

[9] ***, Unmanned aerial vehicle, available at https://en.wikipedia.org/wiki/Unmanned_aerial_vehicle, accessed on 20 Apr. 2016;

[10] Prisacariu V., Boşcoianu M., Luchian A., *Innovative solutions and UAS limits*, Review of the Air Force Academy, 2(26)/2014, Braşov, Romania, ISSN 1842-9238; e-ISSN 2069-4733, p51-58;

[11] ***, Unmanned Aircraft System (UAS) ROADMAP 2005-2030, US, Washington DC, 2005, 213p, available at https://fas.org/irp/program/collect/uav_roadmap2005.pdf;

[12] ***, Advanced Aircraft Analysis software, DAR corporation, available at http:// www.darcorp.com/ Software/AAA/ accessed on 20 Apr. 2016.

REMOTELY AND PILOTED AIRCRAFT SYSTEMS / LAW AND POLICIES

LATERAL GUIDANCE LAWS FOR AUTONOMOUS TRACKING FLIGHT PATHS

Cristian VIDAN

Military Technical Academy, Bucharest, Romania (vidan.cristian@yahoo.com)

DOI: 10.19062/2247-3173.2016.18.1.28

Abstract: *Nowadays, for an UAV it is not enough to fly autonomously, so the latest researches in this domain refers to creating unmanned aircraft systems that are able to take decisions by its elves in that concern the obstacles that encounter in their path and finding the most efficient route towards destination. This paper presents three methods for UAV lateral guidance used for tracking straight-line segments and circular orbits. Each of the threes lateral guidance laws are used by path following block to command UAVs whose path following algorithm should be implemented to drive the UAV on the commanded route and to reach the final destination point. It is important to mention that these methods can be used, also, in presence of wind with accurate path following. Combining lateral guidance law with longitudinal guidance law can result a full guidance strategy which can provide the inputs to the autopilot for a very accurate path following.*

Keywords: *UAV, lateral, law, guidance, path following, straight-line, orbit*

1. INTRODUCTION

High computing power available to modern UAVs makes that the commands received by the aircraft to be processed almost in real time. Therefore, this thing led to the emergence of new challenges imposed to UAVs in terms of autonomous flight control. Tracking algorithms for a flight path becomes more and more complex and, also, requires increasingly more computational power.

In terms of an UAV system design, the following path problem is approached after the autopilot have been designed. Therefore, the altitude command, airspeed command, heading command from path following block are sent towards autopilot inputs.

The main path following problem is concerned with the design of control laws that drive an UAV to reach and follow a geometric path. A secondary goal is to force the object moving along the path to satisfy some additional dynamic specification[6].

In the first section of this paper are presented two lateral guidance strategies for straight-line path following. The first one refers to vector field method and the second one describe a path following algorithm depends on lateral acceleration. The notion of vector fields is similar to that of potential fields, which have been widely used as a tool for path planning in the robotics community. Note that the lateral acceleration algorithm is designed to follow a given path. It can be used to fly between waypoints simply by connecting the waypoints with either straight lines or arcs, but additional algorithms are needed to generate the paths and/or waypoints.

In the second section is presented an orbit following algorithm which is implemented to reduce the distance between UAV inertial position and the center of the orbit to be equal to orbit radius.

These lateral guidance laws for autonomous tracking flight paths are often implemented for different configurations of drones, different sizes and different autopilots.

2. LATERAL GUIDANCE STRATEGIES FOR STRAIGHT-LINE PATH FOLLOWING

2.1. VECTOR FIELD METHOD

Choosing a vector to be the origin of the path and another one to be a unit vector whose direction indicates the desired direction of travel can be described a straight-line path[1]:

$$P_{line}(r,q) = \{x = r + \lambda q, x \in \mathbb{R}^3, \lambda \in \mathbb{R}\} \tag{1}$$

The course angle of path $P_{line}(r,q)$ as measured from north is given by $\chi_q = \arctan 2\frac{q_e}{q_n}$, where $q = (q_n \quad q_e \quad q_d)^T$ expresses the north, east, and down components of the unit direction vector.

Assume that $\Re_i^{P_{line}} = \begin{pmatrix} \cos\chi_q & \sin\chi_q & 0 \\ -\sin\chi_q & \cos\chi_q & 0 \\ 0 & 0 & 1 \end{pmatrix}$ is the transformation matrix from the inertial frame to the path frame and $e_p = \begin{pmatrix} e_{px} \\ e_{py} \\ e_{pz} \end{pmatrix}$ is the relative path error expressed in the path frame. Therefore, the relative error dynamics in the north-east inertial plane, expressed in the path frame, are given by[1]

$$\begin{pmatrix} \dot{e}_{px} \\ \dot{e}_{py} \end{pmatrix} = V_g \begin{pmatrix} \cos(\chi - \chi_q) \\ \sin(\chi - \chi_q) \end{pmatrix} \tag{2}$$

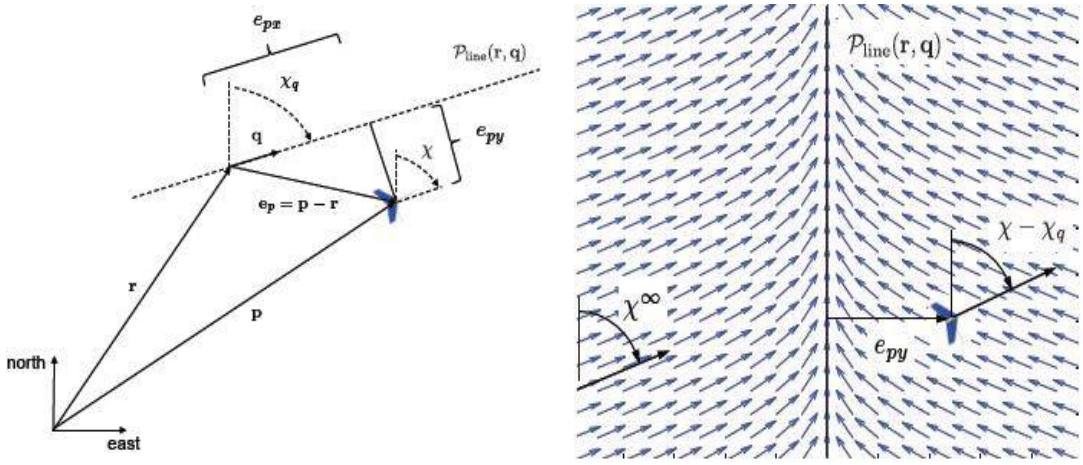

a) b)

FIG.1. a) The configuration of the UAV indicated by (p, χ), and the straight-line path indicated by $P_{line}(r,q)$; **b)** Vector field for straight-line path following.[1]

The lateral straight-line path following problem is to select commanded course χ_c so that $e_{py} \to 0$ when χ_q is known. The relevant dynamics are therefore given by[1]

$$\begin{aligned} e_{py} &= V_g \sin(\chi - \chi_q) \\ \ddot{\chi} &= b_{\chi}(\dot{\chi}_c - \dot{\chi}) + b_{\chi}(\chi_c - \chi) \end{aligned} \tag{3}$$

The objective for this lateral strategy is to select the commanded course angle χ_c in equation (3) so that e_{py} is driven to zero asymptotically. The strategy in this section will be to construct a desired course angle at every spatial point relative to the straight-line path that results in the UAV moving toward the path. The set of desired course angles at every point will be called a vector field because the desired course angle specifies a vector (relative to the straight line) with a magnitude of unity. The strategy is to construct the vector field so that when e_{py} is large, the UAV is directed to approach the path with course angle $\chi^{\infty} \in [0, \frac{\pi}{2})$, and so that as e_{py} approaches zero, the desired course also approaches zero. Thus, the desired course angle of the UAV can be defined as[1]

$$\chi_d(e_{py}) = -\chi^{\infty} \frac{2}{\pi} \tan^{-1}(k_{path} e_{py}) \tag{4}$$

Where: k_{path} - positive constant that influences the rate of the transition from χ^{∞} to zero

Large values of k_{path} result in short, abrupt transitions, while small values of k_{path} cause long, smooth transitions in the desired course.

If χ^{∞} is restricted to be in the range $\chi^{\infty} \in [0, \frac{\pi}{2})$, then clearly

$$-\frac{\pi}{2} < \chi^{\infty} \frac{2}{\pi} \tan^{-1}(k_{path} e_{py}) < \frac{\pi}{2} \tag{5}$$

for all values of e_{py}.

Therefore in this conditions the Lyapunov function $W(e_{py}) = \frac{1}{2} e_{py}^2$ can be used to argue that if $\chi = \chi_q + \chi_d(e_{py})$, then $e_{py} \to 0$ asymptotically, since

$$\dot{W} = -V_a e_{py}^2 \sin(\chi^{\infty} \frac{2}{\pi} \tan^{-1}(k_{path} e_{py})) \tag{6}$$

is less than zero for $e_{py} \neq 0$. The command for lateral path following is therefore given by

$$\chi_c = \chi_q - \chi^{\infty} \frac{2}{\pi} \tan^{-1}(k_{path} e_{py}) \tag{7}$$

2.2. LATERAL ACCELERATION METHOD

This flight path can be represented as interpolated waypoints or a continuous smooth curve. In either case, this path represents the desired location of the vehicle in 3D.

Accordingly, in FIG.2, using a selected reference point (RF) located on the desired path trajectory can be generated a lateral acceleration command(a_{lat}). This lateral acceleration command can be determinate by

$$a_{lat} = 2\frac{V^2}{L}\sin\eta \tag{8}$$

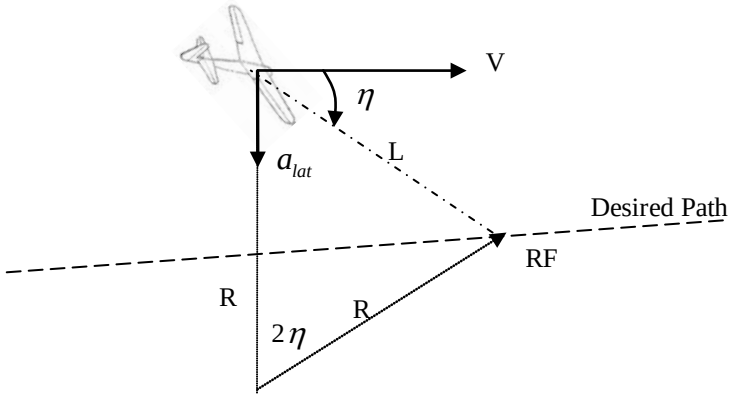

FIG. 2. Guidance algorithm using lateral acceleration

The direction of the lateral acceleration depends of the sign of the angle η. Therefore, if the reference point is to the right side of the UAV, then the UAV tend to align his velocity direction to L line segment direction.

Linearizing the system and assuming that η is small, e is a cross-track error and V is nominal aircraft velocity, the lateral acceleration command can be rewritten[2]:

$$a_{lat} = 2\frac{V}{L}(\dot{e} + \frac{V}{L}e) \tag{9}$$

The guidance law expressed in (8) is very effective and very simple to implement, which makes it to be one of the most used path following method.

Considering ϕ to be the bank angle and assuming that $L\sin\phi = ma_{lat}$ to achieve the desired lateral acceleration and that $L\cos\phi = mg$, then

$$\tan\phi = \frac{a_{lat}}{g} \tag{10}$$

The expression (10) can be used to develop the required bank angle command ϕ_d. Depending on the vehicle, the command ϕ_d is typically saturated at $\pm 15^0$.

3. ORBIT FOLLOWING

A curved path of an object about a point in space is defined as an orbit. Three main parameters can describe the path of the orbit.

$$\Omega_{orbit} = \{o = c + \lambda r(\cos\varphi, \sin\varphi, 0)^T, o \in R^3, \varphi \in [0, 2\pi], \lambda \in \{-1, 1\}\} \tag{11}$$

Where: c – the center of the orbit represented in inertial frame

r – the radius of the orbit

λ - the direction of the orbit ($\lambda = 1$ clockwise orbit, $\lambda = -1$ counterclockwise orbit);

In FIG.3, the distance from the orbit center to the UAV is d, and the angular position of the UAV relative to the orbit is φ.

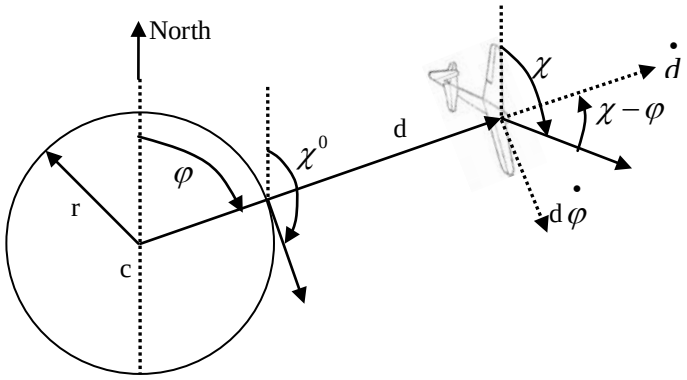

FIG.3. Orbit following algorithm

Assuming that the constant-altitude UAV dynamics in polar coordinates are derived by rotating the differential equations that describe the motion of the UAV in the north and east directions $\dot{p}_n$ and $\dot{p}_e$. Therefore, using the phase angle φ, can be describe the UAV equations of motion in the normal and tangential directions to the orbit:

$$\begin{aligned} \dot{p}_n &= V_g \cos\chi \\ \dot{p}_e &= V_g \sin\chi \end{aligned} \quad \Rightarrow \quad \begin{aligned} \dot{d} &= V_g \cos(\chi - \varphi) \\ \dot{\varphi} &= \frac{V_g}{d}\sin(\chi - \varphi) \end{aligned}$$

Where: V_g represent the ground speed of the UAV.

The control objectives of any orbit following method is to make the distance d similar to the orbit radius ρ and to make the course angle χ to χ^0 in the presence of external disturbances.

Where: $\chi^0 = \varphi + \lambda\frac{\pi}{2}$ - the desired course angle

Like it was shown in section 2.1, it is necessary to construct a course vector field that moves the UAV to the orbit Ω_{orbit}. This course vector field is represented in the following mathematical expression:

$$\chi_d(d-\rho,\lambda) = \chi^0 + \lambda * \tan^{-1}(K_{orbit}(\frac{d-\rho}{\rho})) \tag{12}$$

Where: $K_{orbit} > 0$ is a constant that specifies the rate transition from $\lambda\frac{\pi}{2}$ to zero.

Differentiating the Lyapunov function $W = \frac{1}{2}(d-\rho)^2$ along the system trajectory and assuming that $\chi = \chi_d$ we receive:

$$\dot{W} = -V_g(d-\rho)\sin(\tan^{-1}(K_{orbit}(\frac{d-\rho}{\rho}))) \tag{13}$$

which is negative definite since the argument of sin is in the set $(-\frac{\pi}{2},\frac{\pi}{2})$ for all d>0, implying that $d \to \rho$ asymptotically.

In conclusion the course command for orbit following is given by

$$\chi_c = \varphi + \lambda[\frac{\pi}{2} + \tan^{-1}(K_{orbit}(\frac{d-\rho}{\rho}))]. \quad (14)$$

3. CONCLUSIONS

This paper introduced algorithms for following straight-line paths and circular orbits in the presence of wind. For the first section the idea is to construct a heading field that directs the MAV onto the path and is therefore distinctly different from trajectory tracking, where the vehicle would be commanded to follow a time-varying location.

Methods that I have presented in this paper are much larger debated in [1], [2] and [4]. The purpose of this paper is to describe an integrated approach for developing guidance and control algorithms for autonomous vehicle trajectory tracking.

REFERENCES

[1] Randal W. Beard, Timothy W. McLain , *Small Unmanned Aircraft. Theory and Practice*, Princeton University, 2011;

[2] Kimon P. Valavanis, George J. Vachtsevanos, *The handbook of Unmanned Aircraft Vehicle*, Springer Reference 2014;

[3] D. R. Nelson, D. B. Barber, T. W. McLain, and R. W. Beard, *Vector field path following for miniature air vehicles*, IEEE Transactions on Robotics, vol. 37, pp. 519–529, June 2007.

[4] D. R. Nelson, D. B. Barber, T. W. McLain, and R. W. Beard, *Vector field path following for small unmanned air vehicles*, American Control Conference, (Minneapolis, Minnesota), pp. 5788–5794, June 2006.

[5] I. Kaminer, A. Pascoal, E. Hallberg, and C. Silvestre, *Trajectory tracking for autonomous vehicles: An integrated approach to guidance and control*, AIAA Journal of Guidance, Control and Dynamics, vol. 21, no. 1, pp. 29–38, 1998.

[6] A. Pedro Aguiar, Dragan B. Dacic , Joao P. Hespanha , Petar Kokotovic, *Path-following or reference-tracking? - An answer relaxing the limits to performance,* University of California, Santa Barbara.

DEVELOPMENT OF INTELLIGENT ALGORITHMS FOR UAV PLANNING AND CONTROL

Victor VLADAREANU[*], Elena-Corina BOSCOIANU[**], Ovidiu-Ilie SANDRU[***], Mircea BOSCOIANU[***]

[*]Institute of Solid Mechanics of the Romanian Academy, Bucharest, Romania (vladareanuv@gmail.com)
[**]National Institute for Aerospace Research "Elie Carafoli", Bucharest, Romania
[***] Politehnica University, Bucharest, Romania (oisandru@yahoo.com)
[****]"Henri Coandă" Air Force Academy, Braşov, Romania (boscoianu.mircea@yahoo.com)

DOI: 10.19062/2247-3173.2016.18.1.29

Abstract: *The paper presents a review of intelligent techniques used for the optimization of an UAV mission plan using sensory input. The constrained problem is evaluated using evolutionary algorithms (such as GAs and PSO), while extenics logic is used to evaluate the sensor fusion state. The review is part of a innovative project dealing with swarm UAV missions and AirWing testing.*

Keywords: *UAV, evolutionary algorithms, neutrosophy*

1. INTRODUCTION

Beginning with the 1950s and 1960s, several independent research papers dealt with the possibility of mimicking the basic idea of evolution, as found in nature, to aid in the optimization of engineering problems (Mitchell, 1998) [1]. Thus the field of evolutionary computing was born. Today, population-based meta-heuristic methods such as genetic algorithms (evolutionary algorithm) and particle swarm optimization (swarm algorithm) are beginning to find a place in the optimization of controllers in industry applications [2-4].

In a most interesting and helpful paper, Thomas and Poongodi (2009) argue the benefits of using a genetic algorithm to tune the term gains of a controller in comparison with the classical Ziegler-Nichols scheme [2]. A genetic algorithm is a search algorithm that attempts to improve an initial population of 'chromosomes' (initial solutions) in regards to a user-defined fitness function. Based on the mechanisms of natural selection, the algorithm employs stages of 'selection', 'crossover' and 'mutation' to advance to the next population [1,2]. The authors run a series of simulations on both controllers and find that the GA-tuned system has a much faster response and less steady state error. An interesting idea put forth in the paper is using the classical values as the starting population for the genetic algorithm [2] (while GAs generally start from a random population, it can be specified by the user if so desired (Mitchell, 1998) [1]).

Khan, Abdulazeez et al (2008) delve deeper into the uses of genetic algorithms by attempting to design an optimal fuzzy logic controller [3]. They build upon the work of Byrne (2003) [5] in using a GA to tune the rule base of a fuzzy controller and compare it with a conventional controller. While the subject is treated superficially at times, it does

provide an interesting look into what could be the future of numerical processing as far as controllers are concerned. Byrne himself notes (2003) that classical control, in comparison to a GA-tuned fuzzy, is more prone to faults for a multiple-input multiple-output (MIMO) system [5].

Particle swarm optimization is a newer approach to evolutionary search algorithms which is derived from the natural movement of insects and other 'social' biological organisms (Kennedy, Eberhart, 1995) [6]. Gaing (2004) presents a novel approach using particle swarm optimization to determine the gains of a controller in an AVR system and quotes Fogel (2000) in claiming that 'the premature convergence of genetic algorithms degrades their performance and reduces its search capability' (Gaing, 2004) [7], [8]. He then goes on to compare it with a GA-tuned PID controller, arriving at the conclusion that it provides more robust stability and efficiency, while not suffering from the drawbacks of premature convergence and high computational requirements of the GA-tuned scheme, which obviously also makes it faster [7]. This is perhaps one of the best written papers referenced here and its findings should be of great interest for future research.

2. EVOLUTIONARY ALGORITHMS

Evolutionary Algorithms (EAs) are a type of optimization algorithms which are derived from the evolution of biological populations found in nature. As a search optimization algorithm, it seeks to minimize the value of an objective function supplied by the user in the context of user – defined constraints for the search space, the dimension of which equals the number of independent variables that are part of the objective function (Fogel, 2000) [8].

A Genetic Algorithm (GA) is the most popular type of EA. It mimics the process of natural evolution to obtain a heuristic result for the search problem. In the case of natural selection, constant improvement in a species is brought about through continuous exchange of the genetic makeup of its individuals [5]. This results in fitter, better adapted individuals over the course of a number of generations. A genetic algorithm adapts this process for use in numerical optimization problems.

Prospective solutions are coded as bit strings corresponding to the basic building blocks found in nature, from which they borrow the name of chromosomes. These individuals make up the population of the Genetic Algorithm. In cases where there is some initial knowledge or acceptable estimate of the solution points (for example when we would like to improve an existing heuristic solution), an initial population can be specified for the algorithm. Otherwise, it will be created randomly. Each individual's fitness is tested against the general fitness of the population as part of the process of passing from one generation to the next. This is done by applying the fitness function, which is the function to be minimized, to each individual. A fitter individual will have a higher probability of being selected for reproduction (passing on its genetic information) [5].

The next stage of evolution can then be broken down into selection, crossover and mutation. Selection is the process whereby the individuals from the previous generation are selected probabilistically based on their fitness value into an intermediary population. Crossover is analogous to the act of parenting, producing new individuals from those previously selected by recombining their chromosomes. Mutation means randomly changing a bit within a chromosome with the aim of making the algorithm less susceptible to falsely converging on local minima. In genetic algorithms, mutation is viewed as a background process with a very low probability [5].

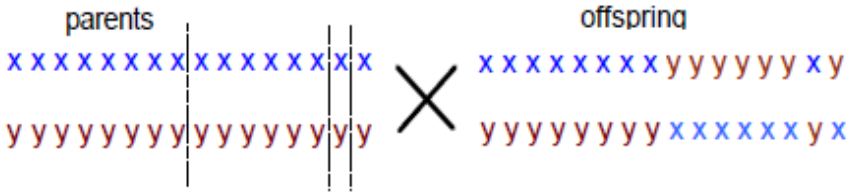

FIG.1. Crossover in a genetic algorithm

While there are a number of options for when a GA should terminate, the most common are specifying a minimum change in the overall fitness function that should be met in order to continue to the next generation, a fixed number of generations for which the program should be run, or both (whichever comes first).

Particle Swarm Optimization (PSO) is another evolutionary algorithm that has seen increased interest in recent years since being introduced by Kennedy and Eberhart in 1995 [6][7]. Instead of using genetic information to modify the individual, the PSO algorithm lets particles traverse a solution space at speeds which are dynamically adjusted according to their track history and other particle's track history. Each particle records a history of the best solution it has found, as well as the best solution found by the overall population. At each time, the velocity of each particle is dynamically changed towards those two bests achieved so far [6].

Although as of this writing there is no standard PSO Toolbox included in Matlab, quite a number of them are readily available on the developer's community website (Rapai, 2008) [9]. The toolbox's implementation and use in Matlab are very similar to those of the GA Toolbox.

There is a lot still to be discovered about evolutionary algorithms in general as well. As mentioned previously, the definition of the objective function is paramount for the use of an evolutionary algorithm, and can, in theory, be weighed differently depending on the preferred system behavior. More complex objective functions, the inner workings of the algorithm itself (mutation rate in GAs, for example) and the impact of various implementation options (such as maximum number of generations, initial population, etc.) amount to virtually limitless opportunities for research in one of the fields found at the forefront of artificial intelligence.

3. ARTIFICIAL NEURAL NETWORKS

Using artificial neural networks and regression implementations to model the information received from the sensor, an accurate reading of the measured sensor array can be obtained without the need for costly components. It also makes the scanner less susceptible to anomalous readings given by the interpolation of different wave signals. For a time-of-flight optical scanner, for instance, this is achieved by using the first three reception trigger signals for the returning wave to estimate the measured distance, rather than having to use a fourth trigger signal on the falling slope, which introduces dead time and may decrease performance due to wave interpolation [10].

There are a great number of methods which can be used to model such an approach. The first step is to test the assumption using linear regression and neural networks on the mean values generated for each point at each of the four triggers. The total sum of differences across all values is called the cost function (J).

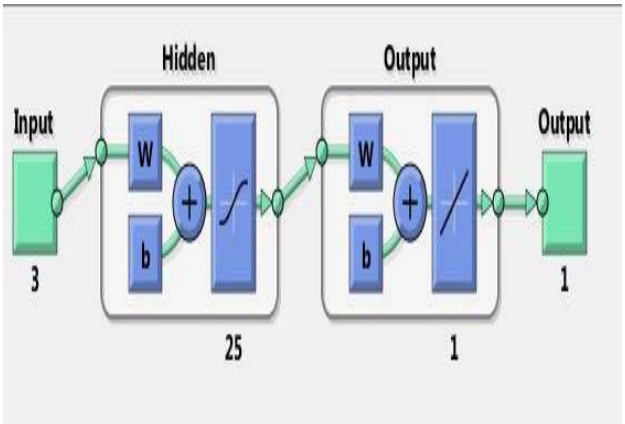

FIG. 2. Artificial neuronal network with one hidden layer (25 neurons)

An artificial neural network consists of a number of 'hidden' features (or neurons) associated with a network of weights, which are improved each iteration until their prognosis is within an accepted tolerance or the number of iterations expires. An example of the investigated network topographies is available in Figure 2.

From the available data, approximately 70% of the examples are used for the actual training of the network. Another 20% is used for cross-validation, whereby the weights are adjusted again based on the observed deviations. The remainder is used as a test for the obtained network, which provides a measure of its accuracy and of whether the network over-fits the available data.

By using the artificial neural network toolbox in Matlab with the obtained data and training a number of network configurations, as well as running through a variety of linear regression models, estimates can be obtained for comparison with the actual mean values derived from the experimental data.

The end result is the selection of an artificial neural network to be implemented into the sensor software with the trained weights obtained in the simulation. This will lead to faster and more robust results being obtained from the raw data, as well as the ability to run more tests using the sensor in actual situations (both static and dynamic).

4. EXTENICS

Extenics is a science whose stated aim is to deal with unsolvable problems. With applications in artificial intelligence, business, marketing, planning, design, control theory and image processing, to name just a few, it is one of the fastest developing new fields of study today.

In his 1983 paper, 'Extension Set and Non – Compatible Problems', Cai Wen put down some of the earlier concepts and established the foundation of what would later become Extenics Theory, a wide – spanning inter-disciplinary science [11](the reference is the 1990 translation). Early papers were few and far between, before the framework of Extenics was established and it became recognized as a field of scientific research in its own right. Further expansion brought important updates both in the formal expressions and the tools used in Extenics. Thus was developed a formalism which would facilitate working within the latest trends of technical processing and whose improvement is still on-going as an important direction in Extenics [12].

One of the first papers to discuss an involved engineering application was published in 1994 by Prof. Wang and entitled 'Extenics control' [13]. It provides a blueprint for the first Extenics controller, which has subsequently undergone numerous modifications and opens up the field of Extenics control proper.

Since the beginning of the new millennium, an expanded research group combined with the years of existing built-up expertise to produce new directions of research in the field. This outlined the beginning of their respective specialized work, making Extenics applications wide-spread in the academic and business world, especially in the Asian continent. In 2012 a monograph work entitled 'Extenics Engineering' was published in English [12] (the previous Chinese version had come out in 2007), marking a very important step to promoting Extenics world-wide.

Extenics is said to be a science combining Mathematics, Engineering and Philosophy [12]. With respect to its application and use it is a trans-disciplinary science, classified as belonging to the wider field of Artificial Intelligence. Extension Logic is purported by the authors to extend fuzzy logic, much in the same way that fuzzy logic extends the classical Cantor logic [11]. This is necessary for work with Extension Sets in contradictory problems and for Extension Strategy Generation Systems (ESGSs)[14]. An example of such strategies is shown in Figure 3.

The main goal of Extenics, as set forth in almost every paper that deals with the issue, as well as throughout its theoretical mainframe, is the generation of solutions to contradictory problems [11]. This is of course very important in and of itself, however in Extenics the process by which this goal is to be achieved is also of great scientific relevance. Contradictory problems, or seemingly impossible problems, have been solved throughout history by using human ingenuity. Extenics studies the creation of such innovative ideas and seeks to develop procedures for understanding and creating new, original thought with the help of modern day advances in computer science. It is partly for this reason that Extenics is classified as part of Artificial Intelligence and is one of the fastest developing new fields of study in the world today [15].

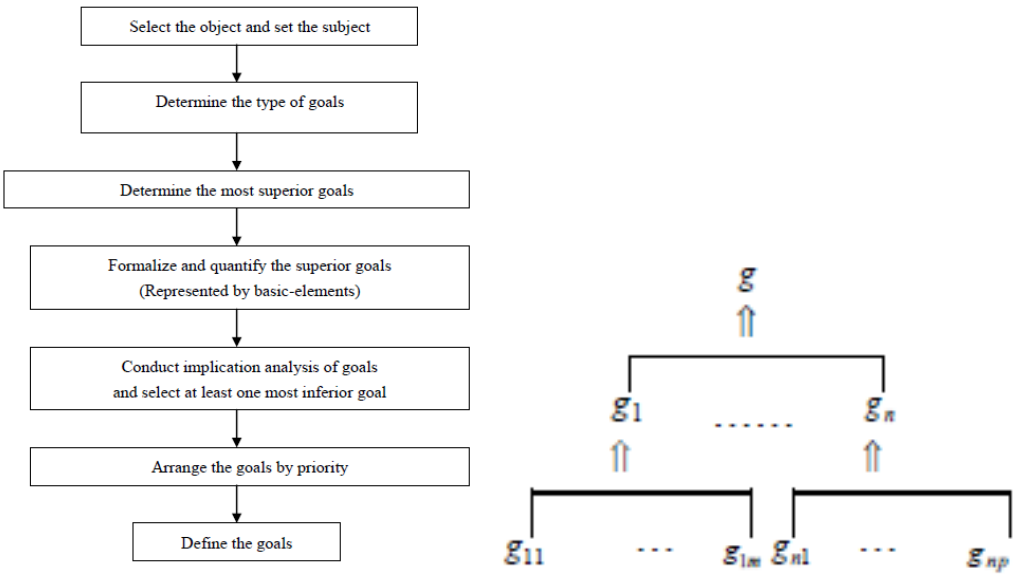

FIG.3. Extenics Strategy Generation and Goal Decomposition

Aside from Extension Sets and Logic, Extension Transformation is one of the core concepts in the theory [12]. It is said that the only constant in life is change, and Extenics emphasizes the need to adapt problem specifications to ever-evolving contexts. Transformation is at the basis of solutions to contradictory problems, both from a theoretical and a practical standpoint. Basic element representations are designed to

support dynamic modelling (as a type of parametric modelling) and solution algorithms consist, for the most part, of iterations of transforms and compound transforms.

CONCLUSIONS

The methods and algorithms presented throughout this paper have been thoroughly studied and simulated and will be used for the implementation of UAV motion strategies in swarm unmanned aviation projects, both in high-level decision algorithms and flight optimization procedures, as well as in lower-level implementations of control and sensor fusion architectures and hierarchies. Further implementation and simulation will also feature software-in-the-loop mission planning and intelligent formation control, of which the algorithms described in this paper will be an integral part.

AKNOWLEDGMENT

This work was accomplished through the Partnerships Program in priority fields - PN II, developed with the support of MEN-UEFISCDI, PN-II-PT-PCCA-2013-4-1349, MASIM project no. 255/2014.

REFERENCES

[1] Mitchell, M., *'An Introduction to Genetic Algorithms'*, First MIT Press, 1998
[2] Thomas, N., Poongodi, P., *'Position Control of DC Motor Using Genetic Algorithm Based PID Controller'*, Proceedings of the World Congress on Engineering 2009, Vol. II, WCE 2009, Jul. 2009
[3] Khan, S., Abdulazeez, S.F., Adetunji, L.W., Alam, Z., Salami, M.J., Hameed, S.A., Abdalla, A.H., Islam, M.R., *'Design and Implementation of an Optimal Fuzzy Logic Controller using Genetic Algorithm'*, Journal of Computer Science 4, 2008
[4] Gaing, Z.L., *'A Particle Swarm Optimization Approach for Optimum Design of PID Controller in AVR System'*, IEEE Transactions on Energy Conversion, vol. 19, no. 2, Jun. 2004[3] T. R. Nail, *A disturbance-rejection problem for a 3-D airfoil exhibiting flutter*, Thesis, Virginia Tech., 2000;
[5] Byrne, J.P., *'GA-optimization of a fuzzy logic controller'*, Master's Thesis, School of Electronic Engineering, Dublin City University, 2003
[6] Kennedy, J., Eberhart, R., *'Particle Swarm Optimization'*, Proceedings of the IEEE International Conference on Neural Networks, vol. IV, 1995
[7] Gaing, Z.L., *'A Particle Swarm Optimization Approach for Optimum Design of PID Controller in AVR System'*, IEEE Transactions on Energy Conversion, vol. 19, no. 2, Jun. 2004
[8] Fogel, D.B., *'Evolutionary Computation: Toward a New Philosophy of Machine Intelligence'*, 2nd ed. IEEE Press, 2000
[9] Rapai, M., *'Particle Swarm Optimization (PSO) Algorithm'* (Matlab code), Nov. 2008, http://www.mathworks.com/matlabcentral/fileexchange/22228-particle-swarm-optimization-pso-algorithm
[10] Iliescu, M., Vladareanu, V., Serbanescu, M., Lazar, M.,*'Product Development of a New 2D Time-of-Flight Scan Laser'*, Journal of Control Engineering and Applied Informatics, submitted for publication, Oct. 2015
[11] Cai Wen. *Extension Set and Non-Compatible Problems [A]. Advances in Applied Mathematics and Mechanics in China* [C]. Peking: International Academic Publishers, 1990.1-21.
[12] Yang Chunyan, Cai Wen, *'Extension Engineering'*, Science Press, Beijing, 2002
[13] Wang Xingyu, Li Jian. *„Extension Control" [J]. Control theory & applications*, 1994, 11（1）: 125-128
[14] Li Lixi, Yang Chunyan, Li Huawen. *Extension Strategy Generation System* [M]. Science Press, 2006.
[15] Boscoianu, M., Cioaca, C., Vladareanu, V., Boscoianu, C., *"An Active Support Instrument for Innovation in Deep Uncertainty – the Strategic Management Ingredients in Robotics and Mechatronics"*, Procedia Computer Science 65 (2015): 210 – 217. ELSEVIER, www.sciencedirect.com, doi:10.1016/j.procs.2015.09.112, www.elsevier.com/locate/procedia, ISSN 1877-0509, ELSEVIER

CAMERA CALIBRATION FOR VISUAL ODOMETRY SYSTEM

Titus CIOCOIU, Florin MOLDOVEANU, Caius SULIMAN

"Transilvania" University, Braşov, Romania (ciocoiutitus@yahoo.com, moldof@unitbv.ro, caiussuliman@yahoo.com)

DOI: 10.19062/2247-3173.2016.18.1.30

Abstract: *Estimating it's ego-motion is one of the most important capabilities for an autonomous mobile platform. Besides odometry ,inertial sensors ,DGPS, laser range finders and so on, vision based algorithms can contribute a lot of information. We want to emphasize the fact that stereo odometry is a chain of several single sub processes where each relies on its predecessor's results. In this paper we will present a stereo camera calibration method and with the help of this we will try to find the intrinsic and extrinsic parameters. The method was implemented with succes in OpenCV.*

Keywords: *intrinsic,extrinsic,odometry,stereo,triangulation,calibration,distorsion.*

1. INTRODUCTION

Camera calibration is a necessary step in 3D vision in order to extract metric information from 2D images.[2][8]

A camera is considered to be calibrated when the parameters of the camera are known (i.e. principal distance, lens distorsion, focal length etc.). For this purpose, in the last twenty years, many calibration algorithms have been developed in the computer vision community. This algorithms are generally based on the perspective camera models. Among themost popular is Robert Tsai's calibration algorithm (Horn, 2000), (Tsai, 1987). His algorithm is based on the pinhole model of perspective projection. The model proposed by Tsai assumes that some of the camera's parameters are given by the are manufacturer, in order to reduce the initial guess of estimation. The algoritm requires n feature points (n> 8) per image and solves the calibration problem with a set of n linear equations based on the radial alignment constraint. A second order radial distorsion model is used while no decentering distorsion terms are considered. This method can be used with either a single image or multiple images of a planar or 3D calibration grid.

Another important and very popular calibration method has been developed by Zhenyou Zhang (Zhang, 1998). His method requires a planar checkerboard grid to be placed in front of the camera at different orientations. The algorithm uses the extracted corner points of the checkerboard to calculate a projective transformation between the image points of the different images. The camera's intrinsic and extrinsic parameters are recovered using a closed-form solution. The radial distorsion terms are recovered within a linear least-squares solution.

The final step is the use of a non-linear minimization of the reprojection error that refines all the recovered parameters. Zhang's method is similar to the oneproposed by Triggs (Triggs, 1998). Zhang's algorithm is the basis behind some popular open source implementations of camera calibration (i.e. Intel's OpenCV and Matlab's calibration toolkit).

2. CONTRIBUTION TO SUSTAINABILITY

Stereo Visual Odometry Systems, as part of Active Vision Systems, is an important concept still to be integrated and supported by novel technologies, promising to expand into most of today's domains, including automotive, autonomous driving, robotics and directly aiming for a new concept, driving and navigation systems with no need of satellites connectivity and GPS position data.

A sustainable key feature that our system provides is given by the very low energy consumption compared with the actual GPS systems, which is caused by eliminating the permanent connectivity between the navigation system and satellites. To expand functionality, we propose two features algorithms that properly manage to help the system to have a much better accuracy. The small dimensions of our proposed stereo odometry system along with its developed control system make the device ideal for future autonomous mobiles needs. Our proposed system manages to reduce the main disadvantage of most of the present day navigation systems – the positioning error of the stereo visual odometry system which in our case is significant lower compared with same parameter of the modern navigation systems in the market.

The goal of the presented system, algorithms and tests is to obtain preliminary data for a complete independent navigation and mapping system that we intend to develop.

The proposed system will help future development of already existing domains by opening a path to new ideas and trends for self-sustained and advanced supportive environments. We anticipate that the results presented in this paper will also contribute to autonomous driving evolution, which represent in our view a small step for sustaining future technologies' development.

3. EXPERIMENTAL RESULTS

A. Stereo Visual Odometry System

In automotive and computer vision, visual odometry is the process of determining the position and orientation of a robot by analyzing the associated camera images.

The project was developed in multiple steps, as it follows. First step was to develop the mechanical model necessary for sustaining the servo motors and web cameras and afterwards it was developed the board data acquisition and control servo motors.

The experimental prototype is made of (Fig.1), acquisition and control board consists of:

- Supply via a laptop charger;
- LM7805 voltage regulators;
- MAX 232 Integrated Circuit;
- ATmega8 microcontroller;
- DB-9 connector;
- 2 Futaba S3305 servo motors;
- 2 Logitech Quick Cam Pro webcams 9000;

First step is to detect key points for each captured frame from the cameras system with two different features detection algorithm (ORB, FAST). After that we eliminate outliers points using RANSAC algorithm and performs stereo correlation.The functional block diagram is the following:

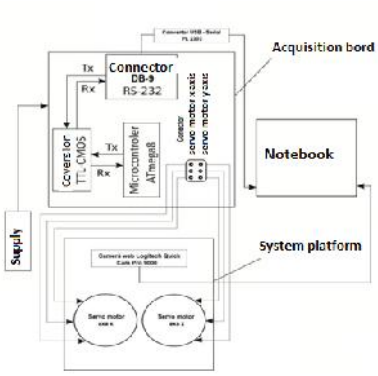

FIG.1. General block diagram of the entire system active vision;

With the remaining points, coordinate transformation is performed from 2D (x,y) to 3D(x,y,z) with the triangulation method (Fig.2).

Having the camera parameters and using the triangulation method, the 3D coordinates of the points are obtained (x_l- coordinate of the feature from the left image, x_r- coordinate of the feature from the left image)[2].

$$Z=bf/(x_l-x_r) \quad (1)$$

The next step is to use the decomposition (SVD method) in order to obtain the values of the rotation matrix (R) and translation (T) of the cameras. To see more easily if the system calculates the correct system trajectory, we introduced additional calculation of the 3 angles of the camera system (roll, pitch, yaw).

To be able to compare the odometry system result, meanwhile the latitude and the longitude of the stereo cameras system are saved for each frame. With those data the system trajectory is created.

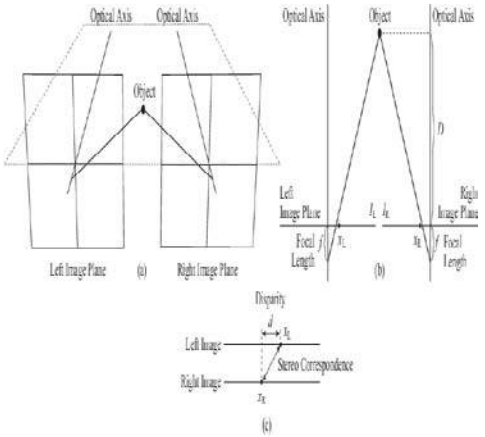

FIG.2. Triangulation method and stereo geometry f- focal length, x_l- coordinate of the feature from the left image, x_r-coordinate of the feature from the right image.

These trajectories are compared in order to determine if the odometry system error is approximately equal to 5% [3].

4. EXPERIMENTAL EVOLUTION

For the experimental evaluation of the above method we have used a wireless CMOS camera. Because the images taken by the camera were very noisy, we needed a filter to remove that noise. The filter used for this purpose was a simple one, the median filter.

The calibration object used for the process consists of two perpendicular planes, in our case we have used two sides of a box. On the two sides we added a calibration pattern consisting of square tiles. The sides of the tiles are 1 cm. Another important step in the calibration process is to choose a convenient world coordinate frame (see Fig.1).[8]

The first step of the calibration process is to set the 3D matrix XYZ, that containts the 3D coordinates of the calibration points. We have chosen those points as follows: as we know the sides of the tiles are 1 cm, so the XYZ coordinates for a point near the origin of the world system are (-1, 0, 1). Then we need to set up the 2D matrix xy, matrix that contains the 2D coordinates of the calibration points. For this purpose we have developed an interactive program that colects the 2D coordinates of these points (see Fig.2).[1][8]

For an accurate calibration process we need between 20 and 30 points. After this step is completed, the estimation of the projection matrix M can be done by applying the method presented early in this work.

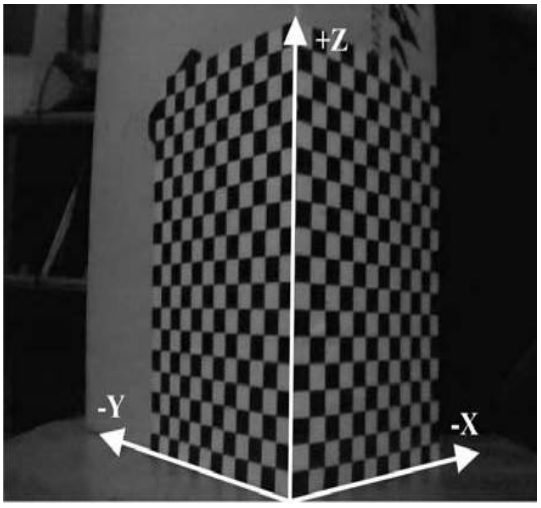

FIG.1. *The calibration object and the chosen world coordinate frame.*

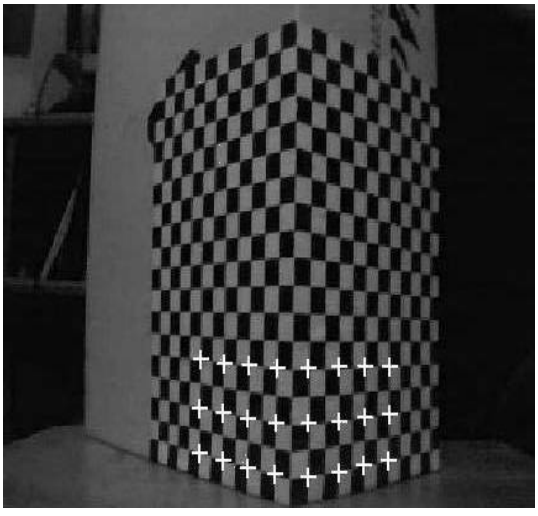

FIG.2. The calibration object and resulting calibration points.

To show that the calibration process was accurate we have considered some cubes with the sides equal to the sides of the tiles and we have put them over the calibration pattern. It can be easily observed the correction of the projection matrix estimation (see Fig.3).

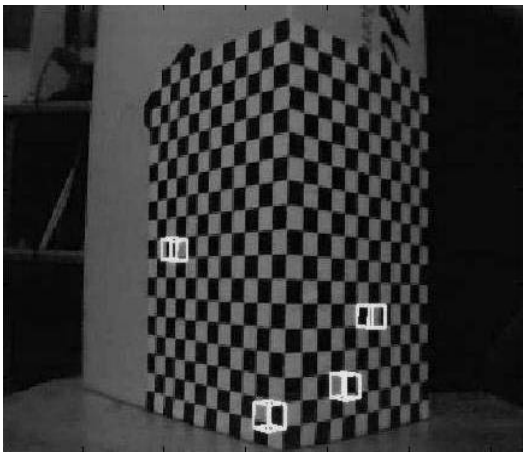

FIG.3. The calibrated camera allows for 3D objects to be drawn in the scene.

In the final step we have computed the estimates for the camera's intrinsic and extrinsic parameters from the projection matrix. The resulting intrinsic parameters are:

$$\begin{aligned} &f_x = 321.0655\,px;\ f_y = 329.5092\,px, \\ &o_x = 156.8256; o_y = 164.7667 \end{aligned} \tag{2}$$

And the camera's extrinsic parameters obtained from the calibration process are:

$$R = \begin{pmatrix} 0.0192 & -0.0070 & 0.9998 \\ 0.7375 & -0.6751 & -0.0189 \\ -0.6750 & -0.7377 & 0.0078 \end{pmatrix} \tag{3}$$

$$T = \begin{pmatrix} -6.2695 \\ -0.6508 \\ 23.9378 \end{pmatrix}$$

The entire calibration process has been implemented in the programming and simulation environment from Intel OpenCV.

CONCLUSION AND FUTURE WORK

The method presented here is a simple calibration method that gets the job done. The precision of the calibration depends on how accurately the image and world reference points are located. The errors on the parameter estimates propagate to the result of the application. The calibration process ultimately depends on the accuracy requirements of the target application. For example, in industry accuracies of submillimeter are required. In other application are accepted even errors of centimeters.

Stereo visual odometry systems remain one of the major research issues for the Autonomus driving and navigation. Creating a totally independent system for the user like an alternative for the standard navigation systems is an important goal to be reached.

As a future development direction we intend to apply a fuzzy logic control algorithm in order to improve the system accuracy. Also we intend to implement a new algorithm with a better accuracy to convert the points from 2D to 3D. Our intention is to research and develop a complete stereo odometry system with application in actual and future areas of interest.

AKNOWLEDGMENT

This paper is supported by the Sectoral Operational Programme Human Resources Development (SOP HRD), ID137070 financed from the European Social Fund and by the Romanian Government.

REFERENCES

[1] Cojocariu, D. „*Acquisition, processing and image recognition*", Ed. University, Craiova Romania 2002.

[2] Corke, P.I. „*Visual Control of Robots: A High-performance Visual Servoing*", Research Studies Press Ltd., John Wiley & Sons Inc, Great Britain 1996.

[3] Gary, B. , Adrian, K. „*Learning Computer Vision with the OpenCV library*", O'Reilly, United States of America 2008.

[4] Constantin, V. „*Image analyze and processing*" , Ed. Politehnica 1999.

[5] Horn, B.K.P. *"Tsai's camera calibration method revisited."* Technical report, MIT Artificial Intelligence Laboratory website 2000.

[6] Jimenez, E.V.C., Navarro, D.Z.,Rojas, R. „*Intelligent Active Vision Systems for Robots*", Cuvillier Verlag, Gottingen, Germany 2007.

[7] Suliman C. Moldoveanu F. *"Single Camera Calibration in 3D Vision "* , IEEE Journal of Robotics and Automation (2009)

[8] Tsai,R.Y.A *"Versatil Camera Calibration for 3D Machine Vision"* In: IEEE Journal of Robotics and Automation, Vol. RA-3, No. 4, p.323-344. (1987).

[9] Trucco,E.,Verri,A.*"Introductory Techniques for 3D computer vision"* Prentice- Hall, Inc., Upper Saddle River, New Jersey, ISBN 0-13-261108-2.(1998).

[10] Zhang, Z. *"A Flexible New Technique for Camera Calibration"* Technical Report MSR-TR- 98-71, Microsoft Research.(1998).

FUZZY LOGIC CONTROL FOR A DC TO DC BUCK CONVERTER

Jenica-Ileana CORCAU, Liviu DINCA

*University of Craiova, Faculty of Electrical Engineering,
Department of Electrical, Energetic and Aerospace Engineering, Craiova, Romania
(jcorcau@elth.ucv.ro, ldinca@elth.ucv.ro)

DOI: 10.19062/2247-3173.2016.18.1.31

Abstract: *In this paper one presents a model and an analysis of a dc-to-dc Buck converter, in closed loop, from 24V to 12 V with a power of 500 W. Model is implemented in MATLAB/SIMULINK toolbox SIMPOWERSYS. Control system is a fuzzy logic one, Mamdani type, and using P.I. configuration. One opted for a fuzzy controller due to its flexibility in its configuration and tuning process, and also because it doesn't need to know a mathematical model for the Buck converter. Fuzzy controller is composed of two sub-controllers in parallel, one for the proportional component and a second for integrative component. One proposes this configuration because fewer inference rules are necessary and also the tuning process is easily accomplished compared to a fuzzy controller with two inputs. Implemented model is validated by numerical simulations and the results are realistic and confirm the possibility to use this type of controller.*

Keywords: *dc to dc buck converter, fuzzy logic controller, analysis*

1. INTRODUCTION

In modern electric power systems, interface between power sources as fuel cells, photovoltaic cells, batteries, and the power bus, and also the control for the power bus voltage are realized by static DC to DC converters. These converters have a wide and continuous development with evolution of power electronic devices. There are many constructive variants with specific destinations as: aircraft, spaceships, telecommunications etc. On aircraft both DC and AC converters are used. In the most situations, input voltage - V_s, for converters is not stabilized, but converter produce a stabilized output voltage - V_{out}, with a different amplitude and possibly with a different polarity than V_s [1]-[2].

Conversion ratio, or voltage gain, in stationary regime $M(d)$ is defined as ratio between output DC voltage V_{out} and input DC voltage V_s [2]

$$M(d)=\frac{V_{out}}{V_s}. \tag{1}$$

so, for the buck converter

$$M(d) = d. \tag{2}$$

Command pulses duty-cycle is

$$d = \frac{t_{on}}{T_s}, \tag{3}$$

where T_S is the switching period.

A wide used method for duty cycle variation is PWM modulation of the command signal of the switching device. The switch is ON when the command signal is '1' and is OFF when the command signal is '0'. PWM generator produce pulses with a specified frequency, e.g. 10 kHz, in this case rectangle pulses, with values '1' and '0'. Input signal for PWM changes between -1 and 1, and duty cycle, of the output pulses, changes between 1 and 0 respectively [3]-[10].

Figure 1 presents DC to DC buck converter in closed loop with a fuzzy logic controller. In figure 2 one presents an equivalent circuit for continuous current regime (CCM) of the buck converter.

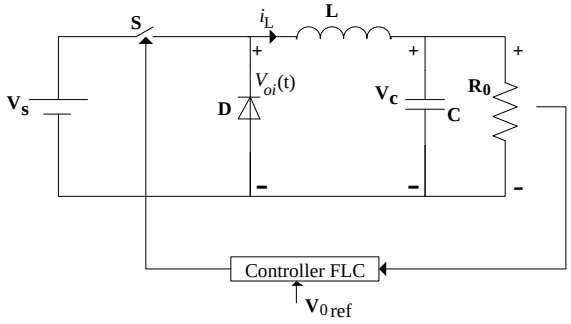

FIG. 1. DC to DC buck converter in closed loop

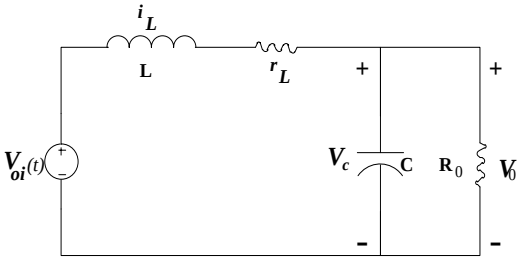

FIG. 2. An equivalent circuit for CCM regime of the buck converter.

Applying Kirchhoff laws for the circuit in figure 2 one obtain the following equations [6]

$$\begin{aligned} r_L i_L + L\frac{\mathrm{d}i_L}{\mathrm{d}t} + V_C &= V_{0i} \\ i_L - C\frac{\mathrm{d}V_C}{\mathrm{d}t} - \frac{V_C}{R} &= 0 \end{aligned}. \tag{4}$$

Automatic control of buck converters was studied in many works, like [3]-[10]. One follows to stabilize output voltage with respect input voltage variations and eventually with respect the converter's load. For Buck converter, static theoretic characteristic is

$$U_{out} = U_{in} \cdot d, \tag{5}$$

where *d* is the duty cycle of the command rectangular signal of the switch. It can vary between 0 and 1 and one observes the output voltage is less than the input.

Classical control like P., P.I., P.D. and P.I.D. need to know a linear mathematical model for the converter.

A modern control technique that doesn't need to know a mathematical model for the converter is fuzzy logic technique. One can to obtain P., P.I., P.D. and P.I.D. fuzzy controllers

2. FUZZY CONTROLLER FOR DC TO DC BUCK CONVERTER

Fuzzy controllers fulfill the same tasks like a classic P.I.D. controller. Fuzzy controller differs from the classic one in that it manages the control complex space in a heuristic manner. However, the fuzzy controller can approximate, with any precision level, linear and non-linear control functions. In many situations is easier to obtain a fuzzy controller with high performance than a classic P.I.D. controller with same performances [11].

Implementation of a fuzzy controller implies control function codification in fuzzy rules set which operates on fuzzy sets resulted in the fuzzyfication of the input and output domains.

Usually, a P.I. fuzzy controller has two inputs and one output. Fuzzy controller in this application consists in two fuzzy sub-controllers (with one input and one output), one for the proportional component and one the second for the integral component. One choose this option due to simplified definition of the inference rules and an easier tuning process. Along side these advantages, this configuration needs a shorter calculus time.

First fuzzy controller is P type with one input (output voltage error) and one output (duty cycle variation). There are 4 membership functions both for input and the output. These membership functions are presented in figures 3.a and 3.b .

Linguistic terms for input (output voltage error) were considered *NAe, NMe , PMe* and *PAe* and for output (duty cycle variation) *YNG, YNMS, YPMS, YPG.* Inference rules were defined as: *IF error is NAe THAN output is YNG; IF error is NMe THAN output is YNMS; IF error is PMe THAN output is YPMS; IF error is PAe THAN output is YPG.* By this way results control function in figure 3.c.

Fuzzy controller for the integrative component considered also 4 membership functions for input and for output. Membership functions were considered trapezoidal, like in figures 3.d and 3.e.

Linguistic terms for the input (output voltage integral) were considered *NAie, NMie , PMie* and *PAie* and for output (duty cycle variation) *YNG, YNMS, YPMS, YPG.* Inference rules were defined as: *IF error is NAie THAN output is YNG; IF error is NMie THAN output is YNMS; IF error is PMie THAN output is YPMS; IF error is PAie THAN output is YPG.* By this way results control function in figure 3.f. Closed loop converter system was implemented in SIMULINK in figure 4. This kind of fuzzy controller was propose by authors in [7].

In the definition of membership functions and inference rules one aimed to obtain a higher slope for the control surface near origin, both for proportional and integrative component. This fact can be observed for the control surfaces in figures 3.c and 3.f.

3. NUMERICAL SIMULATIONS

For a converter with the following parameters - input voltage 24 V, output voltage 12 V, inductance 56.5 μH and capacity 166.7 μF, switching frequency 10 kHz and load

resistance 5 Ω), were performed simulations in SIMULINK, using the fuzzy controller above. As test signals, one used first an input voltage step from 24 V to 27 V, and then a load step from 10 Ω to 5 Ω . Numerical simulations results are shown in figure 5. For the fuzzy controller, in simulations, a refresh rate of 1 kHz was used.

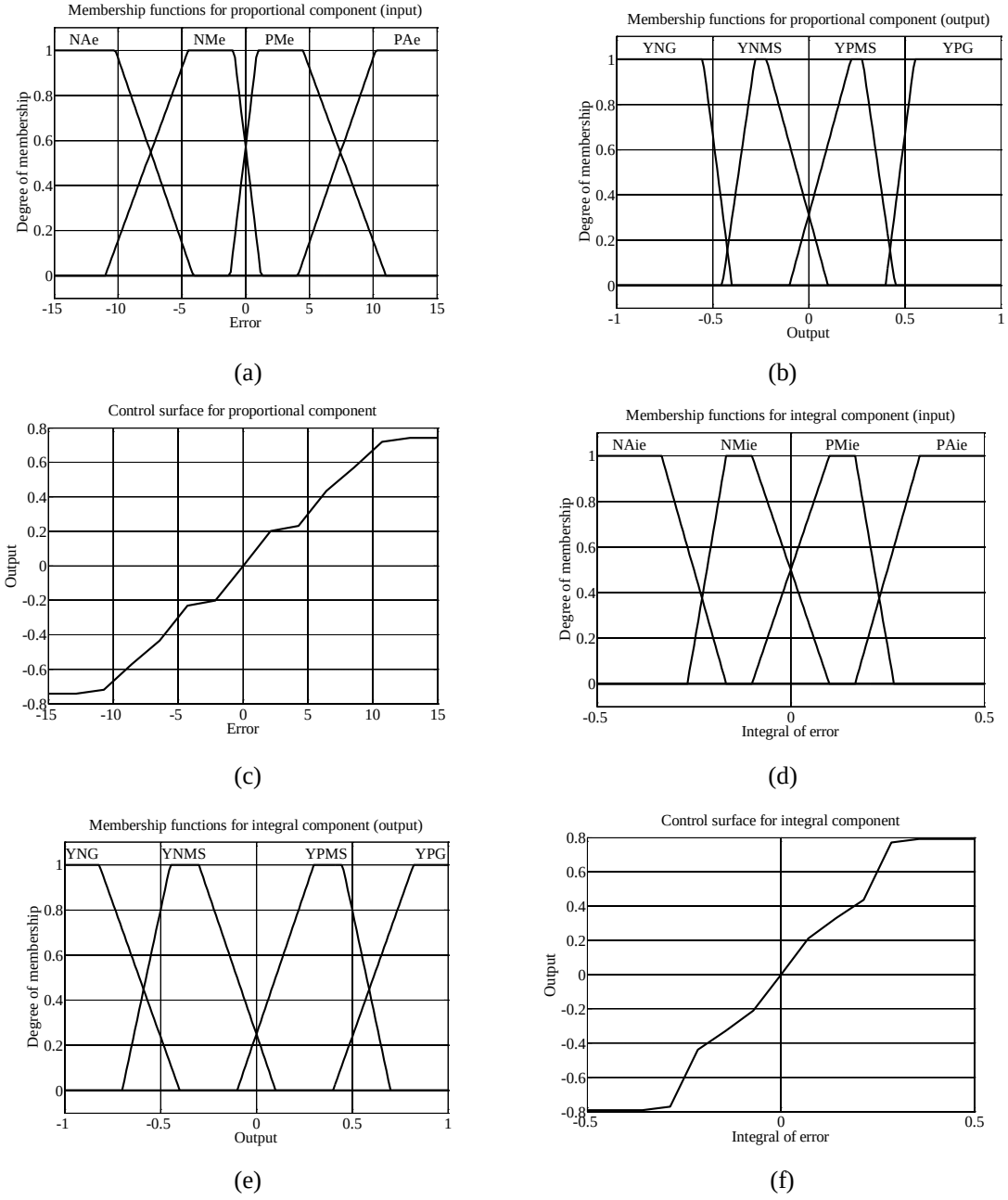

FIG. 3. Fuzzy controller for proportional component and for integrative component

Taking into account the very small variations of the output voltage, one can say this controller can be used for applications that need good output voltage stabilization.

An interesting remark is the presence of some random ripple which is not the simple effect of the switching process but of the interference between the controller and switching process. This ripple decreases with the output current. One can obtain a better behavior of the converter by switching pulses increasing and concurrent improving of the gain and time constant of the fuzzy controller.

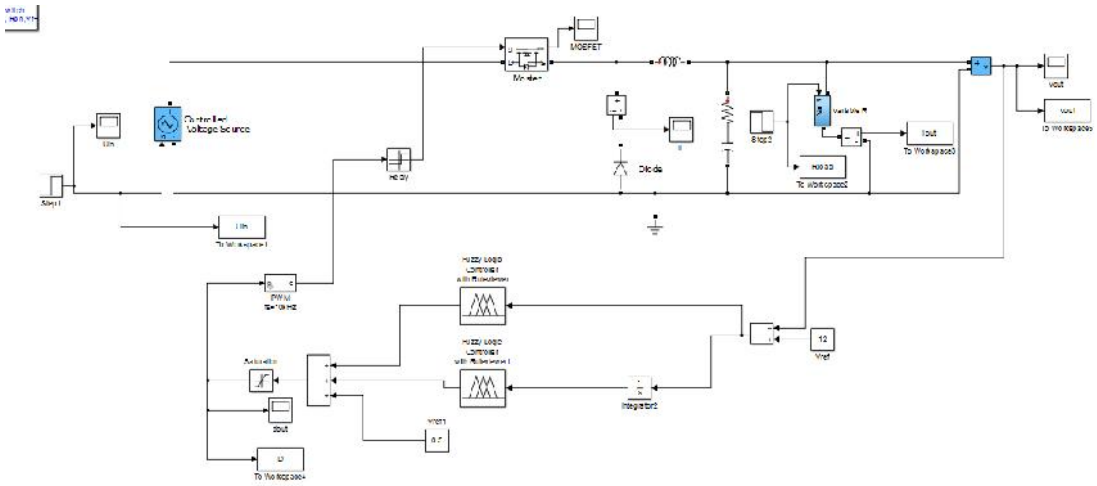

FIG. 4. Matlab/Simulink model for dc to dc buck converter in closed loop

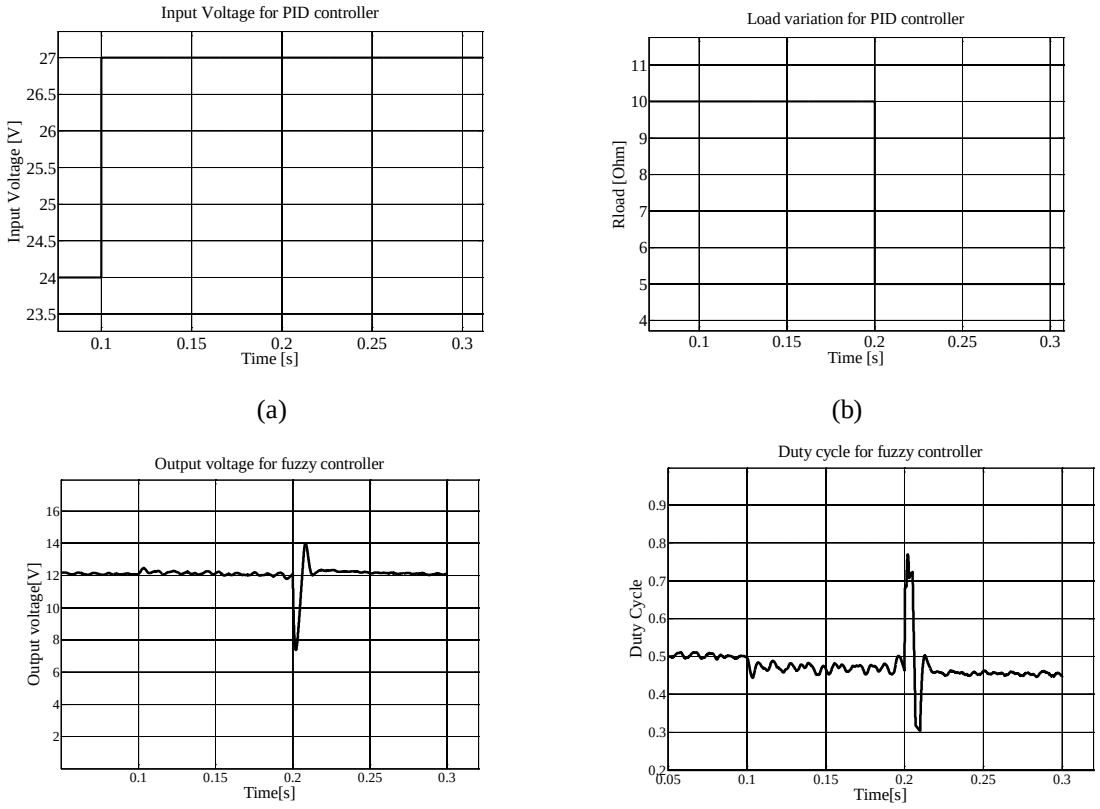

FIG. 5. Behavior of the converter with fuzzy controller

CONCLUSIONS

This paper presents modeling and analysis of a DC to DC buck converter (with a gain lesser one) by numerical simulation. Closed loop model was implemented in MATLAB/SIMULINK toolbox SIMPOWERSYS, and the controller is fuzzy type. This kind of controller was proposed by authors in [7] for a DC-to-DC boost converter. Good behavior of the Buck converter studied in this paper proves the robustness of the fuzzy

controllers. Fuzzy controller shows good stabilization qualities while it doesn't needs to know the mathematical model of the Buck converter in the controller design process. Simplified version with two more simple controllers in parallel, one for the proportional component and one for the integrative component allows simplifying the inference rules definition and the controller tuning. Moreover, the calculus time for this configuration is shorter than the calculus time for a controller with two inputs and one output, due to a smaller calculus volume.

REFERENCES

[1] M. H. Rashid, *Power Electronics Circuits, Devices, And Applications*, 3rd edition, University of West Florida, Pearson Prentice Hall, 2003;

[2] R. W. Erickson and D. Maksimovic, *Fundamentals of Power Electronics*, Second Edition. 912 pp., ISBN 0-7923-7270-0;

[3] G. Feng, W. Zhang, and Yan-Fei Liu, *An adaptive current mode fuzzy logic controller for dc-to-dc converters*, IEEE 2003, page 983-989;

[4] P. Mattavelli, L. Rossetto, G. Spiazzi and P. Tenti, *General-purpose fuzzy controller for dc/dc converters*, APEC, 1995;

[5] A. G. Perry, G. Feng, Yan-Fei Liu and P.C. Sen, *A New Design Method for PI-like Fuzzy Logic Controllers for DC-to-DC Converters*, 2004 35th Annual IEEE Power Electronics Specialists Conference, pp. 3751-3757;

[6] S. Yigang, *Performance Improvement of dc-dc converters using fuzzy logic control (FLC)*. Master of Science Engineering, Ontario Canada, 1999;

[7] L. Dinca and J.I. Corcau, *P.I. Versus Fuzzy Control for a dc to dc boost converter*, SPEEDAM 2016, Paper submitted for publication;

[8] M. Salimi and A. Zakipour, *Direct Voltage Regulation of DC-DC Buck Converter in a Wide Range of Operation using Adaptive Input-Output Linearization*. IEEJ Transactions on Electrical and electronic Engineering,Vol. 10, Iss. 1, pp. 85-91, January 2015, ISSN 1931-4973.

[9] M Sahoo and S. Kumar, *High Gain Step-Up DC –DC Converter For DC Micro-Grid Application.* International Conference on Information and Automation for Sustainability, 2014, ISBN 978-1-4799-4598-6/14;

[10] Monzer Al Sakka, Joeri Van Mierlo and Hamid Gualous (2011). *DC/DC Converters for Electric Vehicles, Electric Vehicles - Modelling and Simulations*, Dr. Seref Soylu (Ed.), ISBN: 978-953-307-477-1, InTech, Available from: http://www.intechopen.com/books/electric-vehicles-modelling-and-simulations/dc-dcconverters- for-electric-vehicles;

[11] Eremia M., Cartina G., Petrica D., s.a. *Artificial intelligence techniques in the management of power systems*. Editura Agir, Bucuresti, 2006.

PERFORMANCE EVALUATION OF THE THERMOELECTRIC GENERATOR

Petru Adrian COTFAS, Daniel Tudor COTFAS, Octavian MACHIDON, Cristina CIULAVU

*Transilvania University of Brasov, Romania (dtcotfas@unitbv.ro)

DOI: 10.19062/2247-3173.2016.18.1.32

Abstract: *The energy produced by the thermoelectric generators is clean and it can be used for the niches application. The paper presents the characterization of the commercial Bi_2Te_3 thermoelectric generator in function of the temperature. The temperature difference between the two parts of the thermoelectric generator is increased using an additional thermoelectric device to heat the hot part, and an aluminum cooler for maintaining the cold part at quasi constant temperature. The I-V and the P-V characteristics of the thermoelectric element are measured at different temperatures. The maxim power, the Seebeck coefficient and the internal electric resistance are calculated. The software to control the devices, to perform the measurements and analyse the data is created.*

Keywords: *thermoelectric generator, Seebeck effect, maxim power, internal resistance*

1. INTRODUCTION

Nowadays it is very important to produce clean energy. There are many types of renewable energy which are mature: solar energy (photovoltaic and thermal energy), wind energy, geothermal energy, micro hydro power, etc. Other types of clean energy have also begun to be used, for example the energy produced by the piezoelectric element and the energy produced by the thermoelectric generator.

The thermoelectric devices can produce a small electric power by converting the thermal energy in electrical energy based on the Seebeck effect and the electrical energy in thermal energy based on the Peltier effect [1-3].

The applications of the thermoelectric devices are destined to cool or heat different things which are coupled at their hot or cold parts [4,5]. The thermoelectric generators can be used in different applications, such as active building envelope [6], heat recovery in automotive, battery charging [7], radioisotope power systems [8], spatial applications, in concentrated solar energy [9] and solar photovoltaic energy [10].

2. THE THERMOELECTRIC GENERATOR

The thermoelectric generator consists of a number of thermoelectric elements that are connected thermally in parallel and electrically in series. The series connection is necessary to increase the generated voltage. The thermal conductivity can be increased if the elements are connected in parallel [1,2]. The structure of the thermoelectric elements consists of: a p type semiconductor connected through a cooper plate with an n type semiconductor, which are placed between two ceramic plates, Fig.1.

The thermoelectric generator can be classified in function of the figure of merit, ZT [11]:

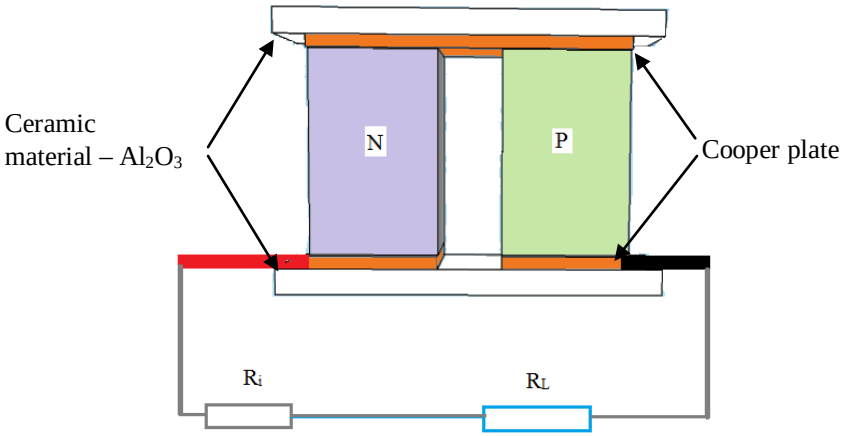

FIG. 1. The structure of the thermoelectric generator

- First generation – ZT < 1.3 and the efficiency of the thermoelectric generator is between 4% and 6%.
- Second generation – $1.3 \leq ZT \leq 1\,8$ and the efficien cy of the thermoelectric generator is between 11% and 15%.
- Third generation – ZT > 1.8 and the estimated efficiency of the thermoelectric generator is greater than15%.

The equation which describes the figure of merit was discovered by Altenkirch in 1911 [11].

$$ZT = \frac{\alpha^2 \sigma}{k} T \tag{1}$$

where σ represents the electrical conductivity, k is the thermal conductivity and α is the Seebeck coefficient.

The efficiency of the thermoelectric generator function of the figure of merit can be calculated with the following equation (2):

$$\eta = \frac{(T_h - T_c)}{T_h} \frac{\sqrt{1+ZT_m}-1}{\sqrt{1+ZT_m}+\frac{T_c}{T_h}} \tag{2}$$

where the first factor of the ratio represents the Carnot efficiency, T_c is the temperature of the thermoelectric element's cold part, T_h is the temperature of the thermoelectric element's hot part and T_m is the average temperature between the T_h and T_c.

The Bi_2Te_3 thermoelectric generator is the most widely used due to the acceptable price, performance and low work temperature. The Bi_2Te_3 thermoelectric generator performance can be improved if it is combined with isomorphic compounds such as PbTe, GeTe and Sb_2Te_3 [12,13].

The temperature distribution in two thermoelectric devices, Bi_2Te_3 and PbTe when a potential by 0.1 V is applied is presented in Fig.2. The simulation was realized using the Comsol multiphysics program.

The thermoelectric generator generated a voltage when there is a temperature difference between the hot and cold parts. The voltage can be calculated using the power balance by equation (3) [14]:

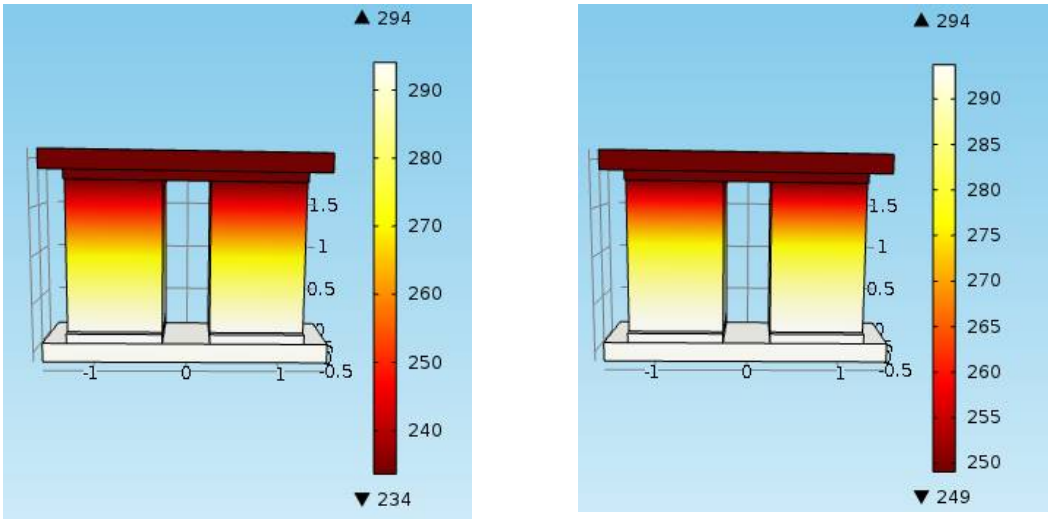

(a) (b)

FIG. 2. The temperature distribution of the two types of thermoelectric generator (a) Bi_2Te_3 (b) PbTe

$$V = \alpha(T_h - T_c) - IR_i \tag{3}$$

where I is the current in the circuit and R_i is the internal resistance of the thermoelectric generator.

The circuit current can be obtained using the following equation (4) and $V=IR_L$:

$$I = \frac{\alpha(T_h - T_c)}{R_i + R_L} \tag{4}$$

where R_L is the load resistance, see figure 1.

Using the equation (5) the electric power generated by the thermoelectric generator can be calculated:

$$P = IV = R_L \frac{\alpha^2 (T_h - T_c)^2}{(R_i + R_L)^2} \tag{5}$$

3. THE EXPERIMENTAL SET-UP

The current voltage characteristic, I-V, is an important tool to characterize the semiconductors, therefore it can be successfully used to analyzed the performance of the thermoelectric generator.

In this work, a commercial Bi_2Te_3 thermoelectric generator, with the dimensions of 6.2 cm/ 6.2 cm / 4.8 mm is analyzed function of the temperature difference between the hot and cold parts.

The temperature difference between the two parts of the thermoelectric generator is realized through maintaining the cold part at quasi constant temperature and increasing the temperature of the thermoelectric generator hot part.

The quasi constant temperature of the cold part is obtained through connecting it with 0.1 mm thermal adhesive tape at an aluminum block, Fig.3a, which is cooled with water.

(a) (b)

FIG. 3. The thermoelectric generator's (a) cold part connected with aluminum block (b) hot part connected with other thermoelectric device

The water flow is monitored with a flowmeter and the water temperature is measured at three points: inlet and outlet of the aluminum block and water tank. The water flow can be changed by controlling the voltage drop on the water pump.

The increasing in temperature of the hot part is obtained by connecting it with 1 mm thermal adhesive tape with the other thermoelectric device, Fig.3b, which is connected at DC programmable power supply.

The I-V characteristics for the thermoelectric generator are measured using a simple electronic load built for this study and the NI cRIO integrated system. NI cRIO (National Instruments compact Reconfigurable Input Output) is an embedded platform which contains a real time processor used for communication and signal processing and a FPGA module that can be programmed by the user for high performance data processing at hardware level. The platform used in our setup is NI cRIO 9074 which has eight slots for connection with C Series I/O Modules which are hot swappable. For measuring the I-V characteristics the NI 9215 module was used which measures the voltage on the thermoelectric generator and the voltage on a resistor with known values for the determination of the current. The NI 9269 module was used for the electronic load and the water pump control.

The temperatures of the thermoelectric generator cold and hot parts are measured with six thermocouples, three for each part, using the NI 9213 thermocouples module of the cRIO integrated system. The positioning of the thermocouples to measure the temperature of the thermoelectric generator can be seen in Fig.3. Three thermocouples were used to have a relatively complete temperature picture.

The experimental set-up to study the behavior of the commercial Bi_2Te_3 thermoelectric generator is presented in Fig.4. The control of the programmable DC power supply, the measurements and the control of the water flow are realized using the software made in the graphical programming language LabVIEW.

4. RESULTS

The I-V characteristics for the thermoelectric generator were measured at different temperature differences between the hot and cold parts. The temperature difference was obtained through power variation on the second thermoelectric device with a DC programmable power supply.

The I-V and P-V characteristics of the thermoelectric generator at different temperature differences are presented in Fig.5a and in Fig.5b.

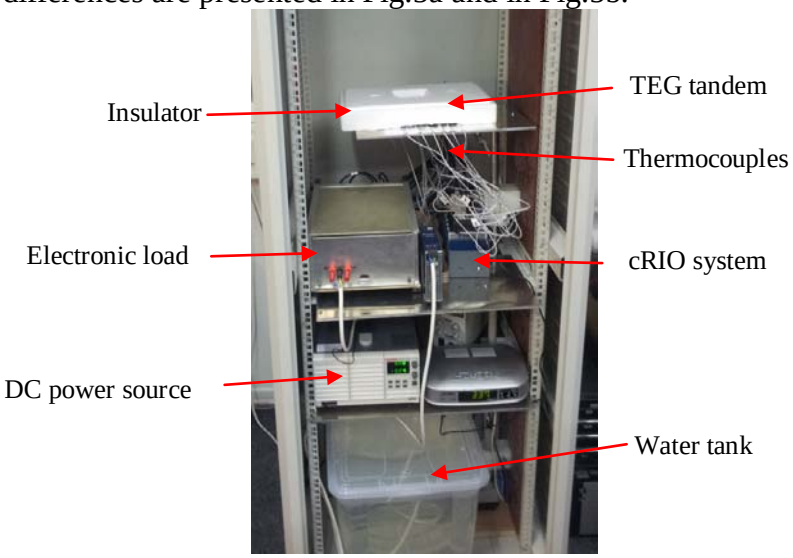

FIG. 4. The experimental set-up to characterize the thermoelectric generator

By analyzing the maximum power generated by the thermoelectric generator in function of the temperature difference, a parabolic dependence can be observed. This dependence is given by the equation (6) obtained by polynomial fitting, Fig.6:

$$P_{max} = 0.039 \cdot 10^{-3} \cdot \Delta T^2 - 0.032 \cdot 10^{-3} \cdot \Delta T - 0.1 \cdot 10^{-3} \quad (6)$$

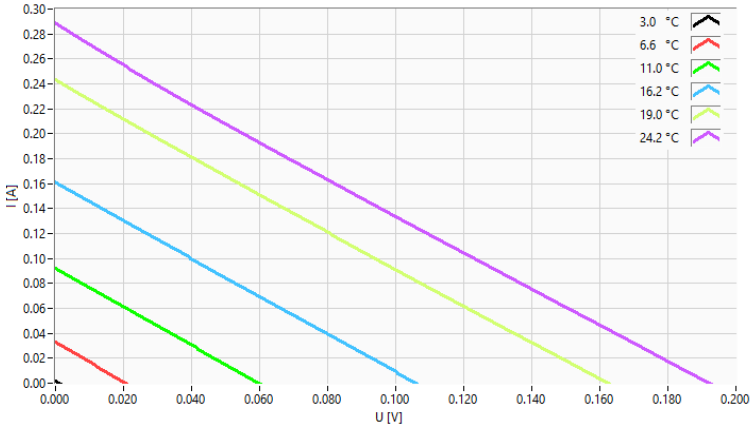

a)

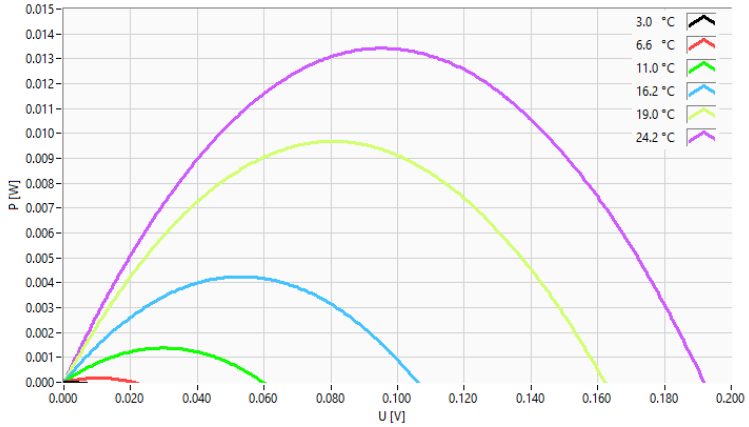

b)

FIG. 5. (a) The I-V characteristic of the Bi_2Te_3 thermoelectric generator in function of the temperature
(b) The P-V characteristic of the Bi_2Te_3 thermoelectric generator in function of the temperature

The equation (3) becomes (7) at the open circuit voltage point where the current is equal to zero:

$$\alpha = \frac{V_{oc}}{T_h - T_c} \tag{7}$$

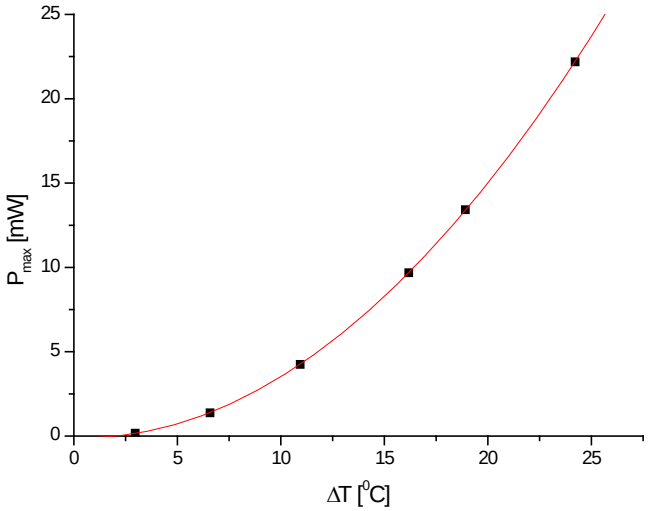

FIG. 6. The P_{max} vs ΔT for the Bi_2Te_3 thermoelectric generator

The Seebeck coefficient can be determined using equation (7), if the temperature of the thermoelectric generator's hot part is varied. The slope of the linear dependence between the open circuit voltage, V_{oc}, and the temperature difference between the hot and cold parts of the thermoelectric generator, is the Seebeck coefficient, see Fig.7. The slope is obtained by linear fitting and the value of the Seebeck coefficient is 10.75 mV/^{o}C.

The internal resistance of the thermoelectric generator increases when the temperature difference increases, see Fig.8. The value of the internal resistance increases with 12% when the temperature difference increases with 21^{o}C.

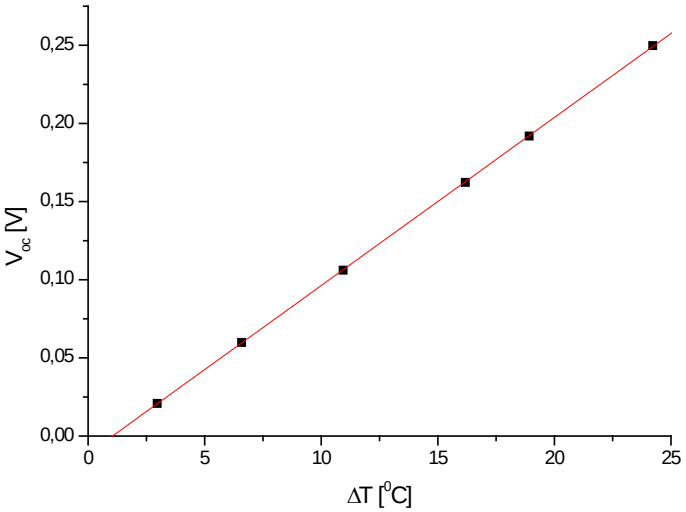

FIG. 7. The V_{oc} vs ΔT for the Bi_2Te_3 thermoelectric generator

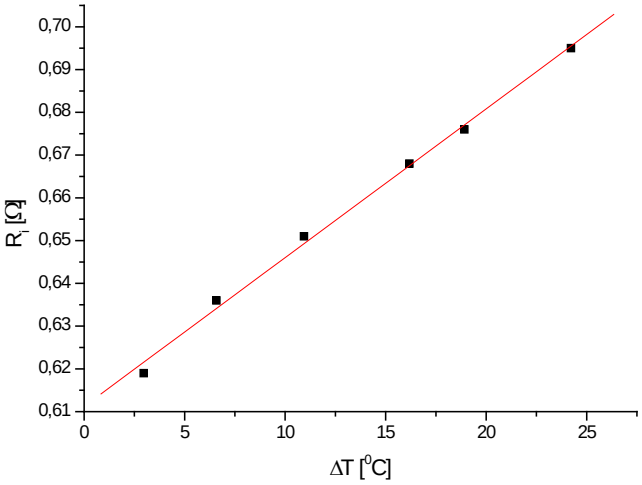

FIG. 8. The R_i vs ΔT for the Bi_2Te_3 thermoelectric generator

CONCLUSIONS

The thermoelectric generators produce renewable energy, but they still have a low efficiency. Using the new types of materials such as the graphene and nanomaterials the efficiency of the thermoelectric generators can be increased and then, the number of their application will also notably increase.

The commercial Bi_2Te_3 thermoelectric generator was analyzed in the paper. The I-V and P-V characteristics at different temperatures were measured and analyzed.

A polynomial model for the maxim power of the thermoelectric generator function of the temperature was identified.

The Seebeck coefficient was determined and the dependence of the thermoelectric generator internal electric resistance function of the temperature was studied.

AKNOWLEDGMENT

This work was supported by a grant of the Romanian National Authority for Scientific Research and Innovation, CNCS - UEFISCDI, project number PN-II-RU-TE-2014-4-1083.

REFERENCES

[1] C.A. Gould, N. Y. A. Shammas, S. Grainger and I. Taylor, *A comprehensive review of thermoelectric technology, micro-electrical and power generation properties*, Proc. 26th international conference on microelectronics (MIEL 2008), Niš, Serbia , 11-14 May, 2008;
[2] R. Ahıska and H. Mamur, A review: Thermoelectric generators in renewable energy, *International Journal of Renewable Energy Research*, vol. 4, no. 1, pp. 128-136, 2014;
[3] S. Karabetoglu, A. Sisman, Z. F. Ozturk and T.Sahin, Characterization of a thermoelectric generator at low temperatures, *Energy Conversion and Management*, vol. 62, pp. 47–50, 2012;
[4] G. Min and D. M. Rowe, Experimental evaluation of prototype thermoelectric domestic refrigerators, *Applied Energy*, vol. 83, pp. 133–152, 2006;
[5] B. J. Huang, C. J. Chin and C. L. Duang, A design method of thermoelectric cooler, *International Journal of Refrigeration*, vol. 23, pp. 208–218, 2000;
[6] X. Xu, S.V. Dessel and A. Messacb, Study of the Performance of Thermoelectric Modules for Use in Active Building Envelopes, *Building and Environment*, vol. 42, no. 3, pp. 1489-1502, 2007;
[7] J. Eakburanatwat and I. Boonyaroonate, Development of a thermoelectric battery charger with microcontroller-based maximum power point tracking technique, *Applied Energy*, vol. 83, pp. 687–704 2006;
[8] R. G. Lange and W. P. Carroll, Review of recent advances of radioisotope power systems, *Energy Conversion and Management*, vol. 49, pp. 393–401, 2008;
[9] S. A. Omer and D. G. Infield, Design and thermal analysis of a two stage solar concentrator for combined heat and thermoelectric power generation, *Energy Conversion and Management*, vol. 41, no. 7, pp. 737-756, 2000;
[10] W. G. J. H. M. Van Sark, Feasibility of photovoltaic— thermoelectric hybrid modules, *Applied Energy*, vol. 88, no. 8, pp. 2785-2790, 2011;
[11] L. D. Zhao,V. P. Dravid and M. G. Kanatzidis, The panoscopic approach to high performance thermoelectrics, *Energy and Environmental Science*, vol. 7, pp. 251-268, 2014;
[12] J. T. Jarman, E. E. Khalil, E. Khalaf, Energy analyses of thermoelectric renewable energy sources, *Open Journal of Energy Efficiency*, vol. 2, pp. 143-153, 2013;
[13] J. C. Zheng, Recent advances on thermoelectric materials, Frontiers of Physics in China, vol. 3, no. 3, pp. 269-279, 2008;
[14] A. Abdelkefi, A. Alothman and M. R. Hajj, Performance analysis and validation of thermoelectric energy harvesters, *Smart Materials and Structures*, vol. 22, pp. 1-9, 2013;

USING MULTI-CARRIER PROBING SIGNALS FOR DETECTING NON-LINEAR OBJECTS

Dilyan DIMITROV, Matei KIROV

National Military University "Vasil Levski", Faculty „Artillery, Air defense and Communication and information system", Shumen, Bulgaria (dilyaniv@abv.bg)

DOI: 10.19062/2247-3173.2016.18.1.33

***ABSTRACT**: In this paper an experimental model of non-linear radiolocation channel and certain calibration methods are shown. An etalon type non-linear object has been used for the calibration of the experimental model.*

***KEYWORDS**: model of non-linear radio location channel, calibration methods, non-linear object.*

1. INTRODUCTION

A major problem with non-linear radars (NLR) is their short range of operation. To increase the range of detection can be used multi-carrier signals [1,2] proposes a technical solution with dual-carrier signal.

Method for synthesis of optimal signal is still not developed. Also the advantage of dual-carrier signals compared to single-carrier signals is not applied yet.

2. SYNTHESIS OFPROBE SIGNALS FORMULTI-CARRIERNLR

The main property non-linear object is the capability of manipulation of signals with traditional frequency convertor. The only difference is the means of multiplexing of both signals. In the case of NLR the multiplexing is carried until the electromagnetic waves propagation medium, which allows the multiplexing of multiple signals with various amplitude, frequency and phase. Another important matters that no working algorithm for frequency conversion the probing signals has been developed yet. All that makes the multicarrier probing in NLR and the effectiveness analysis remain unresolved.

A system of deterministic signals has been considered. Base don't he model of the non-linear radio channel, we can imagine NLR as a set of generator so f monochromatic signals. The probing signal is shown below

$$S_{PS}(t) = \sum_{j=1}^{N} A_j cos\omega_j t \quad (1)$$

Where A_j is the amplitude of the signal with frequency ω_j and N is the number of monochromatic signals.

In particular for dual-carrier probing signal with spectral components frequencies$\omega_1$and$\omega_2$can be written:

$$S_{PS}(t) = \cos(\omega_1 t) + \cos(\omega_2 t) \quad (2)$$

For weak interaction when nonlinear transformation is determined by quadratic

member of the decay of the order of Taylor, the dispersed signal by the object can be represented in the following form:

$$S_{DSPS}(t) = \beta\,(1 + \cos(\Omega t))\cos((\omega_1 + \omega_2)t) \quad (3),$$

Where β is a constant coefficient, and $\Omega = \omega_1 - \omega_2$.

3. SINGLE-CARRIER AND MULTI-CARRIER IRRADIATION OF NONLINEAR OBJECTS

The intensity of the reflected signal $S_{DSPS}(t)$ exceeds one and a half times the intensity of the reflected signal in single-carrier irradiation. In [2] has shown that for transformations of second order deviation of the power of the reflected signal from the average value increases proportionally with the increasing number of monochromatic signals *N* in the probing signal if the following condition:

$$\omega_i - \omega_{i+1} = \omega_{i+1} - \omega_{i+2} \quad (4)$$

I.e. the rate of frequency change of the monochromatic waves is equal. In this case, the elements formation of the spectrum of reflected signal of second order involves more than two spectral components of the probing signal. In particular *N-1* non-linear components with frequencies

$$\omega_n = \omega_1 + \omega_N = \omega_2 + \omega_{N-1} = \omega_3 + \omega_{N-2} \quad (5)$$

are summed coherently.

The equality of average powers of the probing signals can have different interpretations. In particular, if the dual-carrier signal is formed by using two antennas, to compare the energy of the reflected signals at single-carrier and multi-carrier irradiation it is necessary to modify one frequency in a direction or each the other($\omega_1 \rightarrow \omega_2$). In case of equality of the average power of the probing signal flux density in single-carrier irradiation will be greater than the flux density in dual-carrier. This is caused by the increase in the effective area of the antenna twice. For this reason to be correct comparison is important to keep the same area of the antenna system.

In [2] are compared the reflected signals from non-linear objects irradiated with single-carrier and dual-carrier signals using frequency modulated probing signals.

Using directional coupler and power divider one of the signals with average power irradiates through one of the antennas, and the other is delayed and irradiated through the other antenna. In the experiment are compared dual-carrier signal with two antennas and single-carrier signal with one antenna, which proves the significant increase of energy of the reflected signals with multi-carrier irradiation compared to single-carrier.

Multi-carrier irradiation has specific features that should be considered. The first one is the use of ultra wide band width receiver, which in turn leads to reduction of SNR.

Another feature is that the necessary linearity of power amplifiers in wide dynamic range of transmitter has to be provided. It also needs to ensure a uniform gain antenna in a sufficiently wide frequency range.

In [1] is developed on the case by the use of different probing signals from *N* generators with zero phases. Accordingly the phase characteristics of the emitted probing signals do not affect the frequency response of the reflected signals. Matter so f interestare cases where probing signals are not in phase. From this point of view are considered two four-carrier probing signal shown below

$$S_{1PS}(t) = \cos(\omega t) + \cos((\omega + \Omega)t) + \cos((\omega + 2\Omega)t) + \cos((\omega + 3\Omega)t) \quad (6)$$

$$S_{2PS}(t) = \cos(\omega t) - \cos((\omega + \Omega)t) + \cos((\omega + 2\Omega)t) + \cos((\omega + 3\Omega)t) \quad (7)$$

Both $S_{1PS}(t)$and$S_{2PS}(t)$ signals have identical frequency response and the peak-factor (the ratio of the maximum power at any given time-"peak" to the average power) of $S_{1PS}(t)$is greater than the peak-factor of $S_{2PS}(t)$a little more than twice. The intensity of the reflected signal (in the band $2\omega$to$2\omega+6\Omega$) from probing signal $S_{2PS}(t)$is two times smaller compared to the intensity of the reflected signal from probing signal $S_{1PS}(t)$. Moreover, in the spectrum of the reflected signal in the case of using $S_{2PS}(t)$some spectral components vanish.

Increasing the power of the reflected signal N times can be achieved only with maximum possible peak factor, i.e., when all spectral component so f the probing signal are in phase.

When a pulse signal with a duty cycle equal to the required peak-factor (N) the power of the reflected signal is N times greater compared to using a continuous signal while maintaining the same average transmission power for both continuous and pulse signals. The same applies o the power of the reflected signal of multi-carrier radiation if all products in nonlinear frequency range from$2\omega_1$to$2\omega_N$ are taken. It can be concluded that when comparing the performances of different probing signals with the same average power, it is advantageous sin terms of power of the reflected signals the one with greater peak-factor. This applies to the comparison of all statements: using multi-carrier and single-carrier probing signals.

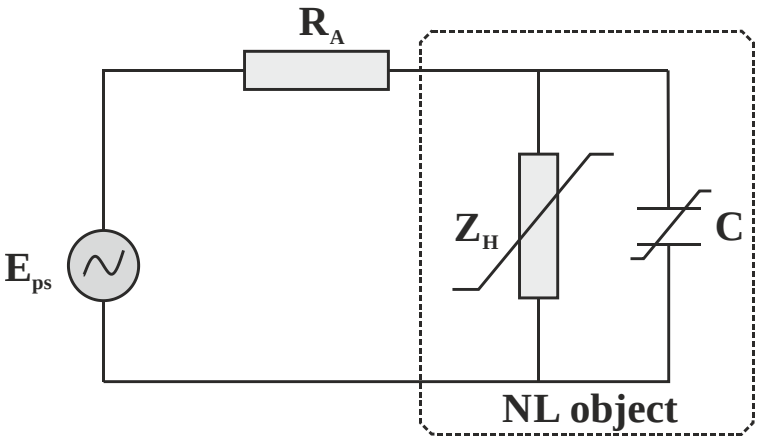

FIG. 1.

FIG.1 shows an equivalent circuit of an ideal non-linear object (*NO*), where in the E_{PS} is the electromotive force caused by the probing signal, R_A is the resistance of the linear portion of the radiation and the U_{NO} is the voltage on the non-linear object. All of these voltages are related with the flowing current I with volt-ampere characteristic $I = f\ (U_{NO})$.

Transmit power of the ideal nonlinear object is

$$P_{NO} = R_A (I_{NO})^2 \quad (8)$$

Of interest is the spectrum of the current flowing through then on linear object. The reforce the relationship between the current flowing through the non-linear object and

current based on probing signal must be determined

$$I = I(E_{PS}) \tag{9}$$

Kirchhoff equation for perfect non-linear object has the form

$$E_{PS} = IR_A + U_{NO} \tag{10}$$

The function $U_{NO} = f^{-1}(I)$ is determined as the inverse volt-ampere characteristic of the nonlinear object. By substituting it with (10) we get

$$E_{PS} = IR_A + f^{-1}(\mathrm{I}) = \mathrm{F}(\mathrm{I}) \tag{11}$$

Function (11) is the inverse relationship of the requested function (9)

$$I = F^{-1}(E_{PS}) \tag{12}$$

Analytical determination of the magnitude of the current in (12) is difficult. In computing environment that corresponds to a conversion of recorded file sand finding their spectrum sing a fast Fourier transform.

CONCLUSIONS

Calculations show that in linear mode of interaction of probing signal with nonlinear object the combined power of the reflected signal for products of second order (second harmonic for each carrier frequency of the probing signal $-2\omega_1$, $2\omega_2$,...,$2\omega_N$) is always equal to the power of the second harmonic of single-carrier signal if the average powers forsingle-carrierandmulti-carrierprobingareequal.Accordingly,the phase differences do not affect the power but influence the shape of the spectrum. Regarding the two signals(6)and(7)the combined power of signals reflected from non-linear object are approximately equal. In modes close to the saturation of then on-linear element the power of the reflected signal increases significantly for probing signals with low peak-factor. This is also valid for single-carrier probing signals with a small peak-factor [3]. Further more, the spectrum of the reflected signal is so blurred that impedes optimal reception of the reflected signal.

As a result of the calculations should not expect higher power of the reflected signal with the use of multi-carrier probing signals compared to single-carrier. That is why for real experiments are mostly used single-carrier probing signals.

REFERENCES

[1].С.В.Ларцов. , *Онелинейномрассеянииприиспользованиимногочастотногоиодночастотногозондирующихсигналов*, Радиотехникаиэлектроника, 2001, том46, с833-838;

[2].Н.С. Вернигоров, А.Р.Борисов, В.БХарин, *Квопросу оп рименениимногочастотногосигнала внелинейнойрадиолокации*, Радиотехникаиэлектроника, 1998.Том43,с 63-66

[3]. D. I. Dimitrov, *Mathematical and simulation models for dispersion of electromagnetic waves from point weld in gof metal so fair craft*, The 32nd International scientific conference of the military technical academy–Modern technologies in the 21st century, Bucharest 2007;

COMPARATIVE ANALYSIS OF TUNING MISSILE AUTOPILOTS USING INTELLIGENT METHODS

Rumen GEORGIEV, Kolyo KOLEV

NMU, Aviation Faculty, Dolna Mitropolia, Bulgaria
(georgievrg@gmail.com, kolev_007@abv.bg)

DOI: 10.19062/2247-3173.2016.18.1.34

Abstract: *This article explores basic technical and design challenges associated with the missile flight control system, including its role in the overall missile system, its subsystems, types of flight control systems, design objectives, and design challenges.*

Keywords: *missile homing loop, feedback control, synthesis techniques for homing guidance.*

1. INTRODUCTION TO MISSILE AUTOPILOTS

Before we go on to discuss any particular type of guidance system, it is necessary to consider first the overall operation of an entire missile guidance and control system; to divide it into convenient groups of units; and to indicate the general function of each major group so that the operation of the particular units may be understood in relation to the operation of the guidance and control system as a whole [1].

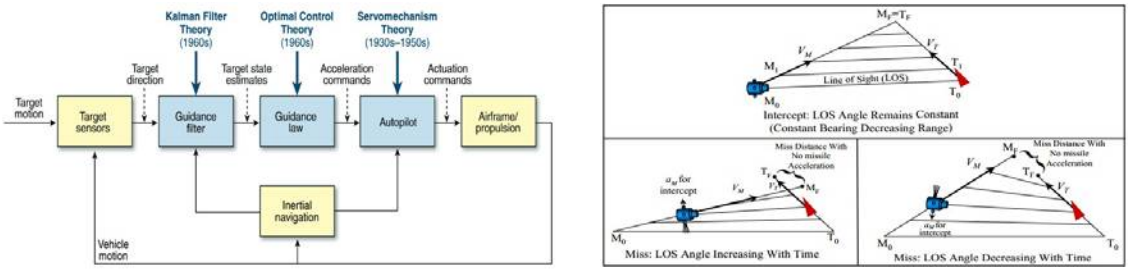

(a) Traditional GNC topology (b) Guidance intercept techniques

FIG. 1. The figure show traditional GNC topology and different guidance intercept techniques

As indicated in Fig. 1. (a), the traditional architecture for all fielded guided missile systems are particular examples of the feedback concept. The GNC topology for a guided missile comprises guidance filter, guidance law, autopilot, and inertial navigation components. The inertial navigation system (INS) provides the position, velocity, acceleration, angular orientation, and angular velocity of the vehicle by measuring the inertial linear acceleration and inertial angular velocity applied to the system. The information from the INS is used throughout missile flight to support guidance and flight control functions. The guidance filter receives noisy target measurement data from the homing sensor and estimates the relevant target states. The guidance law takes the instantaneous target-state estimates as input and determines what the interceptor direction of travel should be to intercept the target. It typically is an anticipatory function in that it generates guidance commands to put the missile on a collision course with the target.

The problem is to design a pitch plane autopilot to track the normal acceleration commanded from the guidance system. The autopilot generates fin angle commands which are sent to the tail surface servos. By deflecting the tail fins, they generate aerodynamic forces and moments that maneuver the missile. Rate gyro and accelerometer measurements are processed by the flight control system to close the feedback control loop.

The principal functions of the guidance system are to detect the presence of the target and track it; to determine the desired course to the target; and to produce electrical steering signals which indicate the position of the missile with respect to the required course. Therefore, you can say that the output of the guidance and control system is the actual missile flight path. If there is a difference between the desired flight path (input) and the one the missile is actually on (output), then the control system operates to change the position of the missile in space to reduce the error.

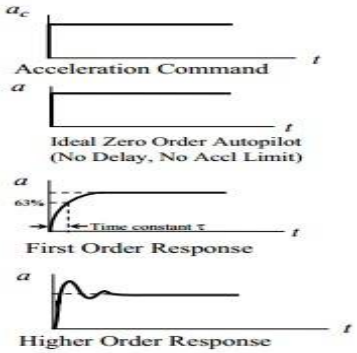

(a) Time response characteristics

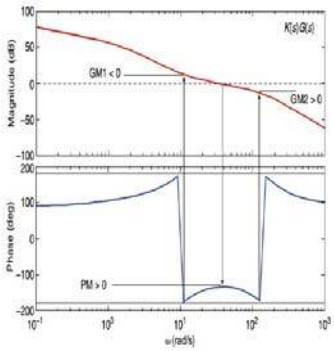

(b) Bode plot open-loop frequency response of an acceleration autopilot

FIG. 2. Traditional approach for developing GNC system -time and frequency characteristics

The purpose of an autopilot is to produce lateral missile acceleration a in response to commanded acceleration a_c as shown in Fig. 2. An autopilot's time constants the approximate time it takes for the missile to achieve commanded acceleration.

The missile motion in space is completely defined by the acceleration normal to the velocity vector and the rate of change of the velocity magnitude. The commanded normal acceleration is the input to a combination of limiters and transfer functions that simulate the autopilot, control system, and aerodynamics, yielding realized accelerations as the output. Specifically, the commanded acceleration is passed to the autopilot in a body frame sense.

2. THE COMMON AUTOPILOT AND MISSILE MODEL

The dynamics of the airframe are governed by fundamental equations of motion, with their specific characteristics determined by the missile aerodynamic response, propulsion, and mass properties. Assuming that missile motion is restricted to the vertical plane (typical for early concept development), the equations of motion that govern the missile dynamics can be developed in straightforward fashion. These equations are sufficient to obtain rough estimates of the impact point. Variations in wind conditions and motor burn as well as heading and attitude control errors would affect actual performance. Adding simple trim aerodynamics with a transfer function representation of the autopilot and a proportional navigation guidance law produces a simulation model.

The gains in the autopilot are scheduled as a function of flight condition to achieve missile stability and command following. The actuator command passes through a second-order transfer function with angle and rate limiters (1).

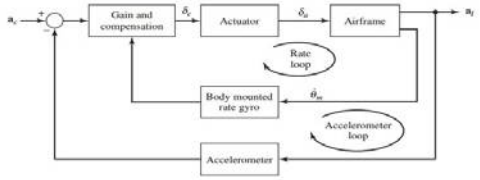

(a) Autopilot block diagram

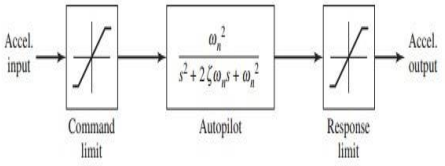

(b) Simple transfer function model for the actuator with angle and rate limiting

FIG. 3. The autopilot acceleration command from the guidance law and the measured acceleration and body rate as inputs to obtain the actuator command.

A "three-loop" autopilot and simple transfer function model for the actuator with angle and rate limiting used to describe these dynamic as in [5] are:

$$\frac{\delta(s)}{\delta_c(s)} = \frac{\omega_a^2}{s^2 + 2\xi_a\omega_a s + \omega_a^2} \tag{1}$$

The application of the longitudinal (vertical plane) flight control system for a bank to turn missile form a single input multioutput design model. The plant outputs are normal acceleration A_z(ft/s^2), and pitch rate q (rad/s), and the plant states are $x = [\alpha \quad q \quad \delta \quad \dot{\delta}]^T$ (angle of attack, pitch rate, fin deflection, and fin rate respectively). The nominal longitudinal airframe dynamics is represented by $G(s)$. The deferential equation used to describe these open loop dynamic as in [5] are:

$$\begin{aligned} \dot{\alpha} &= Z_\alpha\alpha + q + Z_\delta\delta_e \\ \dot{q} &= M_\alpha\alpha + M_\delta\delta_e \\ A_z &= VZ_\alpha\alpha + VZ_\delta\delta \end{aligned} \tag{2}$$

Assuming that the actuator is second order system as:

$$\ddot{\delta}_e = -2\xi\omega\dot{\delta}_e - \omega^2(\delta_e - \delta_c) \tag{3}$$

In the state space form, the airframe dynamics are represented by the following state space triple (A, B, C):

$$\dot{x} = Ax + Bu, \quad y = Cx + Du, \quad A = \begin{bmatrix} Z_\alpha & 1 & Z_\delta & 0 \\ M_\alpha & 0 & M_\delta & 0 \\ 0 & 0 & 0 & 1 \\ 0 & 0 & -\omega^2 & -2\xi\omega^2 \end{bmatrix}, \quad B = \begin{bmatrix} 0 \\ 0 \\ 0 \\ \omega^2 \end{bmatrix}, \quad C = \begin{bmatrix} VZ_\alpha & 0 & VZ_\delta & 0 \\ 0 & 1 & 0 & 1 \end{bmatrix} \tag{4}$$

The transfer function matrix is $G(s) = C(sI - A)^{-1}B$. The longitudinal missile dynamics form a single input multioutput design model from equation 2-5, the transfer function matrix from the elevon fin deflection command δ_c to the normal acceleration A_z and pitch rate q is

$$G(s) = \begin{vmatrix} \dfrac{\omega^2 V(Z_\delta s^2 + Z_\alpha M_\delta - Z_\delta M_\alpha}{(s^2 - Z_\alpha s - M_\alpha)(s^2 + 2\zeta\omega s + \omega^2} \\ \dfrac{\omega^2(M_\delta s^2 + M_\alpha Z_\delta - M_\delta Z_\alpha)}{(S^2 - Z_\alpha S - M_\alpha)(S^2 + 2\zeta\omega s + \omega^2)} \end{vmatrix} = \begin{vmatrix} \dfrac{A_z(s)}{\delta_c(s)} \\ \dfrac{q(s)}{\delta_c(s)} \end{vmatrix} \tag{5}$$

where $Z_\alpha, Z_\delta, M_\alpha, M_\delta$ and M_q are the aerodynamic stability derivatives. The measurements that are available are normal acceleration $A_z = VZ_\alpha\alpha + VZ_\delta\delta$ *(ft/s2), q* pitch rate (rad/s). The scalar control input $u=\delta$ (rad) is the fin angle command. Although these differential equations can be solved numerically, an analytical approach often is desirable to fully understand the missile dynamics. Therefore, the equations of motion are linearized around an operating condition so that linear systems theory can be applied.

The above aerodynamics have been linearized and represented a trim α angle of attack of 16 degrees, Mach number=0.8, V=886.78 (ft/s), an altitude of 4000 (ft.), actuator damping ζ =0.6, and actuator natural frequency ω =113 (rad/s). The following parameters are the nominal values of the dimensional aerodynamic stability derivatives; $Z_\alpha = -1.3046$ (1/s); $Z_\delta = -0.2142$(1/s); $M_\alpha = \pm 47.7109$ (1/s^2) which were taken from [4]. The sign of M_α determines the stability of the open loop airframe. When the M_α is negative the airframe is stable, and when it is positive the airframe is unstable, which occurs when the aerodynamic center of pressure is forward of the center of gravity [5].

3. EXPLORE „THREE-LOOP" AUTOPILOT

The three loop pitch/yaw autopilot is used to most guided tactical missiles today as shown in Fig. 4. It has four gains K_{DC}, K_A, K_R and K_I which are used to control the third order dynamics of the autopilot. These dynamics are due to second order dynamics and an integrator that allows the flight control system to control unstable airframe. The longitudinal autopilot design process is automated to vary the acceleration feedback loop and the pitch rate loop gains and evaluate longitudinal autopilot performance and robustness properties. The performance values examined are the normal acceleration command settling time, the percent undershoot, the percent overshoot and the steady state error.

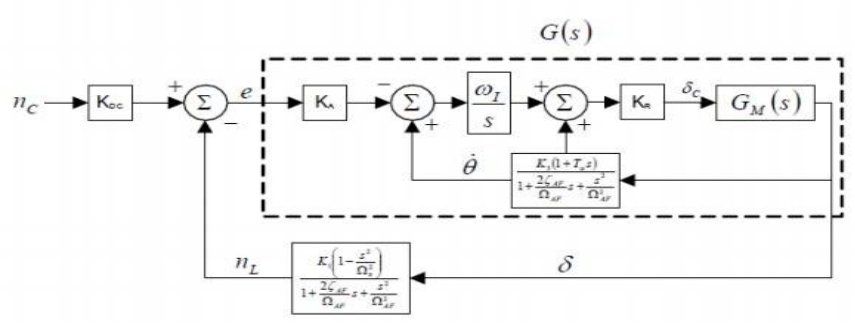

FIG. 4. Standard three-loop autopilot block diagram

The three loop autopilot, it includes an integrator for body rate in order to reduce the steady state error. It should be clear from Fig. 4 that the acceleration feedback loop is a proportional controller acting on the acceleration error. The inner loops form a proportional plus integral (PI) for pitch rate to stabilize the missile body. The outer loop relationship is given by $e = A_{zc}K_{DC} - A_z$ where A_z is the measured output acceleration and A_{zc} is the input acceleration command.

Conventional "three-loop" autopilot and simple transfer function model for the actuator controller does not give acceptable performance for systems with uncertain dynamics, time delays and non-linearity [2]. Hence it is necessary to automatically tune the parameters for obtaining satisfactory response. The automatic tuning gains of

controller has been done using fuzzy logic. Based on expert knowledge a fuzzy logic system transforms a linguistic control strategy into an automatic control strategy [3]. Figure 6 shows the block diagram of a fuzzy controller. The fuzzy controller has been implemented using fuzzy logic toolbox in MATLAB.

4. USING INTELLIGENT FUZZY CONTROLER

The fuzzy controller used in the implementation of Fuzzy longitudinal autopilot design process have fixed rule base and membership functions. The fuzzy controller has basically three main components: scaling factors, membership functions and the rules. The fuzzy controller is formed by the rule base shown as in the figure 5. The inputs to the controller are the error ($e = A_{zc}K_{DC} - A_z$ where A_z is the measured output acceleration and A_{zc} is the input acceleration command.) and the rate of change of error ($\Delta\dot{\theta}$) while the outputs are controller gains K_{DC}, K_A and K_I.

(a) The structure of fuzzy controller (b) Two input three output FLC structure

FIG. 5. Implementation of Fuzzy longitudinal autopilot design process

The structure of fuzzy controller is a two input errors (inner loops and outer loop) - three output controller gains K_{DC}, K_A and K_I. From there the range of the input as well as output membership functions have been found. The membership functions of these inputs fuzzy sets are shown in Figure 6. The linguistic variable levels are assigned as: negative big (NB), negative small (NS), zero (Z), positive small (PS) and positive big (PB). Similarly, the fuzzy set for error change $\Delta\dot{\theta}$ is presented as NB, NS, Z, PS, PB.

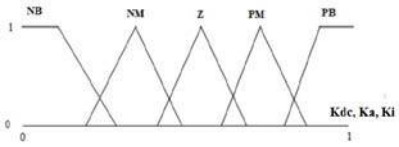

	NB	NM	Z	PM	PB
NB	NB	NB	NM	NM	Z
NM	NB	NM	NS	Z	PM
Z	NM	NM	Z	PM	PM
PM	NM	Z	PM	PM	PB
PB	Z	PM	PM	PB	PB

(a) Fuzzification of the Output; (b) Common Rule Base

FIG. 6. Basic inference mechanism

For the output fuzzy sets the scaling of range has been done corresponding to the formulas:

$$K_{DC} = \frac{K_{DC} - K_{DC\min}}{K_{DC\max} - K_{DC\min}}; K_A = \frac{K_A - K_{A\min}}{K_{A\max} - K_{A\min}}; K_I = \frac{K_I - K_{I\ \min}}{K_{I\ \max} - K_{I\ \min}}. \quad (6)$$

The inference mechanism has two basic tasks [7]: 1) Determining the extent to which each rule is relevant to the current situation as characterized by the two input errors - inner loops and outer loop. This task is called “matching”; 2) Drawing conclusions using the current inputs aid the information in the rule- base, this task is called “inference step”. The defuzzification phase is needed to send the rules which are evaluated in the inference phase as an unique control gains K_{DC}, K_A and K_I to the longitudinal autopilot.

5. SIMULATION RESULTS AND CONCLUSIONS

Simulation results for tracking system show that the fuzzy controller provides the better noise rejection as expected. Step response of the system for fuzzy application is more damped than P and PI control and control variable variations have smaller amplitudes due to the adopted defuzzification method. System setting time to reference input has an acceptable value (approximately 3.3s). The results obtained from this study has led to the further developments in the implementation of Fuzzy longitudinal autopilot design process.

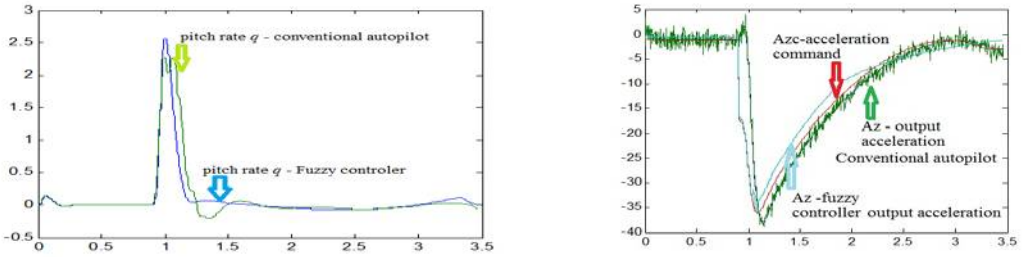

(a) pitch rate *q* (b) normal acceleration *Az*

FIG. 7. Comparison among different methods for tuning longitudinal autopilot performance

The comparison among different tuning methods in terms of various performance specifications such as rise time, settling time, overshoot, undershoot and steady state error using the intelligent and conventional tuning methods has been shown in Table 1. Measure of the efficiency is how quickly the missile will respond to a change in guidance command and also the deviation of the achieved missile motion relative to the command (t is time constant, M_p is peak magnitude, t_p is time to fist peak, t_r is rise time, and t_s is setting time).

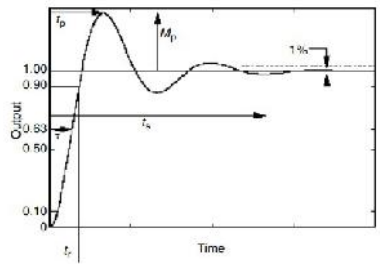

Parameters	Tuning Methods	
	Conventional tuning methods	Fuzzy controller
Rise time t (sec)	0.545	0.771
Setting time t_s (sec)	1.456	1.225
Overshoot M_P (%)	12.35	10.92
Undershoot M_u (%)	8.45	7.35
Steady state error e_{ss}	0	0

(a) Time domain basic objective (b) Table 1

FIG. 8. Comparison among different tuning methods in terms of various performance specifications

The various performance specifications have been improved using the intelligent method except the rise time which is less in case of conventional tuning methods. The steady state error remains zero in all the tuning methods.

GNC algorithms are diverse in type and complexity. The “tuning” process, whereby optimum values for the adjustable parameters are determined.

REFERENCES

[1] Neil F. Palumbo, Homing Missile Guidance and Control, Johns Hopkins APL technical digest, Volume 29, number 1 (2010);
[2] T. J. Ross, Fuzzy Logic with Engineering Applications, Wiley India Edition 2009;
[3] K. S. Tang, K. F. Man, G. Chen, and S. Kwong: An Optimal Fuzzy PID Controller, IEEE Transactions On Industrial Electronics, Vol. 48, No. 4, August 2001 , pp. 757-765;

[4] Fan, L. F., Chen, Y., & Lin, P. (2014). Control analysis for a non-minimum phase static unstably missile. *Proceedings of the 14th International Conference on Control, Automation and Systems* (pp. 947-952).
[5] Wise, K. A., & Eberhardt, R. (1992). Automated gain schedules for missile autopilots using robustness theory. *Proceedings of the First IEEE Conference on Control Applications* (pp. 243-250).
[6] Nesline, F. W., & Nesline, M. L. (1984). How autopilot requirements constrain the aerodynamic design of homing missiles. *Proceedings of the Conference on American Control*.
[7] Passino K.M., Yurkovich S., "Fuzzy Control", Addison Wesley Longman, Inc., California, 1998.

ELECTRICAL AND ELECTRONICAL ENGINEERING / RENEWABLE ENERGY AND ENVIRONMENT

THIN CLIENT FOR REAL-TIME MONITORING OF COMMUNICATION INFRASTRUCTURE

Iulian ILIESCU, Titus BĂLAN, Oana GAROIU, Sorin ZAMFIR

"Transilvania" University, Braşov, Romania (titus.balan@unitbv.ro)

DOI: 10.19062/2247-3173.2016.18.1.35

Abstract: *Monitoring the telecom infrastructure reflects not only a technical perspective but also a business perspective, highlighting, besides possible technical issues, the network areas that need improvements or investments. This paper describes the method for tele-monitoring of communication infrastructure responsible for switching and signaling in the mobile converged core network. The application allows the display of real-time information on a thin client. Thus, decisions related to infrastructure (resource management, optimizations, redeployments) can be taken based on notifications received on a mobile device (e.g. an Android smartphone)*

Keywords: *Real-time monitoring, thin client, Spring Framework, Data Access Objects, REST, Communication Infrastructure*

1. INTRODUCTION

Network operators are dealing with the challenge of reducing operational expenses OPEX and optimize the functionality of distributed infrastructure, within fast response times or methods to predict and avoid network issues, through automatic maintenance solutions.

The purpose of the implementations presented in this paper is to obtain a remote monitoring solution that provides mobility and which has an interface accessible to any user. The user has access to data wherever they are, as long as an Internet connection is available. The scope of the implemented demonstrator is to obtain an intuitive system, easy to set up and use, with the possibility of further development, while providing a very good performance / price ratio. The user has the possibility to view graphs that highlight errors, can analyze detailed view of logs and can perform real-time monitoring of the activities of system responsible with backup actions. Data communication between the server and the Android application is achieved through REST Web services ("Representational State Transfer") [1]. The multiplicity of standards and protocols used in the Internet have made possible the communication between two or more systems connected to the Internet that is a distance from one another. Industry software development, architectural models based on web services are seen increasingly more often, offering numerous advantages, especially when used together with an DAO ("Data Access Objects")[2] type architecture that brings an innovation in the interpretation of data and modeling of data objects. This concept will be detailed later, with examples related to the demonstrations.

2. SPRING FRAMEWORK AND DATA ACCESS OBJECTS

The used architecture is the type Model-View-Controller (MVC Spring framework)[2]. This architectural model allows the isolation of business logic from the

user interface, resulting in an application that allows easy modification of the user interface or even the modification of the lower levels without affecting other layers.

2.1 Spring Architecture

Spring framework was introduced in 2002 by Rod Johnson in "Expert One-on-One J2EE Design and Development" [3] that was initially a simple framework that provides the ability to connect applications together. This framework enables the development and execution of Java applications and offers various organizing features and various APIs (Application Programming Interface - Libraries specialized functions), such as JDBC, JSP, Servlet.

Spring Framework has a well-defined modular structure, consisting of 7 modules[4]:

- Spring AOP (Aspect Oriented Programming) - similar to the idea of object-oriented programming that modularize application in hierarchies of objects, oriented programming aspects breaks the program in aspects.
- Spring ORM (Object Relational Mapping) - is a tool used to connect to databases. It provides APIs for manipulating databases, tools such as JDO, Hibernate and iBatis. In our case, Spring ORM supports DAO pattern.
- Spring DAO (Data Access Objects) - has the role standardization of communication between the web application and database, representing an abstract level between physical data and objects used in the application.
- Spring Web MVC (Model View Controller) architecture implements the MVC web application. Separate application modules in the 3 defined by naming and thus organizing application on 3 levels.
- Spring Web - is a sublevel of Spring Web MVC module.
- Spring Background - is a package built around package "beans" to provide additional sources of APIs
- Spring Core - the most important component of the Spring framework, one that encompasses the injection of outbuildings.

2.2 Model – View – Controller Architecture

Architecture MVC (Model - View - Controller) implements the idea of separating data access and business logic from the user interface. As the name implies, the MVC pattern can be broken down into three components:

- *Model* - is data and data access rules. The software is an approximation of a process of everyday life.
- *View* - returns the contents of a model. Specify exactly how an object should be shown and this presentation is changed whenever the model is changed.
- *Controller* - is performing translation of user interactions with View into actions executed by Model.

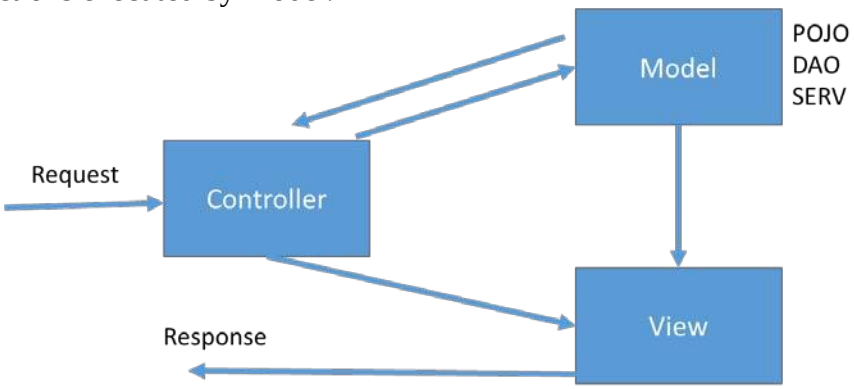

FIG. 1. The Model – View – Controller architecture

3. IMPLEMENTATION SCENARIO FOR MONITORING TELECOM INFRASTUCTURE ELEMENTS

We have chosen to demonstrate the concept by monitoring large Telecom infrastructure elements, main elements for mobile switching center and signaling central elements, that produce a big amount of logfiles, difficult to track and filter:

- EWSD (Elektronisches Wählsystem Digital/Electronic Digital Switching System)[5], produced by Siemens, is one of the most used switching systems, besides having capabilities for advanced Intellginet Networks, offering also services for ISDN (Integrated Services Digital Network), SS7 and Global System for Mobile (GSM).
- The hiS 700 system, developed by Nokia Siemens Networks [6] offers a hardware implementation for the Signaling System number 7 (SS7) used in the core network of mobile communication infrastructure. All the network signaling traffic is routed through this system, positioned in the center of the network, implementing the distribution, conversion and coordination functions for the signaling traffic.

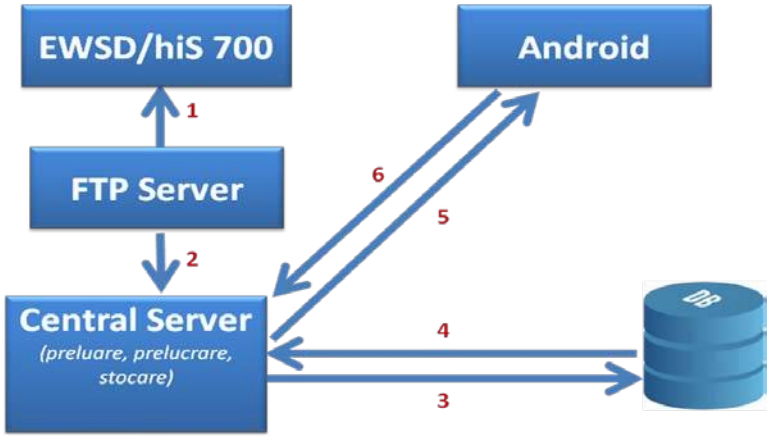

FIG. 2. The working model of the designed system

The system has five main modules that interact through web services of type REST and ORM services. (Fig.2.)
The 5 modules are:

- Switching equipment - these are the system EWSD equipment and signaling system hiS 700
- FTP server - is the server that communicates directly with devices (relationship 1 in Figure 4.1), transferring data via FTP communications and sending them to the web server
- Central Server - is the web server developed in this project, implemented in Java, left running through Apache Tomcat server; is the link between system modules: receiving data from the FTP server via web services (relationship 2 in Figure 4.1), communicated through services ORM to the database (relations 3 and 4 in Figure 4.1), posting data through Android app (5 the relationship of Figure 4.1)
- Database - represented by PostgreSQL, located on the same server as the web application
- Android client - in the project are used two terminals: GenyMotion for simulating mobile device Google Nexus 4 and Samsung I9500 Galaxy S4 smartphone; the data from the server are read by the mobile devices through Retrofit library

4. SOFTWARE SOLUTION ARCHITECTURE

4.1 Web Server

The server is represented by a Java web-developed under Eclipse IDE. This solution is designed to link the physical and application data Client (Android) using REST web services for reading and publishing data received from the server where the data are written. The web server communicates with relational database PostgreSQL through Hibernate ORM libraries [7]. Web services enable communication between the database and Android app.

Initially a *http get* call is performed, to read data from another server (that store physical logs), these data are entered into the database and posted (*http post*) to an IP address that can be accessed by application Client.

Communication via Hibernate ORM database allows access to secure data, by the usage of configuration files. Hibernate ORM enables data modeling and encapsulating them into objects. PostgreSQL is the database that stores application models (objects) in a table form. It is a database accessible from the web that works with SQL.

Transferred data are of two types (*Models*): „procedures" and „logs" (see Fig.3.) MVC architecture, with its elements: model, view, controller allow manipulation of data as objects. Controller is the main functional component of the system, that creates web services responsible for data transfer. Modeling objects with DAO (Data Access Objects) are used to organize communication with the database. For each type of object modeling involves using three different classes which must include:

- Defining the attributes and behavior patterns
- Defining interfaces for database persistence with standard functions (saveOrUpdate, findById, delete, findAll, deleteAll)
- Implement interfaces using the library "org.hibernate" to start the session database

Defining objects is done according to information received from the FTP server and according to what is meant to be inserted into the database.

```java
@Entity
@Table(name = "procedures")
public class Procedures {

    @Id
    @Column(name = "id")
    private int id;

    @Column(name = "element_name")
    private String elementName;

    @Column(name = "begin_timestamp")
    private Date beginTimestamp = new Date();

    @Column(name = "end_timestamp")
    private Date endTimestamp = new Date();

    @Column(name = "procedure")
    private int procedureInt;

    @Column(name = "status")
    private int statusInt;

    @JsonManagedReference
    @OneToMany(fetch = FetchType.EAGER, mappedBy = "procedure")
    private List<Logs> logs;
```

(a)

```java
@Entity
@Table(name = "logs")
public class Logs {

    @Id
    @Column(name = "id")
    private int id;

    @JsonBackReference
    @ManyToOne
    @JoinColumn(name = "procedure_id")
    private Procedures procedure;

    @JsonDeserialize(using = DateDeserializer.class)
    @Column(name = "timestamp")
    private Date timestamp;

    @Column(name = "operation")
    private int operationInt;

    @Column(name = "status")
    private int statusInt;

    @Column(name = "step")
    private int stepInt;

    @Column(name = "command")
    private String command;

    @Column(name = "information")
    private String information;

    private int procedureId;
```

(b)

FIG. 3. Structure of the models for (a) "procedures" and (b) "logs"

4.2 Client Application

Client application interface consists of an application developed for the Android operating system, adaptable to different system version. Is developed in Eclipse IDE plug-in for Android [8], which allows the integration of many bookstores, such as for graphing to web services REST, reading data in predefined formats such as JSON. These libraries will be elaborated further by example and illustration [9].

The same MVC architecture is used to implement Client application model and is defined by the type of data (procedures and logs), vision being implemented in major classes of the Android app (activities). This is the one that uses models as data controller CPC as in the definition of REST web services.

The end user of the developed system accesses data by the use of this application. Security is achieved through the mobile app authentication [10] and access restricted to a web server company level "Intranet". Once authenticated, user can monitor the logs in real time, can produce reports and can supervise the copying files system by viewing the status of orders executed.

5. ANDROID CLIENT IMPLEMENTATION

The purpose of the application is tele-monitoring a system used for storing records retrieved from a switching equipment using an intuitive workflow. A user firstly accesses the application to see if there are uncompleted or completed executions error. To do this, the user must log into the system and access the menu option errors. This option, illustrated in Fig.4., lets the user to view records of procedures executed with error. A list of jobs that are with active error status is displayed and the details of the errors can be expanded, detailed steps are displayed for each job. For each details, steps can be viewed, so the user can know at which stage the error occurred.

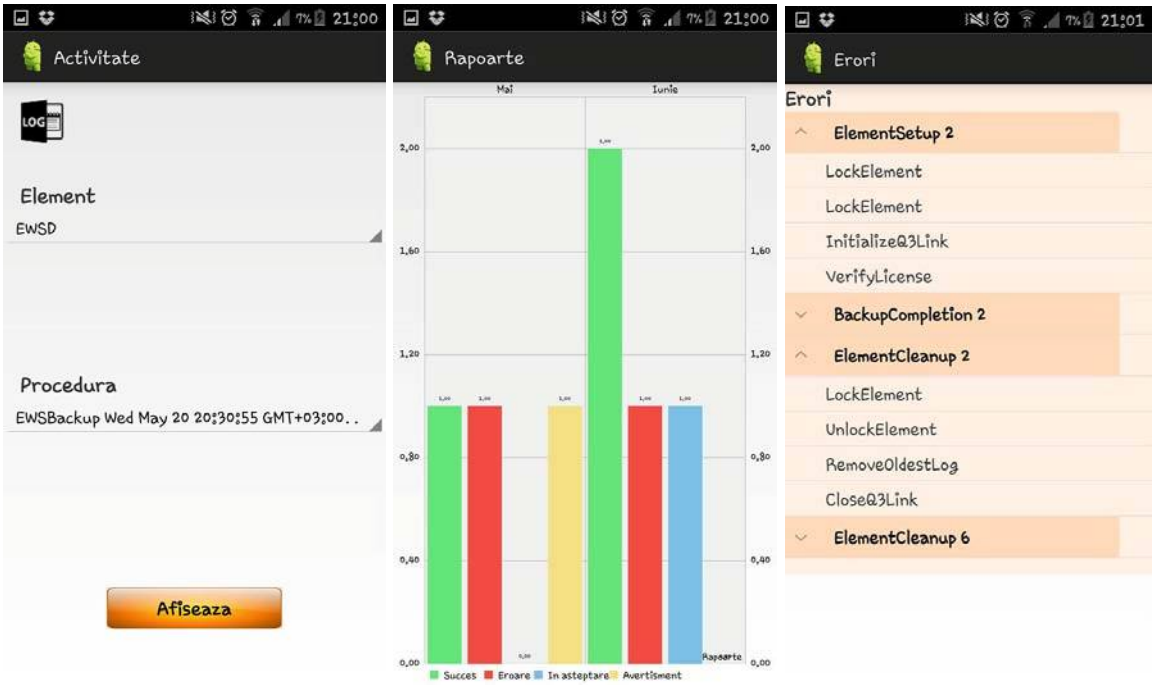

FIG. 4. The Android user application interface: Activity Options, Reports and Execution Errors

If the user wants to watch the entire list of records he will accessed the *Activity* options from menu (Fig.4.) This displays the list of all entries according to criteria chosen by the user (item were executed and procedure executed).

Another functionality of the application is the report generation . The reports can be viewed in two ways:

- Linear graphs with the number of procedures performed each month, depending on their status
- Circular graphs with the total number of procedures, separated according to their status resulting from execution

7. APPLICATION TESTING

Testing of the whole process was achieved by simulating the data transmission-reception.

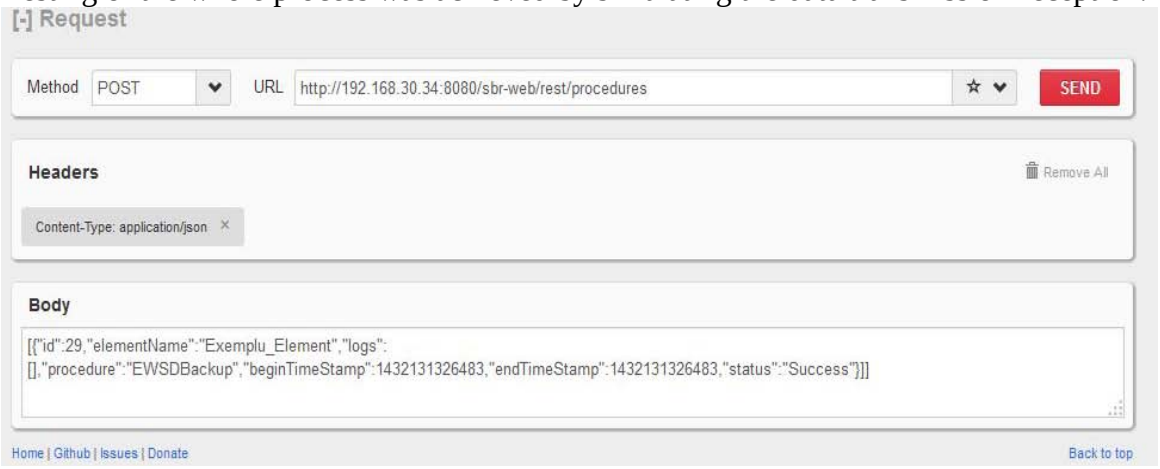

FIG. 5. Simulating a REST client

For transmission, Rest Client application was used from the Mozilla browser by using a sequence of a JSON file. There were two different formats of JSON files, which are retrieved from the server response. REST client interface provided by Mozilla is shown in Fig.5. This allows testing of REST web services and viewing the result. If execution is successful, the outcome is 200 OK.

CONCLUSIONS

The implemented system emphasizes the need for a "console", represented in this case by Smartphone, in monitoring the switching infrastructure of a telecommunications network. "The Console" allows the access to information infrastructure and at the same time provide users mobility.

Client-server model was developed by exploiting the model objects of Object Oriented programming, the data being transmitted and received as models. To transfer data between client and server, REST web services were used for reading and writing files in JSON format and transmitted to the server. Architecture used is the type Model-View-Controller (MVC Spring framework-).

As implementation, the system has two major advantages:

- It is adaptable to the desired execution platform, being developed mainly in Java, whose slogan is "Write once, run anywhere". The system is designed to have as many logical interfaces, not physical, exploiting the idea of class objects.
- The interfaces are generic, allowing modification of the application modules without impacting the system as a whole.

REFERENCES

[1] D. Amritendu, „Spring, Hibernate, *Data Modeling, REST and TDD: Agile Java Design and Development"*, Cathy Reed, 2014
[2] G. Amuthan G, „*Spring MVC: Beginner's Guide"*, Packt Publishing, 2014
[3] R. Johnson, *One-on-One J2EE Design and Development*, Wiley, ISBN: 978-0-7645-4385-2, October 2002
[4] Spring Framework, http://docs.spring.io/spring/docs/current/spring-framework-reference/html/, Accessed March 2016
[5] Siemens Networks LLC, „*Documentation Catalog for EWSD – Digital Electronic Switching System"*, 2006
[6] Nokia Siemens Networks, „*Updated brochure of hiS 700"*
[7] C. Bauer, G. King, G. Gregory, „*Java Persistence with Hibernate"*, Manning Publications Company, 2015
[8] Ziguard Mednieks, Laird Dornin, Blake Meike, Masumi Nakamura, *"Programming Android: Java Programming for the New Generation of Mobile Devices"*, O'Reilly, 2011
[9] Chris Haseman, „*Android Essentials"* Apress, 2008
[10] Ziguard Mednieks, Laird Dornin, Blake Meike, Masumi Nakamura, „*Programming Android: Java Programming for the New Generation of Mobile Devices"*, O'Reilly, 2011

ELECTRICAL AND ELECTRONICAL ENGINEERING / RENEWABLE ENERGY AND ENVIRONMENT

DISPLAYING THE AIR SITUATION THROUGH THE COLLECTION AND PROCESSING OF FLIGHT INFORMATION ON FLIGHTRADAR24 PROJECT

Karina KALAGIREVA, Veselin RADKOV

Department of Aeronautics, Technical University of Sofia, Sofia, Bulgaria
(karina@tu-sofia.bg, vrakov@tu-sofia.bg)

DOI: 10.19062/2247-3173.2016.18.1.36

Abstract: *In the present publication, the sources of flight data collected and processed on the Flightradar24 project are described. A description of the functioning of the system and its advantages, limitations and drawbacks is made. The improvement of Flightradar24 project capabilities by installing a monitoring station at the Technical University of Sofia is also mentioned.*

Keywords: *radar, radar station, ATC, flight safety, ADS-B, MLAT*

1. INTRODUCTION

The discovery of a target (aircraft, surface ships and other objects), the determination of its coordinates and motion parameters is performed by radar devices (radar stations or radars). They are designed to detect the target and determine its coordinates through the generation, transmission and reception of reflected radio signals, and in the case of secondary surveillance radar – by receiving signals transmitted by airborne transceiver (transponder) [1]. Therefore, the following tasks are performed:

1. Finding – establishing the existence of a target;
2. Determination (measurement) of the coordinates of the target;
3. Determination (calculation) of the movement parameters of the target by subsequent radar information processing [2].

Air traffic in the territory of the Republic of Bulgaria and international flights is organized within certain air corridors at which continuous radar surveillance must be established. This requirement appears to be a significant problem when flying over large bodies of water and over land in the presence of vast uninhabited areas where it is impossible to deploy radars (for example in Brazil, Russia etc.). One approach for solving this problem is the simultaneous use of several information sources. This approach is implemented in the Flightradar24 project [7].

2. BACKGROUND RESEARCH

In previous works the authors have studied the parameters and application of GNSS (Global Navigational Systems) and EGNOS (European Geostationary Navigation Overlay Service) in aviation, commercial in particular. Moreover, the radar data is still crucial to combat momentarily unreliable satellite navigation data [8][9]. These systems are irreplaceable in navigation, landing guidance etc. and they have proven sufficient in displaying the air situation by aggregating the data with radar information. However, such

complex systems are unfeasible in monitoring all air traffic, unregulated air traffic in particular [10]. Another problem is that this information is not displayed publicly.

In the current study, an information service called Flightradar24 is described. This service aggregates flight and position data and offers the information to the public. It can be displayed to recreational pilots and UAV operators for situational awareness.

3. INFORMATION SOURCES IN FLIGHTRADAR24

Flightradar24 is a flight tracking service that shows live air traffic from around the world. *Flightradar24* combines data from several sources including ADS-B transponders, US Federal Aviation Administration (FAA) data and Multi-lateration measurements (MLAT).

The ADS-B, MLAT and FAA data is aggregated with schedule and flight status data from airlines and airports to create a unique flight tracking experience on the www.flightradar24.com site.

3.1. ADS-B Technology.

The primary technology Flightradar24 uses to receive flight information is called Automatic Dependent Surveillance-Broadcast (ADS-B) [3]. The ADS-B technology itself is best explained by the image below (Fig.1).

1. Aircraft gets its location from a GPS navigation source (Satellite);
2. The ADS-B transponder on aircraft transmits signal which includes the location of the aircraft among other data;
3. ADS-B signal is picked up by a receiver connected to Flightradar24;
4. Receiver feeds data to Flightradar24;

Data is shown on www.flightradar24.com.

FIG.1. Gathering data in the project Flightradar24 [4]

3.2. FAA data [5].

The flight data is received from the FAA in the United States. Unlike the ADS-B data which is presented in real-time, the FAA data is delayed by roughly 5 minutes due to FAA regulations. On the Flightradar24 map, all aircraft based on FAA data are colored differently.

FAA data is based on radar data (i. e. not just planes with ADS-B transponders) and includes most scheduled and commercial air traffic in the US and Canadian air space as well as parts of the Atlantic and Pacific Ocean.

3.3. Multilateration Tecnology (MLAT) [6].

Many aircrafts still rely on older type transponders (non-ADS-B transponder) to report flight information. A special receiver and the related software are developed for these aircraft within the Flightradar24 project in order to implement MLAT for flights tracking.

Multilateration is a common technique in long-range radio navigation systems, where it is known as hyperbolic navigation. Such systems are relatively simple because they do not require a common clock. A position is determined by measurements of the difference in distance to two transmitters at known locations that broadcast signals at known times.

Unlike absolute distance or angle measurements, measuring the difference in distance between two stations results in an infinite location solutions. When plotted, they form a hyperbolic curve. To locate the exact location, multilateration relies on multiple measurements. A second measurement is made, to a different pair of stations. This measurement will produce a second curve, intersecting with the first. When the curves are compared, a small number of possible locations are revealed, producing a "fix".

3.3.1. MLAT limitations in the Flightradar24 project [7].

For Flightradar24 tracking MLAT requires 4 or more FR24-receivers in a region to receive a signal from the same aircraft. The next step is Time Difference of Arrival (TDOA) measurement – the time it takes the signal to reach the receiver. By comparing how long it takes the signal to reach each of the receivers, it is easy to determine the aircraft's position and speed. MLAT position accuracy is comparable with that of ADS-B.

Flightradar24 team is stating they have achieved an accuracy of 10-20 meters. Speed is also calculated but errors are common in speed data, especially when making turns.

Processing the received MLAT data results in a small delay in the display of the aircraft positions –approximately 30-40 seconds. An issue affecting mainly MLAT flights outside of Europe is the absence of call-sign information, which makes matching the correct flight route information very difficult. Route information is not transmitted by the aircraft, so the call-sign must be compared with flight and schedule databases to determine and display the route. When tracking via MLAT is possible and the call-sign is missing, a difficulty determining the route information is present.

Due to the high frequency used (1090 MHz) the coverage from each receiver is limited to about 250-450 km (150-250 miles) in all directions depending on location. The farther away from the receiver the aircraft is flying, the higher it must fly to be covered by the receiver. The distance limit makes it very difficult to get ADS-B and MLAT coverage over oceans.

3.3.2. MLAT coverage under project Flightradar24.

Most parts of Europe and North America are today covered with MLAT above about 5,000-10,000 feet (1,500-3,000 meters). There is also some MLAT coverage in Mexico, Brazil, South Africa, Japan, Taiwan, Thailand, Malaysia, Indonesia, Australia and New Zealand; MLAT coverage is under continuous expansion in South Africa, South America, China, South Korea, Japan and Russia.

In some locations Flightradar24 project has achieved MLAT coverage below 1500 feet (450 meters), including Amsterdam, Stockholm, Toulouse, Reykjavik, Chicago.

4. FLIGHTRADAR24 PROJECT IN BULGARIA

As stated above, MLAT requires 4 or more FR24-receivers in a region to receive signals from the same aircraft. In general this requirement limits the MLAT's coverage above 5,000-10,000 feet as the probability that four or more receivers can receive the same transponder's signal increases with increased altitude. So it is simple to understand that the number of FR24-receivers located in a region must be high.

Flightradar24 has a network of more than 7,000 ADS-B receivers, shown on Fig. 2.

In March 2015 a FR24-receiver has been installed in the Department of Air Transport at the Technical University of Sofia. The device has been provided by the FR24 team and is part of

the FR24 monitoring network. The equipment installed on the roof of Block 10 of a Technical University consist of (Fig. 3):

- Mode S/ADS-B FR24-receiver;
- Mode S omnidirecional antenna;
- GPS antenna.

The connections between elements is given on Fig. 4.

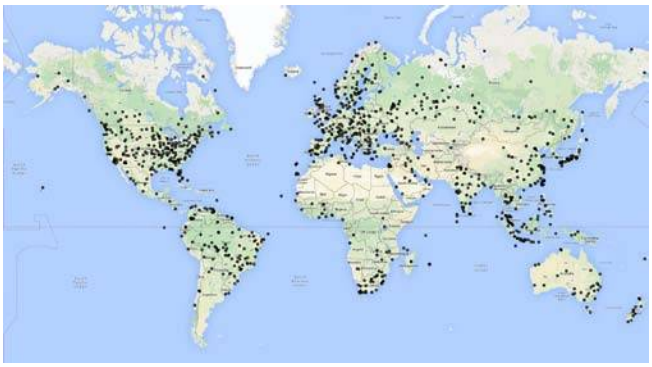

FIG. 2. Map of receivers activated in January-June 2015 [7]

FIG. 3. Specialized equipment to monitor aircraft in real time

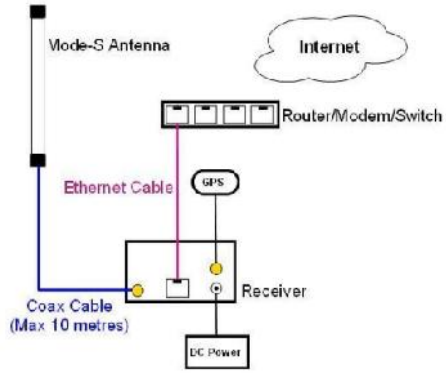

FIG. 4. Schematic diagram

The receiver gets signals from aircraft transponders (ADS-B or older). Received signals are sent to the FR24 data server, where depending on the type of transponder from which the signals are received the necessary processing or measurements is made and the results are displayed on the site in form of moving targets (aircraft, helicopters and more).

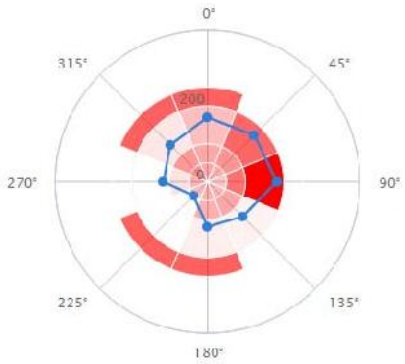

FIG.5. Daily plot of the registered aircrafts by the FR-24 receiver at TU-Sofia (range shown in nautical miles)

Installing the receiver of the Flightradar24 monitoring network at the TU-Sofia have improved the capabilities for monitoring and positioning of aircraft located at altitudes below

450 m significantly, i.e. all departing and landing aircraft at Sofia Airport. This is a particularly valuable contribution, especially having in mind the presence of high natural obstacles as Vitosha Mountain (11 kilometers away from the airport) and limiting the possibility of receiving signals from other monitoring stations in a wide sector in the west direction. A typical polar plot of the range of the daily registered aircrafts by the FR24 receiver at TU-Sofia could be seen on Fig. 5.

CONCLUSIONS

In recent years the unregulated air traffic tends to increase. The rapdly expanding UAV market for the general public neccesitates the creation of a public source of information on all air traffic. Flightradar24 project shows clearly how the opportunities for air situation display in real time are increased by combining flight information from different sources and by appropriate data processing, without the need to use traditional methods for radar surveillance and offering the gathered information to the public.

The only drawback of the Flightradar24 project is the inability to observe and depict aircraft without switched on or with damaged transponders.

By integrating and processing flight information from different sources, the possibilities for monitoring and display of the air situation in real time is improved, including overlarge areas with no radar surveillance. This will significantly improve the opportunities for ATC in these areas, which in turn will lead to increased flight safety.

The introduction of systems that collect and process flight information from different sources is a promising direction, which in many cases may be the only possible solution to ensure the process of ATC over areas without radar coverage.

AKNOWLEDGMENT

The authors want to thank for the technical assistance in the provision of specialized equipment (Mode-S/ADS-B receiver, Mode-S antenna and GPS antenna) to the Flightradar24 project team.

The authors express their gratitude to the Research Sector at the Technical University of Sofia for the financial assistance in publishing the report. The paper is within contract №152PD0028-04 with topic: “Methods for evaluation and comparison of quality indicators of satellite systems”, “Navigation, control and operation of air transport”.

REFERENCES

[1] Korobko, I., *Radiolocation Systems and Devices. Part I – Radiolocation basics*, Sofia, 2002.
[2] Korobko, I., *Radio-technical Systems*, Sofia, 2003.
[3] Radarspotters Team, *Simply about complicated – ADS-B (Automatic Dependent Surveillance-Broadcast)*, http://www.adsbradar.ru, 2013.
[4] Radarspotters Team, *ADS-B Technology (TIS-B, FIS-B)* – photo, http://www.adsbradar.ru, 2013.
[5] Federal Aviation Administration, *About FAA*, http://www.faa.gov, 10 June 2015.
[6] Radarspotters Team, *Multilateration – MLAT*, http://www.adsbradar.ru, 2013.
[7] Flightradar24, *New Flightradar24 Receivers Activated in the First Half of 2015*, New Flightradar24 Receivers Activated January through June 2015 – photo on http://www.flightradar24.com, 2015.
[8] Kalagireva K., Vassilev B., *Comparative Analysis of the Algorithms for Determination of the Egnos Performance Indicators*, 22-nd Saint Petersburg International Conference on Integrated Navigation Systems, 25-27 May 2015.
[9] Kalagireva K., Comparison of the Efficiency of EGNOS Parameter Determination Algorithms, BulTrans-2014 International Conference Proceedings, Sozopol, 2014.
[10] *EGNOS Cost Benefit Analysis in Aviation*, GSA – GNSS Supervisory Authority, 27 July 2009, http://www.lek.com, 2015.

ELECTRICAL AND ELECTRONICAL ENGINEERING / RENEWABLE ENERGY AND ENVIRONMENT

ASPECTS ABOUT FREQUENCY SYNTHESIZERS

Bebe-Bucur MARIN, Adrian NĂSUI, Sebastian SPRINCEANĂ

Ministry of National Defence

DOI: 10.19062/2247-3173.2016.18.1.37

Abstract:*The communications systems objectives consist of maintaining communication depending on different facts like: cruising speeds, subscriber growth, efficient use of the allocated spectrum, expanding geographical coverage, possibility of reconfiguration depending on traffic density, provide new services and achieving affordable costs.*

In this context, effective management of the electromagnetic spectrum has led to the emergence of specific structures capable of stability to disturbance, flexibility and capacity development. These structures, which permit the production of highly stable frequency signal is called frequency synthesizers.The role of frequency synthesizers is very important, it represents the core and customary in transmitting and receiving equipment.

Frequency synthesizers reprezent that class of electronic circuit capable of generating one or more stable frequencies from one or more reference frequencies. The stability of the output frequency is at least equal with the reference frequency.There are two main conventional types of achieving phase/frequency synchronization of the output signal with the reference signal:PLL (phase locked loop) – consist in transfering stability of a highly stable component to a less stable element. Has quite large spectral purity, reproduce with high fidelity a reference signal scaled over a wide frequency range.DDS (direct digital synthesis) - good resolution, low switching times, opportunities for implementing digital modulations,

Keywords: *Frequency synthesizer, PLL, DDS, electromagnetic spectrum, synchronization*

1. INTRODUCTION TO FREQUENCY SYNTHESIZERS

Frequency synthesizer represent the class of electrical circuits capable of generating one or morefrequencies high stability, starting from one or more reference frequencies (fig. 1). Output frequencies stability is at least equal or higher than the input frequency f_0.

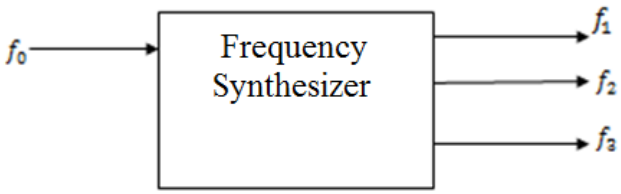

FIG 1. Block diagram of a frequency synthesizer.

Ideally is to obtain from one synthesizer a noise-free sine wave. Actually, this thing never happens, the output signal being affected in some measure by the presence of unwanted disruptive components.

The formula of a pure sine wave is:

$$V(t) = (V_0\ sin(2\pi f_0), \quad (1)$$

If we consider the amplitude fluctuationand the signal's phase, the formula will become:

$$V(t) = (V_0 + v(t))sin(2\pi f_0 t + \phi(t)), \quad (2)$$

where v(t) is the amplitude fluctuation, respectively ϕ(t) fluctuation of the phase.

When designing a frequency synthesizerit is envisaged that it meet certain main features:

-synthesized frequency range signal using a specific portion of the spectrum;

-network spread - the difference between two neighboring frequencies;

-spectral purity of the generated signal - signal to noise ratio is as high as possible;

-switching speed - speed that is reached at a frequency other;

- the number of frequencies generated - fully frequencies depending on the range and the difference;

-the possibility of performing different types of modulation amplitude, modulation in frequency or phase;

-continuity of the phase - phase synchronization maintaining;

-stability of frequency and amplitude output signal - this should not fluctuate greatly, as synthesized signal is lost;

-constructive features - features of some components of a frequency synthesizer;

-power consumption - power in watts of the frequency synthesizer;

-the cost.

2. METHODS OF FREQUENCI SYNTHESIS

PLL Synthesis

A frequency synthesizer using indirect PLL synthesis is based on a circuit that follows and faithfully reproduce a reference signal scaled over a wide frequency.

Frequency synthesizers using method horseback PLL phase generates the desired signal frequency with high enough spectral purity, and also, allows digital output frequency according with specified frequency output.

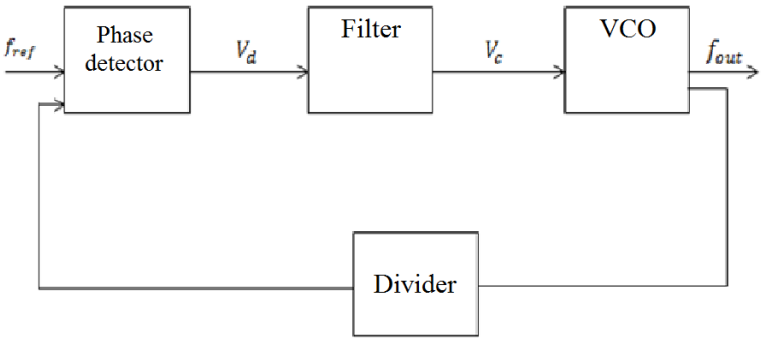

FIG. 2. Block scheme of a PLL synthesizer.

Figure 2. represents a block diagram of a PLL circuit. Initially we have input frequency, that is applied to the input of a phase detector.This generates a voltage outputV_d, whose average value is proportional with the phase difference signal from the detector inlet. The error signal of the phase detector appliess to the input of the loop

filter.This will generate a voltage proportional to the phase error voltage. This voltage control signal is voltage controlled oscillator OCT. In this way the frequency of the output signal f_{out} changes according to the existing momentary error.

GenerallyV$_d$ is:

$$V_d = f(\omega_{int} - \omega_{out}, \theta_{in} - \theta_{out}, \omega_{int} + \omega_{out}, \theta_{in} + \theta_{out}), \quad (3)$$

$$(V_c) = \frac{d\theta_{out}}{dt} \quad (4)$$

PLL architecture is one of the most used among frequency synthesizers because it can be easily integrated into XXI century technologies. One of the main advantages of this method is that it uses a low power consumption. Other advantages of this method are: low production cost, simplicity of construction and permit obtaining relatively fast switching speeds. These advantages make this method very used in a wide range of communications from the audio to the one of the millimeter-wave . PLL method is widely used in wireless communications through its architecture ΔΣ-PLL or fractional-N-method.

The major disadvantage of this method is that it is difficult to obtain digital modulation type and is also difficult to obtain high resolution. Also, good quality oscillators are quite expensive and very bulky leading to restrict their use in a wide variety of communications field such as mobile phones or laptops.

DDS Digital Direct Method

The main elements of the architecture of a direct digital frequency synthesizer are: phase battery, memory, or conversion device using phase-amplitude sine function and digital-to-analog converter. Each of these elements can lead to distort the spectral components of the output signal spectral structure.

At higher operating frequencies, another source of noise consists of transitions that occur when switching from one state to another.

Reduced switching time is required in applications such as frequency hopping radio systems. From this point of view, direct digital synthesis method offers outstanding performance.

DDS architecture out of a battery is related to the entry phase by the following equation:

$$f_{out} = \frac{K}{2^N} \cdot f_{clk}, \quad (5)$$

where N is the length of the arm of a battery, the battery K is the value entry,and frequency control is ff_{clk}. Output frequency range is limited by f_{clk}, thus the maximum output cannot be greater than 400 MHz due to technological limitations.

The total number of possible phases is2^L (L- accumulator size in bits register).

By definition we have:

$2^L=2\pi$ (6)

L represent spread network frequency output achieved.

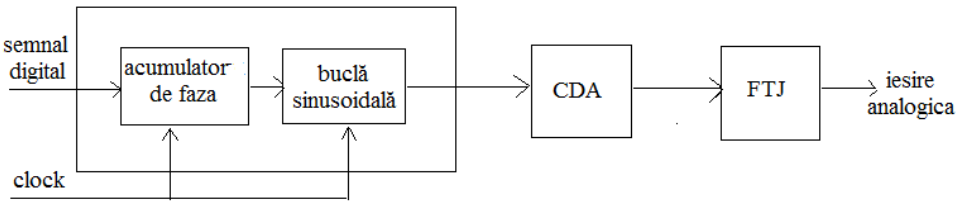

FIG.3 Direct digital synthesis block diagram.

It is shown in Fig.3.block diagram of a synthesizer that uses DDS frequency synthesis method. In the figure above are presented the main elements of an architecture of this kind, namely battery-digital converter and analog sine loop and a low pass filter for filtering signal. The main block is inserted the digital signal so that these enter into Converter. It can have a function sine, cosine, or both. On leaving the furnace signal is filtered by a low pass filter (to improve signal output) following to get the analog signal.

Synthesizers that are based on DDS direct method are used in the Army because it offers many advantages to the military, one of them would be the possibility of implementing any type of modulation. This is possible because it always knows phase, frequency and amplitude of a signal. Also, this method facilitates working in frequency hopping affords great carts, saving network frequencies, rapid scanning of the network, dial a synthesized frequency network, good or very good performance for the unwanted components output.

Also, this method has some less good parts, like for example that the circuits operate at maximum f_{clk}, which means a high energy consumption. Also, a disadvantage of this synthesis is the performance limiting of the digital-to-analog converter, or the occurrence of unwanted spectral components from the effects of truncation, in particular the phase truncation and the operation of the digital-to-analog converter.

Truncates of the bit length value sin (θ) (denoted by W) are stored in memory. The length of the sample phase bits (denoted by D) leads to the appearance of unwanted spectral components in the structure the signal output.

Sizes D and W contribute to increased quantization noise. Signal to noise ratio SNR (Signal Noise Ratio) at a frequency synthesizer can be calculated with the following formula:

$SNR_t = 2^w \cdot \frac{1}{2\pi^2}$, sau în decibeli: $SNR_t(dB) = (6W\text{-}13)\ dB$ (7)

Following the continuity phase generated signal, digital direct synthesis results in performance for digital modulations FSK, QPAK, BPSK, MSK, GMSK, which is impossible with other synthesis methods.

Direct synthesis allows to obtain phase modulation with outstanding frequency performance on precision.

3 ANALYSING THE BEHAVIOR OF A FREQUENCY SYNTHESIZER

For early analysis I selected block diagram of a PLL synthesizer, which is in the figure below.

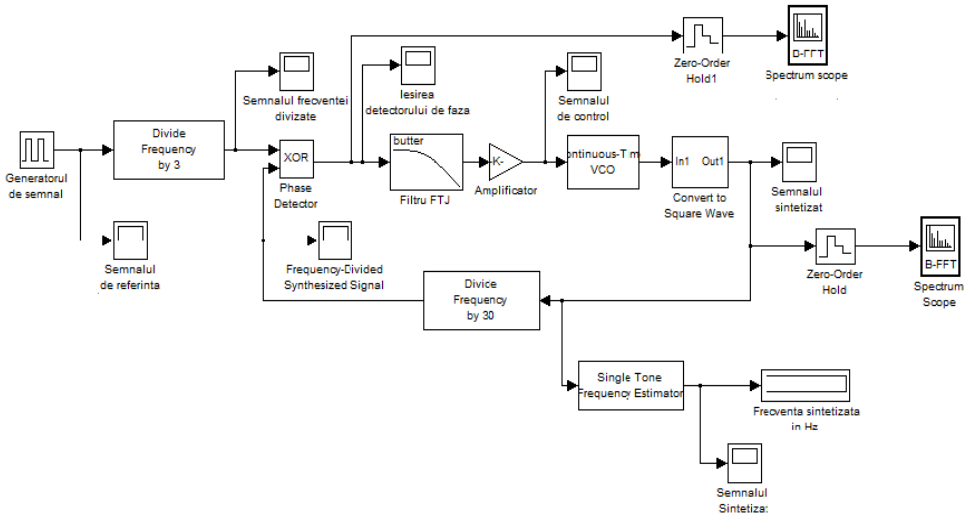

FIG.4. A PLL frequency synthesizer scheme in Simulink.

Figure 4 represents the block diagram of a frequency synthesizer with PLL phase horseback. The reference signal is obtained from the digital signal generator. M frequency divider, divides the frequency reference by m times, after which the signal enters the loop timing.The phase detector apply logical operation "or" to both reference and synthesized divided frequency .The filter is low pass and ensure the voltage needed to trigger the controlled oscillator voltage (with amplifier).It also filters high frequencies. The signal is amplified by an amplifier withconstant size at the output. Voltage controlled oscillator controls the frequency synthesized signal through control signal input. This concerns the output signal of synthesizer.*Voltage controlled oscillator with digital analog converter generates the synthesized signal.*

Value of output signal

$$f_{out} = 10MHz \times 30 \rightarrow \quad f_{out} = 300\ MHz \tag{8}$$

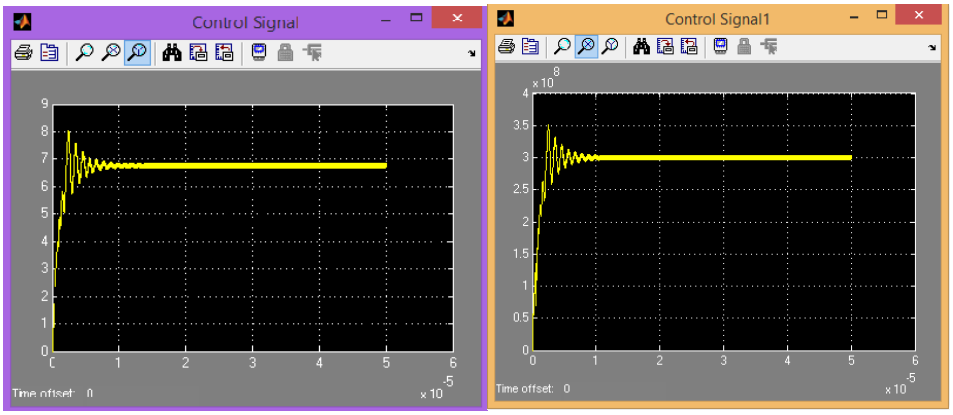

(a) (b)

In the Fig. a it can be seen the control signal that OCT's block receives the input signal frequency to maintain synthesized. This signal fluctuates initially for 10μs, following then to stabilize at constant value of 7/4. This happens when the model reaches an equilibrium.Fig. b is output from the PLL synthesizer. It can be seen that the signal has approximate the same features as the control signal acting OCT site. After amplifying, the signal fluctuates uncontrollably for about 10μs and then stabilizes at the desired frequency of 300 MHz. This synthesizer has a very good stability, an improvement that

can be added to it as time synchronization. The improvement can be done by adding a DDS structure as a reference signal for PLL synthesizer. DDS synthesizer uses the same principle as an NCO. The clock signal has a value of 100 MHz which makes value during sampling be 10^{-8}. Phase accumulator is offering sinusoidal input for signal loop. The accumulator is based on a function mode (mode) totaling values displayed between -1 and 1, and the values which exceed the range of -1 and 1 are not taken into consideration.

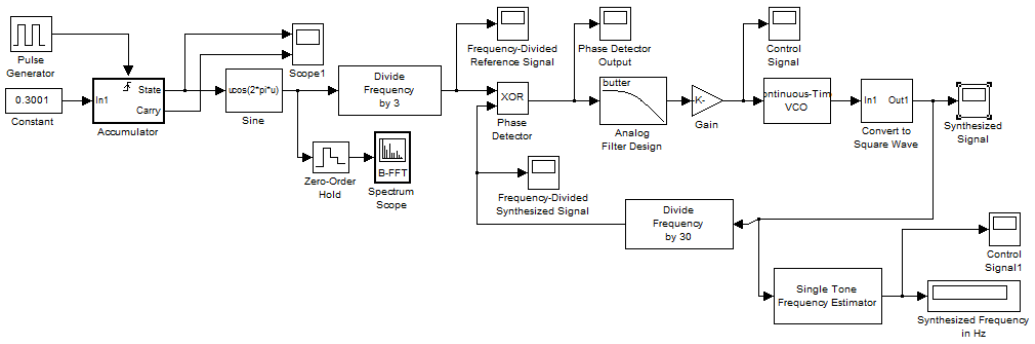

FIG.5.A hybrid frequency synthesizer scheme in Simulink..

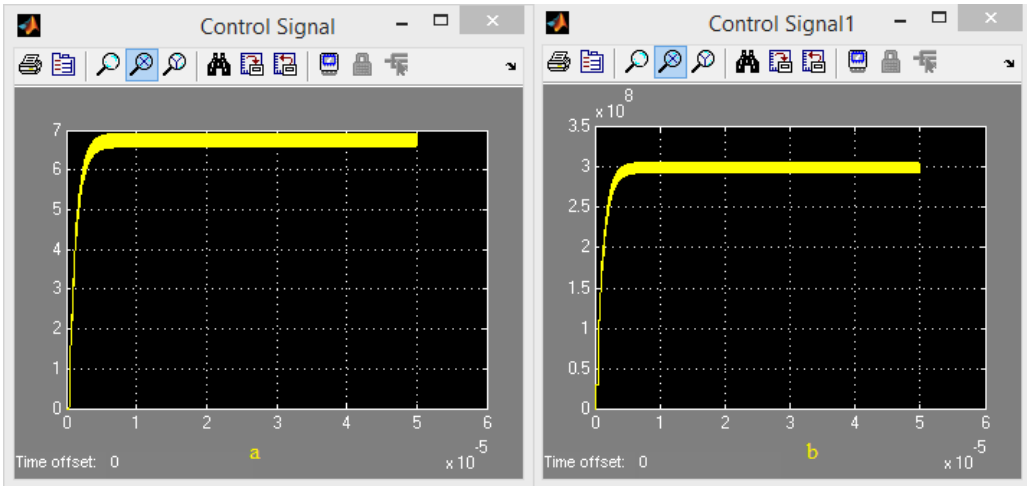

(a) (b)

The amplification of signal at hybrid synthesizer is more direct, which makes the fluctuation to be much smaller, and the time it needs to stabilize is 5μs, instead of 10μs to the PLL synthesizer. Output frequency synthesizer has same value as in the previous section, namely 310 MHz. There is also a little difference for this value in favor of hybrid synthesis by the fact that the calculated value for simulator in PLL synthesizer is 295 MHz.

4. CONCLUSION

Considering all the requirements imposed by choosing this theme and considering everything that was caught during the development of this studywe can say that we presented the main methods of frequency synthesis used in communications, noting and brief analysis of one of the most common methods of frequency synthesizing and, not least, an analysis of a hybrid synthesizer.

We also demonstrated the operation of a PLL frequency synthesizer and how it can generate from any referencefrequency one or more frequencies of any order, and improving that kind of synthesizers by forming a hybrid frequency synthesizer. These ones are much better in terms of the time we live in,by the fact that it provides a much better stability compared with one PLL.

REFERENCES

[1] Bechet, Paul, *Sintetizoare de frecventa*, Sibiu,Academia Fortelor Terestre "Nicolae Balcescu", 2001.
[2] Best, Roland, *Phase Locked Loops: Design, Simulation and Application*, McGrau Hill, 2003.
[3] Liu, Shen, *Analysis and Design of Phase Locked Loops (PLL & DLL*), Taipei, NTUEE, 2000.

ELECTRICAL AND ELECTRONICAL ENGINEERING / RENEWABLE ENERGY AND ENVIRONMENT

FRACTAL STRIPLINE ANTENNA WITH COMBINED ELEMENTS

Gheorghe MORARIU, Mihai MIRON

"Transylvania" University, Brasov, Romania
(gheorghe.morariu@unitbv.ro, mihai.miron@unitbv.ro)

DOI: 10.19062/2247-3173.2016.18.1.38

Abstract: *The paper presents a model of fractal antenna having as resonance elements dipoles obtained by the combination of triangular and discoid surfaces. There are highlighted technical design features and experimental results (reflection coefficient, VSWR, gain). Covering a wide frequency band with a very satisfying gain and having reduced geometric dimensions, antenna is recommended in mobile telephony, digital television and multiservice.*

Keywords: *antenna, fractal, stripline, resonator*

1. INTRODUCTION

Considering the fractal geometrical structure as a combination of virtual capacitors and inductors, it is possible to create a system of resonators for more resonance frequencies which can be selected and corrected by particular fractal pattern, validating the idea that geometry is a core issue in the unique electromagnetic behavior determination of the independent frequency electromagnetic antennas [2].

The antenna contains fractal radiating elements obtained by combination the triangular and discoid surfaces, calculated for specific resonant frequencies.

The combination of butterfly dipoles with different angular opening in a linear and circular network forms a broadband radiant fractal structure (surface tip) with quasi-circularly polarization.

2. ANTENNA DESIGN

The reference resonant frequency of the resonant dipoles is calculated using the formula:

$$f_0 = \frac{c}{\sqrt{\varepsilon_r}} \frac{1}{\lambda}, \tag{1}$$

where $\varepsilon_r = 2.27$ and $c = 3 \cdot 10^8$m/s.

For a chosen wavelength $\lambda = 0.32$m, the resonant frequency is $f_0 = 0.624$GH$_z$.

Being a fractal structure, the antenna covers a frequency domain from $f_0/4$ to $2f_0$, so from 0.156GH$_z$ to 1.248GH$_z$.

Reference spectrum calculation. Considering V_i - angular variation of the phase in the direction of propagation for reception, θ the angle between direction of propagation for reception and antenna surface in the antenna sector $\pm\beta/2$ where wave intensity module direction it is also considered constant, it follows that:

$$V_i = e^{j\theta} \cdot e^{j(\alpha+\gamma R_i)}, \text{ where:} \quad (2)$$

$$\gamma = 2\pi / \lambda \text{ (dephasing coefficient);} \quad (3)$$

$$R_i = R\sqrt{1 \pm \sin(\beta)\cos(\varphi)}; \quad (4)$$

α - attenuation coefficient;

φ - the deviation angle (0 - 90^0) of the radius r of the half-disk resonator in relation to radius R of the fractal sector from dipole in its origin (position where R_i takes the maximum / minimum value) (Fig. 1(a));

$$R_i = R \pm r \quad (5)$$

β - angle of the fractal sector from dipole ($30^0/3$; $45^0/3$; $60^0/3$) (Fig. 1(a)).

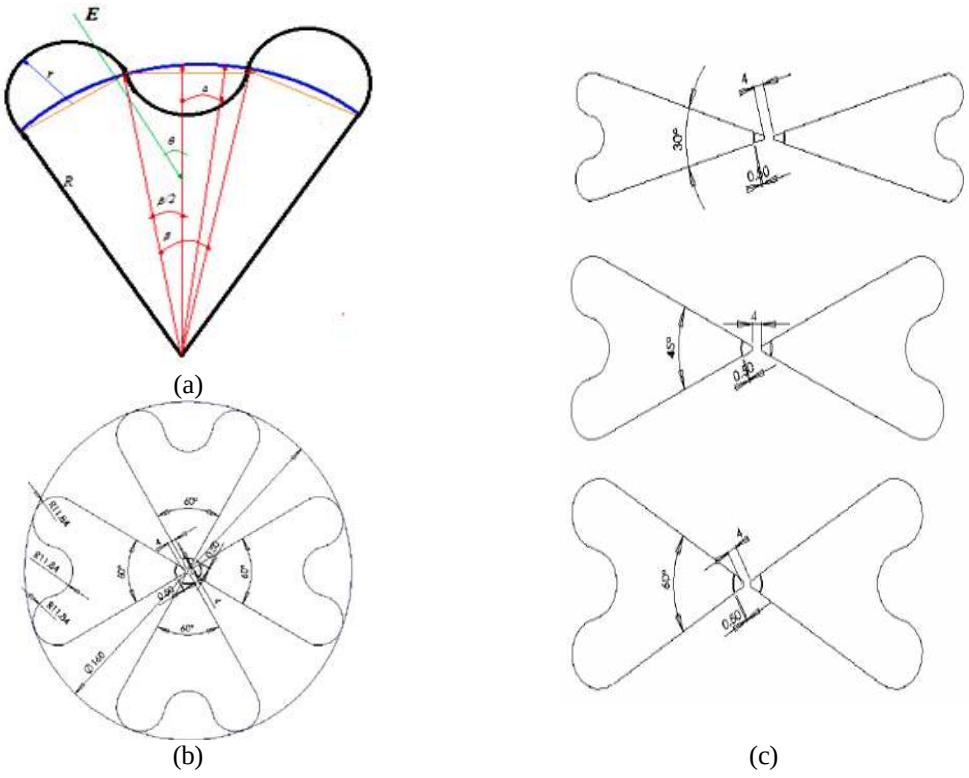

FIG. 1. Fractal stripline antenna with combined elements: (a) Radiant fractal structure – combination of triangular and discoidal surfaces; (b) Central resonator scheme; (c) Butterfly dipoles diagram (λ / 2 = 170mm).

The total phase angle variation is

$$V_0 = \sum V_i, \quad (6)$$

$$V_0 = e^{j\theta} \sum e^{j(\alpha_n + \gamma R_i)} \Big|_{\alpha=0}^{\alpha=\pm\beta/2} \tag{7}$$

so that the wave received (E, H) has the expression:

$$E;H = |E;H| V_0 \tag{8}$$

From total angular phase variation expression (7) it is is observed that basic resonance spectrum covers a bandwidth of (± r / R)*f_0 for each dipole (approximately ± 20%).

In the case of considered central resonator - a compact disk-shaped element, field strength E_T is approximated by the following relationship [1], [2]:

$$E_T = E_0 \left(1 - \left(\frac{\omega \cdot r}{2c} \right)^2 \frac{1}{(1!)^2} + \left(\frac{\omega \cdot r}{2c} \right)^4 \frac{1}{(2!)^2} - \left(\frac{\omega \cdot r}{2c} \right)^6 \frac{1}{(3!)^2} + ... \right) \tag{9}$$

which becomes

$$E_T = E_0 \cdot e^{j\omega t} \cdot J_0 \frac{\omega \cdot r}{c}, \tag{10}$$

where: r - reference disc radius;

J_0 - zero-order Bessel function [7].

Take into consideration a disc radius r = 8cm, the calculated resonant frequency is 1.26GHz (ω·r/c = 2.4).

Technical realization of the antenna. Sizing and framing of antenna elements are presented below, in the figures 2 and 3.

To adapt the resonant elements to the feeder were used line sections with length

$$L = n \cdot \lambda + \frac{\lambda}{4}, \tag{11}$$

where n = 0, 1, 2.

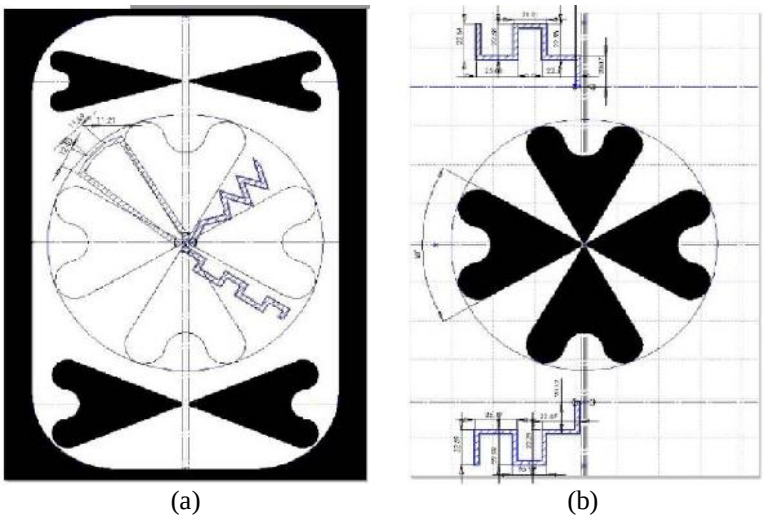

(a) (b)

FIG. 2. Fractal stripline antenna with combined elements – framing of elements: (a) frontal view; (b) rear view.

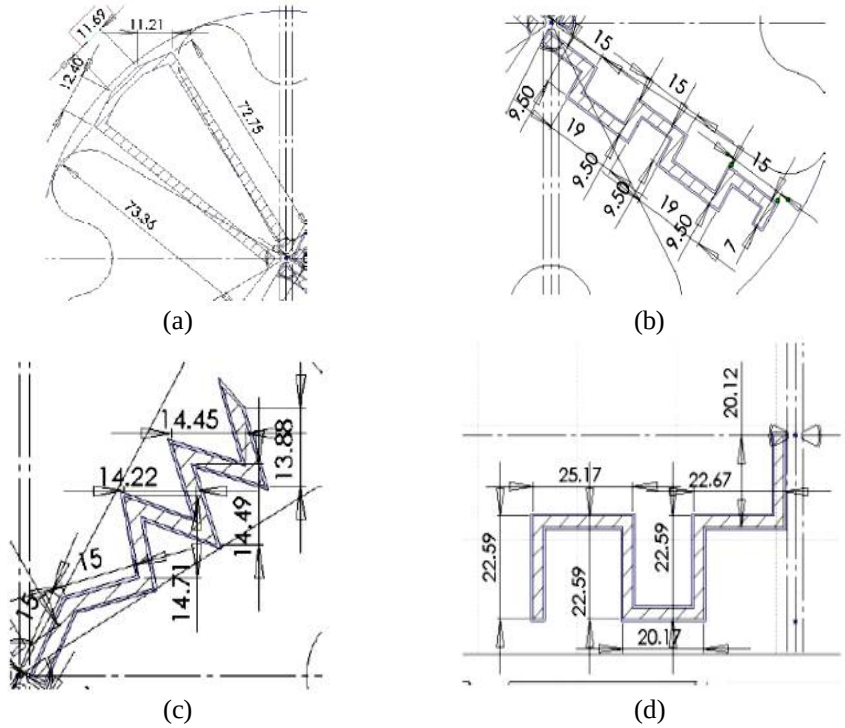

FIG. 3. Fractal stripline antenna with combined elements:
(a) Element of adaptation - phasing line; (b) Element of adaptation (1) to a radiating element with opening of 60º; (c) Element of adaptation (2) to a radiating element with opening of 60º; (d) Element of adaptation to a radiating element with opening of 45º.

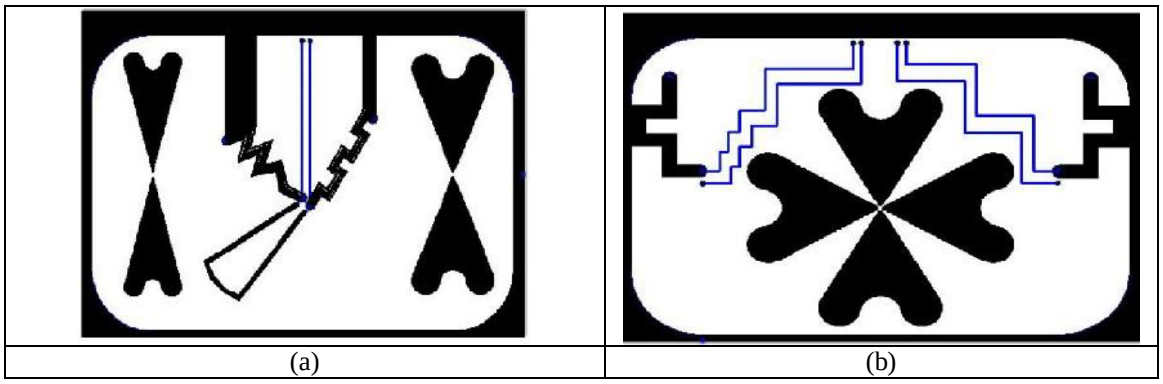

FIG. 4. Fractal stripline antenna with combined elements –
final implementation: (a) frontal view; (b) rear view.

3. EXPERIMENTAL RESULTS

Data on electrical measurements obtained from experiments are presented in sequential order as follows: reflection coefficient variation, standing wave ratio variation, reception diagram with afferent frequency bands, directivity diagrams and antenna gain.

According to the reflection coefficient diagram, Γ=1 for a signal domain from (-27) to (-30)dB, and Γ=0 for a signal domain from (-70) to (-80)dB.

The formula used for voltage standing wave ratio is:

$$VSWR = \frac{1+|r_n|}{1-|r_n|}, \text{ where } r_n = 1, 2, 3. \tag{12}$$

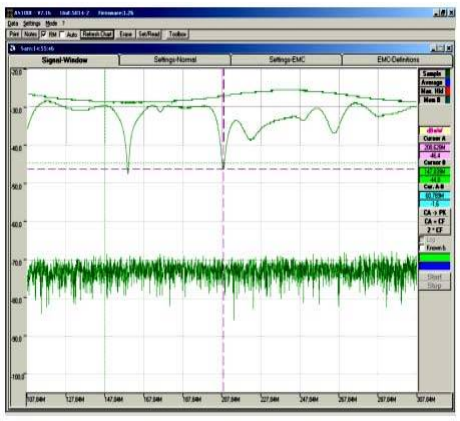

(a)

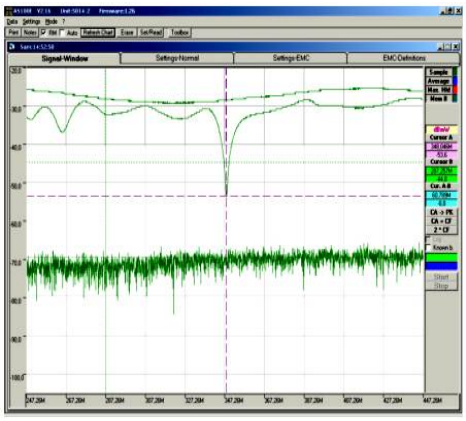

(b)

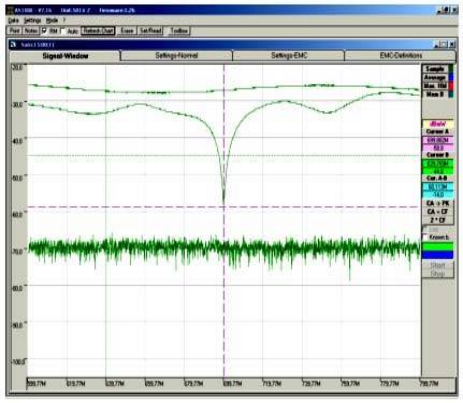

(c)

$$U1 = Ur \cdot 10^{\frac{r1}{20}}\,[mV] = 0.2236 \cdot 10^{\frac{-30}{20}} = 0.2236 \cdot 0{,}031 = 0.007[mV]$$

$$U0 = Ur \cdot 10^{\frac{r0}{20}}\,[mV] = 0.2236 \cdot 10^{\frac{-75}{20}} = 0.2236 \cdot 0.00017 = 0.000039[mV]$$

$$\Delta U_r = U1 - U0 = 0.00697$$

$$x = \frac{\Delta U_r}{100}(mV/div) = 0.0000697(mV/div)$$

$$U_{banda1} = Ur \cdot 10^{\frac{dBvf}{20}} = 0.2236 \cdot 10^{\frac{-46.4}{20}} = 0.2236 \cdot 0.004 = 0.00107$$

$$k = \frac{U_{banda1} - U0}{x} = \frac{0{,}00107 - 0{,}000039}{0{,}0000697} = 14.92$$

(d)

FIG. 5. Reflection coefficient variation: (a) 107-307MHz;
(b) 247.2-447.2MHz; (c) 599.7-799.7MHz; (d) The calculation procedure (Γ=k/100).

Table 1 - Reflection coefficient variation and standing wave ratio.

	Frequency band #1 f_1 = 208,628MHz	Frequency band #2 f_2 = 348,046MHz	Frequency band #3 f_3 = 699,892MHz
Γ - reflection coefficient (k/100)	0.1492	0.06269	0.026839
VSWR - voltage standing wave ratio	1.3507	1.1429	1.0585

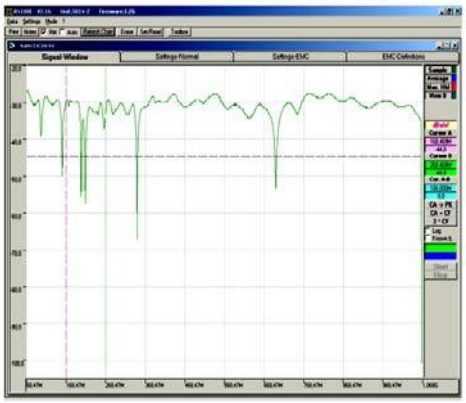

(a)

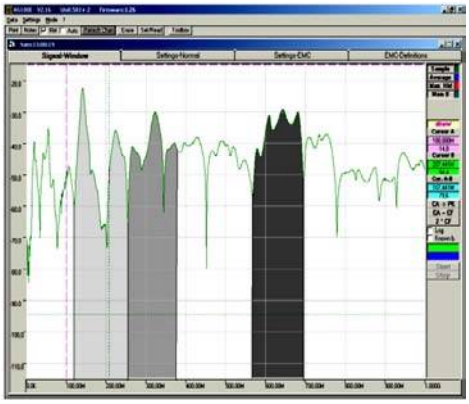

(b)

FIG. 6. VSWR variation (a) and reception diagram with afferent frequency bands (b).

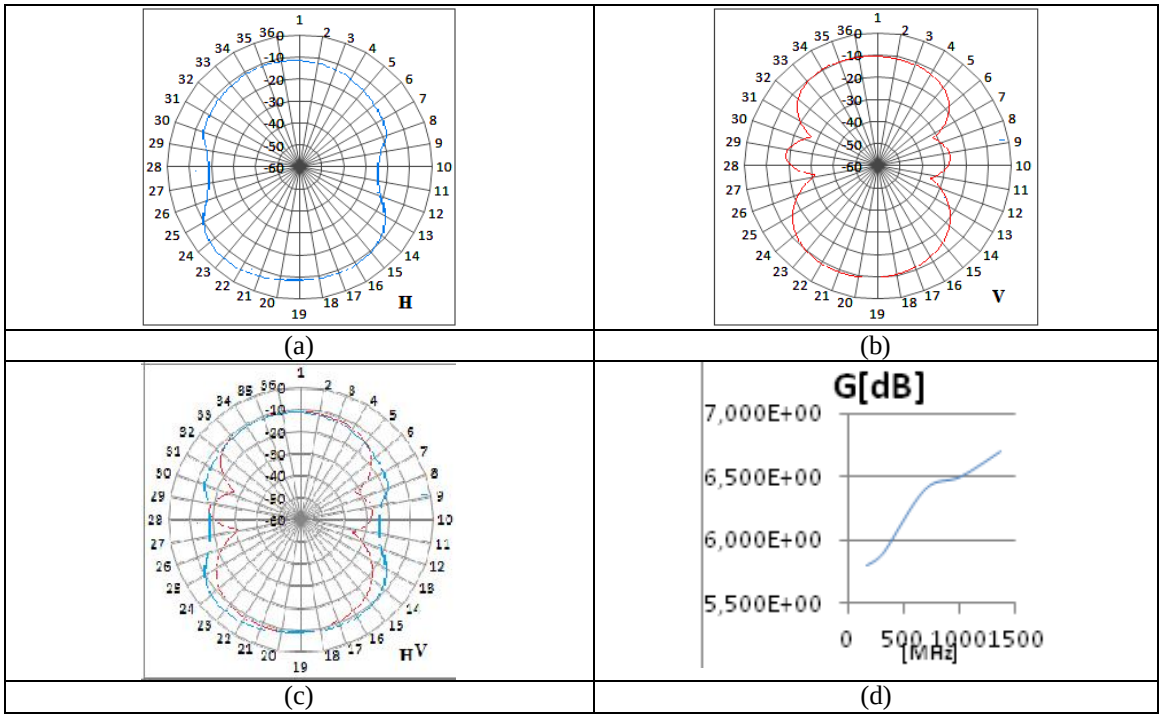

FIG. 7. Fractal stripline antenna with combined elements: (a) Directivity diagram - horizontal polarization; (b) Directivity diagram - vertical polarization; (c) Directivity diagram; (d) Antenna gain.

CONCLUSIONS

Fractal stripline antenna with combined elements at issue belonging to the class of fractal antennas (theoretically independent of frequency antennas) operate in 140MHz - 2.2GHz frequency band with a 6.5dB medium gain.

Note that the standing wave ratio and reflection coefficient decreases with increasing the frequency.

This fractal antenna operates in circular and vertical / horizontal polarization with small differences. Due assessment results, fractal stripline antenna with combined elements can be used in base stations of mobile telephony systems, in RFID systems and wherever it is necessary a microwave broadband communication.

REFERENCES

[1] S. Best, *A Comparison of the Resonant Properties of Small Space-Filling Fractal Antennas*, IEEE Antennas and Wireless Propagation Letters 2 (1), p. 197–200, 2003;
[2] Morariu, G., Alexandru, M., Miron, M., Romanca, M., Machedon-Pisu, M., Dobrescu, A. *Experiment-supported Study on the Bipolar Disk Microstrip Antenna*, DAAAM International Vienna, Austria, Annals of DAAAM & Proceedings, 2009;
[3] R. Kumar and P. Malathi, *On the Design of CPW- Fed Ultra Wideband Triangular Wheel Shape Fractal Antenna*, IJMOT, vol. 5 no. 2, p. 89-93, 2010;
[4] R. Kumar, K. K. Sawant, *On the Design of Circular Fractal Antenna with UShape Slot in CPW-Feed*, Wireless Engineering and Technology, no.1, p. 81-87, 2010;
[5] J. Pourahmadazar, C. Ghobadi, J. Nourinia, *Novel Modified Pythagorean Tree Fractal Monopole Antennas for UWB Applications*, New York, IEEE, 10.1109/LAWP.2011.2154354, 2011;
[6] R. Kumar and Prem Narayan Chaubey, *On the Design of Tree-type Ultra Wideband Fractal Antenna for DS-CDMA System*, Journal of Microwaves, Optoelectronics and Electromagnetic Applications, Vol. 11, no.1, p. 107-121, 2012;
[7] Morariu, G., Miron M., *Fractal Sector Stripline Antenna with Disks*, Review of the Air Force Academy, vol. XII, no. 3(27), 2014.

IOT DIAGNOSTICS FOR CONNECTED CARS

Gheorghe PANGA, Sorin ZAMFIR, Titus BĂLAN, Ovidiu POPA
"Transilvania" University, Braşov, Romania (titus.balan@unitbv.ro)

DOI: 10.19062/2247-3173.2016.18.1.39

Abstract: *Internet of things (IoT) is a relatively new concept identifying various computing devices connected over the internet, differentiated by unique identifiers (IP). Considering the IoT protocols (CoAP, MQTT) as becoming more mature, there is still no generally accepted solution for intelligent management of these devices, though several initiatives are present. Our aim is to demonstrate the versatility of these technologies by implementing a special use-case related to the automotive world, emphasizing the connection between IoT and the connected car. We have chosen the field of automotive diagnostics for our demonstrator considering it represents a crucial path for future intelligent transportation systems.*

Keywords: *IoT, automotive diagnostics, MQTT,Mosquito, Raspberry PI*

1. INTRODUCTION

The idea behind IoT resides in the "thing" term, which includes any natural or artificial object that can be assigned an IP address and provided with the ability to transfer data over a network.[1] As a result we can encounter all sorts of connected devices that are part of this ecosystem.

Even if we talk about an automobile built with fuel sensor capable of alerting the driver when the tank is empty, a pet tracking device or even a heart monitor system implanted inside the body of a patient, the IoT protocols[2] will allow monitoring and controlling remotely [3], over an existing network resulting in improved accuracy, efficiency and security.

In the past decade, because of the new features introduced by the car manufacturers, the vehicles have become increasingly more software driven and at the same time dependent. When it comes to connecting drivers and technology, the auto industry has a longer and richer track record than any other sector by offering a series of improvements aimed not only at safer driving (e.g. ABS, ESP , airbags, cruise control) but also at improving the driving experience overall.

However, diagnostics and maintenance have always been something reserved to the specialized repair shops using custom tools and specific methods, and ultimately these procedures are always related to physical connectivity to the car. It is under this status quo that we take initiativeinto a research project that aims to assure and enhance the car-to-driver and car-to-car communication by studying how IoT can eliminate the need to be in the proximity of a car to perform diagnostics.

By monitoring all the aspects of the car is easier to detect any problem in advance by sending all sensor readings to a certified center where technicians and engineers will apply their expertise to find and predict imminent failures of key systems integrated in the vehicle.

FIG. 1. The Connected Car concept

Besides the diagnostic part, this system would help drivers to keep track of the yearly maintenance, programming service appointments or analyzing the fuel consumption and giving advices for a more eco-friendly driving style.

In a difficult situation like a traffic accident, such a system would be capable to inform the emergency rescue service when the driver is incapacitated, improving the chances for the wounded to live by reducing the overall time of the rescue mission.For the business sector, it can provide an enhanced way to monitor the entire fleet of company cars using open protocols and reducing the costs derived from the already custom solutions on the market.

2. THE IOT PROTOCOL

Our technology choice is MQTT [1] which is alight weight, messaging interchanger protocol based on publish-subscribe model.This pattern is an alternative to the traditional client-server model and requires a message broker (server) which is responsible for distributing messages, over the network to interested clients (devices) based on the topic of a message they are associated with.

The publisher is the client who will send a particular message to a broker and the subscriber is the client who will receive the message from the broker.The publisher and subscriber don’t know about the existence of one another and only way for them to communicate is through the broker, known by both the publisher and subscriber, which filters all incoming messages and distributes them accordingly.

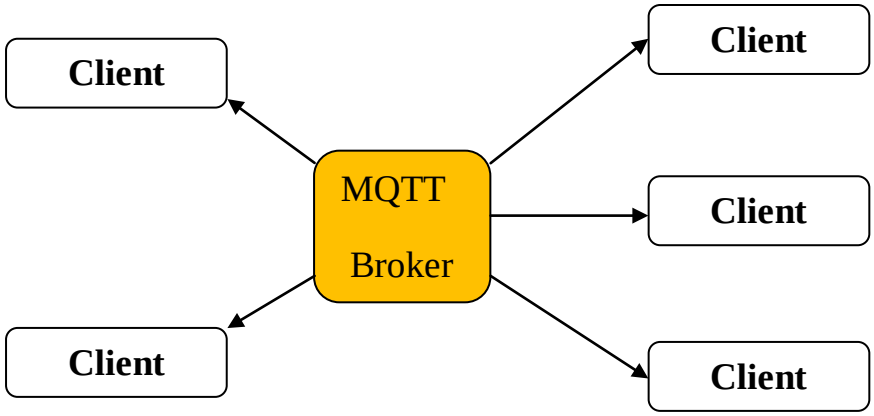

FIG. 2. "Client-Broker" structure of MQTT protocol

One of the most relevant MQTT [2]aspects for this project are decoupling of publisher and subscriber, which can be differentiated in three dimensions:

- *Space decoupling*: It's not necessary that the publisher and subscriber are at same physical location (however a client can be both a publisher and a subscriber at the same time)
- *Time decoupling*: Publisher and subscriber do not need to run at the same time (this is useful for situations when the connection between these two entities is not stable)
- *Synchronization decoupling*: The publishing or receiving operations will not halt any other device operation currently running.

MQTT protocol is designed for interconnecting remote locations where a message is required to have a small footprint or where network bandwidth is very limited. The implemented demonstrator uses Mosquitto[3] as an open source (EPL/EDL licensed) server/broker which implements MQTT protocol.The main advantage and the reason it was chosen for this project was the cross platform capability, Mosquitto offering support for Windows, UNIX kernel based Linux distribution, IOS and Android.

3. THE MONITORING AND CONTROL UNIT

The MCU (monitoring and controlling unit)representsthe car mounted device that connects to the vehicle through OBD-II[4] port and is used for performing the actual diagnostics of the vehicle.

The MCU collects the messages interchanged between ECUs(electronic control unit) and sensor, actuators or any other computers, on the CAN – Bus network, processes them and sends the raw data to a local MQTT client through a serial type communication (RS232/ USB or Bluetooth).By implementing the ISO 9141-2 and SAE J1939 standards of the OBD II protocol, MCU is compatible with a large variety of car manufacturers.

As you can observe in Fig. 3 both standards use a two line communication:

- *K line:* bidirectional line used for initializing the communication between ECU and MCU.
- *L line:* unidirectional line used for data transfer between ECU and MCU.

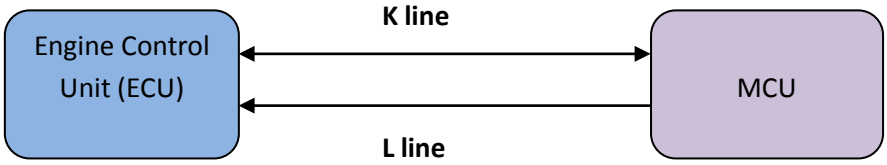

FIG. 3. ISO 9141-2 and SAE J1939communication

Because ISO 9141-2 and SAE J1939 [5] standards are used in theautomotive industry, the reference voltage for the logic levels is 12 V (V_B).

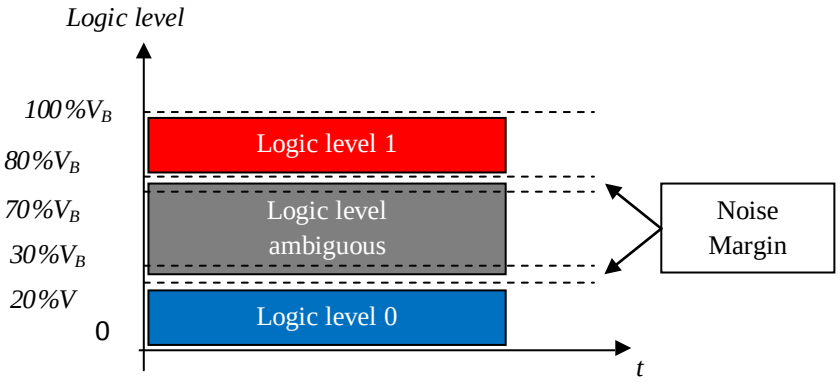

FIG. 4. Logic levels for K line transitions

4. DEMONSTRATOR FOR CONNECTED CAR CONCEPT

4.1 ECU diagnostic stack

The MCU is based on the ELM327[6] chipset capable of interpreting the two CAN based protocols and is triggered by means of an UART interface using AT commands. The following code snippets illustrate how the diagnostic queries are passed to the car:

Table 1. Initialization of the UART interface

```
void uart_init (unsgned int baudrate_init)
 {
       UBRRH=(unsigned char)(baudrate_init>>8);
       UBRRL=(unsigned char) baudrate_init;
       UCSRB|=(1<<TXEN)|(1<<RXEN);
       UCSRC|=(1<<URSEL)|(1<<UCSZ0)|(1<<UCSZ1);

 }
```

After the UART interface has been properly set up the AT commands are sent through the following two methods:

Table 2. Sending and receiving diagnostic through UART

```
void uart_transmit_string(char
*send_string)
 {
while(*send_string)
       {
uart_transmit(*send_string++);

       }
 }
```

```
void uart_recieve_string(unsigned
char *buffer)
{
int s = 0;
while (UCSRA & (1 << RXC))
{
buffer[s] = UDR;
s++;
}
UCSRA |= (1 << RXC);
}
```

4.2 MosquittoMQTT Client

The MQTT client is used mainly as a publisher for the data received from the MCU device. All the sensor related valuesare sent over a mobile network to a broker and from there to a web application where it can be presented in a human readable form.

For the hardware platform a Raspberry PI v3 B is considered to be suitable to sustain the processing power necessary for the system and also because it offers stable development platform.Also,the platform is easily extensible andcould provide real time location through an additional GPS module incorporated in the system for more accurate measurements, real time fleet monitoring for business and companies or for car-to-car signaling of different traffic events like accidents or road blocks.

Another aspect that was considered in the choice of hardware was the limited size and the low power consumption constrains that are usually specific to the automotive sector. The entire client system is car mounted alongside MCU which represents a simple to implement solution for car producers or for any driver who wants to make his car smarter.

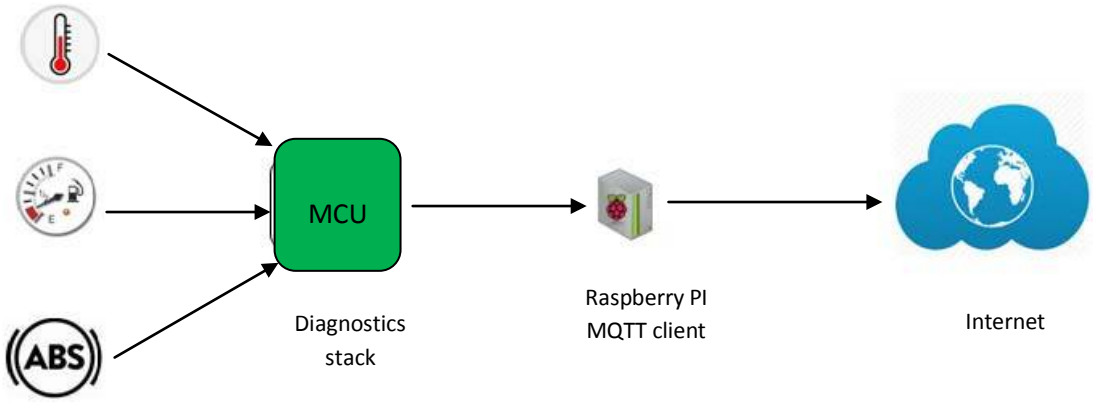

FIG. 5. Connected car client side (car mounted)

Mosquitto MQTT Server

The backend side is represented by theMQTT Server which both the broker and a Web application used for administration purposes. It is used for data interchanging between the publishers (multiple clients)and subscriber and resides in the Internet behaving like a data aggregator.

While a future endeavor would be to create a powerful backend with a rich user interfaces,our focus for the time being revolves on the communication between the car and the internet and more specifically the transmission of diagnostic information by means of an IoT protocol.

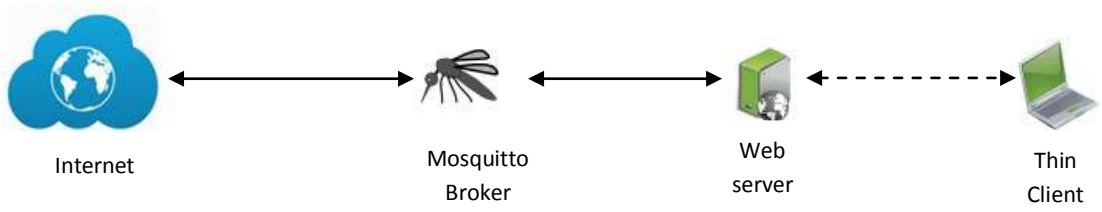

FIG. 6. Connected car server side

5. INTEGRATION AND TESTING SCENARIO

For illustrative purpose we have chosen to present a vehicle use-case signaling an error that was reported by an ECU, but the actual scenario can be carried for several vehicle parameters used in monitoring and diagnostics.

In a real testscenario wehave specifically chosen a vehicle with a known intake manifold problem.This problem is reported by the car ECU as P0103 (Mass or Volume Air Flow Circuit Low Input) error code.

On the CAN-Bus network, data between ECU, sensors and others control modules ispassed using a hexadecimal format. This means that our vehicle under test the intake manifold error message is transmitted to the ECU as: `44000066` which can be translated in a more human readable form as follows:

- first 2 octets represent the mode of operation (in our case mode 03-Diagnostic stored trouble code [7])
- the next 2 octets indicate the power train assembly
- the last 4 octets are the error code, so in our case, this error code has the value 0103

The MCU is connected to CAN-Bus network through OBD-II port placed, usually, under the steering wheel and will interpret the ISO 9141-2 and SAE J1939 specificframe and extract the data of interest.The value P0103extracted from the error message is then sent to Raspberry PI which hosts the Mosquitto client, through RS232 serial communication.

FIG. 7. Client assembly

```
pi@raspberrypi:~ $ mosquitto_pub -t "car/events" -m "P0103" -q 1 -r
pi@raspberrypi:~ $
```

FIG. 8. Mosquitto client publishing the error code message intercepted from CAN-Bus Network

The client will publish (see Fig. 9), using MQTT protocol, the value on /car/events topic on which it is associated and then the broker will assure that the message is delivered to a web application which serves as a remote interface between machine and human factor.

FIG. 9. Mosquitto broker receiving P0103 error code form Moquitto client over the IP network.

Then the web application searches through a local data base in which we store the mapping between the error codes and the human readable format and sends back a full description of the failure message as follows.

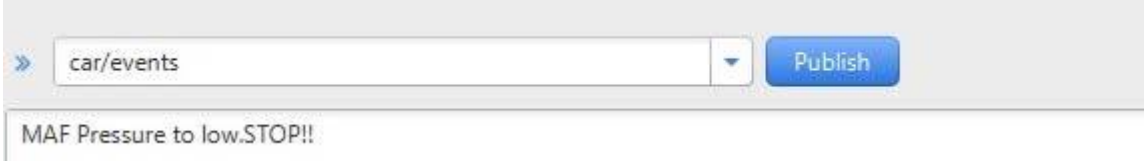

FIG. 10. Mosquitto broker publishing the error description to the topic /car/events.

```
pi@raspberrypi:~ $ mosquitto_sub -t car/events -h 192.168.1.137
MAF Pressure to low.STOP!!
```

FIG. 11. Error alarming via Mosquitto client in subscribe mode

Subsequently, a different client can be used for notification purposes thus informing the person of interest of the available events (in our case the car error code). This notification mechanism could be employed using a smart phone or even a smart watch.

Throughout testing phase we encounter a limitation of our solution: because of fact that the ECU firmware is proprietary we are not able to modify or take actions on the car itself (e.g. resetting the error code, running an extended diagnostic session etc.). Nevertheless the reporting itself is useful for long term analysis and more accurate diagnostics when it comes to sporadic errors, since a mechanic can also take into considerations factors that are not easily reproducible in the repair shop (e.g. temperature, humidity, elevation).

CONCLUSIONS

We were able to illustrate a scenario for IoT Connected Car using MQTT andthe Mosquitto broker where a technical problem, unnoticed by most of the drivers, can represent a serious risk of mechanical failure or even human live threatening situation.Our IoT integrated solution will provide the necessary technical background in order to avoid similar scenarios and even offer a way for remote monitoring the vehicle or traffic events.

Further, our solution can be enhanced; taking benefit of the OMA defined management protocols, by implementing a remote management solution of the MCU allowing functional updates and backend triggered actions.

Due to the factthat the ECU firmware is proprietary we were not able to modify or take actions on the car itself. In order to completely implement the Connected Car concept, including also a reaction loop for remote or self-healing procedures, the implemented solution should be synchronized with the car manufacturer, by creating a trust zone between Engine Control Unit and IoT management devices.

REFERENCES

[1] Giusto D., Iera A., Morabito G., Atzori L. (Eds.): *The Internet of Things*, Springer, 2010
[2] Gubbi J. et al.: Internet of Things (IoT) - *A vision, architectural elements, and future directions, in Future Generation Computer Systems*, 29, pp 1645-1660, (2013)
[3] L. Atzori et al.: The Internet of Things - *A survey, in Computer and Telecommunications Networking 54*, (2010)
[4] Message Queuing Telemetry Transport - v3.1.1. OASIS MQTT TC, http://docs.oasisopen.org/mqtt (2014)
[5] Message Queuing Telemetry Transport Org, http://mqtt.org (2016)
[6] Mosquitto. *Open source MQTT broker*, http://mosquitto.org/
[7] Huan Pan, ISO 9141-2 and J1939 Protocols on OBDII, University of Changaua, 2009.
[8]The OBD home page, http://www.obdii.com/background.html
[9] ELM327 datasheet, http://elmelectronics.com/DSheets/ELM327DS.pdf
[10] Engine codes, http://www.engine –codes.com

CONSIDERATIONS REGARDING THE IMPROVEMENT OF THE MILITARY DRIVER'S SEAT COMFORT FOR THE MILITARY SPECIAL INTERVENTION VEHICLES

Cornel ARAMĂ[*], Marian MITROI[**], Lavinia ARAMĂ[***], Mariana ARAMĂ[*]

[*]"Henri Coandă" Air Force Academy, Braşov, Romania (aramis5791@gmail.com)
[**]Faculty of Mechanical Engineering,"Transilvania" University of Braşov, Romania (ejju_marian@yahoo.com)
[***] freelancer (lavinia_ana@yahoo.com)

DOI: 10.19062/2247-3173.2016.18.1.40

Abstract: *Subjectively speaking, the comfort of vehicles is closely related to a number of factors which together generate a state of comfort and satisfaction of those who are inside it and have the effect of moving safely with a sufficiently high speed, without causing physical and mental fatigue or damage the goods which are being carried. Since seat comfort is a feature of the ergonomics, it has been addressed in various ways by engineering firms, but also by various researchers in the field of ergonomics, who have demonstrated that this feature needs to be thoroughly approached by taking into account the anatomical shapes of the drivers and their needs in relation to the vehicle and the activities performed.*

Keywords: *comfort, vehicle comfort, intervention vehicles, driver seat's ergonomics*

1. THE COMFORT

The comfort feeling could be appreciated as an assembly of mental and physical reactions due to all the factors involved in this state which act on it in different ways.

It could not be said that there is only one widely accepted single criterion which can offer an objective appreciation to evaluate vehicle comfort.

The vehicles comfort is closely connected with the postural stress of the driver and the passengers because of their subjective perceptions on the environmental factors and any mental and physical exposures during missions.

Driving a military vehicle during specific mission is a complex action characterised by the quick succession of the external factors and the reaction rate of the drivers.

The postural comfort is evaluated by taking into account aspects such:

- the distance to the pedals and the necessary forces to act on them;
- the distance to the levers and handles and the necessary force to act on them;
- the type and possibilities to adjust the chair;
- the construction system and the comfort provided by the chair;
- the mode of operation for the rest of the board controls;
- the ventilation and air conditioning system.

The comfort sensation is closely connected to the interior space of the vehicle. The driver working space is calculated by taking into account the anthropometric characteristics and the requirements for a normal evolution of the person in order to accomplish the specific functional assignments [5].

2. THE DRIVER SEAT – GENERAL CONSIDERATIONS

The driver seat is a device which has to ensure a driver's comfortable position during the handling of the vehicle devices and board gadgets. It has to decrease the level of the body vehicles vibrations felt by the driver.

The international standards, such as SAE J941 and J4002, recommend some optimal dimensions for the seats in order to ensure the drivers' and passengers' comfort (Fig. 1), and, from the military point of view, MILSTD-1472 is "The Guide for the Military Vehicles Seat Design".

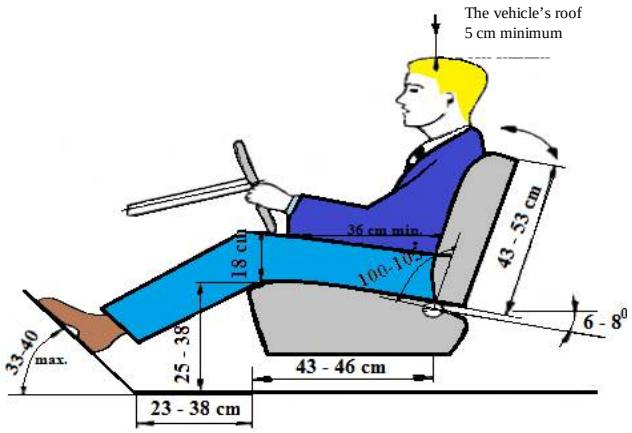

FIG. 1. The main dimensions recommended for the seat driver [5]

FIG. 2. Live images during a demonstrative exercise (the driver is 1,74 m tall)

Another standards which require comfort-specific requests are:

- ISO 3411 – The human physical dimensions and the minimum interior space;
- ISO 6682 – The comfort areas and the minimum necessary spaces for the vehicle handling commands;
- BS ISO 4513:2010 – Road vehicles. Visibility. Methods to determine the driver's visibility area.

The pad and the backrest design do not break to a sufficient extent the vibrations taken over by the chair because of the very large spectre of magnitudes and frequencies.

According to [4], the chair pad provides an decrease in the very frequency of vertical vibrations up to 2,5 Kz towards the vibrations sent by the general structure of the vehicle body. Also, improved vibration isolation could be realised by an elastic supporting structure of the chair.

The chair building implies analysing a large area of characteristics which have to be taken into account during their projecting and building processes. Special details are necessary to be obtained pertaining to biomechanics of the comfort, the pressure distribution on the level of the chair pad, the vibration transmission, the material which has to be used in the fabrication process etc.

3. THE ERGONOMIC SPECIAL FEATURES OF THE DRIVER'S SEAT FOR THE SPECIAL MILITARY INTERVENTION VEHICLE DAC 2.65 FAEG

The driver's seats have, in general, the same shape, but the internal structure and the supplementary systems for comfort differ from one vehicle to another. What is installed on the cars is not common for light trucks or for heavy vehicles, especially for military

vehicles. So, it could be said that the driver's seat ergonomics is realized completely differently and the driver's sensations differ as well.

FIG. 3. The 1-st position for a driver of 1,84 m

FIG. 4. The 2-nd position for a driver of 1,84 m

In the case of the light off-road articulated vehicle, DAC 2.65 FAEG, from the comfort point of view, one can notice the lack of suspension system, thus leading to transporting the crew over a long period of time without fatigue occurrence.

In order to compensate for this aspect, the vehicle driver's seat is located on the body of the vehicle by the means of a mechanic damper which has to damp the random vibrations resulted from the specific off-road tyre rolling conditions (Fig. 4).

Also, another black spot of this vehicle's driver's seat ergonomics is that the driver needs to stay in an uncomfortable position, mainly if the person is over 1,84 m tall (the regular height for a Special Forces soldier). The possible driving positions for a driver of 1,84 m in height can be seen in Fig. 3 and Fig. 4. The person has no special equipment for intervention mission. If they wore a special helmet and bulletproof vest, it would be more difficult to adopt an appropriate position.

In case the driver is 1,74 m tall (Fig. 2), the position behind the steering wheel is easier to be adopted but one has to sit leaning forward in order to have enough power to handle the steering wheel and to have good visibility at the same time.

In order to establish if the requirements for the basic rules of ergonomics are respected (Fig. 1), some measurements have been made for both types of drivers, as it can be seen in Fig. 2. Two models have been used: one driver is 1,84 m tall, and the other one, 1,74 m tall. The results are presented in table 1.

4. CONCLUSIONS

The driver's seat has to be studied very carefully in order to bring it up to the ergonomics dimensions and to delay as much as possible the appearance of the driver's fatigue.

As it could be seen under the former point, in case of DAC 2.65 FAEG vehicle, the ergonomics of the driving seat is far from the standard parameters.

Also, first a study must to be done for each type of vehicle in order to establish the standards for the ergonomics dimensions of the driver's seat. They will depend on the missions which are going to be carried out, the anthropometric dimensions of the soldiers and their special equipment.

Table 1 The results of measurements

Dimensional parameters	Value [cm]			Reviews
	According to SAE J941, J4002	Special Forces driver (1,84 m tall)	Regular height (1,74 m tall)	
a	5	10	15	The driver must lean forward in order to have enough visibility through the windshield
b	43-53	69	64	The chair backrest is extremely small and uncomfortable
c	43-46	34	34	The small chair favours the mobility – the civilian standard must be changed when used for the military vehicles
d	>36	43	43	Inadequate space for a massif soldier equipped with bulletproof vest – the standard must be changed when used for the military vehicles
e	25-38	20	20	The squatting position (of the driver) favours the mobility and… the fatigue
f	18	12	12	Very narrow space for a massif soldier
g	-	35	35	Specific dimensions for this kind of vehicle body
h	-	41	41	
i	23-38	45	45	The pedals are difficult to act on by a driver of regular height
j	-	89	85	The helmet presence influences negatively the mission
k	-	54	54	Specific dimension
l	-	15	12	The bulletproof vest decreases the distance to the steering wheel

Second, the ergonomics specialists will have to collaborate with body designers in order to establish the optimal dimensions of the driver's seat.

Eventually, the effect of the vibrations on the vehicle crew must not be neglected. In this situation, when such vehicles, which lack a suspension system and are compact, rigid and fast, are used for isolated targets intervention, the danger of vibrations can be relieved by using a magnetoreologic damper as a damper between the chair and the vehicle body, as well as a chair made of special materials, for example, ballistic jelly [7].

Applying these technical solutions improves the soldiers' protection, safety and comfort level by increasing the comfort of patrolling and fast intervention vehicles. This is the immediate effect. The most important effect is the increase in combat system viability.

REFERENCES

[1] Aramă, Cornel, Aramă, A., *A Study Regarding the Analysis of the Fulfillment of the Operational Military Requirements by the Light Off-Road Articulated Vehicle, Review of the Air Force Academy*, The Scientific Informative Review, No 1(23)/2013, "Henri Coandă" Air Force Academy Printed House, B+, May 2013;

[2] Aramă, Cornel, *Investigation of Possibilities to Improve the Performances of Special Vehicles, Transylvania* University Braşov, Doctoral Degree thesis, 2006;

[3] Aramă, Cornel, Sava M., Cucu L., *Analysis of the Light Off-Road Vehicle Endowment Possibilities in Order to Use It for Air Force Missions,* The 17th International Conference of Scientific Papers *Scientific Research and Education in the Air Force* AFASES 2015, *Henri Coandă* Air Force Academy, Braşov, Section: *Engineering Sciences-Mechanical Engineering Materials and Technology,* May 2015;

[4] C.W.Stammers, T.Sireteanu – *Semi-active Seat Control For Vehicle Driver Protec ţion*, SISCM, 2001;

[5] Mitroi.M., - Referat nr.3 pentru teza de doctorat *Echipamente şi proceduri destinate evaluării confortului autovehiculelor*, Braşov, 2016;

[6] Mitroi.M., - *Military Seat With Balistic Protection*, National Conference C&I, Brasov, 2015;
[7] N.C.Nicholas, J.R.Welsch, *Balistic Gelatin*, Institute for Non Lethal Defence Technologie, U.S.A., february 2004;
[8] Sava, Mariana, *Analiza viabilităţii radarelor moderne mobile*, Bachelor's Degree thesis, *Henri Coandă* Air Force Academy, Braşov, July 2014.

MECHANICAL ENGINEERING. MATERIALS AND TECHNOLOGY

THE INCREASING ROLE OF USING AIR TRAINING EQUIPMENT IN THE PROCESS OF EDUCATION AND COORDINATION OF THE CREW DUTIES

Sławomir AUGUSTYN, Wioletta ZAWODNIK

National Defence University, Warsaw, Poland, Aviation & Air Defence Institute,
(s.augustyn@aon.edu.pl, wzawodnik@yahoo.com)

DOI: 10.19062/2247-3173.2016.18.1.41

Abstract: *The article shows a new approach to the vision of air training equipment in the process of training for flight and cabin crew. This approach allows for analysis and assessment of particular phases of theoretical and practical training. Moreover, this aspect influences on safety of aircraft and security of passengers.*

Because of a broad context, the subject of the research has been limited to the most significant technical aspects of air training in the crew training process.

Key words*: air training, flight simulator, crew work coordination.*

1. INTRODUCTION

Nowadays we travel more and more. At the same time we are awaiting the highest standards of services. From the very beginning of coming to the airport and finishing in reaching our destination airport. There are various mechanisms, procedures and professionals who take care of particular parts of our trip. They perform their duties, support in necessary situations.It is: pilots, cabin crew, ground staff that is responsible for our safety and comfort. Airlines and aviation companies prepare their employees to work using available technical equipment.

2.THE NEWAPPROACH TOGROUND HANDLING AND CREW WORK COORDINATION

The responsibilities of ground handling staff are very broad. Generally speaking, it is to ensure the safety and comfort of airline passengers and crew members. We can enlist at least checking baggage, cleaning the aircraft, stocking it with refreshments or refueling. People being in charge of defined scope of action at the airport must make sure the ramps, runways or the area nearby is deprived of any debris that could cause damage to the aircraft taking off or landing.

Each group of handling staff is in charge of different area of safety process. It is important to mention that all the actions taken by particular staff is a part of a huge chain process. The various actions include inspecting, storing and transporting luggage, stocking the aircraft with food and drinks that are distributed during flight, cleaning, refueling or preparing passengers to be boarded and begin a comfortable journey.

Good working order of the ground staff is inevitable although for an average passenger it is not so obvious and moreover, it does not have to be. The aim to gain for the passenger is to get to the plane in the shortest period of time. For some people saying

‘time is money’ is extremely true. Therefore, they appreciate their time, spending every free minute working while waiting at the airport [3].

Not all the staff has contact with passengers. Sometimes there is no need to work directly with customers. For example, maintenance staff. They take care of the proper and safe preparing the aircraft to the flight. They follow their own internal organizational procedures which allow us to fly well-maintained planes.On the other hand, we have to mention check-in staff or cabin crew who are on the first line, they are responsible for the image of the company. The image is created by companies’ managers, however the behavior and help of the staff in most cases is invaluable.

The fundamental knowledge of the staff is not enough in fast-developing companies, especially at the biggest airports. Coordination of the smaller actions of workers and first-line employees has to be forced by continuous trainings or workshops. Let us think about the shortage of time and the aircraft full of passengers, the charter flight with the necessity to clean the aircraft. Typical and well know situation. Coordination of the preparing the aircraft to the next flight in time shorter than 20minutes? One could say ‘impossible’. Modern airlines try to have the shortest in-between flights operations. How to do that? The answer is very simple: ‘to have well qualified and well organized staff’.

The cabin crew and the flight crew are the groups of employees who can coordinate almost all the actions nearby the aircraft. Boarding and de-boarding almost at the same time? Of course, it is possible if the cleaning is planned before for certain destinations and the cleaning staff are ready at once without waiting for them. When the so-far passengers leave the aircraft using the rear door, the new passengers can be prepared to be welcomed at the front. Refueling or pre-departure check can be done during the presence of the passengers onboard, however certain circumstances must be filled in. Most companies allow to take passengers with the aircraft being just refueled. There are special procedures defined in so called Standard Operating Procedures (SOP).It provides a flight crew with a step by step guide to effectively and safely carry out operations. SOP's can also be developed and modified when necessary to incorporate improvements based on experience, accidents or innovations from other manufacturers or operators to meet the needs of a particular company.

All in all, we need continuous improvement within air transportation in customer care area. Treating the customer and their needs as a priority is obvious. When we start thinking as of the chain of service which is developing all the time and employees who can foresee some situations or even prevent certain unnecessary stoppage, the companies will always be on time and have only satisfied passengers.

3. AN ENORMOUS ROLE OF THE AIR TRAINING EQUIPMENT IN FLIGHT TRAINING

Working as cabin crew for a major airline is an exciting and challenging experience. In addition to jetting off to exotic destinations, the job also requires a high degree of responsibility and specialization to ensure the safety and comfort of passengers in line with industry regulations.

This job is ideal for young professionals, introducing the skills and responsibilities expected by the world’s leading airlines. Special emphasis is given to customer service and procedures for handling unusual situations during flight.

However, great preparation to the profession means hard work and a lot of trainings. In most cases, the trainings are provided by the airlines who are recruiting the cabin crew. The whole process is quite long and demanding. However, the practical training is the most important and at the same time final phase just before commencing the job.Talking

about the training process of the cabin crew it is similar to flight crew process, however the specification is different.

The practical training include:

- Introduction to Aircraft and Aviation Familiarization
- Crew Member Coordination and Communication
- Customer Service and managing passenger interactions, including e.g. oxygen administration to passengers if necessary
- Safety and emergency procedures, including water survival training, aircraft evacuation, etc.

Using the original aircraft parts we produce a range of very effective, classroom install cabin kits, which can vary in size according to available space and class sizes in your training room.

However, a typical cabin kit would be one side of a narrow body cabin (Boeing 737 or Airbus A320) and four rows of Passenger triple seats, with kits comprising sidewalls, lighting panels, overhead luggage bins and Passenger Service Units (PSU) complete with passenger masks.

Simulators used for training for cabin crew is generally defined as flight simulators with one changing factor only, that is full flight simulator – moving the body cabin being the image of a real aircraft, changing the position of the board while emergency situation. It is electrically driven motion platform shown below:

FIG.3.1 Electrically driven platform of a flight simulator
Source: www.boschrexroth.com

Another type of flight device training for cabin crew is narrow body cabin fixed on not moving frame. However, the height is very important, for Boeing 737 it is approximately 11 meters. Having a real fuselage of the aircraft, the training is very effective. It is possible to exercise using the emergency slide, passenger evacuation or opening the emergency exits [1].

FIG.3.2 CSA flight simulator Source:author's own material

4. THE AIR TRAINING EQUIPMENT IN FLIGHT CREW TRAINING

Air training equipment in flight training is extremely important. New technologies present in modern aircraft place increasing requirements on air personnel, especially on the pilot operatorating an aircraft. Flying itselfis a difficult and a complex task which requires from pilotsvast generalknowledge and technicalexpertise as well asa wide range ofskillsappropriateto the aircraft type andthetasksperformed. Particular attention is currently paidto the development ofairtraining equipment, which is usedin the process ofbasic trainingand professional development of pilots.

Air training equipment is a practical and well tested tool used in assisting theoretical and practical training of pilots:

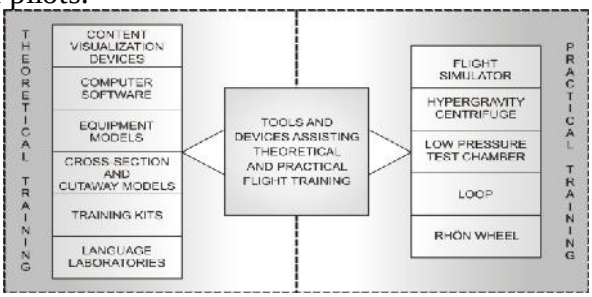

FIG.4.1 Air training equipment Source: Author's own work

Now we will try torefer toair training equipment assistingpracticalflight training, with particular emphasis on aflightsimulator. Specializedtrainingwith the use of airtrainingequipmentis an essentialmethod for exerting the overallimpacton the pilot's abilities. This method brings about a comprehensive psychophysical development of desirable characteristics in the pilot. Diversity ofdemands onpilots of varioustypes of aircraftmeans thatnot all air training equipment can be used in pilot training in the same manner.

Flight simulator is a device or a computer program which simulates the aircraft operation in real flight conditions. Flight simulator types include simple computer gamesto more advancedflightsimulatorsthat arefull-sized functional duplicates ofthe cockpitwith theon-boardsystemsandinstrumentationmounted on ahydraulicplatformor on a hyper gravity centrifugeproducing G-load values reflecting those which are encounteredin variousphases of flight.

The simplest modern flight simulator usually consists of: one or more PC monitorsprovidingvisualization of internaland external (including airport infrastructure, terrain, weather conditions, etc.) environment as well as mission execution environment; aircraftcontroldevices(control stickoryoke, joystick, pedals). The aim of realistic mirror-like conditions is to enterflightcontroldata (pitch, roll, direction); computer systems forinternal and external communications, simulation of soundsthat occurin the aircraft, computer systemsused forprocessing of the input signalsselectedby the pilotin IFR(flight control and navigation instruments, enginecontroldevices, radio navigation systems, etc.). Given thecomplexity of thedesign and the applieddegree of imitation fidelity of the cockpit, equipment and aircraft systems, as well as the simulation ofloadsthat occur during flightmaneuvers Flight Simulation Training Devices (FSTD) may be divided into four major groups[1]:

1.The advanced simulator is Full Flight Simulator (FFS) (Fig.4.2) - the most technologically advanced type of flight simulator. A complete, full-sized and

[1] Part-ORA – Subpart FSTD, CS-FSTD(A)/(H)

functionalreplica of thecockpit ofa given aircraft type, model andseries, combined with the appropriatecomputer systemnecessaryto simulate theaircraft operation on the groundand in the air. The visualization systemprovides aviewoutside thecockpit, and the system ofactuators simulates physicalsensationsassociatedwith motion.Devices of this typeare used, i.a., to traincrewin a dangerousflight conditions, and to develop and reinforce flying habits/currency.

FIG.4.2 Full Flight simulator Source: www.airbus.com

2. Flight Training Device (FTD) (Fig.4.3) is a complete, full-sized and functionalreplica of thecockpit, instruments and control panels ofa given aircraft type, combined with the appropriatecomputer systemnecessaryto simulate theaircraft operation on the groundand in the air. Such devicesdo not necessarily have to beequipped with visualization and motion simulation systems.

FIG.4.3 Flight Training Device (FTD)Source: www.aopa.com

3. Flight and Navigation Procedures Trainer (FNPT) (Fig.4.4) – Cockpitmodelcombined with the appropriatecomputer systemnecessaryto representthe typeor group oftypes of aircraftduringflightoperations. Devices of this type are used, among other things, to train procedural flights and navigation.

FIG.4.4 Flight and Navigation Procedures Trainer (FNPTII)
Source: www.ai.com.pl

4. Basic Instrument Training Device (BITD) is a device which simulates air craft instruments(they can be displayed on the screen) to allow training at least according to the procedural aspects of the IFR flights.

Simulators admitted to be used in the training of licensedflight personnelmust meetthe requirements of Part-ORA (Subpart FSTD).Compliance with theserequirements bythe

deviceis confirmedbythe relevantcertificate issued by an authorizedstateinstitution. In Poland such a certificate is issued by the President of the Civil Aviation Authority.

Regardless of the type of aviationand the stage of flight training/professional development, flightsimulatorsare a widelyusedpilottraining tool. The result ofexperts‘ opinions, flightsimulationstudies, and the author’s own opinionpermit to conclude thatthe essentialbenefits ofthe flight simulator, including those relevant to thepilot'ssituational awarenesscaninclude the following points:

1.*High training effectiveness*. The testsrelated tomeasuring the effectiveness of flight simulation training demonstrated that the traineesdevelopknowledgeand skillsat a level similarto that achievedin a real flight.

2. *Maintaining high standards of training safety.*Due to thenecessity of maintaininga certain level ofsafetyduring training, simulatorssometimes provide the onlyway to learnsome maneuvers, the elementsof air operations performedin the eventof dangerousweather conditions (wind shear, turbulence, icing, jet streams, etc.).

3. *Availability*.The factthat the use of the flightsimulator in flight trainingis not dependenton the current ambient weather conditions, the state of the airport, or the good working condition ofground navigation equipment allows for a moremethodicalapproach to the trainingfrom the human factor perspective.

4. *Repeatability*.The simulator does not require the implementation of the full cycle of a given air operation (pre-flight check, take-off, to discussandrepeata specificpart of the exerciseby the trainee.

5. *Predictability***.** Simulator trainingpreventsthe occurrenceof such dangerousphenomena asair trafficcollision, wind shear, icing, weather deterioration,turbulence, closure of airports, etc.

6.*Learning by mistakes”*– with unlimited possibilities of apply in ga number of ways to solve an in-flight operational problem with"zero" risk level, thesimulatorallows the studentto selectthe solution which is the mostoptimal from his perspective and to test it.

7.*Maintaining pilot currency and proper attention allocation* - systematictraining exerciseson the flight simulatorallows the trainee toconsolidatethe desiredhabits.

8.*Credibility as a tool applied in air accident investigation*.Flightsimulatorsensure accuratereconstructionofflight conditions, the situation onboard, and theevaluation ofthe actions takenby the crew ofthe aircraftin the event ofan undesirable flight-related event.

9.*Simulator scan be used for training for the prototype aircraft under design, or aircraft employing new solutions(systems).*Performingthis task in practice, without the prior simulationand practiceof selected flight maneuverscouldbe associated witha highlevel of riskand, in extremesituations,with high probability of undesirable flight-related event.

10.*High comfort of performing the training tasks by the instructor.*An undoubted advantage ofthe flight simulatorin comparison with theaircraftis the fact that theinstructorcanfocus his attention fully on the traineeand the task performed.

11.*Optimizing the use of financial resources*.The use of the simulatorcan significantly reducethe training costs as compared to thoseincurredforthe use ofthe aircraft [4].

Despite the advantages mentioned above, no simulator can currently be defined as a device that can replace the hands-on trainingin the air. It is stillconsideredas a veryimportant form ofpreparingorsupplementingpractical trainingin the air.

4. CONCLUSION& ACKNOWLEDGMENT

The coordination of the ground handling is inevitable. To get the success there should be well-organized staff being aware of different situation that can happen and to know

how to solve problems before they appear. The well-trained and qualified crew is the fundamental strength of every company. The profession of a pilot, flight attendant or any other person engaged in passenger care ought to be customer oriented approach. Customer care includes among others providing safety during the flight itself and convenience before and afterwards.

The technical systems are one of the mechanisms which are to help us and to make the work easier and more comfortable for the passengers. There is a continuous need to make the air trainings more effective and more and more realistic. They shall reflect as many aspects of real pilot's work as it is possible.

In conclusion, taking into account all aspects mentioned, we can be convinced the better air training is offered the better staff is graduated from aviation training organizations (ATOs). And at the same time we can have highly qualified licensed personnel to fly all over the world.

REFERENCES

[1] Augustyn S., *Human factors in aviation safety investigations.* Kosice: Acta Avionica 2011
[2] Harris K.A., Harris D., *Computer-based simulation as an adjunct to ab initio flight training,* International Journal of Aviation Psychology N° 8/1998, pp. 261–276
[3] Orlansky J., String J., *Cost-effectiveness of flight simulator for military training*(Rep. No. IDA NO. HQ 77-19470), Arlington, VA
[4] Macharella, P.K. Arban, S. M. Doherty, *Transfer of training from flight training devices to flight for ab initio pilots,* International Journal of Applied Aviation Studies N° 5/2005, pp. 25-39
[5] Part-ORA, Subpart FSTD, CS-FSTD(A)/(H), EASA 2012.
[6] Szczepañski C., *Symulatory lotnicze, stan i perspektywy – report,* Warszawa 1998, p. 4
[7] http://www.ai.com.pl/civil/aviation-simulators/?lang=pl
[8] http://www.airbus.com/newsevents/news-events-single/detail/the-first-a350-xwb-full-flight-simulator-is-readied-for-airline-flight-crews/
[9] http://www.boschrexroth.com/en/xc/industries/machinery-applications-and-engineering/motion-simulation-technology/application-areas/cabin-crew-trainers/index
[10]http://flighttraining.aopa.news

MECHANICAL ENGINEERING. MATERIALS AND TECHNOLOGY

THE EXPERIMENTAL ANALYSIS OF THE MEANDERING PHENOMENON GENERATED AT A RAILWAY WAGON

Bogdan CIORUȚA*, Tudor SIRETEANU**

*Faculty of Science, North Univ. Centre at Baia Mare - Tehnical Univ. of Cluj-Napoca, Romania (bciorutza@yahoo.com)
**Institute of Solid Mechanics of the Romanian Academy, Bucharest, Romania (siretimsar@yahoo.com)

DOI: 10.19062/2247-3173.2016.18.1.42

Abstract: *During running, the railway vehicles are subjected to external excitation generating vibrations. These vibrations have a negative impact on the quality of travel, can endanger road safety. Vertical and transverse unevenness of the track and its discontinuities are the main source of vibration from railway vehicles. Another source of vibration is the rolling stock defects such as eccentricity and flatness tread. At the above are added increased speed of movement and increased payload, elements which have imposed the need to describe in a more rigorous way the complex phenomena that occur at the interaction vehicle-runway, vehicle response to irregularities path, implications in improving vehicle stability and comfort.*

Mathematical modeling by random processes of the excitation induced by the path irregularities and dynamic response generated by the vehicle in motion, allows a more accurate description of the interdependence between vehicle vibration and statistical, also spectral properties of path irregularities. This method was used in the dynamics of railway vehicles in the last period, being facilitated by the expansion theory of random vibration and the continuous improvement of equipment, methods of measurement and analysis vibrating mesh that occur in the process of rolling. In the present study we analyzed the phenomenon experimentally. The experimental analysis is based on measuring and machining vibrations measured on a railway wagon by a research team from the Institute of Solid Mechanics.

Keywords: *vibration, railway vehicle, meandering movement, numerical processing*

1. INTRODUCTION

Currently still a significant part of goods and passengers traffic from Europe is carried by rail. The rail system already provides solutions for the transport all over the world, in terms of safety, environment, total journey time, low emissions and low energy. It has the potential to offer attractive urban, regional and long distance mobility [8].

Innovation resulting from technology added value is steadily contributing to strengthen all market segments and their seamless connections, as well as contributes to environmental efficiency, security and safety, and intelligent mobility. The impact of today's rail technology in high-speed is outpacing the increase in aviation for journeys; high-speed trains are therefore the preferred passenger choice for journeys of this distance [8,9]. Intensive development of modern technology and increase goods traffic and speed of travel, the increased noise and vibration level and specific rail transport while traveling. Noise generated during train movements acting adversely on passengers, service personnel and the population in areas crossed by rail.

In addition, intense noise makes it hard to distinguish the sound signals and verbal commands and thereby worsening security conditions rail transport. Railway equipment presents a number of specific issues in terms of shock and vibration, as few vehicles that run on a runway apparently so smooth [9].

Shocks and vibrations from vehicles by rail can occur due to variable speed drive, the game at the ends of the rails, bumps, curves and elasticity ways, taper, eccentricity and deviations from appropriate form of bandages guidance rock rolling on the rail by wheel flange, jerk during braking maneuver and wantonness. The suspension system rolling stock is intended to cushion the shock and vibration, reducing them to acceptable levels [1-3]. Sources of noise and vibration from railway vehicles can be external or internal. The most important sources of noise and vibration are running outside wheel itself, suspension systems and coupling elements, the action of air on the outer walls wagon braking action etc [7]. Rolling noise is produced by all elements in direct contact when running the rails and metal wheels with their bandages [3].

If the suspension chassis is not effective enough, it is possible that the entire steel structure of the wagon to come into vibration. Stoppages and changes speed, the various couplings can become new sources of noise and vibration. Air action against the walls of the wagon produces aerodynamic noise, particularly those giving birth at the front walls and protruding parts of the wagon. Sources of noise and vibrations occur particularly inside the railcars. These sources are the main internal combustion engines, power generators, air compressor and transmission systems (FIG. 1).

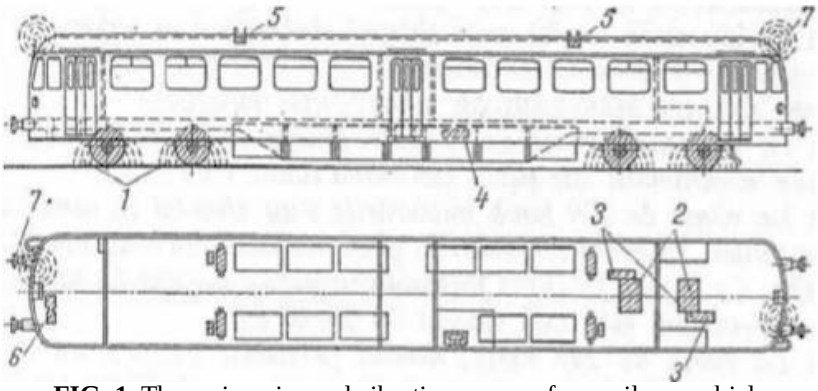

FIG. 1. The main noise and vibration sources for a railway vehicle
1 - rolling and suspension systems; 2 - driving motors; 3 - reducers; 4 - transformator; 5 - exhaust; 6 - air compressor; 7 - horn.
(source: documents.tips/zgomotul-si-vibratiile-la-mijloacele-de-transport-rutier.html)

Noise transmission outside to the inside of the wagon is done in three ways: by air - ventilation channels or other holes and leaks (air noise); the wagon structure as vibration (sound structure of the wagon) and acoustic waves by the action on the dividers exterior of the wagon. Railway wagons required as the noise level in compartments to be as small and yet not be an adjacent track, to avoid disturbing residents concerned. The first problem could be solved largely in the last 15 years, based on systematic research, the constructive nature in various parts of wagons as floors, walls and windows. As normative for new wagons at average speeds of 80 km/h are taken into consideration following noise levels: fast trains 55 dB(A), fast trains 60 dB(A), and 75 dB(A) in tunnels. To double the speed of movement, the noise level increases inside the wagons around 6 dB(A), so the cars fast trains that develops a speed of 200 km/h consider a noise level of 62 dB(A) [10]. On the other hand vertical and transverse unevenness of the track and its discontinuities are the main source of vibration from railway vehicles. Another source of vibration is the rolling stock defects such as eccentricity and flatness tread [11].

Also, due to constructive peculiarities of railway vehicles can generate and support vibrations on the vehicle. The increase in velocity and increased payload imposed also need to describe in a more rigorous way of complex phenomena that occur at the interaction vehicle-runway, vehicle response to irregularities path, with implications for improving vehicle stability and hence the comfort of passengers [5,6].

Modeling processes induced irregularities random excitation path and the vehicle dynamic response allows a more precise description of the interdependence between vehicle vibration and statistical and spectral properties of irregularity path [2].

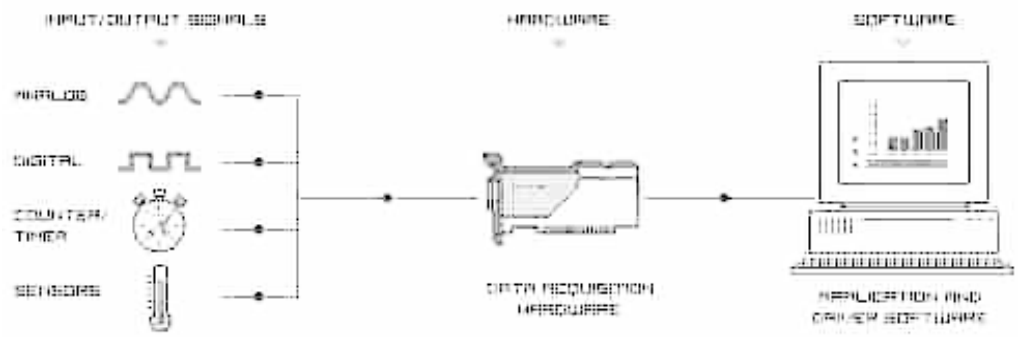

FIG. 2. A system of measurement, acquisition and processing of vibration signals (source: home.hit.no/~hansha/documents/industrial_it_automation.htm)

This method has been increasingly used in vehicle dynamics railway last time, being facilitated by the expansion theory of random vibration and the continuous improvement of equipment, methods of measurement and vibration analysis of low frequency (as presented in FIG. 2) that appear in the tread [4].

2. EXPERIMENTAL ANALYSIS FOR THE MEANDERING MOVEMENT

2.1 Issues concerning realization of vibration records. For experimental analysis of the vibrations have been recorded simultaneously on the magnetic tape acceleration of vibration to the different components of the vehicle at the three levels of interest, the container, bogie and axle of the vehicle in three orthogonal directions. On an additional channel were recorded simultaneously throughout the record, comments on the specific conditions of their time, and details regarding the parameters used.

In FIG. 3 transducer arrangement can be distinguished on the three masses vibrant and measuring system components consisting of transducers T, preamplifiers load and visualization devices and data storage, a tape recorder and a digital oscilloscope.

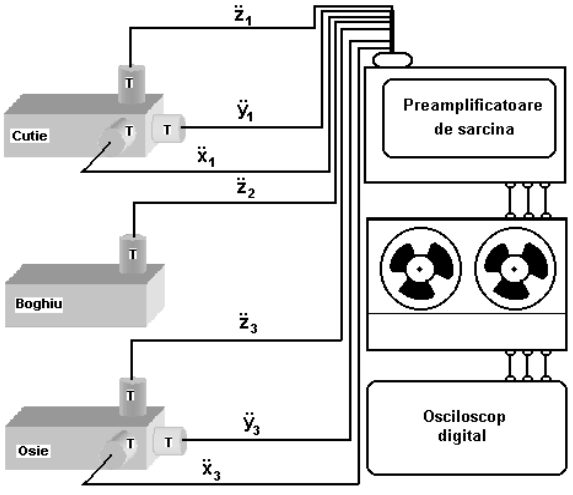

FIG. 3. Measurement scheme of vibration records

The transducers "T" are the type piezoelectric vibrating elements are mounted properly. Before recording, signals were amplified, thus achieving a coarse filter. As I stated earlier, to record and store data has been used a tape Bruel & Kjaer, every time there were three parallel acceleration, one of the channels recording was used for additional comments on rates and the areas where measurements were made. Fluke digital oscilloscope type of measurements used to monitor and ensure their accuracy. For further study in specialized programs is necessary analog-digital conversion of these accelerations. Either $t_1 = 0,\ t_2, ...,\ t_N = T,\ t_k = (k-1)h;\ k = 1,\ 2, ...,\ N$ set of digitized data that are obtained by analog-digital conversion and established a sampling step h. This raises problems because too small a sampling step involves a heavy workload both for data collection and numerical processing them.

On the other hand, a step too large sampling results in an interference between low frequency components and high frequency in the analyzed signal which is a great source of errors in determining the spectral densities of data studied. Since at least two samples are needed in order to define a cycle frequency component of signal analysis that the highest frequency that can be highlighted using the sampling step h is called the Nyquist frequency associated sampling step considered $f_N = \frac{1}{2h} = \frac{N-1}{2T}$. The f_N components of frequencies higher than the analyzed signal will interfere with the frequencies below this frequency. To avoid interference errors there are two methods. The first method is to choose a step sampling small enough so that it is physically impossible analyzed signals contain frequencies higher than the Nyquist frequency associated and it is recommended that this frequency to choose one and a half to two times higher than the frequency of the anticipated maximum, and the second method is the use of low pass filters before they are sampled so that frequencies beyond the range of interest should not be included in the analyzed signal in this case can be chosen f_N equal to the maximum frequency interest.

Whether $u(t)$ a signal measured under the conditions above. Since the frequency range of interest is up to 100 Hz, then consider imposing a sufficient $f = 200\,\text{Hz}$ sampling frequency resulting in a $\Delta t = 0{,}005\,\text{s}$ sampling time to provision and this frequency. And the sampling period $T = 60\,\text{s}$ meaning that the average speed of the train $V = 138\,\text{km/h}$ is the length of the sampling $L = 2{,}3\,\text{km}$. The signals were converted into numerical data using a data acquisition boards National Instruments BNC-2120 and stored in the computer.

2.2 Rail vehicle dynamics problems analyzed the records of vibration at high speeds. Based on measurements of vibration described above can be highlighted a number of important issues for railway vehicle dynamics. The expressions presented below summarizes the main problems that can be studied by processing of vibration measurements performed:

- $\ddot{z}_1, \ddot{z}_2, \ddot{z}_3 \Rightarrow$ Estimating the dynamic forces of the wheel-rail contact
- $\ddot{z}_1, \ddot{x}_1, \ddot{y}_1 \Rightarrow$ Estimating passenger comfort
- $\ddot{x}_3, \ddot{y}_3 \Rightarrow$ Highlighting the movement flexuosity
- $\ddot{z}_3 \Rightarrow$ Tread spectral density estimation (Spectral analysis)

Physical phenomena encountered in the operation are generally characterized by representing the amplitudes while quantities. In this way can be represented sizes and displacements, velocities, accelerations, forces, moments, pressures, temperatures, by varying amplitudes over time.

Much of the physical phenomena can be characterized by temporary diagrams showing a signal a fraction repeatability. In this case the phenomenon is called deterministic and knowing the initial parameters of the signal characterizing the phenomenon investigated, can accurately predict the size desired amplitude at one time located a temporary baseline. Through such simple graphical representation can monitor any deterministic phenomenon, knowing all the data needed to fully characterize the phenomenon studied. Also it can be said that an important part of engineering the physical phenomena of wide interest, not deterministic, ie each graphical representation of the phenomenon considered is unique, unlike any other. In this case it is impossible to say exactly where the amplitude magnitude followed at some point of time. However in this case we can say with sufficient precision, after studying the phenomenon closely, the signal sought does not exceed a certain amplitude but is found behind many records that are within this range, but it is impossible to specify where does to the time it is within that range limitation. Going a little further, you can even make laws which bind the membership and the recorded signal distribution within the range of amplitude. This seemingly illogical expounds allure of a random signal and sets a number of parameters and signal characteristics. For statistical analysis of these signals characterizing the accelerations measured on a railway vehicle that random processes, it took several simplifying assumptions. Thus to reduce the volume of records for characterization widest possible these random processes and thus to reduce the workload required of this operation, it was considered that these signals are of ergodic which had to be shown to reinforce the correctness work on these records that were put under analysis. Data from the measurements are processed in the original program and provides statistical information on the characteristics of these signals, and actual calculations were made in Excel. The repetition of these measurements may also provide statistical information time course of any type of new or existing rail vehicle in operation. One can appreciate the degradation of structures such as vehicles, finding and how it degrades by discovering the causes that produce degradation.

3. NUMERICAL PROCESSING OF RECORDS. RESULTS AND DISCUTIONS

This section illustrates methods of numerical processing carried out simultaneously records of vibration in the vertical direction, the transverse and longitudinal with a triaxial accelerometer mounted on the outer axle grease. By processing these records can reveal flexuosity movement characterized both time domain and frequency. Figures 4, 5 and 6 contains samples of acceleration records made on 3 directions.

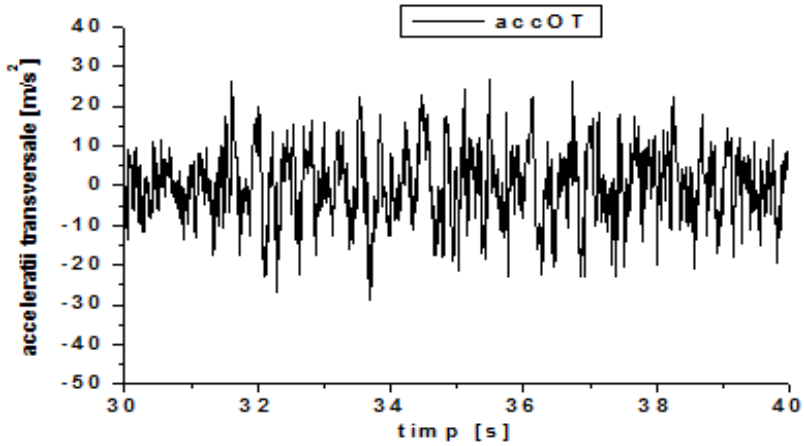

FIG. 4. Samples of records accelerations measured in the transverse direction

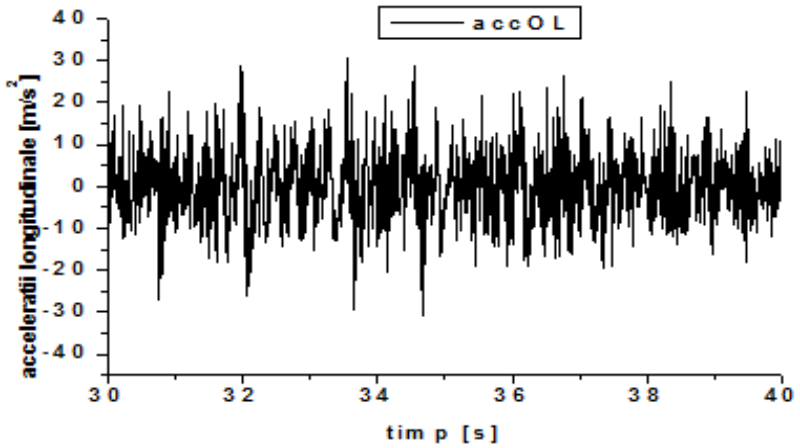

FIG. 5. Samples of records accelerations measured in the longitudinal direction

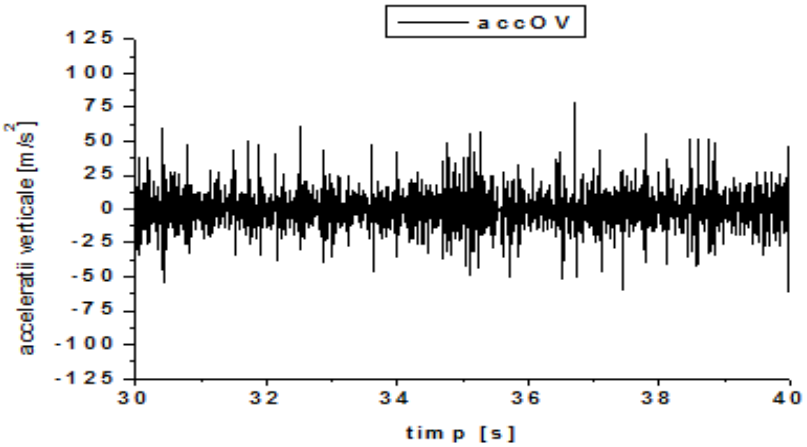

FIG. 6. Samples of records accelerations measured in the vertical direction

Following the calculations were obtained the following correlation coefficients r_{TL} =0.3, r_{TV} = -0.014 and r_{VL} = -0.033. It is noted transverse and longitudinal accelerations That is correlated in a statistically much better than in the horizontal direction Those recorded vertical to the recorded ones.

The F = 3.2Hz frequency is found in the transverse accelerations amplitude spectra (FIG. 7) and longitudinal filtered (FIG. 8), which does not happen if the amplitude spectrum of vertical accelerations filtered (FIG. 9).

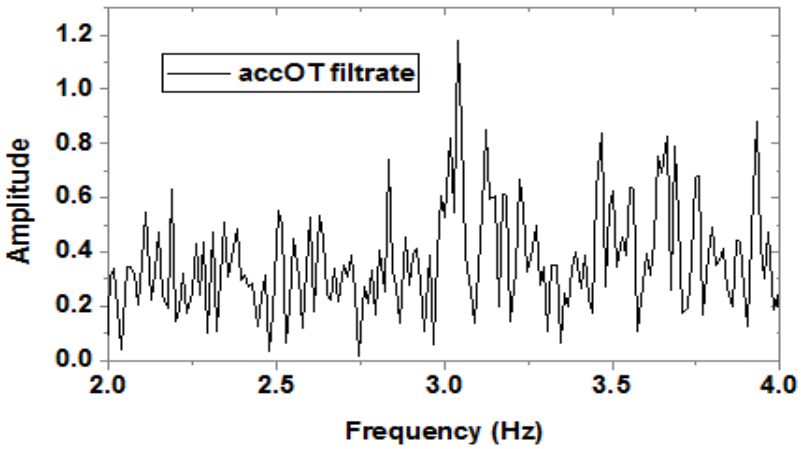

FIG. 7. The spectrum of amplitude transverse accelerations filtered

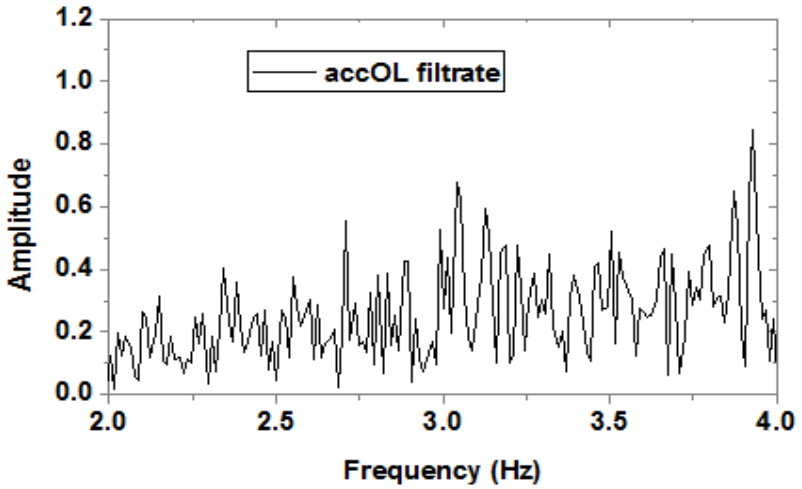

FIG. 8. The spectrum of amplitude longitudinal accelerations filtered

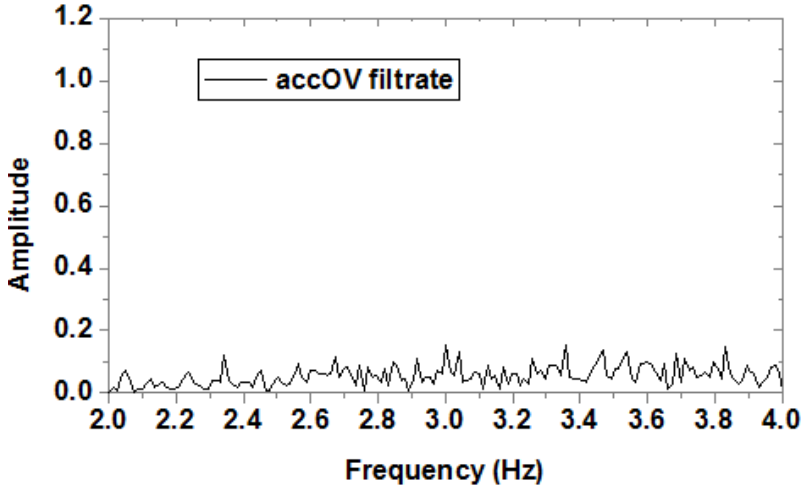

FIG. 9. The spectrum of amplitude vertical accelerations filtered

The values of these correlation coefficients show that transverse and longitudinal accelerations are strongly correlated filtered, while their correlation with vertical accelerations filtered is much weaker, what underlines once again that the movement analyzed in the frequency range 2-4 Hz is movement corresponds flat as meandering phenomenon.

CONCLUSIONS

Simultaneous measurement in three directions (x-longitudinal, y-transversal and z-vertical) of the accelerations at the box axle grease, can provide useful information for highlighting the phenomenon presented. This type of measurement is virtually the only possible real operating conditions since the use of other types of sensors such as travel or gear is not feasible. It is recommended piezoelectric acceleration transducer given that are robust and have a reduced size.

Methods of processing acceleration signals recorded and processed in this paper can reveal flexuosity movement. By determining the amplitude of signals recorded spectra can specify the frequency of occurrence as hunting movement.

By filtering signals in this frequency range it appears clearly as hunting movement, one can determine the dominant frequency sufficiently precise as hunting movement

velocity corresponding to the entries that were made. Method correlation coefficients between measured accelerations in three directions applied for both signals unfiltered and filtered signals especially highlights the strong correlation of acceleration horizontally and poor correlation between them and vertical.

Numerical processing of experimental data is very necessary because the study is done on real situations, that vehicle is studied under realistic conditions, and the results easily contain useful information about both the vehicle studied and about raceway on moving such a vehicle. In case if instead of using a tape recorder and oscilloscope measurement laptop scheme is greatly reduced, the data are digital data processing can be instantaneous. In this way the measurement results can be obtained quickly, reducing working time user. So someday you can check a large number of vehicles and can count the integrity of any vehicle or track on which it runs. The statistical data in a database, obtained by successive measurements over time may provide important information about the sub-assemblies to the vehicle.

For a larger number of vehicles can see which parts fail in a shorter time and the causes of their deterioration, upgrades subsequent vehicle may consist of simple replacement of subassemblies old with new, redesigned that appropriate conduct all claims arising in operation.

REFERENCES

[1] D. Baldovin, T. Sireteanu, S. Nistor, A. Mitu, *Dissipation Effect in the Hunting Motion Stability of Wheel Set with Elastic Joints*, Analele Universităţii "Eftimie Murgu", vol. 17, pp. 167-176, 2010 - anale-ing.uem.ro/2010/18_C.pdf

[2] G. Ene, C. Pavel, *Introducere în tehnica izolării vibraţiilor şi a zgomotului*, MATRIX ROM, Bucureşti, 2012 - www.utilajutcb.ro/uploads/pavel_ene.pdf

[3] I. Sebeşan, *Dinamica vehiculelor de cale ferată*, Editura Tehnică, Bucureşti , 1995 ro.scribd.com/.../Dinamica-vehiculelor-de-cale-ferata

[4] T. Sireteanu, I. Sebeşan, D. Baldovin, *The Influence of Damping Characteristic on the Stabilization Control of Hunting Motion of a Railway Vehicle Wheelset*, Proceedings of the Romanian Academy, Bucureşti, Series A, vol. 11, nr. 4, pp. 355–362, 2010- www.acad.ro/.../09-Sireteanu.pdf

[5] I. Vidican, M. Bejan, *Consideraţii asupra vibraţiilor suspensiilor vehiculelor de cale ferată*, vol. celei de-a XII-a Conferinţă Naţională multidisciplinară "Profesorul Dorin Pavel - fondatorul hidroenergeticii româneşti", Sebeş, 2012 stiintasiinginerie.ro/87 - consideratii asupra vibratiilor.pdf

[6] I. Vidican, M. Bejan, *Consideraţii asupra vibraţiilor din suspensia vehiculelor feroviare şi măsurarea lor*, vol. celei de-a XIII-a Conferinţă Naţională multidisciplinară "Profesorul Dorin Pavel - fondatorul hidroenergeticii româneşti", Sebeş, 2013

[7] *** documents.tips/documents/zgomotul-si-vibratiile-la-mijloacele-de-transport-rutier.html

[8] *** www.kowi.de/Portaldata/2/Resources/fp/railroute-2050.pdf

[9] *** www.maribyrnong.vic.gov.au/files/Passenger_Rail_Infrastructure_Noise_Policy.pdf

[10] *** www.uic.org/IMG/pdf/action_planning_paper_final-2.pdf

[11] *** www.revmaterialeplastice.ro/pdf/SEBESAN.pdf

FACADE OF PERFORATED PLATE: ANALYSIS OF ITS ACOUSTIC BEHAVIOR

Alina-Elena CREȚU

Military Technical Academy, Bucharest, Romania

DOI: 10.19062/2247-3173.2016.18.1.43

Abstract: *This paper was designed to contribute to the application of acoustic solutions in construction. It is presented absorbing behavior of multilayer panels perforated plate, the study was demonstrated by simulating the proposed models using the program Sound Flow. The results were calculated and optimized using simulation software to achieve sound absorption coefficient.*

Keywords: *acoustic, panels perforated, SoundFlow .*

1. INTRODUCTION

Worldwide, the overall noise level is alarmingly high. we live in a noisy society mainly due to the technological environment in which we evolved.

We all know that noise pollution not only makes it hard to relax, but it causes stress and is a real threat to our health. We can not stop development, so any solution to noise will help us improve our physical and mental wellbeing.

All constructive solutions that protect us froma acoustic shock, always have a direct bearing on our quality of life, both physical and mental. Those solutions designed for acoustic enhancement are useful for both new construction and for rehabilitation so as to attenuate any noise and can enjoy the much desired peace and tranquility inside and outside the home.

As discussed in the beginning, the noise is a type of pollution to which we are exposed, that is why this finally master project aims to make the analysis of one of the most important parameters of the acoustic behavior of multilayer panels, as is the sound absorption coefficient. As such, this project focuses on the absorption of low frequency noise (noise from external source); specifically arises absorb noise generated by car traffic, planes and trains.

2. BASIC CONCEPTS

2.2 The Sounds. Sounds are vibrations mainly airborne, which can be perceived by the human ear and interpreted by the brain. They are characterized by its intensity, by the set of frequencies, and any variations thereof in time. People can interpret sounds as signals or noise, distinguishing the former as carriers of useful information, while the latter are undesirable sounds because they interfere with hearing the signal, its intensity or unpleasant frequency, or convey information not desired.

2.1 Frequency. Frequency is a measure of the number of repetitions of a periodic phenomenon per unit time. the international system unit is called hertz frequency and is symbolized by hz, the german physicist heinrich hertz in honor. a frequency of 1hz corresponds to a repetition period of one second. for example, we say of a woodpecker

knocking beak into the bark of a tree 10 times per second, its head oscillates at a frequency of 10 hz.

The audible frequency range for people ranging from 20 to 20,000 Hz. (Cycles per second), although in practice this varies from one person to another, again depending on the age of it. The sounds below 20 Hz are called infrasound and ultrasound 20.000Hz above.

2.3 Intensity. Also called volume or amplitude of the sound. It is the quality that allows us to distinguish between loud and soft sounds. Strong as an ambulance siren and soft as a whisper. This intensity measures the sound pressure level (dB), which carries the sound wave on the particles of the medium through which it propagates.

2.4 Decibels. The intensity of the various noise is measured in decibels (dB), unit of measure of sound pressure. The threshold of hearing is 0 dB (minimum stimulus intensity) and the threshold of pain is 140 dB.

2.5 Sound propagation. Sound is transmitted through materials, solids, liquids or gases but not through empty media. to the sound may reach our ears need a space or propagation medium, this usually is usually the air. In general the speed of sound is higher in the solid and lower in the gases. In gases the particles are further from each other and hence the frequency of interaction is lower than in liquids and solids. The speed of sound in air at 20 ° C is 345 m / s.

2.6 Noise pollution. managing urban noise centered on the control of noise generated by activities in the urban residential land, however, public sensitivity to this form of pollution is increased. So now the environmental management processes involved in management of environmental noise generated mainly railways, traffic, roads, airports, factories, ports, leisure on public roads, municipal services and works.

Environmental noise pollution due to excessive sound that disrupts normal ambient conditions in a given area. While noise does not accumulate, moved or maintained over time as other pollutants, can also cause extensive damage to the quality of life of people if not properly controlled, this, together with the degree of impact caused by a besides noise source depending on its intensity, also depends on the sensitivity to the noise that has the receiver.

Noise pollution is generated by unwanted sounds that negatively affect our quality of life thereby preventing the normal development of our activities.

3. ANALYSIS AND RESULTS OF THE STUDY MODEL

3.1 Input data. All models use a 1.5mm thick plate with holes staggered and placed with airflow resistivity of 5 Kpa.s/m2. In the model which has absorbent material is used in all cases Rockwool wool with properties of density and air flow resistance is 75 kg/m3 to 45kPa.s / m2 respectively. Then discuss the absorption coefficient in each of the models and the changes produced by varying parameters such as the separation distance of the plate from the wall of the facade (d), the diameter of the holes (Ø) and the porosity of the sheet (p). For the analysis we reference the model with separation d = 700mm, holes diameter Ø = 3mm and porosity p = 40%.

3.2 Brief explanation of the software SoundFlow. SoundFlow a simulation software for the calculation of absorption, reflection and transmission of sound in multilayer structures. Allows the modeling of wall structures, floor and ceiling by specifying layer

materials and thickness. In the database these materials are divided into three classes: absorbent, perforated sheets and plates. The classification depends on the mechanisms of sound absorption and for each of the types, different physical properties are used to define it. The program can display the following calculation results:

- Coefficient absorbtion
- Coefficient reflection
- Loss transmission including input impedance real part and imaginary,and the magnitude and phase
- Reflection factor including real and imaginary part and the magnitude and phase.

FIG. 1. *AFMG program window SoundFlow*

Section 1: Definition of the structure:

The pictorial representation of the structure to define the number of layers thickness and material.

Section 2: Properties of the structure:

The content of this window depends on the layer is selected in the structure. When a specific layer is selected edges will turn yellow and in this window properties that may be edited are displayed.

Section 3: Quantities broadband:

The table shows the set of indicators common broadband.

Section 4: Results Window:

The results can be displayed via a chart or by tables. When changes are made to the properties window the results are updated automatically.

3.3 Analysis of model 1: Sheet (1.5mm) + Air + Absorbent (50 mm) + Wall

a. VARIABLE AND SEPARATION WALL PLATE [500 mm, 700 mm, 800 mm, 1000 mm]

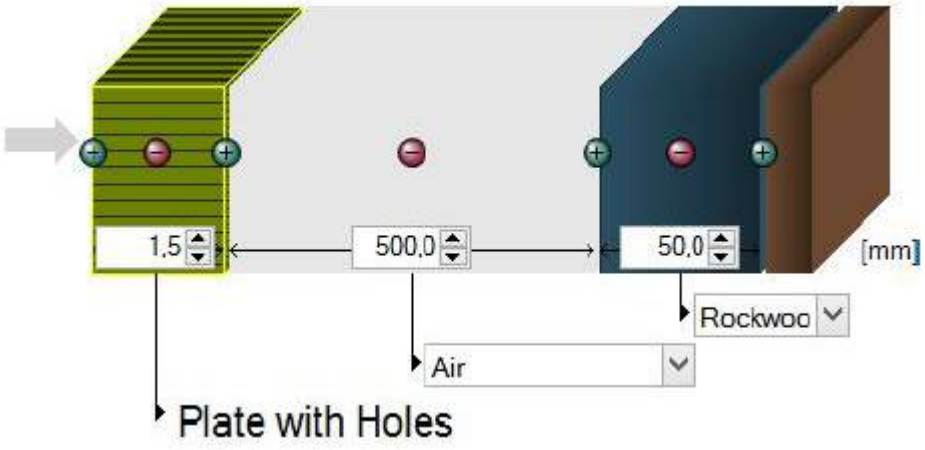

FIG. 2. Results d=500mm. Model 1

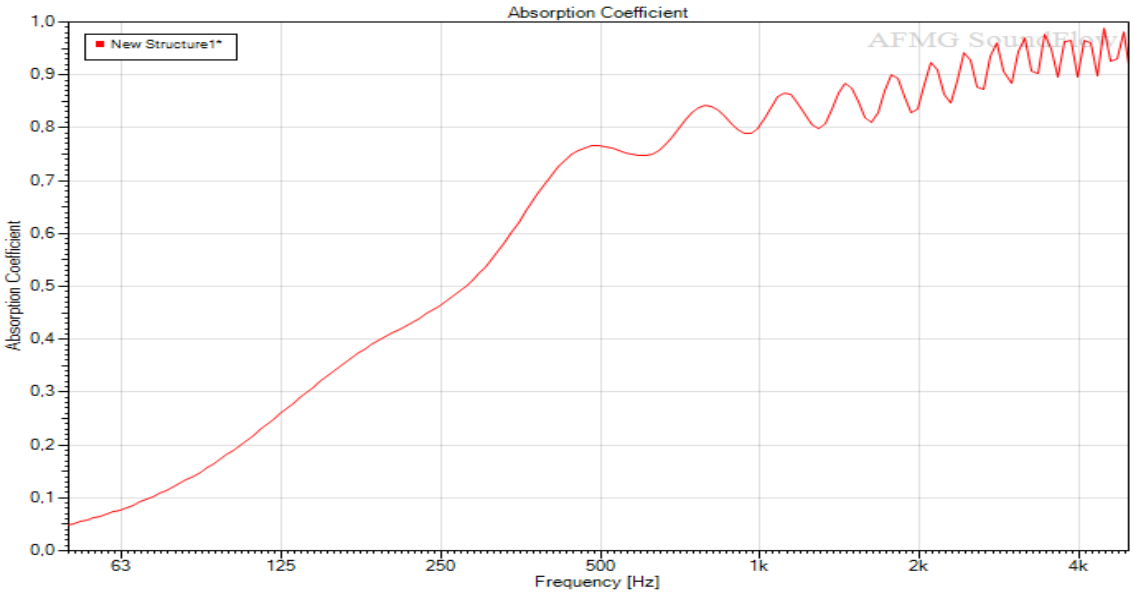

FIG. 3. Results d=500mm. Model 1

ANALYSIS:

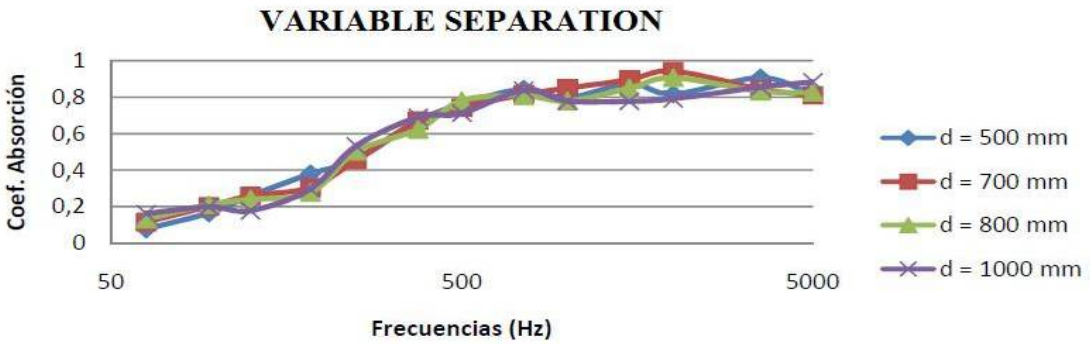

FIG. 4. Analysis influence the separation of the wall plate. Model 1

The trend line that is closest to the graphical representation of our model is a polynomial degree 3 curve. It can be seen to gradually increase as the separation distance of the wall plate to the curve shifts to the left and downward. By example comparing the curves for a distance of 500 to 700 millimeters graphic shifts a frequency of 425 hz with a coefficient of absorption 0734-375 hz with.

An absorption coefficient of 0.672. Namely that is reduced by 11.72% and a frequency coefficient of 8.44% absorption. When the spacing changes from 800 to 1000 mm movement curve is a counterclockwise 32.43% and 35.74% of a downwards. it thus the shift of the curve increases as the gaps they increase.

b. VARIABLE DIAMETER HOLE [1 mm, 3 mm, 5 mm, 10 mm]
ANALYSIS:

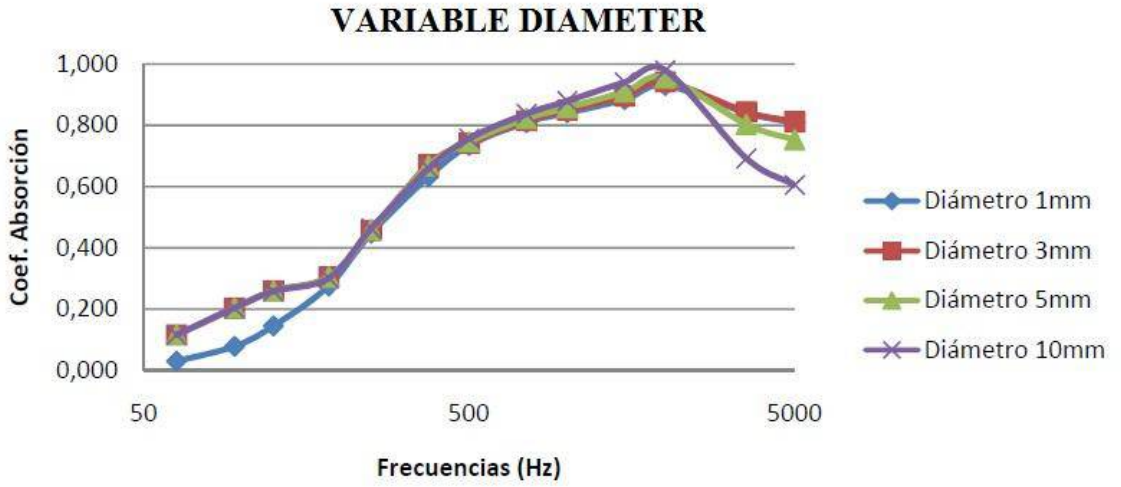

FIG. 5. Analysis influence the diameter of the holes of the plate. Model 1

For frequencies up to 2000 Hz the variation of the absorption coefficient in perforated plates with holes of 3.5 and 10 mm is almost the same, except for a slight increase of 4% around 2000 hz when the hole measured 10mm. from that point diameter growth is a reduction of the coefficient of absorption. From 185 hz plates with holes of 1mm in diameter behave like the others, to that extent its absorption coefficient is a 60% lower.

c. Varying porosity [35%, 40%, 45%, 50%]
ANALYSIS:

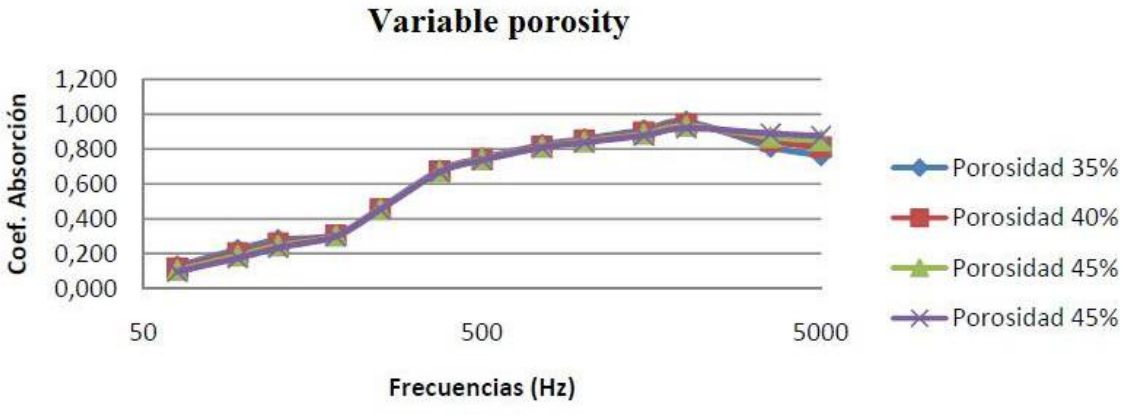

FIG. 6. Analysis influence of the porosity of the sheet. Model 1

4. CONCLUSIONS

Tabel 1.

d	500mm	700mm	800mm	1000mm	700mm				700mm			
Θ	3				1	3	5	10	3			
ρ	40				40				35	40	45	50
5 KPa.s/m2												
Frecuencias	Resulatados											
50	0,049	0.078	0.094	0.122	0.017	0.078	0.078	0.078	0.089	0.078	0.071	0.064
63	0,078	0.116	0.133	0.161	0.031	0.115	0.115	0.116	0.130	0.116	0.105	0.096
80	0,121	0.163	0.178	0.191	0.053	0.163	0.163	0.163	0.181	0.163	0.149	0.138
100	0,182	0.215	0.218	0.197	0.090	0.215	0.215	0.215	0.235	0.215	0.199	0.186
125	0,258	0.259	0.240	0.181	0.145	0.260	0.260	0.260	0.277	0.259	0.245	0.234
160	0,337	0.289	0.253	0.211	0.219	0.289	0.289	0.290	0.299	0.389	0.281	0.275
200	0,405	0.333	0.322	0.376	0.316	0.330	0.329	0.333	0.334	0.333	0.332	0.331
250	0,465	0.458	0.497	0.526	0.448	0.455	0.457	0.456	0.461	0.458	0.455	0.453
315	0,556	0.625	0.622	0.564	0.581	0.631	0.625	0.624	0.636	0.625	0.617	0.610
400	0,691	0.676	0.653	0.700	0.642	0.675	0.676	0.679	0.676	0.676	0.675	0.675
500	0,761	0.739	0.761	0.730	0.733	0.734	0.735	0.734	0.740	0.736	0.732	0.729
630	0,76	0.783	0.774	0.781	0.753	0.783	0.784	0.786	0.783	0.783	0.783	0.783
800	0,828	0.817	0.806	0.811	0.821	0.833	0.817	0.816	0.822	0.817	0.814	0.811
1000	0,815	0.824	0.827	0.830	0.830	0.830	0.824	0.824	0.825	0.824	0.822	0.821
1250	0,831	0.830	0.840	0.832	0.844	0.847	0.831	0.833	0.829	0.830	0.831	0.832
1600	0,852	0.850	0.847	0.851	0.830	0.850	0.850	0.849	0.851	0.850	0.848	0.846
2000	0,877	0.870	0.872	0.869	0.859	0.872	0.871	0.873	0.867	0.870	0.871	0.872
2500	0,901	0.905	0.901	0.904	0.882	0.900	0.906	0.908	0.900	0.905	0.907	0.907
3150	0,931	0.929	0.930	0.931	0.902	0.929	0.931	0.934	0.920	0.929	0.934	0.935
4000	0,939	0.940	0.943	0.941	0.902	0.940	0.943	0.948	0.924	0.940	0.947	0.951
5000	0,947	0.947	0.942	0.959	0.902	0.950	0.951	0.958	0.925	0.947	0.957	0.962

Focusing on the wing we are intterested in increasing the absorbtion acoustics to reduce traffic noise 125 hz,it is concluded that the best separation of the plate to the wall is 700 mm.furthermore most beneficial for increased absorbtion is working with holes 3 mm in diameter. Finally clearly shows that the smaller the porosity is greater than the absorbtion in our cases select the sheet with a percentage of 35% perforated area.

REFERENCES

[1]. *TFG Rocio Olaguibel* „Fachada de chapa perforada: análisis de su comportamiento acústico”
[2]. *Manual del Ruido, Departamento de Construcción arquitectónica,* Ayuntamiento de las Palmas de Gran Canaria, 2006.
[3]. Jornada Criterios Acústicos en el Diseño de Centros Docentes, *Comportamiento acústico de los materiales y edificios,* Centro Tecnológico Labein, Vitoria, Mayo del 2001.

DYNAMICS OF KNOCK-OPEN VALVE FOR GAS GUNS POWERED BY CARBON DIOXIDE

Linh DO DUC[*], Vladimír HORÁK[*], Tomáš LUKÁČ[*], Roman VÍTEK[*] Quang Huy MAI[**],

*University of Defence, Brno, Czech Republic
**Le Quy Don Technical University, Hanoi, Vietnam
(duclinh.do@gmail.com, vladimir.horak@unob.cz, tomas.lukac@unob.cz, roman.vitek@unob.cz, maiquanghuykvk@yahoo.com.vn)

DOI: 10.19062/2247-3173.2016.18.1.44

Abstract: *The paper is focused on the dynamics of knock-open valve used to control the mass flow from a carbon dioxide (CO_2) reservoir. The objective is to formulate the mathematical model simulating dynamics of the knock-open valve system for the gas guns powered by carbon dioxide. The equilibrium discharge mathematical model is overviewed, modified and evaluated to obtain the thermodynamic equilibrium states taking place within the reservoir. The problem is solved using MATLAB environment and results of theoretical solution are verified experimentally. Influence of changes in some design parameters of the knock-open valve system to the mass discharge of CO_2 within the reservoir is comprehensively examined.*

Keywords: *knock-open valve, gas gun, carbon dioxide, airsoft, paintball, pressure reservoir.*

1. INTRODUCTION

In recent years, the knock-open valve is one of the most commonly used gas valves in gas guns technology due to its outstanding reliability, ease of maintenance and long service life. Besides, the only drawback of knock-open valve is extreme sensitivity to working gas pressure. If the reservoir is over-pressurized that means the pressure within the reservoir is higher than the design of the action can accommodate, the valve cannot be opened as far as it should by the hammer, therefore less gas discharges and consequently lower performance. The over-pressurization commonly appears in the case of carbon dioxide reservoir, when the surrounding temperature gets higher than the critical value.

The knock-open valve system plays a critical role in controlling the gun's performance, because its design parameters and set up determine the mass flow from the pressure reservoir into the barrel. In other words, the guns performance controlling problem can be solved, if we are able to discharge the gas out of the reservoir on command.

Hence, it is crucial to obtain a scientific understanding of knock-open valve dynamics and further the dependence of thermodynamic properties within the reservoir on the valve design parameters. In order to satisfy this goal, a comprehensive discharge mathematical model including the knock-open valve dynamics is required.

There is almost no published literature on the topic mentioned above. Several related publications have appeared in the last few years documenting the study of phase behavior of carbon dioxide as the power gas for gas guns [1], in which a comprehensive equilibrium discharge mathematical model for CO_2 has been developed, the complex

internal ballistics models of gas guns were presented in [3,4] and the simulation of the sound effect of RPG-7 anti-tank grenade launcher for shooting training is given in [2]. All these above mentioned works deal with the gas discharge from a pressure reservoir through a control valve system that was treated only as an orifice of a constant cross-sectional area meaning that the dynamics of the valve was neglected.

In this paper, a comprehensive mathematical model simulating the knock-open valve dynamics is formulated. The equilibrium discharge mathematical model for carbon dioxide tanks presented [1] in order to simulate the thermodynamic states taking place inside the reservoir is overviewed and evaluated. For the purpose of verifying the model an experimental setup has been established.

2. PRINCIPLE OF KNOCK-OPEN VALVE OPERATION

Figure 1 shows the basic concept of a knock-open valve consisting of a valve body, a valve stem and a return spring. The valve body is connected with a gas reservoir that in this study is filled with liquefied carbon dioxide. In the case of closed valve, the hammer is held in the back position while the valve is blocking its way by the return spring force and the pressure force generated by the high-pressure CO_2 vapor. In order to prevent gas escaping from the valve through the valve face, a sealing O-ring is used.

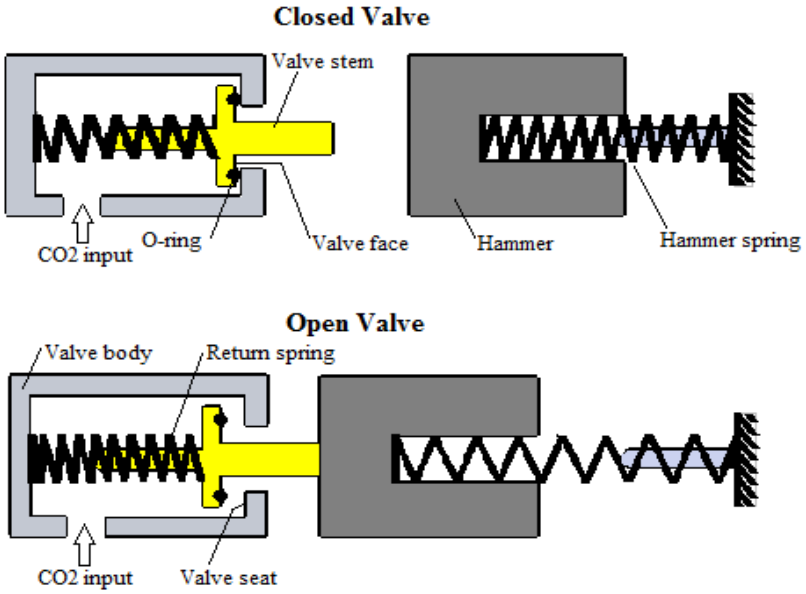

FIG. 1. Schematic of the knock-open valve

Once the hammer is released, it is driven forward by the hammer spring force, then it strikes the end of the valve stem. After that, the valve stem and the hammer move together forward, therefore the contact between the sealing O-ring with the valve face is broken, forcing the valve to open and release the pressurized CO_2 vapor. The valve return spring has been overcome by the power of the hammer, but after a short time, with help of the pressure force of CO_2 vapor in the reservoir, it will reverse the direction of the valve stem and close the valve again to further gas flow.

3. MATHEMATICAL MODEL

As it is seen in Fig. 2a, the reservoir is considered as an open thermodynamic system, in which we assume that CO_2 exists in liquid-vapor equilibrium. The vapor phase occupies the upper part of the reservoir and the bottom reservoir portion is filled by the liquid phase. There exists an interface between the two phases. If all the assumptions provided [1] for the vapor discharge of carbon dioxide tanks are accepted, we are able to apply the equilibrium discharge mathematical model presented in [1] in order to assume the thermodynamic equilibrium states inside the reservoir at every point in time throughout discharging under ambient temperature conditions. This model enables us to determine the time change in pressure and mass.

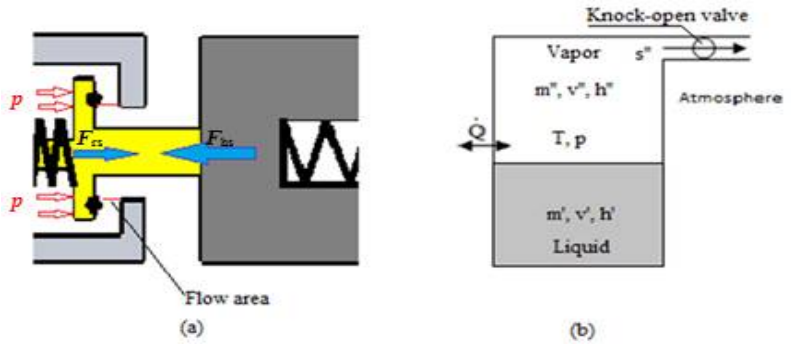

FIG. 2. (a) Schematic of forces acting on the hammer-valve stem system, (b) Reservoir as an open thermodynamic system

The equilibrium discharge mathematical model for the CO_2 reservoir consists of following equations [1]:

$$\frac{dT}{d\tau}=\frac{\dfrac{dQ}{d\tau}-\dot{m}v''\dfrac{L(T)}{\Delta v}}{m\tilde{c}_P(T)-\dfrac{V_R}{T}\dfrac{L(T)}{\Delta v}-L(T)\phi(T)} \tag{1}$$

$$\frac{dx}{d\tau}=-\frac{1}{m}\left(\frac{v}{\Delta v}\frac{dm}{d\tau}-\phi(T)\frac{dT}{d\tau}\right) \tag{2}$$

$$\frac{dm''}{d\tau}=-\frac{v'}{\Delta v}\frac{dm}{d\tau}-\phi(T)\frac{dT}{d\tau} \tag{3}$$

$$\frac{dQ}{d\tau}=\alpha A(T-T_w) \tag{4}$$

$$\frac{dm}{d\tau}=-\dot{m}=-C\frac{vA}{v} \tag{5}$$

where:

T	Temperature of CO_2 within reservoir	V_R	Total volume of reservoir
T_w	Temperature of reservoir wall	α	Heat transfer coefficient

m''	Mass of vapor phase	A	Flow area
m	Total mass of CO_2	C	Discharge coefficient
$\dot{m}$	Mass flow rate through valve system	v	Discharge flow velocity
Q	Heat	Δv	Difference of specific volumes $(v''-v')$
v	Specific volume of CO_2	L	Latent heat
v''	Specific volume of vapor phase	$\tilde{c}_P$	Mixture heat specific capacity
v'	Specific volume of liquid phase	x	Quality of two-phase mixture
v	Discharge flow velocity	ϕ	Substitution function of temperature

In contrast to the equilibrium discharge model provided by the author in [1] flow area A indicated by the read lines in Fig. 2a is not a constant and its size depends on the displacement of the valve stem l_{st}. The value of A can be expressed as follows

$$A = \pi D_{Or} l_{st} \tag{6}$$

where D_{Or} is the sealing O-ring diameter. As it is seen in Eq. (6), to close the mathematical model it is necessary to solve the dynamics of the hammer-valve stem system to obtain the value of the valve stem displacement l_{st}. In order to satisfy this goal, first of all we assume that the collision between the hammer and the valve stem is perfectly elastic collision. It means that the hammer and the valve stem are stick together after the collision and there is no kinetic energy loss. Thus, we can write Newton's Second Law for motion of the hammer-valve stem system in following form

$$\frac{dV_{st}}{d\tau} = \frac{F_{hs} - F_{rs} - F_P}{m_h + \frac{m_{hs}}{3} + m_{st} + \frac{m_{rs}}{3}}, \qquad \frac{dl_{st}}{d\tau} = V_{st} \tag{7}$$

where m_h, m_{hs}, m_{st} and m_{rs} account for the mass of hammer, hammer spring, valve stem and return spring, respectively. The V_{st} denotes for the hammer-valve stem velocity. Here, there are three forces acting on the hammer-valve stem system (see Fig. 2a):

- The return spring force F_{rs} acting on the stem against the hammer spring force F_{hs}. Their value depend on the spring constants, the spring preload and displacement l_{st}.
- The pressure force $F_P = (p - p_a) A_{crs}$, where p is the reservoir pressure, p_a is the surrounding pressure at the knock-open valve output and A_{crs} represents for the cross-sectional area of the valve stem.

In this study, the friction force between the valve moving parts and surfaces is neglected.

Besides, it is needed to take the motion of the hammer before the collision with the valve stem in consideration in order to determine the hammer's impact velocity and further its impact kinetic energy. Before the collision, there is only the spring force acting on the hammer, therefore we apply Newton's Second Law again for hammer motion, we obtain the similar form of the equations of hammer motion as in Eq. (7), in which F_{rs}, F_P, m_{st} and m_{rs} are eliminated.

4. RESULTS OF SOLUTION

The above described problem was solved by numerical integration with MATLAB using the explicit fourth-order Runge-Kutta method. Mathematical model considers a range of input data parameters and boundary conditions (i.e. reservoir volume, initial temperature, the total mass of CO_2 and the percentage of liquid fill within the reservoir, the discharge coefficient, the heat transfer coefficient, etc.). In order to present results of solution, we chose the input data parameters and boundary conditions shown in Tab. 1 that correspond to the design parameters of the knock-valve-hammer system used in Tippmann A5 paintball gun. Results of the solution of the developed mathematical model for this given example are presented from Fig. 3 to Fig. 5.

Table 1. Initial data parameters and boundary conditions

Quantity	**Value**	**Quantity**	**Value**
Initial reservoir temperature (K)	22	Hammer spring constant (N/m)	807
Temperature of reservoir wall (K)	22	Hammer spring mass (g)	2.7
Total reservoir volume ($.10^{-3}m^3$)	0.8	Hammer mass (g)	140
Initial total mass of CO_2 (g)	360	Hammer stroke before collision (mm)	29.5
Initial mass of vapor phase (g)	89	Return spring constant (N/m)	10302
Discharge coefficient	0.7	Return spring mass (g)	1.6
Sealing O-ring diameter (mm)	10	Valve stem mass (g)	4.7

The change in mass of CO_2 within the reservoir is shown in Fig. 3a. Figure 3b indicates the percentage of the vapor phase mass within the reservoir is slightly increasing about 0.02%. It can be explained that, the amount of vapor discharged out of the reservoir is smaller than the amount of vapor generated by the vaporization of the liquid phase for the purpose of maintaining the thermal phase equilibrium inside the reservoir. This phenomena explains the wide range of use of CO_2 in the gas guns community from the point of view of the guns power and the reservoir capacity, i.e. number of shots per fill.

The dynamics of the knock-open valve system is clearly shown in Fig. 4. In the first phase of operation, the hammer is accelerating the beginning until the moment, when it starts colliding with the valve stem. At the end of this phase the hammer reaches the impact velocity v_{ip}. After that, the valve stem and the hammer move together, opening the valve gradually until the hammer is stopped. Then, the hammer changes its direction and moves to the back position that causes the valve to be closed successively. Simulation of the hammer motion after closing the valve is not the aim of this study due to its insignificant influence to dynamics of the knock-open valve.

Results obtained using the described mathematical model enable us to observe influence of changes in various design parameters. The gun's performance is proportional to the amount of CO_2 discharged from the reservoir into the barrel through the knock-open valve during each shots. Figure 5a shows the influence of the hammer impact velocity v_{ip} to the mass discharge of CO_2 (i.e. amount of discharged CO_2). It is seen that the mass discharge reaches its maximum value at the so called critical hammer impact velocity v_{cr}. If the impact velocity oversteps the critical value, it causes the mass discharge to decrease due to decreasing in opening time of the valve (red curve). Figure 6 illustrates the way to choose the correct design value of hammer mass and hammer spring

constant to obtain the required impact velocity. The mass discharge can be also controlled by changing the size of flow area that is function of the sealing O-ring diameter (Fig. 5b).

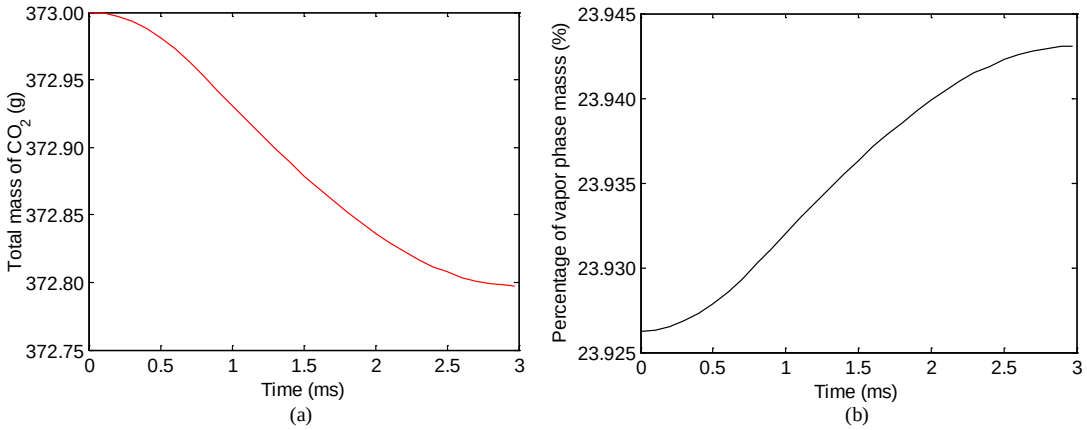

FIG. 3. Time courses of total mass (a) and percentage of vapor phase mass (b) within the reservoir

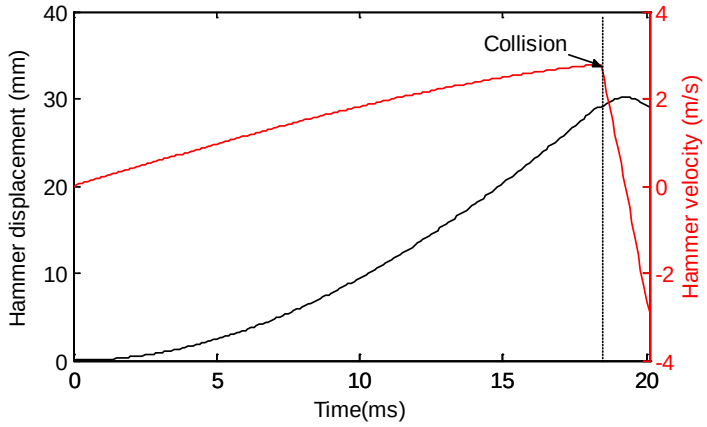

FIG. 4. Hammer displacement (black) and hammer velocity (red) versus time

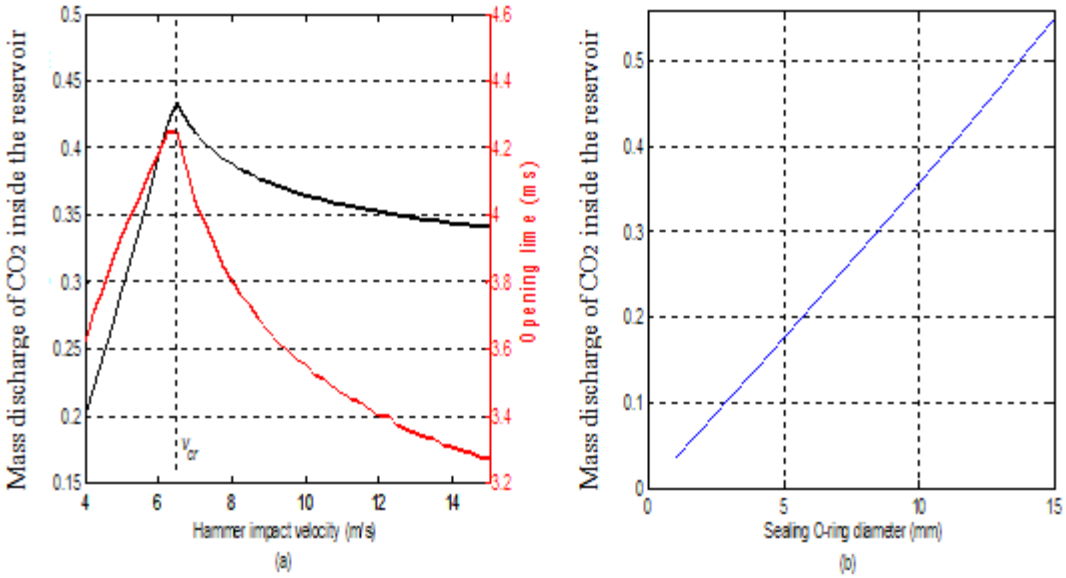

FIG. 5. (a) Influence of the hammer impact velocity and opening time (a) and size of flow area (b) to the mass discharge of CO_2 inside the reservoir

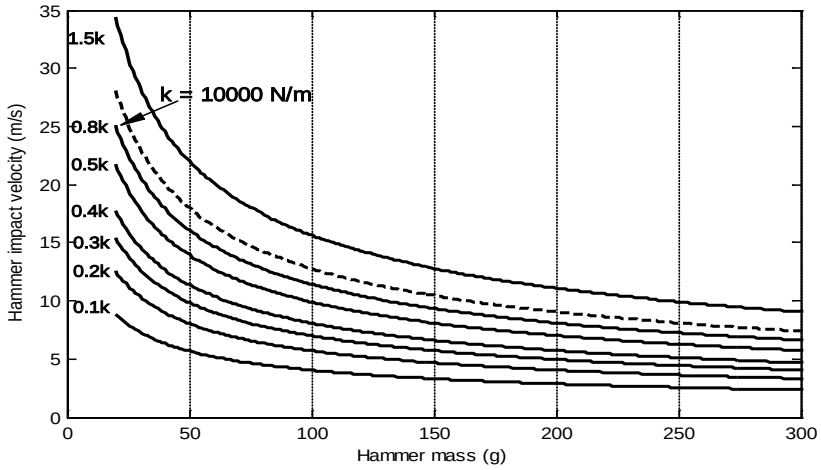

FIG. 6. Hammer impact velocity as a function of hammer spring constant and hammer mass

5. VERIFICATION OF THE MATHEMATICAL MODEL

Results of solution of the hammer and valve stem displacement and the CO_2 mass discharge are compared with the measured values. The displacement of the hammer was measured using high speed camera FASTCAM Mini UX100 type 800K-M-4G, the chosen record rate was 10000 frames per second, the shutter speed was 1/80000 (s). The compassion of calculated and measured time courses of the hammer displacement is shown in Fig. 7.

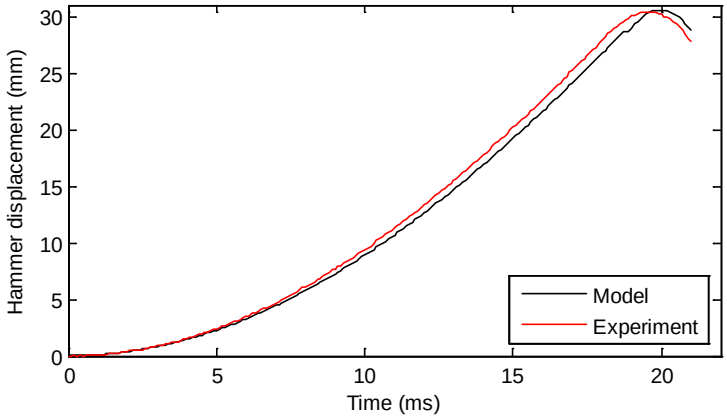

FIG. 7. Hammer displacement vs. time

Table 2. CO_2 mass discharge after opening the valve five times

Hammer mass (g)	CO_2 mass discharge (g)		Difference (%)
	Experiment	Model	
142.6	2.02	1.961	2.92
134.0	2.01	1.960	2.48

The valve is opened five times consecutively and then the CO_2 mass discharge was measured using a precision digital scale. Here two hammers of different masses were used. The calculated and measured mass discharge values are compared in Tab. 2, from

that we can conclude quite good agreement between the results of the mathematical model and experimentally obtained values.

CONCLUSIONS

In this study, the mathematical model for analyzing the dynamics of the knock-open valve system for the knock-open valve has been formulated. The equilibrium discharge mathematical model has been overviewed, modified and evaluated. The problem has been solved in MATLAB environment. Obtained results enable us to analyze various influences of changes in several design parameters. This model can be used as the base for the design and optimization of the knock-open valve system.

The presented mathematical model was verified experimentally by measuring the hammer displacement and the mass discharge of CO_2 within the reservoir. It can be stated that the theoretical solution correspond quite well with experimental measurements. As the future improvement of experimental device, the range of hammer mass will be wider and the flow area size will be changed.

AKNOWLEDGMENT

The work presented in this paper has been supported by the institutional funding DZRO K 201 “VÝZBROJ” and by the specific research project of Faculty of the Military Technology SV16-216.

REFERENCES

[1] L. Do Duc, V. Horák, T. Lukáč, Q. H. Mai, *Study of Phase Behavior of Carbon Dioxide as the Power Gas for Gas Guns*. In KRIVANEK, V. (ed.) *International Conference on Military Technologies, Proceedings ICMT’15*, Brno: University of Defence, p. 29-36, 2015;

[2] Q.H. Mai, V. Horák, L. Do Duc, Sound Effect of RPG-7 Antitank Grenade Launcher for Shooting Training, *Advances in Military Technology*, vol. 9, no. 2, p. 49-60. 2014;

[3] V. Horák, L. Do Duc, R. Vítek, S. Beer, Q.H. Mai, Prediction of the Air Gun Performance, *Advances in Military Technology*, vol. 9, no. 1, p. 31-44, 2014;

[4] L. Do Duc, *Software for thermodynamic and design calculation of gas guns*, Thesis, University of Defence, 2015.

THERMO-ANEMOMETRIC DETERMINATION OF LIQUID WATER CONTENT IN WET AIRSTREAM

Rostislav JANKŮ[*], Vladimír HORÁK[**]

[*]Student of Faculty of Military Technology, University of Defence, Brno, Czech Republic (rostislav.janku@unob.cz)
[**]Department of Mechanical Engineering, University of Defence, Brno, Czech Republic (vladimir.horak@unob.cz)

DOI: 10.19062/2247-3173.2016.18.1.45

Abstract: *The paper is focused on the experimental study of possibilities of the thermo-anemometric analysis for determination of the liquid water content in the stream of wet air. The developed method is based on the measurement and comparison of stream velocity of wet and dry air by the hot-wire thermal anemometric probe. Experiments were performed in the small icing wind tunnel using the standard thermal anemometer Testo 425. There was found the correlation between the liquid water content and the difference in measured velocity of the wet and dry airstreams. The conclusion of the paper pays attention for the interpretation and formulation the final analyses and recommendations.*

Keywords: *liquid water content, aircraft icing, hot-wire sensor.*

1. INTRODUCTION

The liquid water content (*LWC*) is a measure of the amount of water contained in the amount of dry air, usually expressed by grams of water per cubic meter of air (g/m^3). The *LWC* is used for determining of the water content in a cloud. Clouds may contain *LWC* values from of 0.03 g/m^3 for cirrus clouds up to 3 g/m^3 for cumulonimbus clouds. Clouds contain wide range of water droplet sizes with different diameters. The range of diameters usually extends from 15 to 40 μm. Clouds below freezing often contain a mixture of supercooled liquid droplets and small ice crystals. Freezing drizzle size droplets normally extend from 40 to 400 μm. Freezing rain droplets are larger still, extending up to several millimeters in diameter.

The liquid water content, along with airspeed, air temperature, and water droplet size is one of the important parameters that affects icing on aircraft. Therefore, it is crucial to determine a suitable method for measuring the liquid water content in natural clouds or in the stream of air in an icing wind tunnel.

2. MEASURING TECHNIQUES

There are several ways that can be used to measure the liquid water content in clouds or in the flowing airstream.

One way involves cloud remote-sensing techniques. The most known are weather radars. Operational radars were not specifically designed for icing detection, but they may yield information that, when combined with that from other sources such as numerical

weather prediction models, satellite imagery, or surface observations, provides clues to the location and intensity of icing [1].

Cloud water can also be retrieved from passive microwave measurements because of its strong spectral signature and polarization signature. Clouds are semi-transparent allowing for measurement of the total columnar absorption. The absorption is related to the total amount of liquid water in the viewing path, after accounting for oxygen and water vapor absorption [2].

A laser disdrometer measures the reduction of total signal as a hydrometeor passes through a horizontally oriented laser-beam. This signal is proportional to the linear extent of the beam blocked by the hydrometer at this instant in time [3].

The icing blade and rotating cylinder, which are commonly used to measure *LWC* in icing wind tunnels, although there are very simple devices can provide accurate measurements in an icing spray cloud with a median volume diameter less than 50 μm. Both are based on the measure of thickness of ice accreting on the probe surface during the appropriate exposure time [4].

The iso-kinetic probe is less sensitive to droplet splashing, because droplets are drawn iso-kinetically into the probe. The amount of collected water is then weighed to provide a direct *LWC* measurement. The iso-kinetic condition defines a cylindrical stream tube in a spray cloud with a cross-sectional area equal to the probe's inlet area, hence, each measurement represents a discrete point in a spray cloud distribution [5].

Another way is in situ airborne measurements providing the most accurate information about cloud characteristics and detection of icing conditions.

The forward scattering spectrometer probe is an instrument developed for the measurement of cloud droplet size distributions and concentration. This probe detects single particles and size them by measuring the intensity of light that the particle scatters when passing through a focused laser beam. The instrument can size particles from 1 to 50 μm and it is capable of sizing particles having velocities from 20 to 175 m/s [6].

Optical array probe for in situ cloud droplet measurements uses the definition of the cross-sectional sample area within which droplets are detected. The sample volume is derived by multiplying the sample area by the flow velocity and the sample duration. Therefore, a bias in the sample area or in the flow velocity translates directly to a bias in measured droplet concentrations and calculated *LWC*. This probe is used for measure droplets in the range of dimeters from 15 to 450 μm [7].

The hot-wire liquid water sensors are frequently used. The wire is attached to the power supply and is situated on the outside of the airplane. As it moves through a cloud, water droplets hit the wire and evaporate, reducing the temperature of the wire. The resistance of the sensing coil is directly proportional to its temperature. Therefore, the control circuit maintains the sensor at constant temperature by maintaining it at constant resistance. A Wheatstone bridge is formed of four resistances, of which the master coil sensor is one. The power dissipated by the sensor is the product of the current through the sensor and the voltage drop across it. The power dissipation due solely to vaporization can then be estimated, which in turn gives an estimate of liquid water content.

The Johnson-Williams instrument uses two heated wires in a balanced bridge circuit. The main sensing wire is 0.55 mm in diameter and is mounted perpendicular to the airstream. It is heated at a constant voltage to a temperature above the boiling point of water. Cloud droplets impinging on the wire are evaporated, causing the wire to cool and its electrical resistance to decrease. This change in resistance causes an imbalance in the bridge circuit; the degree of imbalance is related to the *LWC*. The second wire is mounted to the airstream and is shielded from droplet impingement. This wire is connected to the

opposite side of the bridge and compensates for small changes in air temperature, air density and speed [4].

The CSIRO-King instrument employs a sensor composed of three wire coils wound around a small hollow tube. The total heat transfer rate from the coil is determined from the power required to keep the sensor coil at a constant temperature. This heat transfer rate is composed of the "dry" term, which is a function of airflow velocity, air density and air temperature, and a "wet" term, which is a function of airflow velocity and *LWC* [4].

The Nevzorov instrument is also a constant temperature device which consists of two separate hot-wire sensor systems that are intended to measure liquid water content and total water content. The sensing elements are mounted on a vane that is designed to keep the sensors aligned into the airflow. Each sensor system consists of two heated wires a sensing wire and a compensating wire. The liquid water content sensor is mounted on the leading edge of the vane and the compensating wire mounted on the trailing edge of the vane. The total water sensor consists of a wire mounted inside a cylindrical cone and the compensating wire wound in a groove around the cylinder. Each set of wires is controlled and monitored by its own set of electronics [4].

3. METHOD OF MEASUREMENT

Prices of the above mentioned systems are too high for using in the small icing wind tunnel, that is used at the University of Defence [8]. Therefore, we were seeking for some simple and less expensive sensor for determining of the liquid water content in the stream of wet air. Hot-wire anemometers have been used extensively for many years as a research tool in fluid mechanics. Measurement of fluid flow velocity is based on the fact that the probe's resistance is proportional to the temperature of the hot wire, which is influenced by the fluid convective heat transfer. If water droplets are present in an airstream, it is supposed that the impacting droplets should substantially increase the hot-wire probe cooling. This phenomenon is then indicated by increasing the measured airflow velocity. This increase in velocity due to water droplets in the wet airstream is examined for various liquid water contents, airflow velocities and temperatures.

The common commercial thermal anemometer Testo 425 was chosen as the instrument for measuring flow velocities and temperatures by means of a permanently connected hot-wire probe. View of the instrument is show in Fig. 1 (a). The hot-wire probe of the thermal anemometer Testo 425 was attached in the center of the test section of the small icing tunnel as shown in Fig. 1 (b).

(a) (b)

FIG. 1. Thermal anemometer Testo 425 (a), hot-wire probe attached in test section (b)

The one nozzle sprayer has been used for the injection of the distilled water into the annular air duct of diameter 120 mm. The resulting liquid water content in the stream of wet air is determined by: the mass of injected water, the duration of water injection, the airflow velocity, and the air duct of diameter. It yields

$$LWC = \frac{\Delta m}{v\, A\, \Delta \tau}, \tag{1}$$

where Δm is the mass (g) of water consumed in a sprayer and $\Delta \tau$ is the time (s) of this consumption, v is the airflow velocity (m/s) and A is the flow cross-sectional area (m^2).

The experiment was performed in such a way that it is possible to find a dependence between the liquid water content and the difference in velocity of the wet and dry airstreams. Differences in velocities of airstreams with and without water droplets injection were examined for various injector modes ensuring *LWC* values from zero to 8 g/m^3. A set of measurements were performed for three airflow velocities v = 5, 8 and 11 m/s and for two air temperatures 0 °C and 24 °C.

4. RESULTS OF EXPERIMENT

Results of measurement as the courses of difference in velocity Δv of the wet and dry airstreams versus the liquid water content *LWC* for three dry airstream velocities v are given in Fig. 2 at the temperature 24 °C and in Fig. 3 at the temperature 0 °C.

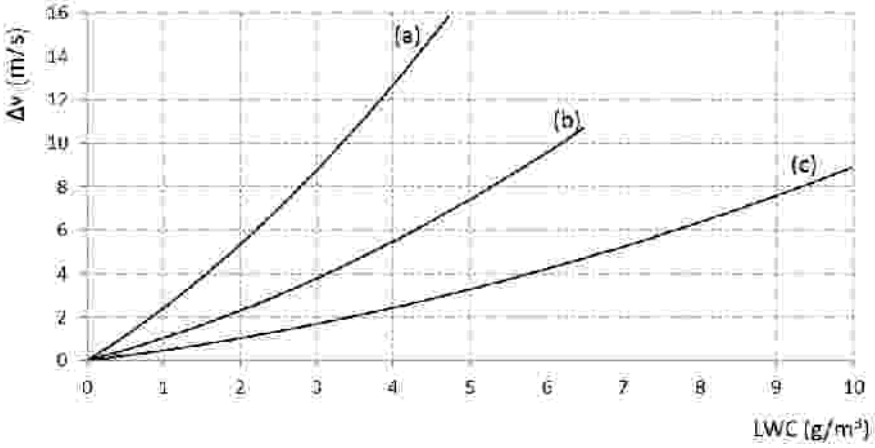

FIG. 2. Difference in velocity of wet and dry airstreams versus liquid water content at temperature 24 °C for airflow velocities: (a) 11 m/s, (b) 8 m/s, (c) 5 m/s

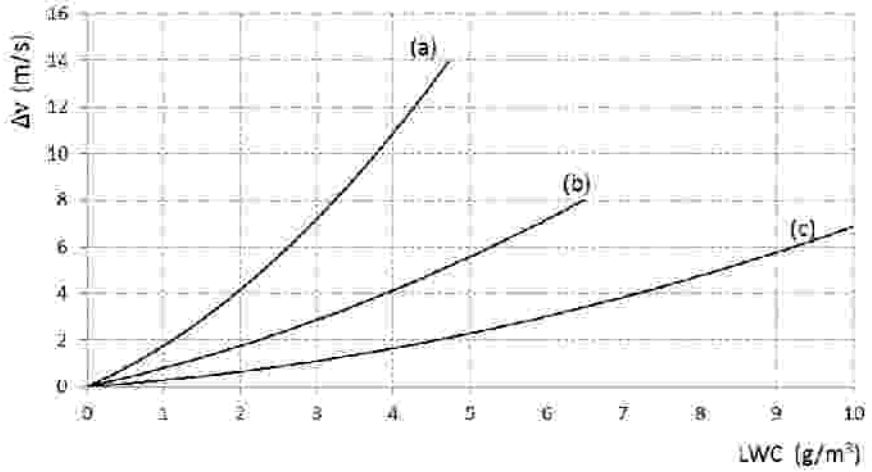

FIG. 3. Difference in velocity of wet and dry airstreams versus liquid water content at temperature 0 °C for airflow velocities: (a) 11 m/s, (b) 8 m/s, (c) 5 m/s

Presented results of measurement show us that the difference in velocity of wet and dry airstreams is a suitable parameter for the determination of the liquid water content with a substantial increase for higher airstream velocities. The influence of the temperature is fairly low.

If we are looking for the correlation between the liquid water content and the given difference in measured velocity, it seems to be rather complicated as seen in Fig. 2 and Fig. 3. However, if we express the difference in measured velocity Δv related to the airflow kinetic energy by $\Delta v/v^2$, we do obtain nearly identical courses for all airflow velocities as shown in Fig. 4. These slight differences are probably given by the measurement accuracy.

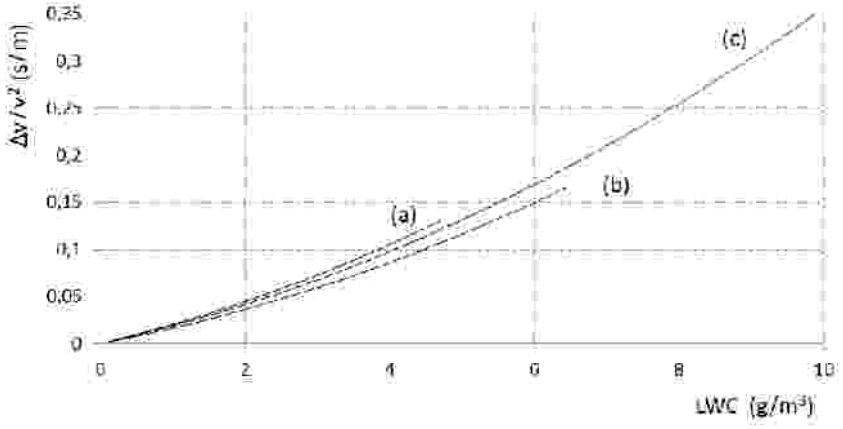

FIG. 4. Difference in velocity of wet and dry airstreams related to airflow kinetic energy versus liquid water content at temperature 24 °C for airflow velocities: (a) 11 m/s, (b) 8 m/s, (c) 5 m/s

5. APPROXIMATION OF RESULTS

An approximation of the measurement results is useful for a computer processing. The dependence of *LWC* versus $\Delta v/v^2$ is plotted for two air temperatures in Fig. 5.

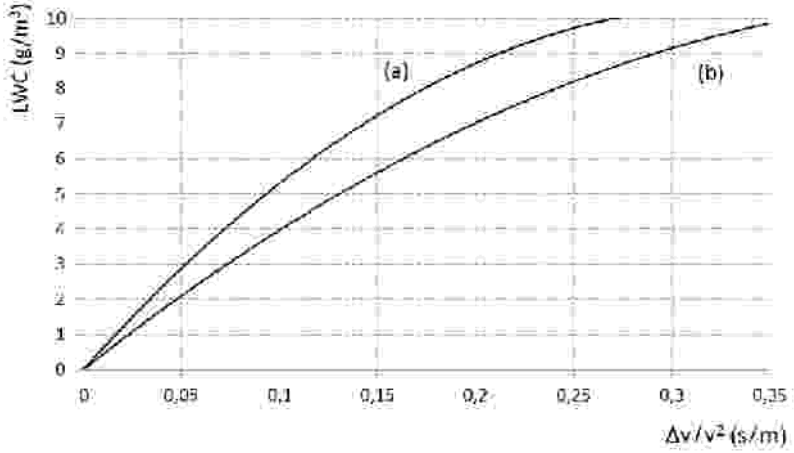

FIG. 5. Liquid water content versus difference in velocity of wet and dry airstreams related to airflow kinetic energy for air temperatures: (a) 0 °C, (b) 24 °C

The best candidate for the approximation of measured results seems to be the polynomial equation in form

$$LWC = x_1\, T^{y_1} \frac{\Delta v}{v^2} + x_2\, T^{y_2} \left(\frac{\Delta v}{v^2} \right)^2, \tag{2}$$

where T is the absolute air temperature (K).

By applying the approximation equation (2) for results of measurement, we can obtain by using the Excel processor the dependence of the liquid water content *LWC* on the difference in measured velocity of the wet and dry airstreams Δv, the airflow velocity v, and the absolute air temperature T valid for the thermal anemometer Testo 425 in form

$$LWC = 4.454\,10^{11}\,T^{-4.045}\,\frac{\Delta v}{v^2} + 2.727\,10^{22}\,T^{-8.4}\left(\frac{\Delta v}{v^2}\right)^2. \tag{3}$$

CONCLUSIONS

The low cost method for the liquid water content quantification in the stream of wet air using the thermal anemometer Testo 425 has been developed. It is possible to use this method for determination of *LWC* in an icing tunnel from differences in measured velocities of airstreams with and without water droplets spray injection.

In principle, it is possible to use the thermal anemometer also for the in situ airborne measurements, if the hot-wire probe would be placed nearby the pitot tube for determining the airspeed of an aircraft. The difference between measured velocities using the thermal anemometer Testo 425 and the pitot tube would be applied by the same way for the determination of the liquid water content.

Results of measurement and their approximation presented in this paper are valid for the given one nozzle water sprayer. The type of water sprayer determines the droplet size diameter. In future, further testing for another water sprayers is supposed.

ACKNOWLEDGMENT

The work presented in this paper has been supported by the institutional funding DZRO K 201 "VÝZBROJ" and by the specific research project of Faculty of Military Technology SV16-216.

REFERENCES

[1] M. K. Politovich, *Aircraft Icing*, Elsevier Science, p. 73, 2003.
[2] Frank J. Wentz, A Well Calibrated Ocean Algorithm for Special Sensor Microwave Imager, *Journal of Geophysical Research*, Volume 102, Issue C4, p. 8703-8718.
[3] M. J. Bartholomew, *ARM's Handbook for the Parsivel2 Laser Disdrometer*. DOE/SC-ARM-TR-137, U.S. Department of Energy, Office of Science, February 2014.
[4] R. F. Ide, *Comparison of Liquid Water Content Measurement Techniques in an Icing Wind Tunnel*, NASA/TM-1999-209643 [Report], December, p. 24, 1999.
[5] J. Tan, M. Papadakis, and S. Muthuswamy, *Development of a Reference Liquid Water Content Probe*, U.S. Department of Transportation DOT/FAA/AR-05/23 [Report], p. 135, August 2005.
[6] *Fast Forward Scattering Spectrometer Probe*. SPEC FCDP Technical Manual, p. 18, March 2011.
[7] S. Lance at al., Water droplet calibration of the Cloud Droplet Probe (CDP) and in-flight performance in liquid, ice and mixed-phase clouds during ARCPAC. *Atmospheric Measurement Techniques*, Vol. 3, p. 1683–1706, 2010.
[8] V. Horák, B. Hoření, D. Rozehnal, and E. Svoboda, Small Icing Wind Tunnel. *ICMT'07, Proceedings of International Conference on Military Technology*. Brno, University of Defence, p. 85-90, May 2007.

EXPERIMENTAL MECHANICAL DEVICE FOR RECOIL SIMUALTION

Tomáš LUKÁČ, Roman VÍTEK, Linh DO DUC, Vladimír HORÁK

Faculty of Military Technology, University of Defence, Brno, Czech Republic
(tomas.lukac@unob.cz, roman.vitek@unob.cz, duclinh.do@unob.cz,
vladimir.horak@unob.cz)

DOI: 10.19062/2247-3173.2016.18.1.46

Abstract: *The paper deals with the development and testing of the experimental, spring powered mechanical device for the simulation of the gun's recoil and further for the obtaining the experimental data for the purpose of research and development of the device for gun's recoil simulation. Several kinds of the present firearm recoil simulation systems and principles of their function are closely described and explained. Measured force diagrams for the experimental mechanical device and for the real assault rifle are presented.*

Keywords: *recoil simulation, assault rifle, SA vz.58, force diagram*

1. INTRODUCTION

Presented experimental mechanical setup was designed to provide an experimental data for the purpose of the research and development of the device for the gun's recoil simulation. The main idea for the design and development is to simulate gun's recoil and behavior as realistically as possible and therein make the training shooting more faithful. Mechanical setup was designed for the purpose of acquisition of the force diagrams provided by the present pneumatic and electromagnetic recoil simulation devices, which use the mechanical impact for the recoil force generation. Obtained force diagrams provide the image of the behavior and dimension of the generated force from the mechanical impact. These force diagrams were used further for the comparison with the real assault rifle force diagrams, obtained from the measurement on a real assault rifle. Czechoslovakian assault rifle SA vz.58 was chosen as a reference firearm.

2. PRESENT RECOIL SIMULATION SYSTEMS

Gun recoil simulation becomes a part of the shooting training firearms and devices, which raises the authenticity of so called "dry shooting". Purpose is to simulate the behavior of the firearm during the shooting more faithful and to train the shooters for the usage of the real gun with the lower costs and higher safety. At present, pneumatic and electromagnetic systems for gun's recoil simulation are used for the professional training.

2.1 Pneumatic recoil simulation systems. The most widespread recoil simulation systems are nowadays the pneumatic systems powered by the compressed air, carbon dioxide or in some cases by compressed nitrogen.

Common design of this systems is in the shape of the additional recoil simulation kit for the real semiautomatic and automatic firearms. With this kit, it is possible to convert real firearm temporarily to the training device, which provides recoil simulation and

sound effect. After a training session, the entire assembly can be quickly removed from the handgun or rifle, making the weapon available again for use with live ammunition [1].

Depending on the type of the reservoir, this kits are made as tethered, where the converted gun is connected to the external reservoir or compressor by the pressure hose, or as tetherless, where the reservoir with the power medium is stored in the firearm, mostly as the replacement of the real magazine. VirTra company provides a small belt clips with compressed air or carbon dioxide for the tethered systems. This allows more mobility than other tethered systems due to the fact that the trainee can have a small and lightweight tank on their belt or back [2].

Some producers use a liquid carbon dioxide reservoirs, located in the weapons magazine instead of pressurized gas tubes. It gives to the user freedom of movement, thus significantly widening the area of its use compared to conventional systems [3].

In the tethered systems, magazine imitation serves as a transition component between the external actuating medium source and the operating cylinder. In this systems, the actuating medium is delivered from the reservoir, or supplied by the compressor, to the cylinder with the movable piston, which replaces a barrel. When the pressure in the cylinder rises, the piston begins to move backwards and shunt the bolt, which is thrown to its rear position, where the bolt impacts to the receiver. Consequential pulse is transferred via the stock to the arm of the shooter as the recoil pulse. Quantization of the actuating medium is provided by the impact valve located in the piston head and activated by the hammer strike via the firing pin. Figure 1 shows the TRS (Tetherless Recoil System) for the pistol, provided by the company Dvorak Instruments[1].

FIG. 1 TRS recoil simulation kit [1]

2.2 Electromagnetic recoil simulation systems. The electromagnetic recoil simulation systems use an electromagnetic field, generated by the coil, to speed up the piston, which is made as the movable coil core, and throw it to the rear position to impact the receiver. In comparison with the pneumatic system, electromagnetic system provides more possibilities in the recoil simulation. The control of the electromagnetic field allows to modify the position and movements monitoring of the piston in the coil and course and size programming of the recoil force, which makes this recoil simulation system very adaptable to the various firearm types, such a pistols, assault rifles or machineguns. Whole system requires less maintenance as the pneumatic system and provides longer service life due to smaller amount of movable parts. [4]

Disadvantage of this system is in the impossibility to design it as the upgrade or a drop-in kit for real firearms. Due to this impossibility, electromagnetic recoil simulation

systems are designed as an imitations of a real firearm types. Another disadvantage is in the mobility of whole simulation system due to relatively high power consumption. Accumulator capacity depends on its dimensions and therefore it's hard to get a suitable battery pack for a longer supplying of whole system.

Therefore a lot of this systems uses an external power source, connected to the imitation firearm through a cable. Trained shooter is in this case limited in movement and the range by the length of the cable. Prospect image of the electromagnetic recoil simulation system for the assault rifle, provided by the Haptech company is shown in the Fig. 2.

FIG. 2 Haptech electromagnetic recoil simulation system [4]

3. ASSAULT RIFLE TESTING

Data for the real firearm force diagram were obtained by the measuring on the Czechoslovakian assault rifle SA vz.58. As a sensor for the force measuring, Kistler, type 9051A, piezoelectric annular force-sensor with the measure range from 0 to 120 kN was used. Whole measurement was realized on the STZA 12 mobile firing rest and data were collected with a ballistic computer, see Fig. 3.

FIG. 3 SA vz.58 assault rifle on the firing rest

Five shots before the measurement were fired due to the rifle stabilization in the firing rest. Next five captured shots shows very similar courses after the rifle stabilization and only small deviations are present, which are caused by the ammunition properties. From this sight, this measurement can be considered as very trustworthy. Figure 4 shows the obtained force diagrams for this five shots.

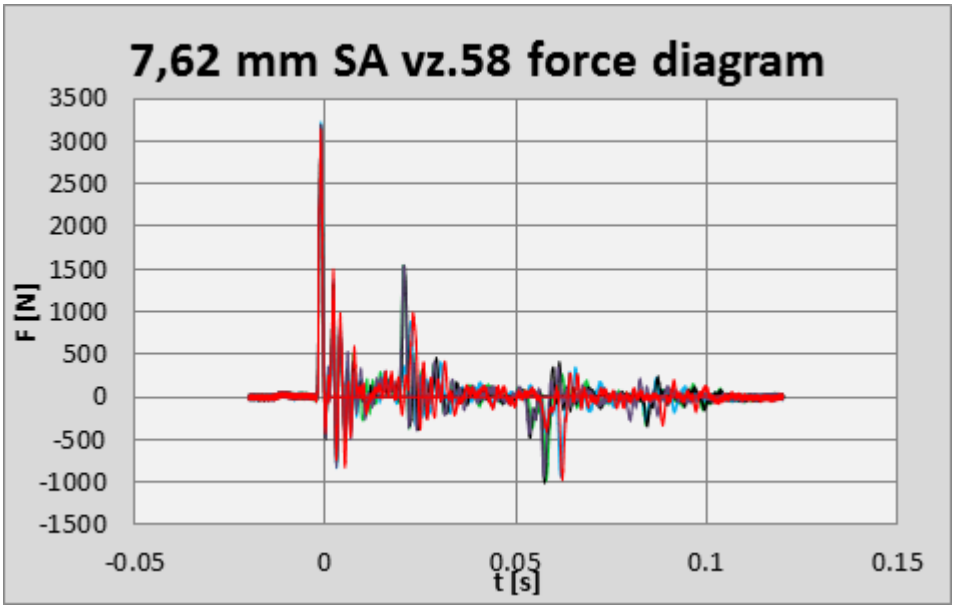

FIG. 4 Measured assault rifle force diagram

Zero time and data recording on the ballistic computer were triggered automatically by the pulse from the optical gate, generated in the point of the projectile crossing through the optical gate. The optical gate was situated 2 m from the barrel muzzle.

The first spike shows the force from the gun-shot itself, caused by the burning of a propellant. After the shot, the bolt carrier is forced to move backwards, unlock the chamber, and in its rear position impacts the receiver, which is represented by the second, smaller spike in the diagram. It's evident that the component of the gun's recoil force, caused by the impact of the bolt carrier in the rear position is comparatively smaller in the comparison with the effect of gun-shot itself.

After the impact, the bolt carrier is forced by the recoil spring to move forwards and in its front position locks the chamber and impacts on the front side of the receiver, which shows the third spike in the opposite direction. This impact is followed by the smaller impact, which shows the fourth spike and it is caused by the repeated impact of the bolt carrier in the front position.

4. MECHANICAL RECOIL SETUP TESTING

The schematics of the experimental, spring powered setup is shown in Fig. 5.

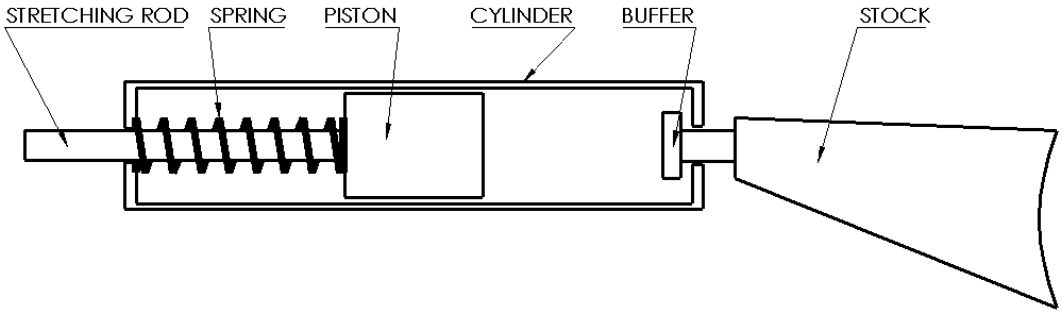

FIG. 5 Mechanical recoil setup schematics

Device consists from the movable piston of a diameter 45 mm with a spring within the closed cylinder. The function stroke of the piston in the cylinder is about 130 mm. The spring stiffness is 4.01 N.mm^{-1} and mass is 142.5 g. In the back side of the cylinder a small movable buffer is inserted, directly connected to a firearm stock. There is a locking mechanism in the front side of the cylinder, which fixes the piston in the front position. The stretching mechanism is provided by the threaded stretch rod, connected with the piston. Four pistons of a different mass are available. The resulting mass of the moving parts in the simulator is given by the formula:

$$m_{mp} = m_p + m_{sr} + \frac{1}{3} m_s \tag{1}$$

where m_p is the mass of piston,
m_{sr} is the mass of stretching rod and
m_s is the mass of the spring.

The individual masses of the movable parts in this configuration are 1321.5 g, 1383.5 g, 1444 g and 1501.5 g. A bronze was chosen as a material for the slip edges, due its better slip properties.

The final view of the experimental setup on the firing rest is shown in Fig. 6.

FIG. 6 Mechanical recoil setup on the firing rest

The measurement was realized with two different pistons with the weight 1321.5 and 1501.5 grams and the same firing rest STZA 12 with the Kistler 9051A force-sensor was used. Several free runs were realized before the measurement due to the device stabilization in the firing rest. Obtained force diagrams for the five runs with heavier piston are shown in Fig. 7.

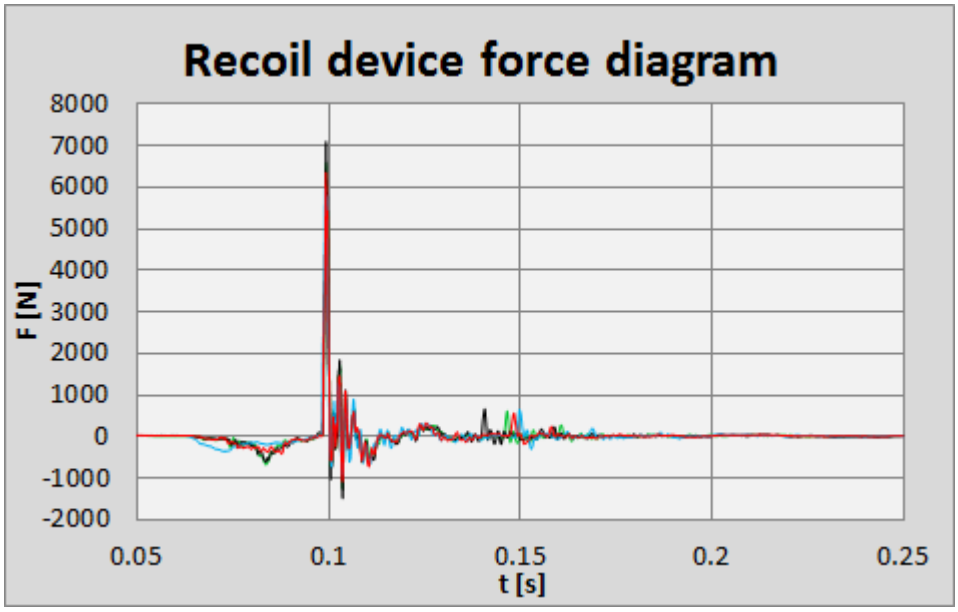

FIG. 7 Mechanical recoil device force diagram(heavier piston)

All captured force diagrams after the initial stabilization shows again almost identical courses, what makes this measurement representative and repeatable. Data capturing was started manually on the ballistic computer.

The straight line in the beginning of the diagram represents the reaction time of the experimental setup operator between the data recording activation and the point of the piston release in the experimental setup after its activation.

The next negative spike is caused by the acceleration of the the piston after its release, due to the closed, spring powered system. During the forced motion of the piston to its rear position, whole setup is forced by the spring to move in opposite direction. This effect is present in every pneumatic and electromagnetic recoil simulation system which uses a movable piston. Duration and the size of this pulse depends on the dynamics of the system and on the length of the piston stroke. Influence of this pulse on the shooter depends on the strength with which is the gun held and it can be very different between the different trained shooters.

The second spike in the diagram is caused by the impact of the piston on the buffer head in its rear position and via the stock is transferred on the arm of a shooter as a recoil pulse. Following small spike in the time about 150 ms is caused by the repeated impact after the reflection of the piston from the buffer head.

Figure 8 shows the five captured force diagrams for the device with the lighter piston installed. The measurement conditions were the same as in the previous measurement with the lighter piston.

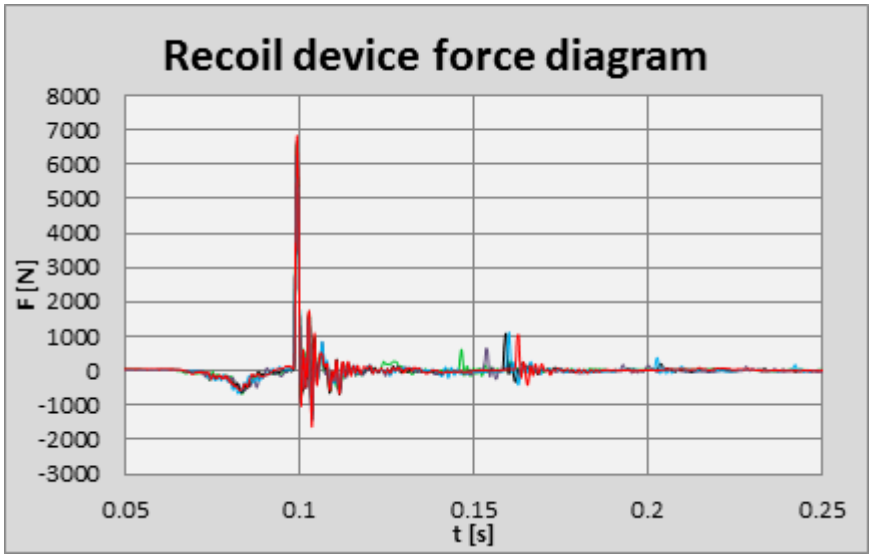

FIG. 8 Mechanical recoil device force diagram(lighter piston)

The course of the force is almost identical in this configuration and proves that the mass of the piston is not critical as expected in this conditions.

CONCLUSIONS

The presented mechanical experimental device represents a first phase in the research and development of the device for gun's recoil simulation, which should simulate the gun's recoil as close as possible. The measurement provided a refreshing results and shows that the mechanical impact of a relatively small piston can provide even bigger force effect than an ordinary assault rifle. In the future work, the spring powered mechanism will be replaced with the carbon dioxide used as a actuating medium. Interaction between the shooter and the firearm will also be studied.

AKNOWLEDGMENT

The work presented in this paper has been supported by the institutional funding DZRO K201 "VÝZBROJ" and by the specific research support project of the Faculty of Military Technology SV16-216.

REFERENCES

[1]Dvorak Product listing and descriptions, *TRS Firearms training systems*, http://www.stressvest.com/pdfs/dvorak_tetherless.pdf [online, retreieved 9.3.2016];
[2] VirTra, *Standard recoil kits – Weapons Simulator*, http://www.virtra.com/tethered-recoil-kits/ [online, retrieved 28.2.2016];
[3] *Recoil simulation equipment*, http://eli.ee/products/1/recoil-simulation-equipment.html [online, retrieved 28.2.2016];.
[4] *Haptech product descriptions*, http://www.haptech.co/products [online, retrieved 2.3.2016].

MECHANICAL ENGINEERING. MATERIALS AND TECHNOLOGY

THE IMPLICATIONS OF RANDOM VIBRATIONS GENERATED BY ROUGH AND HARDLY ACCESSIBLE TRAILS ON MILITARY BODY

MarianMITROI*, Cornel ARAMĂ**

*Faculty of Mechanical Engineering,"Transilvania" University of Braşov, Braşov, Romania (ejju_marian@yahoo.com)
**"Henri Coandă" Air Force Academy, Braşov, Romania (aramis5791@gmail.com)

DOI: 10.19062/2247-3173.2016.18.1.47

Abstract: *During their operation, vehicles are subject to shocks and vibrations that come directly from internal sources and from external sources.The vibrations caused by vehicles tread bumps are random vibration and excitation and response are deterministic processes. Measuring the response involves recording and analyzing the vibration while on the go. If the value is too high amplitudes, vibration may cause temporary or permanent damage to the internal organs of the human body.*

Keywords: *random vibration, limits values, oscillation effects*

1. INTRODUCTION

The vibrations are a mechanical agent, with a toxic action on the military personnel and on the military equipment used by them during the missions and is in general characterized by: frequency, amplitude and period.On the whole vehicle, itself a source of harmful vibrations and oscillations, which propagate in different frequency ranges, manifesting the no suspendedand suspended masses.

The extra-urban displacement in inaccessible terrain or off road specific actionable intervention of special forces,overpower the vehicles to high stresses, create problems for drivers, sometimes there is the need of interrupt the movement.

2. RANDOM VIBRATION

In any travel regime, and on any type of road, vehicle movement is accompanied by the appearance of vibration and shocks.The irregularities of the surface are the main external source of shocks and of vibrations on vehicles.

The way of manifestation of the vibrations and of their damping on the unsuspended and suspended masses is shown in FIG.1.

The unevenness of the driveway creates shocks on the wheel, these being converted to low frequency oscillations through the tire and through the suspension, being subsequently transmitted to the structural frame of the vehicle and hence to the seats.

The perturbations generated by the irregularity of the runway may vary approximately after a law close to the periodical one. The profile of the runaway is characterized by the size (l, h) and by its shape, by the sequence and the frequency of irregularities.

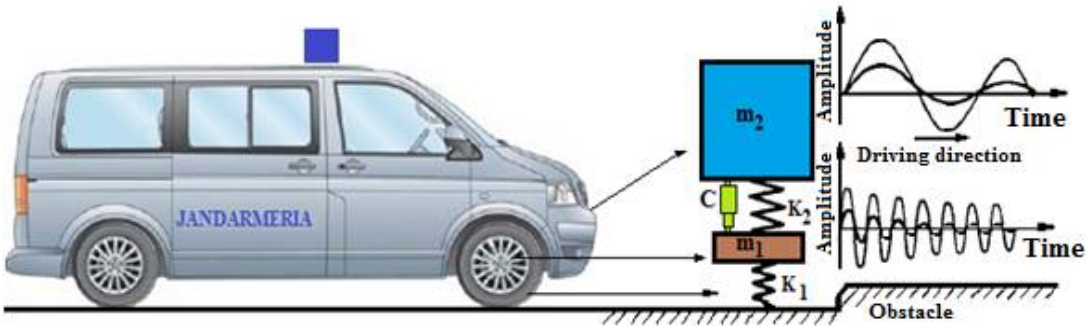

FIG. 1. The depreciation's influence over the suspended and unsuspended masses **[1]**

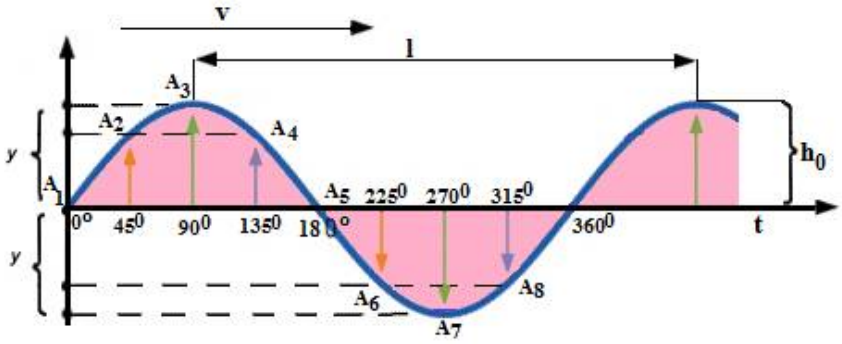

FIG. 2. The sinusoidal profile of the road and representation of the amplitudes**[1]**

Making a simple analysis of it (FIG. 2), we can see:

* If we take into consideration that the irregularities' profile is sinusoidal, the equation of the runaway profile is of the form:

$$h = 1/2h_0(1 - \cos wt) \quad (1)$$

where:

$w = 2\pi v$ the disturbing pulsation; (2)

v = the speed of vehicle;

l = the length of shading.

y = the wave front = A - amplitude;

A_3 = the maximum positive amplitude;

A_7 = the maximum negative amplitude.

* If the irregularities' profile is half sinusoidal, the equation of the tread has the form:

$h = h_0 sin\omega t$ where :ωt∈ [0, T] (3)

However, the road action on road vehicles can be observed based on knowledge of static characteristics of their profiles.

There are situations where the tread has a more complicated form and cannot be described by a simple harmonic function, then are use regular functions expressed by Fourier series:

$$h(t) = b_0 + b_1 \sin(\omega t + \varphi_1) + b_2 \sin(\omega t + \varphi_2) + \cdots + b_n \sin(\omega t + \varphi_n) \quad (4)$$

where:

b_0, b_1, b_2, ..b_n = the amplitudes of harmonic components;

ω = the angular frequency disturbing.

In fact, the interaction between the vehicle's wheel and the road's surface has a random profile, the function

h (t) can be expressed by the equation:

$$h(t) = \int_0^{\infty} b sin(\omega t + \varphi) dt = \int_{\infty}^{\infty} b e^{i\omega t} d\omega \quad (5)$$

This mathematical expression allows the characterization of the tread's action on the vehicle according to its static properties.In the case of such headlands, the main difficulties are related to the rolling resistance force on the wheels' rotation, which occurs between the contactof the tire with the ground deforming it, and between the multitude of oscillations in different amplitudes, which occur during the displacement. The speed of displacement varies depending on the angle of inclination, on the angle of attack of wheels, and on the present weather conditions. In such circumstances it is necessary the prolonged use of a lowergear, to ensure the dynamic factor which is necessary for certain portions of the road, which generates a forced operating regime of the engine and of the transmission, which contributes to increase the oscillations generated by the assembly tire-wheel and in the same time to increase the level of discomfort for the existing staff in the vehicle.

There are situations when the military actions must be conducted suddenly, in a limited time, which requires the acceptance by all participants to the action of a extreme discomfort, where shocks and vibrations transmitted to the body and seats have high values and are even harmful for the human body. [1]

3. LIMIT VALUES OF THE OSCILLATION PARAMETERS

During displacements, the discomfort is felt by people in the vehicle when the level of oscillations transmitted by the vehicle's structure exceeds a certain spectrum frequency and amplitude.

The energy of these vibrations is received by the body and subdued, being absorbed by soft tissues and by internal organs to certain values or amplified according to the mechanical laws of vibrations. The man being fragile being, perceives and manifests differently from one person to another when is exposed to shocks and to oscillatory phenomena, the responses of the human body depending on factors such as bone structure and musculature, its dimensions, the frequency of the oscillations and their amplitude, their duration of exposure, the body posture during the analysis etc.

The individual perception of the fluctuations is a subjective issue so that, the assessing of the effects of vibration can be given by certain baselines:

- The thresholds of perception of oscillations by each individual;
- The individual tolerance thresholds oscillations charged;
- The bothering thresholds.

Exceeding these stages of values causes involuntary and voluntary muscle contractions, local muscle fatigue at the resonance frequency, causes a disorder of the psychological balance etc.

The reactions of the human body are psycho-physiological reactions so that in addition to the structure of the individual it is also important his/her familiarity with such perceptions, the age is particularly important, young individuals supporting different oscillatory phenomena compared to the age and also to sex.

The resonance system values are different for each part of the system, according to the studies of Rasmussen [4]. The mechanical proposed model for the human body is shown in FIG. 3.

According to that system was studied the human body's response to the effect of shocks and oscillations, at different frequencies for standing and seated positions, specific vehicle's positions.

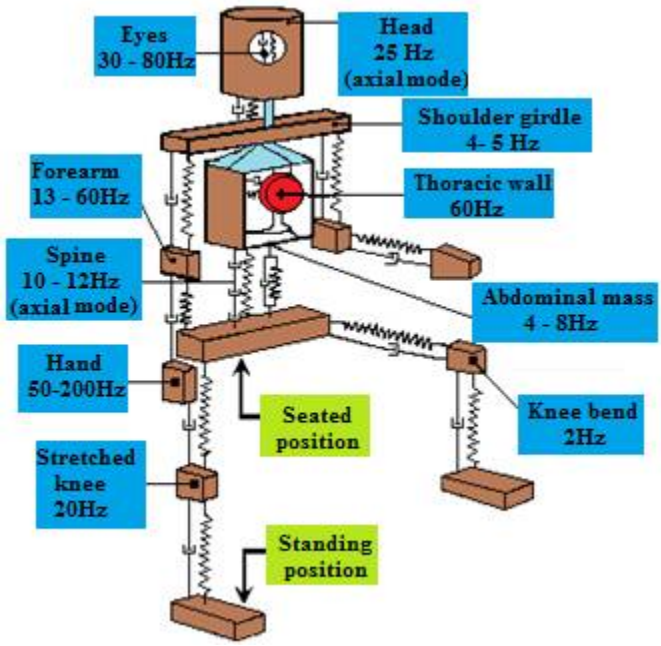

FIG. 3. The resonance frequencies of the human body **[4]**

This linear system, with concentrated parameters can be used with greater precision for low frequencies up to 100 Hz, but also for lower levels of vibration. The analysis has shown that in the longitudinal direction, from feet to head, the body is more sensitive to vibrationsfrom 4-8 Hz range, and in transverse directionto those from 1-2 Hz range[4].

Taking into considerationthe running time through some rough terrain, to fulfill the tasks imposed by missions, the travel done in long periods of time, we can understand that the exposures to fluctuations generated by the route are very important and should be carefully evaluated.

The forces applied achieve the maximum value within a few tenths of a second, manifested in a very short time, can be called forces applied by shock and usually occur in addressing obstacles appeared suddenly along the runway or after collisions. Any biological system may be influenced by vibrations and shocks, if their amplitude is large enough.

The gravity of produced lesions depends on the value of the acceleration taken at the time of the shock's happening and can occur: bruises, broken bones, concussions and crushing tissue.

The pressure generated by the human body on the seat can disrupt the blood's flow on the body and thighs, and in time, creates permanent damage to soft tissue and capillaries. The pressure of distribution on the seat's surface is closely related to the weight of the driver and to the curvature of the seat. Thus, the pressure created at the interface seat - driver is an important factor which affects the state of comfort and relaxation.

In the following image (FIG. 4) are observed the directions of perception of vibrations and shocks through the accelerometer and in the manifestation zone in a seating position.

Taking into account the concrete conditions of the military actions, the specific training of individuals and the used equipment, this model can be radically influenced, as follows:

- Head - the presence of the protection helmet and of specific equipment;
- Pectoral arch – the bulletproof vest collar, the extra weight due to the presence of protection helmet and of accessories and the specific training;
- Chest wall - trained body armor and body;

- Abdominal mass - bulletproof vest and specific military training;
- Feet – the boots' presence and the specific training;
- Hands – the gloves' presence, weaponry and specific training;
- Backbone - bulletproof vest;
- Hearing aid – the presence of ear plugs;
- Visual apparatus - the presence of eye protection.

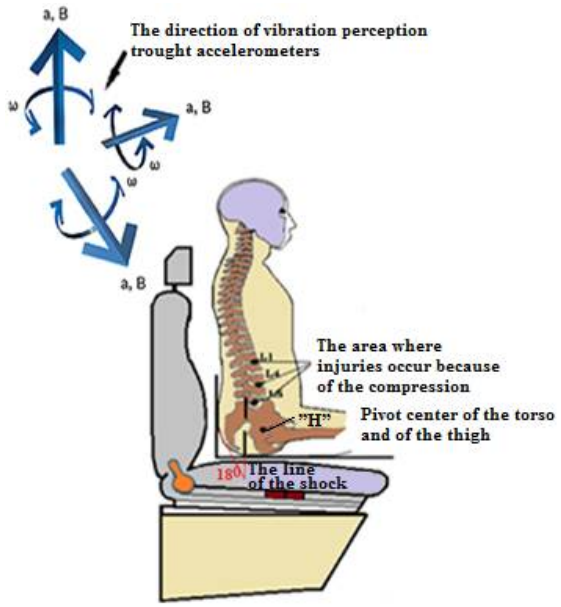

FIG. 4. The line expressions of shock in a seated position **[1]**

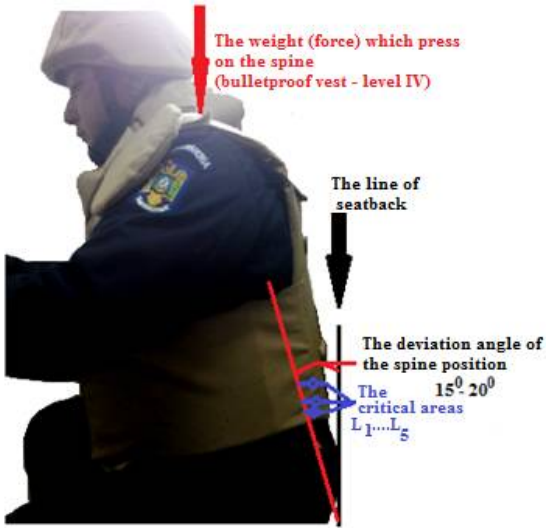

FIG. 5. The changing military position in the car seat **[1]**

As a result of those mentioned in the preceding paragraph, the model proposed by Rasmussen, in the case of soldiers from special forces who move to interventions, there is required to be modified taking into account the reportedelements. There must be taken into consideration the following conditions, which modify the welfare of the body and the influence of vibration on the militaries' body:

- Long journeys and very dangerous routes, after a certain period of time create an oppressive state on the military, which require them to adopt a more convenient seat position in the chair, but medically incorrect. This incorrect position generates the alteration of the zone and causes cervical spondylosis. The position adopted by the military people during long journeys under the influence of runways' vibrations and shocks can be seen in Figure 5.

4. THE VIBRATION AND SHOCK'S EFFECTS ON THE HUMAN BODY

The human behavior under the action of vibrations is influenced by four important characteristic values: intensity, frequency, direction and duration. To study the response of the human factor to the vibrations' action upon itself it must be taken into consideration also the mode of their transmission. There are encountered the following situations:

- Vibrations transmitted simultaneously to the entire surface of the human body or to a major part of it;
- Body vibrations transmitted through aid surfaces (the case of vehicles);
- Vibration transmitted through some body parts: head, hands and feet by hand rails or by the systems of action.

Experiments have shown that the human body due to its anatomical construction tolerates vibrations better in the direct direction than in the lateral one. The sensitivity of the human body is raised from legs to head, to the vibrations in the range of 4-8 Hz, and on the horizontal direction in the frequency range of 1-2 Hz. The attenuation for the vertical position, from toes to the head is 30 dB, and from the body to hands when the steering wheel is used is of 40 dB.[2], [3].

The vibration effects can be seen in various aspects:

* *the physical effect* - occurs due to the direct interfering of the vibration with the physical activity performed by humans, which leads to a reduced performance of certain activities, to hinder some human processes;

* *the mechanical effect* - occurs as a result of exceeding certain limits of propagation and are characterized by the presence of lesions, the most common being those of lung and heart ruptures or the destruction of soft tissues;

* *the biological effect* - occurs due to the stimulation or excitation of the sensorial receptors or of the nervous system and leads to the appearance of fatigue, or to a decreased alertness and of the ability to work, and in some cases to hormonal changes or gastric secretion. This type of effect is also associated with the emotional reactions that lead to behavioral changes of the individuals.

When vibrations are propagated vertically, the unpleasant effects are felt to maximum values of the acceleration for: frequencies f <5 Hz, for maximum speeds between 5 Hz <f <40 Hz and for maximum values of displacement f> 40 Hz. Regarding the vibrations propagated horizontally, the strength of the human body is approximately two times lower, their effects being felt to maximum acceleration for: frequencies up to 2 Hz, to maximum speeds for frequencies between 2 and 25 Hz, and in the moment of traveling to f> 25 Hz. [2], [3].The human exposure to vibrations can be measured by the following criteria, depending on the purpose (Figure 6).

The vibration exposure limits are set differently, depending on the chosen criteria. The sizes and the acceptable limits used in analyzing the influence of vibrations on the human body have been established for sinusoidal oscillations and in situations of random regimes, the assessment of exposure to vibrationsbeing made using static characteristics, such as the square average, the medium value of the maximum levels for a certain period of time.

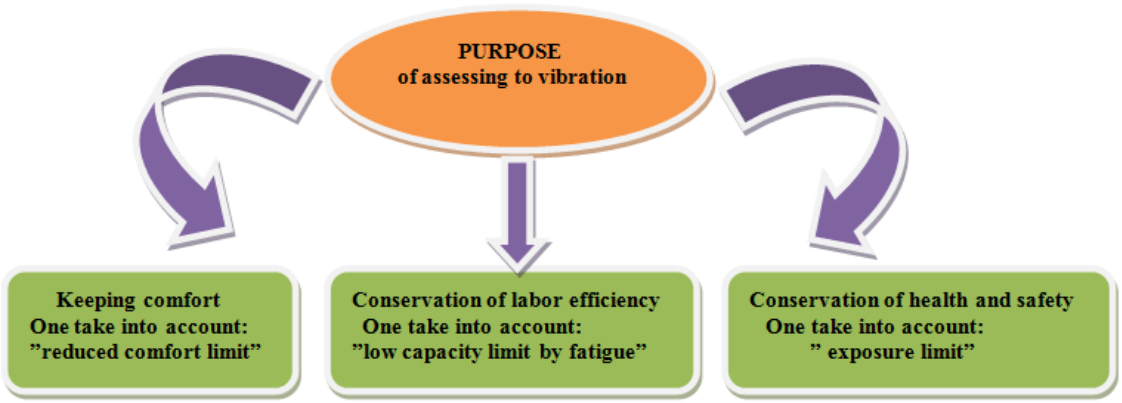

FIG. 6. The purpose of evaluation of human exposure to vibration [1]

5. CONCLUSION

On the human body, the oscillations caused by vehicles have harmful effects, leading to the occurrence of discomfort, fatigue, and in some cases to chronic diseases. The body vibration sensitivity depends on the direction and on nature of the oscillatory movement. The oscillations produced by the vehicle,in different directions,have different frequencies and amplitudes, even in the case of simple sinusoidal excitation. The style of driving of the vehicles is another crucial criterion related to the movement and to the driving comfort offered by them during the move, on different runways,knowing that each individual has hisown temperament, has a certain degree of resistance to stress, has a certain basic knowledge related to moving in different road conditions, related to the properties and to the technical possibilities of the vehicle, factors which influence the degree of comfort during driving.

The base of researches in the field must be developed for higher motor speeds, knowing that a rough road is approached with a slower speed by each driver. The reduction of the values product by these in order to improve the comfort is a very complex issue and requires a thorough analysis of the causes that generated them.

REFERENCES

[1]. Mitroi M., - Report No.3 for thesis *Equipment and procedures to assess comfort of motor vehicles,* Braşov, 2016.

[2]. Panaitescu-Liess R. - *Biomechanical modeling of the human body under the action of vibration*, PhD Thesis, University of Architecture, Faculty de Utilaj Technology, Bucharest, 2013.

[4]. Poddan G.S, Griffin .M.J. - *Evaluation of whole-body vibration the vehicle*, Journal of Sound and Vibration 253 (1), p195-213, 2002.

[5]. Rasmunssen G. - *Human Body Vibration Exposure and Its Measurement*, Bruel&Kjaer brochure 1996.

MECHANICAL ENGINEERING. MATERIALS AND TECHNOLOGY

CAD - CAM PROCEDURES USED FOR RAPID PROTOTYPING OF AN ELECTRIC MOTOR DRIVING SHIELD

Luminita POPA*, Vasile POPA**

*"Transilvania"" University, Brasov, Romania (mluminita2001@yahoo.com)
**" National Defence University ,Carol I" Regional Department for Defense Resources, Bucharest, Romania (vasilepopa2001@yahoo.com)

DOI: 10.19062/2247-3173.2016.18.1.48

Abstract: *The paper presents CAD-CAM procedures used for rapid prototyping of an electric motor driving shield. Computer Aided Design is an activity that uses a computing system in the modification, analysis and optimization of design. The computing system consists of hardware and software optimized design. The prototype models used by CAD/ CAM, allow a rapid improvement and an efficient design. A particular advantage of used CAD/CAM procedures refer to the fact that these components can be adequately and effectively tested before the prototyping, in terms of mechanical stress, due to previous simulations, eliminating all costs which means waste or adjustments.*

Keywords: *CAD-CAM, prototyping, electric motor, driving shield.*

1. INTRODUCTION

In a society of sustainable development, consumption should be streamlined and rationalized and waste production must be minimized. Modern trends require high technologies which afford a higher power density and, therefore, the continuous monitoring of process flow becomes a necessity; In order to increase the reliability, nowadays there is a tendency of CAD-CAM integration tools. Computer technology has greatly influenced the structure of machine tools. The proper product to current requirements should include features that meet the relevant points on ease of assembly, recycling (disposal, reuse, etc.), environment (pollution in the production, use and disposal), user interaction and ease of use (for ergonomic reasons), among others, which do have a significant increase in product time analysis made by different domain designers. Thus, it is necessary to use Computer-Aided Design systems, Computer Aided Engineering, Computer-Aided Manufacturing (CAD, CAE and CAM) and design standardization. These systems are allowing a more efficient communication between different systems [1]

2. THE TECHNOLOGY OF MANUFACTURING OF ELECTRIC MOTORS SHIELDS

The shape is dictated by the design of the shield: the type of used bearing; bearing position on machines; the connection way with the case. An economical way to achieve high dimensional precision of parts is the modeling, simulation and processing CAD technology.CAD technologies have made the transition from traditional power tool to a computerized machine, able to act intelligently.

3. CAD ENVIRONMENT AND CAM PROCEDURES

In the literature, CAD / CAM is an acronym that means using computer design and manufacturing. This innovative technology that uses digital computers to conduct various design and manufacturing functions tends to fully integrate these activities which, traditionally, have been regarded as two distinct and separate functions. Overall, CAD /CAM develop future enterprise advanced technology, full assisted by computer. The computing system consists of optimized for design hardware and software. Within CAD activity, based on executing drawings, were made 3D models of shields. Based on the overall design, taking into account the existing links between the components, it has been established asynchronous motor assembly. CAM includes indirect applications in which the computer has the support role for manufacturing operations.CNC machine tools are designed to change the shape and size of objects in terms of productivity, dimensional accuracy and quality of machined surface. I followed the issues such as energy consumption, process complexity and costs.

The emergence and integration of CAD/CAM systems within the production process, enabled engineers to create 3D CAD project, to generate trajectories in the generic language of CAM system and then to perform conversions in multiple languages.

The CAD and CAM activities are closely interdependent, because CAD is underlying CAM activities.CAD tools are defined based on three concepts: geometric modeling, computer graphics and design tools . CAM tools consist of the intersection of three fields used in manufacturing: CAD tools, network concepts and machine tools. .

Computer-aided manufacturing – CAM is defined as the use of a computer system in planning, management and control of the operations of a plant ,by any direct or indirect interface between the computer and production resources.

4. THREE-PHASE INDUCTION MOTOR

Three-phase induction motor is the most electric motor used in electric drivers (Fig. 1).By means of electromagnetic induction, the rotating magnetic field will induce a voltage in rotor windings. Regardless of the type of engine, it has based on its construction two main components: stator and rotor. Other design elements are shown in Fig. 2:

FIG. 1. Three phase asynchronous motor

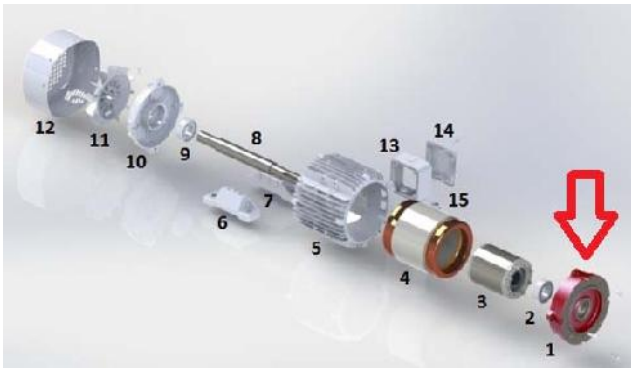

FIG. 2. Motor assembly components:
1- shield drive, 2 and 9 bearings, 3- rotor cage, 4- stator, 5- housing, 6 and 7 feet, 8- rotor shaft, 10- shield fan, 11- fan , 12- protective hood, 13- terminal box, 14- cover, 15- gland.

5. DESIGNING A SHIELD DRIVE IN SOLIDWORKS

For CAD modeling, as software environment, we used SolidWorks and for tool trajectory simulation was used ESPRIT program. SolidWorks software is a CAD software that offers powerful features allowing automating tasks and optimizing the technological process.

For the mark "shield" of the electric motor, the design was executed in Solid Works 3D program, after which the machine codes have been generated using ESPRIT program. The machine code generation is made automatically and the choice of cutting tools required for processing is made manually. To achieve the electric motor driving shield, we were started to outline its section (Fig. 3), following both the casting of blank odds and execution plan quotas (Fig.4).

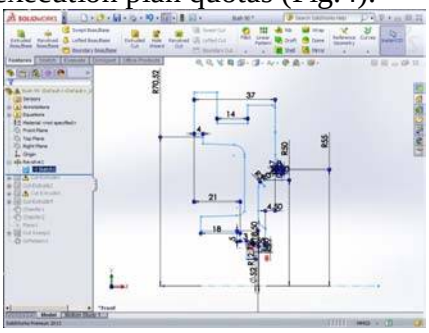

FIG. 3. The outline section of driving shield

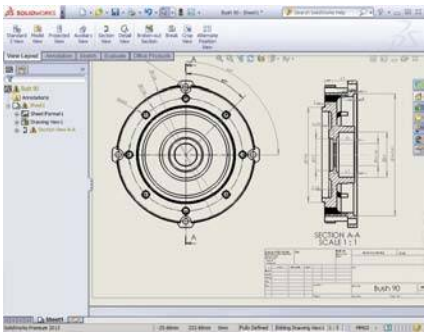

FIG. 4. The execution plan of driving shield.

The next step was to use the REVOLVE command, which has generated the solid body of the piece.

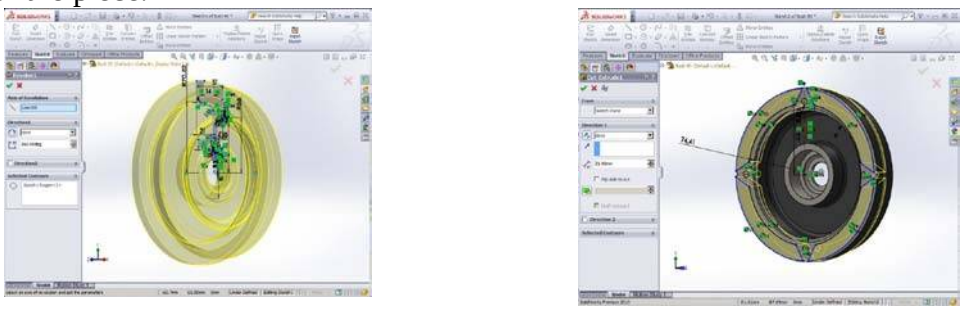

FIG. 5. Generating driving shield lugs

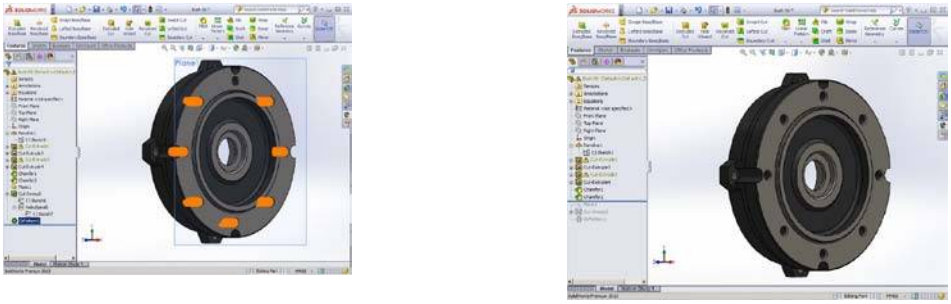

FIG. 6. Making holes

The functions ,,Chamfer 1"and ,,Chamfer 2" had achieved the edges beveling and holes for internal threads execution (Fig. 6).

To mark the processed areas, we have selected their surface by editing surfaces texture. In order to solve this issue, we have chosen from the SolidWorks library texture of the material processed ,, machined steel "(Fig. 7,8).

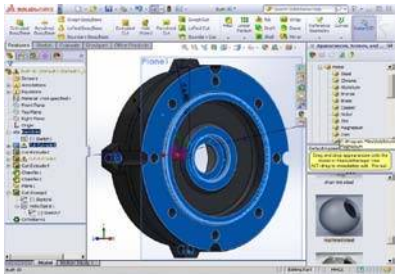

FIG. 7. The outline section of driving shield

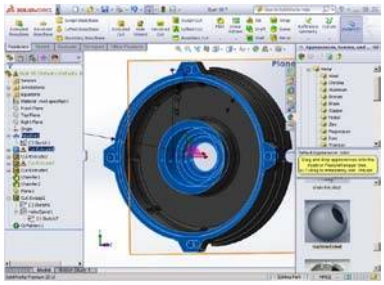

FIG. 8. The execution plan of driving shield.

The final model of piece after completion of design stages (Fig. 9).

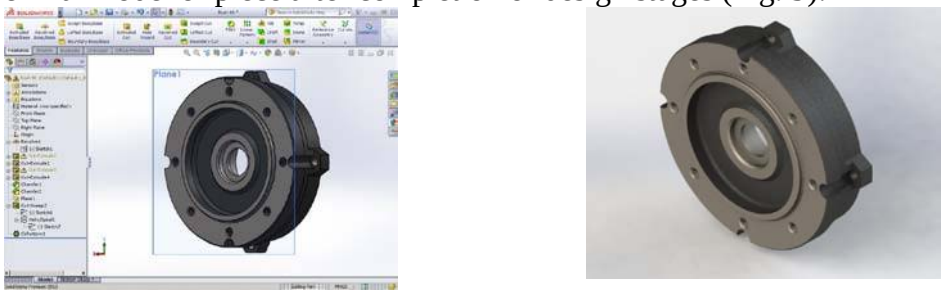

FIG. 9. The final modeling

Using the rendering process I have achieved a realistic image of the piece after modeling phase (Fig. 9).

After we have being obtained CAD models, we can open this model using EspritCam 3D (* .esp)

Since ESPRIT is based on the Paraslid kernel, it is adept at opening a variety of solid model files such as 3D files from other CAD systems as SolidWorks or Pro/ E, files and translated files Such as IGES and Step.

ESPRIT CAM (developed by DP Technology) has developed and adapted a whole library of postprocessors for the whole range of machines OKUMA, has created optimized machining strategies for any type of processing, highlighting the high-technology and OKUMA machinery power, regardless of their configuration. Since the ESPRIT CAM is 100% Windows compatible, can be installed directly on the OSP control of OKUMA machines, can achieve programming, programs testing directly on the machine, and any changes that should be made in the program, can be made directly on CNC's machine without the need to first make the adjustments on your PC and then to be transferred to the machine, thereby reducing setup times of the machine. The manufacturing processes of engine component assembly, made by ESPRIT software are: roughing and finishing on the right part of the face (Fig. 10); milling bay for fixing screws (Fig. 11); lugs drilling for fixing the shield on the electric motor assembly and internal threads pre-drilling (Fig. 12); holes tapping (Fig. 13); roughing and finishing of inner diameter (Fig. 14).

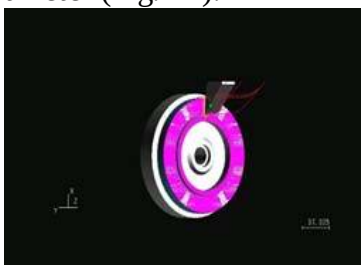

FIG. 10. The outline section of driving shield

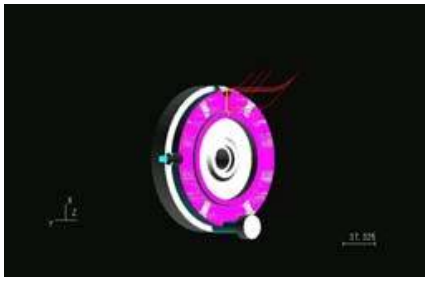

FIG. 11. The execution plan of driving shield.

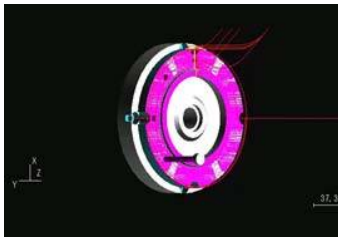

FIG. 12. Lugs drilling

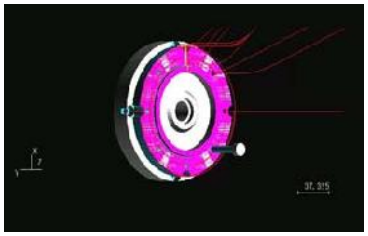

FIG. 13. Holes tapping

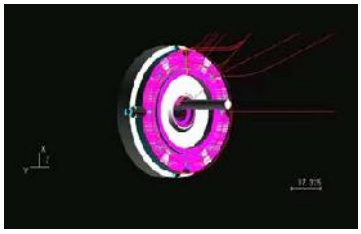

FIG. 14. Roughing and finishing

The program is transferred to Okuma machine as illustrated below (Fig.15):

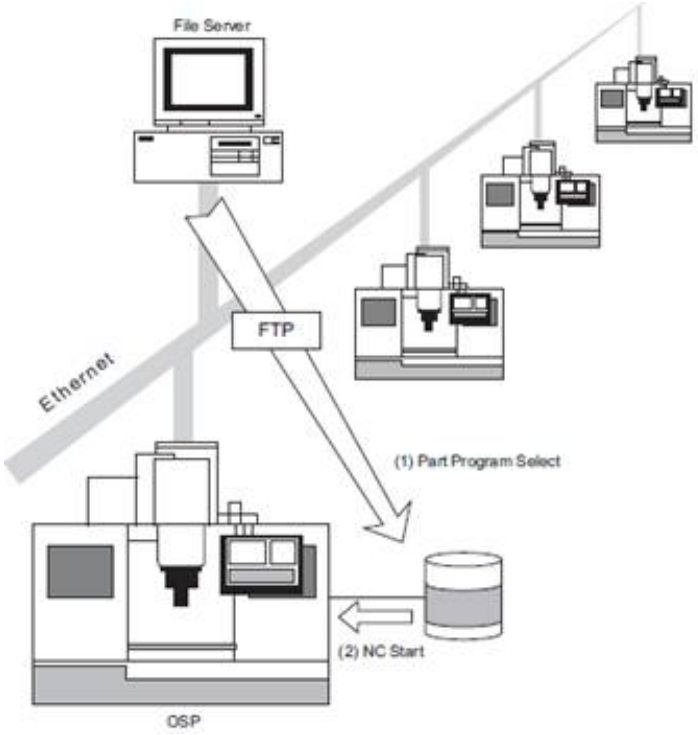

FIG. 15. The program transfer to Okuma machine

5. DETERMINATION OF THE CUTTING REGIME PARAMETERS

Cutting regime parameters are fed into the machine controller and further the process computer determines the cutting regime optimum.

Processing technologies of engine assembly components

The driving shield is made of cast iron and went through several technological operations on a CNC machine tool. The driving shield can be processed by: turning, rotary milling, outside broaching and grinding.

The conical surfaces are manufactured by turning and grinding.

Turning

The lathe is a machine that provides the power for piece turning at a determined rotational speed and for cutting tool advance along and depth of work piece. Turning is accomplished by combining the main rotation movement (usually executed by the piece), with the advance movement of the knife.

The advance movement is generally rectilinear in longitudinal direction, transverse or after an inclined direction, relative to main axis movement (Fig. 16)

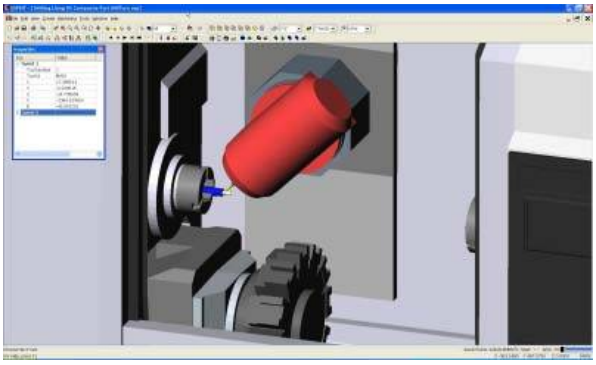

FIG. 16. The advanced movement operation

The machine-tool choice is made on economic criteria: processing operation with minimum value cost price.

The choice of the cutting tool

With the fixing of processing operations, the working tool type is indicated by default. After establishing the cutting tool type and knowing the machining surface and work stage (finishing, semi-finishing or roughing) we choose up the tool with the optimal appropriate geometry. We are choose the cutting tool material taking in consideration the nature of the processed material, its physical and mechanical properties and the adopted cyclonic. If the surface processing can be performed by several versions of the same operation, the choices require the use of different tools; In this case, our tool choice is based on the calculation of the economics compared to the two versions of processing. The cutting tools used for the driving shield processing are: turning knife for outside roughing WNMG, turning knife for outside finishing CNMG, 14mm diameter cutter, 6.8 mm diameter drill, M8 tap, turning knife for inner roughing CCMT. Depending on the destination knives can be: machining knives for roughing or finishing of outer surfaces; machining knives for interior surfaces processing; processing knives for the interior or exterior profile surfaces

Description and operation of CNC machine

FIG. 17. Computerized machine tool

FIG. 18. Components of a CNC machine

A CNC lathe are using mathematics and different coordinate systems for processing received information, following which determines the piece machining process. The precision and accuracy of movement are two important functions of the CNC machine. Most CNC machines have at least two directions of movement during a process (two axes).The axes ensure precise movement and positioning within a movement interval. The machine movements must lead to some machining tool as following: on a certain route; a precise speed of rotation of the shaft; a precise forward speed of the tool.

Components

A CNC machine (Fig. 17,18) consists of two main components: the machine-tool proper (lathe, planer, drill, boring or laser cutting machine, etc.) and data processing unit (controller) required to control machine axes. Also, there are auxiliary components: a computer permanently connected to the machine for the process modeling and simulation and to achieve processing programs.

CNC production process

Programming a CNC machine is achieved by three methods:

Manual - is carried out line by line by the programmer and produce the most compact and optimized processing programs;

Assisted - it is easier way to achieve, because the basic forms are stored in a data library and the programmer only selects those required;

Using a CAM (Computer Aided Manufacturing software - is the most complex form of programming and can be done on a personal computer and transferred directly into the machine's memory.

CNC Modes of operation

CNC machines are provided by default with different operating modes.

The control units are designed to enable the operator to use the machine in three different modes.

These modes have practical uses for production process improvement

The three modes of operation of a CNC machine tool:

The manual operating mode

In this mode, the operator can make manual positioning of the machine, can give the command to references research axes, can start and stop the tool rotation or coolant function. Generally, in manual mode, the operator can operate the various buttons and menus to realize the operations. Any operator order will have immediate response from the machine.

MDI (Manual Data Input) operating mode

The commands which cannot run in *manual operating mode* can be executed in MDI mode. This operating mode allows the operator to enter data into the CNC controller. On the latest generation CNC machines, the MDI technique is used to make manually operated commands. All information is displayed on the programming console display. It should be borne in mind that the operator to be careful when enters a command in MDI mode (Fig. 19), because the command will be executed without validating data entry, there is a danger of collision.

The automatic mode

In this operating mode CNC machine automatically running the programs (Fig. 20,21).

It is the normal operating mode of the machine.. The program is red from the machine's memory.

FIG. 19. MDI mode of Okuma CNC machine

FIG. 20. Automatic mode of Okuma CNC machine

FIG. 21. Collision Avoidance

The driving shield machining made from cast iron was carried out on the Okuma LB 3000 EX II CNC machine tools.

CONCLUSIONS

At present, development and improvement of modeling, simulation and processing technologies have a very important role in machine tools domain, representing an economical method of making parts with high dimensional accuracy. With few exceptions, the most CAD systems have began by implementing geometric tools in two sizes, reaching up to level 5 D. CAM programming can be done relatively quickly for achieving very complex parts. Instead, CAM software can produce 1000 lines of program that are equivalent in terms of effect, with 4- program line achieved manually. Using CAM software - is the most complex form of programming and can be done on a personal computer and transferred directly into the machine's memory. Programming with CAM software allows the user to reach a level of performance far higher than manual programming.

In recent years this way of working has become quite popular, because the CAM software will generate he program in G code which will be transferred directly to CNC machine's memory. Automotive, aviation and shipping are using CAM software because their facilities have comprised a lot of mechanical parts, which are processed very precise

AKNOWLEDGMENT

We hereby acknowledge the structural founds project PRO-DD (POS-CCE, O.2.2.1., ID 123, SMIS 2637, CTR. NO 11/2009) for providing the infrastructure used in this work.

REFERENCES

[1] *** European Aviation Safety Agency. *CS-25, Airworthiness codes for large aero-planes*, October 2003. Available at www.easa.eu.int, accessed on 10 Oct. 2015;
[2] C. Ohtar, A. Fujita, P. N. Nikiforov and M. K Santa, Active flutter suppression for two-dimensional airfoils, *Journal of Guidance, Control and Dynamics*, vol. 14, no. 2, pp. 283-293, 1991;
[3] T. R. Nail, *A disturbance-rejection problem for a 3-D airfoil exhibiting flutter*, Thesis, Virginia Tech., 2000;
[4] J. J. Black and H. Rilliatt, Active control of a structure, *AIAA Paper 99-0036;*
[5] R. Sind and M. Krenner, *Robust aeroservoelastic stability analysis*, Springer, London, 2000;
[6] P. Santorini, *Nonlinear Control Systems*, London, UK, Springer-Verlag, 3rd ed., 2005;
[7] R. Ceaikovski and P. Soznovski, *Neural approximation: a control perspective*, in Neural Network Engineering in Dynamic Control Systems, K. Runt, G. Irwin and F. Warwick (Eds.), Springer, 1995;
[8] F. Rudin, *The method of statistical linearization for nonlinear stochastic vibration*, in F. Ziegler and G. I. Schuller (Eds), *Nonlinear Stochastic Dynamic Engineering Systems*, pp. 45-56, IUTAM Symposium on Nonlinear stochastic dynamic engineering, Innsbruck, Austria, June 21-26, 1987, Springer Verlag, 1988.

DETERMINATION BOMBING ACCURACY FROM LEVEL DELIVERY USING THE EJECTION PRACTICAL BOMB

Stoyko STOYKOV[*], Milen ATANASOV[**]

[*]"Institute for Research and Innovation", National Military University, Veliko Tarnovo, Bulgaria (toki4_1981@abv.bg), [**]"Aviation"Faculty, National Military University, Dolna Mitropolia, Bulgaria (maa_69@abv.bg)

DOI: 10.19062/2247-3173.2016.18.1.49

Abstract: *The bombing delivery systems can improve survivability and delivery accuracy. Despite conventional, wings-level dive bomb delivery can achieve acceptable accuracy an aircraft is vulnerable during maneuvering to weapon release.*

Keywords: *practical bomb, bombing accuracy, ejection*

1. INTRODUCTION

Bombing accuracy is the combination of delivery accuracy and ballistic dispersion. The most common statistical measure from bombing accuracy is the circular error probable (CEP), which is the radius of a circle that should contain one-half (or 50%) of the total number of bomb impacts in a sample. Note that the CEP is applicable only when the distribution is equally proportioned in range and deflection, which is usually not the case when working in the ground plane. The plane where the distribution is equally proportioned is in a plane perpendicular to the bomb trajectory at the time of impact. For most cases, especially level or dive deliveries, the plane perpendicular to the line of sight (i.e., from the aircraft at the time of release to the center of impact) is an adequate approximation to the flight path normal plane to ensure that the distribution is equally proportioned. The delivery accuracy can ascertain of the formula [1, 2, 4, 5, 6]:

$$\begin{aligned} &M[\Delta X_a] = M[\Delta X_d] + M[\Delta X_b]; \\ &\sigma_{Xa}^2 = \sigma_{Xd}^2 + \sigma_{Xb}^2. \end{aligned} \tag{1}$$

where [3]:

$$\begin{aligned} &\tilde{m} = \frac{\sum_{j=1}^{N} \Delta X_j}{N}; \\ &\tilde{\sigma} = \sqrt{\frac{\sum_{j=1}^{N} \left(\Delta X_j - \tilde{m}\right)^2}{N-1}}. \end{aligned} \tag{2}$$

- ΔX_a – bombing error;

- ΔX_d – delivery error;
- ΔX_b – ballistic dispersion;
- $M[\Delta X_a] = m_a$ – sample means the bombing error;
- $M[\Delta X_d] = m_d$ – sample means the delivery error;
- $M[\Delta X_b] = m_b$ – sample means the ballistic dispersion;
- σ_{Xa} – standard deviation for bombing accuracy;
- σ_{Xd} – standard deviation for delivery accuracy;
- σ_{Xb} – standard deviation for ballistic dispersion;

2. MATHEMATICAL MODEL

The structural scheme of the model for determination bombing accuracy using the ejection practical bomb P-50-75 showed fig. 1.

The structural scheme includes these blocks:

- Model at the Aircraft;
- Model at the Aiming System;
- Model at the Bomb;
- Model Error Sources of Information
- Model Determent Ejection Velocity;
- Model Determent Bombing Accuracy.

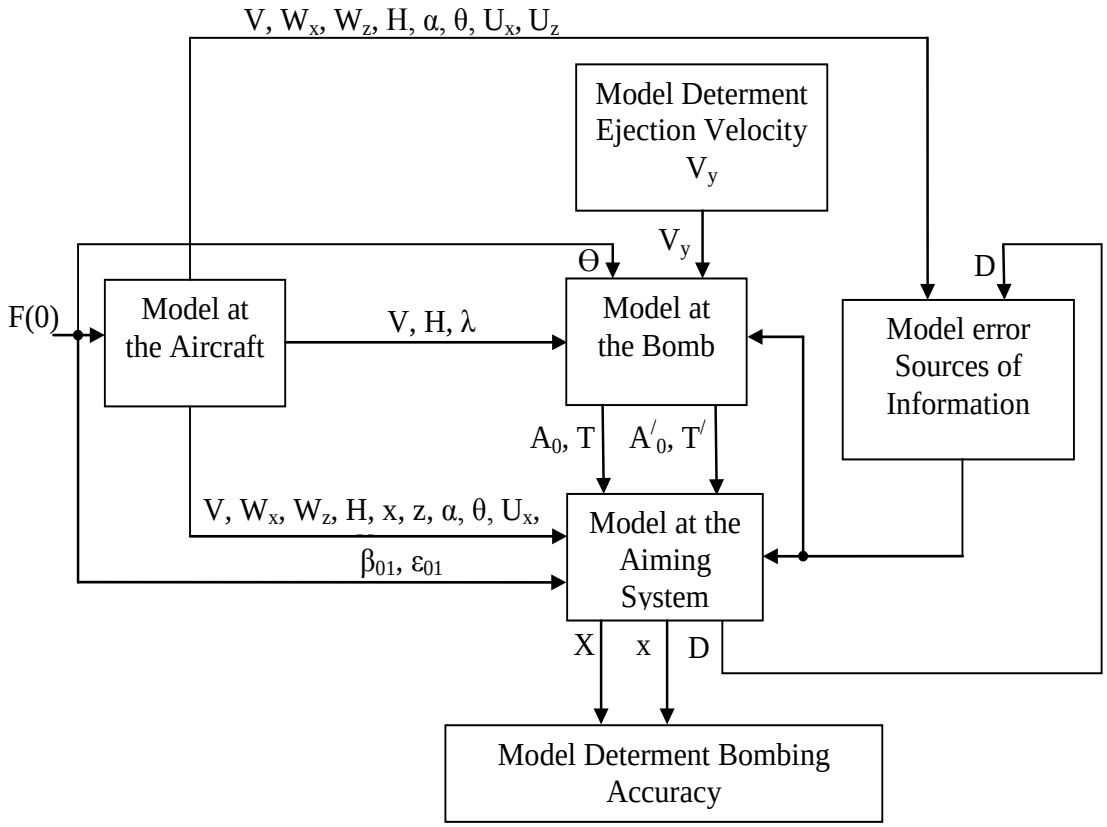

FIG. 1 Structural scheme of the model for determination bombing accuracy

The study for bomb launching in horizontal flight at height and velocity: H=500 – 1500 [m]; V=180 – 260 [m/s], initial vertical bomb velocity - V_y= 2 m/s. Practice Air bomb P-50-75 with technical characteristics: Caliber - 50 kg; Length - 1 065 mm; Body Diameter - 203 mm; Tail fin span - 245 mm; Characteristic time - 21,39 s. is used.

The sight depression angles ε_r (from the fuselage reference line to the target line of sight) at the moment of bomb launching received with mathematical modeling are given in table 1.

Table 1

Level Delivery (λ= 0^0)					
ε_r, deg	**V=180, m/s**	**200**	**220**	**240**	**260**
H=500, m	-20.30	-17.98	-16.13	-14.62	-13.36
750	-24.35	-21.76	-19.68	-17.98	-16.55
1000	-27.53	-24.76	-22.52	-20.67	-19.12
1250	-30.27	-27.37	-25.01	-23.05	-21.40
1500	-32.79	-29.79	-27.33	-25.27	-23.54

We use continuously computed impact point (CCIP) bomb launching mode in implementing the condition $|\varepsilon_r| \leq 18^0$ and when $|\varepsilon_r| > 18^0$ continuously computed release point (CCRP) mode is used.

From the above and table 1 we see that when H=500 [m] and V=220 – 260 [m/s]; and H=750 [m] and V=240 – 260 [m/s] CCIP mode is used. For the remaining conditions CCRP mode is used.

The standard deviation σ_{Xd} for delivery accuracy is changed from 25.23 m to 53.20m (table 2, fig 2). With increasing the height H of bomb launching, σ_{Xd} also increase. When CCIP mode is used, with increasing the velocity V, σ_{Xd} also increase. When CCRP mode is used we see that when V increases, σ_{Xd} decreases, because the time t for velocity integration decreases.

Table 2

Level Delivery **(λ= 0^0)**					
σ_{Xd}, m	**V=180, m/s**	**200**	**220**	**240**	**260**
H=500, m	30.92	25.24	28.79	31.46	34.91
750	33.07	32.14	30.99	32.97	34.32
1000	37.45	36.03	35.97	35.24	34.95
1250	43.92	41.62	40.63	38.87	36.96
1500	53.20	48.79	46.18	44.08	42.52

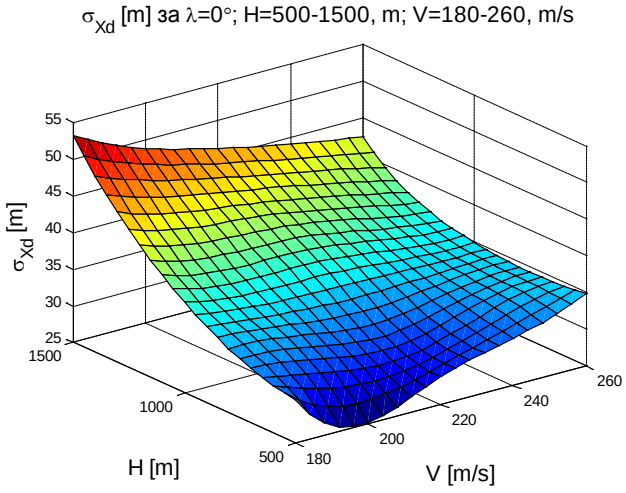

FIG. 2 Depending on σ_{Xd} from V and H

Systematic errors in the sources for information lead to systematic errors in solving bombing problem (table 3). The sample means the bombing error m_d is between 0.15 and 3.02 and the law for its change is the same as in σ_{Xd}.

Table 3

Level Delivery ($\lambda = 0^0$)					
m_d, m	**V=180, m/s**	**200**	**220**	**240**	**260**
H=500, m	0.40	0.16	0.15	0.17	0.19
750	0.97	0.93	0.68	0.69	0.67
1000	1.60	1.56	1.21	1.19	1.15
1250	2.28	2.05	1.74	1.67	1.64
1500	3.02	2.40	2.26	2.14	2.12

Standard deviation σ_{Xb}, sample means m_b determined by solving ballistic problem are shown in table 4, 5 and fig.3.

The standard deviation σ_{Xb} is amended in the range of 2.81 m to 8.94 m. The sample means m_b is amended from 0.7 m to 4.45 m. Height increasing H, σ_{Xb} leads to m_b increasing. Velocity V has slight influence on σ_{Xb} and m_b values.

Table 4

Level Delivery ($\lambda = 0^0$)					
σ_{Xb}, m	**V=180, m/s**	**200**	**220**	**240**	**260**
H=500, m	5.72	2.81	4.15	6.32	6.69
750	6.38	5.87	5.16	6.27	6.89
1000	7.38	6.55	6.47	6.20	5.97
1250	8.24	7.00	6.65	6.70	5.55
1500	8.94	8.77	8.37	7.95	7.52

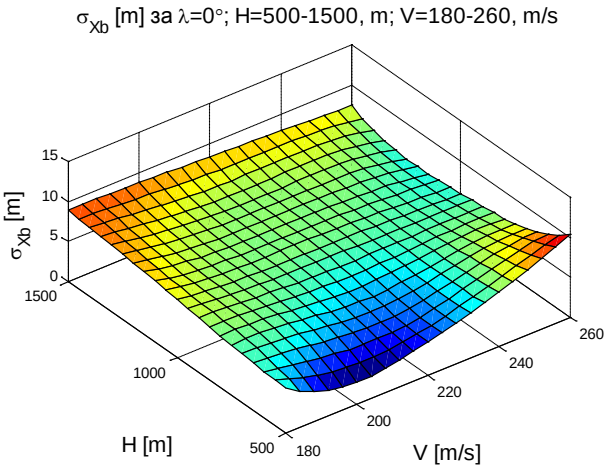

FIG. 3 Depending on σ_{Xb} from V and H

Table 5

Level Delivery ($\lambda = 0^0$)					
m_b, m	**V=180, m/s**	**200**	**220**	**240**	**260**
H=500, m	1.27	0.70	1.77	2.31	2.88
750	1.62	1.62	2.13	1.66	1.19
1000	2.13	2.40	2.53	1.80	0.43
1250	2.80	3.03	2.98	2.73	0.58
1500	3.61	3.53	3.46	4.45	1.65

The standard deviation σ_{Xa}, and sample means m_a are amended: σ_{Xa}=25.40m – 49.57 m; m_a =0.86 m – 6.58 m (table 6, 7 and fig 4).

Table 6

Level Delivery (λ= 0^0)					
σ_{Xa}, m	**V=180, m/s**	**200**	**220**	**240**	**260**
H=500, m	31.44	25.40	29.09	32.17	36.42
750	33.68	32.67	31.42	33.56	35.01
1000	38.17	36.62	36.55	35.78	35.46
1250	44.68	42.21	41.17	39.44	37.38
1500	53.95	49.57	46.93	44.79	43.18

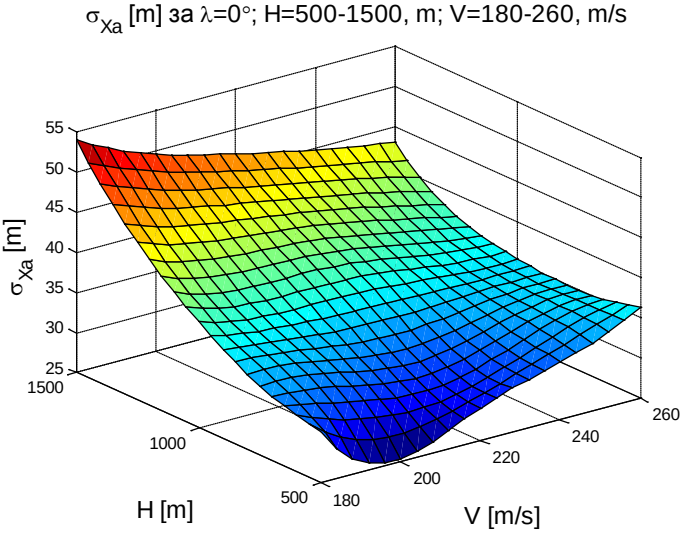

FIG. 4 Depending on σ_{Xa} from V and H

Table 7

Level Delivery (λ= 0^0)					
m_{Xa}, m	**V=180, m/s**	**200**	**220**	**240**	**260**
H=500, m	1.67	0.86	1.92	2.48	3.07
750	2.60	2.55	2.82	2.35	1.86
1000	3.73	3.96	3.75	2.99	1.58
1250	5.08	5.09	4.71	4.40	2.22
1500	6.63	5.92	5.72	6.58	3.78

3. CONCLUSIONS

Standard deviation σ_{Xa} for bombing accuracy, standard deviation σ_{Xd} for delivery accuracy, standard deviation σ_{Xb} for ballistic dispersion for practical bomb P-50-75 pushed out with vertical velocity V_y=2 m/s from horizontal flight for velocity V=180 – 260 [m/s] and height H=500 – 1500 [m] are estimated.

The standard deviation σ_{Xd} for delivery accuracy is changed in the range of 25.23 m to 53.20 m.

The standard deviation σ_{Xb} is amended in the range of 2.81 m to 8.94 m.

The standard deviation σ_{Xa}, and sample means ma are amended: σ_{Xa}=25.40m – 49.57 m.

For practical bomb P-50-75, ballistic dispersion is relatively small; therefore bombing accuracy and delivery accuracy are nearly the same.

REFERENCES

[1] А. Г. Постников, В. С. *Чуйко Внешняя баллистика неуправляемых авиационных ракет и снарядов*, Москва, Машиностроение, (1985).
[2] А. Н. *Беляев Математическое моделирование работы адаптивной замкнутой системы принудительного отделения грузов, Электронный журнал „Труды МАИ“,* Выпуск 61, 2012.
[3] Е. С. Вентцель *Теория вероятностей*, Москва, Наука, 1964 г.
[4] G. M. Siouris, *Missile Guidance and Control Systems*, New York, Springer, 2004.
[5] М. А. *Атанасов Диссертация, Възможности за решаване на задачата на прицелване при бомбопускане по ъглова скорост*, Д. Митрополия, НВУ “В, Левски” 2006 г.
[6] О. С. Стойков *Методи и точност на решаване на задачата на прицелване при бомбопускане*, Д, Митрополия, 2010г.

RESEARCH STUDY ON THE DIMENSIONAL STABILITY OF INTERLOCK 1:1 KNITTED FABRICS MADE OF COTTON YARNS

Monica SZABO, Mihaela DOCHIA, Monica LUNGU

"Aurel Vlaicu" University of Arad, Romania
(szabomonica@yahoo.com, dochiamihaela@yahoo.com, lungu_monica@yahoo.com)

DOI: 10.19062/2247-3173.2016.18.1.50

Abstract: *The study concerns the dimensional changes resulted during the relaxation process after knitting, for tubular fabrics with interlock 1:1 structure, made of cotton yarn, with 50/1 metric count of yarn.*

For the study of the dimensional changes on both directions of the fabric, on the direction of stitches courses and on the direction of stitches courses in vertical direction, can be used a mathematical model with two variables.

The interlock 1:1 structures were obtained through the combined process of knitting, resulting a maximum uniformity of the structural parametres. The parameter's uniformity on entire kittng process is a determinant factor of the dimensional stability. The corelation between the yarn's characteristics, knitting machine's technical characteristics and technological parameters of the kntting process, leads to the achieving of knitted fabrics with minimum dimensional changes.

The interlock 1:1 stuctures which were analyzed in this study, were designed and produced so the final dimensional changes, after chemical finishing, this representing the last phase of the technological process from the knitting department, to be enclosed in the limits of ± 2%, both on the direction of stitches courses and on the direction of stitches courses in vertical direction.

Keywords: *knitted fabric, interlock 1:1 structure, dimensional stability, relaxation shrinkage.*

1. INTRODUCTION

The knitted fabrics are textile structures made of elastic interconnected stitches and characterized by two perpendicular directions, the direction of stitches courses on the direction of stitches courses in vertical direction.

The dimensional stability of the knitted fabrics is reflected in the capability of the products made from these, of maintaining the shape and dimensions in the predetermined limits, after several cicles of washing-wearing process.

The dimensional stability of the knitted fabrics made of cotton is a complex and widely studied issue worldwide. Due to the fact that these are elastic structures, the dimensional stabilization is obtained through the corelation of multiple paramenters, starting with the techological parameters of spinning operation of manufacturig the yarn, the knitting parameters, finishing parameters and finally by studying the washing-wearing behaviour of the clothing products made of these type of fabrics.

For this study,100% cotton yarns were chosen, with 50/1 metric count of yarn and with Z twist sense. Tubular knitted fabrics will be obtained. In this case, the tilt angles of the stitches courses in vertical direction, will become minimal for the tubular fabrics resulted.

The knitting process will be made with uniform alimentation supply for all yarns and on entire process, in order to avoid possible irregularities of the knitted stiches.

The knitted fabrics will be deposited in folded condition for relaxation, for 72 hours in a enclosure that complies with standard parameters (temperature=20^0C, relative humidity=60%, atmosperic pressure=760 mmHg). During this relaxation period, the stitches modify their shape without respecting a predetermined rule, and the final knitted fabrics balancing the internal tensions cumulated during knitting process. In knitting structures situation, the dimensional changes are influenced by the number of the yarn-yarn contat points of the structure's elements, this fact leading to a superior dimensional stability compared to similar knitting structures, in wich the yarn-yarn contact point is smaller.

In table no.1 there are mentioned the technical characteristics of the knitting machines on which the structures were designed, the type and and metric count of the yarn which were used for knitting process and the structure of the fabric.

Table 1

Crt. No.	Knitting machine	Technical characteristics of the knitting machine				Yarn type	Metric count of yarn	Structure of the fabric
		Needle bar diameter [in]	Fineness [E]	Number of systems	Number of needles		[Nm]	
1	MULTIPIQUE TIP 5622-2	30	20	72	2x1872	100% cotton	50/1	interlock 1:1

2. MATERIALS AND METHODS

To determine the influence of techological parameters of knitting process on the dimensional stability, a mathematical model was established in order to define the connection between the relaxation shrinkage, which is considered a dependent variable, and as independent variables, the wale density and the turn of the needle bar.

The results of the practical determination were statistically processed. For the statistically process of the results, for all the knitting structures it was proposed an experimental program with 2 variables x_1 (x of ecuation) and x_2 (y of ecuation) which represent the entry data enclosed. x_{1real} represents the wale density on the knitting machine expressed in stitches/cm, and x_{2real} represents the turn of the needle bar expressed in rotations/minut. The values z_1 and z_2 are the answers.

For the study of the dimensional changes, made on the both directions of the knitted fabric, it is proposed a mathematical model as a rotatable central compound, with two variables. The coefficient's significance was tested with the T test and the adequacy with the Student test.

The experimental program concieved offers information regarding the behaviour of the knitted fabrics from entire variation domain of wale density and turn of the needle bar, proposed.

In table no.2 are represented the encoded and real values for the independent variables, and also the responses for the interlock 1:1 structure made of 100% cotton yarns, with metric count of yarn 50/1.

Table 2

Crt. No.	x_1 enclosed (x)	x_2 enclosed (y)	Wale density [stitches/cm] ($x_{1\ real}$)	Turn of needle bar [rot/min] ($x_{2\ real}$)	Dimensional changes during relaxation on stitch course direction [%] (z_1)	Dimensional changes during relaxation on stitch course in vertical direction [%] (z_2)
1	-1	-1	9,45	10,90	-2,00	-2,30
2	1	-1	11,60	10,90	-0,50	-1,50
3	-1	1	9,45	15,10	-2,50	-2,75
4	1	1	11,60	15,10	-0,75	-1,80
5	-1,414	0	9,00	13,00	-3,00	-3,20
6	1,414	0	12,00	13,00	-0,20	-0,40
7	-1	-1,414	10,50	10,00	-0,90	-1,40
8	1	1,414	10,50	16,00	-0,75	-1,30
9	0	0	10,50	13,00	-0,90	-1,20
10	0	0	10,50	13,00	-0,80	-1,40
11	0	0	10,50	13,00	-0,75	-1,50
12	0	0	10,50	13,00	-0,60	-1,30
13	0	0	10,50	13,00	-0,80	-1,25

Dimensional changes study on stitch course direction (horizontal direction):

The regression ecuation which describes the relaxation process of interlock 1:1 knitted fabrics made of 100% cotton, 50/1 metric count of yarn, stitch course direction is based on following relation (1):

$$f(x,y) := -0.77 + 0.901\cdot x - 0.471\cdot y - 0.067\cdot x^2 - 0.084\cdot y^2 + 0.062\cdot x\cdot y \quad (1)$$

Where: x and y are encoded values

In fig.1 is presented the dependence U=(f,y), in the case of relaxation shrinkage on the stich course direction of the interlock 1:1 fabrics studied.

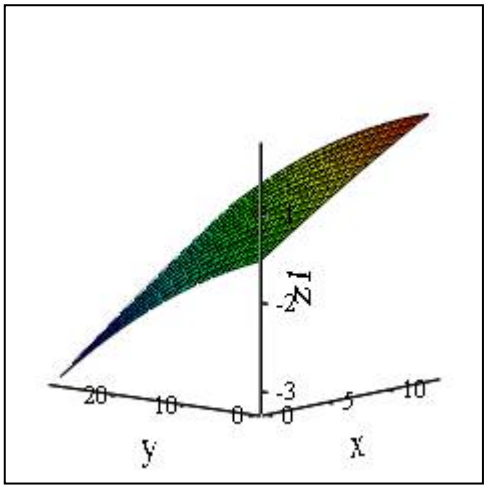

FIG. 1. Response surface in the relaxation shrinkage, on stitch course direction, for the interlock 1:1 knitted fabric

The response surface represented in fig.1 has an elongated saddle shape, and the curve which generates it are hyperbolas.

In fig. 2 there are presented sections through response surface, for the relaxation shrinkage on stitch course direction for interlock 1:1 knitted fabrics studied.

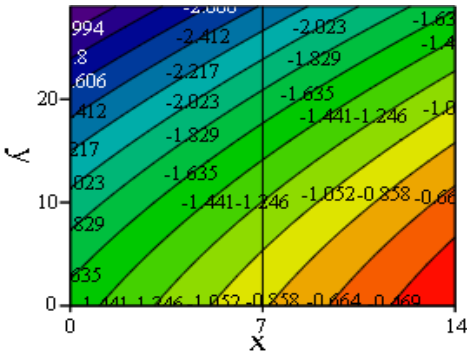

FIG. 2. Sections through response surface in the relaxation shrinkage, on stitch course direction, for the interlock 1:1 knitted fabric

From the graphic representation from fig.2, the level curves can be noticed; these are portions of hyperbolas.

While the wale density increases, the relaxation shrinkage decreases. For the entire field variation of wale density and of the turn of the needle bar, relaxation shrinkage appears (represented by negative values), but in elongation does not appear in any other situations (represented through positive values).

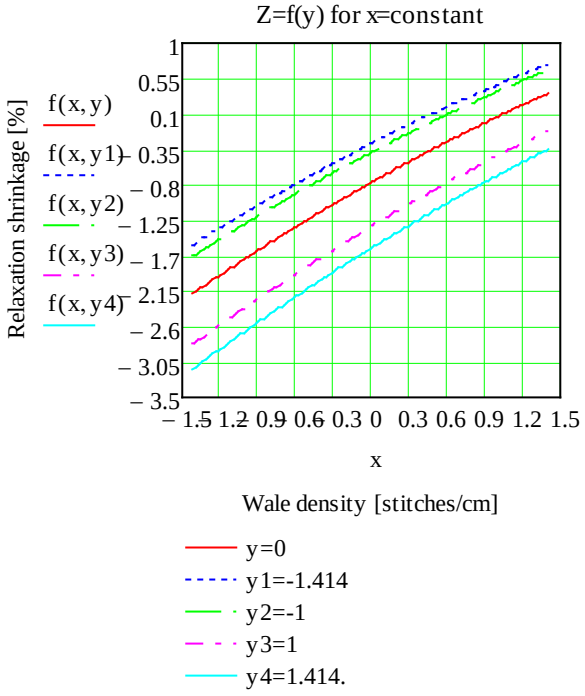

FIG. 3. Variation of Z = f(y) for x = constant in case of dimensional changes after relaxation, on stitch course direction in horizontal direction

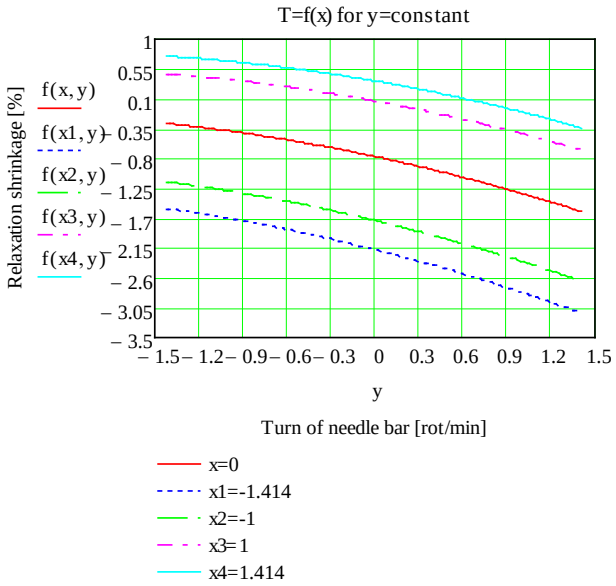

FIG. 4. Variation T=f(x) for y=constant in case of dimensional changes to relaxation, on stitch course direction in horizontal direction

In fig. 3 is represented the dependence of Z = f (y) for x = constant on stich course direction.

From the graphic analyze from fig.3 results that together with the increase of vertical density, the shrinkage to relaxation in the direction of vertical stitches courses decreases, approaching to the 0 value (ideal value). The curves present the same trend for the entire variation domain of vertical density. The switch from one level to another is done with the same effort for the entire variation domain of vertical density.

In fig. 4 is represented the dependence T=f(x) for y=constant.

From the graphic analyze from fig.4, it results that together with the increase of turn of the needle bar, shrinkage to relaxation increases in the direction of vertical stitches courses. The curves present the same trend for the entire variation domain of vertical density. The switch from one level to another is done with the same effort for the entire variation domain of vertical density.

Dimensional changes study on stitch course in vertical direction:

The regression ecuation which describes the relaxation process of the intrelock fabrics made of 100% cotton, 50/1 metric count of yarn, on stich course in vertical direction is given by the following relation (2):

$$f(x,y) := -1.33 + 0.714 \cdot x - 0.363 \cdot y - 0.076 \cdot x^2 - 0.138 \cdot y^2 + 0.037 \cdot x \cdot y \quad (2)$$

In fig. 5 is presented the response surface, which means the dependence U=f(x,y), in the relaxation shrinkage on stitch course in vertical direction of interlock 1:1 fabrics which were studied.

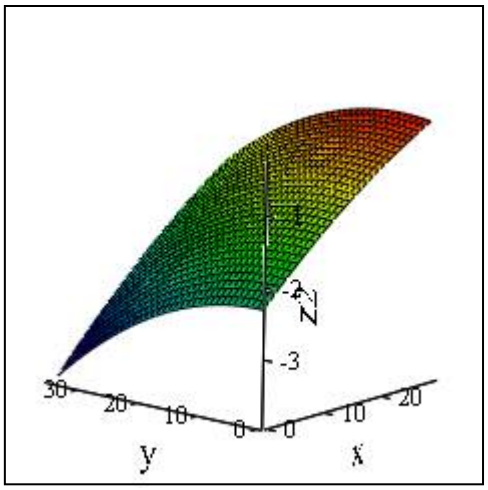

FIG. 5. Response surface in the case of relaxation shrinkage, on stitch course in vertical direction, for interlock 1:1 structures

The response surface has a elongated saddle shape. The curves which generates is are hyperbolas.

In fig. 6 are represented the sections through response surface, in the relaxation shrinkage case, on stitch course in vertical direction, for the interlock 1:1 fabrics studied.

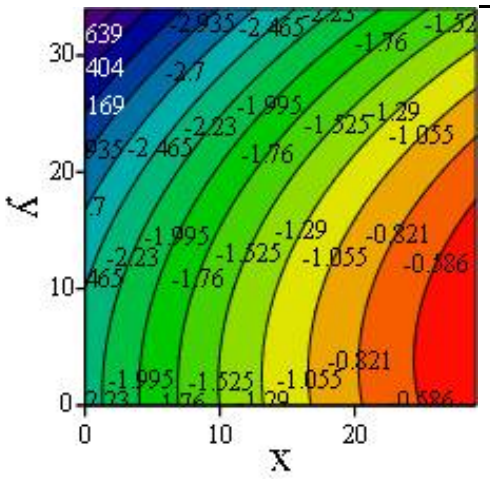

FIG. 6. Sections through response surface in relaxation shrinkage, on stitch course in vertical direction, for interlock 1:1 structures

From the graphic representation from fig.6, the level curves are evidenced, which are portions of hyperbolas.

Together with the increase of the wale density, the relaxation shrinkage decreases. For entire domain of variation of wale density and of turn of the needle bar, the relaxation shrinkage appears on the stitch course in vertical direction (represented by negative values), and in any case does not appear elongation (represented by positive values).

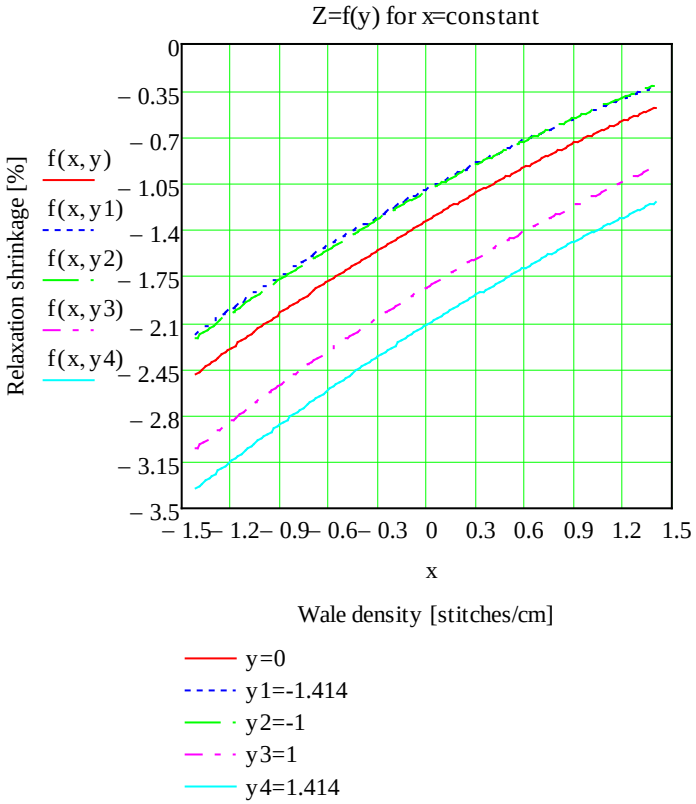

FIG.7. Variation Z=f(y) for x=constant in case of dimensional changes during relaxation, on stitch course in vertical direction

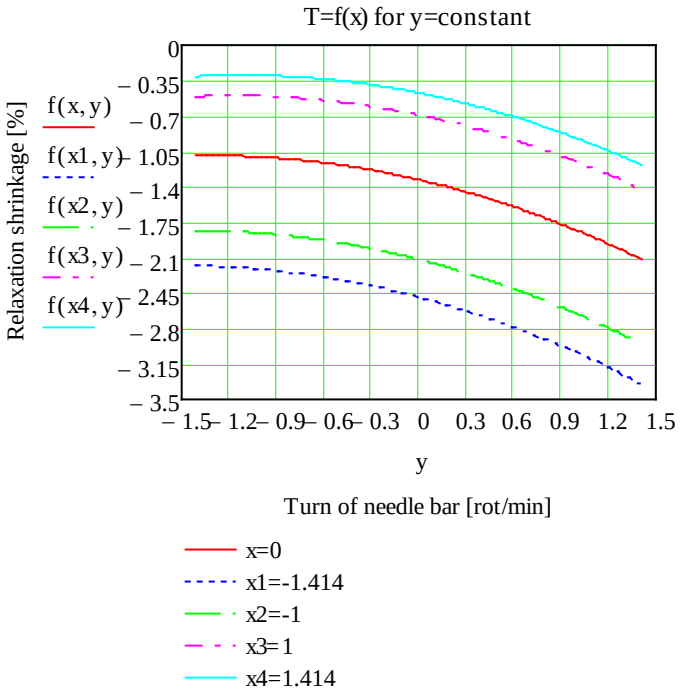

FIG. 8. Variation T=f(x) for y=constant in case of dimensional changes after relaxation on stitch course in vertical direction

In fig.7 is represented the dependence Z=f(y) for x=constant.

For the anlayze of graphic representation from fig.7 can be observed that together with the increase of the wale density, the relaxation shrinkage decreases on stitch course direction for the intrelock structures studied.

In fig. 8 is represented the dependence T=f(x) for y=constant.

From the graphic anlayze from fig. 8 results that together with the increase of the turn if the needle bar, the relaxation shrinkage increases. The curves have the same evolution for entire variation domain of wale density, the tranzit from one level to other is made with the same effort on entire variation domain of wale density.

3. RESULTS AND DISCUSSION

For real values of wale density between 10,5 -12 stitches/cm, the relaxation shrinkage decreases to -0,8% la -0,2%, which are considered very good.

Knitting with big wale densities, over 12 stitches/cm, elongations appear. These elongations appear due to increasing of yarn-yarn contact points, resulting yarn-yarn contact surfaces which lead to modifications of the stitches shape during relaxation period.

The variation of the wale density together with the turn of the needle bar in order to maintain a constant contraction is needed because once with the increase of the turn of needle bar over a certain value, the remanent tensions from the knitted fabric increase also, and in order to maintain the fabric in the same stich shape and at the same values of the structural parameters, the contact surface betewwn the yarns must be increased also.

A too high density does not allow the return through relaxation of the knitted fabric, to a minimum energy state and the remanent tensions manifest through contraction. Also, in the case of big wale densities, the knitted structures loose their elasticity and become.

4. CONCLUSIONS

1. The interlock 1:1 structures made of 100% cotton, 50/1 metric count of yarn studied, were designed so the dimensional chages during relaxation shrinkage to be minimum, this fact having a positive influence on previous procedures applied on knitted fabrics.
2. In order to obtain structures with dimensional stability in the limits of ±2%, the wale density of the knitted fabric determined on the knitting machine, has a major influence.
3. After establishing the optim wale density on the knitting machine, the turn of the needle bar must be set, the other technological parameters of the knitting process having less influence regarding the dimensional changes in un-finished state, of the knitted fabrics.
4. After the relaxation of the knitted fabrics which were released from the knitting machine, minimum contractions are noticed, both on the stitch course direction and on stitch course vertical direction, which concludes to a structure with very good dimensional stability.
5. The use of this method allows with a minimum effort, starting form initial data, which is the fineness of the yarns, technical characteristics of the knitting machine, the wale density, the turn of the needle bar, to predict the final data, more exactly the values of the dimensional changes after relaxation processes.

REFERENCES

[1]. Jiang Tao et al, *Effects of yarn on fabric constructionon spirality of single jersey fabrics*, Textile Research Journal, 1997, 67(1), 57-68
[2]. Hearth, C. N. et al, *Dimensional stability of cotton spandex interlock 1:1 structures under relaxation*, Fibres and Ploymers, 2007, 8(1), 105-110
[3]. Liana M., Abou, N., *The Dimesional Instability of Knitted Structures, International Textile Bulletin*, 2001, 4, 75-80
[4]. Micucioniene, D. Et al, *The influence of drying conditions on Dimensional Stability of Cotton Weft Knitted Fabrics*, Materials Science, 2009, 15, 64-68
[5]. Moghassem, A. R., Tayebi, H.A., *The Effect of Mercerization Treatment on Dimensional Properties of Cotton Plain Weft Knitted Fabric*, World Applied Science Journal, 2009, 7, 1317-1325
[6]. Bayazit, M., *Dimensional and Phisical Properties of Cotton/Spandex Single Jersey Fabrics*, Textile Research Journal, 2003, Vol. 73, No. 1, p. 11-14
[7]. Dhingra, R. C., Chan, C.K., Abbas, M. S., Tao, J., *Effects of Yarn and Fabric Construction on Spirality of Cotton Single Jersey Fabrics*, Textile Research Journal, 1997, Vol. 67, No. 1, p. 57-68
[8]. Souza, A. A. U. et al., *Prediction of dimensional changes in circular knitted cotton fabric, Textile Research Journal*, 2010, Vol. 80, No. 3, p. 236- 252
[9]. Ahmed, M. E., Abdel, Z. M., *The Effect of Machine Setting on Weft Knitted Fabric Properties, Journal of Applied Sciences Research*, 2008, Vol. 4, No. 11, p. 1371-1379

MECHANICAL ENGINEERING. MATERIALS AND TECHNOLOGY

DETERMINATION OF MAXIMUM ANGLE SLOPE THROUGH NORMAL REACTIONS TO THE WHEELS, IN STATIC AND DYNAMIC REGIME

Adrian ȘOICA, Stelian ȚARULESCU

"Transilvania" University of Brasov, Romania (a.soica@unitbv.ro, s.tarulescu@unitbv.ro)

DOI: 10.19062/2247-3173.2016.18.1.51

Abstract: *Crossing ability is the quality of the vehicle to travel on roads or in off road terrain and to overcome obstacles. Special purpose vehicles and the 4x4 require much improved performance, especially on climbing slopes. The paper aims to provide a method for determining the maximum slope angle that can climb a vehicle with two axel, starting from normal reactions to its wheels, in static and dynamic regime.*

Keywords: *vehicle dynamics, maximal road slope, normal static reaction, normal dynamic reaction.*

1. INTRODUCTION

Establishing the forces, reaction and moments on the vehicle axle are topics treated in various forms in [1-6]. Particular aspects for determining carrying capacity, maximum slope that can be climbed are treated in [1, 5, 6].

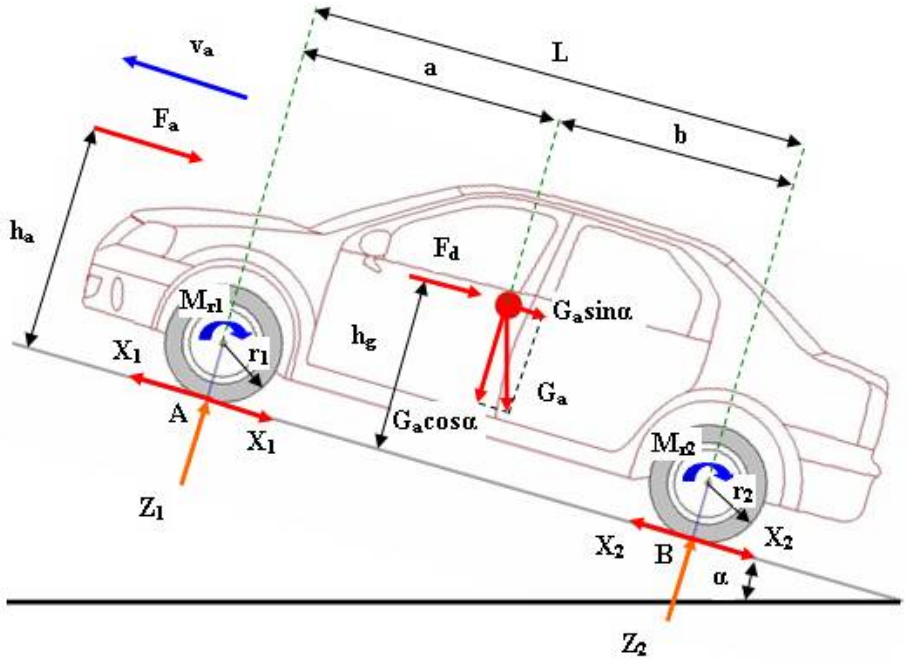

FIG. 1. Forces, reaction and moments on the vehicle with two axle

Forces, moments and reactions acting on the vehicle are shown in Fig. 1; the following notations have been made: G - weight of the vehicle; Fa - air resistance; Fd - resistance to acceleration; X1 and X2 - tangential reactions to the front and rear axle; MR1 and MR2 - rolling resistance torque for the front and rear axle; a and b - longitudinal coordinates of the center of mass; hg - height of the center of mass; ha - height of the center of pressure. Under stationary vehicle conditions, the static reactions, considered as normal to the two axles, may be determined from the equations of moments in relation to the points of contact between the wheel and the road surface, A and B. In this case we have Fa = 0; Fd = 0; MR1 and MR2 = 0 = 0. By writing the equation of moments in relation to the rear axle, the point B, the following relation obtained:

$$Z_1 \cdot L = G_a \cdot \cos(\alpha) \cdot b - G_a \cdot \sin(\alpha) \cdot h_g \tag{1}$$

where having the weight G_a as common factor the following relation is obtained:

$$Z_1 = G_a \frac{b \cdot \cos(\alpha) - h_g \cdot \sin(\alpha)}{L} \tag{2}$$

If we write the equation of moments in relation to the front axle, the point A, the following relation is obtained for the reaction on the rear axle:

$$Z_2 \cdot L = G_a \cdot \cos(\alpha) \cdot a + G_a \cdot \sin(\alpha) \cdot h_g \tag{3}$$

and by grouping the terms:

$$Z_2 = G_a \frac{a \cdot \cos(\alpha) + h_g \cdot \sin(\alpha)}{L} \tag{4}$$

Relations 2 and 4 depend on the angle of the slope where we have the vehicle and they do not depend on the coefficient of adhesion (the vehicle is stationary). From the graph in Fig. 2 it is noticed that the front axle reaction has a decreasing trend along with increasing angle α, while the rear axle loads for the same variation of the slope angle.

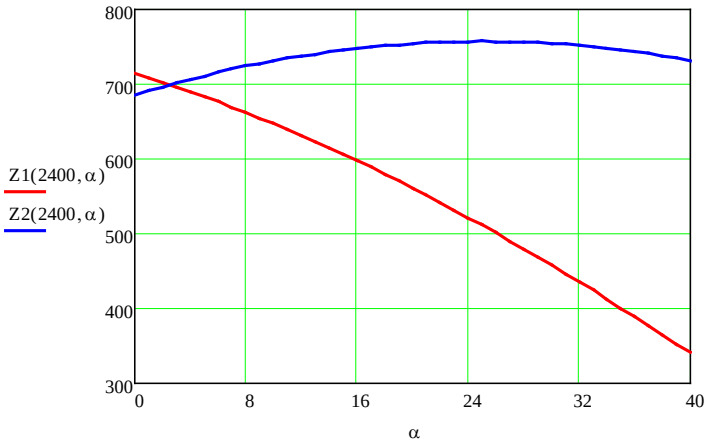

FIG. 2. Variation of vertical static reactions in case of the two axle vehicle with front axle traction, depending on the slope angle

2. VEHICLE WITH TWO AXLES MOVING ON SLOPE

In order to determine the normal dynamic reactions to the road surface, we considered the general case of a vehicle running up a ramp with trim α, in uniformly accelerated motion.

While the vehicle is running, the normal reactions to the front and rear axles change according to the type of motion. We start from the general case of a vehicle with traction or braking system applied on both axles; we then detail particular cases considering the motion and the number and position of axles. Tangential reactions X_1 and X_2 are oriented depending on the axle position: traction or braking.

As calculus assumptions for the determination of normal reaction to the two axels we consider that the vehicle is a rigid body, without taking into account the additional movement that occurs due to suspension oscillations. In order to determine the normal reaction Z_{1d} and Z_{2d} will write equations of moments in relation to the points of contact between the wheel and the road, i.e. B and A respectively, considering all the forces and moments acting on the vehicle.

By writing the moment equation in relation to point B, we obtain:

$$Z_{1d} \cdot L + M_{r1} + M_{r2} + G_a \cdot \sin(\alpha) \cdot h_g + F_d \cdot h_g + F_a \cdot h_a - G_a \cdot \cos(\alpha) \cdot b = 0 \quad (5)$$

The sum of forces perpendicular to the road surface is given by the relation:

$$Z_{1d} + Z_{2d} = G_a \cdot \cos(\alpha) \quad (6)$$

Viewing that $r_1 = r_2 = r$ şi $f_1 = f_2 = f$, we have:

$$M_{r1} + M_{r2} = f_1 \cdot r_1 \cdot Z_{1d} + f_2 \cdot r_2 \cdot Z_{2d} = f \cdot r \cdot G_a \cdot \cos(\alpha) \quad (7)$$

Where r_1 and r_2 - are the working radius of the wheels on the front and rear axle; f_1 and f_2 - rolling resistance coefficients for the wheels on the front and rear axle. Considering the relation 7, the equation 5 will be:

$$Z_{1d} \cdot L + f \cdot r \cdot G_a \cdot \cos(\alpha) + (G_a \cdot \sin(\alpha) + F_d) \cdot h_g + F_a \cdot h_a - G_a \cdot \cos(\alpha) \cdot b = 0 \quad (8)$$

from where:

$$Z_{1d} = \frac{G_a \cdot \cos(\alpha) \cdot (b - f \cdot r)}{L} - \frac{(G_a \cdot \sin(\alpha) + F_d) \cdot h_g + F_a \cdot h_a}{L} \quad (9)$$

In order to determine the normal reaction to the rear axle, Z_{2d} we take an analogue approach and we write the equation of moments in relation to point A.

$$Z_{2d} \cdot L - M_{r1} - M_{r2} - G_a \cdot \sin(\alpha) \cdot h_g - F_d \cdot h_g - F_a \cdot h_a - G_a \cdot \cos(\alpha) \cdot a = 0 \quad (10)$$

By substituting the expression 7 in the relation 10 we obtain:

$$Z_{2d} = \frac{G_a \cdot \cos(\alpha) \cdot (a + f \cdot r)}{L} + \frac{(G_a \cdot \sin(\alpha) + F_d) \cdot h_g + F_a \cdot h_a}{L} \quad (11)$$

The normal reactions from relations of Z_{1d} and Z_{2d} reveal that they depend on:
- type of vehicle movement;
- road characteristics;
- construction characteristics of the vehicle.

These relations are valid regardless the direction and the value of X_1 and X_2 tangential reaction forces and their distribution on axles.

Since tangential reactions are limited by adhesion, normal reaction to axles cannot exceed certain limits. From equilibrium of forces in the direction of the vehicle traveling speed, we obtain the relation:

$$\pm X_1 \pm X_2 = G_a \cdot \sin(\alpha) + F_a + F_d \tag{12}$$

giving:

$$G_a \cdot \sin(\alpha) + F_d = (\pm X_1 \pm X_2) - F_a \tag{13}$$

Taking into account the relation 13, the expressions 9 and 11 of normal reaction Z_1 and Z_2 will be written as:

$$Z_{1d} = \frac{G_a \cdot \cos(\alpha) \cdot (b - f \cdot r)}{L} - \frac{\left[(\pm X_1 \pm X_2) - F_a\right] \cdot h_g + F_a \cdot h_a}{L} \tag{14}$$

and, respectively:

$$Z_{2d} = \frac{G_a \cdot \cos(\alpha) \cdot (a + f \cdot r)}{L} + \frac{\left[(\pm X_1 \pm X_2) - F_a\right] \cdot h_g + F_a \cdot h_a}{L} \tag{15}$$

Relations 14 and 15 will be further particularized for a vehicle with front axle traction.

3. TWO AXLE VEHICLE WITH FRONT AXLE TRACTION

In this case in relations 14 and 15 the following replacements are made in order to determine $Z_{1dtf.}$

$$\begin{cases} X_1 = \varphi \cdot Z_{1d} \\ X_2 = -f \cdot Z_{2d} = -f \cdot G_a \cdot \cos(\alpha) + f \cdot Z_{1d} \end{cases} \tag{16}$$

and to determine Z_{2dtf} respectively:

$$\begin{cases} X_1 = \varphi \cdot Z_{1d} = \varphi \cdot G_a \cdot \cos(\alpha) - \varphi \cdot Z_{2d} \\ X_2 = -f \cdot Z_{2d} \end{cases} \tag{17}$$

giving

$$Z_{1dtf} = \frac{G_a \cdot \cos(\alpha) \cdot \left[b + f \cdot (h_g - r)\right]}{L + h_g \cdot (\varphi + f)} - \frac{F_a \cdot (h_a - h_g)}{L + h_g \cdot (\varphi + f)} \tag{18}$$

$$Z_{2dtf} = \frac{G_a \cdot \cos(\alpha) \cdot (a + f \cdot r + \varphi \cdot h_g))}{L + h_g \cdot (\varphi + f)} + \frac{F_a \cdot (h_a - h_g)}{L + h_g \cdot (\varphi + f)} \quad (19)$$

We can estimate that the height of the center of mass hg is equal to the height of the center of pressure ha and the force of air resistance F_a is lower at lower speeds. Thus, under conditions of maximum traction, the second term from the numerator of relations 18 and 19 may be neglected. The dynamic reactions depend on the road slope and the coefficient of adhesion φ.

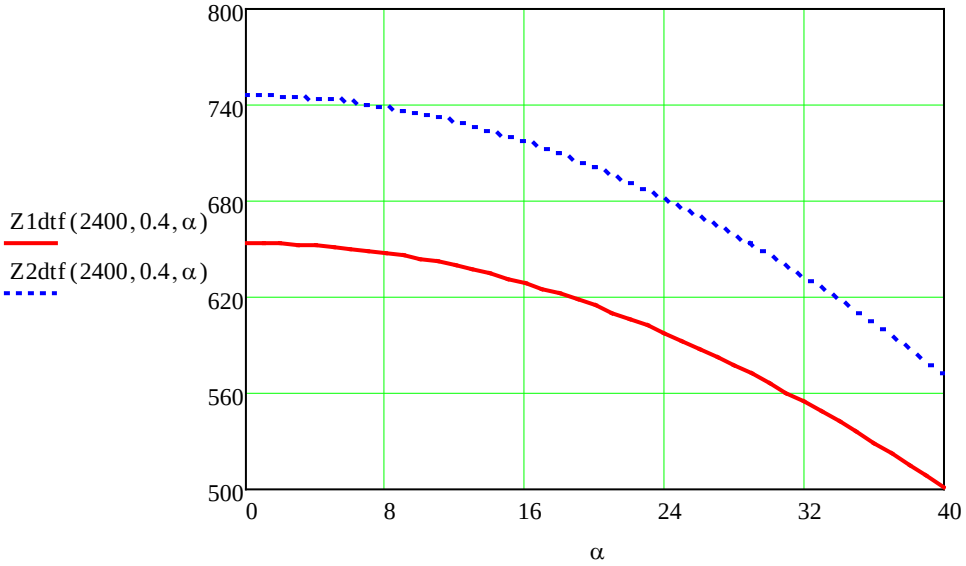

FIG. 3. Variation of vertical dynamic reactions in case of the two axle vehicle with front axle traction, depending on the slope angle

From relations 18 and 19 we notice a decreasing trend of vehicles normal reactions to axles as the slope angle α increases, Fig. 3.

Provided the same graph presents the dynamic and static vertical reactions on an inclined road, Fig. 4. shows that for a particular adhesion coefficient and a particular slope angle the static and dynamic reactions intersect.

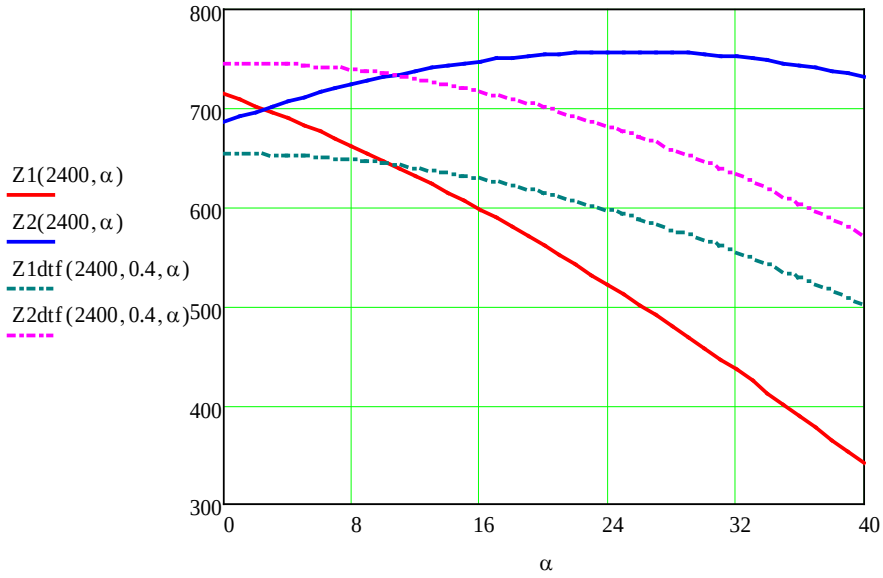

FIG. 4. Variation of vertical dynamic and static reactions in case of the two axle vehicle with front axle traction, depending on the slope angle

This means that for an angle α the static reactions are equal to those generated in dynamic conditions. Furthermore, for the reactions to both front and rear axle the intersection angle is the same. We may conclude that when the relation between normal dynamic reactions and static normal reactions is equal to 1, $Z_{1dtf}/Z_1=Z_{2dtf}/Z_2=1$, we obtain the maximum slope angle at which a vehicle may run up, as seen in figure 6.4. If $m_1= Z_{1d}/Z_1$ and $m_2= Z_{2d}/Z_2$, the values for m1 and m2, illustrated on the graph on the right of the maximum slope angle value cannot be obtained as this would result in $m_1>1$ and $m_2<1$, which is impossible to obtain in case of any type of vehicle, as seen in Fig. 5.

Figure 4 Variation of vertical dynamic and static reactions in case of the two axle vehicle with front axle traction, depending on the slope angle.

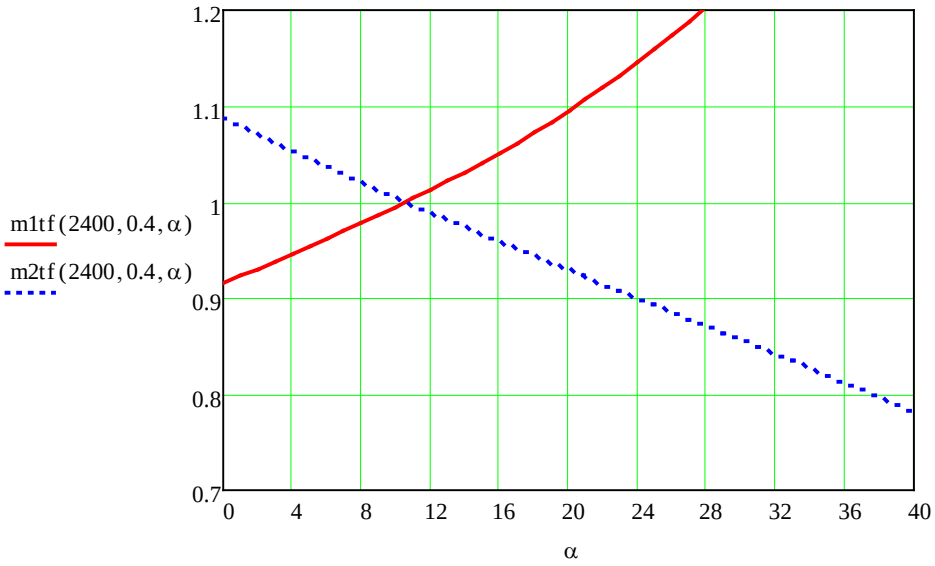

FIG. 5. Variation of dynamic change coeficient of reactions to axles in case of a vehicle with front axle traction depending on the slope angle

4. COMPARISON OF METHODS USED TO DETERMINE THE MAXIMUM SLOPE

The classical method to determine the maximum slope that a vehicle may climb, considering that the vehicle cannot roll and without taking into account the rolling resistance, uses the following formulae for 4x2 vehicles under different traction systems.

Thus, for a vehicle with front axle traction, the following formula is used:

$$\alpha_{max} = a\tan\left(\frac{b}{\frac{L}{\varphi}+h_g}\right) \tag{20}$$

Knowing the dynamic and static reactions, the maximum slope may be determined by solving the equation described by the equality $Z_{1d}/Z_1=1$ by defining two functions $h(\alpha)$, $g(\varphi,\alpha)$ and $h(\alpha) = g(\varphi,\alpha)$:

$$g(\varphi,\alpha) = \frac{\left[b+f\cdot\left(h_g-r\right)\right]\cdot G_a\cdot\cos(\alpha)}{L+\left(\varphi+f\right)\cdot h_g}$$
$$h(\alpha) = \frac{G_a\cdot b\cdot\cos(\alpha)-G_a\cdot h_g\cdot\sin(\alpha)}{L} \tag{21}$$

and by applying the root function that may be used to determine the maximum slope angle at which a vehicle may run up depending on the parameter φ.

The root function can only solve one equation in one unknown:

$$Rampa\max 1(\varphi,\alpha) = root(h(\alpha)-g(\varphi,\alpha),\alpha) \tag{22}$$

By comparing the result we actually notice an overlap of the values of the maximum slope angle at which a vehicle may climb under different adhesion conditions.

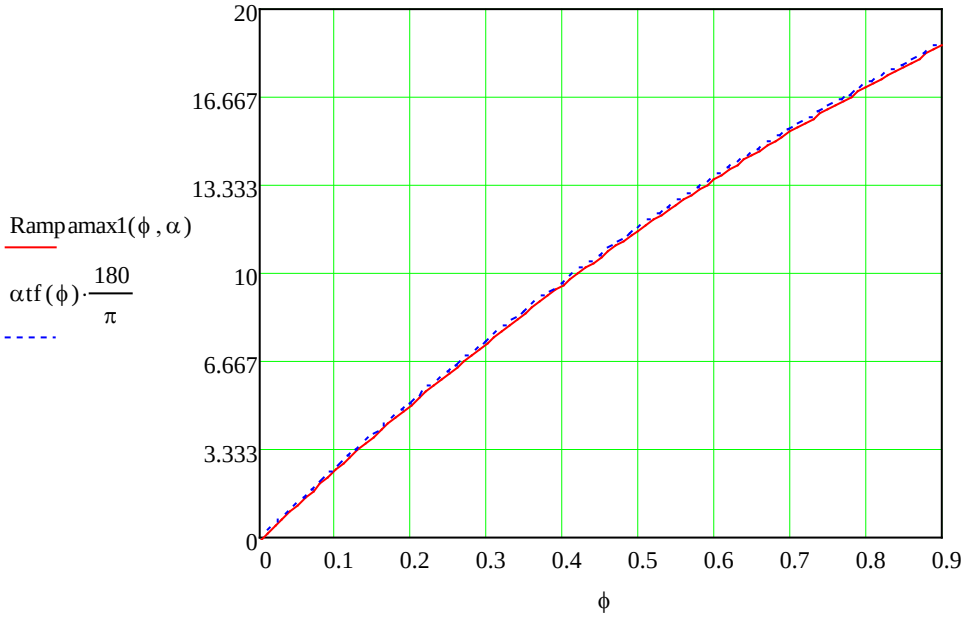

FIG. 6. Comparison of the maximum slope angle at which a vehicle may climb

CONCLUSIONS

Determination of maximum slope angle that can be climbed to a vehicle with two axle from normal static and dynamic reactions to the axle, offers similar results with other methods, for all possible traction configurations 4x2 and 4x4.

REFERENCES

[1] Preda, I., *Aspects regarding the wheel loads of tractor-semitrailer road train*, CAR 2005, The International Congress on Automotive, Pitesti, Romania, 2005.
[2] Genta, G., *Motor vehicle dynamics : modeling and simulation*, ISBN 9810229119, World Scientific Publishing Co. Pte. Ltd., 2003.
[3] Gillespie, T., *Fundamentals of Vehicle Dynamics*, Society of Automotive Engineers, 1992.
[4] Rajesh Rajamani, Vehicle Dynamics and Control, ISBN 978-1-4614-1432-2, Springer Science+Business Media, 2012.
[5] Gaiginschi, R., s.a., *Road Safety*, Editura Tehnica, 2007.
[6] Stoicescu, A.P., *About motor vehicle Center of Gravity Position Determination,* Ingineria Automobilului, pp.20-22, 2015.

RESEARCHES ON COMBUSTION QUALITY FOR A GDI EXPERIMENTAL ENGINE

Stelian ȚÂRULESCU, Radu ȚÂRULESCU, Adrian ȘOICA*

*"Transilvania" University of Brașov, Romania (s.tarulescu@unitbv.ro, radu.tarulescu@unitbv.ro, a.soica@unitbv.ro)

DOI: 10.19062/2247-3173.2016.18.1.52

Abstract: *The present paper presents researches on combustion quality for a gasoline direct injection engine. The tests ware made on an AVL single cylinder test bed for gasoline and diesel engines. In this case, it was used a AVL 475 cc GDI Single Cylinder Research Engine Type 5405.The quality of the combustion for this engine was analyzed and compared with the theoretical principles. During the test was noticed that the main engines parameters are variable for 100 engine cycles. The variation occurs in function of the air temperature, air/fuel mixture formation, cooling system variation, combustion start moment and several engine design parameters. In order to increase the combustion quality, some measures can be applied: using an injection strategy with two or three phases; varying the advance angle of the spark related to TDC; varying the quantity of fuel injected per engine cycle; optimization of combustion chambers.*

Keywords: *combustion, quality, engine, direct injection.*

1. INTRODUCTION

The vehicles equipped with internal combustion engines are the main air pollution souse from transportation system. Also, internal combustion engine emissions contributed to the global warming and other environmental impacts. World-wide, various emission legislation have been put in action in a concerted effort of motivating vehicle manufacturers to produce relatively cleaner and more fuel efficient engines [1]. The new Euro 6 regulations regarding CO_2 emissions and regulated emissions including NO_x, CO, HC, and particulate matter (PM) are demanding advanced internal combustion engines with greatly improved combustion processes. Gasoline Direct Injection (GDI) is an increasingly popular type of fuel injection system employed in modern four-stroke gasoline engines. The major advantages of a GDI engine are lower emission levels, increased fuel efficiency and higher engine power output. The cooling effect of the injected fuel and the more evenly dispersed combustion mixtures allow for improved ignition timing settings which are an equally important system requirement [4].

In Fig. 1 are presented the constructive differences between Multi Point Injection (MPI) and Gasoline Direct Injection (GDI) [3]. The main improvement for GDI represents the fuel/air mixture formation. The petrol/gasoline is highly pressurized and injected by high voltage driven injectors via a common rail fuel line directly into the combustion chamber of each cylinder as opposed to conventional single or multi-point fuel injection that happens in the intake manifold tract or cylinder port. In some applications gasoline direct injection enables stratified fuel charge combustion for improved fuel efficiency and reduced emission levels at low load. The major advantages

of a GDI engine are lower emission levels, increased fuel efficiency and higher engine power output [1].

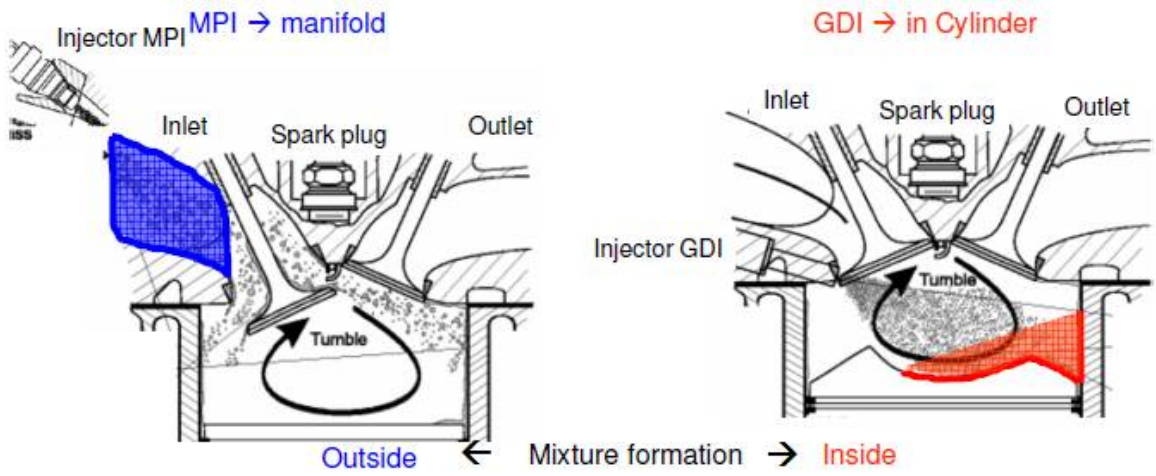

FIG. 1. The difference between Multi Point Injection (MPI) and Gasoline Direct Injection (GDI) [3]

In order to obtain data and optimize solutions for GDI engines, a research program was developed at Transilvania University of Braşov, ICDT - Research & Development Institute. The research stand is an AVL single cylinder test bed for gasoline and diesel engines. For the present paper, the tests was made on a AVL 475 cc GDI Single Cylinder Research Engine 5405. The single cylinder can be setup in several configurations (with multipoint injection, with direct injection, with turbocharger). The mixture formation and combustion processes of the fuel can be monitored through the test bed component software, AVL FIRE Commander 7.06c - IAV [2]. In Figure 2 is presented the Single cylinder test bed cell that was used for the researches.

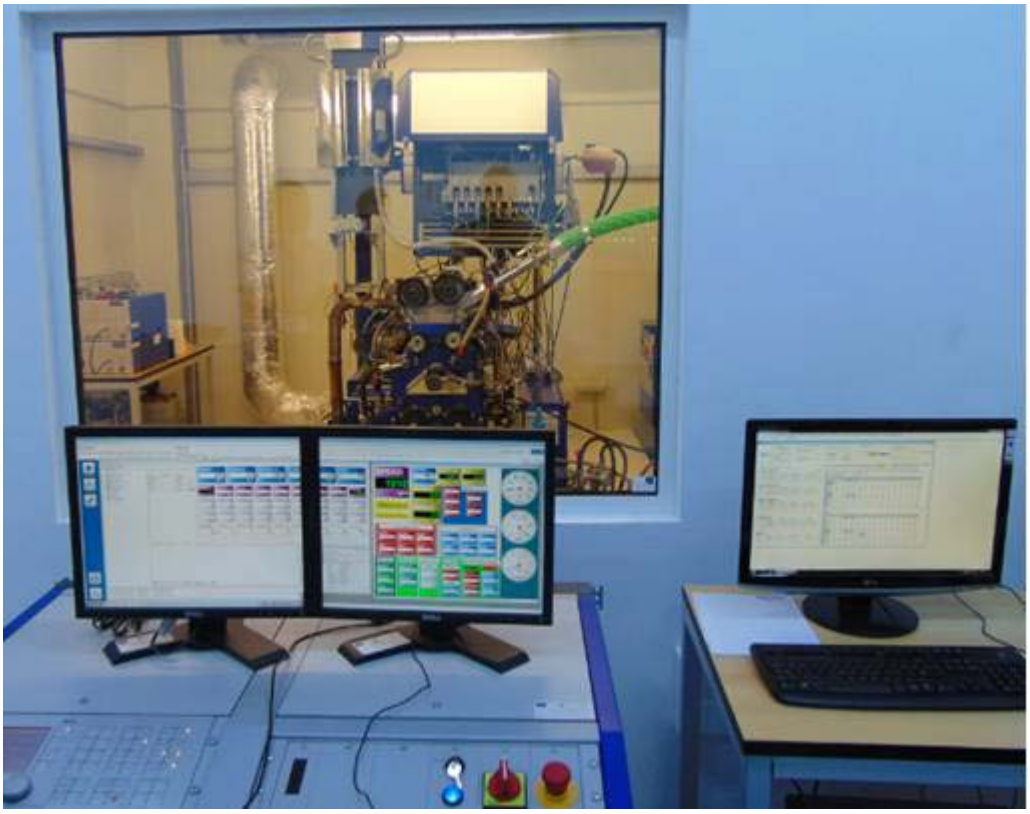

FIG. 2. The tested engine and necessary autoimmunization and software

2. COMBUSTION QUALITY EVALUATION FOR SPARK IGNITION ENGINES

The combustion of spark ignition engines can be divided into three frames: ignition and flame development; flame propagation; flame termination. Flame development is generally considered the consumption of the first 5% - 10% of the combustible mixture. During the flame development period, ignition occurs and the combustion process starts, but very little pressure rise is noticeable and little or no useful work is produced (Fig. 3). Just about all useful work produced in an engine cycle is the result of the flame propagation period of then combustion process. This is the period when the bulk of the fuel and air mass is burned (80-90%). During this time, pressure in the cylinder is greatly increased, and this provides the force to produce work in the expansion stroke. The final 5% - 10% of the mixture which burns is classified as flame termination. During this time, pressure quickly decreases and combustion stops [5].

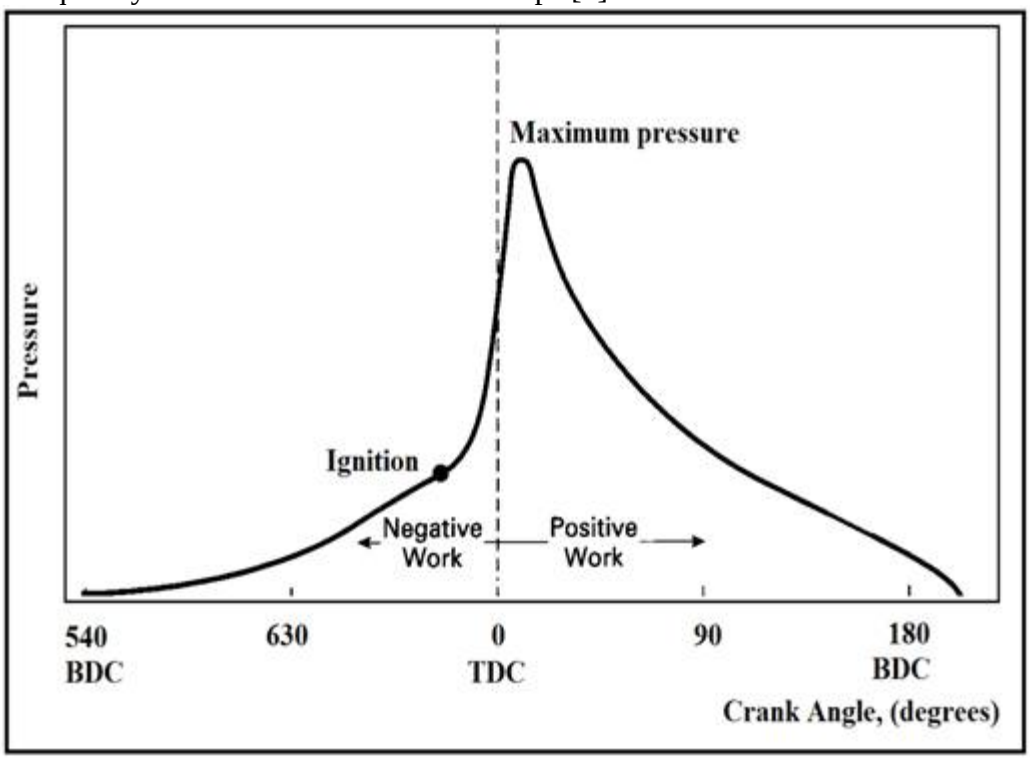

FIG. 3. Theoretical cylinder pressure curve for spark ignition (SI) engines

Theoretically, combustion would be exactly the same for every engine cycle, and there would be no cycle-to-cycle variation. This does not happen due to several variations that occur in the intake system and within the cylinder. Even if no variations occurred before combustion, the turbulence within the cylinder would cause statistical variations to occur during combustion. Temperature differences in the runners cause variations in the evaporation rates, and this causes variations in the air-fuel ratio. More fuel vapor in a hotter runner will displace more air and give a richer mixture and lower volumetric efficiency. Also, the evaporative cooling causes temperature differences and density differences. Passage of air around the throttle plate breaks into two flows, causing vortices and other variations that will then affect all downstream flow [6].

Local variations and incomplete mixing, near the spark plug, cause the initial discharge across the electrodes to vary from the average, which then initiates combustion differently cycle-to-cycle. Once there is a difference in the start of combustion, the entire following combustion process will be changed. Figure 4 shows how pressure varies as a

function of time for 10 consecutive cycles in a single cylinder spark ignition engine. The ensuing combustion process for these cycles will be quite different [7].

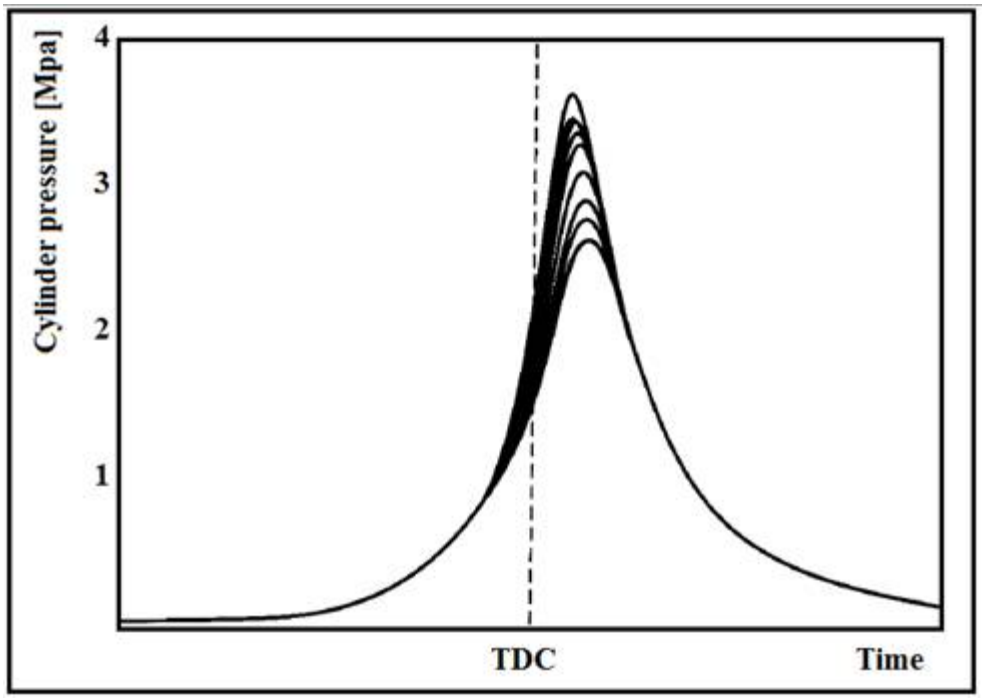

FIG. 4. Real cylinder pressure curve for spark ignition (SI) engines

3. USED EQUIPMENTS

The researches presented in the present paper ware made on a Single Cylinder Research Engine 5405 with following specifications:

- Bore: 82 mm; Stroke: 90 mm; Displacement: 475 cm^3;
- Max. speed: 6000 rpm;
- Rated power: 20 kW natural aspirated;
- Rotation inertia approx. 0,4 kgm^2;
- Combustion concept: Homogeneous, λ=1;
- Compression ratio: 11.5:1.

The test bed have some other components and systems: AVL Engine Control Unit (AVL ETU 427); Coolant and conditioning Unit 577; AVL Fuel mass flow meter - Type Flex Fuel; AVL Fuel temperature control; Intake Air Consumption Measurement Device; Particle Evaluation - Micro Soot Sensor Continuous Measurement of Soot Concentration; AVL PUMA Open Test bed Automation [8].

The used software for intake and combustion process optimization is AVL FI2RE Commander 7.06c – IAV. AVL FIRE was developed to solve the most demanding flow problems in respect to geometric complexity and chemical and physical modeling. FIRE offers a comprehensive computational fluid dynamics solution: a powerful set of modules, features and capabilities, pre-and post-processing integrated in a common environment and workflows and methods effectively supporting the use of the software to solve any problem accurately [2].

The software used for engine parameters monitoring is AVL Indicom software. During cycle based data acquisition the value of cycle time must vary all the time.

3. RESEARCH METHODOLOGY

The engine was tested in controlled laboratory conditions. The used fuel was Petrom 95 gasoline. The atmospheric temperature was constant maintained at 18 ºC.

The test was made for a load corresponding with 613 mbar manifold pressure and for 1520 rpm engine speed. The intake parameters are controlled by set the number of injections (first, second or third direct injection and one indirect injection). In this case it was used only one direct injection. The fuel mixture was adjusted by varying the amount of fuel injected per cycle (injection period - μs). The ignition time was set in crank angle degrees before top dead center. The engine combustion quality was tested for 100 engine cycles.

The parameters changes were made to obtain an optimal single cylinder pressure curve and more optimal combustion (no detonations). In the Figure 5 are presented the intake, ignition and combustion features for 475 cc GDI Single Cylinder Research Engine.

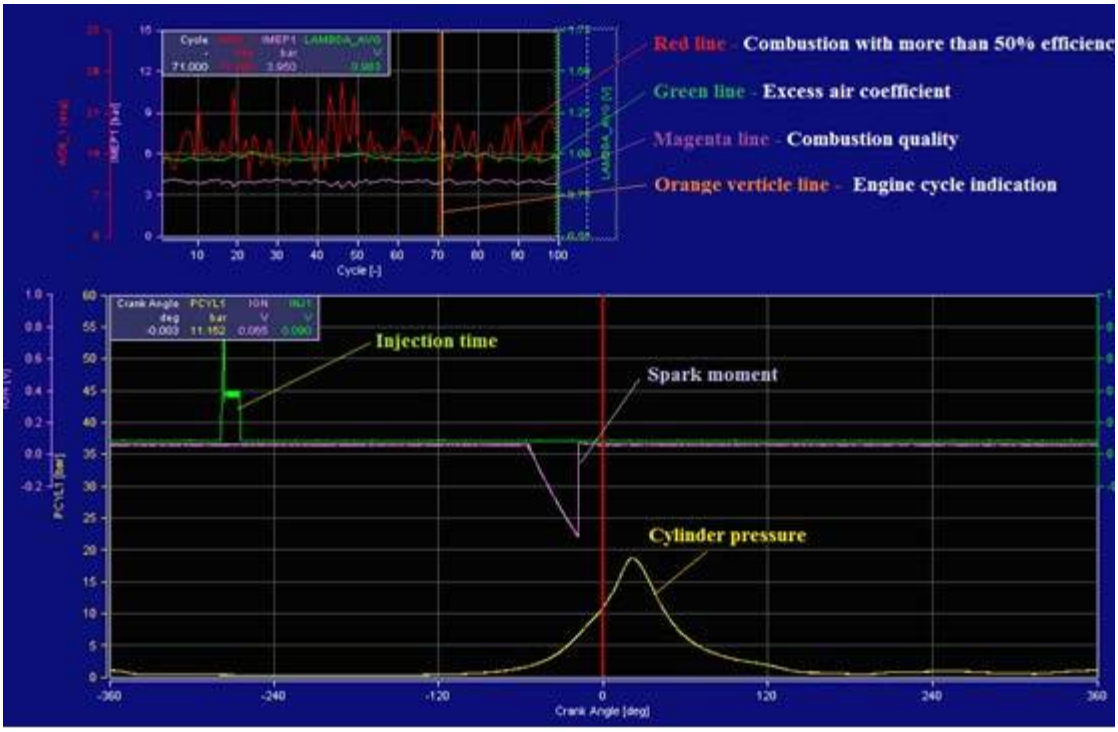

FIG. 5. Experimental cylinder pressure curve and combustion parameters for tested GDI engine

Engine combustion quality can be analyzed using a set of data from the 100 engine cycles recorded. In the top right window (Fig. 5), the combustion quality is represented by the following curves:

- A red line that represents combustion with more than 50% efficiency. The combustion is more efficient when the curve has a high amplitude.
- A green line that represents the excess air coefficient variation. The excess air coefficient (lambda) for this engine is approximately 1. If the line is almost strait the variation is low and the engine runs properly.
- A magenta line that represents the combustion quality. If this line is almost strait the combustion quality is constantly good and the engine runs properly.
- An orange cursor that indicates the actual engine cycle. This position is related to the main interface window that presents the cylinder pressure.

In the main window are presented the parameters for engine test intake, ignition and combustion. The three curves represent:

- A green curve that represents the fuel intake duration. This curve is situated at a relative distance from top dead center (TDC). In this case the advance is - 280 Crank angle degrees.

- A magenta curve that represents the ignition moment (spark propagation). This curve is also situated at a relative distance from top dead center (TDC). In this case the advance is - 50 Crank angle degrees.

- A yellow curve that represents the cylinder pressure curve for the analyzed engine, for one cycle.

For the 100 engine cycles we can observe the cylinder pressure variation. These are related to the fluctuant engine running. In figure 6 and 7 are presented two example engine cycles: cycle no. 46 and cycle no. 80.

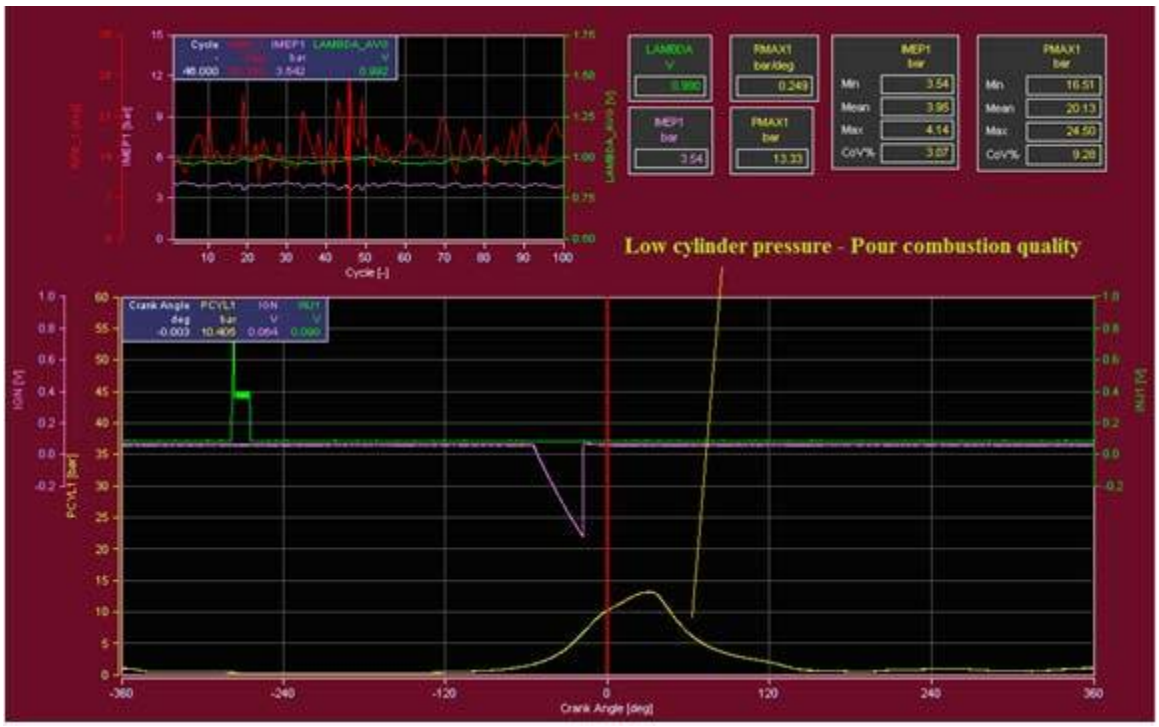

FIG. 6. An abnormal combustion engine cycle (Example: Cycle no. 46)

In Figure 6 is exemplified a motor cycle with a pour quality of combustion. It can be seen a reduced amplitude of the curve of the engine cylinder pressure. For this situation excess air coefficient is 0.990, indicated mean effective pressure is 3.54 bars and the maximum cylinder pressure is 13.33 bars.

In Figure 7 is shown an engine cycle which has a higher combustion quality. The curve of the cylinder pressure has a normal evolution, corresponding to a normal maximum cylinder pressure. For this situation excess air coefficient is 0.983, indicated mean effective pressure is 4.10 bars and the maximum cylinder pressure is 24.50 bars.

For this two examples it can be noticed the variation of the excess air coefficient (air/fuel mixture) and the indicated mean effective pressure that influence the quality of the combustion and the value for the maximum cylinder pressure.

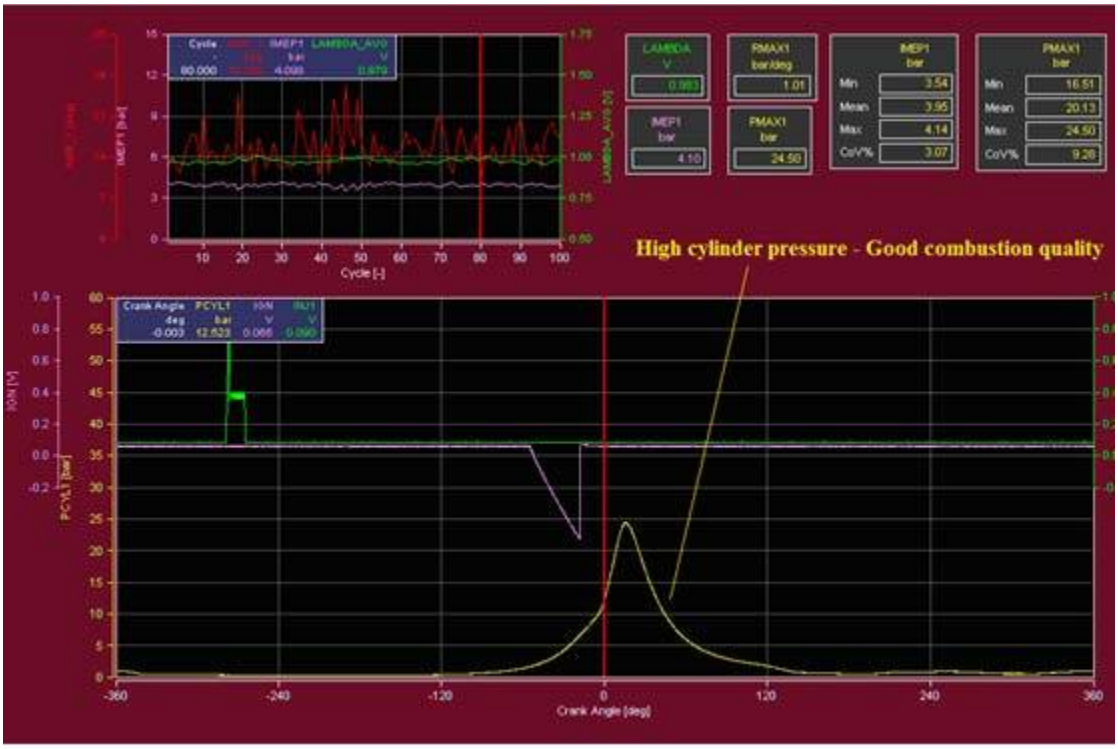

FIG. 7. An optimal combustion engine cycle (Example: Cycle no. 80)

CONCLUSIONS

In the research tests made on the experimental engine, a large set of data were collected for the analysis of combustion quality and efficiency. The combustion quality can be expressed by a set of graphical parameters, among which the most important is the engine cylinder pressure. For functional conditions (for a load corresponding with 613 mbar manifold pressure and for 1520 rpm engine speed) there were recorded 100 engine cycles. It was observed a variation of cylinder pressure curve in function of the excess air coefficient and indicated mean effective pressure.

In order to optimize engine operation and for a high quality of combustion we can take the following measures:

- using an injection strategy with two or three phases;
- varying the advance angle of the spark related to TDC;
- varying the quantity of fuel injected per engine cycle.
- optimization of combustion chambers.

All these strategies can be tested using the software component AVL FI2RE Commander 7.06c – IAV. In Figure 8 is shown the interface for AVL FI2RE Commander software [8].

Another set of measures can be related to modelling the combustion chambers. There has always been extensive debate over the optimum SI engine combustion chamber design. There are a large number of options for cylinder head and piston crown shape, spark plug location, size and number of valves, and intake port design. The major combustion chamber design objectives which relate to engine performance and emissions are: a fast combustion process, with low cycle-by-cycle variability, over the full engine operating range; a high volumetric efficiency at wide-open throttle; minimum heat loss to the combustion chamber walls; a low fuel octane requirement [9].

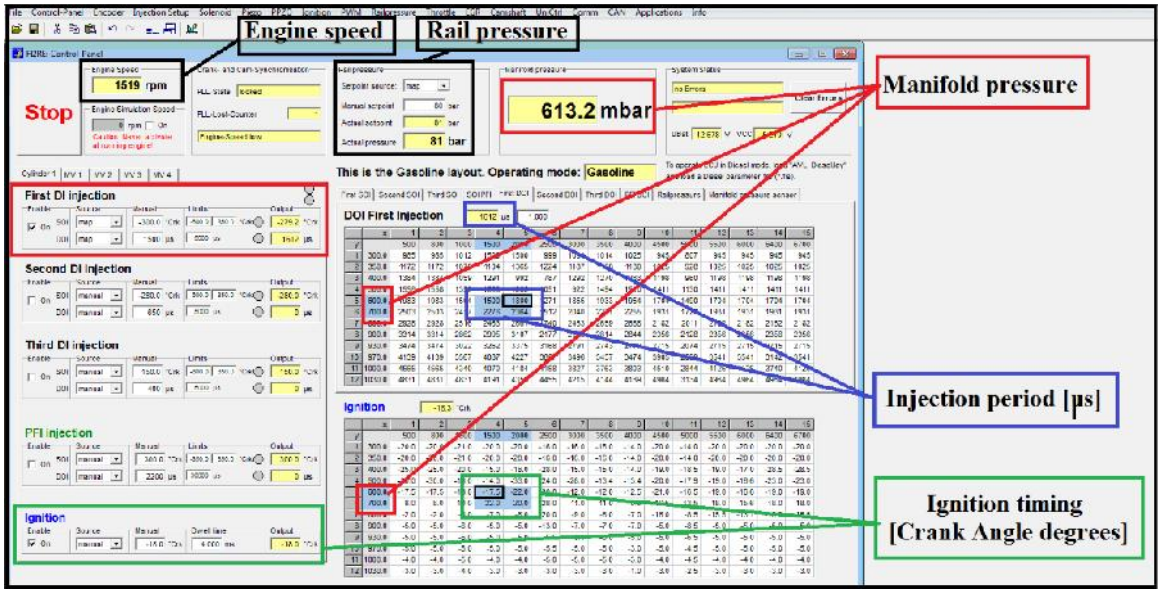

FIG. 8. AVL FI2RE menu - engine map parameters

The research can be extended to multi cylinder engines testing (engines that equip road vehicles). It seeks to improve engines processes and reduction of polluting emissions.

AKNOWLEDGMENT

We hereby acknowledge the structural founds project PRO-DD (POS-CCE, O.2.2.1., ID 123, SMIS 2637, ctr. No 11/2009) and Transilvania University of Brasov for providing the infrastructure used in this work.

REFERENCES

[1] A. K. Singh, A. M. Lanjewar, A. Rehman, Direct Fuel Injection System in Gasoline Engine - A Review, *International Journal of Innovative Technology and Exploring Engineering (IJITEE)*, ISSN: 2278-3075, Volume-4 Issue-4, September 2014;
[2] AVL - Tutorials and books for Engines Test Cell equipments usage, 2013;
[3] O. Fritz, GDI engine development according EU 6, *AVL Tutorials and books for Engines Test Cell*, 2013;
[4] P. K. Gajbhiye, S. P. Chincholkar, Review on Electronically Assisted Gasoline Direct Injection 4-Stroke Single Cylinder Engine System, *International Journal of Science and Research (IJSR)*, India Online ISSN: 2319-7064;
[5] W. Pulkrabek, Engineering Fundamentals of the Internal Combustion Engine, University of Wisconsin-Platteville;
[6] E. F., Obert, Internal Combustion Engines and Air Pollution. New York: Harper and Row, 1973;
[7] J. A. Gatowski, , E. N. Balles, K. M. Chun, F. E. Nelson, J. A. Ehchian, J. B. Heywood, Heat Release Analysis of Engine Pressure Data, *SAE paper 841359, SAE Trans.*, vol. 93, 1984;
[8] S. Ţârulescu, R. Ţârulescu, C.I. Leahu, Optimizing Combustion in an Single Cylinder GDI SI Engine, *Proceedings of the European Automotive Congress EAEC-ESFA 2015, Springer Cham Heidelberg New York Dordrecht London*, ISBN 978-3-319-27275-7 ISBN 978-3-319-27276-4 (eBook), DOI 10.1007/978-3-319-27276-4, Library of Congress Control Number: 2015955888 p. 395-404.
[9] J. B. Heywood, Internal Combustion Engine Fundamentals, ISBN 0-07-028637-X, printed McGraw-Hill, Inc., 2000 Edition.

THE TURBINE INLET TEMPERATURE AND COMPRESSOR PRESSURE RATIO, THE SIAMESE TWINS OF THE GAS TURBINE ENGINES

Béla VARGA, Gyula ÓVÁRI, László KAVAS

National University of Public Service, Budapest, Hungary (varga.bela@uni-nke.hu, ovari.gyula@uni-nke.hu, kavas.laszlo@uni-nke.hu)

DOI: 10.19062/2247-3173.2016.18.1.53

Abstract: *When we read the technical data of any kind of gas turbine engines in most cases besides the performance data we get two important data, namely the Turbine Inlet Temperature (TIT) and Compressor Pressure Ratio (CPR) usually for take-off rate of power. But considering a certain TIT there is a range of CPR which is suitable for this TIT. This range of CPR depends on the TIT itself but the engine component efficiencies also has effect on the possible CPR. In this paper we intended to examine how this range of CPR can be determined, the range itself, how it is affected by the component efficiencies and the operational point of today existing turboshaft engines between the minimum and maximum possible CPR-s. To answer these questions we developed a gas turbine thermal mathematical model.*

Keywords: *take-off operational point, turbine inlet temperature, compressor pressure ratio, specific net work output, thermal efficiency*

1. INTRODUCTION

To achieve the above mentioned results we theoretically determined the possible terms of minimum and maximum CPR-s considering a certain TIT. Surely we have to tie the CPR extremes to some kind of optimum points of the gas turbine engines.

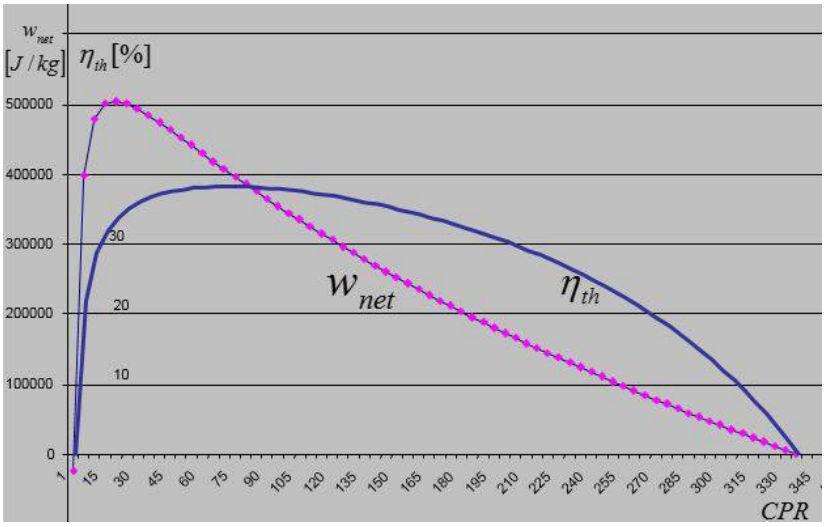

FIG. 1. The Specific Net Work Output and Thermal Efficiency of a gas turbine cycle as a function of Compressor Pressure Ratio [1]

We can presume that the Specific Net Work Output (SNWO or w_{net}) and Thermal Efficiency (TE or η_{th}) of the gas turbine engine cycles, both of which are primary performance indicators and suitable for the evaluation of any kind of gas turbine engines, can define these extremes. It is quite clear that their maximum value are at different CPRs, but lower CPR than that of the CPR of maximum SNWO and higher CPR than that of the CPR of maximum TE is illogical because out of this range both of them decrease, see Fig.1.

2. BUILDING UP THE THERMAL MATHEMATICAL MODEL

To build up the thermal mathematical model we used three basic equations of gas turbine engine cycles (1), (2), (3). All three energy transfers to or from the cycle are the function of CPR, considering given "T_0-T_3" temperature range and component efficiencies [1]. Where "T_0" is equivalent of the International Standard Atmosphere temperature at Main See Level.

Important to note, that the gas properties are also functions of CPR through the actual temperature range of compression or expansion.

$$w_c(\pi) = \left(c_{pa} T_0 / \eta_m\right) \cdot \left(\pi^{(\kappa_a - 1)/\kappa_a \cdot \eta_{polc}} - 1\right) \tag{1}$$

$$w_e(\pi) = c_{pg} T_3 \left(1 - 1/\left(\sigma\pi\right)^{\left((\kappa_g - 1)\eta_{pole}\right)/\kappa_g}\right) \tag{2}$$

$$q_{in}(\pi) = \left(c_{pb} / \eta_b\right) \cdot \left(T_3 - T_0 \pi^{(\kappa_a - 1)/\kappa_a \cdot \eta_{polc}}\right) \tag{3}$$

This equations are suitable to determine the chosen performance indicators, namely the SNWO and the TE.

$$w_{net}(\pi) = w_e(\pi) - w_c(\pi) \tag{4}$$

$$\eta_{th}(\pi) = w_{net}(\pi) / q_{in}(\pi) \tag{5}$$

here: $w_{net}(\pi)$ - SNWO [J/kg]; $\eta_{th}(\pi)$ - TE [-]; $w_c(\pi)$ - specific compression work [J/kg]; $w_e(\pi)$ - specific expansion work [J/kg]; $q_{in}(\pi)$ - specific input heat [J/kg]; π - CPR [-]; T_0 - intake inlet temperature [K]; T_3 - TIT [K]; κ_a - adiabatic exponent for compression [-]; κ_g - adiabatic exponent for expansion [-]; c_{pa} - isobaric specific heat for compression [J/kgK]; c_{pg} - isobaric specific heat for expansion [J/kgK]; c_{pb} - isobaric specific heat for combustion [J/kgK]; σ - pressure loss for the whole engine (air intake, combustor, exhaust pipe, others) [-]; η_{polc} - polytrophic efficiency of compression [-]; η_{pole} - polytrophic efficiency of expansion [-]; η_m - mechanical efficiency including power off take [-]; η_b - combustion efficiency [-].

SNWO ($w_{net}(\pi)$) is the desired output of the thermodynamic cycle. In accordance with the second law of thermodynamics the mechanical work is always less than the input heat and in addition the friction in the real gas turbine elements causes some more heat loss. This heat is dissipated as wasted heat into the environment.

TE ($\eta_{th}(\pi)$), in general, energy conversion efficiency is the ratio between the useful output of a device and the input, in energy terms. For thermal efficiency, the input ($q_{in}(\pi)$) to the device is heat, or the heat content of the fuel that is consumed.

In accordance with (4) and (5) the real gas turbine engine cycles, at given "T_0-T_3" temperature range and component efficiencies, have two optimums, namely the maximum of the SNWO and TE, but the related CPRs are significantly different from each other. In accordance with it, it is impossible to produce the maximum SNWO and the maximum TE in the same time. Using this programme, described in this paper, the user can determine the CPRs of the maximum SNWO and the maximum TE and their actual value.

To determine these special CPRs related to the above mentioned engine properties, equations (4) and (5) needs to be analysed as functions, looking for their local extreme. In this case it is the local maximum we are looking for and can be found by using the first derivative test. SNWO and TE maximums are, where their first derivative is zero, see (6) and (7).

$$w_{net}(\pi) \text{ is maximum, where}: w_{net}'(\pi) = 0 \tag{6}$$

$$\eta_{\text{th}}(\pi) \text{is maximum, where}: \eta_{\text{th}}'(\pi) = 0 \tag{7}$$

The model produces:

- The characteristic curves in TIT versus CPR diagram for any kind of combination of engine component efficiencies;
- Calculates the distinguished CPR values;
- It takes into consideration the change of compressor polytrophic efficiency as a function of blade length giving possibility to evaluate its effect on the distinguished CPRs, TE and SNWO;
- It provides the analyses and evaluation of existed turboshaft engines.

To process the above listed examinations, Microsoft Excel was used with Visual Basic programming. Microsoft Excel Worksheet provides the communication platform of the created Visual Basic programme [3].

3. TE AND SNWO CHARACTERISTICS IN CPR VERSUS TIT DIAGRAM

In Fig. 2 (a) the TE curves can be shown from 20 to 36%, while in Fig. 2 (b) the SNWO curves from 100 to 500 kJ/kg. In both cases the component efficiencies are shown in the bottom left corner. Three curves from left to right represent the CPRs of the maximum SNWO (green), maximum TE (red) and as a compromise between them as the maximum value of their multiplication (blue). The two curves (green and red) really gives the possible range of CPR at this given component efficiencies and at any TIT.

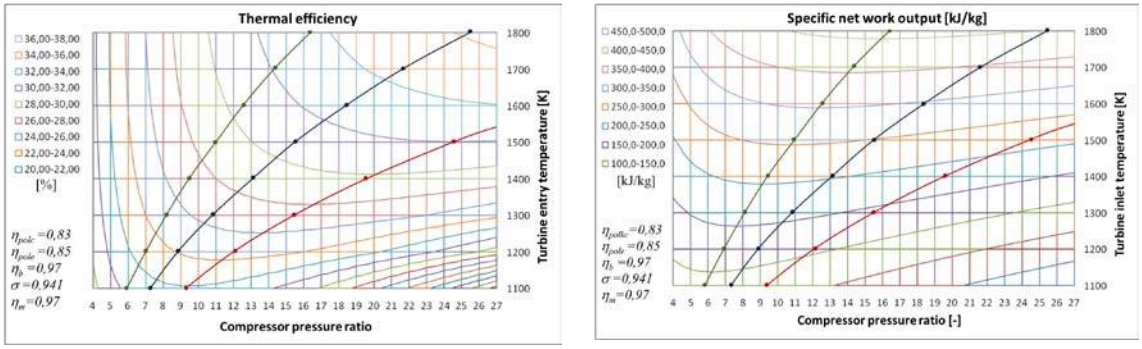

(a) (b)

FIG. 2. The TE and SNWO curves in TIT versus CPR diagram [1]

In accordance with it these charts give general information at a certain component efficiencies what TE and SNWO can be expected and what the possible range of CPR. The model can produce that for every variety of component efficiencies and losses.

What is clearly visible that at a given TIT and at low CPRs both examined engine properties worsen heavily. It can be proven by simple mathematical deduction. Neglecting the deduction we have to recognise that both functions are rational functions with vertical asymptotes, where at decreasing CPR both functions go to infinity.

4. IDEAS ABOUT THE POSSIBLE OPERATIONAL POINT

Presuming, the designers in most cases can work with given engine components, which mostly determine the component efficiencies and turbine entry temperature. In this case the only thing they can vary, is the CPR. Of course, the CPR must not be out of the above defined limits, namely the CPR of maximum SNWO and TE. At a low TIT and consequently low SNWO it is reasonable to position the take-off operational point close to the lower eligible CPR. It is even more justified if the raise of CPR causes significant deterioration of compressor polytrophic efficiency, because in this case the lower compressor polytrophic efficiency can consume the hoped advantage of higher TE. At higher turbine entry temperature, consequently higher SNWO there is larger space for the designers to play with the CPR. One reason that a small drop of the SNWO, from a relatively high value, is not so painful like at originally low SNWO. In addition at this range the deterioration of SNWO at increasing CPR is not so significant like at lower TIT. Consequently, we presumed, that at older turboshaft engines with lower TIT the take-off operational point is positioned in the first part of possible CPR range, between the green and blue line, by Figure 1 and 2. At newer engines with higher turbine entry temperature it is more likely tending to the upper limit of CPR even accepting the deterioration of compressor polytrophic efficiency, however it decreases this upper limit of CPR. In the next part of paper we check these ideas analysing some existing turboshaft engines.

5. ANALYSES OF EXISTING TURBOSHAFT ENGINES

First step for the above mentioned analyses is to collect all possible available performance data of some existing turboshaft engines [3,4,5,6,7,8,9,10]. Of course, there are numerous turboshaft engines, but the companies are not eager to share too much data. Choosing the turboshaft engines we preferred the middle category considering their shaft power. There is only one exception. This one is the LM 2500 turboshaft which is used rather as an industrial and marine gas turbine with much larger size and shaft power comparing to the chosen helicopter turboshaft engines.

During the evaluation I concentrated for five important data:

- Shaft power of take off RPM (P_{shaft});
- TIT (T_3) (or any other temperature in hot section);
- CPR (π);
- Engine mass flow rate $(\dot{m})$;
- Specific fuel consumption (SFC) or thermal efficiency (η_t).

Shaft power, SFC and CPR was almost always available. The TIT caused the strongest uncertainty as either missing or clearly deformed data. It did not thwart the examination but

weaken the verification of results. During the evaluation process the shaft power and the compressor pressure ratio were the two fixed data in the process. The mass flow rate and specific fuel consumption were the two data I used to smooth the model using TIT and component efficiencies as variables. I continued changing the variables until both above mentioned data $(\dot{m}; SFC)$ of the model and the existing engine became equal, which was the requirement to accept the final results of model. As I mentioned earlier, the turbine entry temperature in some cases were confusing. Finding exact data was easier in case of two Russian (ex-Soviet) helicopter engines, TV2-117A and TV3-117, because of their available maintenance manuals. Their turbine inlet temperature only slightly differed from the result of the model. From this conformity I concluded that in case of missing TIT or when it is clearly out of reasonable range I accept the result of thermal model. To be honest I did not try to achieve totally precise results analysing the existing turboshafts. The reason was the relatively large number of analysed engines. To collect all engine data would have been time consuming and sometimes futile. The second reason was that my main object was rather to present how this thermal model works practically.

Table 1. Results of the engine analyses

	TV2-117A	**TV3-117VM**	**T58-GE-100**	**MTR 390E**	**T800-LHT-801**	**RTM 322-01/9**	**LM 2500**
P_{sh} *[kW]*	1103	1699	1118	1043	1166	1799	24000
T_3 *[K]*	1168	1250	1269	1627	1444	1507	1504
$\dot{m}$ *[kg/s]*	6,8	8,75	6,35	3,6	4,53	5,79	70,3
π_{wh}-$\pi_{\eta t}$ π_{op} *[-]*	6,24-9,97 6,6	7,18-12,2 9,45	6,52-10,22 8,4	9,45-16,73 14	8,92-16,41 15	10,36-20,81 14,7	12,38-29,64 18
Poz. [%]	9,58	45,28	50,73	62,48	81,19	41,56	32,58
η_{pole} *[-]*	0,848	0,846	0,824	0,815	0,849	0,857	0,872
η_{polc} *[-]*	0,824	0,824	0,798	0,774	0,808	0,822	0,858
η_t *[%]*	22,58	25,66	22,59	27,83	29,85	32,26	36
w_{net} *[kJ/kg]*	162,3	190,8	176	303,47	257,3	310,8	341,451

here: P_{sh} – shaft power [kW]; $\dot{m}$ - mass flow rate [kg/s]; π_{wh}-$\pi_{\eta t}$ – CPRs of the SNWO and TE maximums at a given turbine entry temperature [-]; π_{op} – take off operational point (CPR) [-]; *Poz. [%]* – position of the operational point between the CPRs of the SNWO and TE maximums [%]; *SFC* – Specific Fuel Consumption [kg/kWh].

Considering the above mentioned operational points (CPRs) it is well demonstrated, that all the operational CPRs are between the SNWO and TE maximums but these positions does not show any significant order, which would allow to draw any deeper conclusions. Their positions are in percentage of the whole CPR range and can be seen in line 5 of Table 1 (*Poz. [%]*).

CONCLUSIONS

Having gone through the analysis process we got other interesting results about the turboshaft engines. It is clear that the helicopter engines (Table 1), like the other fields of aviation have gone through huge evolution. The increased CPR, TIT, and the FADEC system (used by all new engines) improved their performance, although much less than we experience in other gas turbine engine categories. The main reason is that the average turboshafts provide about 250–2500 kW shaft power with 2–12 kg/s air mass flow rate. Accordingly their compressors are relatively small, which causes short rotor blade length,

especially in rear stages (or last centrifugal stage). This effect has been heightened by the development trend to increase the SNWO decreasing the engine dimensions and weight. This fact considerably penalizes mainly the compressor polytrophic efficiency [2]. It is the reason that in some cases compressor and turbine polytrophic efficiency of a newer engine is not significantly higher, what is more sometimes lower comparing to an older engine. It means the CPR is usually not higher than ~15, and the resulted maximum TE is less than 32%, while at bigger (new) gas turbine engines (where air mass flow is over 30 kg/s) the TE is usually over 40%. Good example is the LM 2500, which TE does not achieve 40%, but its TE is considerably higher than the efficiency of the much smaller turboshafts.

The better component efficiencies and the high CPR and TIT of the new generation RTM-322-01/9 presents the best overall features. This is clearly shows us that good performance indicators cannot be achieved only by increasing the CPR and TIT. To keep the component efficiencies, especially compressor polytrophic efficiency as high as possible, has the same importance.

Of course, increasing the TIT and CPR without higher or even sometimes with lower element efficiencies, higher SNWO and TE can be achieved. Without being precise, about 100 K TIT and 2.5-3 CPR raise gives (absolute) 2% TE and 50 kJ/kg SNWO increment. That is the situation today in turboshaft category. Analyzing the performance of turboshaft engines, chosen one category (by shaft-power) we experience that the higher SNWO and TE is mainly coming from the higher TIT and CPR. It is almost a catch-22. Considering the same shaft-power output getting higher SNWO the result is smaller and smaller engine (lower mass flow rate is needed) preventing to achieve (significantly) higher engine element efficiencies or sometimes resulting even lower values [2].

The advantage of this thermal mathematical model that for any variations of the engine element efficiencies and TITs the changes of TE, SNWO and the related CPRs can be followed and vice versa being known the estimated element efficiencies and the desired TE and SNWO the user can determine the necessary TIT and CPR [1].

REFERENCES

[1] B. VARGA, *Gázturbinás hajtóművek teljesítmény és hatásfok növelésének műszaki technológiai háttere, és ezek hatása a katonai helikopterek korszerűsítésére*, PhD értekezés, Budapest, 2013, http://uni-nke.hu/downloads/konyvtar/digitgy/phd/2013/varga_bela.pdf, p. 47-81
[2] E. PÁSZTOR, *Szállító repülőgépek gázturbinás hajtóművei nyomásviszonya növelésének termikus problémái*, 2007, Repüléstudományi Közlemények, p. 36-45
[3] Klimov, url: http://en.klimov.ru/production/helicopter/TV2-117/ , (15.03.2013)
[4] GE Delivers LM2500 Gas Turbines to Austal USA, e-doc, url: http://www.marinelink.com/news/delivers-turbines-austal348871.aspx, (15.03.2013)
[5] GE Aviation, url: http://www.geaviation.com/engines/military/t58/, (15.03.2013)
[6] Data for some military gas turbine engine, e-doc, url: http://www.aircraftenginedesign.com/TableB1.html, (15.03.2013)
[7] MTU Aero Engines, url: http://www.mtu.de/en/products_services/military_business/ programs /mtr390/ index.html, (15.03.2013)
[8] Rolls-Royce, url: http://www.rolls-royce.com/defence/products/tactical_aircraft/t800.jsp, (15.03.2013)
[9] Rolls-Royce, url: http://www.rolls-royce.com/Images/RTM322_tcm92-6703.pdfhttp://www.rolls-royce.com/ Images/RTM322_tcm92-6703.pdf, (15.03.2013)
[10]GE Aviation, url: http://www.geaviation.com/engines/marine/lm2500.html, (15.03.2013)

DYNAMIC CONTROL OF PNEUMATIC ACTUATOR SYSTEM

Ionel Cristian VLADU, Daniela ROȘCA, Nicu BÎZDOACĂ, Viorel STOIAN

University of Craiova, Romania (cristian.vladu@ie.ucv.ro, drosca2003@yahoo.com, nicu@robotics.ucv.ro, stoian@robotics.ucv.ro)

DOI: 10.19062/2247-3173.2016.18.1.54

Abstract: *Pneumatic actuators are among the most used non-electric drive systems. The cost, simplicity of control and mechanical structure are some of the advantages they impose. The main disadvantage of this type of drives consists in unable control of intermediate positioning and dynamic movement. The paper also presents a hybrid drive system, with the actuator pneumatic piston and magnetorheological element for control. This drive system allows complete control of piston displacement and movement dynamics. We also present the experimental results obtained in order to determine the parameters of magnetorheological element for different operating modes.*

Keywords: *unconventional drives, pneumatic, magnetorheological, dynamics*

1. INTRODUCTION

A. Pneumatic actuator

A pneumatic actuator mainly consists of a piston, a cylinder, and valves or ports. The piston is covered by a diaphragm, or seal, which keeps the air in the upper portion of the cylinder, allowing air pressure to force the diaphragm downward, moving the piston underneath, which in turn moves the valve stem, which is linked to the internal parts of the actuator. Pneumatic actuators utilize compressed air to generate the operating energy. These actuators are quick to respond, but are not ideal for environments under high pressures, as gas is compressible. Because of the compressibility of the working environment, pneumatic pistons allow displacements only between extreme positions (zero displacement or maximum displacement), so we cannot achieve partial displacements. Also, the dynamic movement is heavily dependent on the pressure and flow rate of the working and load.

B. Magnetorheological fluid

Magneto-rheological (MR) fluids, generally consisting of small magnetic particles dispersed in a liquid, are material systems whose rheological properties are controllable through the application of an external magnetic field (Fig.1 (a)). Under a high magnetic field, the magnetic particles have been observed to aggregate into elongated clusters aligned along the magnetic field direction. This macro-structure is responsible for the solid like rheological characteristics and is hereby denoted the ground state of the MR fluids at the high field limit. One of the main applications is the stop-valve (Fig.1 (b)).

C. Stop-valve

Since the phenomena occurring during flow of viscous rheological fluids are very complex and difficult, for mathematical modeling is necessary to determine the experimental parameters, global descriptive rheological stop-valve.

Mathematical models proposed for fluids, applied to rheological systems go from ideal operating premises and therefore cannot fully describe a real system.

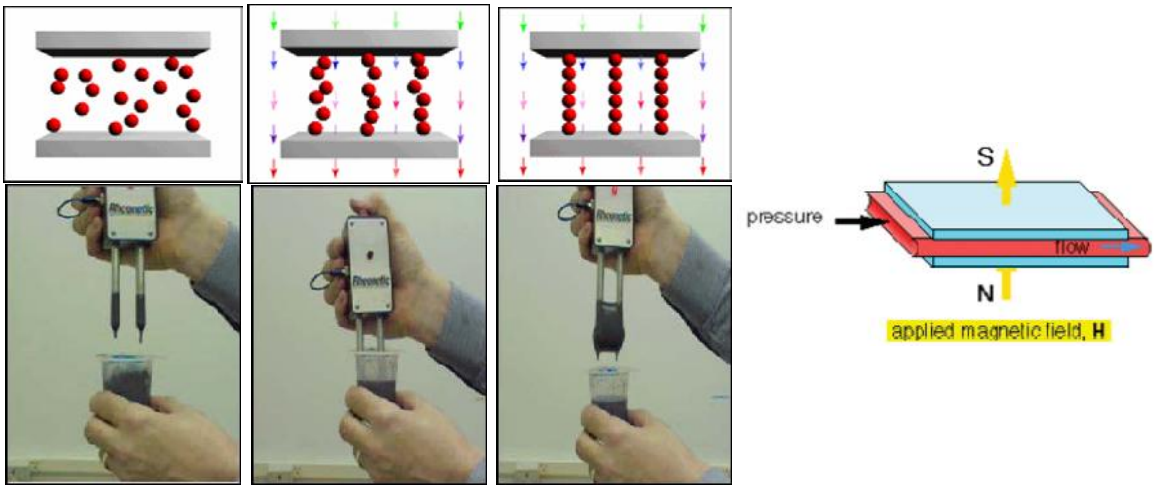

(a) (b)

FIG. 1. Magnetorheological fluid in a magnetic field (a) Magnetorheological stop-valve

Therefore part of the system parameters must be approximated on the basis of preliminary experiments.

Thus for a system with valve-stop depending on the type and size of valve, the constructive rheological parameters are determined experimentally. The mathematical model that describes the behavior in electrical and magnetic field will be based on them.

2. HYBRID DRIVE

A. General description

The paper presents a hydraulic cylinder which is divided in four rooms interconnected with the pressure generator and the MR valve.

For the assurance and the control of the pressure from the cylinder rooms, a generator of controlled pressure built around of a MR stop-valve is used (Fig. 2)[7].

The pressure P (maximum admitted by system) is transmitted in a controlled manner to system through a MR stop-valve. The system consists of the tank with gas under pressure 9, the lines of pressure between tank and cylinder 7 and 8, the double piston 4 and the stop-valve with MR 3. The cylinder 4 is divided transversal in 4 identical rooms by the piston 6. Each among these is divided in two parts by a piston which can displace across cylinder. MR fluid can be found in both central rooms that communicate with the MR valves through pipelines 5. In the rooms from the ends of cylinder gas can also be found and trough the valves; these communicate with the tank with gas under pressure 9 by the pipelines 7 and 8, or they can free the gas in outside cylinder trough other valves.

We suppose the movement is accomplished on the left. Therefore pressure is released in pipeline 7 from the tank of pressure 9. Consequently the piston 6 is displaced on the down. Due to this movement the volume of the MR liquid from internal cylinder is modified and it appears as a circulation of the liquid between cylinder and valve MR 3. This depends on the applied magnetic field which controls the movement piston; it may or may not modify the fluid volume in the room. The movement in opposite direction is analogously made after the release of the pressure of the gas from the rooms by cylinder.

B. Description of MR valve

The magneto-rheological liquids are intelligent smart fluids which modify their physical and chemical properties under the magnetic field action. We modify the fluid

viscosity under the influence of the magnetic field. One of the main applications of this effect is the structure of stop-valve.

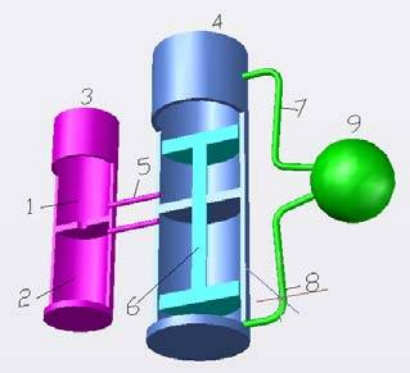

FIG. 2. The hybrid drive – schematic

A stop-valve consists in two lateral walls in which the sources of magnetic field can be found. If the liquid which flows among electrodes is a MR type, then the pressure decreases longitudinally and thus, the difference of pressure on the admission valve or the flow can be controlled through the intensity variation of the applied magnetic field.

The net advantage of this type of admission valve consists in a gradient type control of the resulted pressure. Because the dynamic model must describe the fluid viscid flow (which presents non-Newtonian flow) and because it differs substantially from one geometric valve's model to another, as well as depending on the type of fluid, the difference of pressure on valve according with the intensity of the magnetic field is experimentally determined establishing a tabular correspondence.

3. PROBLEM SOLUTION

A mathematic model for applications and a physical platform for determining stop-valve parameters have been created [1] [2] [3] [4].

Considering that the fluid is an one-dimensional type and that the strength of body and convection effects are negligible, when applying conservation we obtain a differential first degree differential equation between viscosity gradient and axial pressure gradient.

The solution of this equation leads to a linear distribution of viscosity, independent of the type of material existing between the poles.

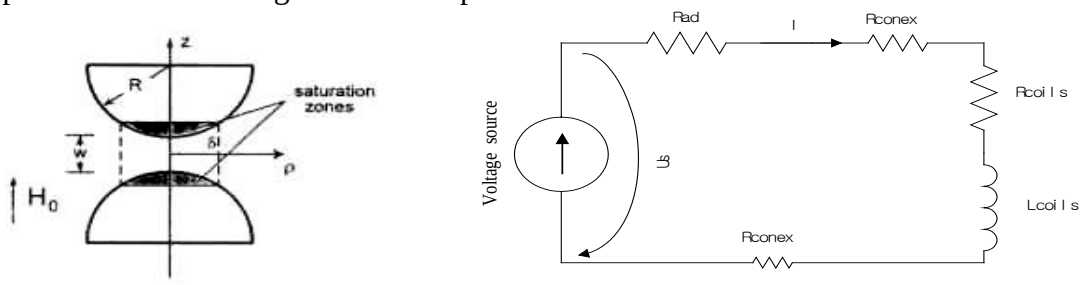

(a) (b)

FIG. 3. Stop-valve MR parameter (a), Simple control circuit (b)

When the material has a characteristic viscosity gradient, such as MR fluid, it will flow until the resulting pressure gradient will increase to a level that it becomes greater

than the dynamic viscosity opposition. In this case, the critical pressure gradient, amplitude, for fluid flow is:

$$\left|\left(\frac{dp}{dx}\right)_c\right| = \frac{2\tau_y}{h} \tag{1}$$

If the pressure gradient is equal to or greater than this critical value, and the fluid in the immediate vicinity of the stimulant poles, where the apparent viscosity maximum, we will have all conditions for the fluid to flow. Near the center, where the apparent viscosity is identical to zero, there will be an area with non-active material, characterized by an uniform axial velocity similar to that of free flow. Its modifications in pressure tubes (based on the formula of d'Arcy for circular tube) are

$$\Delta P_{short\_pipes} = f\frac{l}{d}\frac{\rho}{2A^2}Q^2 = \frac{64}{\mathrm{Re}}\frac{l}{d}\frac{\rho}{2A^2}Q^2 = \frac{K}{K_1}Q^2 \approx K_{\Delta P}Q^2 \tag{2}$$

l - length of tube [m] d - inside diameter of tube [m] - fluid density [kg/m^3], A - area of the tube section [m^2]; Q - flow rate [m^3/sec] f - friction factor ; Re - Reynolds number or the most frequently used form (meaning the change of nozzle or valve):

$$Q = \pi d\Delta x\sqrt{\frac{2}{\rho}}\sqrt{\Delta P} \tag{3}$$

After calculations we obtain:

$$\frac{d}{dt}\left(\frac{\Delta Q}{Q_0}\right) + a_1\frac{\Delta Q}{Q_0} = a_2\frac{\Delta H}{H_0} \tag{4}$$

where

$$a_1 = \frac{12\eta}{g^3 w\rho} - \frac{Q_0}{A^2 wgL} \quad a_2 = \frac{\alpha cm}{g\rho Q_0}H_0^m \tag{5}$$

Using relationship between the magnetic field intensity and the number of spiral coil we obtain

$$\frac{d}{dt}\left(\frac{\Delta Q}{Q_0}\right) + a_1\frac{\Delta Q}{Q_0} = a_2\frac{\Delta I}{I_0} \tag{6}$$

The structure of the most simple control circuit includes a source of current / voltage with additional resistors and coils:

$$\left(R_{ad} + R_{conex} + R_{coils}\right)I + L_{coils}\frac{d}{dt}I = U_s \tag{7}$$

To simplify the electrical circuit, resistance winding with the auxiliary connections can be neglected in comparison with Rad. Using the same technique, with the equivalent circuit that has a dynamic system of order we have:

$$\frac{d}{dt}\left(\frac{\Delta I}{I_0}\right) + a_3\frac{\Delta I}{I_0} = a_4\frac{\Delta U_s}{U_{S0}} \tag{8}$$

where

$$a_4 = \frac{U_{S0}}{I_0 L_{coils}} \quad a_3 = \frac{R_{ad} + R_{conex} + R_{coils}}{L_{coils}} \approx \frac{R_{ad}}{L_{coils}} \tag{9}$$

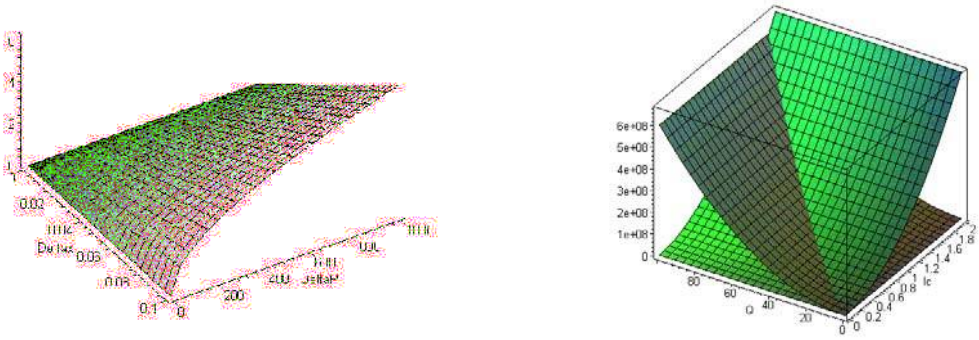

(a) (b)

FIG. 4. Changes in pressure tubes (a), Dependent flow of intensity magnetic field (b)

4. EXPERIMENTAL STAND

The presented platform is designed to determine the experimental parameters of magneto-rheological electro-valves for hybrid actuator.

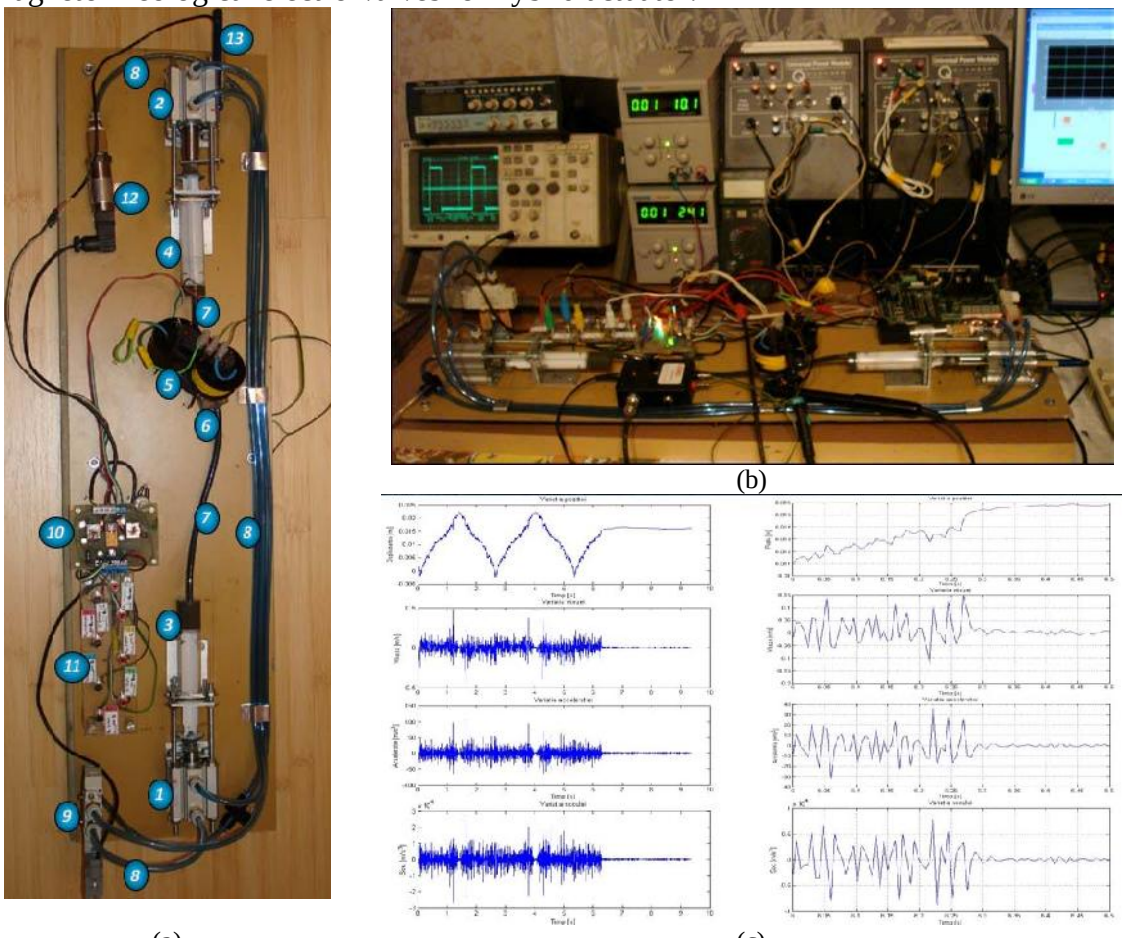

(a) (b) (c)

FIG. 5. Experimental stand (a) (b), Experimental results - stop-valve parameters for step signal (from up to down: the displacement, the speed, the acceleration, the shock; evolution and detail from left to right)(c)

As a concept, the platform is composed of a block which moves rheological fluid, the block which generate the excitation field and the MR electro-valve [5][6]. The experimental stand is shown in figure 5 (a)(b).

Block 1 is composed of two pistons, both with the same shaft, a pneumatic piston and a hydraulic piston. The pneumatic plunger has the role of motion generator, while the other piston trains the magneto-rheological liquid. The second block has a similar construction and operates the same way. I have to mention that the movement is generated only in one of the blocks 1 or 2 at a time. Therefore a block has the role of motor, the other having the role of a generator. These are in series to the block 3 - the magneto-rheological stop-valve. Electro-valve energy may be influenced by the utilization of an electromagnetic element composed of a framework for ferrite winder - block 4. The command is given for the both pistons in a positive or negative direction of the axis. By applying magnetic field to the electro-valve MR we control the speed of MR fluid. The final result depends on ~~of~~ the speed of movement of the rheological fluid, which ~~is~~ also depends on the power energy which generates the magnetic field.

The order of displaced pistons from blocks 1 and 2 is done by the electro-valve with pneumatic drawer - block 5. Depending on its supply voltage (0V and 24V) a movement is generated for pistons from block 1 and block 2).

By using PC with a Simulink algorithm command and by interfacing the computer with the platform, the acquisition board from Quanser system is used. The order stand is made by Quanser acquisition system using a PC. Control laws are implemented through a custom Simulink Quanser model. This model allows modeling of the voltage generator excitation control according to a law implemented and the process repeated a sufficient number of times to obtain average values of the parameters real valve.

CONCLUSIONS

The presented actuator has a simple construction having all the features of a pneumatic drive. The motion control is precise by using the stop-valve MR. Only a little volume of MR fluid is used in the circuit controller of pressure.

Although mathematic modeling can be difficult and although it depends on the actuator model and on the used material, it can easily establish a tabular correspondence for sizes that we concern, using experimental methods.

REFERENCES

[1] Aboudi, J. – *Effective behavior and dynamic response modeling of electro-rheological and magneto-rheological fluid composites*, Smart Mater. Struct., 8, 1999, 106-115

[2] Bîzdoacă, N., Ivănescu, M., Vladu, I.C., Other, (2009), *Control and integration of smart materials and structures technological.* vol 1-5, Universitaria Publishing House, Craiova, 2009

[3] Bîzdoacă, N., Diaconu, I, *Magnetorheological (MR) Fluids. Basic Mathematical Models For MR Applications – 39 Week of the Syrian Science – 6-11 Nov.*, Damascus, 1999

[4] Jianwei Zhang, Xiuqing Gong, Chun Liu, Weijia Wen, and Ping Sheng, *Electrorheological Fluid Dynamics, Physical review letters*, volume 81, number 7, 7 NOVEMBER 2008

[5] Vladu I., Strîmbeanu D., Ivănescu M., Vladu I. C., Bîzdoacă E. N., *Experimental results for magneto-rheological stop-valve,* Sinaia, Romania, Octomber 12-14, 2012, 16th International Conference on System Theory, Control and Computing (ICSTCC)

[6] Vladu I., Vladu I. C., *Experimental determination of parameters descriptive Of magneto-rheological valve*, Craiova, Romania, Octomber 11-15, 2011, 8th International Conference on Electromechanical and Power Systems (SIELMEN)

[7] Vladu I.C., Ravigan F., *Magnetorheological Actuator with PWM Control Modelled using Simhydraulics*, Brasov Romania, 25-27 May, 2009, Proceedings of 18th International Workshop on Robotics in Alpe-Adria-Danube Region (RAAD)

COLLABORATIVE LEARNING USED IN TEACHING THE INFORMATION TECHNOLOGIES CONCEPTS

Tiberiu BULIGA, Ștefan-Gheorghe PENTIUC

MintViz Lab, MANSiD Research Center,
Faculty of Electrical Engineering and Computer Science, Suceava, University "Stefan cel Mare" of Suceava, Romania (tibi81@yahoo.com, pentiuc@usv.ro)

DOI: 10.19062/2247-3173.2016.18.1.55

Abstract: *The article briefly presents a review about the Computer-Supported Collaborative Learning. Will be introduced different elements for CL, a few principles of using CL and what is a Collaborative Virtual Environment (CVE). In the second part will be discussed about how to use the CL to teach fundamental concepts from IT. The study case presented uses CL concepts to teach the Merge Sort algorithm.*

Keywords: *E/Learning, Computer-supported collaborative learning: CSCL, Collaborative Virtual Environment: CVE*

1. INTRODUCTION

The Romanian educational context has changed under the influence of socio-political factors and the progress of Information Technologies. The education pattern has changed the paradigm of learning based on progressive retention of information (ancient type) to the modern learning paradigm based on experiential learning (skills acquisition) and social interaction.

This article concerns the concept of collaborative learning (CL), where the full term is Computer-Supported Collaborative Learning (CSCL).

CSCL is a sub-branch of science education that is concerned with studying how people can learn together through mediated systems.

Panitz thought to a similar definition and added only that the teacher must control documents after the educational planners with very clear objectives. Kagan has developed learning activity subject adding a targeting component of social interaction. Johnson, Johnson and Holubec (1993) say that collaborative learning leads to maximize learning for all educational actors. Slavin (1996) stresses the element of collaboration: teamwork and common goals of the team. ipei. By G. Stahl [et. the] quoted by Traian Rebedea – in "Collaborative learning", "it is important to view CSCL as a vision of possibilities that computers hide and a bundle of research directions that should be followed, rather than an established lab practice and teaching widely accepted ".

2. CSCL EVOLUTION

More avant-garde projects such as: project ENFI - Gallaudet University, the project CSILE - University of Toronto and the "5th Dimension" - University of California - have led to the concept of CSCL. All three projects have included and tested new ways to develop reading and writing through technology. The ENFI project led to one of the first

software to communicate through text (now chatting) "CSCWriting" (Gruber, Peyton & Bruce, 1995).

The CSILE project (Computer Supported Intentional Learning Environment - Learning Environment mediated by computers) later known as the Knowledge Forum fashioned a new pedagogy for perceiving classrooms as small communities that develops knowledge.

The "5thD" was developed with the idea of developing reading and writing skills.

All these projects have used computer systems and information technology in the interest of education and for developing new activities introduced in the training of social organization. Thus were laid the foundations of CSCL. A seminar in 1989 Maratea, Italy is considered the start of the CSCL because it was the first international public meeting that sugested the term "computer supported collaborative learning". CSCL first conference was held in US in 1995 marking a suite of many other annual conferences that followed and which developed this research field. Among the most popular papers we can notice: Bruffee - Collaborative Learning (1993), Crook - Computers and the Collaborative Experience of Learning (1994), Dillenbourg - Collaborative Learning: Cognitive and Computational Approaches (1999), Bereiter - Education and Mind in the Age knowledge (2002). Since 1996 the area was regularly enriched with various articles published by the International Journal of Computer Supported Collaborative Learning. In 2015 was published an anniversary article : "A decade of CSCL" by Gerry Stahl -known author.

Collaboration vs. Cooperation CL

Cooperation (cooperation or joint work) is achieved through collaboration ("action of work and its outcome. In collaboration (with ...) = participating actively through an effective contribution to a work jointly and together (with ...) "); by Oxford dictionary definition of cooperation is “the action or process of working together to the same end” with the origin late middle English: from Latin cooperatio(n-), from the verb cooperari (see cooperate); later reinforced by French coopération.

Many dictionaries retain these two terms as synonyms but we can differentiate two slightly distinct meanings understanding through cooperation "a form of relationship between students consisting of solving problems of common interest, they each contribute actively and effectively" (Dr. Loretta Handrabura, 2003) and cooperation "a form of learning, study, interaction, interpersonal/intergroup depending on time legth and resulting from mutual influences from the agents involved" (Dr. Loretta Handrabura). Panitz stresses that collaborative learning is a personal philosophy, not just a classroom technique. The basic premise in collaborative learning is consensus -between cooperative group members thus avoiding competition where the most equipped outweigh other weaker group members. Collaborative learning is defined by a set of processes that help educational actors interact to achieve a specific goal or develop a final product. Although there are many group type analysis and different insights the fundamental approach in collaborative learning is teacher-centered while classic educational process is student-centered. Therefore, cooperative learning requires joint action of several people (students, teachers) in pursuit of common goals by influences that benefit everyone involved. Collaborative Learning focuses on the tasks involved in relationship but cooperation is the process of achieving those tasks. "(Oprea, Crenguţa - Lăcrămioara, 2003). The same author points out that "collaborative learning integrates cooperative learning." (Oprea, Crenguţa - Lăcrămioara, 2003).

3. MAIN ELEMENTS AND PRINCIPLES OF CL

According to Johnson & Johnson, Johnson & Holubec 1989 and 1998, there are five fundamental elements that characterize this type of learning:

1. Positive Interdependence

According to this principle the group's success depends on the effort in the task by all members. Students are directed towards a common goal, stimulated by a collective assessment and the result is the sum of all efforts.

2. Individual responsability

According to this principle each group member takes responsibility to solve the task.

3. Training and development of social skills

According to this principle young students follow along stimulating interpersonal intelligence, namely the ability to communicate among themselves, to seek and receive support when needed, to provide innovative ideas and solve other conflict situations in everyone's interest.

4. Face to face Interacting

This principle is about seeking direct contact within working group members, also seating arrangement so that they can create small groups of interaction or even software methods by which children would encourage and help each other.

5. Group task division

According to this principle we should reserve time to reflect on how they will solve all the tasks by each individual member and also by the collective group.

The main CL Principles are the following:

1. Enhance the capability of students in retention
2. Increase a positive attitude towards learning
3. Develop social skills

4. Maximum using of different learning styles of all children

5. Performance improvement for the weaker children when they are grouped with the other children.

It is important to bear in mind that progress will not ever stop and new tools and strategies will occur and will refine permanently. Innovation is the precursor to a permanent connection to current ideas.

The collaboration will bring added value to the company and a product (even educational) more valuable to final beneficiaries.

CL reduces stress, makes education seem much easier, it gives freedom of expression and in general makes people happiest.

4. COLABORATIVE VIRTUAL ENVIRONMENTS(CVE)

A. From AI to CSCL

CSCL can be seen in contrast with earlier approaches to using computers in education. Koschmann (1996) has identified an historical sequence of approaches:

(a) Computer assisted training

It was a behaviorist approach that dominated the early years of modern education (1960). In this perspective, learning is seen as a store of facts. The fields of knowledge were organized bottom up type, from basic literacy students who were presented in a logical sequence through computerized training and exercises. Many commercial educational software still follows this approach.

(b) Artificial intelligent systems (AI)

AI started from a cognitive philosophy analysis learning by accurate mental models and potentially faulty mental representations. It thus rejected the behaviorists who said that learning should not be concerned with how students represent and process gained knowledge. This approach seemed particularly promising in the 1970s and created computer models of student response actions (event-based programming) which identified errors in user's mental models.

(c) Logo

This paradigm of the 1980s approach is claiming that sujects must themselves build their own knowledge stimulating the desire for exploration and use of your own judgment (functions, subroutines, loops, recursion, etc.).

(d) CSCL

CSCL approach was initiated in 1990. It explored how computers could bring students together to learn working together in small groups and learning communities. Motivated by social constructivist theories this paradigm offers opportunities for mutual support in educational construct. Here began AI era that was carried forward by the concept of CSCL. Within CSCL learning focus is on collaboration with other colleagues rather than learning directly from the teacher. This way the role of the computer shifts from mere provision of knowledge - whether in the form of eLearning tutorials or as feedback by IS - to supporting collaboration by providing channels of communication and interaction scaffolding.

The primary form of collaborating is networking based support (email, chat, forums, videoconferencing, instant messaging, social networks and newest 3D environments).

B. Collaborative E-Learning Systems

E-Learning systems that promote learning in a collaborative virtual environment (CVE) can be:

a) Immersive Simulators
b) Virtual Learning Environment
c) Serious Games

C. 3d Virtual worlds

3D virtual worlds are "practical tools for virtual reality" (E. Castranova, 2005). Unlike the paradigm of virtual reality technology that makes use of expensive hardware and creates an artificial environment, Virtual 3D environments are built in environments, something that may offer access to the user itself. Virtual worlds can be accessed by multiple users simultaneously (MMOG - Massively Multiplayer Online Games). A multiuser 3D virtual world (3D MOVIE) is an environment where you can interact via avatars.

Most authors who studied virtual worlds emphasized their persistent character between different working sessions.

Among the variety of 3D virtual worlds we distinguish: Open Wonderland, Open Qwak, Active Worlds, Vastpark, Multiverse, Worlds, Reaction Grid, Second Life (including open source Open Sim).

3dMUVE is the new media that could be used in education. Persistence feature allows resumption of social interaction such as collaborative learning.

D. Linking learning and 3D virtual worlds

One of the most used LMS platforms (learning management system) is Moodle platform (open source type). It is implemented in various educational institutions and companies that support training. Although this platform is very flexible and allows for

better content management and assessment tools, its weak point is interactivity and interaction between users. Therefore CVE remains more efficient solution for modern training. Why CVE?

(a)Social Learning: students can meet each other (whether part of the same school or from partner schools).

(b)Inspiring Learning: 3D virtual environments allow exploration on real or imaginary locations.

(c)Creative Learning: Some virtual worlds allow students to build easy real or virtual objects. There is therefore unlimited opportunities for collaboration with other students in order to undertake tasks of design and construction.

(d)Relevant Learning: Virtual meetings can be their real-life counterparts and so students will benefit from practicing skills needed in the 21st century in a 3D virtual environment.

5. STUDY CASE

It was designed a lesson about the Merge Sort algorithm applying the principle of Cl. In the lesson are involved a server and a number of mobile devices by the students. The stages of the lesson are the following:

- the students make login in to the server
- the server firstly generates randomly an array of integers, and after divide this array into a number of sub-arrays that are sent to the student devices
- the students try to sort their sub-arrays and try to sent the result to the server
- the module communicating with the server check if the subarray is in the correct order and if OK it send the sub-array to the server
- the server make the merge operation with the received sub-arrays and display the final (sorted) array

In a more suitable version the problem will be solved on much more levels. Some students will have the possibility to divide their sub-arrays into small ones and to send these to their colleagues. These students will make after the merge sort and will sent the merged sub-array to the next higher level.

6. CONCLUSION

Computer systems continue to play a central role in supporting education based on student collaboration. It identifies and develops new methods and theories for wide group collaboration, also new methods of learning and assessment.

Education increasingly use new technologies in learning and computer-supported collaborative learning tends to be accepted as a basic form of learning and would be widely adopted.

The Collaborative Learning seems to be very usefull to be used for teaching fundamental concepts of computer science, especially those where multi-processing or parallel processing may be involved.

AKNOWLEDGMENT

This research was supported by the project "Integrated center for research, development and innovation in Advanced Materials, Nanotechnologies, and Distributed Systems for fabrication and control", No. 671/09.04.2015, Sectorial Operational Program

for Increase of the Economic Competitiveness, co-funded from the European Regional Development Fund.

REFERENCES

[1] Stahl, G., Koschmann, T., & Suthers, D. (2006). *Computer-supported collaborative learning: An historical perspective*. In R. K. Sawyer (Ed.), Cambridge handbook of the learning sciences (pp. 409-426). Cambridge, UK: Cambridge University Press. Available at http://GerryStahl.net/cscl/CSCL_English.pdf in English, Învăţarea colaborativă sprijinită de calculator: O perspectivă istorică - Traducere de Traian Rebedea, revăzută de Ştefan Trăuşan-Matu http://GerryStahl.net/cscl/CSCL_Romanian.pdf in Romanian

[2] Johnson David W., Johnson Roger T. (2001). *Making Cooperative Learning* Work Available at http://bama.ua.edu/~stjones/ph582/johnson.pdf

[3] Rebedea, T., Dascălu, M., Trăuşan -Matu, Şt., Teodorescu, A., Ene, A. *Analyzing Collaborative Learning Processes Automatically: Exploiting the Advances of Computational What is cooperative learning?* Available at http://www.academia.edu/4424158/_Traian_Rebedea_Mihai_Dasc_%C4%83lu_%C8%98tefan_Tr%C4%83u%C8%99an

[4] Panitz, Theodore (1999). *Collaborative versus Cooperative Learning: A Comparison of the Two Concepts Which Will Help Us Understand the Underlying Nature of Interactive Learning* Available at http://files.eric.ed.gov/fulltext/ED448443.pdf

[5] Gruber, Peyton & Bruce,"*CSC Writing"* (1995), in Stahl, Gerry (2010). Global Introduction to CSCL, p.62, Available at http://gerrystahl.net/elibrary/global/global.pdf

[6] G. Stahl (2015). *A decade of CSCL*, Available at http://paperity.org/p/74623182/a-decade-of-cscl

[7] Panitz, Theodore (1999). *Collaborative versus Cooperative Learning: A Comparison of the Two Concepts*, Available at http://files.eric.ed.gov/fulltext/ED448443.pdf

[8] Oprea, Crenguţa (2003). *Pedagogie. Alternative metodologice interactive*. Bucureşti: Editura Universităţii din Bucureşti, ISBN 973-575-776-1

[9] Gaylor R. (2013). 12 *Principles of Collaboration*, http://westxdesign.com/2013/04/collaboration/

[10] Hoan C., Lim K. Y. T. (2015). *Effectiveness of collaborative learning with 3D virtual worlds*, http://onlinelibrary.wiley.com/doi/10.1111/bjet.12356/abstract

[11] Johnson, D.W., Johnson, R. (review 2009). *Making cooperative learning work*, Available at http://www.tandfonline.com/doi/abs/10.1080/00405849909543834?journalCode=htip20

[12] Hebbel-Seeger, A., Reiners, T., Shaffer, D. (Springer, 2014). *Synthetic Worlds: Emerging Technologies in Education and Economics*, https://books.google.ro/ books? id=5ee3BAAAQBAJ&pg=PA273&lpg=PA273&dq=Synthetic+Worlds:+Emerging+Technologies+in+Education+and+Economics&source=bl&ots=5WVlHHYi0Y&sig=x_FGuj4baSQp-EjKLPCdbh6OgCI&hl=ro&sa=X&ved=0ahUKEwjb8f7OwsLMAhWH7BQKHWPqApEQ6AEIKjAC#v=onepage&q=Synthetic%20Worlds%3A%20Emerging%20Technologies%20in%20Education%20and%20Economics&f=false

[13] Qvortrup L. (Springer, 2001). *Virtual Interaction: Interaction in Virtual Inhabited* 3D Worldshttps://books.google.ro/books?id=jkLtBwAAQBAJ&pg=PA115&lpg=PA115&dq=Qvortrup+L.++Virtual+Interaction:+Interaction+in+Virtual+Inhabited+3D+Worlds,+Springer&source=bl&ots=6U8NLVJy76&sig=N2QcoTDCDdTeoZEZjVVqPzYHf8c&hl=ro&sa=X&ved=0ahUKEwin0dmdw8LMAhVDzRQKHdwmDYEQ6AEIPTAE#v=onepage&q=Qvortrup%20L.%20%20Virtual%20Interaction%3A%20Interaction%20in%20Virtual%20Inhabited%203D%20Worlds%2C%20Springer&f=false

REGARDING THE POPULATION DYNAMICS INVESTIGATION USING ENVIRONMENTAL INFORMATION SYSTEMS

Alin-Andrei CIORUȚA, Bogdan CIORUȚA

Faculty of Science, North Univ. Center at Baia Mare - Technical Univ. Cluj-Napoca, Baia Mare, Romania (aciorutza@yahoo.com, bogdan.baiamare@gmail.com

DOI: 10.19062/2247-3173.2016.18.1.56

Abstract: *The growth of organisms in a favorable environment is typically modeled by a simple exponential function, in which the population size increases at an ever-increasing rate. This is because the model, at their most simple, assume a fixed net "birth" rate per individual. This means that as the number of individuals increases, so does the number of individuals added to the population. This description of population change pre-supposes that resources for growth are always adequate, even in the face of an ever-increasing population. In the real world, resources become limiting for growth, so that the rate of population growth declines as population size increases.*

There are several numerical (bio-mathematical) models that simulate this behaviour, and here we will explore a model termed generalized "logistic" growth. The generalized logistic differential equation, dealt with in this paper, is a classical, but still useful model for describing the dynamics of a one-species population in an environment with limited resources.

This paper deals with the theoretical analyse (definition, properties) and some applications of the dynamic systems treated under the generalized logistic equation formalism. Also, there are presented a variety of growth curves based on extended forms of the classical Verhulst logistic growth equation and some applets realised in Wolfram Mathematica.

Keywords: *Environmental Informatics, population dynamics, growth models*

1. INTRODUCTION

Science and scientific knowledge of the world is at the base of everything that mankind has gradually accomplished, for the last century. Nowadays society would have had probably another view without mankind considerable scientific activities and revelations (discoveries). As time went by, these discoveries helped reshape our culture and society progress [5,6].

The importance of discoveries (e.g. Artificial Intelligence, Environmental Informatics) is evaluated by its economic impact or by the benefit that brings for a large number of people. Data transferring, modern transport, electricity and many others, are the "mature fruit" of epochal discoveries, purely scientific [5].

Environmental Informatics, as a scientific discovery, applies methods and information technologies for the collection, analysis, interpretation, dissemination and use of the environment's information. It also includes a wide range of disciplines that can be used to understand the specific environment issues: *artificial intelligence*, *neural networks*, *geographic information systems (GIS)*, *remote sensing*, *mapping services*, *data storage technologies (databases)*, *software engineering*, *mobile technology* and *the Internet*.

The main goal of Environmental Informatics is the creation of a research infrastructure related to the integration of research projects in key areas of academic and research activities [6]:

- *environmental science*: geology, geophysics, meteorology, biogeography;
- *chemistry* related fields: environmental chemistry, biochemistry, biotechnology, enzymology, chemistry technology, analytical chemistry;
- *biology* with related fields: ecology, ethology,'s biomonitoring, ecotoxicology;
- *physics* with related areas: environmental physics, biophysics, physics of solids;
- *mathematics* and the related fields: mathematical modeling, biostatistics, applied mathematics;
- *computer sciences* with related areas: artificial intelligence - soft computing, parallel computing and distributed, computational mathematics, bioinformatics.

The modern society (information society) in accordance with the actual changes and preocupations in the environment domain has provided various types of informatics resources (tools, methodologies, procedures) to manage and support the ideas and actions related to the environmental issues [4], as presented in Fig. 1.

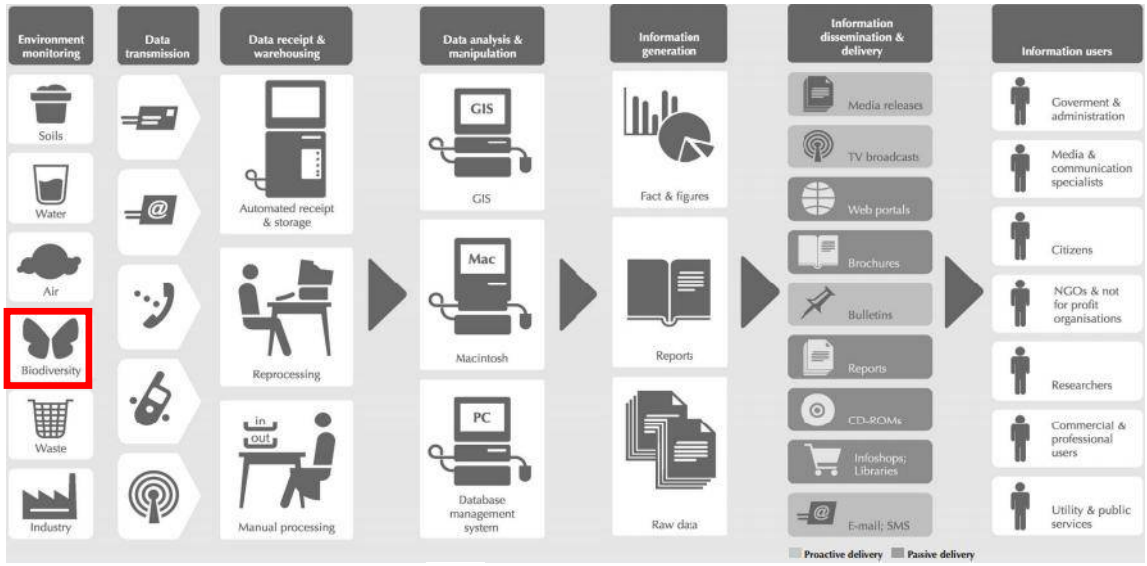

FIG. 1. The schematic diagram for EIS [10]

Population grows over time as well as the modern technology implication in everyday life. Informatics become essential for all the fields related to technology and environment protection. Informatics resources are becoming nowadays more and more important for environmental management, planning and decision-making [4].

An exhaustive analysis of the environmental hazards in terms of physical, chemical, biological, geological, hydro-meteorological processes and their interactions is becoming critical, and not so extraordinary made without the support offered by the environmental information systems (EISs) and environmental informatics [4].

2. INTRODUCTION

Nowadays, significant efforts are required to analyze relevant data and environment information, simulate related processes, evaluate resulting impacts or scenarios and generate viable decision alternatives. The informatics resources developed in the last 3-4 decades have enabled and help us to investigate the complex interactions between the natural systems and engineered ecosystem, and also to search for sustainable strategies

for a harmonious development. Environmental information and environmental information systems play an important role in decision-making in the field, being closely linked with environmental requirements in decades [7], and with environmental research methodologies [5]. The discussion on EISs as particular environmental research methodologies aims to identify characteristic attributes that allowed passage of environmental data to environmental information and from EISs to Environmental Informatics.

In the contemporary society the dynamism of the changes in all the domains of the social, cultural, economic and ecologic life is one of dominant constants. These transformations of the society represent solicitations and challenges that the academic structure and the mankind have to deal with; both through the way in which it organizes the knowledge and the learning, through the quality of the results in the end, and also through the ways in which it distributes them in the society, using, in most cases, the correspondence between the real world and the mathematical world [8] (Fig. 2).

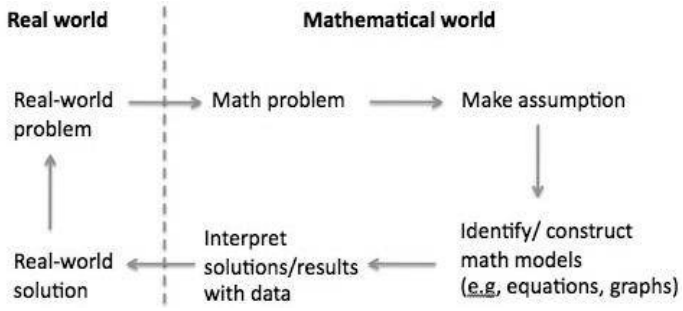

FIG. 2. Mathematical models as a relation between real and mathematical world

According to all the equations presented before it is essential to notice that every population models seems to be derived from the generalized logistic growth model [1], with different values for the α, β and γ parameters [3,11], as presented in the Fig. 3.

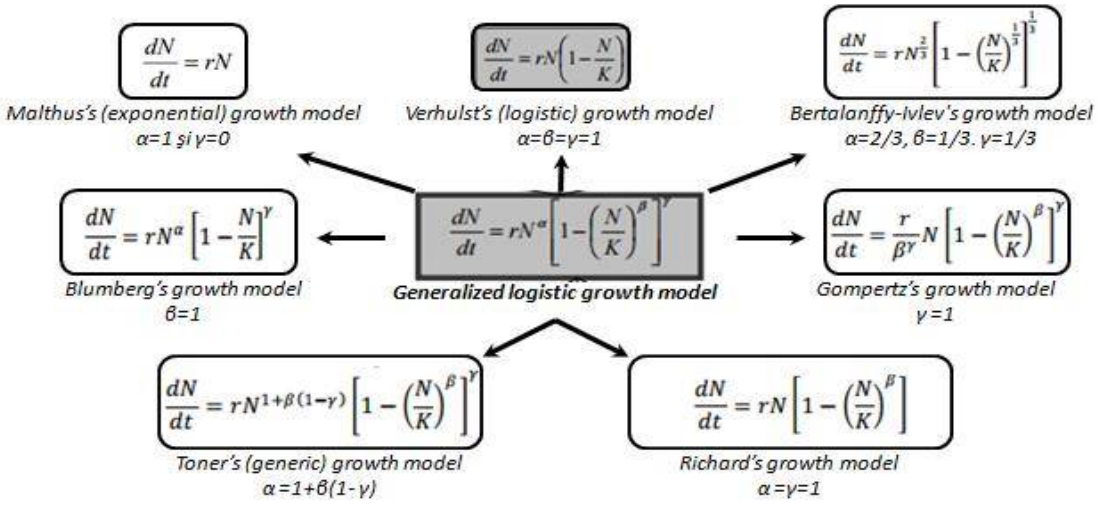

FIG. 3. The generalized logistic curve and its derivative models [11]

During recent decades the stirring up of the processes of globalization, practically in all spheres of present day civilization, has aggravated and brought numerous problems resulting from nature-society interactions. To overcome these problems, it is necessary to develop and adopt new concepts and techniques to study and evaluate the changes occurring on the earth ecosystem [2]. For this, application of information technology via Environmental Information Systems is the best option.

Due to pressure from natural selection which involves achieving a high efficiency of the reproduction process, can be fairly easily notice that the general populations trend is to grow numerically. Because the main function of living organisms that grow in terms of numbers is the reproduction in order to perpetuate the species, any model that would try to describe the dynamics of a population should include reproduction [8]. There are two important models of population growth that are based on the reproductive process: the exponential and logistic models (Fig. 4).

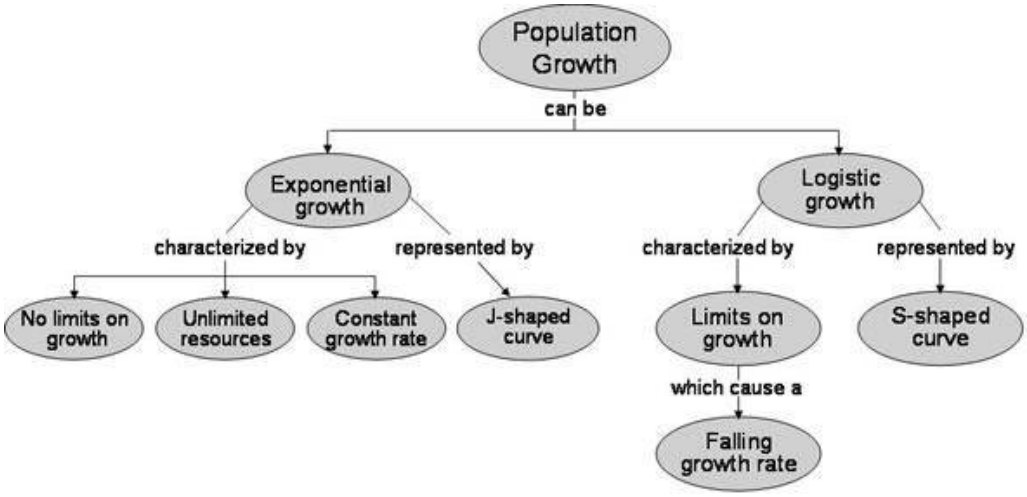

FIG. 4. The main mathematical models of population growth and their properties (source: www.goldiesroom.org)

Since we especially brought to discussion the mathematical modeling as the main vector used in ecological analytical research for studying the complex behavior of dynamic ecological systems, as there are populations, in the following we will present some applications (applets) realized in Wolfram Language of Mathematica software.

Designed for the new generation of programmers, the Wolfram Language, the world's most productive programming language, has a vast depth of built-in algorithms and knowledge, all automatically accessible through its elegant unified symbolic language.

In the following examples we used the *manipulate* function, because it gives immediate access to a huge range of powerful interactive capabilities. For any expression with symbolic parameters, the mentioned function automatically creates an interface for manipulating the parameters, according to the Computable Document Format (CDF) created by Wolfram Research company.

```
Manipulate[
 Plot[K/(1 + (K/N - 1) Exp[-r Kt]), {t, 0, 20},
  PlotRange -> {-5, 100},
  AxesLabel → {t, population}, Axes -> True,
  ImagePadding -> {{15, 15}, {15, 15}},
  ImageSize -> {400, 220}],
{{N, 0.1, "Initial population (N)"}, 0.001, 100,
  Appearance -> "Labeled"},
{{r, 0.15, "Rate of increase (r)"}, .01, 4,
  Appearance -> "Labeled"},
{{K, 4, "Carrying capacity (K)"}, .01, 90,
  Appearance -> "Labeled"},
 ControlPlacement → Top]
```

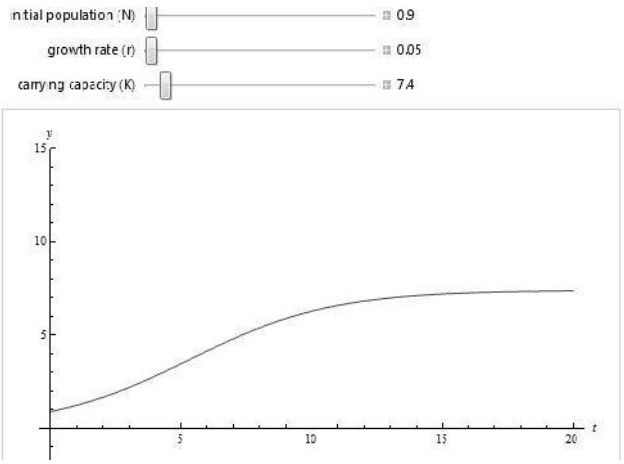

FIG. 5. A simple logistic equation model considering *N*, *r* and *K* parameters

As it can be observed, the simplified form of the logistic equation (Fig. 5) is a powerful expression for a single population dynamics. It can lead to population size prediction in reasonable intervals, if there is a sufficiently large number of data about population size in time and space, at least 3 parameters: N - initial population at time t_0, r - rate of increase and K - the carrying capacity of the environment. To the same extent, we obtain the same graphic if considering a particular family of curves (Fig. 6).

```
Manipulate[If[fam,
  Plot[Evaluate[Table[x[t, N, r], {N, 0.01, 1, 0.1}]], {t, 0, 10},
   ImageSize -> {450, 300},
   PlotRange -> {0, 1},
   PlotStyle -> Table[{Thickness[0.007],ColorData["SunsetColors"][i]}, {i, 0.01, 1, 0.1}],
   AxesLabel -> {Style["t", Italic, 12], Style["x(t)", Italic, 12]}],
  Plot[x[t, N, r], {t, 0, 10},
   ImageSize -> {450, 300}, PlotRange -> {0, 1},
   PlotStyle -> {Thickness[0.01]},
   AxesLabel -> {Style["t", Italic, 12], Style["x(t)", Italic, 12]}]],
  {{N, 0.067,"Initial population (N)"}, 0.01, 1, Appearance -> "Labeled",
  Enabled -> Dynamic[ !fam]},
 {{r, 0.96, "Rate of increase (r)"}, -2, 2, Appearance -> "Labeled"},
  {{fam, True, "Family of curves"}, {True, False}}, ControllerLinking -> True,
  Initialization :> ({x[t_, x0_, r_] := 1/(1 + (1/x0 - 1)*Exp[(-r)*t])};
   ReleaseHold[HoldComplete[{x[t_, x0_, r_] := 1/(1 + (1/x0 - 1)*Exp[(-r)*t])}]])]
```

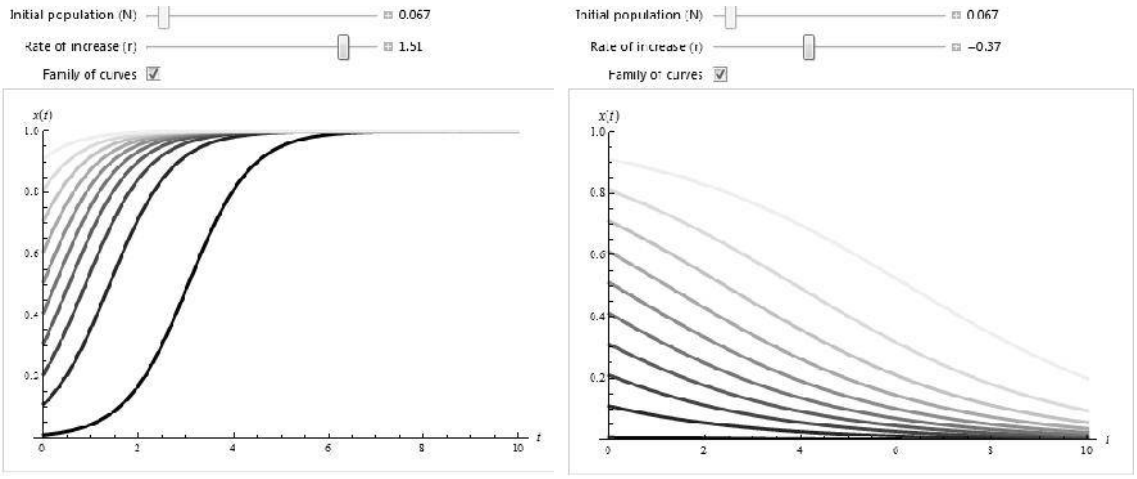

FIG. 6. The logistic equation behavior considering a particular family of curves

CONCLUSIONS

Nowadays, much attention is being paid to the problem of population growth and this has led also to an increase of interest in mathematical ecology. The growth of organisms in a favourable environment is usually modeled by a simple exponential function, in which the population size increases at an ever-increasing rate.

In the real world, resources become limiting for growth, so that the rate of population growth declines as population size increases. There are several numerical (bio-mathematical) models that simulate this behaviour, and we explore the generalized "logistic" growth model, which is a classical, but still useful model for describing the dynamics of a one-species population in an environment with limited resources.

Population modeling became of particular interest to biologists. The logistic population model, the Lotka–Volterra model of community ecology, life table matrix modeling, the equilibrium model of island biogeography and variations there of are the basis for ecological population modeling today.

REFERENCES

[1] ***, *Introduction to functions and models*: web.anglia.ac.uk/ functions_and_models/logistic.pdf

[2] Arnold D., Cavallini F., *Fitting a Logistic Curve to Data*, College Mathematics Journal, vol. 24, no. 3, pg. 247-253, 2002 www.math.hmc.edu/~depillis/logistic.pdf

[3] Asfiji S., Isfahani R., Dastjerdi R., Fakhar M., *Analyzing the Population Growth Equation in the Solow Growth Model Including the Population Frequency*, International Journal of Humanities and Social Science, vol. 2, no. 10, pg. 134-144, 2012 www.ijhssnet.com/special_issue.pdf

[4] Cioru□a B., Coman M., Cioru□a A., *Studying Environmental Problematics and Hazards with help of Informatics Applications*, International Conference "Scientific Research and Education in the Air Force", 22-24 mai 2014, Braşov, vol. 2, pg. 289-292, 2014 www.afahc.ro/afases/2014/studying.pdf

[5] Cioruța B., Coman M., *Incursiune în cercetarea ştiinţifică modernă a mediului înconjurător. De la SIM la Informatica Mediului*, Journal of Environmental Research and Protection (Ecoterra), Universitatea Babeş-Bolyai Cluj-Napoca, nr. 29, pg. 17-20, 2011 www.ecoterra-online.ro/.../5124.pdf

[6] Coman M., Cioruța B., *Environmental Information Systems as a possible solution for strategic development of local and regional communities*, Conferința Internațională „Aerul şi Apa – componente ale mediului", 22-23 martie 2013, Cluj-Napoca, Editura Presa Universitară Clujeană, pg. 516-523, 2013 aerapa.conference.ubbcluj.ro/2013/coman_cioruta 516-523.pdf

[7] Coman M., Cioruța B., *Evoluția, definiția şi rolul Sistemelor Informatice de Mediu în dezvoltarea strategiilor pentru protecția mediului*, Journal of Environmental Research and Protection (Ecoterra), Universitatea Babeş-Bolyai Cluj-Napoca, nr. 27, pg. 11-14, 2011 www.ecoterra-online.ro/.../1401.pdf

[8] Dr. Malcolm S., *BIOS 6150: Ecology*, Western Michigan University, Department of Biological Sciences, 2007 homepages.wmich.edu/~malcolm/BIOS6150-Ecology/Lectures/6150Week04.pdf

[9] Nwabudike A., *A model for population forecasting* (project for M.Sc in computer sciences), Faculty of Physical Sciences, Department of Computer Sciences, University of Nigeria, pg. 61, 2014 www.unn.edu.ng/publications/Nwabudike Augustine.pdf

[10] Rerep., *Snapshot of Environmental Information Systems in South Eastern Europe: Current Progress and Future Priorities*. The Regional Environmental Reconstruction Programme for South Eastern Europe, 2003 documents.rec.org/publications/SnapshotEnvInfSystems.pdf

[11] Tsoularis A., *Analysis of logistic growth models*, Res. Lett. Inf. Math. Sci, vol. 2, pg. 23-46, 2001 http://modelosysistemas.azc.uam.mx/logisticmodels.pdf

A NEW eBOOK CONCEPT AND TECHNOLOGY DEDICATED TO GEOGRAPHICAL INFORMATION

Dan CRISTEA[*], Ștefan-Gheorghe PENTIUC[**]

[*] "Alexandru-Ioan Cuza" University of Iasi, Faculty of Computer Science, Iasi, Romania (dcristea@info.uaic.ro), [**] "Stefan cel Mare" University of Suceava, Faculty of Electrical Engineering and Computer Science, Suceava, Romania (pentiuc@usv.ro)

DOI: 10.19062/2247-3173.2016.18.1.57

Abstract: *The paper presents the concept of MappedBook, the heart of preoccupations and the advances of the project MappingBooks - Jump in the book!. A MappedBook presents a real multi-dimensional interpretation of a book content: textual, graphical, geographical and temporal information, dependence from the localization of the reader and augmented reality, in short, an adequate disclosure of the reader. This kind of eBook "understands" part of the text, recognizes entity mentions with a correspondent in the reality, knows where the reader is and what are the real entities nearby. In the designed technology a MappedBook will be able to draw on the map a route which is described in the book, to upload and use geographical data. The technology is based on a client-server architecture.*

Keywords: *e-book, natural language understanding, mobile computing.*

1. INTRODUCTION

A MappedBook is an interactive electronic book (eBook) connected to the reader, and which could be instantly responsive to the location where the user (reader) is, via a mobile phone or a tablet. This eBook could provides information about events in the real or virtual location, about places' names and other named entities contained in the original book. The system will enrich the existing text links with contextual knowledge for completing readers with additional information beyond the text itself so the eBook becomes an interactive and enjoyable reading.

The main issue will be a 2D or 3D hypermap as described in [1]. These hypermaps, which are in fact multimedia systems referencing Romanian geographical information, can help to increase the visibility of Romanian tourism potential to an international public or to potential customers.

The structured information of a hypermap covers some basic levels with continuous coverage superimposed levels as discrete data, raster and vector, multimedia and hyperlinks.

For the implementation of a Mapped Book, the initial processing of the original text with artificial intelligence tools is essential. The basic text analysis includes at least: recognition of the language, text classification, tokenization, tagging of parts of speech, lemmatization, recognizing noun phrase groups and mentioned entities, sentence-level

segmentation and anaphora resolution. All of them are well known techniques, which have reached technological maturity for Romanian[1].

2. MAPPEDBOOK – A SHORT DESCRIPTION

Mainly a MappedBook is an interactive eBook having the following features:

- it is connected to the reader and the real world
- it is sensitive to the location where the reader is
- incorporates elements of mixed reality, by dynamically setting text over the images captured by the camera of the user's mobile device.

The information provided will be differentiated in time and space.

The eBook let users navigate in multimedia data sets, not only ordered by theme but also spatially. The concept discussed here is supplemented by a prototype developed in an authorware environment.

The platform addresses mainly two categories of readers:

i) middle school, high school students and students of Romanian universities,
ii) tourists visiting Romania.

For the first category of users the MappedBooks will be a geographical textbook, and for the second category – touristic guides. The end product for both categories of users represents an innovative interactive technology, for now dedicated only to the Romanian language, but extendable in the future to other languages [2].

For example, if the user reads about a museum and its position happens to be close to the user location, the system will try to find on the web its visitation schedule. If there is sufficient time for a visit, it will notify the user that possibility.

Interactive social gaming features can be imagined, children/students engaged in learning activities or traveling, same as tourists visiting Romania, can be put in relation to each other.

Moreover, by using mixed reality technologies, over the image captured by the mobile device (tablet or smartphone) tourist information about the various objectives sought can be overlapped.

An example is shown in Fig. 1 where a user situated nearby Suceava, looking at the image captured by her phone camera, could see instantaneously in what direction are the main localities situated at a maximum distance of 50 km around her position. If he will turn around, the image captured will be updated with the names of another localities. The system make possible the configuration by the user of the main parameters for vizualization (distance, angles, methods for filtering the points of interest).

This function will be available online or offline (the later, in cases when the phones are not connected to Internet). In the online case, if the user touches a locality on the screen, the server will sent a short description of the locality and other supplementary information if required, in order to be displayed over the image.

The online regime is built as a client-server architecture, where the server will be able to provide web services, feeding with textual and geographical information the clients assumed to be mobiles (smartphones, tablets, laptops).

[1] For more references, see the pages of the NLP-Group@UAIC-FII at http://nlptools.info.uaic.ro/.

FIG.1. Information on the point of interest superposed on the image captured with the camera of the mobile device

On the other hand, meaningful linguistic data achieved in the project will be stored in public archives to be useful for future research, that will handle the implementation / development of processing technologies of the Romanian language, as well as the development of electronic dictionaries. An example of this is the extensive list of Romanian geographical names acquired during the project, which will become instances of the Romanian WordNet [3] concepts. Moreover, the structure, content and design of hypermaps will be contextualized. The project has created an inventory of public information and educational tourism in a catalogue metadata space by using geocoded public data available.

3. MAIN MODULES

As an eBook will be based firstly on text (and hypertext) information, the textual data providers will be, generally, publishing houses, which, based on partnership agreements, will offer the primary texts (electronic forms of manuals and travel guides) to the partners in this project. On the server, the texts are subject to a linguistic processing chain followed by a geographical processing and crawling the web for relevant connected information. The overall structure of the system was proposed in [4] and [5] and later developed in [6].

The main modules of the system are the following (see Fig. 2):

1. Text Analytics (TA) – by accessing the NLP services of the NLP-Group&UAIC-FII;
2. Name Entity Recognition (NER) – by using a gazetteer (a large collection of entity names) and a collection of patterns identifying classes;
3. Entity Crawling (EC) – for now, only on a list of predetermined sites;
4. Relations Detection (RD) – namely space relations, based on a list of patterns;
5. Geography (GEO) – exploiting GIS data;
6. Maps & Trajectories (M&T) – for positioning geo-names and journey paths on maps;

7. Augmented Reality – a module running on the client, dealing with orientation of the camera and placing of information in real time;

8. Interfaces – implementing interfaces adequate for different types of devices;

9. Client-Server – responsible for the communication between server and client's device;

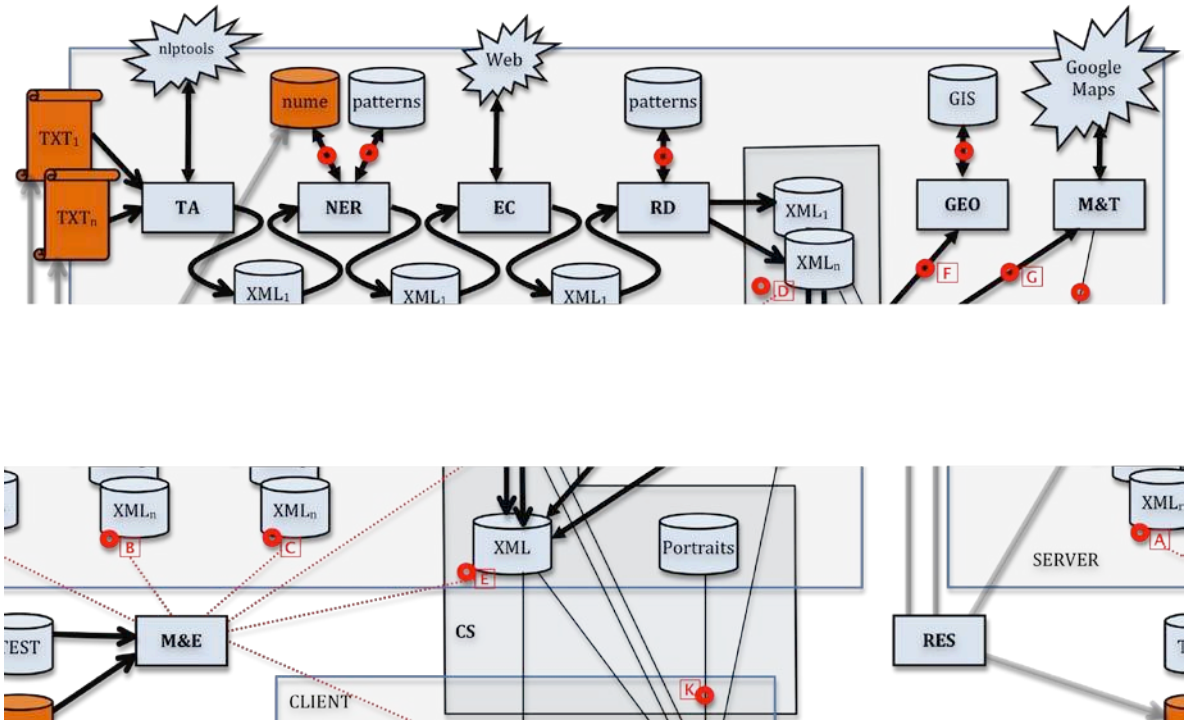

FIG.2. Relations between the main components of the MappingBooks system

MappingBooks will be able to recognize and annotate different types of entities, linking those statements in the book with data from the real and virtual world, and synchronize by applying artificial intelligence techniques [7], [8] for linking references found in the book with actual images captured with the user's mobile device.

CONCLUSIONS

The MappingBooks technology addresses a new concept of an eBook dedicated to geographical subjects in an integrated manner [9], [10]. When ready, the project will be of help to different types of users, from school children to students, and from travellers to people eager to discover touristic places in Romania, in an interactive, attractive manner. The technology processes texts of manuals of geography and travelling guides.

The feasibility of the technology for automatic annotation of texts described above is very much dependent on the maturity of language technologies modules. The more accurate are the annotations obtained automatically, the less expensive the whole production cycle will be for a new book, because manual correction of massive annotations obtained automatically will be avoided.

ACKNOWLEDGMENTS

The paper benefits by the financial support of the project MAPPINGBOOKS - JUMP IN THE BOOK!, in the frame of PARTNERSHIPS - Collaborative Projects Applied Research - Competition 2013 (PCCA 2013). The consortium is composed of "Alexandru-Ioan Cuza" University of Iasi – as coordinator, SC SIVECO Romania SA., and the "Stefan cel Mare" University of Suceava.

REFERENCES

[1] Kraak, M.-J., Rico, V.D. (1997): *Principles of hypermaps, Computers & Geosciences*, 23(4), pp. 457-464.

[2] Anechitei, Daniel, Cristea, Dan, Dimosthenis, Ioannidis, Ignat, Eugen, Karagiozov, Diman, Koeva, Svetla, Kopeć, Mateusz, Vertan Cristina (2013): *Summarizing Short Texts Through a Discourse-Centered Approach in a Multilingual Context.*, in Neustein, A., Markowitz, J.A. (eds.), Where Humans Meet Machines: Innovative Solutions to Knotty Natural Language Problems. Springer Verlag, Heidelberg/New York.

[3] Dan Tufiş, Dan Cristea, Sofia Stamou (2004). BalkaNet: Aims, Methods, Results and Perspectives. A General Overview. In *Romanian Journal of Information Science and Technology*, Romanian Academy, Bucharest, Romania, Dan Tufis (ed.) Special Issue on BalkaNet, July, 7(1-2), ISSN 1453-8245, pages 9–43.

[4] Dan Cristea, *MappingBooks- Let me jump in the book! Structure proposal*, Communication at The 7th International Conference on Speech Technology and Human-Computer Dialogue "SpeD 2013", Cluj-Napoca, October 16-19, 2013.

[5] Dan Cristea, ț Ionu Cristian Pistol (2014). *MappingBooks Jump in the book!* Communication at ConsILR – Craiova, 18-19 September 2014

[6] Dan Cristea, Eugen Ignat, *Linking Book Characters. Toward A Corpus Encoding Relations Between Entities*, Invited paper: The 7th International Conference on Speech Technology and Human-Computer Dialogue, "SpeD 2013", Cluj-Napoca, October 16-19, 2013.

[7] Florea A., Pentiuc, Gh. Şt., Kayser, D. (2004): *Intelligence artificielle et agents intelligents*, Ed. Printech, Bucharest, ISBN 973-652-976-2, 420 p.

[8] Dan Cristea, Ionț -Cristian Pistol (2014). *MappingBooks: Linguistic Support For Geographical Navigation Systems*. In Mihaela Colhon, Adrian Iftene, Verginica Barbu Mititelu, Dan Cristea, Dan Tufiş (eds.) (2014). Proceedings of the 10th International Conference "Linguistic Resources And Tools For Processing The Romanian Language, Craiova, 18-19 September 2014", „Alexandru Ioan Cuza" University Publishing House, pag. 189-198

[9] Longley, P. A., Goodchild, M. F., Maguire, D. J. & Rhind, D. W. (2005): *Geographical information systems and science*, p. 511.

[10] Kraak, M.-J. & Ormeling, F. (2010): *Cartography. Visualization of Spatial Data*, Prentice Hall.

APPLIED MATHEMATICS, COMPUTER SCIENCE, IT&C

SATELLITE TRACKING USING NORAD TWO-LINE ELEMENT SET FORMAT

Emilian-Ionuţ CROITORU, Gheorghe OANCEA

Transilvania University of Braşov, Braşov, Romania
(emil.ca2651@yahoo.com, gh.oancea@unitbv.ro)

DOI: 10.19062/2247-3173.2016.18.1.58

Abstract: *This paper presents the study of satellite tracking using the NORAD Two-Line Element (TLE) set format. In this research, the mathematical model for the determination of the osculating orbital elements of the selected satellite is presented and one computer program is developed for the satellite tracking using the application Matlab, a platform for solving engineering and scientific problems. The NORAD TLE represents the input data for the developed program, while the output data takes the form of a graphical representation of the satellite track around planet Earth.*

Keywords: *satellite tracking, NORAD, two-line element, orbital elements, Matlab, application*

1. INTRODUCTION

The Space Age started with Sputnik 1's lonely 3 month journey in orbit around Earth. Thus, October 4, 1957 became the first step to space exploration. Starting with this point, many more spacecraft – unmanned and, later, manned – have followed and created history for mankind. History which is now described as satellites into Earth's orbit, around and on the Moon, around the Sun or other planets of our Solar System, and even going further and breaking the boundaries towards other Systems in our Universe [1].

Thus, for young researchers who did not witness this history in its making, two questions appear: how many objects of any kind are in space and who keeps track of them. The answer to the first question is: 1071 operational satellites in orbit around Earth – with more than 50% launched and places into orbit by the United States – and over 170 million space debris objects with dimensions larger than 1 mm – from which 670000 objects are larger than 10 mm and 29000 objects larger than 100 mm [2]. Of course, the numbers are rising from one month to another as more and more countries have joined in on this space race, and furthermore, private companies are developing programs for future space tourism.

While the first question has a simple answer, the second proves to be quite a challenge even with the increasing number of applications dedicated towards satellite and space debris tracking [3]. Although these applications are proving to be a step forward in objects tracking around Earth and not only, they can be used only by experts who possess the theoretical knowledge and practical background and are not suited for common use.

The current paper presents the development and usage of one application for satellite tracking around Earth. The mathematical model for the determination of the osculating orbital elements of the selected satellite is presented and one simple computer program is developed for the satellite tracking using the application Matlab with input from the NORAD Two-Line Element Set Format.

2. SATELLITE TRACKING WORKFLOW

In order to complete the task of developing one application for satellite tracking for common use, a series of objectives are defined:

- user-friendly interface of the application;
- easy access for satellite data;
- graphical display of all performed operations;
- graphical display of complete satellite data;
- complete separation of input and output data;
- tables for conclusions regarding satellite orbit;

The steps taken for the development of the desired application corroborated with the completion of the objectives presented beforehand are:

a) reading of the NORAD Two-Line Element Set Format for the chosen satellite;

b) extraction of necessary information such as: satellite name, eccentricity, inclination, argument of periapsis, mean anomaly, longitude of the ascending node and mean motion;

c) mathematical calculations of necessary input for the application;

d) starting point determination, all points of the satellite track being characterized by vector radius and vector speed;

e) differential calculus in order to obtain the satellite's orbit;

f)projection of satellite's orbit onto Earth's surface, without and with revolution movement;

g) mathematical determination of the satellite's rate of decay;

h) graphical display in Earth's atmosphere for the last two steps;

Thus, the required information for the application to function and perform the desired operations are the NORAD Two-Line Element Set Format and the mathematical model for satellite orbits.

3. NORAD Two-Line Element Set Format

Firstly, the NORAD Two-Line Element Set Format is a data format used to transmit one coded set of orbital elements that perfectly describe the satellite's orbit around Earth. An application could use this set in order to compute the exact position at any moment of the tracked satellite. This TLE format is a specific one used by NORAD and NASA. Also, these formats are distributed freely around the world by means of the Internet and contain three lines: one title line and two lines of coded text.

For a better understanding of the NORAD Two-Line Element Set Format coding, a visual description using the International Space Station TLE is performed:

```
ISS (ZARYA)
1 25544U 98067A   04236.56031392  .00020137  00000-0  16538-3 0  9993
2 25544  51.6335 344.7760 0007976 126.2523 325.9359 15.70406856328903
------------------------------------------------------------------------
12345678901234567890123456789012345678901234567890123456789012345678901234567890   reference number line
         1         2         3         4         5         6         7
```

FIG. 1. International Space Station TLE [4]

Table 1. International Space Station TLE – description [4]

Line 0		
Columns	Example	Description
1-24	ISS (ZARYA)	Object common name based on information from the Satellite Catalog.
Line 1		
Columns	Example	Description
1	1	Line Number
3-7	25544	Satellite Catalog Number
8	U	Elset Classification
10-17	98067A	International Designator
19-32	04236.56031392	Element Set Epoch (UTC) *Note: spaces are acceptable in columns 21 & 22
34-43	.00020137	1st Derivative of the Mean Motion with respect to Time
45-52	00000-0	2nd Derivative of the Mean Motion with respect to Time (decimal point assumed)
54-61	16538-3	B* Drag Term
63	0	Element Set Type
65-68	999	Element Number
69	3	Checksum
Line 2		
Columns	Example	Description
1	2	Line Number
3-7	25544	Satellite Catalog Number
9-16	51.6335	Orbit Inclination (degrees)
18-25	344.7760	Right Ascension of Ascending Node (degrees)
27-33	0007976	Eccentricity (decimal point assumed)
35-42	126.2523	Argument of Perigee (degrees)
44-51	325.9359	Mean Anomaly (degrees)
53-63	15.70406856	Mean Motion (revolutions/day)
64-68	32890	Revolution Number at Epoch
69	3	Checksum

From fig. 1 and table 1 presented above, it can be clearly seen that the line of interest for the desired application is line 2, especially columns 9 to 63. Based on the data coded in this line – which are actually the orbital elements of the satellite's orbit – a complete tracking of the satellite can be performed. Adding the mathematical model of the application, the user-friendly interface and the graphical display of all satellite data, the objectives of the desired application will be achieved.

4. ORBITAL ELEMENTS

Orbital elements are the parameters required to identify in a unique manner the orbit of a specific satellite. In space mechanics, these orbital elements are generally considered in classical two-body systems. These systems are using the classical Keplerian orbit description which is derived from Newton's laws of motion and Newton's law of universal gravitation. Many different way to describe the same orbit from a mathematical point of view exist, but certain schemes – which have become more popular due to their simple way of use – each consisting of a set of six parameters, are commonly used in orbital mechanics.

The Keplerian orbit is just an idealization, a mathematical approximation at a particular time, while a real orbit (and its elements) change over time due to perturbations by other objects – gravity of those object as an example – and the effects of relativity.

Five independent quantities entitled orbital elements are sufficient to completely describe the size, shape and orientation of an orbit. In fig. 2 the classical set of orbital elements are shown:

- a – semi-major axis; this element defines the size of the orbit;
- e – eccentricity; this element gives the shape of the orbit;
- i – inclination; this element represents the orientation of the orbit with respect to Earth's equator;
- ω – argument of periapsis; this element defines where the low point, called perigee, of the orbit is with respect to the Earth's surface;
- Ω – longitude of the ascending node; this element represents the location of the ascending and descending orbit locations with respect to the Earth's equatorial plane;
- ν_o – true anomaly at epoch; this element notes where the satellite is within the orbit with respect to the perigee;
- t_o – time at epoch;
- T – time at periapsis passage;
- Π – longitude at periapsis;

$$\Pi = \varpi + \Omega \tag{1}$$

- u_o – argument of latitude at epoch;

$$u_o = \varpi + \nu_o \tag{2}$$

- l_o – true longitude at epoch;

$$l_0 = \Omega + \varpi + \nu_o = \Pi + \nu_o = \Omega + u_o \tag{3}$$

- p – semi-latus rectum;

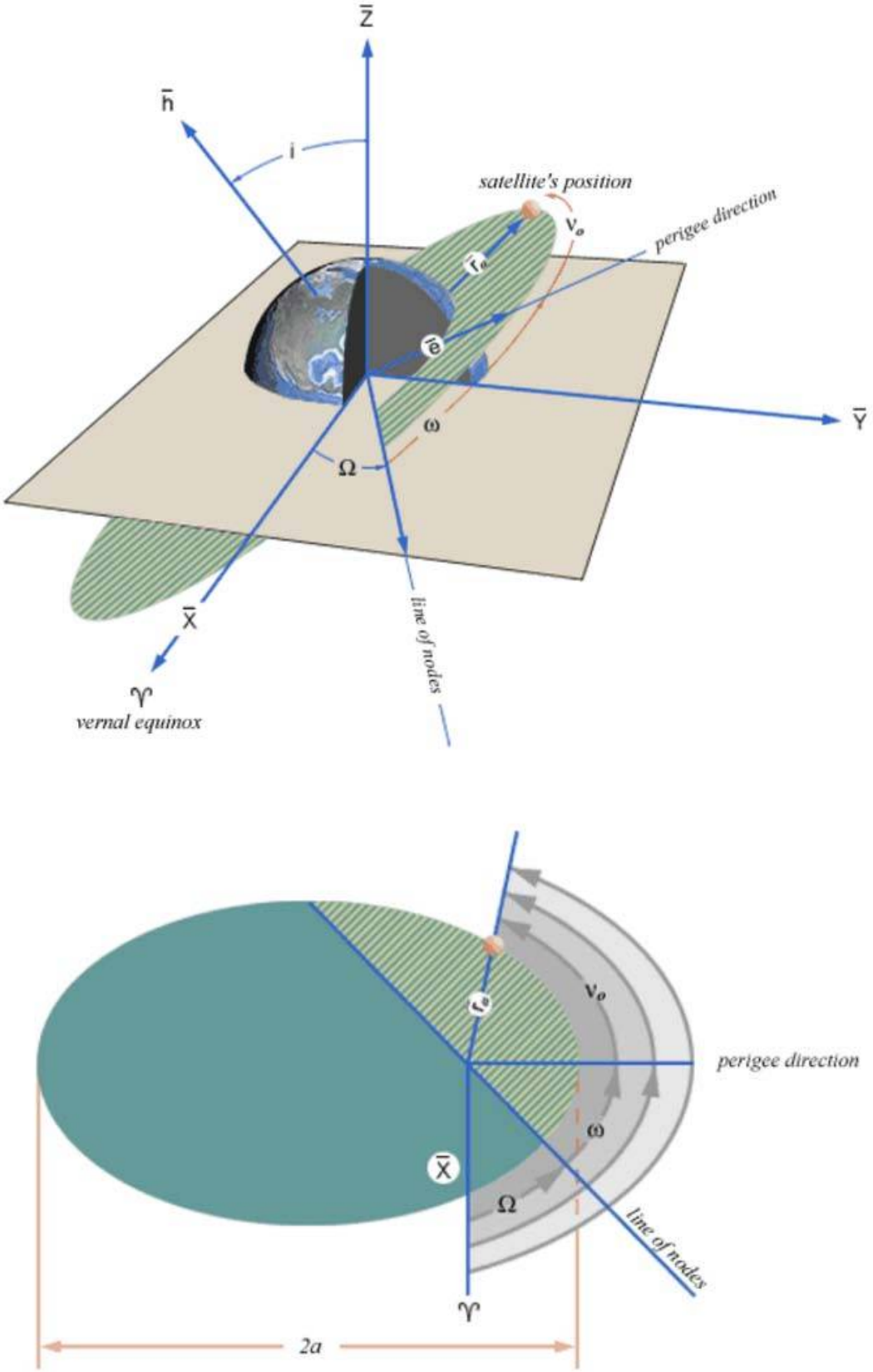

FIG. 2. Orbital Elements - Visual Description [5]

Alongside this orbital elements, three fundamental vector are also required:

a) angular momentum, h; it is the vector normal to the orbital plane

$$\vec{h} = \vec{r} \times \vec{v} = \begin{bmatrix} \vec{I} & \vec{J} & \vec{K} \\ r_x & r_y & r_z \\ v_x & v_y & v_z \end{bmatrix} = h_x \cdot \vec{I} + h_y \cdot \vec{J} + h_z \cdot \vec{K} \tag{4}$$

b) node vector, n; it is the vector pointing along the line of nodes in the direction of the ascending node;

$$\vec{n} = \vec{K} \times \vec{h} = \begin{bmatrix} \vec{I} & \vec{J} & \vec{K} \\ 0 & 0 & 1 \\ h_x & h_y & h_z \end{bmatrix} = n_x \cdot \vec{I} + n_y \cdot \vec{J} + n_z \cdot \vec{K} = -h_y \cdot \vec{I} + h_x \cdot \vec{J} \tag{5}$$

c) eccentricity vector, e; it is the vector which points from the center of the earth (focus of the orbit) towards the perigee with a magnitude exactly equal to the eccentricity of the orbit;

$$\vec{e} = \frac{1}{\mu} \cdot \left[(v^2 - \frac{\mu}{r}) \cdot \vec{r} - (\vec{r} \cdot \vec{v}) \cdot \vec{v} \right] \tag{6}$$

5. MATHEMATICAL MODEL OF APPLICATION

With all these elements in place, the problem of determining the vector for radius and speed of the satellite, when the orbital elements are known, can be solved. Assuming the following orbital elements are given: p, e, i, Ω, ω and v, the radius vector can be written in the perifocal system [6]:

$$\vec{r} = r \cos \nu \vec{P} + r \sin \nu \vec{Q} \tag{7}$$

where:

$$r = \frac{p}{1 + e \cos \nu} \tag{8}$$

Thus, considering equation (7), the speed vector can be written in the perifocal system as:

$$\begin{aligned} \vec{v} &= \frac{d\vec{r}}{dt} \\ \vec{v} &= \sqrt{\frac{\mu}{p}} \left[-\sin \nu \vec{P} + (e + \cos \nu) \vec{Q} \right] \end{aligned} \tag{9}$$

The transformation between perifocal system and geocentric system is needed:

$$\begin{bmatrix} a_I \\ a_J \\ a_K \end{bmatrix} = \tilde{R} \begin{bmatrix} a_P \\ a_Q \\ a_W \end{bmatrix} \Leftrightarrow \vec{a}_{IJK} = \tilde{R} \vec{a}_{PQW} \tag{10}$$

where:

$$\tilde{R} = \begin{bmatrix} \cos\Omega\cos\varpi - \sin\Omega\sin\varpi\cos i & -\cos\Omega\sin\varpi - \sin\Omega\cos\varpi\cos i & \sin\Omega\sin i \\ \sin\Omega\cos\varpi + \cos\Omega\sin\varpi\cos i & -\sin\Omega\sin\varpi + \cos\Omega\cos\varpi\cos i & -\cos\Omega\sin i \\ \sin\varpi\sin i & \cos\varpi\sin i & \cos i \end{bmatrix} \quad (11)$$

The mathematical model is established, the NORAD Two-Line Element Set Format coding is explained and the application presentation follows in the next chapter.

6. APPLICATION PRESENTATION

Incorporating all of the above into the Matlab application [7], the results for the data mentioned in fig. 1 are shown below:

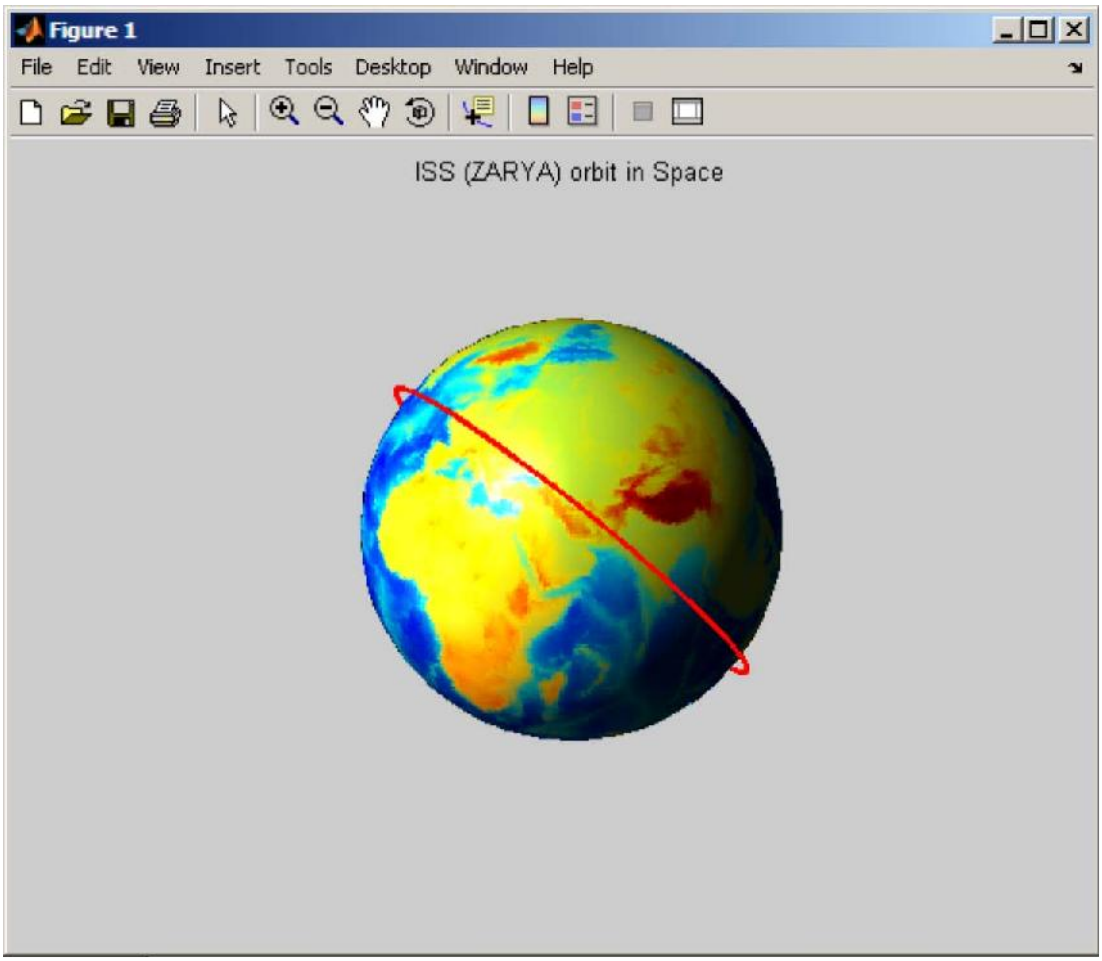

FIG. 3. International Space Station Orbit

The next step is given by performing the projection of the satellite's orbit on the Earth's surface, at first without considering the rotation of the Earth (fig. 4a) and after with this consideration (fig. 4b), and the calculation and display of the rate of decay of the same satellite (fig. 5).

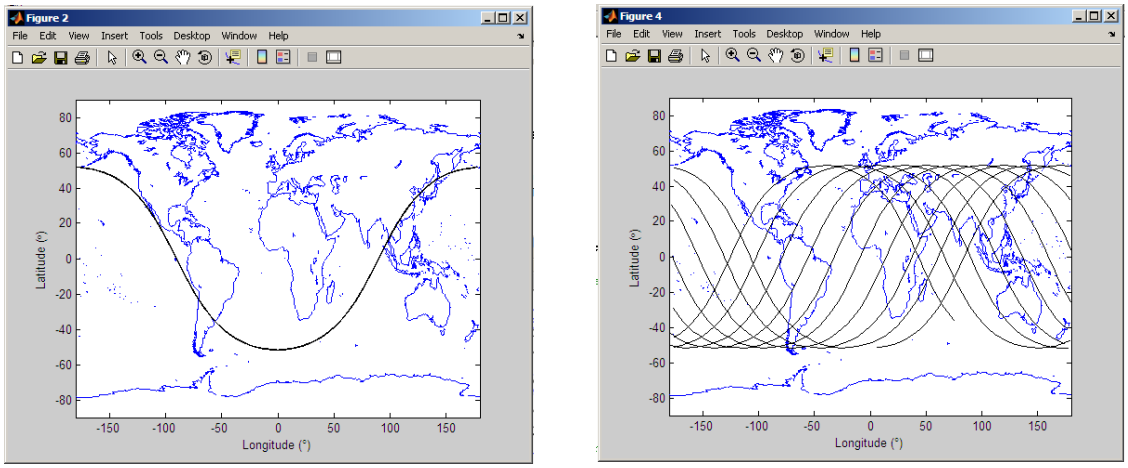

(a) (b)

FIG. 4. International Space Station Orbit Projection on Earth's Surface:
a – without Earth's rotation; b- with Earth's rotation

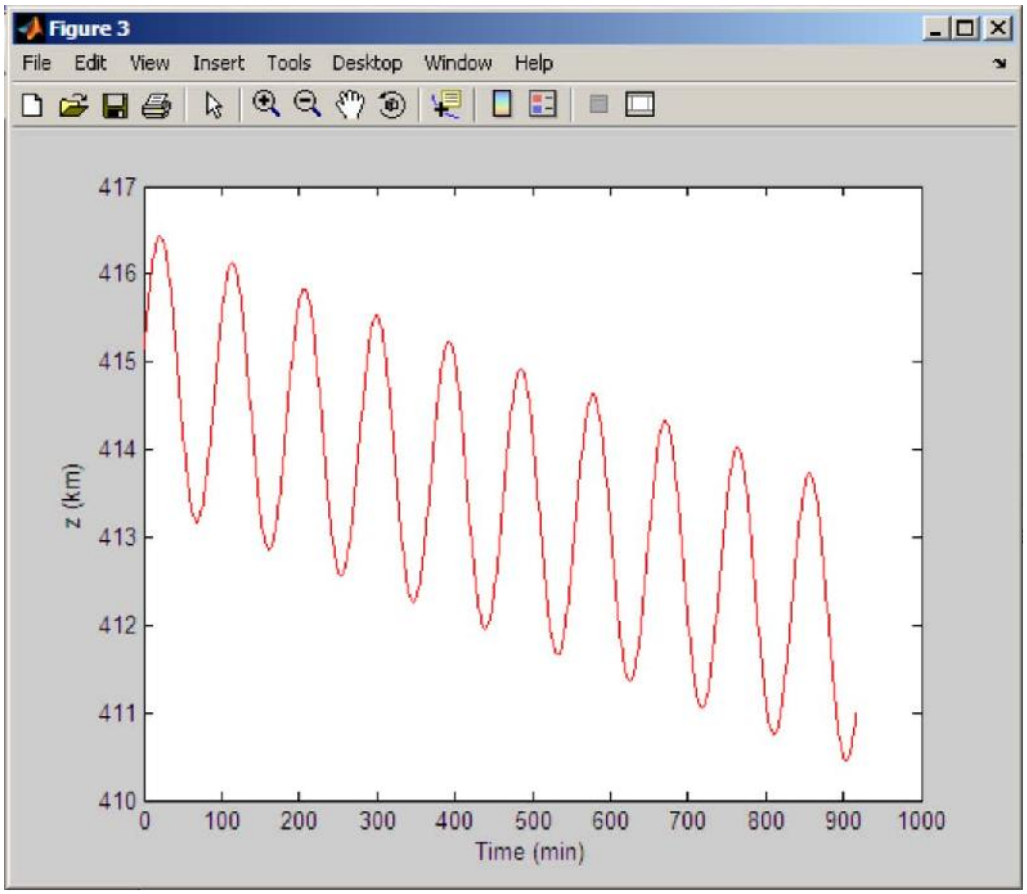

FIG. 5. International Space Station Rate of Decay

CONCLUSIONS

One can imagine that in order to track the increasing number of satellites and space debris objects, the human and computational effort is very high without a specialized, and at the same time simple, application like the one presented by this paper. And although awareness regarding this subject is on the rise thru different state or private funded programs [8], more solutions are needed in order to have a clean sky to look upon at night.

REFERENCES

[1] *** Universe Today – Space and Astronomy News, *How many satellites are in space?*, October 2013. Available at http://www.universetoday.com/, accessed on 9 April 2016.
[2] *** European Space Agency, *How many space debris objects are currently in orbit?*, July 2013. Available at http://www.esa.int/Our_Activities/Space_Engineering_Technology/, accessed on 9 April 2016.
[3] *** CelesTrack, *Satellite Tracking Software Index*, April 2016. Available at https://celestrak.com/software/satellite/sat-trak.asp/, accessed on 9 April 2016.
[4] *** Space Track, *Basic Description of the Two Line Element (TLE) Format*. Available at https://www.space-track.org/documentation#/tle/, accessed on 10 April 2016.
[5] *** National Aeronautics and Space Administration, *Orbital Elements*, October 2012. Available at http://spaceflight.nasa.gov/realdata/elements/graphs.html, accessed on 10 April 2016.
[6] H. Curtis, *Orbital Mechanics for Engineering Students*, Elsevier Aerospace Engineering Series, Oxford, 2005.
[7] *** MathWorks, *MATLAB – The Language of Technical Computing*, April 2016. Available at http://www.mathworks.com/products/matlab/, accessed on 22 April 2016.
[8] *** Lyndon B. Johnson Space Center, *Orbital Debris Education Package*, April 2008. Available at http://www.orbitaldebris.jsc.nasa.gov/library/EducationPackage.pdf, accessed on 22 April 2016.

APPLIED MATHEMATICS, COMPUTER SCIENCE, IT&C

A NUMERICAL ANALYSIS OF COMBUSTION PROCESS IN AN AXISYMMETRIC COMBUSTION CHAMBER

Alexandru DUMITRACHE*, Florin FRUNZULICA**

*Institute of Mathematical Statistics and Applied Mathematics, Bucharest, Romania (alexandru.dumitrache@ima.ro)
**Politehnica University, Bucharest, Romania (ffrunzi@yahoo.com)

DOI: 10.19062/2247-3173.2016.18.1.59

Abstract: *Combustion phenomenon is one of the most important problems involved in different industries, such as gas turbines, combustion chamber, melting of metals, etc. In this paper, combustion process of methane downstream of an axisymmetric sudden expansion in a circular pipe with a constant wall temperature has been studied. The conservation equations of mass, momentum, energy, and species as well as additional equations due to turbulence modeling have been numerically solved. The standard k-ε model and eddy dissipation combustion model has been used to simulate the turbulence and combustion phenomenon, respectively. Properties of gaseous mixture have been computed using the ideal gas equation of state. The governing equations have been discretized using a finite volume approach and power law scheme and the resulting set of algebraic equations has been solved simultaneously using the SIMPLER algorithm on a non-uniform staggered grid system. The numerical results have been compared with the other's numerical results and experimental data.*

Keywords: *combustion chamber, CFD, methane combustion, turbulent flow*

1. INTRODUCTION

The design of combustion chambers is of great importance. The geometry of these chambers may change gradually or suddenly. When the fluid path is changed abruptly, flow parameters, flow characteristics and the heat transfer rate are altered consequently. On the other hand, turbulent flows through axisymmetric sudden expansions are influenced by many parameters. Among these are inlet geometry, inlet flow Reynolds number, expansion ratio, step height, inlet turbulence intensity and inlet boundary condition. The interaction between turbulence and combustion is very important in the design of combustion chamber. Combustion phenomenon and the important design parameters are governed by this interaction.

Numerical simulation is becoming a powerful means in understanding combustion process and designing or optimizing combustion systems. The mathematical modeling of turbulent combustion has been outlined by Magnussen et al. [1]. They have developed the eddy dissipation concept for modeling of combustion. Turbulent non-reacting flows have been briefly studied by Ramous [2]. He, later, developed a mathematical model to study turbulent, confined, swirling flows under reacting non-premixed condition [3]. It is observed that the dimensions of the recirculation zone are larger for non-premixed reacting flows than for incompressible conditions. This seems to be caused by the heat released from the chemical reaction, which affects the density, centrifugal forces and radial pressure gradient.

Two fast-chemistry models, the eddy dissipation concept (EDC) and the conserved scalar (CS) approach, have been analyzed [4]. In this work turbulence is simulated by three types of k - ε models. The equations are discretized using a hybrid scheme and the SIMPLE algorithm is employed to solve the resulting algebraic equations.

Ohtsuka has performed the numerical study of reacting and non-reacting flows using the Reynolds stress differential [5]. He has modeled mixing of air and helium and also the combustion of propane.

In this work, combustion of methane in turbulent flow is studied. It is assumed that the fuel and air enter the cylindrical chamber with abrupt expansion as confined coaxial jets.

2. GOVERNING EQUATIONS

The combustion chamber geometry under study is shown schematically in Fig. 1. This geometry consists of two confined, coaxial jets; the inner jet contains pure fuel (methane) and the outer jet contains air. It is assumed here that the methane and air react by means of a one-step overall and irreversible chemical reaction rather than through a multitude of elementary reaction steps. It is assumed that the flow is statistically stationary and axisymmetric.

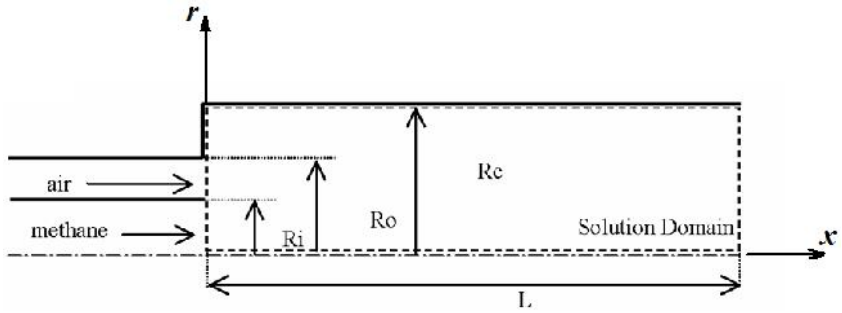

FIG. 1. Schematic of flow geometry and solution domain

The hydrodynamic equations governing the statistical stationary, axisymmetric, turbulent flow field in the geometry shown in Fig.1 can be written as:

·Continuity

$$\frac{\partial}{\partial x}(\rho u)+\frac{1}{r}\frac{\partial}{\partial r}(r\rho v)=0 \tag{1}$$

·Axial momentum component

$$\frac{\partial}{\partial x}(\rho uu)+\frac{1}{r}\frac{\partial}{\partial r}(r\rho vu)=\frac{\partial}{\partial x}\left(\mu_{eff}\frac{\partial u}{\partial x}\right)+\frac{1}{r}\frac{\partial}{\partial r}\left(r\mu_{eff}\frac{\partial u}{\partial r}\right)+S_u \tag{2}$$

where,

$$S_u=-\frac{\partial p}{\partial x}+\frac{\partial}{\partial x}\left(\mu_{eff}\frac{\partial u}{\partial x}\right)+\frac{1}{r}\frac{\partial}{\partial r}\left(r\mu_{eff}\frac{\partial v}{\partial r}\right)-\frac{2}{3}\frac{\partial}{\partial x}\left(\mu_{eff}\nabla V+\rho k\right) \tag{3}$$

·Radial momentum component

$$\frac{\partial}{\partial x}(\rho uv)+\frac{1}{r}\frac{\partial}{\partial r}(r\rho vv)=\frac{\partial}{\partial x}\left(\mu_{eff}\frac{\partial v}{\partial x}\right)+\frac{1}{r}\frac{\partial}{\partial r}\left(r\mu_{eff}\frac{\partial v}{\partial r}\right)+S_v \tag{4}$$

where,

$$S_v = -\frac{\partial p}{\partial r} + \frac{\partial}{\partial x}\left(\mu_{eff}\frac{\partial u}{\partial r}\right) + \frac{1}{r}\frac{\partial}{\partial r}\left(r\mu_{eff}\frac{\partial v}{\partial r}\right) - 2\mu_{eff}\frac{v}{r^2} - \frac{2}{3}\frac{\partial}{r\partial r}\left[r\left(\mu_{eff}\nabla V + \rho k\right)\right] + \frac{2}{3}\frac{1}{r}\left(\mu_{eff}\nabla V + \rho k\right) \tag{5}$$

·Scalar equation

The scalar variables k (turbulent kinetic energy), ε (turbulent dissipation rate), H (specific total enthalpy), Y_f (mass fraction of fuel) and Y_m (mass fraction of species m) satisfy the following equation (substitute generic variable φ):

$$\frac{\partial}{\partial x}\left(\rho u\varphi\right) + \frac{1}{r}\frac{\partial}{\partial r}\left(r\rho v\varphi\right) = \frac{\partial}{\partial x}\left(\Gamma_{eff}\frac{\partial \varphi}{\partial x}\right) + \frac{1}{r}\frac{\partial}{\partial r}\left(r\Gamma_{eff}\frac{\partial \varphi}{\partial r}\right) + S_\varphi \tag{6}$$

where, the source term, S_φ for Y_m and H is zero and for Y_f [1], k, ε, are as follows:

$$S_{Y_f} = -\rho\frac{\varepsilon}{k}\min\left(A\cdot Y_f, A\cdot\frac{Y_{O2}}{S}, A\cdot B\cdot\frac{Y_{\Pr}}{S+1}\right),\ S_k = P - \rho\varepsilon,\ S_\varepsilon = \left(C_1 P - C_2\rho\varepsilon\right)\frac{\varepsilon}{k} \tag{7}$$

where,

$$P = 2\mu_{eff}\left[\left(\frac{\partial u}{\partial x}\right)^2 + \left(\frac{\partial v}{\partial r}\right)^2 + \left(\frac{v}{r}\right)^2\right] + \mu_{eff}\left(\frac{\partial u}{\partial r} + \frac{\partial v}{\partial r}\right)^2 \tag{8}$$

$$\mu_t = C_\mu\rho\varepsilon k^{1/2},\ \mu_{eff} = \mu + \mu_t,\ \Gamma_{eff} = \frac{\mu_{eff}}{\sigma_\varphi} \tag{9}$$

$$\nabla\cdot V = \frac{\partial u}{\partial x} + \frac{1}{r}\frac{\partial}{\partial r}\left(rv\right) \tag{10}$$

and the constants for the turbulence model [6] and combustion model [1] are:

$$C_1 = 1.44,\ C_2 = 1.92,\ C_\mu = 0.09, \sigma_k = 1.0,\ \sigma_\varepsilon = 1.3,\ \sigma_T = 1.0,\ A = 4.0,\ B = 0.5,\ S = 4.0 \tag{11}$$

Remark: A and B are model constants [1] which depend on both the structure of the flame and the reaction between the fuel and oxygen; Y_f, Y_{O_2} and $Y_{\Pr}$ are the mass fraction of fuel, oxygen and products; S is the stoichiometric mass ratio of oxygen to fuel.

·Chemical reaction equation:

The overall reaction can be written as:

$$CH_4 + 2\left(O_2 + 3.76N_2\right) \rightarrow CO_2 + 2H_2O + 2\times 3.76N_2 \tag{12}$$

The mean density of mixture is calculated from the ideal gas equation of state:

$$\rho = p \Big/ RT \sum_{i=1}^{N_S} \frac{Y_i}{M_i} \tag{13}$$

where, R, N_s, and M_i are the universal gas constant, the number of species and the molecular mass of specie i, respectively.

The specific heat at constant pressure for the mixture is computed as:

$$Cp_m = \sum_{i=1}^{N_S} Y_i Cp_i,\ Cp_i = \frac{R}{M_i}\left(a_i + b_i T + c_i T^2 + d_i T^3 + e_i T^4\right) \tag{14}$$

in which, Cp_i is the specific heat of the specie i and a_i ,b_i ,c_i ,d_i ,and e_i are constants for each specie that can be determined from tabulated data [7].

The temperature of gas, T, is obtained from:

$$T = \left(H - Y_f H_R\right) / Cp_m \tag{15}$$

where, H_R is the enthalpy of combustion.

3. BOUNDARY CONDITIONS

To solve the governing equations, boundary conditions must be applied to the inlet, outlet, solid walls and centerline of the solution domain.

A brief description of these boundary conditions is as follows.

Two flows were assumed to have zero radial velocities at the inlet and enter the combustion chamber with uniform but different axial velocities and temperatures. The inlet turbulence kinetic energy and its dissipation are taken as $k = I^2 u^2$ and $\varepsilon = C_\mu k^{1.5} / 0.03l$, respectively, in which I is the inlet turbulence intensity and l is either the radius of the fuel inlet flow, or annular height of the air inlet flow. The flow is assumed to leave the combustion chamber with zero axial gradients of flow quantities. At the solid walls, the no slip condition for normal velocity component was applied while the wall function [6, 8] was employed to calculate the tangential velocity near the wall and heat transfer rates. At the combustion chamber centerline, radial velocity component is zero, and the radial gradients of other flow quantities are zero because of symmetry.

4. NUMERICAL PROCEDURE

The conservation equations for mass, axial and radial momentum, energy, species, kinetic energy of turbulence and its dissipation rate, are discretized using the finite volume method and the power law scheme [9]. For this purpose, the computational domain is considered as a non-uniform staggered grid, which covers the whole solution domain.

The grid has a higher node concentration at the annulus-mixing layer between the fuel and the air stream, in the recirculation zone near the inlet and near the wall where steep gradients of the flow variables are expected. The values of scalar variables are calculated at the grid nodes, while the axial and radial velocity components are calculated at the grid midpoints in order to have a conservative finite-difference algorithm.

The resulting algebraic equations are coupled and are simultaneously solved by Tri-Diagonal Matrices Algorithm (TDMA). The SIMPLER algorithm is used to introduce pressure gradient in the momentum equations.

In order to prevent the divergence of non-linear equations, the suitable under relaxation factors are used.

Because of intensive influence of temperature and pressure changes on density, the density is assumed to be constant at the first 500 iterations to prevent divergence. Then the resulting flow variables are taken as initial quantities to solve equations simultaneously. Therefore the equations are solved iteratively until a prescribed convergence criterion is achieved.

The criterion for convergence of numerical solution was that the total normalized residual is less than 10^{-3}. This convergence was achieved in about 1800 iterations.

5. RESULTS AND DISCUSSIONS

The geometrical and dynamical parameters of the combustion chamber and the flows have been chosen as to be comparable with those in [10]. The length, L, of the combustion chamber is 1.7 m, and the radius, R_c, is 0.06115 m. The inner radii of the fuel, R_i, and air, R_o, inlets are 0.0295 m and 0.0465 m, respectively. The fuel and air mass flow rates are 7.2 gr/s and 137.0 gr/s, which yield an air/fuel velocity ratio of approximately 20:1. The temperatures of combustion chamber walls, T_w, fuel inlet, T_i, and air inlet, T_o, are 500K, 300K and 600K, respectively.

To ensure the precision of computations, the numerical procedure has been thoroughly checked.

First, the sensitivity analysis has been done. The proper choice of grid size has been examined in [11]; solutions have been performed with different grid densities and grid points to ensure a grid-independent solution. The axial velocity at the centerline of combustion chamber (central velocity) for two different grid points (80×60, 200×120) has been compared. It has been observed that the difference between them is less than 5%. Then, it was found that a grid consisting of 200×120 points is sufficient in providing a grid-independent solution.

Typical fluid flow and streamlines are shown in Fig. 2a, b. Two recirculation zones are observed; one, appears at the centerline immediately downstream of the fuel inlet which was produced due to high momentum flux ratio of the air and fuel flows and resulting in flame stabilization, the other, appears near the outer wall because of the sudden expansion. Figure 3 shows the results for a grid with 1700 x 140 nodes (I=7%) using Fluent solver.

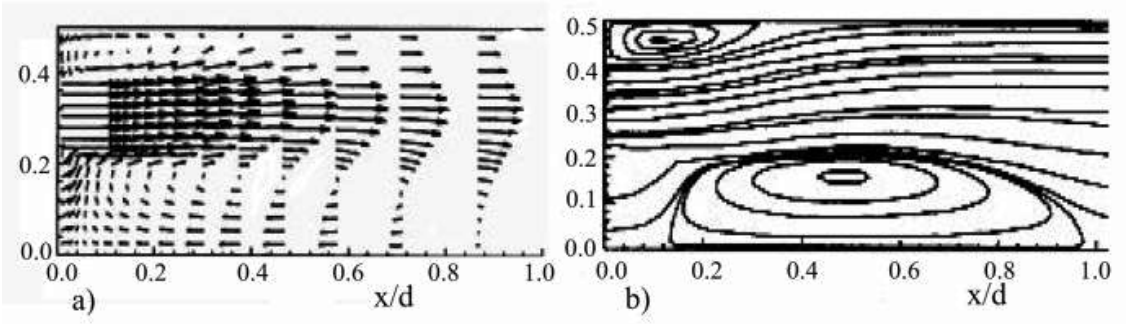

FIG. 2. (a) Fluid flow near the inlet of combustion chamber; (b) Streamlines near the inlet of combustion chamber

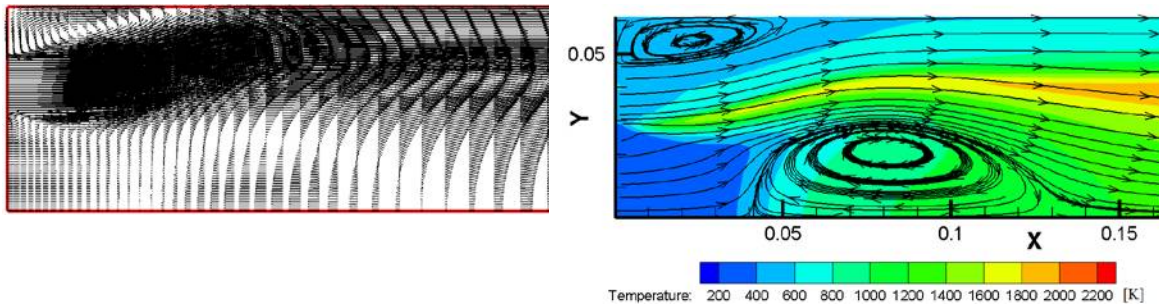

a. b.

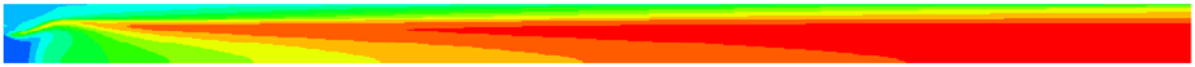

c. Isothermal contours – full chamber

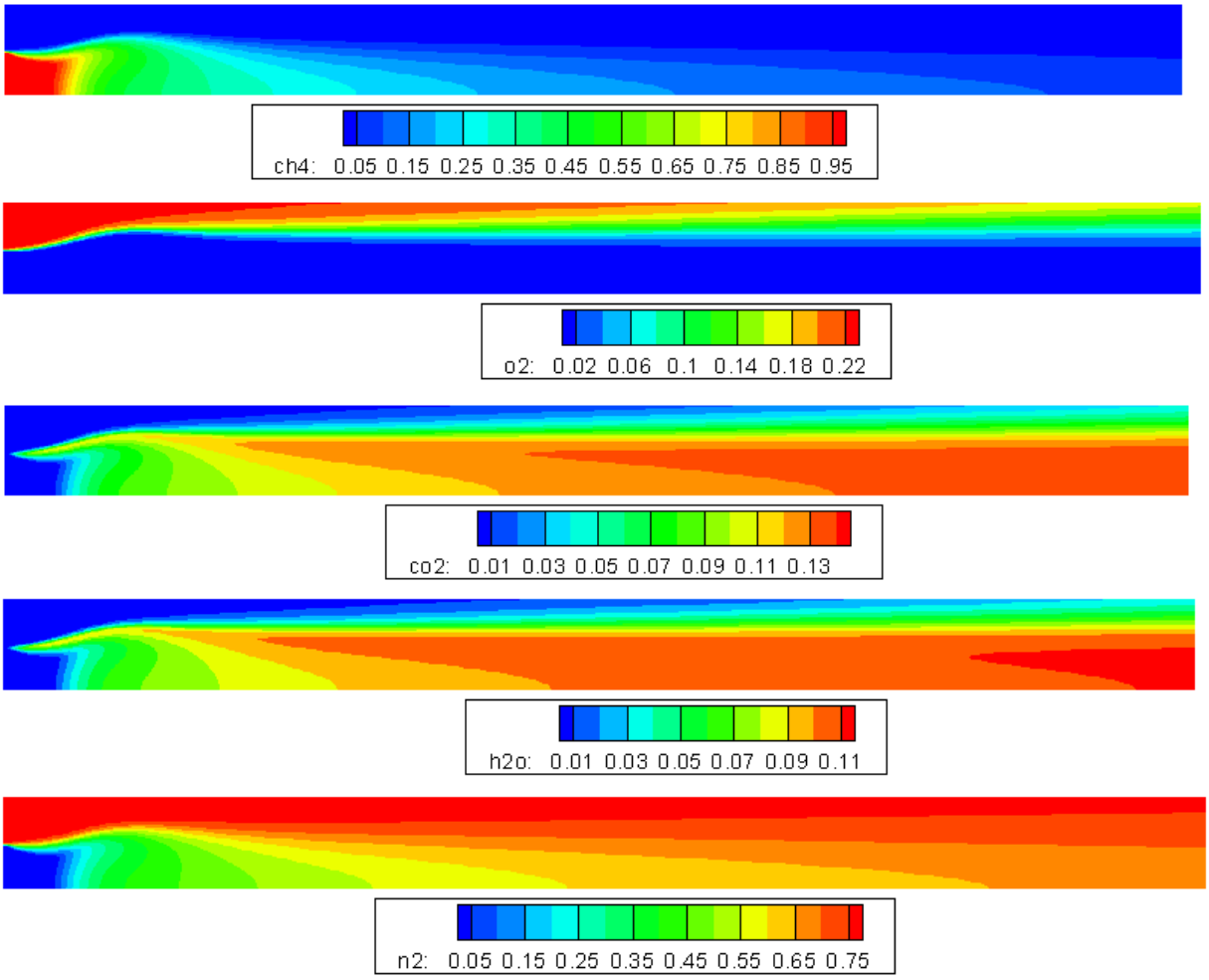

FIG. 3. Results for a grid with 1700 x 140 nodes (I=7%) using Fluent solver: (a) Fluid flow; (b)Streamlines and isothermal contours; (c) Isothermal contours – full chamber; (d) Mass participations of components in combustion chamber (CH_4, O_2, CO_2, H_2O, H_2)

Moreover the published experimental and numerical results [4, 10] have been used to verify the correctness of the numerical procedure. In Fig. 4, the temperature profiles at different sections of combustion chamber are compared with EDC model results [4] and experimental results [10]. It is observed that the results of this study are in good agreement with experimental data.

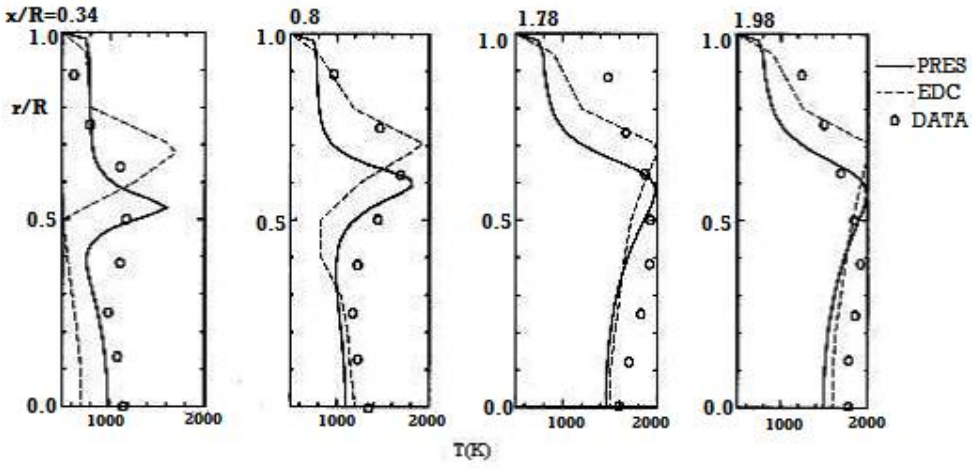

FIG. 4. Temperature profiles at different sections of combustion chamber

Also it is observed that, increasing turbulence intensity decreases the dimensions of recirculating zone. The central velocity at different conditions are compared with each other in Fig. 5:

(1) using the existing model and I= 7%,
(2) using the existing model and I=17%,
(3) using the existing model without combustion (cold flow),
(4) using the EDC model
(5) using the FLUENT model EDC, and
(5) using experimental data.

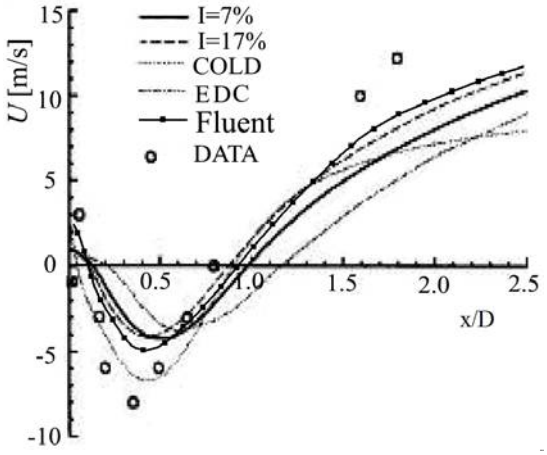

FIG. 5. Central velocity at different conditions (two different turbulence intensities)

It is observed that, the existing model is more effective in prediction of recirculation zone than the EDC model. Also the axial velocity profiles for cold flow (without combustion) and hot flow (with combustion) at different axial sections of combustion chamber are compared with experimental data (Figure 6). It is observed that the flow is expanded due to high temperature caused by combustion reaction. Numerical results are in good agreement with experimental data especially at downstream of recirculation zone.

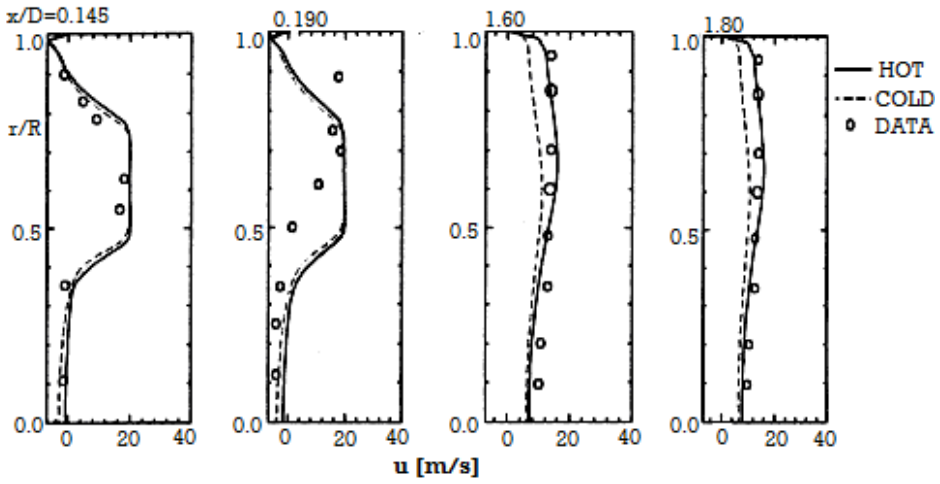

FIG. 6. Velocity profiles at different sections of combustion chamber

CONCLUSIONS

The model can predict the velocity, pressure, temperature, fuel mass fraction, mixing mass fraction and combustion products mass fraction distributions. Using these distributions, one can estimate the critical values of the above properties. As an example, using the pre-mentioned conditions, the maximum temperature of the combustion products turns out to be approx. 2000K. Because of high temperatures caused by combustion reaction, fluid flow is expanded. Increasing the turbulence intensity decreases the dimensions of recirculation zone.

REFERENCES

[1] B. F. Magnussen and B. H. Hjertager, On mathematical modeling of turbulent combustion with special emphasis on soot formation and combustion, *Sixteenth Symposium (International) on Combustion*, The Combustion Institute, pp. 719-729, 1978;

[2] J. I. Ramos, Turbulent non-reacting swirling flows, *Technical Notes*, *AIAA J* , pp. 846-847, 1983;

[3] J. I. Ramos, Numerical solution of non-premixed reactive flows in a swirl combustor model, *Eng. Comput.*, vol. 1, pp. 173-182, 1984;

[4] J. Nisbet, L. Davidson and E. Olsson, *Analysis of two fast-chemistry combustion models and turbulence modeling in variable density flow*, Computation Fluid Dynamics Conf., vol. 1, pp. 557-563, 1992;

[5] M. Ohtsuka, Numerical Analysis of swirling non-reacting and reacting flows by the Reynolds stress differential methode, *Int. J. Heat Mass Transfer***,** vol. 38, pp. 331-337, 1995;

[6] B. E. Launder and D.B. Spalding, The Numerical computation of turbulent flows, *Comp. Meth. Appl. Mech. Eng.*, vol. 3, pp. 269-289, 1974;

[7] Y. A. Cengel and M. A. Boles, *Thermodynamics an engineering approach*, Second Edition, McGrow-Hill, New York, 1989.

[8] C. L. V. Jayatilleke, The Influence of Prandtl number and surface roughness on resistance of the laminar sublayer to momentum and heat transfer, *Progr. Heat Mass Transfer*, vol. 1, pp. 193-329. 1969.

[9] S. V. Patankar, *Numerical heat transfer and fluid flow*, McGraw-Hill, Washington,1980.

[10] F. K. Owen, L. J. Spaddacini, and C. T. Bowman, Rept. EPA-600/2-76-247a, Washington, 1976.

[11] M. Mirmoosavi, *Numerical investigation of combustion in cylindrical tube*, M. Sc. Thesis, Dep of Mechanical Eng., Shahid Bahonar University of Kerman, 1998.

THE STABILITY OF THE CONTROLLABILITY BY TWO SCALE HOMOGENIZATION

Mihaela DUMITRACHE

University of Piteşti, Piteşti, Romania (mihaela_dumitrache_1@yahoo.com)

DOI: 10.19062/2247-3173.2016.18.1.60

Abstract: *In this paper we use the HUM method and we performed an exact internal control which operates on the border of the holes from an ε - periodic perforated domain. Using the two-scale convergence method, we obtain a homogenized hyperbolic problem controlled this time on the whole homogenized domain (without holes) by a surface integral from the limit of the control.*

Keywords: *ε -periodic perforated domain, two-scale convergences, HUM method, exact internal control, homogenization.*

1. INTRODUCTION

In this article, we study a stability problem: what becomes a hyperbolic problem on an ε - periodic perforated domain which is controlled on the border of the holes? Will the property of controllability by homogenization be kept after $\varepsilon \to 0$ (where ε is the distribution period of the holes in the domain) ?

The initial control is found with the HUM method, but, now, it is applied on a perforated domain.

The answer to the last question is an affirmative one. The novelty of the result consists in the fact that the surface integral from the limit of the control is the exact internal control for the homogenized hyperbolic problem – the limit of the hyperbolic initial problem which has got an exact control. Another difference, from other similar articles dealing with the same topic, is the two-scale method, in contrast with the energetic method of Tartar in [8], which cannot be applied in the case of the perforated domain, from this article, a domain which has the property that the holes intersect the border of the homogeneous domain (without holes).

2. THE GEOMETRY OF THE DOMAIN

Let be Ω an open bounded domain from $\mathbb{R}^n (n \geq 3)$ with smooth border $\partial\Omega$. Let be the representative cell of the following form, $Y = (0, l_1) \times \cdots \times (0, l_n)$, from $\mathbb{R}^n$. We use the following notation from [3] for defining the ε - periodic perforated domain. Let be $T \subset Y$ an open domain so that $\overline{T} \subset Y$. T is called hole.

For any $\varepsilon > 0$ and $k \in \mathbb{R}^n$ we denote by $T_\varepsilon^k = \varepsilon(kl + T)$ are the holes in $\mathbb{R}^n$, where $kl = (k_1 l_1, ..., k_n l_n)$. We denote by $T_\varepsilon = \bigcup \left\{ T_\varepsilon^k \,\middle|\, T_\varepsilon^k \cap \Omega \neq \varnothing, k \in \mathbb{R}^n \right\}$ that represent the holes which are in Ω or these intersect the border of Ω. We denote by $\Omega_\varepsilon = \Omega \setminus \overline{T}_\varepsilon$ the ε -

periodic perforated domain. The set $\Sigma_\varepsilon = \bigcup \left\{ \partial T_\varepsilon^k \,\middle|\, T_\varepsilon^k \cap \Omega \neq \varnothing, k \in \mathbb{Z}^n \right\}$ represents the border of the holes, the difference from [3] consists in the fact that the holes intersect $\partial\Omega$. We denote by $Y^* = Y \setminus \overline{T}$.

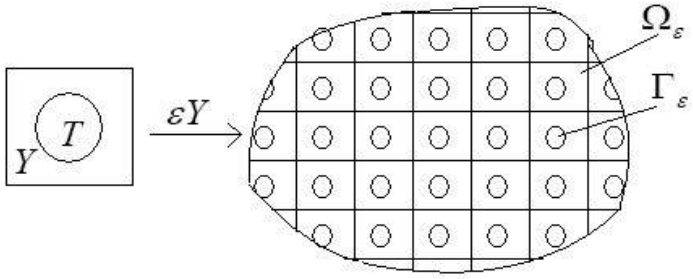

FIG. 1. The structure.

3. THE STATEMENT OF THE PROBLEM

Using the HUM method we obtain the problem that is verified by the exact internal control in the domain $\Omega_\varepsilon \times (0,T)$:

$$\begin{aligned} u_\varepsilon'' - \frac{\partial}{\partial x_i}\left(a_{ij} \frac{\partial u_\varepsilon}{\partial x_j} \right) + q_\varepsilon u_\varepsilon = 0, \text{ in } \Omega_\varepsilon \times (0,T) \\ u_\varepsilon = 0, \text{ on } \partial\Omega \times (0,T) \\ u_\varepsilon(0) = u_\varepsilon^0,\ u_\varepsilon'(0) = u_\varepsilon^1 \text{ on } \Omega_\varepsilon \end{aligned} \tag{1}$$

where $u_\varepsilon^0 \in U_\varepsilon$, $u_\varepsilon^1 \in L^2(\Omega_\varepsilon)$, $q_\varepsilon \in L^2(\Omega_\varepsilon)$ and U_ε is the Hilbert space defined by $U_\varepsilon = \bigcup \left\{ u \in H^1(\Omega_\varepsilon) \,\middle|\, u = 0 \text{ on } \partial\Omega \right\}$ with the associated norm:

$$\|u\|_{U_\varepsilon} = \left(\sum_{i=1}^{n} \int_{\Omega_\varepsilon} \left(\frac{\partial u}{\partial x_i} \right)^2 dx \right)^{\frac{1}{2}} \tag{2}$$

The coefficients a_{ij} are constant and elliptic. With Lax-Milgram theorem the problem (1) has a unique solution. Also, the application $\left(u_\varepsilon^0, u_\varepsilon^1\right) \mapsto \frac{\partial u_\varepsilon}{\partial \nu_\varepsilon}$ is linear and continuous from the space $U_\varepsilon \times L^2(\Omega_\varepsilon)$ to the space $L^2\left(0,T; L^2(\Gamma_\varepsilon)\right)$, so $\frac{\partial u_\varepsilon}{\partial \nu_\varepsilon} \in L^2\left(0,T; L^2(\Gamma_\varepsilon)\right)$. We have to remind ourselves that $\frac{\partial u_\varepsilon}{\partial \nu_\varepsilon}$ represents the derivative of u_ε with respect to the outside normal ν_ε at Γ_ε and it is defined as:

$$\frac{\partial u_\varepsilon}{\partial \nu_\varepsilon} = a_{ij} \frac{\partial u_\varepsilon}{\partial x_j} n_i \tag{3}$$

where $\nu_\varepsilon = (n_1, ..., n_n)$ are the components of the normal.

We denote the exact internal control by $\varphi_\varepsilon = \dfrac{\partial u_\varepsilon}{\partial \nu_\varepsilon}$ and it controls the following hyperbolic problem:

$$\begin{aligned} v_\varepsilon'' - \frac{\partial}{\partial x_i}\left(a_{ij}\frac{\partial v_\varepsilon}{\partial x_j}\right) + q_\varepsilon v_\varepsilon = 0, \text{ in } \Omega_\varepsilon \times (0,T) \\ \frac{\partial v_\varepsilon}{\partial \nu_\varepsilon} = \varepsilon\varphi_\varepsilon, \text{ on } \Gamma_\varepsilon \times (0,T) \\ v_\varepsilon = 0, \text{ on } \partial\Omega \times (0,T) \\ v_\varepsilon(T) = v_\varepsilon'(T) = 0, \text{ in } \Omega_\varepsilon \end{aligned} \tag{4}$$

With the Lax-Milgram theorem, the problem (4) has a unique solution so that $(v_\varepsilon(0), v_\varepsilon'(0)) \in L^2(\Omega_\varepsilon) \times (U_\varepsilon)'$, where $(U_\varepsilon)'$ is the dual of U_ε. More than this, the application $(u_\varepsilon^0, u_\varepsilon^1) \mapsto (v_\varepsilon(0), v_\varepsilon'(0))$ is linear and continuous from $U_\varepsilon \times L^2(\Omega_\varepsilon)$ to $L^2(\Omega_\varepsilon) \times U_\varepsilon'$.

In next section we homogenize these two problems using the idea from [6] and the two-scale convergence method introduced in [1] and [7].

4. THE HOMOGENIZATION AFTER $\varepsilon \to 0$

The homogenized problems for (1) and (4) are:

$$\begin{aligned} (measY^*)u'' - \frac{\partial}{\partial x_i}\left(A_{ij}^{\hom}\frac{\partial u}{\partial x_j}\right) + qu = 0, \text{ in } \Omega \times (0,T) \\ u = 0, \text{ on } \partial\Omega \times (0,T) \\ u(0) = \frac{u^0}{measY^*}, \; u'(0) = \frac{u^1}{measY^*} \text{ in } \Omega \end{aligned} \tag{5}$$

where we have the next convergences:

$$\begin{aligned} &\chi_{\Omega_\varepsilon}(x)u_\varepsilon(x) \xrightarrow{2s} \chi_{Y^*}(y)u(x) \\ &\chi_{\Omega_\varepsilon}(x)q_\varepsilon(x) \xrightarrow{2s} \chi_{Y^*}(y)q(x) \\ &\chi_{\Omega_\varepsilon}(x)u_\varepsilon^0(x) \xrightarrow{2s} \chi_{Y^*}(y)u^0(x) \\ &\chi_{\Omega_\varepsilon}(x)u_\varepsilon^1(x) \xrightarrow{2s} \chi_{Y^*}(y)u^1(x) \end{aligned} \tag{6}$$

where

$$\chi_{\Omega_\varepsilon}(x) = \begin{cases} 1, x \in \Omega_\varepsilon \\ 0, x \notin \Omega_\varepsilon \end{cases} \tag{7}$$

is the characteristic function of Ω_ε and

$$\chi_{\Omega_\varepsilon}(x) = \chi_{Y^*}\left(\frac{x}{\varepsilon}\right). \tag{8}$$

The homogenized coefficients $A_{ij}^{\hom}$ are given in [2] and [4, 5].

The homogenization of the problem (4). The homogenized controlled problem is:

$$\begin{aligned} \left(measY^*\right)v'' - \frac{\partial}{\partial x_i}\left(A_{ij}^{\hom}\frac{\partial v}{\partial x_j}\right) + q(x)v(x) =_\varepsilon v_\varepsilon = 0, \text{ in } \Omega_\varepsilon \times (0,T) \\ \frac{\partial v_\varepsilon}{\partial \nu_\varepsilon} = \varepsilon\varphi_\varepsilon, \text{ on } \Gamma_\varepsilon \times (0,T) \\ v_\varepsilon = 0, \text{ on } \partial\Omega \times (0,T) \\ v_\varepsilon(T) = v'_\varepsilon(T) = 0, \text{ in } \Omega_\varepsilon \end{aligned} \quad . \tag{9}$$

where

$$\begin{aligned} &\chi_{\Omega_\varepsilon}(x)v_\varepsilon \xrightarrow{2s} \chi_{Y^*}(y)v(x) \\ &\varepsilon\chi_{\Omega_\varepsilon}(x)\varphi_\varepsilon(x) \xrightarrow{2s} \varphi(x,y) \end{aligned} \tag{10}$$

and $\varphi(x,y)$ is the limit of the control.

CONCLUSIONS

By comparing the controlled problem by φ_ε and the homogenized problem of it, we can observe: the limit of the control – which operates on the border of the holes – in homogenized problem acts via a surface integral on the whole homogeneous domain (without holes) Ω.

REFERENCES

[1] G. Allaire, *Homogenization and two-scale convergence*, SIAM J, Math. Anal. 23,6, 1482-1518,1992;
[2] D. Ciorănescu, J. Saint Jean Paulin, *Homogenization of reticulated structures*, Springer Verlag (New Zork), 1999;
[3] C. Conca, J. I. Diaz, A. Linan, C. Timofte, *Homogeniyation in chemical reactive flows*, Electronic Journal of Differential Equations, No. 40, 1-22, 2004;
[4] C. Gheldiu, *L'homogeneization d'equation des ondes pour structures renforcees*. Buletin Ştiinţific, Universitatea din Piteşti, Nr. 15, 29-38, 2009;
[5] C. Gheldiu, *L'homogeneisation de probleme des ondes pour structures reticulees renforcees vers l'epaisseur du materiau. Controlabilite exacte pour structures reticulees renforcees*, Buletin Ştiinţific – Universitatea din Piteşti, Seria Matematică şi Informatică, Nr. 17 (2011).
[6] V. Komornik, *Exact controllability and stabilization. The multiplies method*, Masson, Paris, 1994;
[7] G. Nguetseng, *Asymptotic analisys for a stiff variational problem in mechanics*, SIAM J, Math. Anal. 21,6, 1394-1414, 1990;
[8] L. Tartar, *Problemes d'homogeneization dans les equations aux derivees partielles*, in Cours Pecot, College de France, 1977;

USING THE ANALOGY IN TEACHING TETRAHEDRON GEOMETRY

Adriana-Daniela GURGUI

"Ovidius"High School, Constanta, Romania (adrianagurgui@yahoo.com)

DOI: 10.19062/2247-3173.2016.18.1.61

Abstract: *In the teaching tetrahedron geometry, we often meet similar properties to those of the triangle and that is why it is good to emphasize and use this analogy. The result will develop in students not only the functional thinking, but also the analog thinking.*

Keywords: *comparative studies, elementaryproblems in Euclidian geometries.*
MSC2010: *97D10, 51M04*

1. INTRODUCTION

While the triangle is determined by three non-collinear points, the tetrahedron is defined by four non-coplanar points. In the following we will make a brief, but very useful parallel between the two geometric notions.

2. PARALLEL BETWEEN TRINGLE AND TETRAHEDRON

We will follow Table 1, where we will find the properties of the triangle and tetrahedron:

Table 1.

No.	TRIANGLE	TETRAHEDRON
1.	$Area = \frac{B \cdot h}{2}$	$Volume = \frac{A_b \cdot h}{3}$
2.	The center of gravity in the triangle is distanced at 1/3 from the base and 2/3 from the peak.	The center of gravity in the tetrahedron is distanced at 1/4 from the base and ¾ from the peak.
3.	The center of the inscribed circle in the triangle is determined by the intersection of bisectors and $r = \frac{S}{p}$ where r is radius of the circle, $S$is the area and $p$is the semiperimeter of the triangle.	The center of the inscribed sphere in the tetrahedron is determined by the intersection of bisecting planes of the dihedral angles and $r = \frac{3V}{S}$ where r is radius of the sphere, $V$is the volume and $S$is the total area of the tetrahedron.
4.	The center of the circumscribed circle of the triangle is determined bythe intersection of perpendicular bisectors.	The center of the circumscribed sphere of the tetrahedron is determined by the intersection of the median planes of tetrahedron edges.

5.	In an equilateral triangle the three medians have equal lengths.	In a tetrahedron with equiareal faces the four medians have equal lengths.
6.	In an equilateral triangle the three altitudes have equal lengths.	In a tetrahedron with equiareal faces the four altitudes have equal lengths.
7.	Triangle angle bisector theorem: A bisector of an angle of a triangle divides the opposite side in two segments that are proportional to the other two sides of the triangle.	Dihedral angle bisector theorem in tetrahedron: A bisector half-plane of an dihedral angle in tetrahedron divides the opposite edge in two segments that are proportional to the other two surfaces of the dihedral angle.
8.	Cathetus theorem in the right triangle ABC with $m(\angle A)=90^\circ$ and $AD \perp BC$: $AB^2 = BC \cdot BD$ and similars.	An analogue of the Cathetustheorem in the tetrahedron $VABC$, with $VA \perp VB \perp VC \perp VA$ and $AH \perp (ABC)$: $A^2_{\Delta VAB} = A_{\Delta ABC} \cdot A_{\Delta HAB}$ andsimilars.
9.	The right triangle altitude theorem in the right triangle ABC with $m(\angle A)=90^\circ$ and $AD \perp BC$: $AD^2 = DC \cdot DB$ and similars.	An analogue of the right triangle altitude theorem in the tetrahedron $VABC$, with $VA \perp VB \perp VC \perp VA$ and $AH \perp (ABC)$: $A^2_{\Delta VCD} = A_{\Delta CAD} \cdot A_{\Delta HBC} = A_{\Delta CBD} \cdot A_{\Delta HAC}$ andsimil ars.
10.	Pithagorean theorem in the right triangle ABC with $m(\angle A)=90^\circ$: $BC^2 = AB^2 + AC^2$	An analog of the Pithagorean theorem in an tetrahedron $VABC$, with $VA \perp VB \perp VC \perp VA$ and $AH \perp (ABC)$: $A^2_{\Delta ABC} = A^2_{\Delta VAB} + A^2_{\Delta VBC} + A^2_{\Delta VCA}$

In the following there will be proved some of the theorems presented in the previous table. The numbering will be kept and it will only refer to the theorems of the tetrahedron.

Now we will prove 7. from the Table 1. (A bisector half-plane of an dihedral angle in tetrahedron divides the opposite edge in two segments that are proportional to the other two surfaces of the dihedral angle).**(FIG. 1.)**

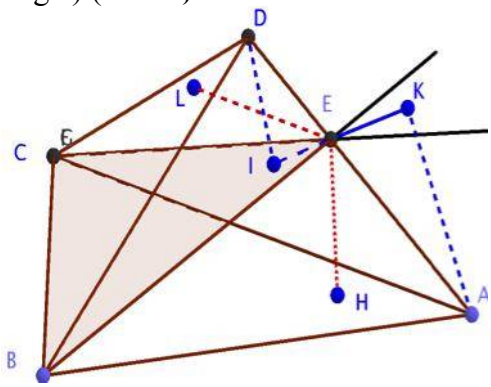

FIG. 1.

Let be E the point where the bisector half-plane intersects the opposite edge of the tetrahedron and $EL \perp (BCD), EH \perp (ABC)$. Because (BCE) is the bisector-half plane, the distances to the faces of the dihedral angle are the same, therefore $EL = EH$.

$$V_{DBCE} = \frac{S_{BCD} \cdot EL}{3}, V_{ABCE} = \frac{S_{ABC} \cdot EH}{3}$$

$$\frac{V_{DBCE}}{V_{ABCE}}=\frac{\frac{S_{BCD}\cdot EL}{3}}{\frac{S_{ABC}\cdot EH}{3}}=\frac{S_{BCD}}{S_{ABC}}\cdot\frac{EL}{EH}=\frac{S_{BCD}}{S_{ABC}} \quad (1)$$

Let $DI\perp(BCE), AK\perp(BCE)$. Therefore $DI\|AK$. We will prove that I,E,K are collinear. Let $\beta=(DI,AK)$ From $E\in AD\subset\beta$ and $E\in(BCE)\Rightarrow E\in\beta\cap(BCE)$.

But $I,K\in\beta\cap(BCE)$ and then $I,E,K\in\beta\cap(BCE)$, so they are collinear.

Volumes of the two tetrahedrons can also be expressed by:

$$V_{DBCE}=\frac{S_{CBE}\cdot DI}{3}, V_{ABCE}=\frac{S_{CBE}\cdot AK}{3}, \quad \frac{V_{DBCE}}{V_{ABCE}}=\frac{\frac{S_{CBE}\cdot DI}{3}}{\frac{S_{CBE}\cdot AK}{3}}=\frac{DI}{AK} \quad (2)$$

$$\text{From } DI\|AK\Rightarrow\Delta DIE\approx\Delta AKE\Rightarrow\frac{DI}{AK}=\frac{IE}{KE}=\frac{DE}{AE} \quad (3)$$

$$\text{And from (1),(2)si (3)}\Rightarrow\frac{S_{BCD}}{S_{ABC}}=\frac{DE}{AE}.$$

Now we will prove that in tetrahedron $VABC$ with $VA\perp VB\perp VC\perp VA$ the orthogonal projection of point V on the plane (ABC), H, is the orthocenter of the triangle ABC and the validity of the statements 8.9.10. from the Table 1:(**FIG. 2.**)

$$A^2_{\Delta VAB}=A_{\Delta HAB}\cdot A_{\Delta ABC} \text{ (for 8.)} \quad (4)$$

$$A^2_{\Delta VCD}=A_{\Delta CAD}\cdot A_{\Delta HBC} \text{ (for 9.)} \quad (5)$$

$$A^2_{\Delta ABC}=A^2_{\Delta VAB}+A^2_{\Delta VBC}+A^2_{\Delta VCA} \text{ (for 10.)} \quad (6)$$

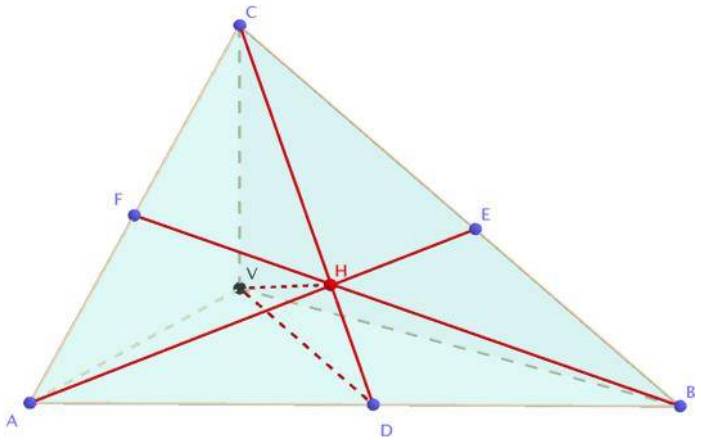

FIG. 2.

Let $VH\perp(ABC)$. We will prove H is the orthocenter of the triangle ABC. First we will prove that $CH\perp AB$. From $VC\perp VB$ and $VC\perp VA\Rightarrow VC\perp(VAB)\supset AB\Rightarrow VC\perp AB$.

From $VH\perp(ABC)\supset AB\Rightarrow VH\perp AB$

From $VC\perp AB$ and $VH\perp AB\Rightarrow AB\perp(VCH)\supset CH\Rightarrow AB\perp CH$

Similarity it can demonstrated that $BH \perp AC$ and then H is the orthocenter of the triangle ABC.

Now we will prove that the validity of the statement 8. fromthe Table 1 .

From $A^2_{\Delta VAB} = \left(\frac{AB \cdot VD}{2}\right)^2$ $A_{\Delta HAB} = \frac{AB \cdot HD}{2}$, $A_{\Delta ABC} = \frac{AB \cdot CD}{2}$

Using Cathetus Theorem in ΔVCD: $VD^2 = HD \cdot CD$ we have:

$$A^2_{\Delta VAB} = A_{\Delta HAB} \cdot A_{\Delta ABC} \Leftrightarrow \left(\frac{AB \cdot VD}{2}\right)^2 = \frac{AB \cdot HD}{2} \cdot \frac{AB \cdot CD}{2} \Leftrightarrow$$

$$\Leftrightarrow \frac{AB^2 \cdot VD^2}{4} = \frac{AB^2 \cdot (HD \cdot CD)}{4}$$

It will prove the validity of statement 9. From the Table 1:

From (4) Cathetus Theorem in the right triangle ΔVCD: $CV^2 = CD \cdot CH$ and $VD^2 = AD \cdot BD$ (The right triangle altitude theorem in the right triangle ΔVAB)

$$A^2_{\Delta VCD} = A_{\Delta CAD} \cdot A_{\Delta HBC} \Leftrightarrow \left(\frac{CV \cdot VD}{2}\right)^2 = \frac{CD \cdot AD}{2} \cdot \frac{CH \cdot BD}{2} \Leftrightarrow$$

$$\Leftrightarrow \left(\frac{CV \cdot VD}{2}\right)^2 = \frac{(CD \cdot CH) \cdot (AD \cdot BD)}{2} \Leftrightarrow \left(\frac{CV \cdot VD}{2}\right)^2 = \frac{CV^2 \cdot VD^2}{4}$$

Finally it will prove the validity of statement 10. from the Table 1:

From $A^2_{\Delta VAB} = A_{\Delta HAB} \cdot A_{\Delta ABC}$, $A^2_{\Delta VBC} = A_{\Delta HBC} \cdot A_{\Delta ABC}$, $A^2_{\Delta VAC} = A_{\Delta HAB} \cdot A_{\Delta ABC}$

Then $A^2_{\Delta VAB} + A^2_{\Delta VBC} + A^2_{\Delta VCA} = A_{\Delta HAB} \cdot A_{\Delta ABC} + A_{\Delta HBC} \cdot A_{\Delta ABC} + A_{\Delta HAC} \cdot A_{\Delta ABC} =$

$A_{\Delta ABC} \cdot (A_{\Delta HAB} + A_{\Delta HBC} + A_{\Delta HAC}) = A^2_{\Delta ABC}$.

CONCLUSIONS

The few analogies studied in this work open the way to the comparative study between plane geometry concepts and the concepts of the space geometry. Therefore, the knowledge of the plane geometry is not just an adjunct to the geometry of space, but also a rich source of inspiration and analogies.

REFERENCES

[1] ***GeoGebra 5. Available at http:/.geogebra.en.softonic.com/mac, accessed on March 23, 2016;
[2] D. Branzei, M. Miculita, *Tetrahedron triangle analogies,* Paralela 45, Pitesti 2000;
[3] L. Nicolescu, V. Boskoff, *Applied Geometry Problems*EdituraTehnica, Bucuresti 1990;
[3] H. V. Stoiculescu, I.M. Popa, I. Popa *Geometry and Trigonometry fotXth Grad,* Didactic and Pedagogic Publishing, Bucuresti, 1990

MULTICOPTER LANDING

Jaromir HOSEK

"University of Defence, Faculty of Military Technology, Brno, Czech Republic
(jaromir.hosek@unob.cz)

DOI: 10.19062/2247-3173.2016.18.1.62

Abstract: *Paper presents the methods to help the landing of the Unmanned Aerial Vehicle. There are mentioned two other methods and depicted method based on the Neural network. The main idea of that approach is described. The paper solves landing of the Unmanned Aerial Vehicle by means of camera only.*

Keywords: *unmanned aerial vehicle, unmanned ground vehicle, landing problem.*

1. INTRODUCTION

The new term used in these days is the Unmanned Aerial Vehicle (UAV). Strictly speaking, it is an aircraft without human pilot aboard and we can say it is the Unmanned Aircraft System (UAS). Nowadays, public use the term drone widely, because there is a big similarity to sound of the flying male bee.

The Unmanned Aerial Vehicles (UAV) are used in private sector and, of course, in security branch. The private sector have many types of the UAV from small miniature weighting to 1kilogram up to very heavy UAV weighting tens kilograms. There are used fixed-wing and rotary-wing UAV. The smaller types we can buy in a children stores and playing with them to attract children to study technical branches. The higher types are used in commercial. The examples of using are:

Power engineering – the UAVs are equipped by cameras and they serve to monitoring wind power stations, refineries, opencast mines, photovoltaic power stations, gasworks, etc.

Agriculture – monitoring of crop, an insects, the fungal diseases, moving the wild animals, etc.

Building industry – check of a roof condition, the high smokestacks, the transmissions towers and nowadays very important measurement of the heat losses, etc.

Environment – measurement of the atmosphere, the atmosphere pollution and monitoring hazardous waste dumps, etc.

Culture and entertainment – propagation of the cities, the historical sights, the interest places, the sport and culture actions, etc.

Transport industry – monitoring the streets, the highways, the floods, the snow calamities, etc.

There are many other and other field where the UAV can be used to improving and speeding up some activities. The main field of using is in the security branch, it is meant the search and rescue systems, the reconnaissance for military and police, for observing demonstrations and big sport actions (football matches, etc.), searching the lost persons and guarding of dangerous areas like the ammunitions storages, the chemical factories or damaged nuclear power stations (Fukushima, Chernobyl).

We can find many other ways to divide the UAVs, this is according to a number of motors, UAVs weight, equipment on board etc., it depends on authors and their preferences.

2. COOPERATION BETWEEN UAV AND UGV

There are many types of the UAV which are used in security branches. We have small UAV (multicopter) with rotary-wing, type Y6 which is equipped by three servomotors and its weight is about 1,5kg and payload is 0,400kg. Its main advantage is ability to vertical takeoff and landing and of course to hover above or in front of interesting place. This UAV can hide behind a tree, a building or any obstacle to observe important things. The advantages of these multicopters are small dimensions and because of that to operate quietly and of course furtively and if necessary secretly.

The big problem of such small multicopter is mainly energy. They can be in the air about 10-15 minutes, this is flying range about two kilometres. We can use another battery pack but a payload will be decreased.

The unmanned ground vehicles (UGV) are very popular too. Their control is nearly the same, remotely control, they use GPS, accelerometers, rate gyroscopes, magnetometers and other sensors based on the MEMS technology. They range is longer and they have not any problem with energy source and their payload is incomparable with the UAV. The UGV has smaller ability to discover large area in a short time. The question is: can we use an advantages of both unmanned vehicles? The answer is why not. The UGV can serve like carrier of the UAV and if necessary to charge its batteries. The problem is that both vehicles are remotely controlled and operators must cooperate during landing on the UGV. The operator controls multicopter by means of camera and after some stressful mission the landing manoeuvre is very difficult. As mentioned above multicopter use visual (VIS) and infrared (IR) cameras. These cameras are primary used for information to user and for navigation, guidance and control, the same like primary guidance sensor of birds, insects, etc. The main idea is to use untapped potential of the cameras for automatic landing on UGV ramp.

3. OTHER APPROACHES TO SOLUTION

The landing problem is solved by many ways and by many researches. I was interested in two ways of solving this problem.

3.1 Assisted landing. At first it is very interesting to take advantage of control system of the UGV. The idea comes from using onboard VIS and IR cameras to recognize the UGV carrier and by means of visual data to control landing. The authors proposed to place the light blinking diodes on an UAV bottom. The UGV ramp will be equipped by a camera. This camera tracks the position of diodes and microprocessor counts distance and orientation of an UAV and counts differences this is coordinates Δx, Δy, Δz and angle $\Delta\alpha$, as shown in Fig.1. The counted differences are led to the UGV control system which turn vehicle to right position due to the UAV.[1]

3.2. Landing by means of beacons. The main idea is nearly the same, the landing place is very small and multicopter use a camera for measuring of all parameters of the control system for landing. The signal wall for landing is placed on ground in vertical position and it is equipped by the radiations sources (beacons). The sources are tracked by the camera fixed on an UAV. The one radiation source do not enable the landing Fig.2a. The four sources enable landing but undirected landing, Fig.2b. Due to the authors use five radiation sources which are arranged as shown in Fig.2c. The inputs of a camera are

convert through threshold method to binary picture by means of MATLAB function *graythresh* to rectangular grid and occupied fields in the grid are positions of beacons and control system can determine its position to source's wall. [2]

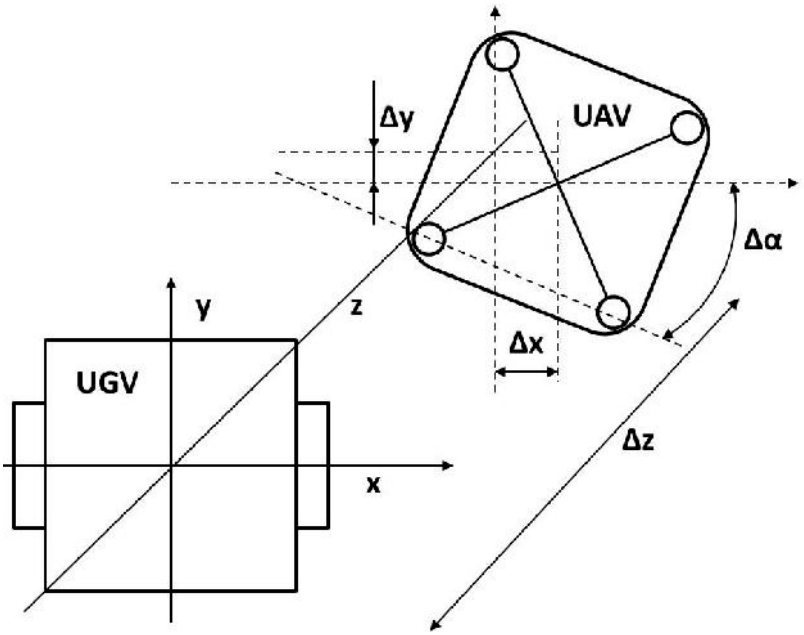

FIG.1., Basic coordinates between UGV and UAV

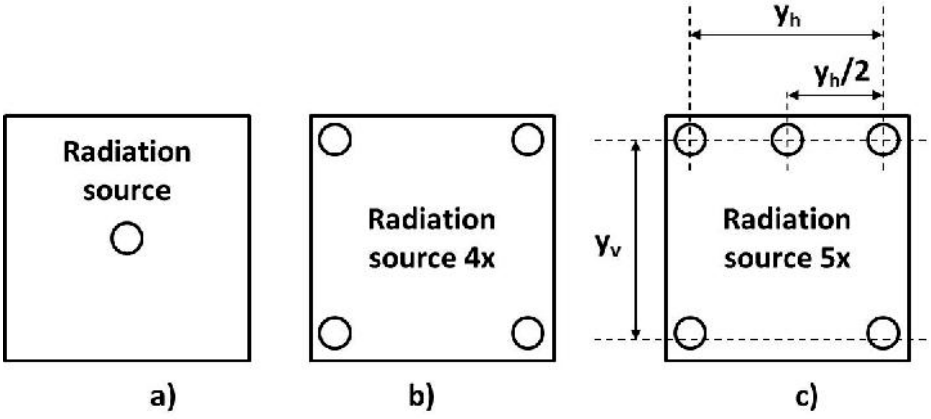

FIG.2., Placement of the radiation sources

4. NEURAL NETWORKS AS DECISION ELEMENT

There are many variants how to solve takeoff and landing of the small multicopter. The one of the variants is to use neural networks.

The big problem during using of the multicopter is landing. We assume the small multicopter equipped with a camera and landing on a determine place for example a ramp. The ramp is equipped by passive element which enables to gain the landing parameters for control system of the multicopter. The suitable element is the circle, Fig.3a. The circle drawn on a ramp enable only landing but without orientation because of that it is needed to add other elements. These elements are other circles but smaller and placed in determinate pattern. There is chosen triangle of which vertexes are small circles

as shown in Fig3b. The patterns can be various and the circles can be arranged in shape of big letter L Fig.3c or can be used five circles etc.

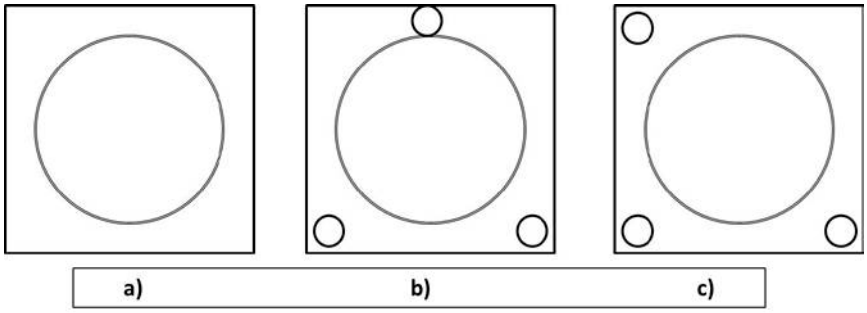

FIG.3., Pattern on a ramp

Main idea is that when we see on the circle from any angle we see the ellipse. We assume that the camera approaches and an ellipse changes to a circle, Fig.4. The landing without orientation can approach from every course and control system evaluates changes from an ellipse to a circle, and when a multicopter is above a ramp the control system see the circle and can land. The oriented landing needs other information about the front part of a ramp. When a multicopter is above a ramp and see a circle the control system must detect three circles in a vertexes of triangle and rotate in accordance with them.

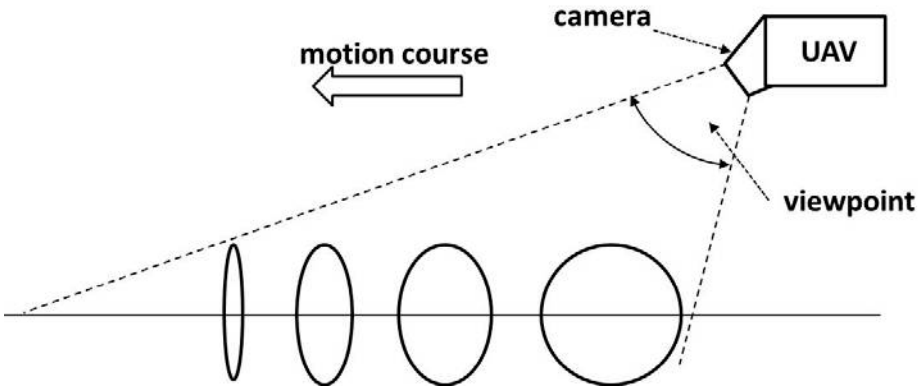

FIG. 4. Changes ellipse to circle

The decision element of the control system is the neural network. The neural net is trained on recognition of the various shapes of the ellipses. The motion course and a velocity of a multicopter depends on the shape of the ellipses. The shapes are divided into 4 main categories. The first category, the ellipse is very narrow and it means basic approach to a ramp. The second, when an ellipse is wider, the velocity is decreased and the course is the same. The third one, the ellipse is wider again and a velocity is decreased again too. The last stage is when an ellipse is (nearly) the circle, the velocity is stopped and multicopter is prepared to landing and a neural net recognize three additional circles to determine orientation of the multicopter, Fig.6. The output of the neural network may be set in accordance to a ratio of a small half-axis to a big half-axis. The neural network output setting depends on the type and the size of the multicopter, Fig.5.

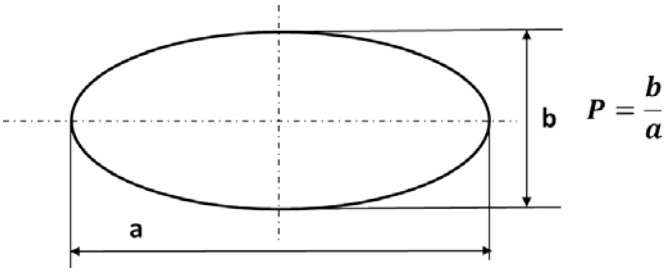

FIG.5. Neural Network setting

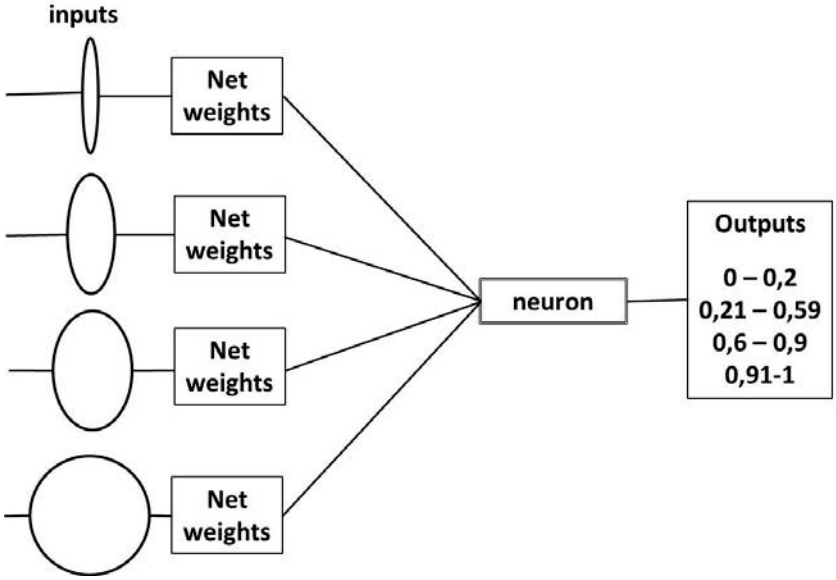

FIG.6, Neural network

CONCLUSIONS

The modern UAV are used for an entertainment and for more important things like searching or guarding. The last ones require long time operation this is long time flight above interesting area. To make flight longer we can use cooperation between the UAV and the UGV. The presented method for using neural network during landing can increase of an effectivity of the UAV using. When the visibility is sufficient the circles can be passive, on the other hand during unfavourable weather conditions the circles must be active, for example light up circles or circles must shine.

REFERENCES

[1] Y. Bergeon, R. Doskocil, V. Krivanek, J. Motsch, A. Stefek, *UAV Assisted Landing on Moving UGV*, ICMT2015, Brno, May 19 – 21. 2015, University of Defence, p.611-615, ICMT 978-80-7231-976-3;
[2] M. Polasek and J. Nemecek, *The utilization of the videocamera for the unmanned aerial vehicle control*, ICMT2015, Brno, May 19-21. 2015, University of Defence, ICMT 978-80-7231-976-3;
[3] J. Wesley Hines, *Neural Approaches in Engineering (MATLAB supplement)*, John Wiley and Sons, New York, 1997;
[4] M. Novak, *Umělé neuronové sítě*, C. H. Beck, Praha 1998, ISBN 80-7179-132-6;
[5] S. Russel, P. Norvig, *Artificial Intelligence a Modern Approach*, Third Edition, Pearson Education Limited, 2014, ISBN 978-1-292-02420-2;

APPLIED MATHEMATICS, COMPUTER SCIENCE, IT&C

SUBJECT INFORMATION TECHNOLOGY IN MILITARY EDUCATION – CIVILIAN STUDY

Miroslav HRUBÝ

University of Defence, Brno, Czech Republic (miroslav.hruby@unob.cz)

DOI: 10.19062/2247-3173.2016.18.1.63

Abstract: *The paper deals with the new experience connected with the subject "Information Technology" which was gained at the Faculty of Military Technology, University of Defence, Brno, Czech Republic. The attention is focused on the new civilian Bachelor's degree study programme "Technologies for Defence and Security" where the subject "Information Technology" is included in the first semester of studies.*

Keywords: *algorithms, computer networks, information technology, university, programming*
MSC2010: *68W01, 68N15, 68P05, 97Q60.*

1. INTRODUCTION

Although the Faculty of Military Technology (FMT) of the University of Defence (UoD) main focus is on military students for the Czech Armed Forces, the FMT is also realizing civilian study programmes. It enables better usage of the human and technical resources of the FMT. The text of the article follows [1] where the subject "Information Technology" was for the first time introduced but that subject was tailored for military students of the FMT UoD. Now the different subject "Information Technology" which was prepared for civilian students of the FMT UoD, is introduced.

The goal of the paper is to introduce the study plan of the subject, its teaching methods and rules for passing the exam. The findings from the first semester of the subject teaching are included.

2. NEW UNIVERSITY OF DEFENCE CIVILIAN STUDY PROGRAMME

Since 2015, the FMT UoD has been started the new civilian Bachelor's degree study programme "Technologies for Defence and Security". It covers three fields of study: "Communication and Information Technologies", "Technologies for Protection of Assets and People" and "Weapons and Ammunition". Two new fields of study are being prepared for accreditation process. These are: "Aviation Techniques" and "Geography and Meteorology for Defence and Security". The subject of "Information Technology" is included in the winter semester of the first year of studies.

3. SUBJECT "INFORMATION TECHNOLOGY" CONTENT

The subject of "Information Technology" is a mandatory subject for all FMT UoD civilian students in the first semester of their Bachelor's degree study programme since 2015. The guarantor of the subject is Department of Communication and Information

Systems(CIS) but Department of Military Geography and Meteorology is also involved in its teaching. Three main part of the subject are described in Table 1.

Table 1 – Content of the subject "Information Technology" for the civilian students FMT UoD:

Programming	Introduction into algorithms, data types and data structures, statements of a high level programming language, structure of a program.	Lectures 6 hours
	JavaScript program running, input and output in JavaScript, usage of an array in JavaScript, string processing, user defined functions, buttons and input field on a webpage.	Laboratory exercises 26 hours
Computer Networks	Introduction into computer networks, history, division, forms of realization, network architecture reference model ISO/OSI, model TCP/IP, local computer networks including wireless networks, Ethernet, fundamental suite of TCP/IP protocols, planning of the address space, CIDR, VLSM, routing, safety.	Lectures 14 hours
	Basic configuring of network devices, realization of simple networks and their diagnostics.	Laboratory exercises 8 hours
Geography	State coordination Systems S-JTSK and WGS 84, approaches to expression of location, digital geographical data, their formats, methods of their obtaining	Lectures 4 hours
	Geographical Information Systems (GIS)	Laboratory exercise 2 hours

The subject Information Technology is immediately followed in the next semester by the subject "Modeling and Simulation". This subject is focused on the software

Matlab&Simulink [2, 3] and its content is divided into 16 hours of lectures and 32 hours of laboratory exercises.

4. TEACHING METHODS USED

The subject of "Information Technology" was for the first time studied by civilian students FMT UoD in the winter semester of the academic year 2015/2016. Lectures were provided in a high capacity lecture hall for all students at the same time. Lectures focused on each of the three main parts of the subject were realized by appropriate vocational specialist. Laboratory exercises were provided for the groups of maximum 20 students. The most of students worked on their own notebooks during the laboratory exercises focused on programming. They respected the recommendation of the lecturer to use their own computers which they were familiarized with.

In the academic year 2015-2016 four members of CIS Department academic staff and two members of Department of Military Geography and Meteorology took part in the subject teaching. The teaching process was coordinated by the guarantor of the subject and no serious problems occurred.

Programming tasks were especially focused on the array data structure and statements of branching, switch and cycles. Students were practically acquainted with the basics of event programming on the web page. Examples of programming assignments were similar to them as published in [1] for the FMT UoD military students.

The stress were put on the fact that students should be fully familiarized with three basic control structures (sequence, branching and cycle) and their use in writing algorithms by JavaScript programming language.

Each assignment was step by step analysed and programmed. Finally, the students were asked to prepare a simple protocol in MS Word. The protocol had always four parts:

- Assignment;
- HTML file content;
- JavaScript file content;
- Documentation from program run preferably in more than one web browser.

The concrete example of that is shown in Fig. 1, Fig. 2, Fig. 3, Fig. 4 and Fig. 5.

> Put random data into two vectors named Alex and Ben which have 5 elements with indexes 0 to 4. Vectors have to contain whole numbers from the interval <1;7>. Realize the button on the webpage and assign a user defined function to it. This function will calculate the scalar product and the result will be displayed by alert window.

FIG. 1. Text of assignment

```
<html>
  <head>
     <title>Programming in JavaScript</title>
  </head>
  <body>
     <h1>Assignment 13: Work with Arrays</h1>
     <p>Scalar product of vectors:</p>
     <button id="btnScalProd">Calculate scalar product</button>
     <br>
     <script src="script13.js"></script>
  </body>
</html>
```

FIG. 2. Content of HTML file

```
var Alex=[], Ben=[], i;

btnScalProd.onclick = function() {
var spv=Alex[0]*Ben[0];;
for (i=1; i<5; i++) {
spv=spv+Alex[i]*Ben[i];
}
alert("Scalar product of vectors Alex and Ben: "+spv);
};

document.write("<br>Content of vector Alex:<br>");
for (i=0; i<5; i++) {
Alex[i] = Math.floor(Math.random() *7)+1;
document.write("vector component with the index "+i+": "+Alex[i]+"<br>");
}
document.write("<br>Content of vector Ben:<br>");
for (i=0; i<5; i++) {
Ben[i] = Math.floor(Math.random() *7)+1;
document.write("vector component with the index "+i+": "+Ben[i]+"<br>");
}
```

FIG. 3. Content of script file

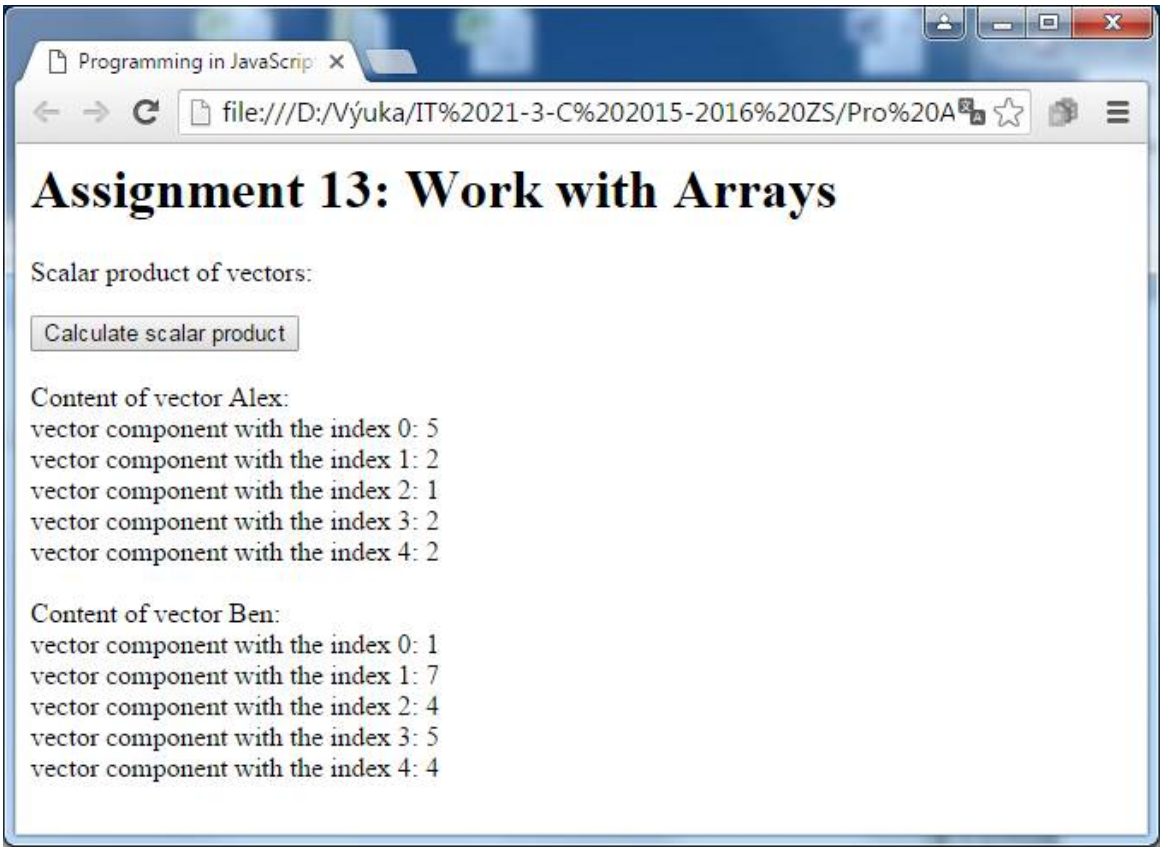

FIG. 4. Screenshot (a) (b) - script run in Google Chrome environment

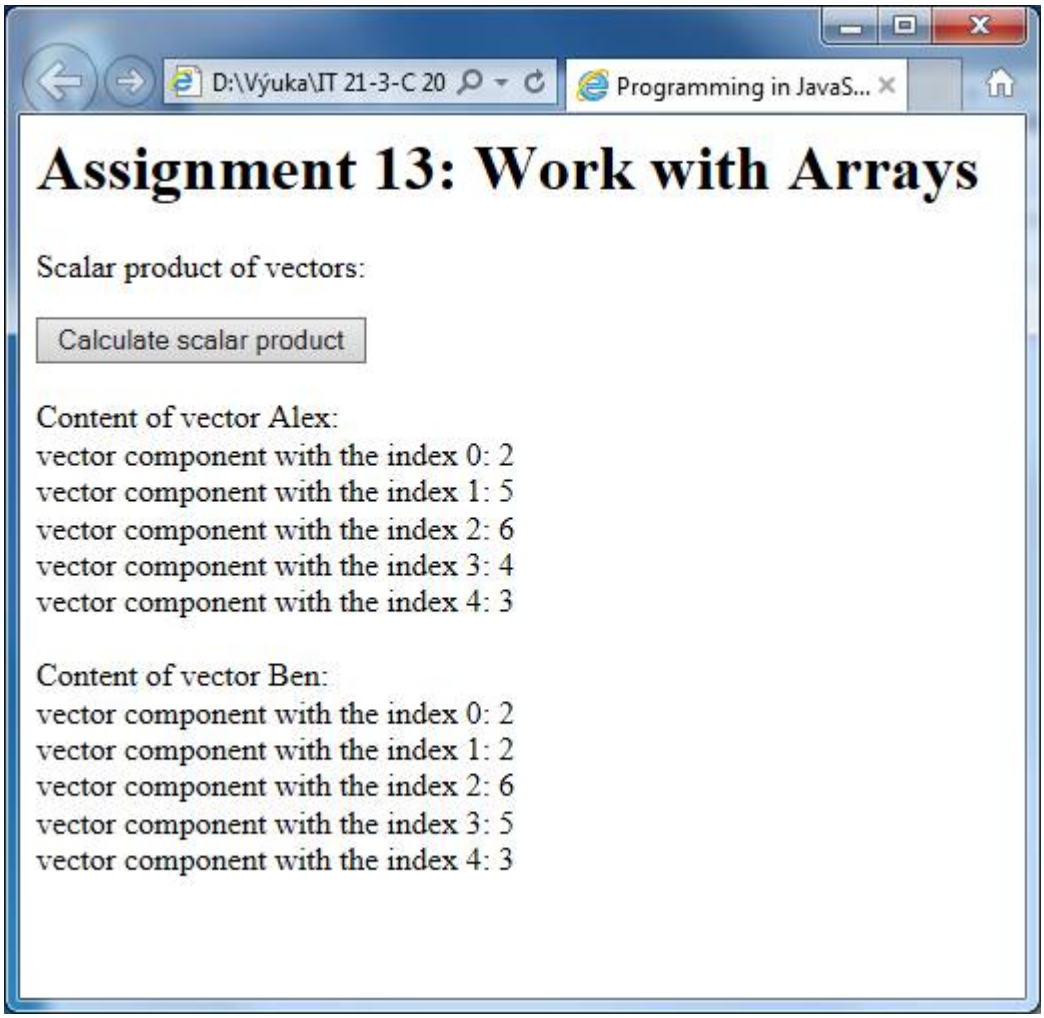

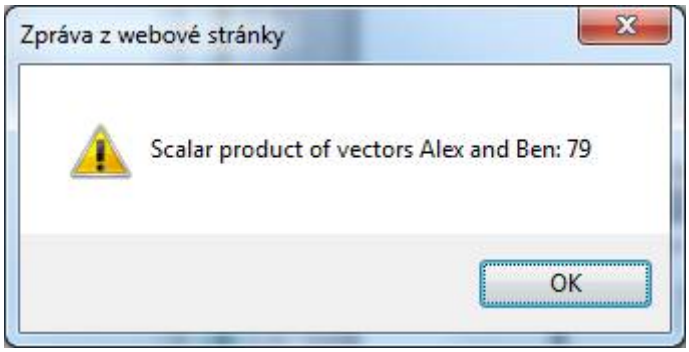

FIG. 5. Screenshot (a) (b) script run in Microsoft Internet Explorer 11 environment

Many good information sources connected with JavaScript programming language can be found at the Internet [4, 5, 6]. Teachers and students can access them according to their needs.

5. SUBJECT EXAMS

In the winter semester of the academic year 2015/2016 the students' knowledge and skills gained were for the first time tested. The author of the article had to test 37 students. Keeping in mind that students had to pass other 4 subject exams (Mathematics I,

Physics I, Basic of Electrical Engineering, Basics of Mechanical Engineering), final semester exam was done with respect to the following rules.

Firstly, the students had to pass the written test from the part 2 and the written test from the part 3 of the subject, that is from "Computer Networks" and from the "Geography". This written tests were done during the semester independently. Then, the final subject exam was only focused on "Programming" part of the subject.

The final exam from the "Programming" had written part and oral part. During the written part students answered ten questions focused on programming terminology, connections among terms and explaining small parts of code in JavaScript language. The oral part contained discussion on written part and additional questions to students programming assignment, which was done at home and sent to the examiner before. Students solved three programming assignments at home which had to respect three groups of topic.

Finally, the students required grades according to the result of their written test from "Computer Networks" part and the result of their exam from "Programming" part.

6. GAINED EXPERIENCE

6.1 Target group input characteristics. Let's have data sample of 30 students from the total number of 31 students who started the study field "Weapons and Ammunition". Input questionnaire survey of the author has given important information for the teaching and learning process.

Almost all students finished high-quality and suitable secondary schools: 4 students passed their leaving examination at eight-year long grammar schools and 11 students passed leaving examination at four-year long grammar schools, 12 students at secondary technical schools, 1 student at the Police Academy, 1 student at an economic Lyceum and 1 student at an art school.

Total number of 7 students gained some experience in studies at other universities, 6 students tried to study at the other university but they stopped their study, 1 student graduated from the Faculty of Economics of another technical university.

There was no student in the sample without his/her own PC or notebook.

There were 16 students who gained some experience in programming before their studies at the FMT UoD but only 4 of them felt some basic knowledge from that times.

6.2 Subject exam results. The number of students who passed the final subject exam during the examination period was 18. At the end of the examination period 9 students from these 18 students had 100 % of credits and 9 students from these 18 students had 67 % to 87 % credits and they can continue their studies conditionally; they must pass all missing exams during the first 4 weeks of the summer semester. It is interesting that all these students passed the exam from the subject of "Information Technology".

The number of students who had to stop their studies at the FMT UoD is 13 students. They got only 13 % to 50 % of credits but the minimum limit was 60 % of credits. It is interesting that no one from these unsuccessful students tried to pass the exam from the subject of "Information Technology".

The author assume that step by step fulfilment of assignment by students during the semester brought a very positive effect on the exams from the subject of "Information Technology".

6.3 Interpretation of the results from the author's point of view. According to target group input characteristics and final exams results it is possible to formulate gained

experience as follows. The most suitable secondary schools for the successful studies at the FMT UoD are eight-year long grammar schools, high-quality four-year long grammar schools and high-quality technically oriented secondary schools. The failure in studies at another university can often be a prerequisite for the failure at the FMT UoD. Programming experience gained before entering the FMT UoD is useful even though the most of the students with this experience feel a low effect for their current knowledge. Computer ownership can be recognized as a current study standard. The key prerequisites for the successful studies are motivation and personal qualities.

CONCLUSIONS

Contemporary gained experience lead to possible next development of the subject "Information Technology". The subject requires significantly different demands due to the previous knowledge and skills of students. The teacher should meet the input characteristics of the target group.

Inclusion of the subject of "Information Technology" in the education of all FMT UoD civilian students in the 1st semester of their studies is the optimal time. Algorithmic thinking of the technical fields students should be formed as soon as possible.

It will be suitable to discuss the experience gained during the first semester of implementation and maybe to slightly modify the second part of the subject content, that is the content of "Computer Networks". This part of the subject seemed to be extremely difficult for the students.

The current number of a maximum of 20 students in the laboratory seems to be acceptable. If possible, students should use their own notebooks.

Oral exams are very important. Discussion with the students is irreplaceable. Written exams do not give complete feedback. Group programming assignment before exams is useful. It enables programming skills exchange among the students.

AKNOWLEDGMENT

The paper was supported by the partial development plan for the organization Faculty of Military Technology, University of Defence, Brno, Czech Republic.

REFERENCES

[1] M. Hrubý, *Subject Information Technology in Military Education*, in AFASES 2015, Brasov, Romania, May 28-30, 2015;

[2] *** MathWorks. *MATLAB*. Available at http://www.mathworks.com/products/matlab/?requestedDomain=www.mathworks.com, accessed on 31 March 2015;

[3] *** MathWorks. *SIMULINK*. Available at http://www.mathworks.com/products/simulink/, accessed on 31 March 2015;

[4] M. Haverbeke, *Eloquent JavaScript: A Modern Introduction to Programming*. Available at http://eloquentjavascript.net/, accessed on 31 March 2015;

[5] *** w3schools.com. *JavaScript Tutorial*. Available at http://www.w3schools.com/js/default.asp, accessed on 31 March 2015;

[6] M. Moncur,. *Sams Teach Yourself JavaScript in 24 Hours*. Pearson Education, Informit. Available at http://www.informit.com/library/library.aspx?b=STY_JavaScript_24_hours, accessed on 31 March 2015.

SOME RESULTS ACCORDING THE INTERLACING THE ZEROS OF A FUNCTION

Ana-Maria LUCA (RÎTEA), Florența Violeta TRIPŞA

*"Transilvania" University, Braşov, Romania (ana_ritea_maria@yahoo.com, florentatripsa@yahoo.com)

DOI: 10.19062/2247-3173.2016.18.1.64

Abstract: *The goal of this article is to present some results concerning Markov interlacing property of zeros for some kind of polynomials. We first present an equivalent lemma referring to T-systems from Borislav Bojanov's point of view and some extensions to more general classes of functions studied by Losko Milev and Nikola Naidenov. As a corollary we obtain that Markov's lemma holds true also in the case of logarithmic polynomials* $\sum_{k=0}^{n} a_k ln^k x$.

Keywords: *Chebyshev approximation, sum product algorithm*
MSC2010: *08A40, 41A50, 26C10, 35C11*

1. INTRODUCTION

During his research, the professor Borislav Bojanov was preoccupied to study and to bring new results referring Markov's lemma. He established an equivalent lemma concerning Chebyshev-systems in [1].

First of all, we give the definition of Chebyshev-systems.

Definition 1 [1] *Let* $\bar{\varphi} := \{\varphi_1(x), \varphi_2(x), \dots, \varphi_n(x)\}$ *be an arbitrary system of continuous functions on the interval* $[a, b]$. *The system* $\bar{\varphi}$ *is a* ***Chebyshev-system*** *(or briefly* ***T-system****) on* $[a, b]$, *if*

$$det \begin{bmatrix} \varphi_1(t_1) & \cdots & \varphi_n(t_1) \\ \vdots & \ddots & \vdots \\ \varphi_1(t_n) & \cdots & \varphi_n(t_n) \end{bmatrix} \neq 0 \quad (1)$$

for each $t = (t_1, t_2, \dots, t_n)$ *such that* $a \leq t_1 < t_2 < \dots, < t_n \leq b$. *Assume in addition, that the functions* $\{\varphi_1(x), \varphi_2(x), \dots, \varphi_{n-1}(x)\}$ *also constitute a T-system on* $[a, b]$.

We shall now consider the algebraic polynomials of degree at least equal to n.

Lemma of Markov [5] *Let* $p(x) = (x - x_1) \dots (x - x_n)$ *and* $q(x) = (x - y_1) \dots (x - y_n)$ *two polynomials that have the zeros* $x_1 < \dots < x_n$, *respectively,* $y_1 < \dots < y_n$ *that satisfy the interlacing conditions*

$$x_1 \leq y_1 \leq x_2 \leq y_2 \leq \dots \leq x_n \leq y_n \quad (2)$$

Then the zeros $t_1 \leq t_2 \leq \dots \leq t_{n-1}$ *of* $p'(x)$ *and the zeros* $\tau_1 \leq \tau_2 \leq \dots \leq \tau_{n-1}$ *of* $q'(x)$ *are interlacing too, i.e.*

$$t_1 \leq \tau_1 \leq t_2 \leq \tau_2 \leq \dots \leq t_{n-1} \leq \tau_{n-1} \quad (3)$$

Moreover, if $x_1 < \dots < x_n$ *and at least one of the inequalities* $x_i \leq y_i, i = 1, \dots, n$ *is strict, then all inequalities in* (3) *are strict.*

Remark 1. The lemma of Markov is called also ***Markov interlacing property***.

2. EQUIVALENT RESULTS

In the paper [5], Lozko Milev and Nikola Naidenov formulated a condition (denoted by (**P**)), such that if a T-system satisfies (**P**), then there occurs Markov's lemma:

We consider now, $\{u_0, u_1, \dots, u_n\}$ be a T-system on $\mathbb{R}$, with $u_i \in C^n(\mathbb{R})$, for $i = 0,1,\dots,n$, and every non-zero of polynomial $u = \sum_{i=1}^{n} a_i u_1$, where $(a_0, a_1, \dots, a_n) \in \mathbb{R}^{n+1}$ have at most n real zeros. We establish

$U_n := span\{u_0, u_1, \dots, u_n\}$,

and

$X = \{(x_1, x_2, \dots, x_n) \in \mathbb{R}^n : x_1 < \cdots < x_n$

Being $\bar{x} \in X$ a given point, we define

$$f(\bar{x}, t) := \begin{bmatrix} u_0(t) & \dots & u_n(t) \\ u_0(x_1) & \dots & u_n(x_1) \\ \vdots & \ddots & \vdots \\ u_0(x_n) & \dots & u_n(x_n) \end{bmatrix}. \quad (4)$$

Obviously, $f(\bar{x}, t)$ is a polynomial from U_n, which has zeros $x_1, x_2, \dots, x_n$. Note that if $g \in U_n$ is any other polynomial having the same zeros, then there exists a constant C such that $g(t) = Cf(\bar{x}, t)$. In general, we shall say that $f \in U_n$ is an *oscillating polynomial* if it has n distinct real zeros.

Applying Rolle's theorem to a polynomial $f(\bar{x}, t) \in U_n$, we observe that $f'(\bar{x}, t)$ admits at least one zero in each of the intervals $(x_i, x_{i+1}), i = 1, 2, \dots, n-1$. We shall suppose that the system U_n has the following property (**P**):

(**P**) *There exist numbers* δ_0 *and* δ_n *in* $\{0, 1\}$ *such that for every* $\bar{x} = (x_1, x_2, \dots, x_n) \in X, f'(\bar{x}, t)$ *admit exactly:*

- δ_0 *zeros in* $(-\infty, x_1)$;
- *one zero in each of the interval* $(x_i, x_{i+1}), i = 1, 2, \dots, n-1$;
- δ_n *zeros in* $(x_n, +\infty)$.

In the following, we introduce the set of index $J(U_n) \subset \{0, 1, \dots, n\}$, which corresponds to the zeros of $f'(\bar{x}, t)$. The definition of (U_n) is as follows: *the set* $\{1, \dots, n-1\}$ *is contained in* $J(U_n)$ *and if* $\delta_i = 1$ *for some* $i \in \{o, n\}$ *then* $i \in J(U_n)$.

For the results that will be presented, we need to introduce the following theorem, which relates to the T-general systems which have the property (**P**).

Theorem 1 [5] *Assume that* $U_n := span\{u_0, u_1, \dots, u_n\}$ *is a T-system on the real line, which satisfy the property (**P**). Let* $\bar{x} = (x_1, x_2, \dots, x_n)$ *and* $\bar{y} = (y_1, y_2, \dots, y_n)$ *be two arrays from* X*, that are interlacing, in the following order*

$$x_1 \le y_1 \le x_2 \le y_2 \le \cdots \le x_n \le y_n \quad (2)$$

Then the zeros $\{t_i\}_{i \in J(U_n)}$ *of* $f'(\bar{x}, t)$ *and the zeros* $\{\tau_i\}_{i \in J(U_n)}$ *of* $f'(\bar{y}, t)$ *are interlacing in the same order:*

$$t_m \le \tau_m \le t_{m+1} \le \tau_{m+1} \le \cdots \le t_M \le \tau_M, \quad (5)$$

where $m := min J(U_n), M := max J(U_n)$. *Even more, if* $\bar{x} \neq \bar{y}$, *then all the inequalities from* (5) *are strict.*

Lemma 1 [5] *Let* $\{u_0, u_1, \dots, u_n\}$ *be a T-system on* $\mathbb{R}$ *and let* f *and* g *be two oscillating polynomials from* $U_n := span\{u_0, u_1, \dots, u_n\}$ *with the zeros* $\bar{x} \in X$ *and respectively,* $\bar{y} \in X$. *If* $\bar{x}$ *and* $\bar{y}$ *are interlacing and* $\bar{x} \neq \bar{y}$, *then* $f^{|}$ *and* $g^{|}$ *cannot have any common zero.*

Lemma 2 [1] *Every zero* η *of the derivative of an algebraic polynomial* $p(x) = (x - x_1)...(x - x_n)$ *is an increasing function* x_k *from the domain* $x_1 < \cdots < x_n$.

3. MARKOV'S INTERLACING PROPERTY APPLIED ON OTHER TYPE OF POLYNOMIALS AND MAIN RESULTS

One of the natural objectives of mathematicians is to extend the Markov interlacing property on several general classes of functions. In researches that have been performed recently, Lozko Milev and Nikola Naidenov have established that Markov interlacing property of zeros occurs also in the case of exponential polynomials of the form $\sum_{i=0}^{n} b_i e^{\alpha_i x}$ and in the case of linear combinations of the Gaussian kernels (normal) $\sum_{i=0}^{n} b_i e^{-(x-\beta_i)^2}$ in the paper [5]. Other authors have demonstrated that Markov's lemma is maintained also in the case of orthogonal polynomial functions, trigonometric polynomial functions, etc.

We consider now the real numbers $\alpha_0 < \alpha_1 < \cdots < \alpha_n$ and we define

$$V_n(\bar{\alpha}) := span\{e^{\alpha_0 x}, e^{\alpha_1 x}, \dots, e^{\alpha_n x}\}. \quad (6)$$

It is known the fact that $V_n(\bar{\alpha})$ is a T-system on $(-\infty, +\infty)$. Let

$$J(\bar{\alpha}) := \begin{cases} \{0, 1, \dots, n-1\}, \alpha_0 > 0; \\ \{1, 2, \dots, n\}, \alpha_n < 0; \\ \{1, 2, \dots, n-1\}, \alpha_0 \le 0 \le \alpha_n. \end{cases} \quad (7)$$

In the following theorem, we establish the Markov's interlacing property for the system $V_n(\bar{\alpha})$.

Theorem 2 [5] *Let* f *and* g *be two oscillating polynomials from* $V_n(\bar{\alpha})$ *that admit the zeros* $\bar{x} \in X$ *and* $\bar{y} \in X$, *respectively satisfy the inequalities* (2). *Then the zeros* $\{t_i\}_{i \in J(\bar{\alpha})}$ *of* $f^{\cdot}$ *and zeros* $\{\tau_i\}_{i \in J(\bar{\alpha})}$ *of* $g^{\cdot}$ *are interlacing in the same order:*

$$t_i \le \tau_i \le t_{i+1} \le \tau_{i+1}, \text{ for } i, i+1 \in J(\bar{\alpha}). \quad (8)$$

More, if $\bar{x} \ne \bar{y}$, *then inequalities from* (8) *are strict.*

In addition, if $\alpha_0 < \alpha_1 < \cdots < \alpha_n < 0$ *then for every natural number* k, *the zeros* $\left\{t_i^{(k)}\right\}_{i=1}^{n}$ *of* $f^{(k)}$ *and zeros* $\left\{\tau_i^{(k)}\right\}_{i=1}^{n}$ *of* $g^{(k)}$ *are interlacing also:*

$$t_1^{(k)} \le \tau_1^{(k)} \le t_2^{(k)} \le \tau_2^{(k)} \le \cdots \le t_n^{(k)} \le \tau_n^{(k)}.$$

A similar enunciation is true also for $0 < \alpha_0 < \alpha_1 < \cdots < \alpha_n$.

Proof.

Consult [5] p. 674.

Remark 2. We will omit the proofs of the presented theory, they can be consulted in referred papers of each theorem/lemma/corollary.

Milev Lozko with Nikola Naidenov described the interlacing property of zeros for linear combinations of Gaussian kernels, in the following corollary:

Corollary 1 [5] *Let* f *and* g *be two oscillating polynomials of the form* $\sum_{i=0}^{n} b_i e^{-(x-\beta_i)^2}$, $(\beta_0 < \cdots < \beta_n)$ *which admit the zeros* $\bar{x}$, *respectively* $\bar{y}$. *We consider that* $\bar{x}$ *and* $\bar{y}$ *are interlacing in the order of relation (1). Then the zeros* $\{t_i\}_{i=0}^{n}$ *of* $f^{\cdot}$ *and the zeros* $\{\tau_i\}_{i=0}^{n}$ *of* $g^{\cdot}$ *are interlacing in the same order. More, if* $\bar{x} \ne \bar{y}$, *then the interlacing is strict.*

Proof.

Consult [5] p. 676.

The author aims is to show that the Markov's interlacing property of zeros takes place in the case of logarithmic polynomials, by the following corollary:

Corollary 2 *Let f and g be two logarithmic polynomials of the form $\sum_{k=0}^{n} a_k \ln^k x$ that admit the zeros $\bar{x} = (x_1, \dots, x_n)$, respectively $\bar{y} = (y_1, \dots, y_n)$. We assume that $\bar{x}$ and $\bar{y}$ are interlacing in the order of relation (2). Then the zeros $\{t_i\}_{i=0}^{n}$ of f' and the zeros $\{\tau_i\}_{i=0}^{n}$ of g' are interlacing in the same order. Even more, if $\bar{x} \neq \bar{y}$, then the interlacing is strict.*

Proof.

First, we need to emphasize that the polynomial logarithmic with the form $\sum_{k=0}^{n} a_k \ln^k x$ is equivalent with the polynomial $\prod_{k=1}^{n}(\ln x - x_k)$. Therefore, since this is a product composed of increasing factors with functions (regardless of the actual values of x_k), we obtain a polynomial function admitting n real solutions, like:

✓ t

o the function $f:(0;+\infty)\to\mathbb{R}, f(x)=\prod_{k=1}^{n}(\ln x - x_k)$, if we attach the equation $f(x)=0$, we will have

$$(\ln x - x_1)(\ln x - x_2)\dots(\ln x - x_n) = 0 \Rightarrow \begin{cases} (\ln x - x_1) = 0 \\ (\ln x - x_2) = 0 \\ \dots \\ (\ln x - x_n) = 0 \end{cases} \Rightarrow \tag{9}$$

$$\Rightarrow \begin{cases} \ln x = \ln e^{x_1} \\ \ln x = \ln e^{x_2} \\ \dots \\ \ln x = \ln e^{x_n} \\ \text{fc. ln is injective} \end{cases} \Rightarrow \bar{x} = (e^{x_1}, e^{x_2}, \dots, e^{x_n})$$

therefore the polynomial solutions of f are of the form $\bar{x} = (e^{x_1}, e^{x_2}, \dots, e^{x_n})$, and those of g are of the form $\bar{y} = (e^{y_1}, e^{y_2}, \dots, e^{y_n})$. We insist to underline that these solutions are unique, that is resulting from the fact that this logarithmic function is injective over the entire domain of definition. Here, we shall attach the graph of the function $f:(0;+\infty)\to\mathbb{R}, f(x)=\prod_{k=1}^{n}(\ln x - x_k)$, to outline the idea that Lemma 2 is carried also in the present case (by changing the variable $x \longrightarrow \ln x$), i.e. algebraic solutions $\bar{x}$ and $\bar{y}$ of polynomials f, respectively g are increasing functions from the domain $x_1 < \dots < x_n$.

$$f(x) = \prod_{k=1}^{n}(\ln x - x_k) \tag{10}$$

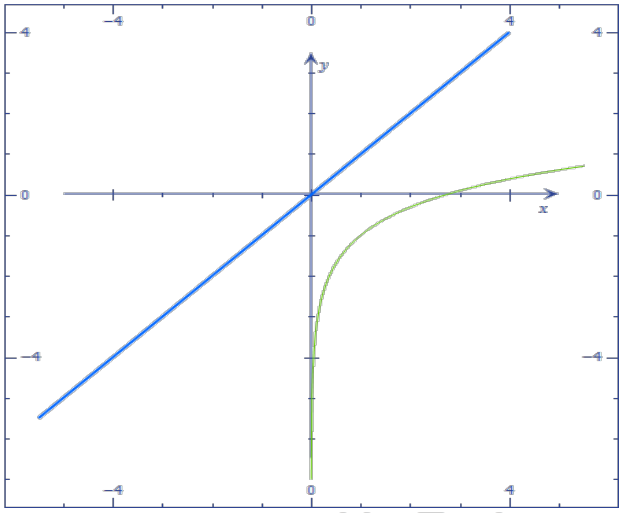

FIG. 1. The graph of function $f(x)=\prod_{k=1}^{n}(\ln x-x_k)$

We now consider, $\{a_0\ln^0 x, a_1\ln^1 x, a_2\ln^2 x, \dots, a_n\ln^n x\}$ a T-system on $\mathbb{R}$, with $\ln^i x \in C^n(\mathbb{R})$, for $i=0,1,\dots,n$, and every non-zero of polynomial $\sum_{i=0}^{n} a_i \ln^i x$, where $(a_0,a_1,\dots,a_n)\in\mathbb{R}^{n+1}$ it has at most n real zeros. We set

$$U_n := span\{a_0\ln^0 x, a_1\ln^1 x, a_2\ln^2 x, \dots, a_n\ln^n x\} \tag{11}$$

and

$$X=\{(e^{x_1},e^{x_2},\dots,e^{x_n})\in\mathbb{R}^n: e^{x_1}<e^{x_2}<\dots<e^{x_n};\ x_1<\dots<x_n\}. \tag{12}$$

Given a point $\bar{x}\in X$, we define

$$f(\bar{x},t) := \begin{bmatrix} \ln^0(t) & \dots & \ln^n(t) \\ \ln^0(e^{x_1}) & \dots & \ln^n(e^{x_1}) \\ \vdots & \ddots & \vdots \\ \ln^0(e^{x_n}) & \dots & \ln^n(e^{x_n}) \end{bmatrix}. \tag{13}$$

Evidently, $f(\bar{x},t)$ is a polynomial from U_n, which has the zeros $e^{x_1},e^{x_2},\dots,e^{x_n}$. We emphasize that if $g\in U_n$ is another logarithmic polynomial that has the zeroes $\bar{y}=(e^{y_1},e^{y_2},\dots,e^{y_n})$. We have then $f\in U_n$ and $g\in U_n$ being two oscillating polynomials that have n real distinct zeros.

Applying Rolle's theorem to the polynomial $f(\bar{x},t)\in U_n$, with

$$f(x)=\sum_{k=0}^{n} a_k\ln^k x \Leftrightarrow f(x)=\prod_{k=1}^{n}(\ln x-x_k)\Rightarrow$$

$$\Rightarrow f'(x)=\frac{1}{x}a_1+\frac{2}{x}a_2\ln x+\frac{3}{x}a_3\ln^2 x+\dots+\frac{n}{x}a_n\ln^{n-1}x \Leftrightarrow f'(x)=$$

$$=\frac{1}{x}(\ln x-x_2)(\ln x-x_3)\dots(\ln x-x_n)$$
$$+\frac{1}{x}(\ln x-x_1)(\ln x-x_3)\dots(\ln x-x_n)+\dots$$
$$+\frac{1}{x}(\ln x-x_1)(\ln x-x_2)\dots(\ln x-x_{n-2})(\ln x-x_n)$$
$$+\frac{1}{x}(\ln x-x_1)(\ln x-x_2)\dots(\ln x-x_{n-2})(\ln x-x_{n-1})\Rightarrow$$

$$\Rightarrow f'(x)=\frac{1}{x}\sum_{k=1}^{n} a_k \ln^{k-1} x \Leftrightarrow f'(x)=$$
$$=\frac{1}{x}[(\ln x-x_2)(\ln x-x_3)\dots(\ln x-x_n)$$
$$+(\ln x-x_1)(\ln x-x_3)\dots(\ln x-x_n)+\cdots$$
$$+(\ln x-x_1)(\ln x-x_2)\dots(\ln x-x_{n-2})(\ln x-x_n)$$
$$+(\ln x-x_1)(\ln x-x_2)\dots(\ln x-x_{n-2})(\ln x-x_{n-1})]$$

where $\frac{1}{x}\neq 0, \forall x\in(0,+\infty)$.

We can observe that the derivative $f'(\bar{x},t)$ is another logarithmic polynomial function of degree $n-1$, which admits at least one zero in each of the intervals (x_i,x_{i+1}), $i=1,2,\dots,n-1$, on the form $e^{t_1},e^{t_2},\dots,e^{t_n}$, respectively $g'(\bar{y},t)$ admits at least one zero in each of the intervals $(y_i,y_{i+1}), i=1,2,\dots,n-1$, on the form $e^{\tau_1},e^{\tau_2},\dots,e^{\tau_n}$; and the system U_n admits the property (**P**), therefore by theorem 1, it happens the interlacing of the zeros of $f'(\bar{x},t)$ and $g'(\bar{y},t)$ like this

$$e^{t_1}\leq e^{\tau_1}\leq e^{t_2}\leq e^{\tau_2}\leq\cdots\leq e^{t_n}\leq e^{\tau_n}. \quad (14)$$

We must point out that, according to Lemma 1, f' and g' do not have any common zero.

We want now to justify the strictly intercalation, as follows: because $\bar{x}\neq\bar{y}$, thanks to the exponential function to be strictly monotone, respectively injective; it follows therefore that the interlacing is strict

$$e^{t_1}<e^{\tau_1}<e^{t_2}<e^{\tau_2}<\cdots<e^{t_n}<e^{\tau_n} \quad (15)$$

which finish the proof of the corollary.

Corollary 3 *Let f and g be two logarithmic polynomials of the form $\sum_{k=0}^{n} a_k \ln^k x$ that admit the zeros $\bar{x}=(x_1,\dots,x_n)$, respectively $\bar{y}=(y_1,\dots,y_n)$. We assume that $\bar{x}$ and $\bar{y}$ are interlacing in the order of relation (1). Then the zeros $\{t_i\}_{i=0}^{n}$ of derivative of order (k) of f, noted by $f^{(k)}$ and the zeros $\{\tau_i\}_{i=0}^{n}$ of derivative of order (k) of g, noted by $g^{(k)}$ are interlacing in the same order. Even more, if $\bar{x}\neq\bar{y}$, then the interlacing is strict.*

Proof.

The proof can be done by induction, with the particular case $k=1$ demonstrated in corollary 2. (with $k=1$ we discuss about the first derivative of the polynomials f and g, i.e. f' respectively g').

CONCLUSIONS

The studies of Borislav Bojanov referring the lemma of Markov, have applications in algebra, approximation theory, statistics, etc. The author aims to expand the two corollaries presented aforesaid, in the probability theory. Maybe it can be find a connection with statistical distributions, like the logarithmic – exponential distribution.

REFERENCES

[1] B. Bojanov, Markov Interlacing Property for Perfect Splines, *Journal of Approximation Theory*, no. 100, pp. 183-201, 1999;

[2] P. Borwein, A. T. Erdely, J. Zhang, Muntz systems and orthogonal Muntz-Legendre polynomials, *Transactions of the American Mathematical Society*, vol. 342, april 1994;

[3] I. Georgieva, C. Hofreither, G. Nikonov, R. Uluchev, Interpolation of mixed type data by bivariate polynomials, *Constructive Theory of functions: in memory of Borislav Bojanov (2010)*, Sozopol, pp. 69-79, prof. Marin Drinov Academic Publishing House, Sofia,, 2012;

[4] O. Kounchev, Multidimensional Chebyshev Systems (Haar systems), *Functional Analysis and Applications, available at http://arxiv.org/abs/0808.2213v2*, 2011;

[5] L. Milev, N. Naidenov, Markov interlacing property for exponential polynomials, *Journal of Mathematical Analysis and Applications*, no. 367, pp. 669-676, 2010.

APPLIED MATHEMATICS, COMPUTER SCIENCE, IT&C

OPTIMAL CONTROL IN STABILIZING THE DYNAMICS OF SHIPS AND MULTI-PROPELLED MISSILES

Dedicated to math Gheorghe Radu, PhD, on his 65-th anniversary

Mircea LUPU[*], Gheorghe RADU[**], Cristian-George CONSTANTINESCU[**]

[*]"Transilvania" University Braşov (m.lupu@unitbv.ro), [**]"Henri Coanda" Air Force Academy Brasov (gh.radu@gmail.com)

DOI: 10.19062/2247-3173.2016.18.1.65

Abstract: *This paper deals with automatic stabilization of rockets, submarines or satellites dynamics. This stabilization is based on relay-type automatic regulators, by using the minimal time criterion for optimal control with the Pontreagiune extremal principle. In this study, the state variables are the rotation angles and the control function has 2 components, which are appearing because of lateral rolling perturbations. Finaly, numeric-analytical studies are approached, and the results are graphically presented.*

Key words: *optimal control, control function, extreme principle of Pontreaguine, absolute stability.*

MSC2010: *34H05, 49K35, 93C15, 93C73, 93D10.*

1. INTRODUCTION

The goal of an optimal control problem (O.C.P.) of a dynamic system is to determine a set of state variables, of certain control and driving functions satisfying an optimization criterion, performing the extremization of a quality index in this way. This performance index is a functional depending on these elements and time and spatial restrictions.. Practical applications requirements for these functionals are optimal controls of the following type: achievement of minimal time, minimum fuel consumption, energy, to achieve extreme performance [4,10,13]. Dynamical systems from different domains are generally represented generally by nonlinear equations with parameters, while internal or external disturbances occur leading to unstable solutions related to a free balance state. The stabilization of these regimes is done by using automatic controls that actually fast reacts for optimal control and routing [3, 5-7, 12, 14]. Lurie [8], [4], [13] and Popov [11], [4], [3] methods are known to automatically adjust the absolute stabilization, with applications. This paper, for optimal control of stabilizing angular velocities of aircraft and missiles, deals with the "Minimum Time Criteria" and the Pontreaguine extremal [9], [1], [7], with results and studies in different applications [5], [6], [7]. The optimal control function will have 2 components: $u(u_1, u_2)$.

2. OPTIMAL CONTROL IN ANGULAR SPEED STABILIZATION REGARDING FLUVIAL OR SPATIAL NAVES

We will consider a multi-propelled nave with axial-cylinder symmetry, as in figure 1. We choose a system of axes ($Ox_1x_2x_3$) as principal axes of inertia, where O is the masses, as a solid body rigidly fixed in point O. The nave rotate with the angular velocity

$\overline{\omega}(\omega_1, \omega_2, \omega_3)$, where ω_i are the rotation speeds around the axes Ox_i, $i = \overline{1,3}$; Ox_3 is the axis of longitudinal symmetry.

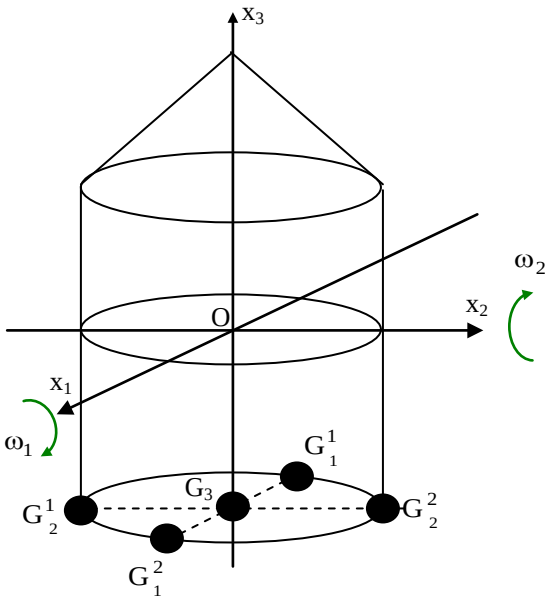

FIG. 1: A multi-propelled nave

Symmetrical with these axes the ship has turbojet propulsion generators $G_1(G_1^1, G_1^2)$ on Ox_1 with two nozzles, $G_2(G_2^1, G_2^2)$ on Ox_2 and generator G_3 on Ox_3, with traction purpose. These reactive nozzles can create moments, being accompanied by gas dynamics wings, integrating gyroscopes, small jet shutters that can help to guide and stabilize the angular velocities regime. The controller [3], [5-7] is equipped with sensors and microprocessors for data processing and it may (with a rapid response) control the disrupted regime for optimal stabilization [12], [14]. Disturbances considered here may be due to turbines fuel, meteo external agents or environmental density. These naves may be rockets, spacecraft, capsule, modules, mega-drones or submarines, torpedoes, etc [8], [12], [14].

The angular velocities are $\omega_1 = x_1(t)$, $\omega_2 = x_2(t)$, $\omega_3 = x_3(t)$, the inertia momentums of the body are I_1, I_2, I_3 - symmetrically $(I_1 = I_2 = I)$, see figure 1.

We write the equations of angular velocities disturbed by external moments $M_i(t)$ [10], [12], [14]:

$$\begin{cases} I_1\dot{x}_1 = (I_2 - I_3)x_2x_3 + M_1(t) \\ I_2\dot{x}_2 = (I_3 - I_1)x_1x_3 + M_2(t) \\ I_3\dot{x}_3 = (I_1 - I_2)x_1x_2 + M_3(t) \end{cases} \quad (1)$$

We suppose that moments $M_i(t)$ are caused by propelling forces $G(g_1, g_2, g_3)$:

$$h_1 = l \cdot g_1(t),\ h_2 = l \cdot g_2(t),\ h_3 = h \cdot g_3(t) \quad (2)$$

Taking into consideration the symmetry: $I_1 = I_2 := I$, we have:

$$\begin{cases} \dot{x}_1 = \dfrac{I - I_3}{I} x_2x_3 + \dfrac{l}{I} g_1(t) \\ \dot{x}_2 = -\dfrac{I - I_2}{I} x_3x_1 + \dfrac{l}{I}\ g_1(t) \\ \dot{x}_3 = \dfrac{h}{I_3} g_3(t) \end{cases} \quad (3)$$

System (1) with $M_i(t) = 0$ is in stable equilibrium around $O(0,0,0)$ (undisturbed).

Let's suppose that at $t_0 = 0$ we have the disturbed position

$$x_1(0) = \alpha_1,\ x_2(0) = \alpha_2,\ x_3(0) = \alpha_3 \quad (4)$$

If the traction $g_3(t)$ is known, than we have

$$x_3(t) = \alpha_3 + \int_0^t \frac{h}{I_3} g_3(\tau)d\tau \quad (5)$$

This shows that x_3 can be controlled independently of x_1 and x_2, but x_3 can influence in (3) variables x_1 and x_2. We suppose that the rapid reaction response time is short and x_3 may be considered constant $x_3 = \alpha_3$, so $g_3 \cong 0$. We also suppose that forces g_1, g_2 are bounded

$$|g_1(t)| \le L,\ |g_2(t)| \le L \tag{6}$$

In this case the system (3) is linearized and we introduce the control function $u(u_1(t), u_2(t))$ to control optimum stabilization of disturbed solution to O(x_1=0, x_2=0) for system (7) in minimal time.

$$\begin{cases} \dot{x}_1 = \omega x_2 + k u_1(t) \equiv f_1 \\ \dot{x}_2 = -\omega x_1 + k u_2(t) \equiv f_2 \end{cases} \tag{7}$$

where:

$$\begin{cases} \omega = \dfrac{I - I_3}{I}\alpha_3;\ \omega > 0 \\ k = \dfrac{l}{I}L; \qquad k > 0 \\ u_i(t) = \dfrac{g_i(t)}{L};\ \ i = 1,2 \end{cases} \tag{7'}$$

We note that state equations (7) in the phase space $(x_1 O x_2)$, $X(x_1(t); x_2(t))$, with control parameters $(u_1(t); u_2(t))$satisfy the conditions:

$$\begin{cases} -1 \le u_1(t) \le 1 \\ -1 \le u_2(t) \le 1 \end{cases};\qquad U := [-1,1] \tag{8}$$

and hence the allowable plan U (u_1Ou_2) is a compact square.

The technical sense in equations (7) for U_i (t) is to find forces $g_i(t) \leftrightarrow u_i(t)$ to reduce speeds $(x_1, x_2) \to (0,0)$ on optimal paths starting from $M_0(\alpha_1, \alpha_2)$ at time t_0 to reach the final target O(0, 0) at the time $t_f > t_0$ so the transfer time to be minimal (o.c.p.) [2], [3], [9], [7].

3. MINIMAL TIME CRITERION. EXTREMUM PRINCIPLE

Let's consider a system described by the state equations

$$\dot{x}_i = f_i(t, x(t), u(t)), t \in [t_0, t_1] \subseteq \mathbf{R}_+, i = \overline{1,n} \tag{9}$$

where the state function is $x(t) = (x_1, x_2, ..., x_n), x_i \in X \subset \mathbf{R}^n$ and the control function $u(t) = (u_1, u_2, ..., u_m) \subset U \subset \mathbf{R}^m$ with $m \le n$.

Functions f_i meet the regularity conditions and U is the allowable domain of parameters $u_i(t)$. System (9) respects the given initial conditions (I):

$$\text{(I)}\ x_i(t_0) = x_i^0 \in R, i = \overline{1,n} \tag{10}$$

determining the disturbed initial state $X^0 \in S^0$, where S^0 is the variety on which X^0 is fixed.

Assuming that Cauchy problem (9) (10) has $x_i = x_i(t, t_0, x^0, u), t \ge t_0$ as unique solution, we request that this trajectory transfer the system in the state $X^1 \in S^1$, where X^1 is fixed on S^1 (target (final) state - usually steady state in the final moment $t_1 = t_f$ horizon pool) - $t_0 \le t_1$:

$$\text{(F)}\ x_i(t_1) = x_i^1 \in R, i = \overline{1,n} \tag{11}$$

The final moment t_1 will be determined using "minimal time criterion" - rapid response $\min_{u\in U}(t_1 - t_0) = t^*$, extremizing the performance index J = J [u] [1], [2], [9].

Let's consider the index functional, see [1], [9], [10]:

$$J(u) = \int_{t_0}^{t_1} f_0(x, u, t)dt \tag{12}$$

where f_0 is a characteristic function (Lagrangean) with:

$$\dot{x}_0(t) \equiv f_0(t, x, u); x_0(t_0) = C_0 \tag{13}$$

The optimal control problem (P.C.O.) is to determine an optimal admissible command $u^* \in U$ to extremize (12) so that the original system (9) (10) (I) is transferred to the final system (11) (F) in minimal time (minimum criteria).

"Extreme Pontriaguine principle" (P.E.) will be calling to solve it. We auxiliary introduce the multipliers $\lambda(t) = (\lambda_0(t), \lambda_1(t), ..., \lambda_n(t))$ as non-null solution of the adjunct system [1] [9] [7] [10]:

$$\dot{\lambda}_i = -\sum_{j=0}^{n}\left(\frac{\partial f_j}{\partial x_i}\right)_0 \lambda_i \ ; \ \lambda_i(t_0) = c_i, i = \overline{1,n} \tag{14}$$

associated with (9)…(13) with arbitrary constants c_i (but not all of them arbitrary), which will finally become the controller parameters.

We note that (14), if it's linearized: $\dot{X} = AX + BU$ in the final null position (O) vicinity, $A = (a_{ij}) = \left(\frac{\partial f_i}{\partial x_j}\right)_0$ i.e. $\dot{\lambda} = -A'\lambda$, where $\dot{\lambda} = -A'\lambda$, A' is the transposed matrix.

We consider the lagrangean like f_0 and (12) :

$$L(t, x(t), u(t)) \equiv f_0(x, u, t) \equiv 1, \dot{x}_0 = f_0 \equiv 1 \tag{15}$$

$$J(u) = \int_{t_0}^{t_1} Ldt = t_1 - t_0 ; \min_u J(u) = J(u^*) = \min_u (t_1 - t_0) = t^* \tag{16}$$

We build the generalized Hamiltonian [9] [10] associated with (11) (12) (13) (14):

$$H(t, x(t), \lambda(t), u(t)) = \lambda_0 \dot{x}_0 + \sum_{i=1}^{n} \lambda_i \dot{x}_i \tag{17}$$

where $\dot{x}_0 = f_0 \equiv 1$, with $\dot{\lambda}_0 = \left(\frac{\partial f_0}{\partial x}\right)_0 \lambda \equiv 0, \lambda_0 \equiv C_0$

From (11) and (17) we have:

$$H \equiv \lambda_0 + \sum_{i=1}^{n} \lambda_i f_i(t, x, u) \tag{18}$$

and we built the canonic attached and adjunct system [1] [2] [7] [9]:

$$\dot{x}_i = \frac{\partial H}{\partial \lambda_i} \tag{19}$$

$$\dot{\lambda}_i = -\frac{\partial H}{\partial x_i}, i = \overline{1,n}, t \in [t_0, t_1] \tag{20}$$

with $u_i \in [-1,1]$ and initial conditions $x_i(t_0) = x_i^0$, $\lambda_i(t_0) = c_i$. This system is:

$$\dot{x}_i = f_i(t, x, u); \dot{\lambda}_i = -\lambda_i \sum_{j=1}^{n}\left(\frac{\partial f_j}{\partial x_i}\right)_0 \tag{21}$$

with 2n unknowns: x_i, λ_i and 2n conditions, where u* is previously and optimal chosen.
"Pontreaguine minimum principle" theorem ([1] [2] [9]): A necessary condition for the existence of an optimal solution $u^* \in U$ $(x_i \in [-1,1])$ minimizing (11), $\min_u J(u) = J(u^*) \equiv \min_u (t_1 - t_0) = t^*$ associated with (9), (10), (11), (18), where $\min_u H(t, x, \lambda, u) = H^*(t, x, \lambda, u^*) = 0, \forall (t, x, \lambda)$ is that trajectories x_i, λ_i respect (19), (20), (21) $\forall t \in [t_0, t^*]$ with:

$$H(t, x, \lambda, u) \geq H^*(t, x, \lambda, u^*) \geq 0; \min(H) = H^*(t^*, x^*, \lambda^*, u^*, C) = 0 \quad (22)$$

Remarks:

1) We may take $\lambda_0 = c_0 \equiv 1$ and H(t) is minimized determining the vector $\lambda = (\lambda_1, \lambda_2, ..., \lambda_n)$ so that the speed $\dot{X} = (\dot{x}_i)$ projection on λ vector to be minimum: $\min\left(\sum_{i=1}^{n} \lambda_i \dot{x}_i\right)$.

2) After building H, (17) and (18) with H = H(u), we find u* with $-1 \leq u_i \leq 1$, generally with $\frac{\partial H}{\partial u} = 0$; but, if H is linear in u, $H = a + bu_1 + cu_2$, then, according to linear programming with $H \geq 0$ in compact square $u(t) \in U$ included in (H, u1, u2) space, the minimum H(u*)=0 will be in the square tips $u^* = \{(u_1^* = -1, u_2^* = 1), (u_1^* = 1, u_2^* = -1)\}$; the solutions will be $x = x(t, u^*), \lambda = \lambda(t, u^*)$.

.

4. ANGULAR SPEEDS STABILIZATION OPTIMAL CONTROL

We still apply the algorithm (9) - (22) to (1) – (8); and build Hamiltonian (17) (18) associated with the system (7):

$$H = 1 + \lambda_1 \dot{x}_1 + \lambda_2 \dot{x}_2 = 1 + \lambda_1 \omega x_2 - \lambda_2 \omega x_1 + \lambda_1 k u_1 + \lambda_2 k u_2 \geq 0 \quad (23)$$

We note that $H = H(u_1, u_2) = a + bu_1 + cu_2$ is linear and positive in the compact square $u_1(t) \in [-1;1]$, $u_2(t) \in [-1;1]$; so in the space (H, u_1, u_2) H has a null minimum in the square tips: $H \geq H_{\min_{k \in U}} = H(u_1^*, u_2^*) = 0$

So, if $u_1^* = -\text{sgn}(\lambda_1); u_2^* = -\text{sgn}(\lambda_2)$ (24)

the trajectories $C_1^{\pm}(u_1 = 1, u_2 = -1)$ or $C_1^{\mp}(u_1 = -1, u_2 = 1)$ will be obtained, and they will tend to origin $O(x_1 = 0, x_2 = 0)$.

The system is autonomic and u^* is pulse-type. It results that the controller will be a relay-type one, acting with or without commutation [1] [2] [7]. We solve the canonic system (13)(14), effectively (7) with initial conditions $x_i(t_0 = 0) = \alpha_i, i = 1, 2$ and $u \in U$:

$$\begin{cases} \omega x_1 - u_2^* k = (\omega \alpha_1 - u_2^* k)\cos \omega t + (\omega \alpha_2 + u_1^* k)\sin \omega t \\ \omega x_2 + u_1^* k = -(\omega \alpha_1 - u_2^* k)\sin \omega t + (\omega \alpha_2 + u_1^* k)\cos \omega t \end{cases} \quad (25)$$

$$\left(x_1 - \frac{u_2^* k}{\omega}\right)^2 + \left(x_2 + \frac{u_1^* k}{\omega}\right)^2 = \left(\alpha_1 - \frac{u_2^* k}{\omega}\right)^2 + \left(\alpha_2 + \frac{u_1^* k}{\omega}\right)^2 \quad (26)$$

We note that these trajectories are circles with centers $O^*\left(\frac{u_2^*k}{\omega},-\frac{u_1^*k}{\omega}\right)$ and radius $R^2=\left(\alpha_1-\frac{u_2^*k}{\omega}\right)^2+\left(\alpha_2+\frac{u_1^*k}{\omega}\right)^2$, but they are not reaching the target point O(0,0) for $\forall(\alpha_1,\alpha_2)$. If in (26) $x_1\equiv 0, x_2\equiv 0$, we will get for $(\alpha)=(x)$ the compatible circles – a bi-local problem.

$$\left(\omega x_1-u_2^*k\right)^2+\left(\omega x_2+u_1^*k\right)^2=2k^2;R=\frac{k\sqrt{2}}{\omega};O_0^*\left(\frac{u_2^*k}{\omega},-\frac{u_1^*k}{\omega}\right) \tag{27}$$

$$\begin{cases} x_1-\frac{u_2^*k}{\omega}=\frac{k\sqrt{2}}{\omega}\cos\theta \\ x_2+\frac{u_1^*k}{\omega}=\frac{k\sqrt{2}}{\omega}\sin\theta \end{cases};\ \theta=\theta_0+\omega(t-t_0) \tag{28}$$

We note that the origin is on the circles from this family and their centers are on the first bisecting line (Oz_1) of the system x_1Ox_2 or on the second one (Oz_2), with the (z_1Oz_2) axis system, see figure 2a. Choosing the optimal circles depends on the optimal control u* so that $H^*(u^*)\geq 0$; if the X system would be rotated with $\frac{\pi}{4}$: $z\to z=x\cdot e^{i\frac{\pi}{4}}$, we note that from $H(u^*)\geq 0$, with (23) and (24) it results the trajectory on the upper (towards Oz_1) half-circles $\{C_1^*\}$ from the first quadrant and the lower half-circles, $\{C_2^*\}$ from the third quadrant, i.e.: $\{C_{10}^{\mp}:u_1^*=-1,u_2^*=1\}\cup\{C_{20}^{\pm}:u_1^*=1,u_2^*=-1\}$, with centers respectively: $O_{10}^{\mp}\left(\frac{k}{\omega},\frac{k}{\omega}\right)$ and $O_{20}^{\pm}\left(-\frac{k}{\omega},-\frac{k}{\omega}\right)$. Choosing the initial point $M^0(\alpha_1^0,\alpha_2^0)\in C_{10}^{\mp}$ in the moment t_0, corresponds to the angle θ_0 towards Ox_1:

$$\tan\theta_0=\frac{\alpha_2^0-\frac{k}{\omega}}{\alpha_1^0-\frac{k}{\omega}};$$

It may be observed on figure 2a that $\theta_0\in\left[\frac{\pi}{4},\frac{5\pi}{4}\right]$, with $\theta=\omega t+\frac{\pi}{4}$.

$$\theta_0\in\left[\frac{\pi}{4},\frac{5\pi}{4}\right],t_0\in\left[0,\frac{\pi}{\omega}\right],t^*=\frac{1}{\omega}\left(\frac{5\pi}{4}-\theta_0\right),\alpha_1^0>0,\alpha_2^0>0 \tag{29}$$

Analog and asymmetrically for the circle $C_2^{\pm}$.

Remark: The optimal trajectories are periodical $T=\frac{2\pi}{\omega}$; $\{C_{1j}^{\mp}\}\cup\{C_{2j}^{\pm}\}$ are tangent half-circles, with centers $O_{1j}^{\mp}\left((2j+1)\frac{k}{\omega},(2j+1)\frac{k}{\omega}\right),O_{2j}^{\pm}\left(-(2j+1)\frac{k}{\omega},-(2j+1)\frac{k}{\omega}\right)$, $j=0,1,2,...$ and radius $R=\frac{k\sqrt{2}}{\omega}$; for example, if the starting point is $M_{0j}\in C_{1j}^{\mp}$, then the minimal time will be $t^*=j\frac{k}{\omega}+\frac{1}{\omega}\left[\frac{5\pi}{4}-\theta_0(M_{0j})\right]$, without relay commutation.

There are situations when the starting point is not on the small half-circles, for example $P_0(\gamma_1,\gamma_2)$ in the third quadrant in figure 2b. In this case we choose from $C_{2j}^{\pm}$ a half-circle $O_{2j}^{\pm}$ with radius R_Γ denoted $\Gamma^{\pm}$. This circle crosses one of the half-circles $C_{1j}^{\mp}$. This is the commutation moment $(u_i \to -u_i, i=1,2)$, the new trajectory starting from Q and ending in origin.

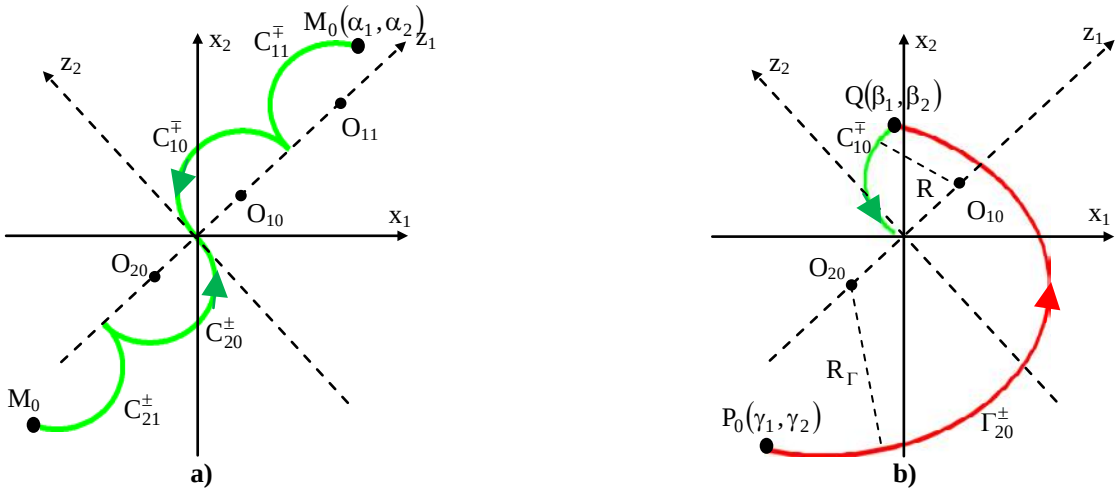

FIG. 2: Optimal trajectories
a) With no relay commutation b) with relay commutation

We solve the adjunct system (14-20) with H from (23):

$$\dot{\lambda}_1 = -\omega\lambda_2, \dot{\lambda}_2 = \omega\lambda_1, \lambda_1(t=0) = c_1^+, \lambda_2(t=0) = c_2^- \tag{30}$$

$$\lambda_1 = c_1\cos\omega t + c_2\sin\omega t; \lambda_2 = c_1\sin\omega t - c_2\cos\omega t \tag{31}$$

$$\lambda_1^2 + \lambda_2^2 = c_1^2 + c_2^2; \lambda_1 = \sqrt{c_1^2+c_2^2}\cos(\omega t - \varphi_0); \lambda_2 = \sqrt{c_1^2+c_2^2}\sin(\omega t - \varphi_0) \tag{32}$$

$$\tan\varphi_0 = \frac{c_2}{c_1}; \varphi_0 = a\tan\left(\frac{\lambda_2^0}{\lambda_1^0}\right) \tag{33}$$

We note that the adjunct system solution (31) describes a circle (32) and the period is the same as $C_{10}^{\mp}$, $C_{20}^{\pm}$ semicircles one, so $C_{10}^{\mp}$ semicircle description coincides with the description in the same direction of the semicircle upper $\lambda_2 > 0$ and $C_{20}^{\pm}$ description coincides with lower semicircle $\lambda_2 < 0$ in the plane $(\lambda_1 O\lambda_2)$.

Choosing the signs for u* and λ, c_1, c_2 was determined by interpreting the semi-circles in (z_1Oz_2) as follows:

$$\left.\begin{array}{l}\{C_{10}^{\mp}; u_1^* = -1; \lambda_1 > 0; c_1 > 0; u_2^* = 1; \lambda_2 < 0; c_2 < 0 \text{ pentru } z_2 \ge 0\} \text{ și}\\ \{C_{20}^{\pm}; u_1^* = 1; \lambda_1 < 0; c_1 < 0; u_2^* = -1; \lambda_2 > 0; c_2 > 0 \text{ pentru } z_2 \le 0\}\end{array}\right. \tag{34}$$

4.1. Optimal Control of the Un-commutated System [1], [2], [7]

Let's suppose that in the initial moment t_0 the system is in $M_0(\alpha_1,\alpha_2)$ on $C_{10}^{\mp}$ or $C_{20}^{\pm}$, and must reach the (target point) $O(0.0)$ in minimum time t_1^*; $\alpha_1 > 0$, $\alpha_2 > 0$ or

$\alpha_1 < 0$, $\alpha_2 < 0$, α_i given in the system (x_1Ox_2) on $C_{10}^{\mp}$ or $C_{20}^{\pm}$ (without relay switching).

$$C_{10}^{\mp}: \left(x_1 - \frac{k}{\omega}\right)^2 + \left(x_2 - \frac{k}{\omega}\right)^2 = \left(\frac{k\sqrt{2}}{\omega}\right)^2 ; u_1^* = -1; u_2^* = 1; t \in \left[0; \frac{\pi}{\omega}\right] \quad (35)$$

M_0 corresponds to the angle:

$$\theta_0 = \begin{cases} a\tan\dfrac{\alpha_2 - \frac{k}{\omega}}{\alpha_1 - \frac{k}{\omega}} & \dfrac{\pi}{4} \le a\tan\dfrac{\alpha_2 - \frac{k}{\omega}}{\alpha_1 - \frac{k}{\omega}} \le \dfrac{\pi}{2} \\ \pi + a\tan\dfrac{\alpha_2 - \frac{k}{\omega}}{\alpha_1 - \frac{k}{\omega}} & -\dfrac{\pi}{2} \le a\tan\dfrac{\alpha_2 - \frac{k}{\omega}}{\alpha_1 - \frac{k}{\omega}} \le -\dfrac{\pi}{4} \end{cases} ; \frac{\pi}{4} \le \theta_0 \le \frac{5\pi}{4} \quad (36)$$

We find $t_0 = \dfrac{\theta_0}{\omega}$ and as in $O(0.0)$ $t_f = \dfrac{\theta_f}{\omega} = \dfrac{5\pi}{4\omega}$, it results $t_{min}^* = \dfrac{1}{\omega}\left(\dfrac{5\pi}{4} - \theta_0\right)$ (37)

$$H_0^*\left(t_f, X^*, U^*, \lambda^*\right) = 1 + k\lambda_2 - k\lambda_1 = 0 \quad (38)$$

With (23), (31-33): $H_0^*(c_1, c_2) = 1 + k\sqrt{c_1^2 + c_2^2}\left(\sin\left(\omega t^* - \varphi_0\right) - \cos\left(\omega t^* - \varphi_0\right)\right) = 0$, by choosing characteristic values c_1, c_2 with (33) on microprocessors. Analog if the system starts with $M_0 \in C_{20}^{\pm}$.

4.2. Optimal Control of the Commutated System

Let's suppose that trajectories (26) are starting at t_0 from $P_0(\gamma_1, \gamma_2)$, $P_0 \in \Gamma_2^{\pm}$, not reaching in O; they intersect with the switching curves $C_1^{\mp}$ in Q and will optimally arrive in $O(0.0)$. P_0 is in the third quadrant, $\gamma_1 < 0$, $\gamma_2 < 0$, with $\theta_0(P_0) \in \left[\dfrac{5\pi}{4}, \dfrac{9\pi}{4}\right]$. We consider the circle $\Gamma_{20}^{\pm}$ (figure 2b), with center $O_{20}\left(-\dfrac{k}{\omega}, -\dfrac{k}{\omega}\right)$ and radius $R_\Gamma^2 = \left(\gamma_1 + \dfrac{k}{\omega}\right)^2 + \left(\gamma_2 + \dfrac{k}{\omega}\right)^2$; $\dfrac{k\sqrt{2}}{\omega} < R_\Gamma < \dfrac{3k\sqrt{2}}{\omega}$. It results the equation:

$$\Gamma_{20}^{\pm}: \left(x_1 + \frac{k}{\omega}\right)^2 + \left(x_2 + \frac{k}{\omega}\right)^2 = \left(\gamma_1 + \frac{k}{\omega}\right)^2 + \left(\gamma_2 + \frac{k}{\omega}\right)^2 \quad (39)$$

The Trajectories (39) $\Gamma_{20}^{\pm}$ will intersect (35) $C_{10}^{\mp}$ in $Q(\beta_1, \beta_2)$, i.e. the commutation point. We solve the system (39)(35): by subtracting the equations the radical axis (A) is obtained, so we'll solve the system {(35), (A)} [1][2][7].

$$(A)\ x_1 + x_2 = \frac{\omega}{4k}\left(\gamma_1^2 + \gamma_2^2 + + \frac{2k}{\omega}(\gamma_1 + \gamma_2)\right) := E > 0; x_1 > 0; x_2 > 0 \quad (40)$$

From (35) and (40) it results $x_1 = \beta_1$; $x_2 = \beta_2$; $Q(\beta_1, \beta_2)$

$$x_1 = \frac{1}{2}(E - \delta) > 0;\ x_2 = \frac{1}{2}(E + \delta) > 0, \text{ where } \delta = \sqrt{\frac{4k}{\omega}E - E^2} \quad (41)$$

Generally, $\theta = \omega t + \frac{5\pi}{4}$; we will find $t_0(P_0)$ and $\theta_0(P_0)$, then $t_1(Q)$ and $\theta_1(Q)$:

$$\theta_0(P_0) = \begin{cases} \pi + a\tan\dfrac{\gamma_2 + \frac{k}{\omega}}{\gamma_1 + \frac{k}{\omega}} & \dfrac{\pi}{4} \le a\tan\dfrac{\gamma_2 + \frac{k}{\omega}}{\gamma_1 + \frac{k}{\omega}} \le \dfrac{\pi}{2} \\ 2\pi + a\tan\dfrac{\gamma_2 + \frac{k}{\omega}}{\gamma_1 + \frac{k}{\omega}} & -\dfrac{\pi}{2} \le a\tan\dfrac{\gamma_2 + \frac{k}{\omega}}{\gamma_1 + \frac{k}{\omega}} \le -\dfrac{\pi}{4} \end{cases} ; \frac{5\pi}{4} \le \theta_0 \le \frac{9\pi}{4} \tag{42}$$

$$\theta_1(Q) = 2\pi + a\tan\frac{\beta_2 + \frac{k}{\omega}}{\beta_1 + \frac{k}{\omega}} \tag{42'}$$

$$t_1^* = t_1^1 - t_0^1 = \frac{1}{\omega}\left[\theta_1(Q) - \theta_0(P_0)\right] \tag{43}$$

which is the P_0Q arc travel time.

With $Q(\beta_1, \beta_2)$ determined, we pass on arc QO (on the circle $C_{10}^{\mp}$) respecting the determinations (35) – (38) and replacing (α_1, α_2) with (β_1, β_2) in the second stage.

$$\theta_0^2(Q) = \begin{cases} a\tan\dfrac{\beta_2 - \frac{k}{\omega}}{\beta_1 - \frac{k}{\omega}} & \dfrac{\pi}{4} \le a\tan\dfrac{\beta_2 - \frac{k}{\omega}}{\beta_1 - \frac{k}{\omega}} \le \dfrac{\pi}{2} \\ \pi + a\tan\dfrac{\beta_2 - \frac{k}{\omega}}{\beta_1 - \frac{k}{\omega}} & -\dfrac{\pi}{2} \le a\tan\dfrac{\beta_2 - \frac{k}{\omega}}{\beta_1 - \frac{k}{\omega}} \le -\dfrac{\pi}{4} \end{cases} ; \frac{\pi}{4} \le \theta_0^2 \le \frac{5\pi}{4} \tag{44}$$

$$t_0^2(Q) = \frac{\theta_0^2}{\omega};\ t_2^*(Q) = \frac{1}{\omega}\left(\frac{5\pi}{4} - \theta_0^2\right) \tag{44'}$$

The final minimal time for the trajectories (35) and (39) is

$$t^* = t_1^* + t_2^* \tag{45}$$

and $H^*(O) \equiv 0$, $H^*\left(t_2^*, X^*, U^*, \lambda^*\right) = H(c_1, c_2) \equiv 0$ is used after (38).

Numerical and graphic applications were developed for the two above mentioned situations.

Remark:

If the speeds system is amortized - resistance terms (elastic damped oscillator) appear - trajectories are spiral arcs. The study of this case is analogous to those presented in the paper.

REFERENCES

[1] Barbu, V., *Mathematical methods in optimization differential equations*. Bucharest, Romanian Academy Press, in Romanian (1989).

[2] Belea, C., *The system theory – nonlinear systems.* Bucharest: Ed. Did. Ped., in Romanian (1985).

[3] Dumitrache, I., *Automatica - vol. I.* Bucharest: Romanian Academy Press, in Romanian (2009).

[4] Lupu, C., Lupu, M., Optimized solution for ratio control structures. Multiple propulsion systems case study. *Proceedings of Conference on Fluid Mechanics and its Technical Applications*, INCAS and Institute of Mathematical Statistics and Applied Mathematics of the Romanian Academy, pp. 67-77 (2013).
[5] Lupu, M., Florea, Ol., Lupu, C., Criteria and applications of absolute stability in the automatic regulation of some aircraft course with autopilot. *Proceedings of Conference on Fluid Mechanics and its Technical Applications*, INCAS and Institute of Mathematical Statistics and Applied Mathematics of the Romanian Academy, pp. 109-120 (2011).
[6] Lupu, M., Florea, Ol., Lupu, C., Studies and Applications of Absolute Stability of the Nonlinear Dynamical Systems. *Annals of the Academy of Romanian Scientists*, Serie Science and Technology, vol. 2, 2(2013), pp. 183-205.
[7] Lupu, M., Radu, G., Constantinescu, C.G., Airplanes Or Ballistic Rockets Optimal Control And Flight Absolute Stabilization In Vertical Plane By Using The Criterion Of Minimal Time Or Fuel Consumption, ROMAI Journal, vol. 11, 2015.
[8] Lurie, A.Y., *Nonlinear problems from the automatic control*. Moskow: Ed. Gostehizdat, in Russian (1951).
[9] Pontreaguine, L. & Co., *Theorie mathematique des processus optimeaux*. Moscou: Editions Mir (1974).
[10] Popescu, M.E., *Variational Transitory Processes, Nonlinear Analysis in Optimal Control*. Bucharest: Ed. Tehnica, in Romanian (2007).
[11] Popov, V.M., *The hyperstability of automatic systems*. Bucharest: Ed. Academiei Romane 1966). Moskow: Ed. Nauka (1970). Berlin: Springer Verlag (1973).
[12] Pratt, Roger W., *Flight Control Systems*. I.E.E. British Library, A.I.A.A. USA (2000).
[13] Rasvan, Vl., Stefan, R., *Systemes nonlineaires*. Bucharest: Ed. PRINTECH, in Romanian (2004).
[14] Stengel, Robert F., *Flight Dynamics*. Oxford: Princeton University Press (2004).

IDENTIFYING DATA AFFECTED BY ABERRANT ERRORS OBTAINED IN THE MANUFACTURING OF SPECIAL ALLOYS

Ioan MILOSAN

Transilvania University, Brasov, Romania (milosan@unitbv.ro)

DOI: 10.19062/2247-3173.2016.18.1.66

Abstract: *The paper presents an example of calculation to identify data affected by aberrant errors and removing these data from the values of hardness (HB), strength (R_m) elongation (A) and impact strength (KCU) of Ni austempered ductile iron, by applying the r_{max}/r_{min} and Romanowski tests. By studying all the data presented in this paper, following remarkable conclusion: both tests had identified as data affected by aberrant errors for the same values of the mechanical properties. In this way, the experimental results obtained are validated with a statistical confidence level of 95%.*

Keywords: *data affected by aberrant errors, r_{max}/r_{min} test, Romanowski test*

1. INTRODUCTION

By analyzing a number of experimental data it can happen that some abnormal values to be higher or lower than the rest of the results. These non-conforming values are often referred to as: aberrant errors, abnormal, anomalous, outliers, discordant observation, exceptions, surprises, peculiarities or contaminants in different application domains [1].

The question which arises is to use statistical tests to identify abnormalities and removing these data because of incorrect information about the study that they can induce.

The paper presents an example of calculation to identify data affected by aberrant errors and removing these data from the values of hardness (HB), strength (Rm), elongation (A) and impact strength (KCU) of Ni austempered ductile iron, by applying the r_{max}/r_{min} and Romanowski tests.

2. IDENTIFYING DATA AFFECTED BY ABERRANT ERRORS

Identifying data affected by aberrant errors can be accomplished by applying the r_{max}/r_{min} and Romanowski tests.

Solving the two tests is done in the following steps [2 - 4]:

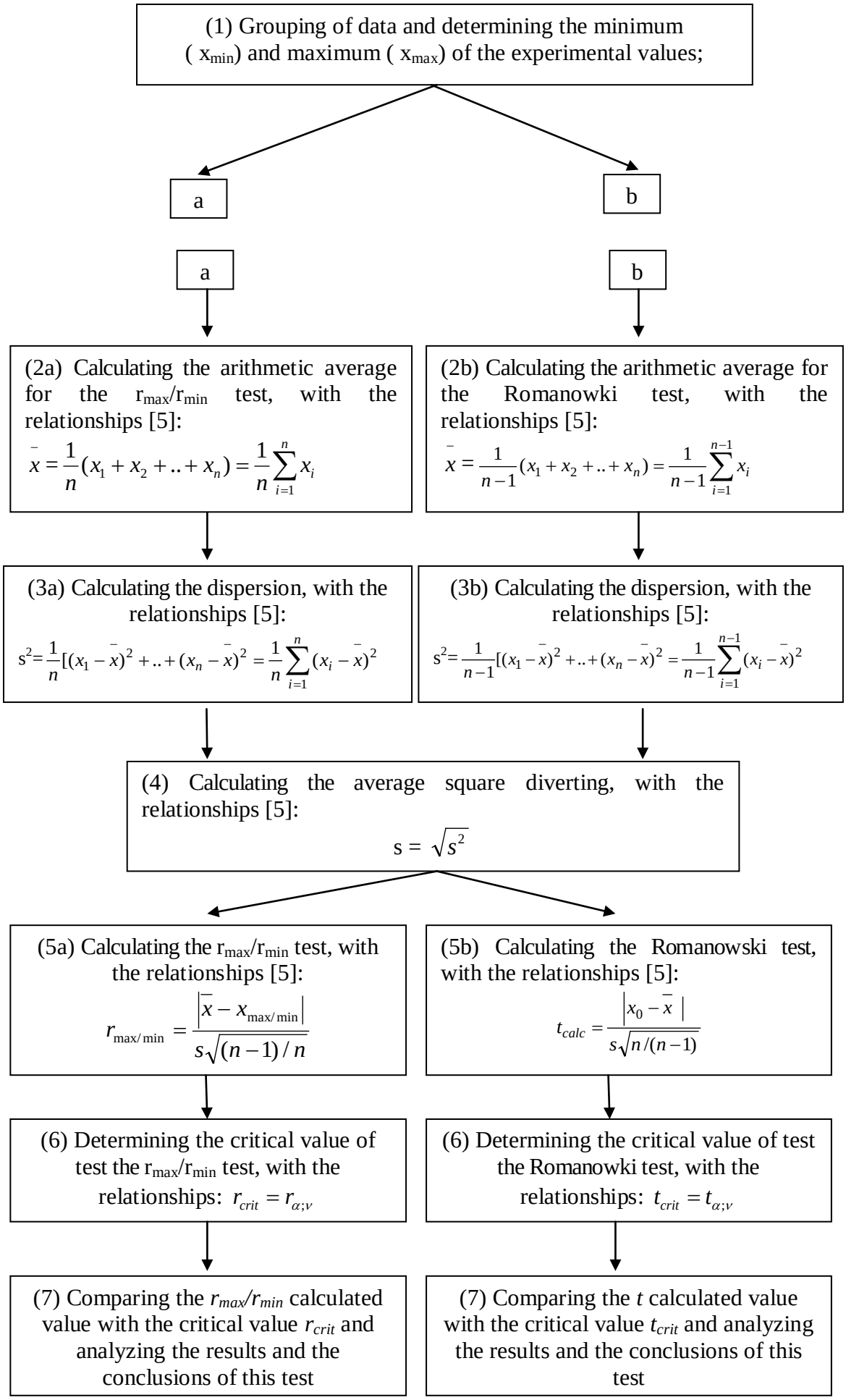
(1) Grouping of data and determining the minimum (x_{min}) and maximum (x_{max}) of the experimental values;
a
b
a
b
(2a) Calculating the arithmetic average for the r_{max}/r_{min} test, with the relationships [5]:
$\bar{x} = \frac{1}{n}(x_1 + x_2 + .. + x_n) = \frac{1}{n}\sum_{i=1}^{n} x_i$
(2b) Calculating the arithmetic average for the Romanowki test, with the relationships [5]:
$\bar{x} = \frac{1}{n-1}(x_1 + x_2 + .. + x_n) = \frac{1}{n-1}\sum_{i=1}^{n-1} x_i$
(3a) Calculating the dispersion, with the relationships [5]:
$s^2 = \frac{1}{n}[(x_1 - \bar{x})^2 + .. + (x_n - \bar{x})^2 = \frac{1}{n}\sum_{i=1}^{n}(x_i - \bar{x})^2$
(3b) Calculating the dispersion, with the relationships [5]:
$s^2 = \frac{1}{n-1}[(x_1 - \bar{x})^2 + .. + (x_n - \bar{x})^2 = \frac{1}{n-1}\sum_{i=1}^{n-1}(x_i - \bar{x})^2$
(4) Calculating the average square diverting, with the relationships [5]:
$s = \sqrt{s^2}$
(5a) Calculating the r_{max}/r_{min} test, with the relationships [5]:
$r_{max/min} = \frac{|\bar{x} - x_{max/min}|}{s\sqrt{(n-1)/n}}$
(5b) Calculating the Romanowski test, with the relationships [5]:
$t_{calc} = \frac{|x_0 - \bar{x}|}{s\sqrt{n/(n-1)}}$
(6) Determining the critical value of test the r_{max}/r_{min} test, with the relationships: $r_{crit} = r_{\alpha;\nu}$
(6) Determining the critical value of test the Romanowki test, with the relationships: $t_{crit} = t_{\alpha;\nu}$
(7) Comparing the r_{max}/r_{min} calculated value with the critical value r_{crit} and analyzing the results and the conclusions of this test
(7) Comparing the t calculated value with the critical value t_{crit} and analyzing the results and the conclusions of this test

where:

n = the number of experimental determinations;

$\bar{x}$ = the arithmetic average of the experimental data. For Romanowski test, the average value $\bar{x}$ is calculated without considering the value x_0 which is analyzed;

s^2 = the dispersion of the experimental data;

s = the average square diverting of the experimental data;

x_0 = the liable data to be affected by aberrant errors for the Romanowski test;

r_{crit} = the critical value for the r_{max}/r_{min} test [3];

t_{crit} = the critical value for the *t* test is the tabular value on the basis of the number of values in the series of data and confidence interval [5];

α = the coefficient of statistical confidence level, α = 0.95 [6];

ν = the number of degrees of freedom, $v = n-2$ for the r_{max}/r_{min} test and $v = n-1$ for the Romanowski test;

Comparing the r_{max}/r_{min} calculated value with the critical value r_{crit} and analyzing the results for the r_{max}/r_{mi} test, two situations can occur:

a) If $r_{max}/r_{min} < r_{crit}$ the values of the minimum (x_{min}) and maximum (x_{max}) of the experimental values are normal for our experimental research;

b) If $r_{max}/r_{min} > r_{crit}$ the values of the minimum (x_{min}) and maximum (x_{max}) of the experimental values are identified as data affected by aberrant errors for our experimental research;

Comparing the *t* calculated value with the critical value t_{crit} and analyzing the results for the Romanowski test, two situations can occur:

a) If $t < t_{crit}$ the values of the liable data to be affected by aberrant errors (x_0) of the experimental values are normal for our experimental research;

b) If $t > t_{crit}$ the values of liable data to be affected by aberrant errors (x_0) of the experimental values;

In both cases when determining abnormal after removing them, the calculations will made using new parameters required analysis.

3. EXPERIMENTAL INVESTIGATION

3.1. Materials

The studied materials, was a Ni-Cr cast iron with the following composition (% in weight): 3.75 %C; 2.14 %Si; 0.40 %Mn; 0.014%P; 0.004 %S; 0.05 %Mg and 0.48 %Ni.

This cast iron was made in an induction furnace. Nodular changes were obtained with the "In mold" method, with the help of prealloy FeSiMg with 10-16% Mg, added into the reaction chamber in a proportion of 1.1% of the treated cast iron.

This materials were subjected to a heat treatment whose parameters have been:

- the austenizing temperature, T_A = 830 [°C];
- the maintained time at austenizing temperature, τ_A = 60 [min];
- the temperature at isothermal level, T_{iz} = 300[°C] for lot A and 400[°C] for lot B;
- the maintained time at the isothermal level, τ_{iz} = 10, 20, 30, 40, 50 and 60 [min], corresponding to the first stage for obtaining bainitic structure.

All these experimental specimens, were performed at isothermal maintenance in salt-bath (55% KNO3+45% NaNO3), being the cooling after the isothermal maintenance was done in air.

From this material, 24 typical test specimens were done: 12 typical test specimens for hardness (HB), strength (R_m) and elongation (A) and 12 typical test specimens for impact strength (KCU)

3.2. Results

The values of the mechanical results are presented in tables 1.

Table 1. Data Analysis of HB, R_m KCU and A values

Lot	T_A [°C]	τ_A [min]	T_{iz} [°C]	τ_{iz} [min]	HB	R_m [N /mm^2]	KCU [J/cm^2]	A [%]
A	830	60	300	30	451	1400	54	2
				60	426	1370	58	2,3
				90	415	1350	63	2,5
				120	408	1300	65	2,7
				150	390	1190	63	2,6
				180	383	1130	64	2,6
B			400	30	375	1020	73	4,2
				60	321	930	78	4,8
				90	306	890	77	5,3
				120	302	860	79	5,6
				150	298	850	77	5,4
				180	292	815	76	5,3

It can be certainly observed a normal evolution of the values for mechanical characteristics [7]:

-when maintaining time at the isothermal level is growing then R_m and HB are decreasing and A with KCU are increasing;

-when maintaining time at the same temperature of the isothermal level is increasing than R_m and HB are decreasing, A and KCU are increasing;

- less maintaining time for the isothermal variation provides higher values of HB and R_m but lower of A and KCU;

This evolution of the mechanical properties is determined by the structural changes reported to the parameters of the heat treating. This evolution of the mechanical properties is determining by the structural constituents for each heat treatment.

In the case of lots A structure can be constituted of inferior bainite, residual austenite and martensite .These constituents are determining high values for R_m and HB, and less high for A and KCU.

This can be explained by the time of the isothermal level maintenance, followed by air cooling at the room temperature, is increasing the proportion of martensite, a constituent which is determining higher values for R_m and HB and lower for A and KCU in the structure of the lots.

In the case of lots B structure can be constituted of superior bainite, residual austenite and the martensite will disappear. These constituents are determining high values for A and KCU, and less high for R_m and HB [7].

4. IDENTIFYING DATA AFFECTED BY ABERRANT ERRORS

Experimental data of HB, R_m KCU and A presented in table 1 are processed by one of the 2 tests the r_{max}/r_{min} and Romanowski tests.

4.1. Data processing using the r_{max}/r_{min} test

The r_{max}/r_{min} test was applied following calculation steps above. Data resulting are presented in table 2. It was selected the coefficient of statistical confidence level, $\alpha = 0.95$ (the default is 5% or 0.05). According [3] for an accuracy of 95%, the value of r_{crit} = 1,996

Table 2. r_{max}/r_{min} test for data sets

Lot	Properties	x	Measured values	$\bar{x}$	s	r_{calc}	r_{crit}	Values remains Yes/No
A	HB	x_{max}	451	412.167	22.608	1.875	1.996	Yes
		x_{min}	383			1.408		Yes
	R_m	x_{max}	1400	1290	98.169	1.227		Yes
		x_{min}	1130			1.785		Yes
	KCU	x_{max}	65	61.167	3.891	1.079		Yes
		x_{min}	54			2.017		*No*
	A	x_{max}	2.7	2.467	0.249	1.026		Yes
		x_{min}	2			2.057		*No*
o	HB	x_{max}	375	315.667	27.992	2.322		*No*
		x_{min}	292			0.926		Yes
	R_m	x_{max}	1020	894.167	66.484	2.070		*No*
		x_{min}	815			1.304		Yes
B	KCU	x_{max}	79	76.667	1.886	1.330		Yes
		x_{min}	73			2.090		*No*
	A	x_{max}	5.6	5.1	0.469	1.168		Yes
		x_{min}	4.2			2.102		*No*

Comparing the r_{max}/r_{min} calculated value, r_{calc} with the critical value r_{crit} and analyzing the results for the r_{max}/r_{mi} test, two situations can occur:

a) If $r_{max}/r_{min} < r_{crit}$ the values of the minimum (x_{min}) and maximum (x_{max}) of the experimental values are normal for our experimental research, in this case it noted with a *Yes;*

b) If $r_{max}/r_{min} > r_{crit}$ the values of the minimum (x_{min}) and maximum (x_{max}) of the experimental values are identified as data affected by aberrant errors for our experimental research, in this case it noted with a *No;*

By studying all the data presented in this table, following a general remarkable conclusions: all values are accepted as correct data (Yes) with exception the following values noted with No, which have been identified as data affected by aberrant errors :

- the value of x_{min} =54, from the impact strength (KCU) data of lot A, r_{calc} = 2.017, r_{crit} = 1.996 so $r_{calc} > r_{crit}$;
- the value of x_{min} = 2, from the elongation (A) data of lot A, r_{calc} = 2.057, r_{crit} = 1.996 so $r_{calc} > r_{crit}$;
- the value of x_{max} = 375, from the hardness (HB) data of lot B, r_{calc} = 2.322, r_{crit} = 1.996 so $r_{calc} > r_{crit}$;
- the value of x_{max} = 1020, from the strength (R_m) data of lot B, r_{calc} = 2.070, r_{crit} = 1.996 so $r_{calc} > r_{crit}$;
- the value of x_{min} = 73, from the impact strength (KCU) data of lot B, r_{calc} = 2.090, r_{crit} = 1.996 so $r_{calc} > r_{crit}$;

- the value of x_{min} = 4.2, from the elongation data of lot B, r_{calc} = 2.102, r_{crit} = 1.996 so $r_{calc} > r_{crit}$;

For this six experiments it was eliminated the value affected by aberrant errors and recovery the test without these values, until they finally obtain a value that confirms initial relationship: $r_{max}/r_{min} < r_{crit}$. These new experimental value is normal for our experimental research and in this case it noted with a *Yes* for the column of the table representing values remains.

4.2. Data processing using the Romanowski test

The Romanowski test was applied following calculation steps above. Data resulting are presented in table 3. It was selected the coefficient of statistical confidence level, α = 0.95 (the default is 5% or 0.05). According [2, 5] for an accuracy of 95%, the value of t_{crit} = 1,92.

The values of the Romanowski test for the data sets are presented in tables 3.

Table 3. Romanowski test for data sets

Lot	Properties	x	Measured values	$\bar{x}$	s	t_{calc}	t_{crit}	Values remains Yes/No
A	HB	x_{max}	451	404.4	24.375	1.746	1.92	Yes
		x_{min}	383	418	20.890	1.768		Yes
	R_m	x_{max}	1400	1268	93.038	1.290		Yes
		x_{min}	1130	1322	73.593	2.383		Yes
	KCU	x_{max}	65	60.4	3.826	1.098		Yes
		x_{min}	54	62.6	2.417	3.250		*No*
	A	x_{max}	2.7	2.40	0.248	0.111		Yes
		x_{min}	2	2.54	0.136	3.624		*No*
B	HB	x_{max}	375	303.8	9.765	6.659		*No*
		x_{min}	292	320.4	28387	0.914		Yes
	R_m	x_{max}	1020	869	38.781	3.556		*No*
		x_{min}	815	910	61.664	1.407		Yes
	KCU	x_{max}	79	76.2	1.720	1.487		Yes
		x_{min}	73	77.4	1.019	3.942		*No*
	A	x_{max}	5.6	5	0.452	1.212		Yes
		x_{min}	4.2	5.28	0264	3.737		*No*

Comparing the t calculated value, t_{calc} with the critical value t_{crit} and analyzing the results for the Romanowski test, two situations can occur:

a) If $t_{calc} < t_{crit}$ the values of the minimum (x_{min}) and maximum (x_{max}) of the experimental values are normal for our experimental research, in this case it noted with a *Yes;*

b) If $t_{calc} > t_{crit}$ the values of the minimum (x_{min}) and maximum (x_{max}) of the experimental values are identified as data affected by aberrant errors for our experimental research, in this case it noted with a *No;*

By studying all the data presented in this table, following a general remarkable conclusions: all values are accepted as correct data (Yes) with exception the following values noted with No, which have been identified as data affected by aberrant errors :

- the value of x_{min} =54, from the impact strength (KCU) data of lot A, t_{calc} = 3.250, r_{crit}= 1.92 so $t_{calc} > t_{crit}$;

- the value of $x_{min} = 2$, from the elongation (A) data of lot A, $r_{calc} = 2.057$, $t_{crit} = 1.92$ so $t_{calc} > t_{crit}$;

- the value of $x_{max} = 375$, from the hardness (HB) data of lot B, $t_{calc} = 3.624$, $r_{crit} = 1.92$ so $t_{calc} > t_{crit}$;

- the value of $x_{max} = 1020$, from the strength (R_m) data of lot B, $r_{calc} = 6.659$, $t_{crit} = 1.92$ so $t_{calc} > t_{crit}$;

- the value of $x_{min} = 73$, from the impact strength (KCU) data of lot B, $r_{calc} = 3.942$, $t_{crit} = 1.92$ so $t_{calc} > t_{crit}$;

- the value of $x_{min} = 4.2$, from the elongation data of lot B, $r_{calc} = 3.737$, $t_{crit} = 1.92$ so $t_{calc} > t_{crit}$;

For this six experiments it was eliminated the value affected by aberrant errors and recovery the test without these values, until they finally obtain a value that confirms initial relationship: $t_{calc} < t_{crit}$. These new experimental value is normal for our experimental research and in this case it noted with a *Yes* for the column of the table representing values remains.

CONCLUSIONS

By studying all the data presented in this paper following remarkable conclusions:

(a) When maintaining time at the isothermal level is growing then R_m and HB are decreasing and A with KCU are increasing;

(b) When maintaining time at the same temperature of the isothermal level is increasing than R_m and HB are decreasing , A and KCU are increasing;

(c) Less maintaining time for the isothermal variation provides higher values of HB and R_m but lower of A and KCU;

(d) The evolution of the mechanical properties is determined by the structural changes reported to the parameters of the heat treating and this evolution of the mechanical properties is determining by the structural constituents for each heat treatment;

(e) In the case of lots A, structure can be constituted of inferior bainite, residual austenite and martensite .These constituents are determining high values for R_m and HB, and less high for A and KCU;

(f) In the case of lots B, structure can be constituted of superior bainite, residual austenite and the martensite will disappear. These constituents are determining high values for A and KCU, and less high for R_m and HB;

(g) By using the two statistical tests (the r_{max}/r_{min} and Romanowski tests) were removed normal results of experimental research;

(h) By studying all the data presented in the table 2 and 3, following a general remarkable conclusions: all experimental data as correct were noted with *Yes* and all experimental data as aberrant errors resulting from application, were noted with *No*;

(i) Both tests had identified as data affected by aberrant errors for the same values of the mechanical properties;

(j) Both tests will be recalculated until are done the conditions for acceptance.

REFERENCES

[1] M. R. Costescu, Identifying Data Affected by Aberrant Errors. Applied Program, *Economic Informatics*, vol. 12, no. 1, pp. 52 - 22, 2008;

[2] M. Banica and N. Medan, Statistical analysis of the experimental data obtained in studying of water jet cleaning, *Academic Journal of Manufacturing Engineering*, vol. 13, no. 1, pp. 6-10, 2015;

[3] D. Taloi, *Optimization of metallurgical processes*, E.D.P. Bucharest, 1983;

[4] T. Laurian and R. F. Mirică, *Paper 3-Eliminating aberrant values*, 2014. Available at http://www.omtr.pub.ro/didactic/fsm/lab/fsm03.pdf, accessed on 28 April 2016;
[5] I. Tanasescu, *Statistical control of processes and products*, E.D.P. Bucharest, 1987;
[6] M. Bulgaru and L. Bolboaca, *Quality engineering. Quality management, statistics and control measurements in 3D*, Alma Mater, Cluj-Napoca, 2001;
[7] J. M. Chou, M. H. Hon. and J. L. Lee, The austenite transformation in ferritic ductile cast iron, *Materials Science and Engineering A*, vol. 158, no. 2, pp. 241-249. 1992.

STATISTICAL PROCESSING OF EXPERIMENTAL DATA USING ANALYSIS OF VARIANCE

Ioan MILOSAN

"Transilvania" University, Brasov, Romania (milosan@unitbv.ro)

DOI: 10.19062/2247-3173.2016.18.1.67

Abstract: *The differences between samples of observations made by statistics is called analysis of variance (ANOVA). Being an extension of analysis of variance, the two-way ANOVA compares the mean differences between groups that have been split on two independent variables. This method is similar to the process of comparing the statistical difference between two samples, in that it invokes the concept of hypothesis testing. The paper presents an example of calculation for two-way analysis of variance repeated measures applied for the results of strength (Rm) and impact strength (KC) of Ni-Cu and Ni-Cu-Cr austempered ductile iron. Two-factor ANOVA / Two-way ANOVA: is an experiment with two independent variables, call them factor 1 (in our case, the auxiliary alloying elements: Ni-Cu and Ni-Cu-Cr) and factor 2 (in our case, the maintained time at the isothermal level, t_{iz}) that has three levels: t_{iz} = 5, 30 and 60 minutes. It was selected the level of significance (the default is 5% or 0.05).*

Keywords: *statistics, analysis of variance, strength, impact strength*

1. INTRODUCTION

Any technological process operates simultaneously on several factors, random and systematic, each having an influence on the process performance.

By analysis of variance (ANOVA) are separate effects of random variation factors of the effects of systematic factors (technological parameters), the separation taking place by decomposition of the total variance components and estimate their dispersions [1].

Analysis of variance usually refers to statistical analysis involving simultaneous comparison of multiple sets of observations, not just the comparison of two averages [2].

ANOVA creates a way to test several null hypothesis at the same time. The logic behind this procedure has to do with how much variance there is in the population [3].

In situations where the influences are tested simultaneously to two factors and their interactions on the performance of a technological process, using two factors variance analysis (Two-way ANOVA). Based on research results are selected significant factors and interactions that come as variables in the mathematical model of the process [4, 5].

The paper presents an example of calculation for two-way analysis of variance repeated measures applied for the results of strength (Rm) and impact strength (KC) of Ni-Cu and Ni-Cu-Cr austempered ductile iron.

2. THE STEPS OF THE TWO-WAY ANALYSIS OF VARIANCE

Solving Two-Way Analysis of Variance is done in the following steps [1, 2]:

(1) Enter experimental data

(2) Calculation of the Sum of squares for A factor, SS(A), (i.e. sum of the squared deviations from the mean) is done with the relationship:

$$SS(A) = r * b \sum_{i=1}^{a} (\bar{y}i - \bar{y})^2$$

(3) Calculation of the Sum of squares for B factor, SS(B), (i.e. sum of the squared deviations from the mean) is done with the relationship:

$$SS(B) = r * a \sum_{j=1}^{b} (\bar{y}i - \bar{y})^2$$

(4) Calculation of the Sum of squares for AB factors, SS(AB) is done with the relationship:

$$SS(AB) = r * \sum_{i=1}^{a} * \sum_{j=1}^{b} (\bar{y}ij - \bar{y}i - \bar{y}j + \bar{y})^2$$

(5) Calculation of the captures variability within each group SS(Within) is done with the relationship:

$$SS(Within) = \sum_{i=1}^{a} * \sum_{j=1}^{b} * \sum_{k=1}^{r} (\bar{y}ijk - \bar{y}ij)^2$$

(6) Calculation of the Total sum of squares, SS(Total), is done with the relationship:

$$SS(Total) = \sum_{i=1}^{a} * \sum_{j=1}^{b} * \sum_{k=1}^{r} (\bar{y}ijk - \bar{y})^2$$

a

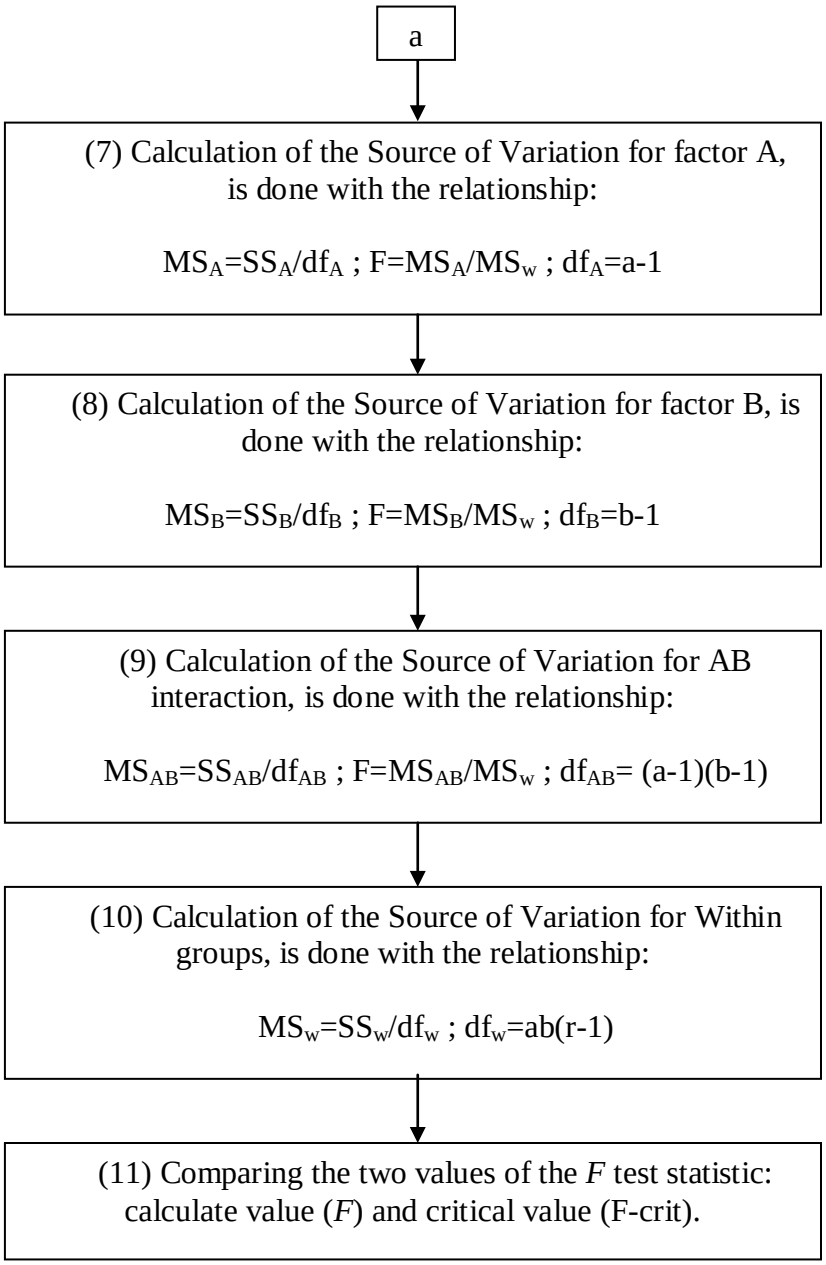

where:

Factor A has 1, 2, ..., a levels;

Factor B has 1, 2, ..., b levels;

SS(A) = Sum of squares for A factor (i.e. sum of the squared deviations from the mean);

SS(B)= Sum of squares for B factor (i.e. sum of the squared deviations from the mean);

SS (AB)= Sum of squares for AB factors (i.e. sum of the squared deviations from the mean);

AB = the interaction between A and B.

SS(Within)= captures variability within each group;

SS(Total)= Total sum of squares

a = levels for A factor;

b = levels for B factor;

r = total number of observations for each interaction;
abr = n = the total number of observations;
Y = process performance;
$\bar{Y}$ = average of process variable;
i = levels of A factor;
j = levels of B factor;
k = levels of interactions;
df = the degrees of freedom is equal to the sum of the individual degrees of freedom for each sample.
abr = n = the total number of observations;
SS = Sum of squares (i.e. sum of the squared deviations from the mean);
MS = Mean square;
F = the calculated value of the Fischer criteria;
F-crit = is the critical value of the Fischer criteria: for the level of significance, α = 0.05 (the default is 5% or 0.05.), the critical value for F;
P-value is determined from the F ratio and the two values for degrees of freedom;

3. EXPERIMENTAL INVESTIGATION

3.1. Materials

The first studied materials (Lot A), was a Ni-Cu cast iron with the following composition (% in weight): 3.80 %C; 2.60 %Si; 0.45 %Mn; 0.005 %P; 0.001 %S; 0.072 %Mg; 0.40 %Ni and 0.18 %Cu. The second materials (Lot B), was a Ni-Cu-Cr cast iron with the following composition (% in weight): 3.61% C; 2.67% Si; 0.53 % Mn; 0.011%P; 0.005%S; 0.06%Mg; 0.45% Ni; 0.22%Cu and 0.20% Cr.

This materials were subjected to a heat treatment whose parameters have been:

- the austenizing temperature, T_A = 900 [°C];
- the maintained time at austenizing temperature, τ_A = 30 [min];
- the temperature at isothermal level, T_{iz} = 300 [°C];
- the maintained time at the isothermal level, τ_{iz} = 5, 30 and 60 [min], corresponding to the first stage for obtaining bainitic structure.

All these experimental specimens, were performed at isothermal maintenance in salt-bath (55% KNO3+45% NaNO3), being the cooling after the isothermal maintenance was done in air.

From this material, 36 typical test specimens were done: 18 typical test specimens for strength (Rm) determination and 18 typical test specimens for impact strength (KC) determination. For each Rm and KC determination it was done three parallel determinations (r = 3).

3.2. Results

The values of the mechanical results are presented in tables 1.

It can be certainly observed a normal evolution of the values for mechanical characteristics [6, 7]:

-when maintaining time at the isothermal level for both Lots (A and B) is growing, then strength (R_m) decreases and impact strength (KC) (unnotched samples) increases;

-when maintaining time at the same temperature of the isothermal level is increasing, then Rm decreases and KC increases;

Table 1. Data Analysis of R_m and KC values for T_A= 900°C and T_{iz}=300°C

Materials	τ_{iz} [min]	R_m [N /mm^2] parallel observations			KC [J /cm^2] parallel observations		
		Obs. 1	Obs. 2	Obs. 3	Obs. 1	Obs. 2	Obs. 3
Ni-Cu (Lot A)	5	1420	1425	1423	56	57	56
	30	1390	1390	1393	61	60	61
	60	1300	1309	1311	67	68	68
Ni-Cu-Cr (Lot B)	5	1454	1450	1450	47	46	46
	30	1425	1425	1421	53	54	52
	60	1395	1390	1390	57	56	56

- comparing the 2 groups, we see that for the same parameters of heat treatment, Lot B (Ni-Cu-Cr) has sensible superior values for strength and inferior values for impact strength comparing with Lot A (Ni-Cu).

This evolution of the mechanical properties is determined by the structural constituents for each chemical composition, which can be constituted of inferior bainite, residual austenite and martensite. By allying with additional Cr, the complexes carbides made, will induce higher values sensitive to strength (R_m) and lower for impact strength (KC).

4. CALCULATION OF TWO-WAY ANOVA

Two-factor ANOVA / Two-way ANOVA: is an experiment with two independent variables, call them factor 1 (in our case, the auxiliary alloying elements: Ni-Cu and Ni-Cu-Cr) and factor 2 (in our case, the maintained time at the isothermal level, t_{iz}) that has three levels: t_{iz} = 5, 30 and 60 minutes.

It was selected the level of significance (the default is 5% or 0.05). The R_m and KC Summary Table of the ANOVA- Two Factor With Replication are presented in Tables 2 and 3.

Table 2.Summary Table of the R_m ANOVA- Two Factor With Replication

SUMMARY	**Sample 5**	**Sample 30**	**Sample 60**	**Total**
Ni-Cu (lot A)				
Count	3	3	3	9
Sum	4268	4173	3920	12361
Average	1422,667	1391	1306,667	1373,444
Variance	6,333333	3	34,33333	2707,278
SUMMARY	**Sample 30**	**Sample 60**	**Sample 90**	
Ni-Cu-Cr (lot B)				
Count	3	3	3	9
Sum	4354	4271	4175	12800
Average	1451,333	1423,667	1391,667	1422,222
Variance	5,333333	5,333333	8,333333	673,4444
TOTAL	**Sample 30**	**Sample 60**	**Sample 90**	
Count	6	6	6	
Sum	8622	8444	8095	
Average	1437	1407,333	1349,167	
Variance	251,2	323,4667	2184,567	

Table 3.Summary Table of the KC ANOVA -Two Factor With Replication

SUMMARY	**Sample 5**	**Sample 30**	**Sample 60**	**Total**
Ni-Cu (lot A)				
Count	3	3	3	9
Sum	169	182	203	554
Average	56,33333	60,66667	67,66667	61,55556
Variance	0,333333	0,333333	0,333333	24,77778
SUMMARY	**Sample 30**	**Sample 60**	**Sample 90**	
Ni-Cu-Cr (lot B)				
Count	3	3	3	9
Sum	139	159	169	467
Average	46,33333	53	56,33333	51,88889
Variance	0,333333	1	0,333333	19,86111
TOTAL	**Sample 30**	**Sample 60**	**Sample 90**	
Count	6	6	6	
Sum	308	341	372	
Average	51,33333	56,83333	62	
Variance	30,26667	18,16667	38,8	

The Source of Variation of the ANOVA- Two Factor With Replication are presented in Tables 4 and 5, where:

F is the calculated value of the Fischer criteria; F_{Sample}= MS_{Sample} / MS_{Within}; $F_{Columns}$= $MS_{Columns}$ / MS_{Within}; $F_{Interaction}$= $MS_{Interaction}$ / MS_{Within};

F-crit = is the critical value of the Fischer criteria: for the level of significance, $\alpha = 0.05$ (the default is 5% or 0.05.), the critical value for F;

F-crit for Sample with df (1, 16) is 4.493998;

F-crit for Columns with df (3, 16) is 3.238872;

F-crit for Interaction with df (3, 16) is 3.238872.

Table 4.Source of variation of the R_m ANOVA, T_A = 900°C and T_{iz}=300°C

ANOVA						
Source of Variation	SS	df	MS	F	P-value	F-crit
Sample	10706,72	1	10706,72	1025,112	5,44E-13	4,747225
Columns	23956,33	2	11978,17	1146,846	1,99E-14	3,885294
Interaction	2964,111	2	1482,056	141,8989	4,46E-09	3,885294
Within	125,3333	12	10,44444			
Total	37752,5	17				

Table 5.Source of variation of the KC ANOVA, T_A = 900°C and T_{iz}=300°C

ANOVA						
Source of Variation	SS	df	MS	F	P-value	F-crit
Sample	420,5	1	420,5	946,125	8,75E-13	4,747225
Columns	341,4444	2	170,7222	384,125	1,32E-11	3,885294
Interaction	10,33333	2	5,166667	11,625	0,001556	3,885294
Within	5,333333	12	0,444444			
Total	777,6111	17				

In figure 1 is presented the influence of the source of variation over the values of the Fischer Criteria.

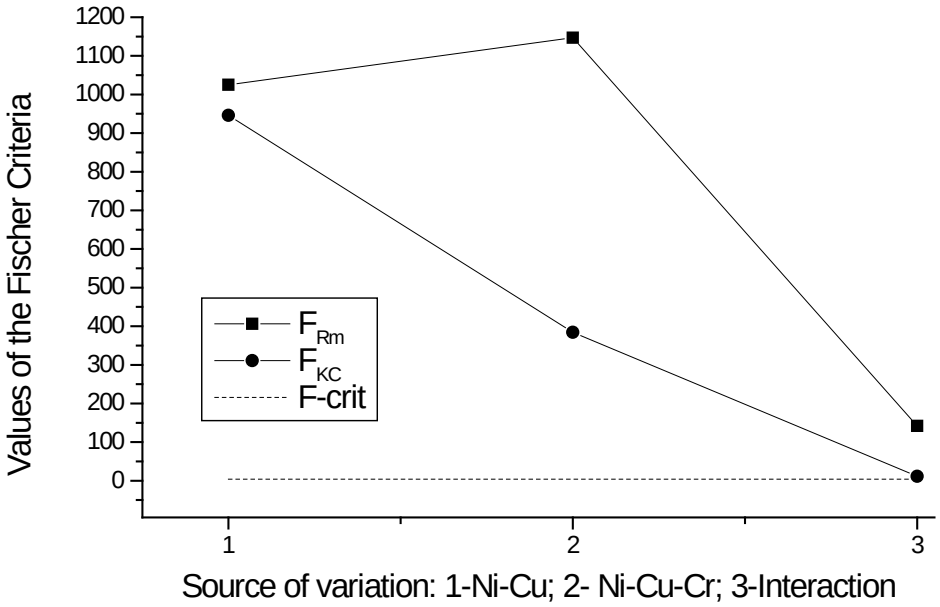

FIG. 1. The influence of the source of variation over the values of the Fischer Criteria.

The following observations can be made after analyzing the results presented in table 4, 5 and figure 1:

(a) From table 4, source of variation of the R_m ANOVA- Two Factor With Replication, T_A = 900°C and T_{iz}=300°C, it was compares the two values of the F test statistic: calculate value (F) and critical value (F-crit). Note that in this case the calculated value (F) is greater than the critical value (F-crit), i.e.:

- analyzing the Lot A, is observed for Ni-Cu alloying, that the calculated value F = 1025.112 is greater than the critical value (F-crit) = 4.747225 (1025.112 > 4.747225), therefore, the effect of the first independent variable is significant;

- analyzing the Lot B, observed for Ni-Cu-Cr alloying, that the calculated value F = 1146.846 is greater than the critical value (F-crit) = 3.885294 (1146.846 > 3.885294), therefore, the effect of the first independent variable is also significant;

- analyzing the effect of interaction between the two lots, we see that for Rm, the calculated value F = 141.8989 is greater than the critical value (F-crit) = 3.885294 (141.8989 > 3.885294), therefore, so both lots are the parameters for the technological process.

(b) From table 5, source of variation of the KC ANOVA- Two Factor With Replication, T_A = 900°C and T_{iz}=300°C, it was compares the two values of the F test statistic: calculate value (F) and critical value (F-crit). Note that in this case the calculated value (F) is greater than the critical value (F-crit), i.e.:

- analyzing the Lot A, is observed for Ni-Cu alloying, that the calculated value F = 944.125 is greater than the critical value (F-crit) = 4.747225 (944.125 > 4.747225), therefore, the effect of the first independent variable is significant;

- analyzing the Lot B, observed for Ni-Cu-Cr alloying, that the calculated value F = 384.125 is greater than the critical value (F-crit) = 3.885294 (384.125 > 3.885294), therefore, the effect of the first independent variable is also significant;

- analyzing the effect of interaction between the two lots, we see that for Rm, the calculated value F = 11.625 is greater than the critical value (F-crit) = 3.885294 (11.625 > 3.885294), therefore, so both lots are the parameters for the technological process.

(c) From table 4, 5 and figure 1, the following observations can be made:

- the values of the Fischer Criteria for the Rm properties is bigger for all the source of variation comparing with the values of the Fischer Criteria for the KC properties;

- both values of the Interaction are bigger than the critical value from the Fischer Criteria (F-crit = 3,885294), so both variables are technological factors for the studied materials (lot A and lot B).

CONCLUSIONS

By studying all the data presented in this paper following remarkable conclusions:

(a) Analysis of variance usually refers to statistical analysis involving simultaneous comparison of multiple sets of observations, not just the comparison of two averages;

(b) In situations where the influences are tested simultaneously to two factors and their interactions on the performance of a technological process, using two factors variance analysis (Two-way ANOVA).

(c) The evolution of the mechanical properties is determined by the structural constituents for each chemical composition, which can be constituted of inferior bainite, residual austenite and martensite. By allying with additional Cr, the complexes carbides made, will induce higher values sensitive to strength (R_m) and lower for impact strength (KC).

(d) Analyzing the effect of interaction between the two independent variables, we see that:

- the values of the Fischer Criteria for the Rm properties is bigger for all the source of variation comparing with the values of the Fischer Criteria for the KC properties;

- both values of the Interaction are bigger than the critical value from the Fischer Criteria (F-crit = 3,885294), so both variables are technological factors for the studied materials (lot A and lot B).

REFERENCES

[1] K. Hae-Young, Statistical notes for clinical researchers: Two-way analysis of variance (ANOVA)-exploring possible interaction between factors, *Restor Dent Endod.*, vol 39, no. 2, pp. 143-147, 2014;

[2] R.A. Armstrong, F. Eperjesi and B. Gilmartin, The application of analysis of variance (ANOVA) to different experimental designs in optometry. *Ophthalmic and Physiological Optics*, vol. 22, no. 3, pp. 248-256, 2002;

[3] D. Taloi, *Optimization of technological processes*, E.A. Bucharest, 1984;

[4] J. Budde, Variance analysis and linear contracts in agencies with distorted performance measures. *Management Accounting Research*, vol. 20, no. 3, pp. 166-176, 2009;

[5] K.T. Wing, Using enhanced cost models in variance analysis for better control and decision making, *Management Accounting Quarterly*, vol. 4, no. 2, pp. 27-35, 2005;

[6] R.A. Harding, The production, properties and automotive applications of austempered ductile iron. *Kovove Materialy*, vol. 45, pp.1-16, 2007;

[7] A. Rimmer, DI solutions aid vehicle design, *The Foundry Trade Journal*, vol. 2, pp. 54-56, 2004;

STOCHASTIC APPROXIMATION FOR RELIABILITY PROBLEMS

Florența Violeta TRIPŞA, Ana-Maria LUCA (RÎTEA)

Transilvania University, Braşov, Romania (florentatripsa@yahoo.com, ana_ritea_maria@yahoo.com)

DOI: 10.19062/2247-3173.2016.18.1.68

Abstract: *The article discusses the mathematical model for the stochastic approximation of reliability problems and an optimality system for the stochastic approximation plan given by M.T. Wasan. The end of the paper defines the concept of adapted stochastic approximation plan (SA).*

Keywords: *stochastic approximation, random variables, reliability, probability*

1. INTRODUCTION

In many probability theory applications the random variables occur and they depend on one or more parameters. Thus, in the reliability theory, there is the problem of the time variation study of the characteristics of a certain system (automobile, computer or any type of machine, etc.), time being in this case a parameter.

Such situations can be studied with the help of stochastic processes, these representing a current research direction of the probability theory, just because of the fact that they have new and numerous practical uses.

Stochastic approximation algorithms, introduced by H. Robbins and S. Monro since 1950 have been the subject of rich literature due to its wide applicability area.

A field where stochastic approximation algorithms is present is the reliability theory, whose purpose is to determine the laws of emergence of the problems in a system, with the probability of fulfilling the functions with certain performances and without problems, in a certain time interval and specified exploitation conditions.

2. THE ENUNCIATION OF THE GENERAL PROBLEM OF STOCHASTIC APPROXIMATION

A stochastic approximation problem may be synthetized as following:

Take an experiment whose results depend on a t *variable and mark* $Y(t)$ *the random variable corresponding to those results.*

Pick a random value t_1 *that leads to the observed value* $Y(t_1)$ *of the random variable* $Y(t)$.

Mark $F(t) = EY(t)$, E *being the random variable average* $Y(t)$.

The result should be the determination of a t^* *value to verify the equation* $F(t^*) = \alpha$, *where* $\alpha \in R$ *randomly chosen.*

The solution of this problem will be found with an iterative procedure.

Choose a non-rising series of positive numbers $(a_n)_n$ $(a_n \geq a_{n+1}, \forall n \in N)$ and establish a recursion, for the purpose of selecting another t value, for the following experiment:

$$t_{n+1} = t_n - a_n\left[y(t_n) - \alpha\right] \tag{2.1}$$

An *n* number of experiments is assumed to have been made, obtaining a result, therefore the values of t_n and $y(t_n)$ are already known.

Then, using the recursion relation (2.1) the value of t used in the number (n+1) experiment can be determined.

If in the relation (2.1) $\alpha = 0$ is chosen, this is reduced to

$$t_{n+1} = t_n - a_n y(t_n) \tag{2.2}$$

In the relation (2.2) if $y(t_n) > 0$ then $t_{n+1} < t_n$, and if $y(t_n) < 0$ then $t_{n+1} > t_n$.

These observations are important for the solution in the equation $F(t^*) = \alpha$.

The conclusion is that if $y(t_n) > 0$, then the t value for the (n+1) step should drop; if $y(t_n) < 0$, then the chosen t for the (n+1) step should rise.

What is interesting is the condition that the array $(t_n)_n$ should converge in a mean square value, with probability 1, for the t^* value.

3. REAL STOCHASTIC APPROXIMATION FOR RELIABILITY PROBLEMS

We analyze the functionality of a "system" that has a certain t "lifespan", with a corresponding $F(t)$ distribution function.

The system is examined at $t_1, t_2, ..., t_n$ time. If the inspection reveals the fact that the robot is not operative, then it is repaired (if possible) or replaced (if it cannot be fixed).

The general problem is the selection of an inspection plan $t_1, t_2, ..., t_n$, in an optimum way.

Next, an optimality criterion is defined and it is proven that the stochastic approximation plan fulfills this criterion.

If the system's "lifespan" is a continuous random variable, with an exponential repair, then the distribution function becomes:

$$F(t) = \begin{cases} 0, & if < 0 \\ 1 - e^{-\lambda t}, & if\ t \geq 0 \end{cases} \tag{3.1}$$

where $\lambda > 0$ is an unknown parameter with a known positive interval, that is $\lambda \in (\lambda_1, \lambda_2)$ with $0 < \lambda_1 < \lambda_2$ given.

The distribution function is differentiable for any $t > 0$ and $F'(t) = \rho(t)$ is the probability density.

Mark $T_i = t_i - t_{i-1}$, $i = 2,3,....$, $T_1 = t_1$, the time interval between two consecutive inspections.

Take the array $\{t_n\}_n$ as an arbitrary array of random variables, having the distribution depending on a real parameter, different from λ.

Consider a random variables array $(Y_n)_n$, defined as:

$$Y_i = \begin{cases} 1, & with\ probability\ e^{-\lambda T_i} \\ 0, & with\ probability\ 1 - e^{-\lambda T_i} \end{cases} \tag{3.2}$$

That is, if at moment t_i verification, the system is not functional, then $Y_i = 0$, or $Y_i = 1$.

Take f_n a measurable function, of *n* variables $Y_1, Y_2, ..., Y_n$, with real values which does not depend on λ.

The time intervals between two consecutive inspections are given by the following relations:

$$T_1 = \max\{0, v_1\}$$
$$T_{n+1} = \max\{0, f_n(Y_1, Y_2, ..., Y_n) + v_n\},\ n = 1,2,... \tag{3.3}$$

Intuitively, after the *n* number of inspections, the next inspection, defined by T_{n+1}, depends on the past observations $(Y_1, Y_2, ..., Y_n)$ with f_n.

M.T. Wasan suggests an optimality criterion that takes into consideration the information about λ, this becoming unavailable after inspection procedures.
The information average is defined after applying a I plan of *n* inspections with the relation:

$$J_n(I,\lambda) = n^{-1}E\left[\frac{d}{d\lambda}\log L_n(\lambda)\right]^2, \tag{3.4}$$

where $L_n(\lambda)$ is the probability function of λ when $(Y_1, Y_2, ..., Y_n)$, respectively $(T_1, T_2, ..., T_n)$ are known

Then,

$$J(I,\lambda) = \liminf_{n\to\infty} J_n(I,\lambda), \tag{3.5}$$

is called the medium limit of the information obtained after a I plan.
The next problem is that of maximizing $J_n(I,\lambda)$ and $J(I,\lambda)$ after a correct selection of the I plan. The following theorem gives a result, concerning the efficient estimation of λ.

Theorem 3.1
For each value of n,

$$J_n(I,\lambda) \le \lambda^{-1}\cdot T_\lambda(2-\lambda T_\lambda),\ \forall\lambda, I \tag{3.6}$$

where T_λ represents the solution of the equation

$$e^{-\lambda T} = 1 - \frac{1}{2}\lambda T \tag{3.7}$$

Observation: $T_\lambda = -\frac{\log p}{\lambda}$ and T_λ is the value of the distribution function in $x = 100(1-p)$, of the exponentially distributed variable, where $p \approx 0{,}203$.

Demonstration
The probability conditioned by the observations $Y_1, Y_2, ..., Y_n$, when $(v_1, v_2, ..., v_n)$ are known is:

$$\prod_{i=1}^{n}\left(e^{-\lambda T_i}\right)^{Y_i}\left(1-e^{-\lambda T_i}\right)^{1-Y_i} \tag{3.8}$$

As the distribution of $(v_1, v_2, ..., v_n)$ is independent of λ, then,

$$\frac{d}{d\lambda}\log L_n(\lambda) = -\sum_{i=1}^{n} T_i Y_i + \sum_{i=1}^{n}\frac{(1-Y_i)T_i e^{-\lambda T_i}}{(1-e^{-\lambda T_i})} =$$

$$= -\sum_{i=1}^{n}\frac{T_i(Y_i - e^{-\lambda T_i})}{(1-e^{-\lambda T_i})} \tag{3.9}$$

Mark $\frac{T_i(Y_i - e^{-\lambda T_i})}{1-e^{-\lambda T_i}} = X_i$

Using the relation (3.2) the result is

$$E(X_i X_j) = E\left\{X_i T_j\left(1-e^{-\lambda T_j}\right)^{-1}\cdot E\left[\left(Y_j - e^{-\lambda T_j}\right)\left(Y_1, ..., Y_{j-1}, T_1, ..., T_j\right)\right]\right\} = 0, \text{ for } j > i \tag{3.11}$$

Further on, the result is

$$E\left[\frac{d}{d\lambda}\log L_n(\lambda)\right]^2 = \sum_{i=1}^{n} E(X_i^2) = \sum_{i=1}^{n} E\left\{T_i^2\left(1-e^{-\lambda T_i}\right)^{-2}\cdot E\left[\left(Y_i - e^{-\lambda T_i}\right)^2 \middle| Y_1, ..., Y_{i-1}, T_1, ..., T_i\right]\right\} =$$

$$= E\sum_{i=1}^{n} T_i^2\left(1-e^{-\lambda T_i}\right)^{-1} e^{-\lambda T_i} \le n T_\lambda^2\left(1-e^{-\lambda T_\lambda}\right)^{-1} e^{-\lambda T_\lambda} \tag{3.11}$$

which shows that the function $T^2\left(1-e^{-\lambda T}\right)^{-1} e^{-\lambda T}$ is maximized for $T = T_\lambda$, hence it results the required enunciation.
Equality is obtained in (3.11) only and only if $p(T_i = T_\lambda) = 1, \forall i$.

If λ is known, then the inspection plan for the purpose of maximizing $J_n(I,\lambda)$, for each n and λ is called a periodical inspection plan with a T_λ time interval between two consecutive inspections. Aside from an array of the unknown values of λ, there is no optimal plan to obtain equality for.

Defining the adapted stochastic approximation plan

Definition 3.1

A I inspection plan is called adapted (related to $J(I,\lambda)$) if the following equality occurs:

$$J(I,\lambda) = \lambda^{-1} \cdot T_\lambda (2 - \lambda T_\lambda) \tag{3.12}$$

The following plan called the stochastic approximation plan (SA) is based on the Robins-Monro method and uses the fact that T_λ corresponds to the $100(1-p) \approx 79{,}7$ value of the exponential distribution, independent of λ.

If the T_1 is selected in the $\left[T_{\lambda_1}, T_\lambda\right]$ interval and the $(T_1, T_2, ..., T_n)$ is considered to be defined, then the following can be defined:

$$\lambda_n = T_n^{-1} \log p$$

$$A_n = \lambda_n^{-1} \cdot p^{-1} = -T_n (p \log p)^{-1}$$

$$T_{n+1} = \max\left[T_{\lambda_2}, \min\left\{T_\lambda, T_n + n^{-1} \cdot A_n (y_n - p)\right\}\right], \text{ for } n = 1,2 \tag{3.13}$$

Wasan establishes the following result with the condition that the defined relations are fulfilled.

Theorem 3.2

The SA plan described by the relations (3.13) is adapted (the demonstration is based on the convergence verification in the probability of the array $(T_n)_n$ to T_λ).

This result represents one of the usages of the stochastic approximation method for the resolution of applied problems.

REFERENCES

[1] Orman, V., G.: *Handbook of limit theorems a stochastic approximation.* Braşov. *Transilvania* University Publishing.
[2] Wasan, M., T.: *Stochastic approximation.* Cambridge University Press. 1969
[3] Robbins, H., Monro: *Stochastic approximation methods.* Ann. Math. Stat. 1951.
[4] Bailey, B., A., *Approximation theory,* Springer Proceedings in Mathematics. 2012.
[5] Bhattacharya Rabi, N., Waymire Edward, C., *Stochastic processes with applicatioons,* Siam edition. 2009.